



TECHNISCHE
UNIVERSITÄT
WIEN

DISSERTATION

DEVELOPMENT OF CARBONYL-SENSING ASSAYS FOR THE APPLICATION IN FLUORESCENCE-ACTIVATED DROPLET SORTING

ausgeführt zum Zwecke der Erlangung des akademischen Grades eines
Doktors der technischen Wissenschaften unter der Leitung von

Associate Prof. Florian Rudroff

&

Univ. Prof. Marko D. Mihovilovic,

Institut für Angewandte Synthesechemie, E163

eingereicht an der Technischen Universität Wien

Fakultät für Technische Chemie

von

Dipl.-Ing. Sebastian Hečko

Wien, 10.09.2021

*“Zweifel ham wa nicht ...
...brauch ma nicht.”*
— [Leon Goretzka](#)

*“There is nothing noble in being superior to your fellow man;
true nobility is being superior to your former self.”*
— [Ernest Hemingway](#)

Pre maminu

For my mother

Declaration

Erna Zukic contributed to establishing the expression system for Squalene hopene cyclase mutants derived from *Zymononas mobilis* and *Alicyclobacillus acidocaldarius* and their application for the biotransformation of citronellal analogs in C 1.1.2.

Albin Vadakkechira contributed to the synthesis of substrates and products for the study on the Squalene hopene cyclase catalyzed Prins reaction of citronellal analogs described in chapter C 1.1.1 and his bachelor thesis.

Stefan Giperakis contributed to the synthesis of substrates and products for the study on Squalene hopene cyclase catalyzed Friedel Crafts acylations of alkylated 3-(3-hydroxyphenyl)propanoic acids towards the respective indanones described in chapter C 1.2.

Astrid Schiefer contributed significantly with the optimization of the (5-amino-4-(N'-hydroxycarbamimidoyl)-2-methoxyphenyl)phosphonic acid 4-P,5-MeO-ABAO [148] synthesis, as well as the evaluation of its optical and kinetic properties in different pH systems described in chapter C 1.5.2.

Verena Scheibelreiter contributed to the synthesis of the parent 2-amino-N'-hydroxybenzimidamide ABAO [LIV], which enabled comparison of its kinetic and spectroscopic properties with synthesized ABAO- analogs described in chapter C 1.5.2.

Frederick Mortzfeld contributed to the synthesis of the (4-amino-5-(N'-hydroxycarbamimidoyl)-2-methoxyphenyl)phosphonic acid 5-P,4-MeO-ABAO [153] for the evaluation of its fluorometric properties in the amino benzamidoxime (ABAO) assay for the detection of aldehyde producing enzymes described in chapter C 1.5.2.

Front Matter

Table of Contents

Declaration	4
Front Matter	i
Table of Contents	i
Acknowledgments	vi
Abstract	ix
Kurzfassung	x
A Synthetic Schemes	12
A I Synthesis of citronellal analogs for SHC catalyzed Prins-reactions	12
A II Synthesis of fluorogenic substrates for SHC catalyzed Friedel-Crafts reactions	15
A III Synthesis of alkylated 3-(3-hydroxyphenyl)propanoic acids for SHC catalyzed Friedel-Crafts acylation	17
A IV Studies towards the synthesis and evaluation of fluorogenic adducts with NBD-H-type reagents	18
A V Improving water solubility of NBD-H / -HA reagents	20
A VI Improving water solubility of ABAO reagents	22
B Introduction	25
B I Prelude	25
B II Protein engineering in biocatalysis	26
B II.1 Directed evolution	26
B II.2 Squalene hopene cyclase (SHC)	28
B II.3 Carboxylic acid reductase (CAR)	31
B III Ultra-high-throughput screening (uHTS) for protein engineering	32
B III.1 Fluorescence-based assays	34
B III.1.1 Functional group assays	36
B III.1.1.1 Aldehyde selective assays	38
B III.1.1.2 Ketone selective assays	42
B IV Fluorescence-activated droplet sorting	45
B IV.1 Limitations	48
B IV.2 Applications in protein engineering efforts	49
B V Objectives	50
C Results and discussion	52
C I.1 Part I – SHC catalyzed Prins reaction	52
C I.1.1 Synthesis of citronellal derivatives	53
C I.1.2 Biotransformation with citronellal analogs	60

C I.2	Part II – Friedel-Crafts reaction of alkylated 3-(3-hydroxyphenyl)propanoic acids	66
C I.3	Part III – Synthesis of fluorogenic substrates for SHC catalyzed Friedel-Crafts acylation reactions	68
C I.4	Part IV – Substrate independent approach for the detection of carbonyl compounds using NBD-type reagents	77
C I.5	Part V – Improving the water solubility of assay compounds for carbonyl detection	99
C I.5.1	Nitrobenzoxadiazole (NBD) reagents	99
C I.5.2	Amino benzamidoxime (ABAO) reagents	111
C I.1	Part VI – Fluorescence-activated droplet sorting	135
C I.1.1	Optical assembly	136
C I.1.2	Manufacturing of microfluidic PDMS chips	140
C I.1.3	Droplet encapsulation	144
C I.1.4	Droplet sorting	146
C I.1.4.1	Proof of concept (unsuccessful at the point of writing)	153
D	Conclusion and Outlook	154
E	Experimental part	157
E I	Materials and methods – chemical synthesis	157
E I.1	Chromatographic methods	157
E I.2	NMR spectroscopy	158
E I.3	UV-Vis & Fluorescence spectroscopy	158
E I.4	Specific rotation	159
E I.5	Melting point	159
E I.6	HR-MS	160
E II	General procedures	160
E II.1	General procedure A: Wittig reaction and deprotection of citronellol derivative precursors	160
E II.2	General procedure B: Swern oxidation of citronellol derivatives	161
E II.3	General procedure C: BAIB/TEMPO oxidation of citronellol derivatives	162
E II.4	General procedure D: Negishi coupling of naphthyl derivatives with activated 4-ethoxy-4-oxobutylzinc bromide	163
E II.5	General procedure E: Alkylation of phenylpropionic acid, methyl esters	164
E II.6	General procedure F: Saponification of alkylated phenylpropionic acid, methyl esters	165
E II.7	General procedure G: Alkylation of 5-hydroxy-1-indanones	165
E II.8	General procedure H: Sulfonamidations of [1,2,5]-benzoxa- / benzthiadiazole sulfonyl chlorides.	166
E II.9	General procedure I: Nucleophilic aromatic substitution of sulfonamide aryl chloride and bromides with ethyl N-hydroxyacetimidate	167
E II.10	General procedure J: Quaternarizations of sulfonamide derivatives	168
E II.11	General procedure K: Palladium-catalyzed phosphinE-Carbon coupling of decorated ABAO precursors	169
E II.12	General procedure L: 2-Amino benzamidoxime (ABAO) synthesis by nucleophilic addition	170
E II.13	General procedure M: Lewis-acid promoted phosphonate deprotection of P-ABAO derivatives	171
E III	Chemical Synthesis	172
E III.1	Part I – Synthesis of citronellal analogs for SHC catalyzed Prins-reactions	172
E III.1.1	6-((Tert-butyldimethylsilyloxy)hexan-1-ol [2]	172
E III.1.2	6-((Tert-butyldimethylsilyloxy)hexanal [3]	173
E III.1.3	Hept-6-en-1-ol [5]	174
E III.1.4	7-Methyloct-6-en-1-ol [7]	175
E III.1.5	8-Methylnon-6-en-1-ol [9]	176
E III.1.6	6-Cyclopentylidenehexan-1-ol [11]	177
E III.1.7	7-Methyloct-6-enal [13]	178
E III.1.8	8-Methylnon-6-enal [14]	179
E III.1.9	6-Cyclopentylidenehexanal [15]	180
E III.1.10	(S)-Tert-butyl((3,7-dimethyloct-6-en-1-yl)oxy)dimethylsilane [17]	181
E III.1.11	(S)-6-((Tert-butyldimethylsilyloxy)-4-methylhexanal [18]	182
E III.1.12	(S)-3-Methylhept-6-en-1-ol [19]	183
E III.1.13	(S)-3,8-Dimethylnon-6-en-1-ol [20]	184
E III.1.14	(S)-6-Cyclopentylidene-3-methylhexan-1-ol [21]	185
E III.1.15	(S)-3-Methylhept-6-enal [22]	186
E III.1.16	(S)-3,8-Dimethylnon-6-enal [23]	187

E III.1.17	(<i>S</i>)-6-Cyclopentylidene-3-methylhexanal [24]	188
E III.1.18	(<i>R</i>)-Tert-butyl((3,7-dimethyloct-6-en-1-yl)oxy)dimethylsilane [26]	189
E III.1.19	(<i>R</i>)-6-((Tert-butyl)dimethylsilyloxy)-4-methylhexanal [27]	190
E III.1.20	(<i>R</i>)-3-Methylhept-6-en-1-ol [28]	191
E III.1.21	(<i>R</i>)-3,8-Dimethylnon-6-en-1-ol [29]	192
E III.1.22	(<i>R</i>)-6-Cyclopentylidene-3-methylhexan-1-ol [30]	193
E III.1.23	(<i>R</i>)-3-Methylhept-6-enal [31]	194
E III.1.24	(<i>R</i>)-3,8-Dimethylnon-6-enal [32]	195
E III.1.25	(<i>R</i>)-6-Cyclopentylidene-3-methylhexanal [33]	196
E III.1.26	(<i>S</i>)-4,8-Dimethylnon-7-enal [36]	197
E III.1.27	(<i>S</i>)-3,7-Dimethyloct-6-enal oxime [37]	198
E III.1.28	(<i>S</i>)-3,7-Dimethyloct-6-enenitrile [38]	199
E III.1.29	(<i>S</i>)-3,7-Dimethyloct-6-en-1-yl methanesulfonate [39]	200
E III.1.30	(4 <i>S</i>)-4,8-Dimethylnon-7-en-2-ol [40]	201
E III.1.31	(<i>S</i>)-3,7-Dimethyloct-6-enoic acid [41]	202
E III.1.32	<i>S</i> -Ethyl (<i>S</i>)-3,7-dimethyloct-6-enethioate [42]	203
E III.2	Part II – Synthesis of fluorogenic substrates for SHC catalyzed Friedel-Crafts reactions	205
E III.2.1	7-Bromonaphthalen-2-ol [44]	205
E III.2.2	2-Bromo-7-methoxynaphthalene [45]	206
E III.2.3	7-Methoxy-2-naphthaldehyde [46]	207
E III.2.4	1-(7-Methoxynaphthalen-2-yl)ethan-1-ol [48]	208
E III.2.5	1-(7-Methoxynaphthalen-2-yl)ethan-1-one [49]	209
E III.2.6	(2-Carboxyethyl)triphenylphosphonium bromide [51]	210
E III.2.7	6-Methoxynaphthalen-1-ol [53]	211
E III.2.8	6-Methoxynaphthalen-1-yl trifluoromethanesulfonate [54]	212
E III.2.9	4-(7-Methoxynaphthalen-2-yl)butanoic acid [56]	213
E III.2.10	6-Methoxy-2,3-dihydrophenanthren-4(1 <i>H</i>)-one [57]	214
E III.2.11	4-(6-Methoxynaphthalen-1-yl)butanoic acid [58]	215
E III.2.12	7-Methoxy-3,4-dihydrophenanthren-1(2 <i>H</i>)-one [59]	216
E III.3	Part III – Synthesis of alkylated 3-(3-hydroxyphenyl)propanoic acids for SHC catalyzed Friedel-Crafts acylation	217
E III.3.1	Methyl 3-(3-hydroxyphenyl)propanoate [61]	217
E III.3.2	(<i>S</i>)-3,7-Dimethyloctan-1-ol [62]	218
E III.3.3	(<i>S</i>)-1-Iodo-3,7-dimethyloctane [63]	219
E III.3.4	(<i>S</i>)-8-Iodo-2,6-dimethyloct-2-ene [64]	221
E III.3.5	Methyl 3-(3-(octyloxy)phenyl)propanoate [66]	222
E III.3.6	Methyl (<i>S</i>)-3-(3-((3,7-dimethyloctyl)oxy)phenyl)propanoate [67]	223
E III.3.7	Methyl (<i>S</i>)-3-(3-((3,7-dimethyloct-6-en-1-yl)oxy)phenyl)propanoate [68]	224
E III.3.8	3-(3-(Octyloxy)phenyl)propanoic acid [69]	225
E III.3.9	(<i>S</i>)-3-(3-((3,7-Dimethyloctyl)oxy)phenyl)propanoic acid [70]	226
E III.3.10	(<i>S</i>)-3-(3-((3,7-Dimethyloct-6-en-1-yl)oxy)phenyl)propanoic acid [71]	227
E III.3.11	5-Hydroxy-2,3-dihydro-1 <i>H</i> -indanone [72]	228
E III.3.12	5-(Octyloxy)-2,3-dihydro-1 <i>H</i> -inden-1-one [73]	229
E III.3.13	(<i>S</i>)-5-(3,7-Dimethyloctyl)oxy)-2,3-dihydro-1 <i>H</i> -inden-1-one [74]	230
E III.3.14	(<i>S</i>)-5-(3,7-Dimethyloct-6-en-1-yl)oxy)-2,3-dihydro-1 <i>H</i> -inden-1-one [75]	231
E III.4	Part IV – Studies towards the synthesis and evaluation of fluorogenic adducts with NBD-H-type reagents	232
E III.4.1	4-(1-Methylhydrazineyl)-7-nitrobenzo[c][1,2,5]oxadiazole (NBD-MH) [77]	232
E III.4.2	4-Hydrazineyl-7-nitrobenzo[c][1,2,5]oxadiazole hydrazine adduct (NBD-H) [78]	233
E III.4.3	(<i>E</i>)-4-(2-Benzylidenehydrazineyl)-7-nitrobenzo[c][1,2,5]oxadiazole [80]	234
E III.4.4	(<i>E</i>)-4-Nitro-7-(2-(1-phenylethylidene)hydrazineyl)benzo[c][1,2,5]oxadiazole [82]	235
E III.4.5	(<i>E</i>)-4-(2-(3,4-Dihydronaphthalen-1(2 <i>H</i>)-ylidene)hydrazineyl)-7-nitrobenzo[c][1,2,5]oxadiazole [84]	236
E III.4.6	O-(7-Nitrobenzo[c][1,2,5]oxadiazol-4-yl)hydroxylamine [86]	237
E III.4.7	(<i>E</i>)-1-Phenylethan-1-one O-(7-nitrobenzo[c][1,2,5]oxadiazol-4-yl) oxime [88]	238
E III.4.8	(<i>E</i>)-3,4-Dihydronaphthalen-1(2 <i>H</i>)-one O-(7-nitrobenzo[c][1,2,5]oxadiazol-4-yl) oxime [89]	239
E III.5	Part V – Improving water solubility of NBD-H /-HA reagents	241
E III.5.1	7-Chlorobenzo[c][1,2,5]oxadiazole-4-sulfonyl chloride [94]	241
E III.5.2	2-((7-Chlorobenzo[c][1,2,5]oxadiazole)-4-sulfonamido)- <i>N,N,N</i> -trimethylethan-1-aminium formiate [96]	242
E III.5.3	7-Chloro- <i>N</i> -(2-(dimethylamino)ethyl)benzo[c][1,2,5]oxadiazole-4-sulfonamide [98]	243
E III.5.4	Ethyl (<i>E</i>)- <i>N</i> -((7-(<i>N</i> -(2-(dimethylamino)ethyl)sulfamoyl)benzo[c][1,2,5]oxadiazol-4-yl)oxy)acetimidate [99]	244

E III.5.5	(E)-2-((7-(((1-Ethoxyethylidene)amino)oxy)benzo[c][1,2,5]oxadiazole)-4-sulfonamido)-N,N,N-trimethylethan-1-aminium iodide [100]	245
E III.5.6	7-Chloro-N-(2-(dimethylamino)ethyl)-N-methylbenzo[c][1,2,5]oxadiazole-4-sulfonamide [102]	246
E III.5.7	Ethyl (E)-N-((7-(N-(2-(dimethylamino)ethyl)-N-methylsulfamoyl)benzo[c][1,2,5]oxadiazol-4-yl)oxy)acetimidate [103]	247
E III.5.8	(E)-2-((7-(((1-Ethoxyethylidene)amino)oxy)-N-methylbenzo[c][1,2,5]oxadiazole)-4-sulfonamido)-N,N,N-trimethylethan-1-aminium iodide [104]	248
E III.5.9	7-Bromobenzo[c][1,2,5]thiadiazole-4-sulfonyl chloride [106]	249
E III.5.10	7-Bromo-N-(2-(dimethylamino)ethyl)-N-methylbenzo[c][1,2,5]thiadiazole-4-sulfonamide [107]	250
E III.5.11	Ethyl (E)-N-((7-(N-(2-(dimethylamino)ethyl)-N-methylsulfamoyl)benzo[c][1,2,5]thiadiazol-4-yl)oxy)acetimidate [108]	251
E III.5.12	(E)-2-((7-(((1-Ethoxyethylidene)amino)oxy)-N-methylbenzo[c][1,2,5]thiadiazole)-4-sulfonamido)-N,N,N-trimethylethan-1-aminium iodide [109]	252
E III.5.13	2-((7-Bromo-N-methylbenzo[c][1,2,5]thiadiazole)-4-sulfonamido)-N,N,N-trimethylethan-1-aminium iodide [110]	253
E III.5.14	2-((7-Hydrazineyl-N-methylbenzo[c][1,2,5]thiadiazole)-4-sulfonamido)-N,N,N-trimethylethan-1-aminium iodide [111]	254
E III.5.15	(E)-2-((7-(2-Benzylidenehydrazineyl)-N-methylbenzo[c][1,2,5]thiadiazole)-4-sulfonamido)-N,N,N-trimethylethan-1-aminium iodide [112]	256
E III.5.16	(E)-2-((7-(2-(3,4-Dihydronaphthalen-1(2H)-ylidene)hydrazineyl)-N-methylbenzo[c][1,2,5]thiadiazole)-4-sulfonamido)-N,N,N-trimethylethan-1-aminium iodide [113]	257
E III.6	Part VI – Improving water solubility of ABAO reagents	259
E III.6.1	5-Methoxy-2-amino benzamidoxime (5-MeO-ABAO) [124]	259
E III.6.2	Diethyl (3-amino-4-cyanophenyl)phosphonate [127]	260
E III.6.3	Diethyl (3-amino-4-(N'-hydroxycarbamimidoyl)phenyl)phosphonate [128]	261
E III.6.4	(3-Amino-4-(N'-hydroxycarbamimidoyl)phenyl)phosphonic acid (4-P-ABAO) [129]	262
E III.6.5	Diethyl (4-amino-3-cyanophenyl)phosphonate [131]	263
E III.6.6	Diethyl (4-amino-3-(N'-hydroxycarbamimidoyl)phenyl)phosphonate [132]	264
E III.6.7	(3-Amino-4-(N'-hydroxycarbamimidoyl)phenyl)phosphonic acid (5-P-ABAO) [133]	265
E III.6.8	Dibenzyl (3-amino-4-cyanophenyl)phosphonate [135]	266
E III.6.9	4-(Benzyloxy)-3-methoxybenzotrile [137]	267
E III.6.10	4-(Benzyloxy)-5-methoxy-2-nitrobenzotrile [138]	268
E III.6.11	2-Amino-4-hydroxy-5-methoxybenzotrile [139]	269
E III.6.12	4-Hydroxy-5-methoxy-2-nitrobenzotrile [140]	270
E III.6.13	Dibenzyl (4-cyano-2-methoxy-5-nitrophenyl) phosphate [141]	271
E III.6.14	4-Cyano-2-methoxyphenyl trifluoromethanesulfonate [142]	272
E III.6.15	4-Carbamoyl-2-methoxy-5-nitrophenyl trifluoromethanesulfonate [143] and 4-cyano-2-methoxy-5-nitrophenyl trifluoromethanesulfonate [144]	273
E III.6.16	4-Cyano-2-methoxy-5-nitrophenyl trifluoromethanesulfonate [144]	275
E III.6.17	Diethyl (4-cyano-2-methoxy-5-nitrophenyl)phosphonate [145]	276
E III.6.18	Diethyl (5-amino-4-cyano-2-methoxyphenyl)phosphonate [146]	277
E III.6.19	Diethyl (5-amino-4-(N'-hydroxycarbamimidoyl)-2-methoxyphenyl)phosphonate [147]	278
E III.6.20	(5-Amino-4-(N'-hydroxycarbamimidoyl)-2-methoxyphenyl)phosphonic acid (4,5-P-MeO-ABAO) [148]	279
E III.6.21	2-Amino-5-bromo-4-methoxybenzotrile [150]	280
E III.6.22	Diethyl (4-amino-5-cyano-2-methoxyphenyl)phosphonate [151]	281
E III.6.23	Diethyl (4-amino-5-(N'-hydroxycarbamimidoyl)-2-methoxyphenyl)phosphonate [152]	282
E III.6.24	(4-Amino-5-(N'-hydroxycarbamimidoyl)-2-methoxyphenyl)phosphonic acid [153]	283
E III.6.25	2-Amino-3-bromo-5-methoxybenzotrile [154]	284
E III.6.26	Diethyl (2-amino-3-cyano-5-methoxyphenyl)phosphonate [155]	285
E III.6.27	Diethyl (2-amino-3-(N'-hydroxycarbamimidoyl)-5-methoxyphenyl)phosphonate [156]	286
E III.6.28	(2-Amino-3-(N'-hydroxycarbamimidoyl)-5-methoxyphenyl)phosphonic acid (3,5-P-MeO-ABAO) [157]	287
E III.6.29	N-(2-cyano-4-methoxyphenyl)acetamide [159]	288
E IV	Biotransformation of SHC variants	289
E IV.1	Standard media preparations	289
E IV.2	<i>Zymomonas mobilis</i> (Zmo)	289
E IV.2.1	Expression of the <i>Z. mobilis</i> SHC variants in <i>Escherichia coli</i>	289
E IV.2.2	Cell treatment before the biotransformation	290
E IV.2.3	Biotransformation	290

E IV.2.4	Biotransformation of (S)-6-cyclopentylidene-3-methylhexanal [24] with ZMO variant F486C to (1S,2R,5S)-2-(cyclopent-1-en-1-yl)-5-methylcyclohexan-1-ol [161]	291
E IV.2.5	Biotransformation of (R)-6-cyclopentylidene-3-methylhexanal [33] with ZMO variant F486C to (1R,2R,5R)-2-(cyclopent-1-en-1-yl)-5-methylcyclohexan-1-ol [162]	292
E IV.2.6	Biotransformation of (R)-6-cyclopentylidene-3-methylhexanal [33] with ZMO variant W555Y to (1S,2R,5R)-2-(cyclopent-1-en-1-yl)-5-methylcyclohexan-1-ol [163]	293
E V	Assembly and application of the FADS system	294
E V.1	Equipment set-up	294
E V.1.1	Optical alignment	297
E V.1.2	Flow controller pressure connection	301
E V.2	Manufacturing of microfluidic PDMS chips	302
E V.2.1	Master mold fabrication	302
E V.2.2	PDMS chips fabrication	305
E V.2.3	Chip preparation and electronics	306
E V.2.3.1	Silanization	306
E V.2.3.2	Electrode manufacturing	307
E V.2.3.3	Electrical connectivity	307
E V.3	Droplet encapsulation	308
E V.4	Droplet sorting	310
E V.5	(Failed) Proof of sorting	312
F	Appendix	313
F I	List of materials for the FADS	313
F II	Gene sequences	316
F III	List of abbreviations	319
F IV	Curriculum vitae	320
F V	References	322

Acknowledgments

Die Jahre meines PhDs haben mich durch viele Superlative geführt – sie waren die lehrreichste, aufregendste, stressigste, aber auch lustigste Zeit in meinem bisherigen Leben. Den unzähligen Menschen, die mich durch diesen Abschnitt meiner Ausbildung geführt haben, will ich in den nächsten Zeilen danken.

Lieber Marko, ich danke dir, dass du mir bereits schon im Diplomstudium dein Vertrauen entgegengebracht hast und mich für meinen PhD in deine Gruppe aufgenommen hast. Insbesondere möchte ich mich bedanken, dass ich die Chance bekommen habe, an so einem spannenden, aber auch riskantem Thema arbeiten zu dürfen. Du hast mir stets die Freiheiten gelassen, mich akademisch auszutoben und ich hatte immer das Gefühl, dass ich bei dir bei jeglichen Entscheidungen die wissenschaftliche und persönliche Rückendeckung habe.

Lieber Flo, obwohl ich nicht von Anfang an die Ehre und das Vergnügen hatte mit dir zusammenzuarbeiten, bin ich wirklich sehr froh dich ab der Halbzeit meines PhDs meinen wissenschaftlichen Chaperon nennen dürfen zu haben. Über die letzten Jahre sind wir denke ich zu einem ausgezeichneten Team herangewachsen und haben dadurch viele wissenschaftliche, aber auch sportliche Erfolge einstreichen konnten. Deine Tür war stets offen für fachlichen Input, sowie auch gelegentliche hopfenhaltige Plaudereien. Die Wildsauläufe und auch etliche Weihnachtsfeiern unter deiner Schirmherrschaft werden mir ganz sicher unvergesslich bleiben.

Ein großes Danke gilt auch Christian Stanetty und Michael Schnürch, die stets mit frischen Denkanstößen in Seminaren und zwischen Tür und Angel zu meiner wissenschaftlich, aber auch persönlichen Weiterentwicklung beigetragen haben.

Vielen Dank auch Irena und UFlo für ihren Einsatz die Gerätschaften auf der TU Wien in Betrieb zu halten. Weiters auch ein großes Danke Christian Hametner für das Messen von herausfordernden NMR-Studien. Auch ein Danke an Frank Johannes von TU Wien Werkstatt für die Mithilfe bei der Planung auf Aufbau des FADS-Grundgerüsts. Ich möchte mich auch bei Mario Rothbauer und Sarah Spitz aus der Forschungsgruppe von Prof. Ertl bedanken, die mir bei der Herstellung der PDMS Chips mit ihrer tatkräftigen Hilfe zur Seite gestanden sind. Ein großes Danke gilt auch Erna Zukic, ohne die die SHC Methodologie in der Arbeitsgruppe niemals so Fuß gefasst hätte.

Die Wissenschaft ist jedoch nur ein Teil des PhDs – das Miteinander innerhalb der Forschungsgruppe ein anderer wichtiger Part. Ich bin unglaublich dankbar eine solch freundliche und familiäre Arbeitsatmosphäre erlebt haben zu dürfen. Die Erfolge in dem PhD wären in dieser Form sicher nicht möglich gewesen ohne meine zwei Mitstreiter im „Droplet“-Team. Freddy und Astrid, ihr wart mit Sicherheit mitentscheidend für den Fortschritt und den Spaß, den die Arbeit mit sich gebracht hat. Die Laserwunden, mühseligen Klempner- und Maschinenbauarbeiten und langen, langen Nächte waren (und das trotz unserer ganz unterschiedlichen Musikgeschmäcker) irgendwie durchzuhalten, weil wir uns stets gemeinsam den Rücken gestärkt haben.

Die Aktivitäten in der Koch-, Lauf- oder Bouldertruppe sowie die unzähligen Weihnachts- und Oktoberfeste und Apres-Synthesebiere haben dazu beigetragen, dass sich viele meiner Kollegen zu meinen engsten Freuden entwickelt haben. Insbesondere meine Mitstreiter im Labor „G20“ haben miteinander viel gelitten und viel gefeiert. Einen besonderen Dank gilt dir El Capitano, Elektro-Italo-DJ, Wein-Gourmand Drasi Drasko Draskovitser – die unzähligen Segelurlaube und Feiern werden mir sicher (un)vergesslich bleiben. Vielen, vielen Dank für deinen immerwährenden Beistand sowohl in als auch außerhalb des Labors – ich hoffe wir werden noch einige Geburtstage zusammen ausrichten. Lieber Hubert (Hubs(ch)i – es musste sein), als Benchpartner waren wir zu Zeiten unsere gegenseitigen Pls

sowie auch Kummerkästen. Vielen Dank für viele entspannte Afterwork-Biere und einige befreiende Gespräche bei Rick&Morty Filmabenden. Mein Monsterlieferant Clemens – die unzähligen Wochenenden, die wir gemeinsam im Labor verbracht haben und über das Leben philosophiert haben werde ich nicht vergessen. Ich danke auch unseren neuen G20-Mitgliedern, insbesondere dir Christoph – immer ein Mann der Tat, bewaffnet mit Computer, 3D-Drucker und Boulderschuh. Dr. Hollywood Dreier – ich weiß nicht, ob dein übermäßiger Pasta- und Pesto-Konsum der Gesundheit förderlich war, aber ich muss mich ganz besonders bei dir bedanken, da du einer der ersten warst der mich unglaublich herzlich in die Gruppe willkommen geheißen hat. Unsere gemeinsamen TEDx-Zeiten haben mich ganz eindeutig persönlich unglaublich weitergebracht – ich danke dir für die damalige Chance etwas außerhalb der Unilandschaft zu bewegen. Ein generelles Danke zählt allen derzeitigen und damaligen Mitgliedern des G20 Labors mit Kathi, Laszlo und Philipp.

Mein liebes Cousinchen Dani – ich glaube, dass wir erst über den PhD so richtig (oder wieder) zueinander gefunden haben. Ich habe unsere ehrliche, direkte und manchmal für Außenstehende unpassenden Art miteinander zu reden wahrlich im Labor vermisst. And also, my dear Resi-mu – you started from being this inapproachable Italian girl who spoke at least 5-times as fast as any average Austrian to being one of my dearest friends. I hope we'll get to have many more evenings celebrating with a little "Damenspitz". David auch dir danke für deine immer aufmunternden Worte und deine go-to Arbeitsmentalität, die doch immer dazu bewogen hat, doch noch das letzte Quäntchen rauszuholen – möge deine Beautyfarm in Fülle gedeihen. Danke auch dir Tom für die letzten Jahre in denen du trotz deines Sprachhandicaps dennoch das Wissen über die Unsterblichkeit und die Klempnerlehre unter das Volk gebracht hast. Lydia danke für die verrückten Diskussionen die während meiner Zeit hinter der Tastatur geklemmt, oft das Schreiben erleichtert haben – ich hoffe, dass du in deinen letzten Jahren im PhD doch noch den Avocado-Dieb findest – pusinka. Ein großes Danke auch dir Kathi, die du mich in der Zeit, in der diese Arbeit Formen angenommen hat, immer wieder mit deiner charmanten, unvergleichlichen Art motivieren konntest und mir gut zugesprochen hast – ohne unseren zwischenzeitlichen Tratsch wäre die Zeit sicher nicht so schnell vergangen. Ein Danke auch die alteingesessenen Mädels des G10er und Biolabs, Jo, Nina und Julia – ihr schafft es immer in den tristen Alltag des Labors einen gewissen Charme zu bringen, sodass einem eigentlich nie langweilig wurde – auf dass doch viele XXL-Töpfe gefüllt und noch einige (virtuelle) Berge beklommen werden. Vielen Dank auch der Burschenverstärkung des „Mädls-Labs“ – und die immer wiederkehrenden spannenden Diskussionen in der Küche mit Viktor, Dominik, Richy und Stefan.

Vielen Dank auch den vielen Menschen außerhalb unserer Forschungsgruppe – insbesondere der lieben Nicole (langes i) – was haben wir schon gemeinsam gefeiert, gelacht und auch einiges geweint, Babsi (Bobschi oder Terminatorⁱⁿ) – wir holen uns noch ganz sicher einen gemeinsamen Marathon in Spitzenzeit, Michi (Michael Schumacher Ferrari) – irgendwann wird's noch ein Kran (was auch immer das heißen soll) sowie meinem Work-husband Wilko – ich freu mich schon auf viele, viele Kulturdates und Kulturmenüs während unserer gemeinsamen Zeit in der Startup-Szene.

Ein großes Danke auch an meine ehemaligen und derzeitigen Studenten, Matthias Schöbinger, Albin Vadakkechira, Johanna Zieher, Stefan Giparakis und Lorenz Gruber für ihren Beitrag zu dieser Arbeit.

Zu guter Letzt möchte ich meiner Familie und insbesondere meiner Mutter danken – ohne deine immerwährende Unterstützung und der Sicherheit, dass du immer hinter mir stehst, würde ich nicht dort stehen, wo ich gerade bin. Ich danke für die ganzen kleinen wiederkehrenden Erinnerungen auch in der tiefsten Nacht, dass ich doch ja genug trinken, schlafen und mich doch einmal bitte ausruhen soll. Dadurch wusste ich immer, dass du immer über mich wachst! Vielen, vielen Dank!

Abstract

Enzymes have intrigued chemists to pursue their catalytic utility ever since their first reports. Due to their unparalleled versatility and selectivity, they provide an efficient and environmentally benign alternative to conventional organic synthetic methodology. Especially with the surge in recent identifications of new catalytically active proteins enabled by bioinformatics and developments in protein engineering, their use has increasingly found its place in the catalytic landscape. Herein *de novo* designed proteins derived by computational methods or directed evolution approaches using randomized structural mutations allow the chemist to delve into uncharted reaction territory. Especially the latter, however, requires sophisticated screening tools which can cope with the immense numbers of variants created by truly randomized approaches. Novel ultra-high-throughput screening (uHTS) systems enable the assessment of libraries of up to 10^7 samples using microfluidic devices and highly sensitive assays.

Among these approaches, fluorescence-activated droplet sorting (FADS) systems entrap aqueous single-cell chemical reactors in pL sized droplets in perfluorinated media. Simultaneously encapsulated assay components interact with the target of choice enabling sensitive detection *via* laser-induced fluorescence (LIF). With the use of surfactants, coalescence of the droplets is prevented, and the readout can be directly correlated to individual enzymatic activity. However, a substantial water solubility of the assay components – correlated to logD values – was shown to be a prerequisite to impair the transport of fluorescent products between singular droplets through the continuous phase.

This thesis aimed to develop analytical toolsets that would enable rapid evaluation of directed evolution libraries for two promiscuous enzymes using the FADS approach, namely the squalene hopene cyclase (SHC) and carboxylic acid reductase (CAR). In both cases, the envisioned enzymatic transformations were to yield carbonyl compounds that were either inherently fluorescent or detected *via* downstream conjugation with suitable fluorogenic reporters targeting the reactive carbonyl moiety.

Initially, based on the recently discovered carbonyl activation mode of the SHC, a set of known citronellal derivatives were used to establish the novel biocatalytic system in the research group and elaborate its catalytic promiscuity for an enzymatic Prins reaction. Building upon these results, we targeted harnessing its Brønsted acidic catalytic machinery for an analogous cyclization of suitable fluorogenic aryl nucleophiles in a formal Friedel-Crafts acylation (FCA). Due to the lack of initial hits for the non-native transformation, we pursued an ultra-high-throughput approach to implement a carbonyl-selective sensor. Herein two distinct approaches were explored using already established carbonyl-specific assay tools based upon NBD (7-nitro-2,1,3-benzoxadiazole) and ABAO (amino benzamidoxime) reagents and adapted to be applicable in a FADS regime. This was achieved with the incorporation of hydrophilic groups, which minimized leakage across the droplet interface. Both synthesized water-soluble derivatives were proven to exhibit similar positive optical and kinetic profiles.

Complementing the development of the chemical carbonyl assays, a novel custom-built FADS system was established at the TU Wien, covering the optical and optomechanical hardware assembly, installation of the microfluidic flow controller, the manufacture of microfluidic chips, and the writing of the LabView code for the final sorting process.

Kurzfassung

Enzyme haben aufgrund ihrer unvergleichlichen Selektivität und Versatilität Chemiker seit Beginn an verleitet, ihren katalytischen Nutzen zu erforschen. Sie bieten eine effiziente und umweltfreundliche Alternative zu herkömmlichen organischer Synthesemethodik. Vor allem durch die zunehmende Identifizierung neuer Biokatalysatoren mittels Einsatzes von Bioinformatik und weitreichenden Entwicklungen im Protein-Engineering Bereich, hat ihre Verwendung einen stetig wachsenden Platz in der katalytischen Landschaft eingenommen. Mithilfe von gerichteter Evolution, in welcher zufällige Mutationen in die Struktur von Proteinen eingebaut werden, können Chemiker noch unerforschte Reaktionen realisieren. Die immense Anzahl an Enzymvarianten, die durch randomisierte Mutation erzeugt werden, erfordert jedoch ausgefeilte Selektions-Werkzeuge. Neuartige Ultra-Hochdurchsatz-Screening-Systeme ermöglichen die Untersuchung von Bibliotheken mit bis zu 10^7 Enzymvarianten durch Einsatz von mikrofluidischen Geräten und hochempfindlichen Fluoreszenz-Assays. Zu diesen Ansätzen gehört das Fluorescence-Activated Droplet Sorting (FADS), worin einzelne Zellmutanten in pL-großen wässrigen Tröpfchen mit perfluorierten Medien umschlossen werden. Gleichzeitig interagieren miteingeschlossene fluorogene Assay-Komponenten mit dem gewünschten enzymatisch-hergestellten Produkt und ermöglichen so einen empfindlichen Nachweis der gewünschten Reaktionen mittels laserinduzierter Fluoreszenz (LIF). Durch die Verwendung von Tensiden wird die Koaleszenz der Tröpfchen verhindert, und die Messwerte können direkt mit der individuellen enzymatischen Aktivität in Zusammenhang gebracht werden. Es hat sich jedoch gezeigt, dass eine hohe Wasserlöslichkeit der Testkomponenten - korreliert mit logD-Werten - eine Voraussetzung ist, um den Transport der fluoreszierenden Produkte zwischen einzelnen Tröpfchen durch die kontinuierliche Phase zu beeinträchtigen.

Ziel dieser Arbeit war es, analytische Werkzeuge zu entwickeln, die eine schnelle Evaluierung von Bibliotheken mit gerichteter Evolution unter Verwendung des FADS-Ansatzes für zwei promiskuitive Enzyme, die Carbonsäurereduktase (CAR) und die Squalen-Hopenzyklase (SHC), ermöglichen würden. In beiden Fällen führten die geplanten enzymatischen Umwandlungen zu Carbonylverbindungen. Diese waren entweder inhärent fluoreszent oder wurden durch nachgeschaltete Konjugation mit geeigneten fluorogenen Reportern nachgewiesen.

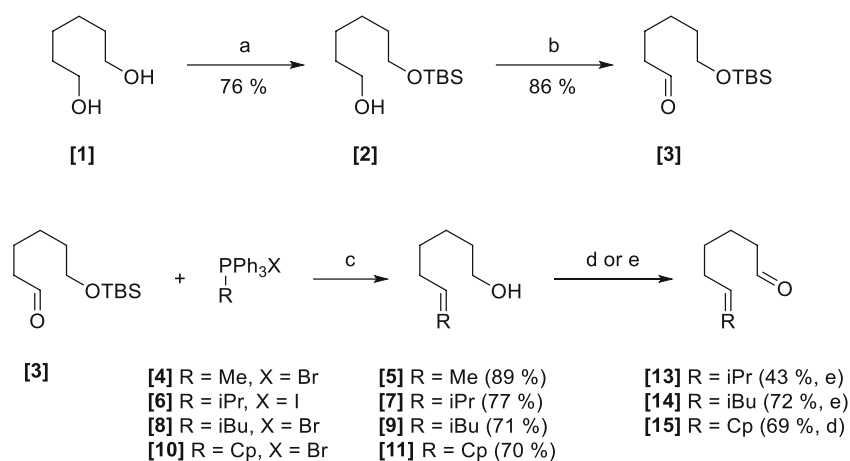
Zu Beginn wurde die SHCs als neues biokatalytisches System in der Forschungsgruppe etabliert. Hierzu wurde eine Reihe bekannter Citronellal-Derivate synthetisiert, um die katalytische Promiskuität einiger SHC Mutanten für die enzymatische Prins-Reaktion zu eruieren. Aufbauend auf diesen Ergebnissen wurde versucht die Brønsted-saure katalytische Maschinerie für eine analoge Cyclisierung geeigneter fluorogener Arylnukleophile in einer formalen Friedel-Crafts-Acylierung (FCA) nutzbar zu machen. Aufgrund der Inkompatibilität der Enzyme für diese nicht-natürliche Transformation wurde eine Mutationsstudie mittels gerichteter Evolution beabsichtigt. Die Identifizierung von positiven Mutanten sollte mittels Ultra-Hochdurchsatz-Screenings durch Implementierung eines carbonylselektiven Sensors möglich gemacht werden. Hierbei wurden zwei verschiedene Ansätze unter Verwendung bereits etablierter carbonylspezifischer Assay-Tools auf der Basis von NBD- (7-Nitro-2,1,3-benzoxadiazol) und ABAO- (2-Aminobenzamidoxim) Reagenzien erforscht und so angepasst, dass sie in FADS-Systemen anwendbar gemacht werden können. Dies wurde durch den Einbau hydrophiler

Gruppen erreicht, die einen möglichen Austritt über die Tröpfchengrenzfläche minimieren. Die synthetisierten wasserlöslichen Derivate wiesen nachweislich unverändert positive optische und kinetische Eigenschaften auf. Ergänzend zur Entwicklung der chemischen Carbonyl-Assays wurde an der TU Wien ein individuell konfigurierbares FADS-System etabliert. Der Aufbau des Instruments beinhaltet die optische und optomechanische Hardware-Montage, die Installation des mikrofluidischen Durchflussreglers, die Herstellung der mikrofluidischen Chips sowie das Schreiben des auf LabView basierenden Codes, welcher für die Steuerung des Sortierprozesses verantwortlich ist.

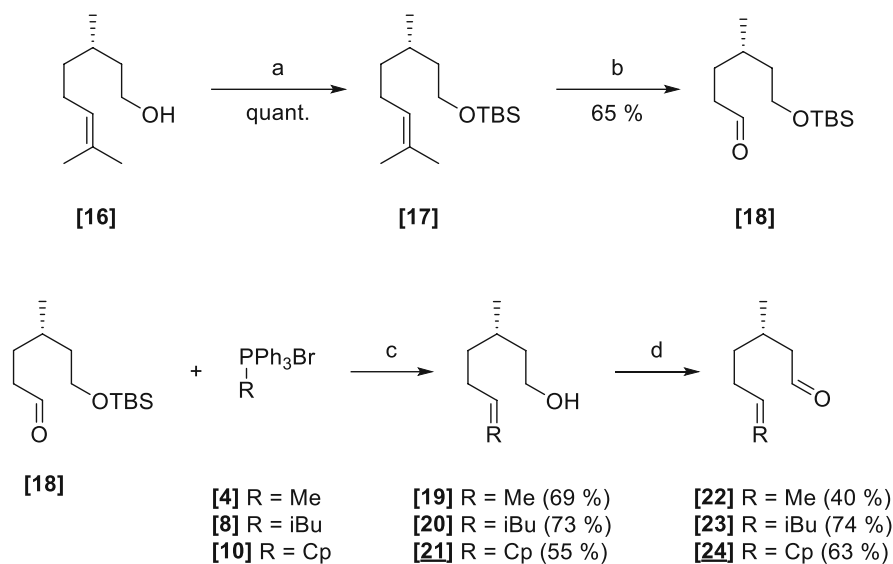
A Synthetic Schemes

All compounds prepared or used as starting materials in this thesis are numbered in bold Arabic numerals. Compounds unknown to the literature are additionally underlined>. Compounds referred to the literature or presented hypothetically are numbered in Roman numerals - Structures presented within the introduction are numbered in lowercase roman numerals.

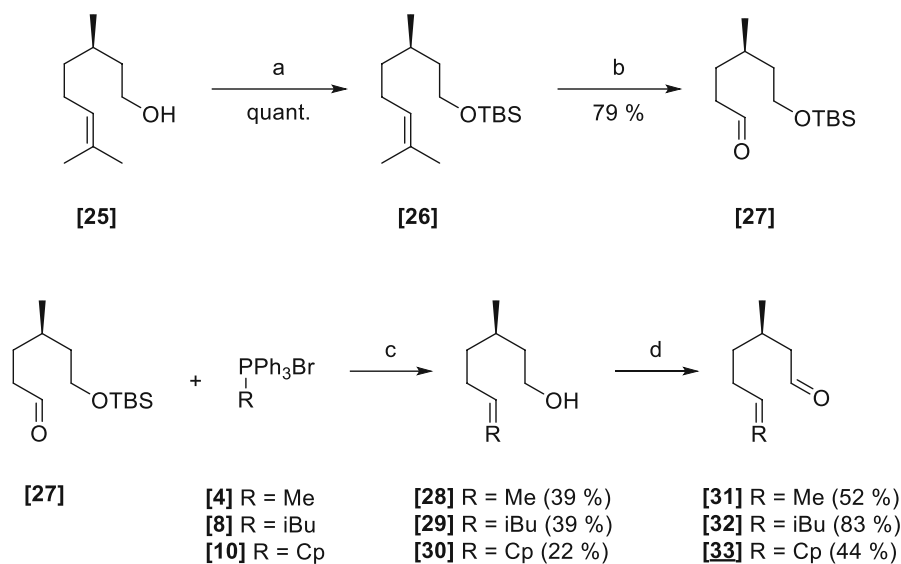
A I Synthesis of citronellal analogs for SHC catalyzed Prins-reactions



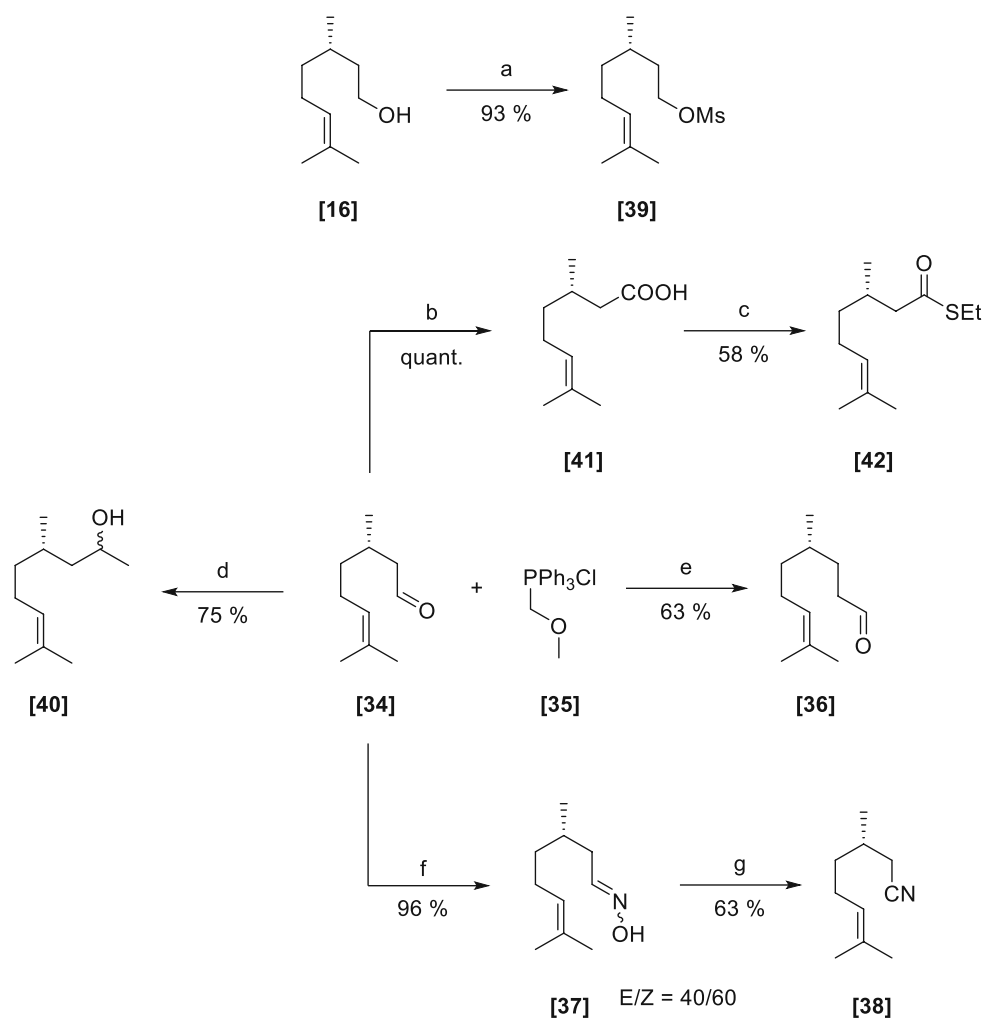
Scheme A-1: Reagents and conditions: a) TBSCl, imidazole, dry DMF, 0 °C to rt; b) (COCl)₂, dry DMSO, dry NEt₃, dry CH₂Cl₂, -78 °C to rt, Ar; c) n-BuLi, 0 °C to rt then 1M TBAF in THF, dry THF, rt, Ar; d) (COCl)₂, dry DMSO, dry NEt₃, dry CH₂Cl₂, -78 °C to rt, Ar; e) BAIB, cat. TEMPO, MeCN/H₂O (pH 7), 0 °C to rt.



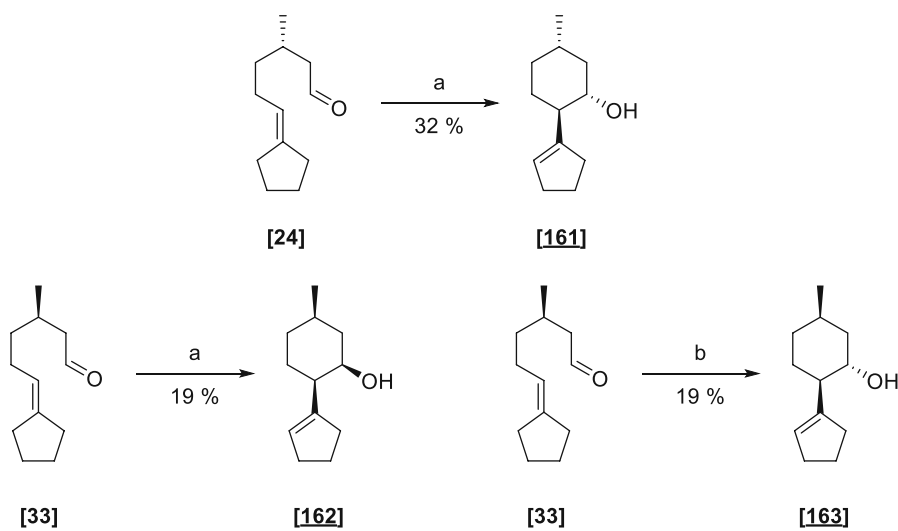
Scheme A-2: Reagents and conditions: a) TBSCl, imidazole, dry CH_2Cl_2 , 0 °C to rt, Ar; b) O_3 , 1:1 dry $\text{CH}_2\text{Cl}_2/\text{MeOH}$, -78 °C then Me_2S , -78 °C to rt, Ar; c) n-BuLi, 0 °C to rt then 1M TBAF in THF, dry THF, rt, Ar; d) $(\text{COCl})_2$, dry DMSO, dry NEt_3 , dry CH_2Cl_2 , -78 °C to rt, Ar.



Scheme A-3: Reagents and conditions: a) TBSCl, imidazole, dry CH_2Cl_2 , 0 °C to rt, Ar; b) O_3 , 1:1 dry $\text{CH}_2\text{Cl}_2/\text{MeOH}$, -78 °C then Me_2S , -78 °C to rt, Ar; c) n-BuLi, 0 °C to rt then 1M TBAF in THF, dry THF, rt, Ar; d) $(\text{COCl})_2$, dry DMSO, dry NEt_3 , dry CH_2Cl_2 , -78 °C to rt, Ar.

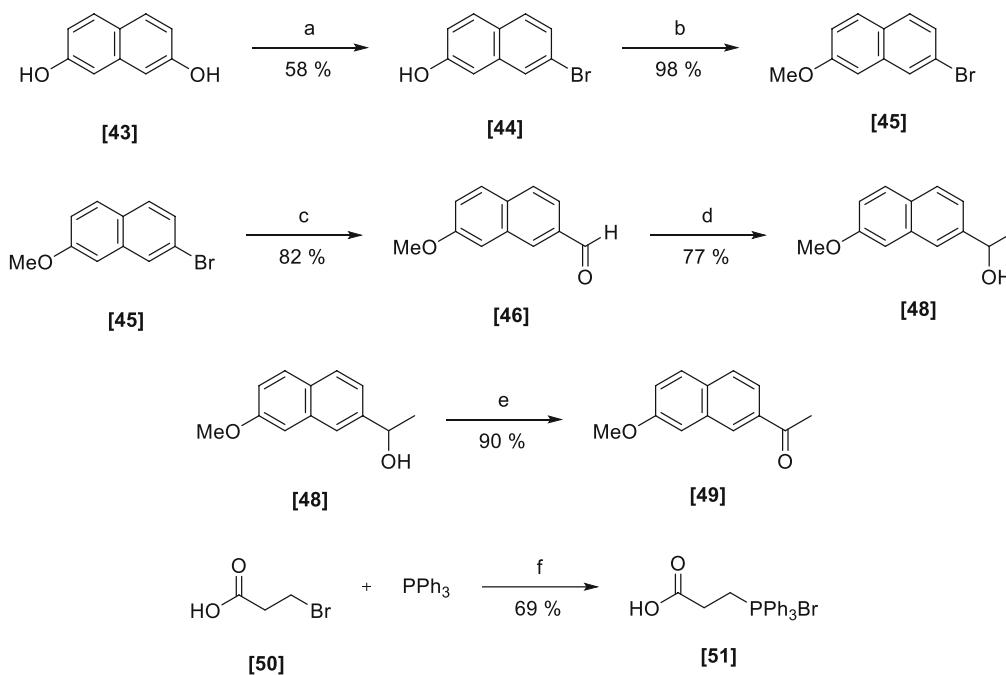


Scheme A-4: Reagents and conditions: a) MsCl, dry NEt_3 , dry CH_2Cl_2 , 0 °C to rt, Ar; b) AgNO_3 , NaOH, H_2O , 0 °C to rt; c) EDCI.HCl, dry DIPEA, 10 mol% DMAP, EtSH, dry CH_2Cl_2 , 0 °C to rt, Ar; d) 3M MeMgCl in THF, dry THF, 0 °C to rt, Ar; e) KOTBu , 0 °C to rt, dry THF, Ar then 3:1 THF/1 M HCl, rt; f) $\text{NH}_2\text{OH}\cdot\text{HCl}$, Na_2CO_3 , $\text{H}_2\text{O}/\text{MeOH}$, rt; g) 5 mol% $\text{Cu}(\text{OAc})_2$, MeCN, rt.

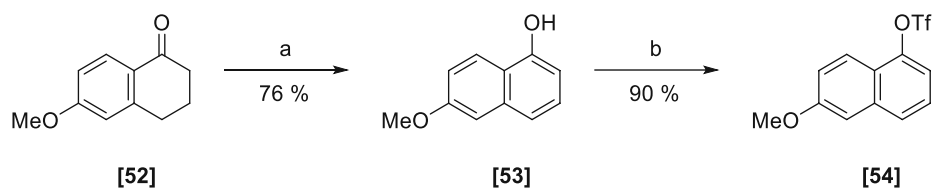


Scheme A-5: Reagents and conditions: a) ZMO F486C, 50 mM pH 6.0 citrate buffer, 24 h; b) ZMO W555Y, 50 mM pH 6.0 citrate buffer, 24 h.

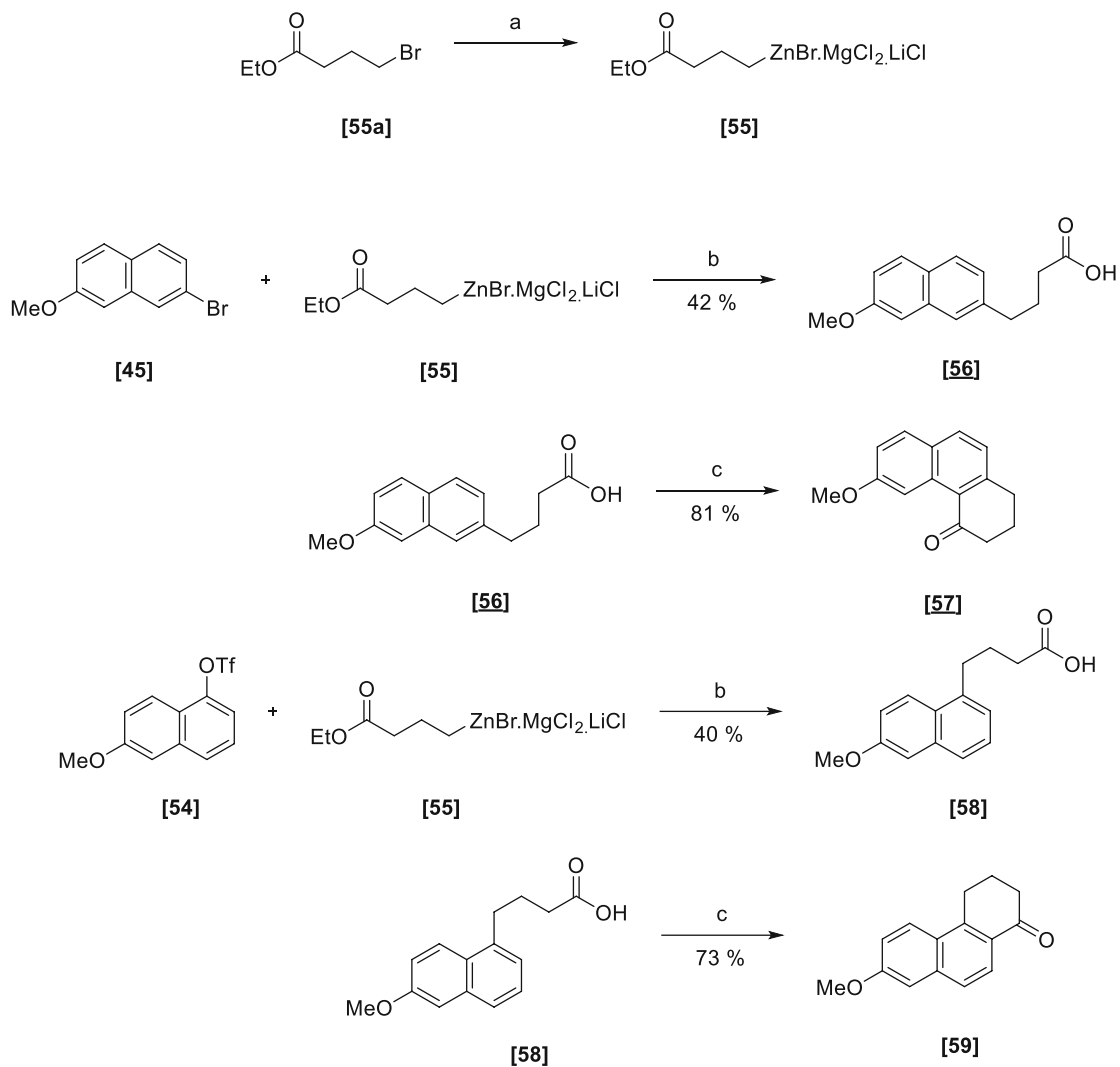
A II Synthesis of fluorogenic substrates for SHC catalyzed Friedel-Crafts reactions



Scheme A-6: Reagents and conditions: a) PPh₃, Br₂, 0 °C to rt, MeCN then dihydroxynaphthalene, 70 °C, 1 h, evaporate then 250 °C, 1 h; b) CH₃I, K₂CO₃, dry acetone, rf, Ar; c) nBuLi, -78 °C, dry THF, Ar then dry DMF, -78 °C to rt, THF, Ar; d) 1M MeMgBr in Et₂O, dry Et₂O, 10 °C to rt, Ar; e) DMP, dry CH₂Cl₂, rt, Ar; f) MeCN, rf.

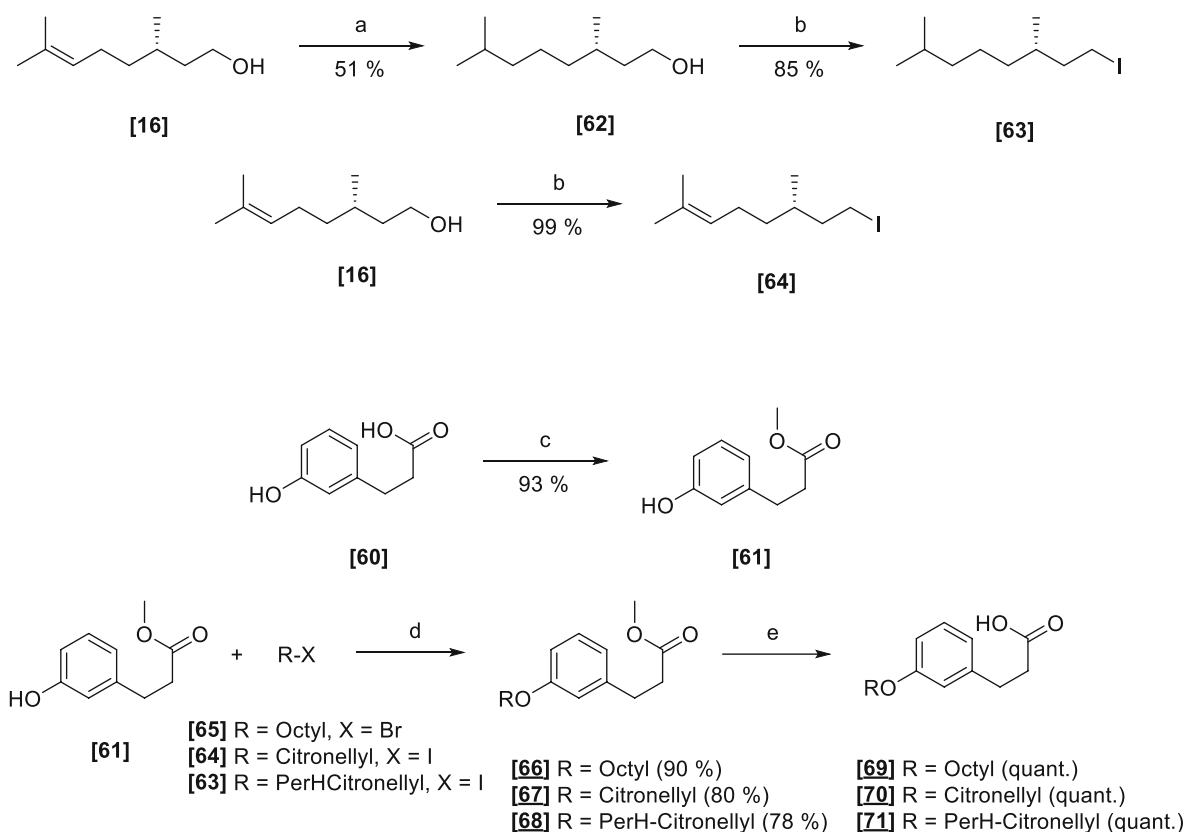


Scheme A-7: Reagents and conditions: a) 1. Br₂, cat. HCl, dry Et₂O, < 5 °C then LiBr, Li₂CO₃, DMF, rf, Ar; b) Tf₂O, dry NEt₃, dry CH₂Cl₂, -40 °C to rt, Ar.

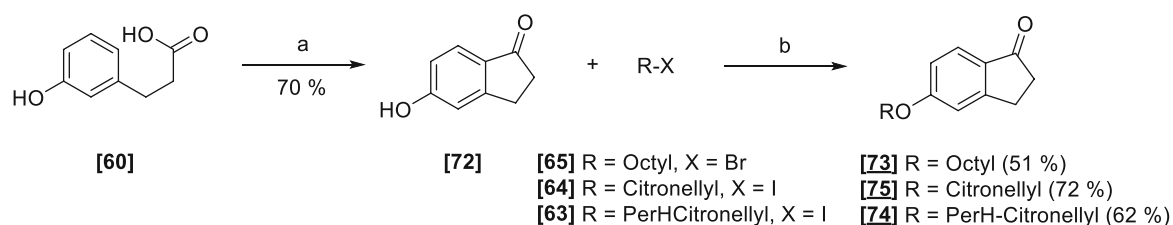


Scheme A-8: Reagents and conditions: a) LiCl, ZnCl₂, Mg, 4-bromobutanoate, dry THF, 3 h; b) Pd(PPh₃)₄, dry THF, rt to 50 °C, then KOH, H₂O/THF, rf; c) (COCl)₂, cat. DMF, dry CH₂Cl₂, rt, Ar.

A III Synthesis of alkylated 3-(3-hydroxyphenyl)propanoic acids for SHC catalyzed Friedel-Crafts acylation

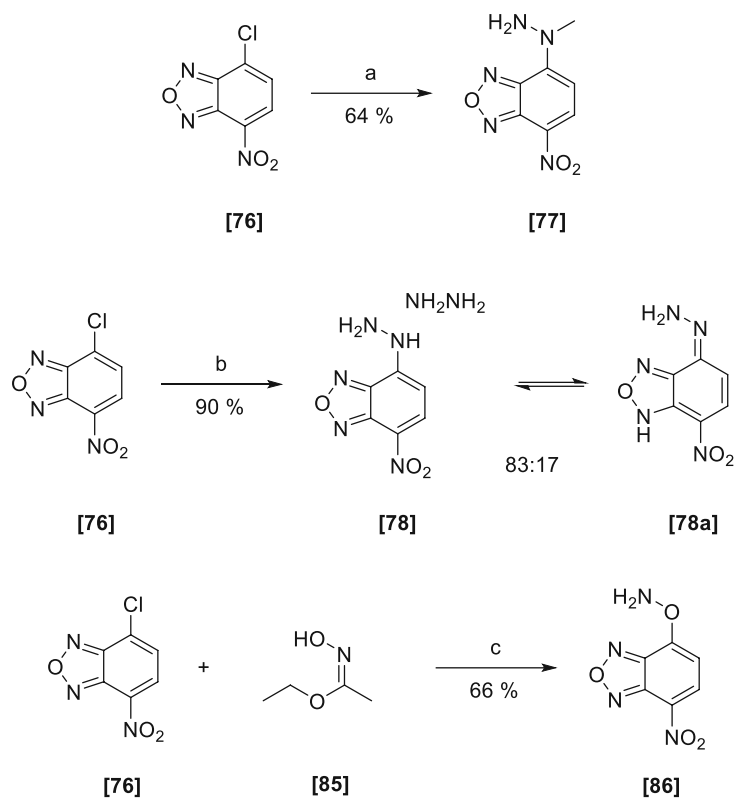


Scheme A-9: Reagents and conditions: a) 10 wt% Pd/C, H₂, MeOH; b) PPh₃, imidazole then I₂, CH₂Cl₂, 0 °C to rt, Ar; c) H₂SO₄, dry MeOH, 50 °C; d) K₂CO₃, dry, degassed DMF, 80 °C, Ar; e) 2N KOH, THF, rf.

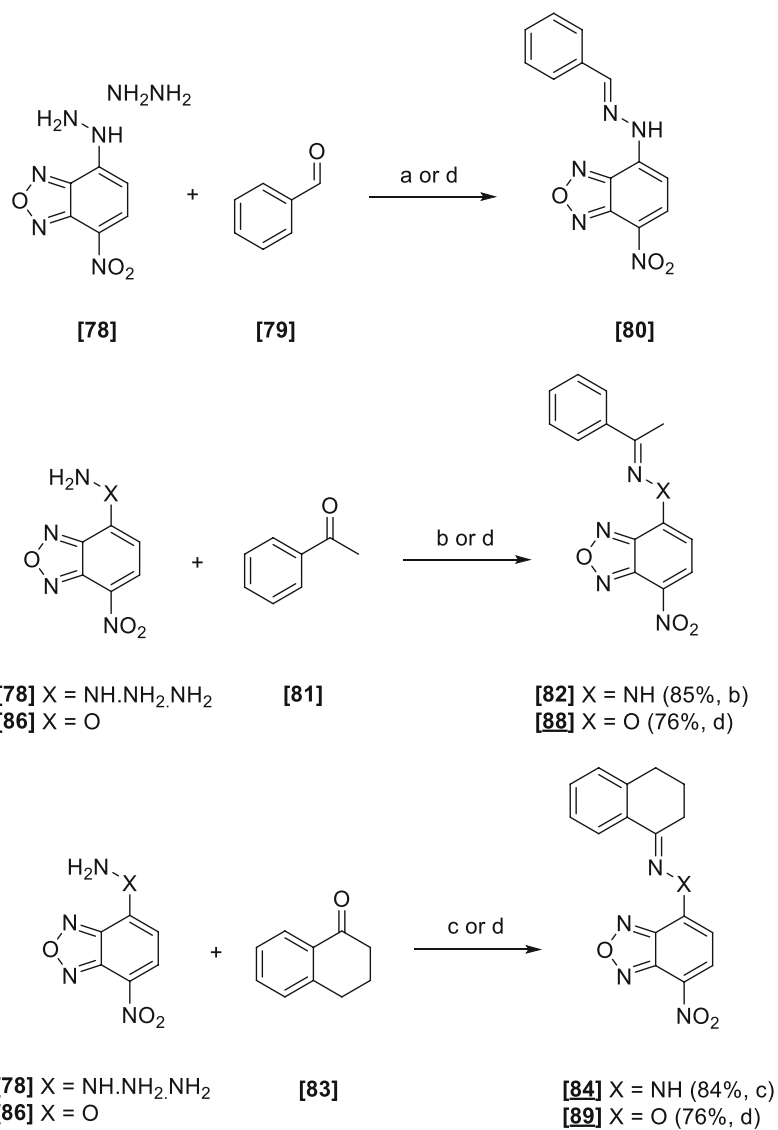


Scheme A-10: Reagents and conditions: a) NaCl, AlCl₃, 180 °C, 1 h; b) K₂CO₃, dry, degassed MeCN, reflux, Ar.

A IV Studies towards the synthesis and evaluation of fluorogenic adducts with NBD-H-type reagents

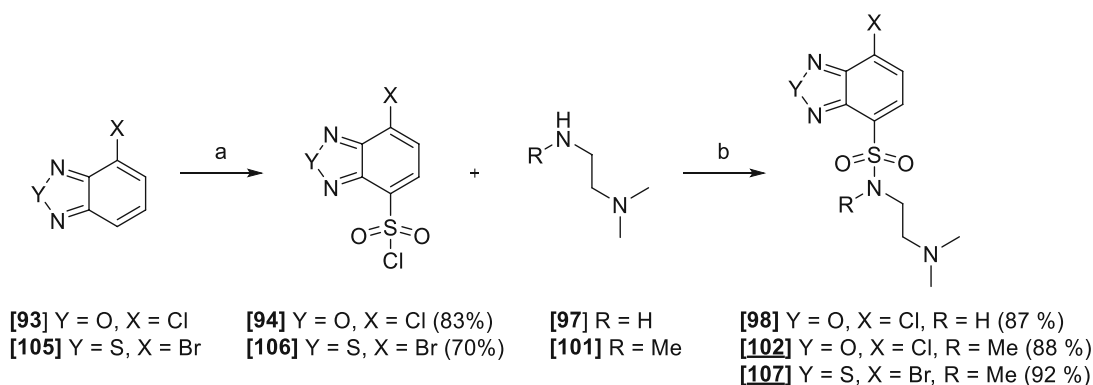


Scheme A-11: Reagents and conditions: a) monomethylhydrazine in MeOH, MeOH/CHCl₃, rf, Ar; b) NH₂NH₂·H₂O in MeOH, CHCl₃, rt; c) Na₂CO₃, H₂O, rt then TFA / H₂O, rt.

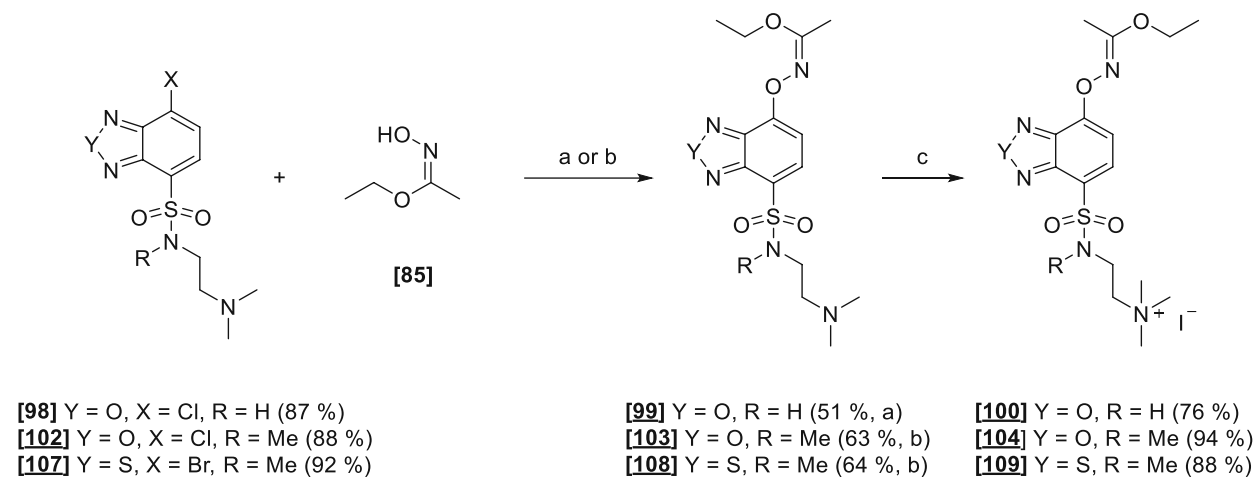


Scheme A-12: Reagents and conditions: a) MeOH, rt; b) 0.1 equiv. PTSA, MeOH, rt; c) 1.0 equiv. PTSA, MeOH, rt; d) Et₂O, rt.

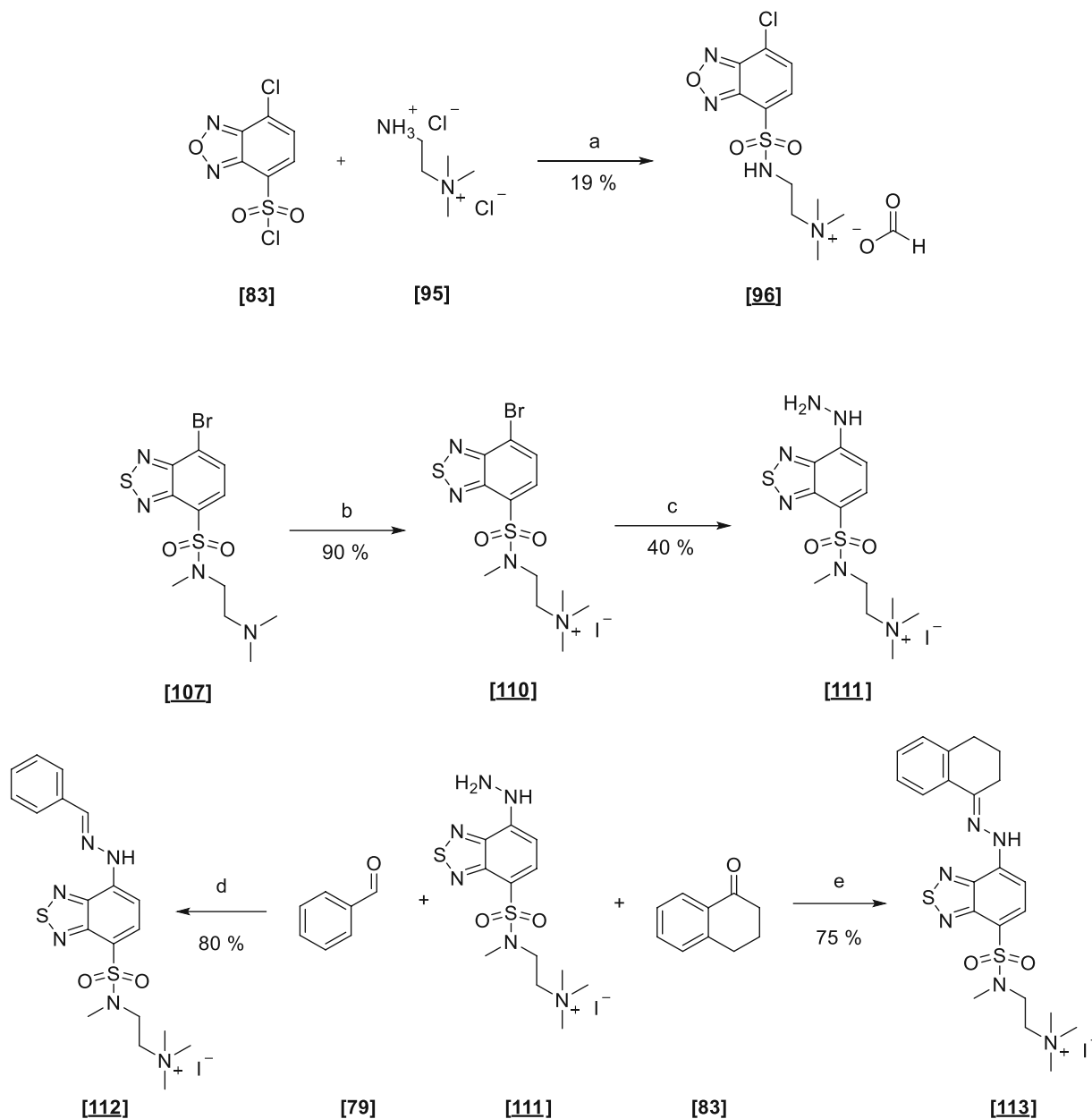
A V Improving water solubility of NBD-H / -HA reagents



Scheme A-13: Reagents and conditions: a) HSO_3Cl , neat, 0°C to 150°C ; b) dry NEt_3 , dry CH_2Cl_2 , 0°C to rt, Ar.

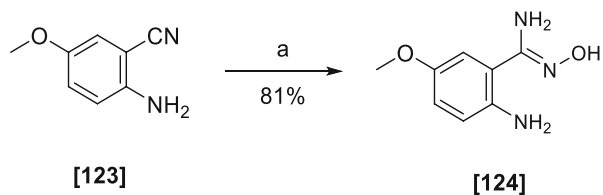


Scheme A-14: Reagents and conditions: a) 2.5 eq. NaH , 2.5 eq. **[85]**, dry DMF , 0°C to rt, Ar; b) 1.2 eq. NaH , 1.2 eq. **[85]**, dry DMF , 0°C to rt, Ar; c) CH_3I , MeOH , rt, Ar.

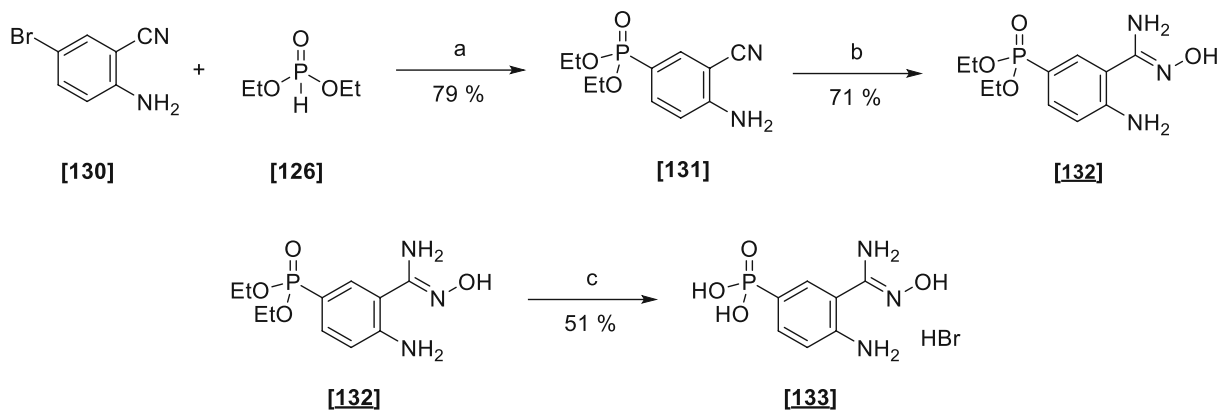
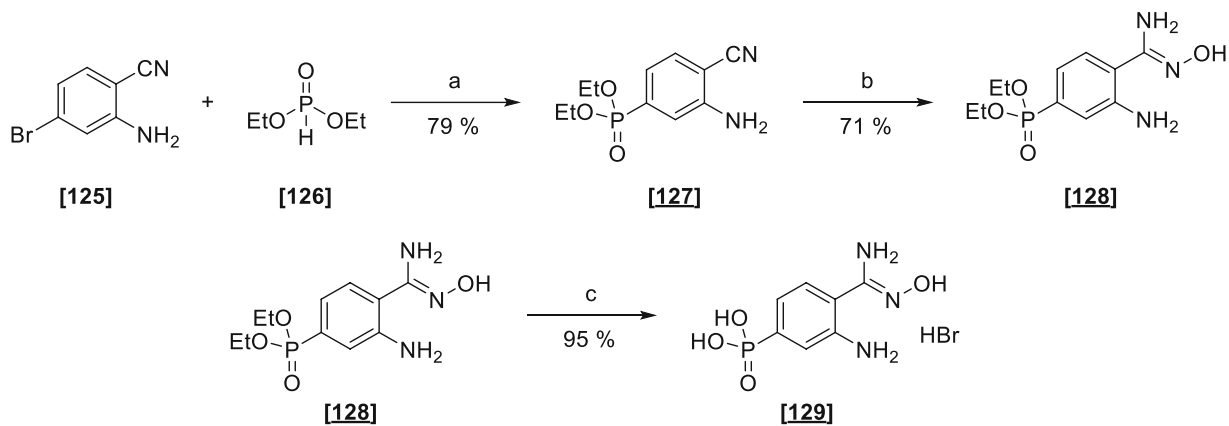


Scheme A-15: Reagents and conditions: a) NEt_3 , $\text{MeCN}/\text{H}_2\text{O} = 6:1$, rt then preparative HPLC; b) CH_3I , MeOH , rt, Ar; c) $1\text{M NH}_2\text{NH}_2$ dry MeCN , 50°C , Ar; d) 50°C , $10\text{ vol}\% \text{H}_2\text{O}/\text{MeCN}$, Ar; e) cat. pTSA , 50°C , $10\text{ vol}\% \text{H}_2\text{O}/\text{MeCN}$, Ar.

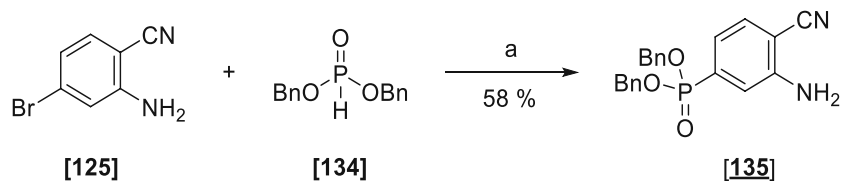
A VI Improving water solubility of ABAO reagents



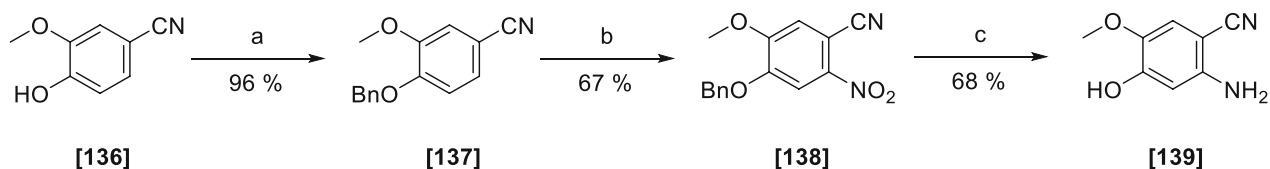
Scheme A-16: Reagents and conditions: a) $\text{NH}_2\text{OH}\cdot\text{HCl}$, NaHCO_3 , dry EtOH, rf.



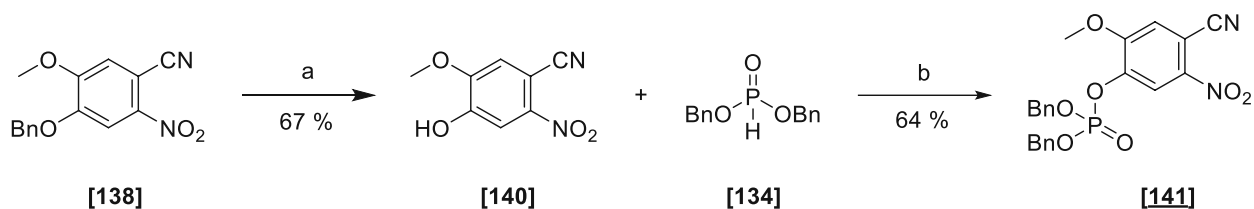
Scheme A-17: Reagents and conditions: a) 4 mol% $\text{Pd}(\text{OAc})_2$, 12 mol% PPh_3 , Cy_2NMe , degassed, dry EtOH, rf, Ar; b) $\text{NH}_2\text{OH}\cdot\text{HCl}$, dry NEt_3 , dry EtOH, rf, Ar; c) TMSBr, HPLC grade MeCN, rt, Ar then evaporate and HPLC grade MeOH, rt, Ar.



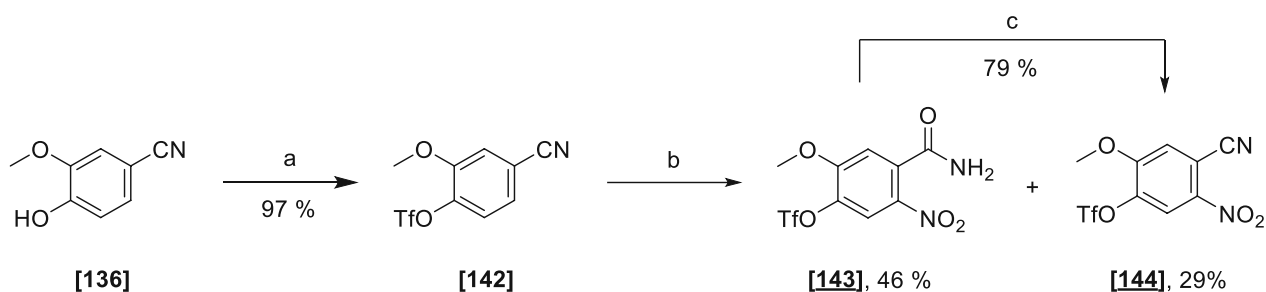
Scheme A-18: Reagents and conditions: a) 5 mol% $\text{Pd}(\text{PPh}_3)_4$, Cs_2CO_3 , dry THF, 120 °C, 10 minutes, Monowave reactor®.



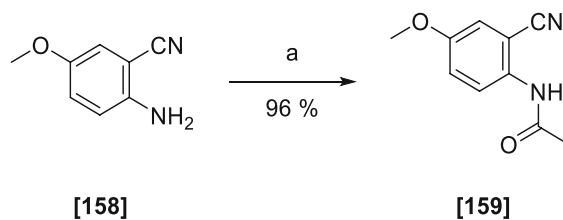
Scheme A-19: Reagents and conditions: a) BnBr, K₂CO₃, dry DMF, rt, Ar; b) HNO₃, Ac₂O, 0 °C to rt; c) 10 wt% Pd/C (10%), 1 atm H₂, dry EtOAc.



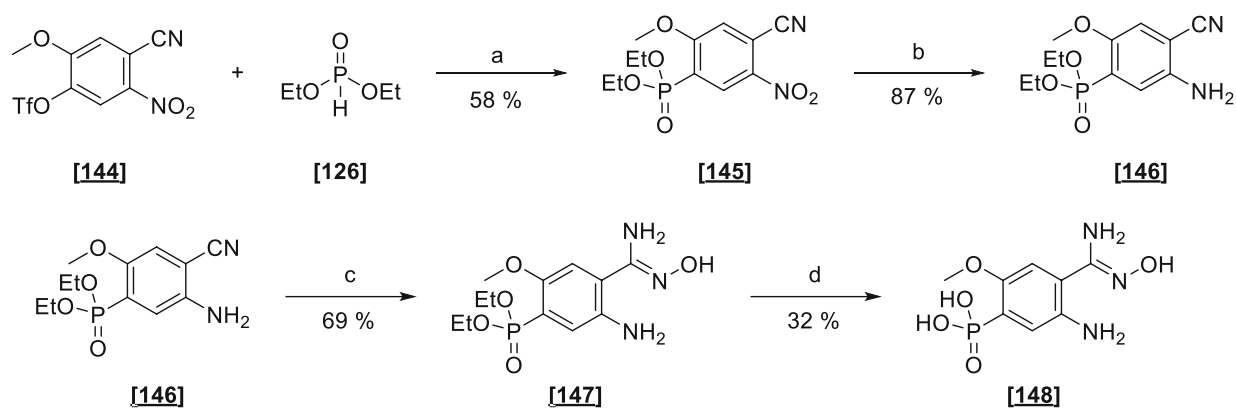
Scheme A-20: Reagents and conditions: a) TFA, rt, 3 d; b) CCl₄, DIPEA, DMAP, dry MeCN, -15 °C, Ar.



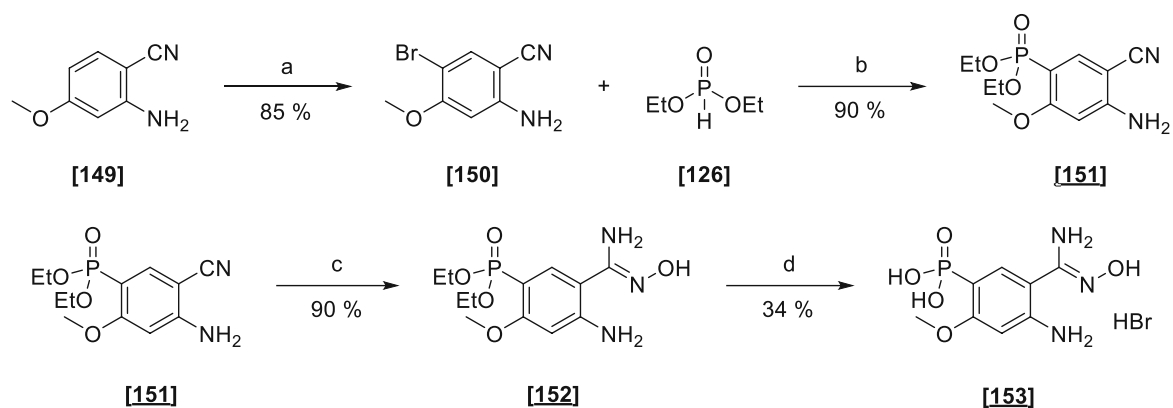
Scheme A-21: Reagents and conditions: a) Tf₂O, dry NEt₃, dry CH₂Cl₂, -78 °C to rt, Ar; b) 100 % HNO₃/H₂SO₄, H₂SO₄, 0 °C; c) 1 mol% PPh₃O, (COCl)₂, dry NEt₃, dry MeCN, 0 °C to rt.



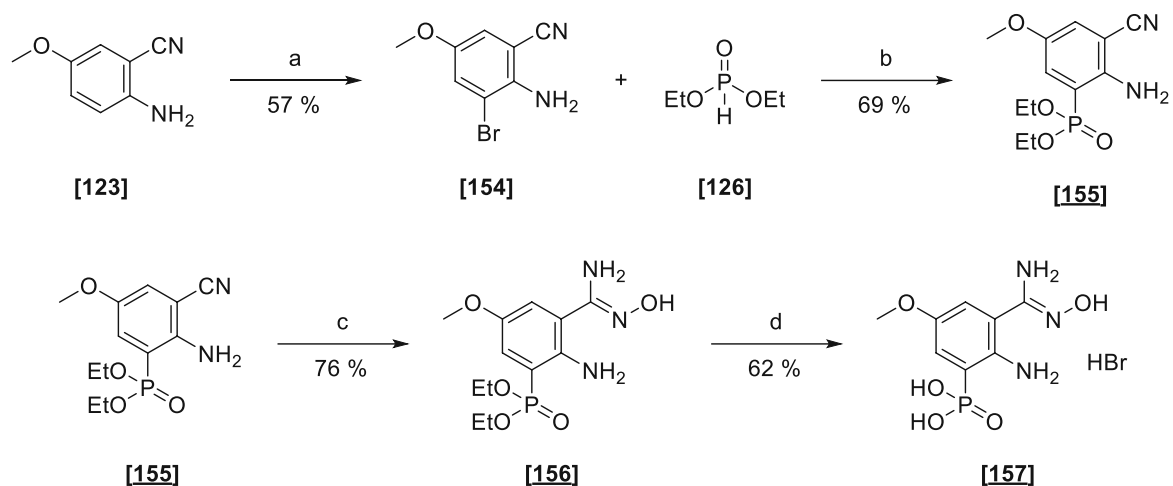
Scheme A-22: Reagents and conditions: a) Ac₂O, dry CH₂Cl₂, rt, Ar.



Scheme A-23: Reagents and conditions: a) Pd(PPh₃)₄, Cy₂NMe, degassed EtOH, microwave, Ar; b) Fe, AcOH, dry MeOH, reflux; c) NH₂OH.HCl, dry NEt₃, dry EtOH, reflux, Ar; d) TMSBr, HPLC grade MeCN, rt, Ar then evaporate and HPLC grade MeOH, rt, Ar.



Scheme A-24: Reagents and conditions: a) NBS, dry CH₂Cl₂, rt, Ar; b) Pd(PPh₃)₄, Cy₂NMe, degassed EtOH, microwave, Ar; c) NH₂OH.HCl, dry NEt₃, dry EtOH, reflux, Ar; d) TMSBr, HPLC grade MeCN, rt, Ar then evaporate and HPLC grade MeOH, rt, Ar.



Scheme A-25: Reagents and conditions: a) NBS, dry CH₂Cl₂, 0 °C to rt, Ar; b) Pd(PPh₃)₄, Cy₂NMe, degassed EtOH, microwave, Ar; c) NH₂OH.HCl, dry NEt₃, dry EtOH, reflux, Ar; d) TMSBr, HPLC grade MeCN, rt, Ar then evaporate and HPLC grade MeOH, rt, Ar.

B Introduction

B I Prelude

Since the first example set by Louis Pasteur for an enzymatic resolution of racemic tartaric acid in 1858¹, chemists have pursued to harness the power of nature to enable chemical transformations. Fischer's seminal work introducing the lock and key model² laid the foundation for understanding enzymatic interactions in biocatalysis. Michaelis and Menten's equations describing enzyme reaction kinetics³ a few years later represented another theoretical landmark explaining the behavior of substrate binding and enzymatic catalysis long before these theories became accepted fact. Or Buchners report⁴ that exemplified that cell-free extracts could be essentially used for fermentation processes decoupling the catalytic utility from intact organisms. All these initial reports culminated in developments in biocatalysis that could be summarized in several waves of groundbreaking research and technological innovations.⁵ Whereas "first wave" researchers mostly applied serendipitously discovered components in living cells for chemical reactions^{6,7}, the second wave involved already structure-based modifications of biocatalysts to enable their application for a broader range of non-natural transformations and substrates.^{8,9} Emerging with pioneering work Pim Stemmer¹⁰ and Frances Arnold¹¹, researchers began developing techniques that guided the third wave of biocatalyst development which, among other advances, led to the advent of directed evolution methodology. The accelerated simulation of classical Darwinian evolution enables rapid optimization of enzymes for an application in non-native conditions¹² (non-neutral pH¹³, high amount of organic co-solvent¹⁴ or increased thermostability¹⁵), increased enzymatic substrate promiscuity¹⁶, inverted or altered (stereo- or regio-)selectivity^{17,18} or empowered researchers to trigger a complete exchange of native functionality¹⁹. Detection of beneficial evolution events, however, requires tools that pinpoint desired positive changes to the protein structure. Especially for highly randomized mutagenesis experiments, libraries that span several millions of entries need to be assessed in a time-effective way while maintaining high selectivity in the screening process. FACS (fluorescence-activated cell sorting)²⁰⁻²² and FADS (fluorescence-activated droplet sorting)²³⁻²⁵ systems were already proven to be viable solutions to the problem, assessing these libraries in hours instead of days or weeks without relying on expensive robotic platforms. However, these speeds come with a caveat – a need for sufficiently sensitive assays compatible with the underlying screening procedure²⁶. Although immense efforts have been undertaken to optimize gene mutagenesis²⁷ and thus quality of the generated libraries, certain bottlenecks can still be found in appropriate assay development as the plethora of directed evolution studies still rely on admittedly established but outdated methodology. As we are now on the verge on the fourth wave of novel biocatalysts to be designed²⁸, further research should be directed at the development of these tools that complement the success story of biological innovation.

B II Protein engineering in biocatalysis

Protein engineering involves the design and evolution of proteins with a specific, desired functionality.²⁹ For synthetic applications, these efforts generally involve changes in substrate specificity, enhancements in enzymatic activity, or improvements in stability (pH, thermal, proteolytic).³⁰ These modifications culminate in the goal to complement or at best depart from traditional organic chemistry. Herein biocatalysts provide an efficient and environmentally benign alternative to conventional synthetic methodology. Due to their unparallel enantio-, regio- and chemoselectivity, they offer significant advantages in comparison. For instance, reactions can be performed without the tedious protection and deprotection steps commonly employed in enantio- and regioselective organic synthesis. In the case of a proven active catalyst, side reactions are practically suppressed, and thus, desired product isolation is rendered more facile. Unfortunately, collective synthetic demands do not necessarily go in line with nature's enzymatic repertoire.³¹ Consequently, tools for the optimization and the development of novel enzymatic catalysts had to be established (Fig. 1).

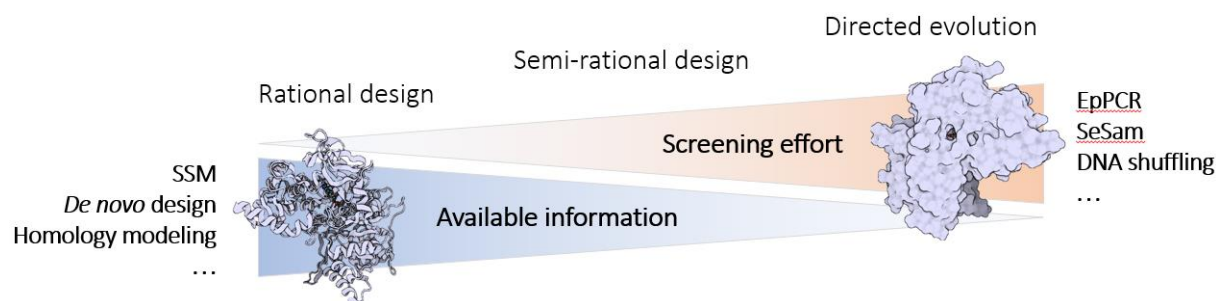


Fig. 1: Spectrum of protein engineering techniques depending on the underlying knowledge about the target protein. Screening efforts scale inversely proportional to the available information. SSM (site saturation mutagenesis), EpPCR (error-prone-PCR), SeSam (sequence saturation mutagenesis).

Rational approaches involving structure-based and *de novo* enzyme designs were developed in recent years. These efforts already broadened substrate range led to improved catalytic performance and the emergence of novel functionalities to obtain products with high added value for industrial applications.³² However, in-depth knowledge about the selected protein is generally necessary to identify a priori beneficial changes to the protein structure. In contrast, randomized methods are employed when no prior knowledge of protein structure is available or novel reactivity is sought after.^{26,33,34} These efforts are subsumed under the term “directed evolution” pioneered since 1990 and led to the awarding of the Nobel Prize in 2018.³⁵

B II.1 Directed evolution

Directed evolution experiments represent a fast-tracked, stimulated Darwinian evolution in a laboratory environment. They comprise iterative cycles (Fig. 2) of diversity generation events and high-throughput screenings selecting for improved phenotypical properties (reactivity, selectivity, stability). Favorable mutations at the protein level are thus accumulated, which can be translated back to the nucleobase sequence. Contrasting natural evolution, which aims to enhance traits for survival or

reproduction, directed evolution is carried out at much higher mutation and recombination rates to screen for the desired biological function.

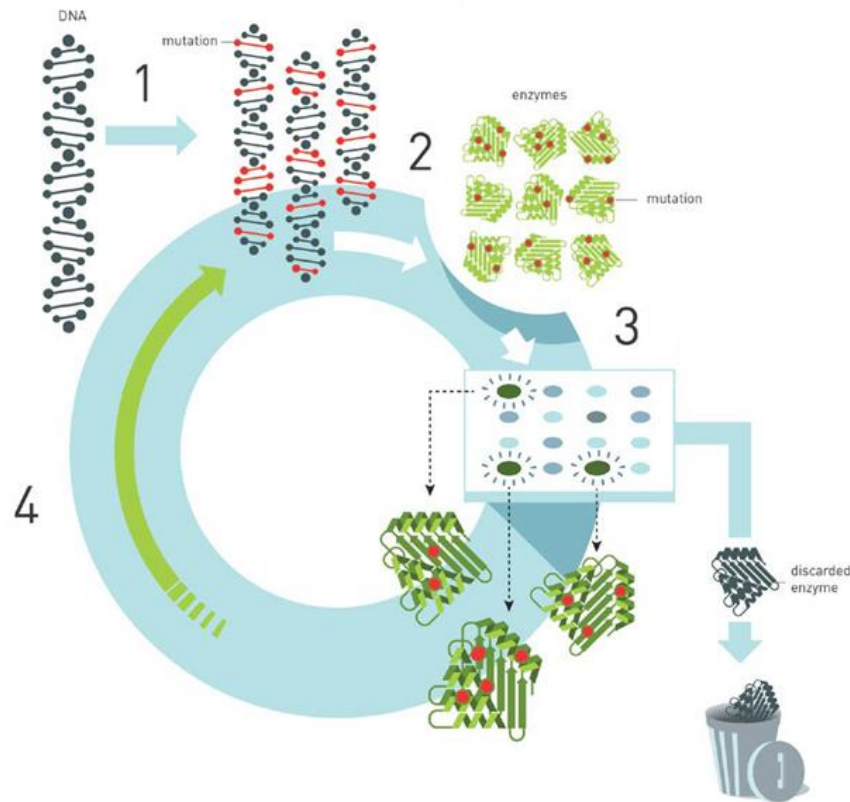


Fig. 2: Work-flow for directed evolution: 1 - library of mutants is generated using appropriate gene mutagenesis methodology, 2 – genetic information is translated to corresponding enzyme variants expressed in suitable hosts, 3 – protein library is screened for a defined phenotypical read-out (stability, yield, selectivity, ...) typically coupled to spectroscopic assays, 4 – improved mutants are isolated and corresponding genetic variants serve as a new starting point for the next round of evolution. Adapted from: Advanced information. NobelPrize.org. Nobel Prize Outreach AB 2021 - accessed September 2021.

Typically, several rounds of evolution using various library generation methods are applied to obtain positive screening results, necessarily creating large numbers of enzyme variants. As a numerical example: To cover the whole sequence space of an average protein encompassing 300 amino acid residues with random mutations at three positions, 2.5×10^9 clones would have to be screened.³⁶ However, as most studies try to maintain a target enzymatic functionality stemming from its active site constitution, only a fraction of structural changes needs to be frequently evaluated. Generally, 10^3 to 10^6 mutants are assessed to afford a sufficient threshold for positive hits. These libraries need to be inevitably screened with suitable high-throughput assays (HTA) using appropriate selection tools.³⁷

The generation of those libraries represents one of the most crucial challenges. Most widely, *in vitro* gene diversification, using random mutagenesis methods like epPCR (error-prone PCR) or recombination-based DNA shuffling, are applied to reach the desired coverage of sequence space. EpPCR introduces random mutations into a defined segment of DNA by using the inherently low fidelity of Taq polymerase with an increased mutation rate (1-3 per kilobase). Alteration of the reaction buffer composition or using unequal dNTP concentrations further increases the error probability. DNA shuffling, on the other hand, involves the digestion of parental DNA strands into randomized fragments. Reassembly of those homologous genes with primerless PCR at sequences with sufficient similarity gives access to combinatorial libraries. This imitated process of homologous recombination can be

additionally coupled with epPCR to further diversify the genetic information. Building upon these initial strategies, plenty of methods have been introduced over the last three decades using either *in vivo* or *in vitro* gene diversification.²⁷

Initial directed evolution studies dealt with the enhancement of enzymatic tolerance in biocatalytic applications. Exemplified by seminal reports from Arnold's group, the methodology was successfully applied to improve the organic solvent compatibility³⁸ and thermostability¹⁵ of a para-nitrobenzyl esterase. Further advances in the field were made to couple the use of enzymes in industrial processes^{34,39} or for the synthesis of active pharmaceutical intermediates.⁴⁰ Recent trends have, however, moved to tackle the engineering of promiscuous enzymes for transformations classically attributed to organic synthesis. Hilvert *et al.* used a combination of targeted mutagenesis, computational refinement, and subsequent directed evolution to create a highly active Diels-Alderase.⁴¹ In another approach, highly promiscuous hemoproteins were adapted to facilitate abiological carbene and nitrene transfer reactions, thus enabling cyclopropanations, C-H insertions, and aldehyde olefinations, among others.⁴² These representative approaches had two common denominators – a well-defined starting point for evolutionary studies and underlying promiscuity of the target protein. Although one enzyme had been artificially created, the ultimate dramatic improvements in activity and specificity were enabled using directed evolution methodology substantiating the efficiency of the process if parent enzymes are chosen correctly. However, this also comprises suitable assays that pinpoint to the desired enzymatic variants.

Two different promiscuous enzyme classes were chosen as targets for this thesis, namely the SHC (squalene hopene cyclase) and CAR (carboxylic acid reductase). Even though these biocatalysts do not share similar substrate and product profiles, both were envisioned to be applied for the production of carbonyl compounds using their unique catalytic machinery (see following chapters). With the thus converging functionality of target products, a suitable screening methodology for directed evolution studies based on carbonyl sensors was to be established.

B II.2 Squalene hopene cyclase (SHC)

-hopene cyclases (SHC) belong to a class of monotopic membrane enzymes of the terpene cyclase/mutase family. Their name stems from its native activity to catalyze the cyclization of linear squalene [i] into the pentacyclic triterpenes hopene [ii] and hopan-22-ol [iii], using its Brønsted acidic catalytic machinery.⁴³ Spatial arrangement of the highly conserved active site of SHCs causes the central aspartic acid proton to adopt an anti-orientation towards the carbonyl functionality (Fig. 3). Due to the surrounding apolar cavity, the low solvation causes a dramatically increased acidity compared to its syn-conformer⁴⁴. The thereby facilitated protonation of squalene isoprene units triggers the cationic cyclization cascade towards their steroidal products.⁴³

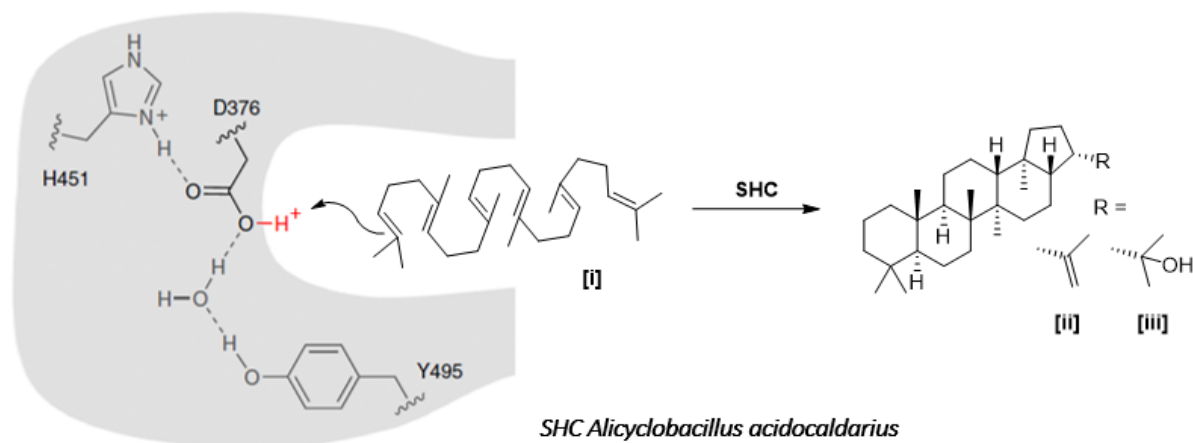
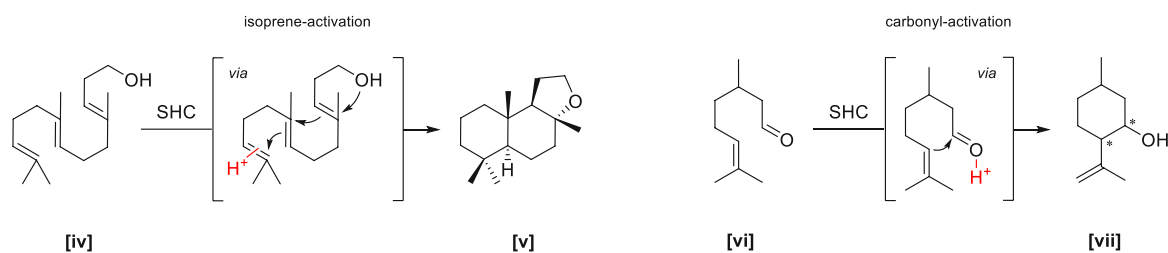


Fig. 3: Active site of the SHC from thermoacidophilic *Alicyclobacillus acidocaldarius* wild-type exemplifying the amino-acid network forcing the proton of aspartic acid D376 into anti-configuration, which catalyzes the cyclization of squalene [i] into its cyclic steroidal products hopene [ii] and hopan-22-ol [iii].

The mechanistic intricacies of this cyclization were studied in depth by the group of Hoshino⁴⁵⁻⁴⁷ and Hauer⁴⁸⁻⁵³, whereas the latter challenged the native catalytic machinery with many squalene analogs bearing different nucleophiles trapping the terminal carbocation. Interestingly truncated⁵⁴ as well as elongated⁵⁵ compounds bearing a similar isoprene motif were accepted by different families of SHCs. Terminal ketones, carboxylic acids, and alcohols, among others, were found to act as suitable nucleophiles.⁵⁰ The latter was applied for the synthesis of (-)-ambroxan [v] from homofarnesol [iv], an important and expensive fragrance compound normally isolated from the excretion of the sperm whale *Physeter macrocephalus*.⁵⁰



Scheme 26 - left: SHC catalyzed stereoselective cyclization of homofarnesol [iv] towards (-)-ambroxan [v]; right – SHC catalyzed Prins reaction of (±)-citronellal [vi] towards isopulegol [vii].

In succeeding studies, starting from the best-studied and structurally known SHC_{Acc}, several to that day known SHCs were challenged with (±)-citronellal [vi], which albeit bearing a similar double bond motif, showed exclusive protonation only at the carbonyl functionality. Herein especially, SHCs stemming from the *Zymomonas mobilis* family efficiently catalyzed the Prins reaction of citronellal [vi] to its isopulegol isomers [vii].^{48,51}

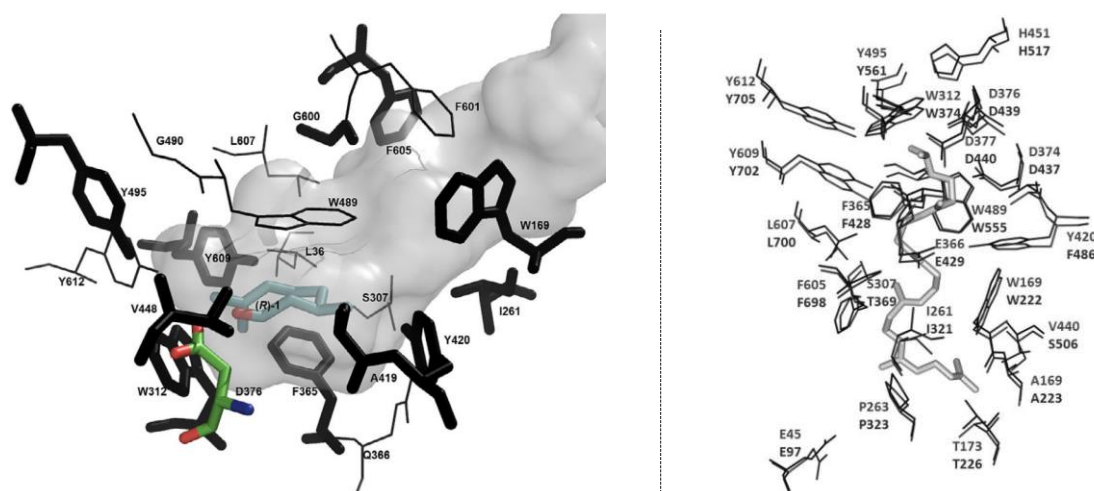
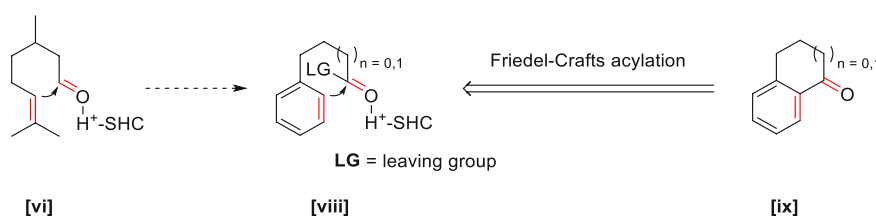


Fig. 4 - left: Representation of the activation of (*R*)-citronellal in the active site of the SHC_{Aac} – catalytically active aspartic acid D376 is highlighted in green. Residues chosen for targeted mutagenesis in the study by Bastian *et al.* are marked in bold⁵²; **right:** Comparison of the active sites of SHC_{Aac} and SHC_{Zmo_1548}: Crystal structure of SHC_{Aac} was obtained by co-crystallization with the inhibitory substrate 2-azasqualene (depicted in grey).⁵⁶ Alignment of amino acid residues of SHC_{Zmo_1548} (54 % overall amino acid similarity) with SHC_{Aac} displayed almost structural identity of the active site and substrate binding pocket.⁵¹

Incited by the novel activation mechanism, both promising SHCs (*Aac* and *Zmo*) families were screened for this novel activity. Herein, cyclases stemming from the organism *Zymomonas mobilis* were shown to outperform its thermoacidophilic counterpart as wild-types. Initial evolution studies using SSM at known active-site residues for the SHC_{Aac} discovered several beneficial hot spots which triggered increased activity or selectivity upon mutation, as depicted in Fig. 4 left.⁵² Several of these could be translated to homologs *Zmo* residues (Fig. 4. right) as well as further expanded.^{51,57} The most promising candidates used for non-native transformations were found in the SHC_{Aac} bearing mutations A419G/Y420C/G600A or I261A, in homologous positions of two SHC_{Zmo} families with F438C_{Zmo_0872} and F486C_{Zmo_1548} as well as a novel mutation for the later family with W555Y_{Zmo_1548}. These showed activity for the original transformation but additionally exhibited promiscuous reactivity towards truncated and elongated substrates and the carbonyl functionality.

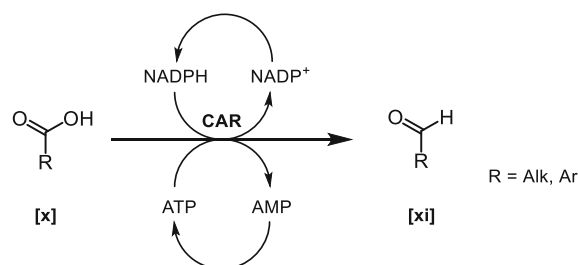


Scheme 27: Hypothesized enzymatic Friedel-Crafts acylation using the Brønsted acidic catalytic machinery of the SHC.

Building upon the broad substrate acceptance of the SHC, we targeted harnessing its Brønsted acidic catalytic machinery. Analogous to the carbonyl protonation for the Prins reaction depicted in Scheme 26, a similar cyclization mechanism was hypothesized using suitable aryl nucleophiles [viii] (Scheme 27). The resulting cyclized aryl-ketone products [ix] would be derived *via* formal enzymatic Friedel-Crafts acylation (FCA). As no randomized mutational studies have been published on this enzymatic system to date, the promiscuous nature of the enzyme class would enable an improved starting point for any protein engineering efforts for this novel transformation.

B II.3 Carboxylic acid reductase (CAR)

Carboxylic acid reductases (CAR) are large multi-domain enzymes that catalyze the ATP- and NADPH-dependent reduction of carboxylic acids [x] to the corresponding aldehydes [xi] (Scheme 28)^{58,59}. These proteins feature three different functional domains: the N-terminal adenylation domain (A-domain), a central phosphopantetheine binding domain (T-domain), and the C-terminal reduction domain (R-domain) (see. Fig. 5). The CAR itself requires a PPTase-mediated activation enabling binding of a phosphopantetheine arm, which facilitates the transition of the substrate between A- and R-domain active sites.



Scheme 28: Overview of the ATP- and NADPH-dependent CAR catalyzed reduction of carboxylic acids [x] to their corresponding aldehydes [xi]. In vivo systems enable the regeneration of both co-factors by the cellular machinery.

The proposed mechanism of CAR can be divided into four distinct steps (Fig. 5). Upon binding of ATP and the respective carboxylic acid (1), the carbonyl species is initially activated by ATP, forming an acyl-adenylate complex with the nucleophilic attack of the carboxylate (2). The reactive intermediate is readily trapped by the thiol functionality of the phosphopantetheine arm, forming the respective thioester while concomitantly releasing AMP (3). Using the flexible arm, the activated ester is transferred to the R-domain, whereupon reduction with NADPH, the resulting aldehyde and NADP^+ are expelled (4) while returning the arm into its thiol form.

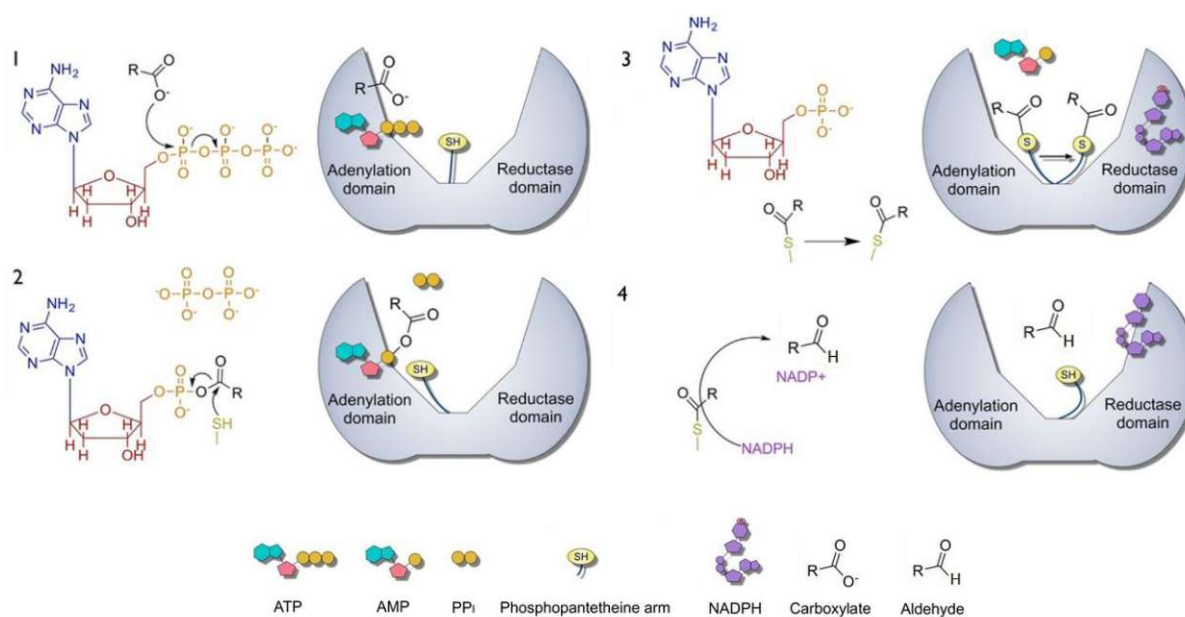


Fig. 5: Mechanism for the enzymatically catalyzed reduction of carboxylic acids using the three-domain assembly of the CAR enzyme.⁵⁹

Carboxylic acid reductases have shown acceptance for a broad range of substrates, enabling reductions of aryl, as well as aliphatic carboxylic acids.⁶⁰ Interestingly, a counter-intuitive enhanced activity was observed for electron-rich aromatic compounds. These systems would theoretically render the carbonyl functionality less electrophilic. However, studies on related non-ribosomal peptide synthetases (NRPs) have shown that the initial adenylation step was rate-limiting and therefore imposed the most significant impact on substrate specificity and selectivity.⁶¹ Decreased activity was thus observed for compounds bearing electron-withdrawing substituents in resonance to the carboxylate group as well as ortho-substituted aromatic systems due to steric interference.⁶²

Particular bottlenecks for the reactivity of the protein were also found for very small aliphatic substrates (acetic and propionic acids) and amino acids^{63,64}, which were hardly accepted by the approximately 30 known CAR enzymes to date. This general trend for bulkier substrates was ascribed to the large A-domain binding pocket, which showed improved interactions to aromatic or long-chained aliphatic structures.⁵⁸ Recent studies have dealt with the expansion of substrate scope as well as optimization using mostly site-directed mutation approaches. Stolterfoth *et al.* triggered an improved substrate specificity towards larger aliphatic acids by enlarging the binding pocket of the A-domain of ncCAR by selective alanine exchanges.⁶⁵ A different strategy used MD (molecular dynamics) simulations of a srCAR domain crystal structure to identify 17 latent residues for a possible enhancement of enzymatic activity. SSM was used to create an extensive library of 340 variants which were individually expressed and screened. GC-analysis of all single-point mutants identified K542W as well as A937W to enhance benzoic acid conversion by a factor of 7⁶⁶. This study revealed mutations at the R-domain to modify mainly the activity of the reductase. Variations at the A-domain, on the other hand, were shown to determine overall substrate specificity.

Prompted by the promiscuity of the CAR and problematic conversions for sterically more demanding aromatic aldehydes, our group took a randomized approach. Using ABAO reagents as chromogenic aldehyde sensors (see. B III.1.1.1), a library of 6000 epPCR derived niCAR mutants were screened for an improved activity for over 20 aldehydes.⁶⁷ The A-domain mutation Q283P prompted a 9-fold increase in K_M value and improved typically low conversions of several ortho-substituted benzoic acids.^{62,67} This study, in particular, highlighted the power of suitable assay tools to enable rapid expansion of sequence space through targeted identification of positive candidates. In light of the positive outcome of this investigation, albeit having constraints imposed on the size of the mutein library by the applied screening throughput of the robotic platform, we were prompted to pursue the field of ultra-high-throughput screenings using the same assay methodology.

B III Ultra-high-throughput screening (uHTS) for protein engineering

Ultra-high-throughput screenings (uHTS) in the protein engineering field are applied to rapidly identify beneficial attributes of enzymatic variants in more extensive libraries generated by randomized mutagenesis. Herein “ultra-high-throughput,” although not uniformly defined, is generally understood as testing of at least 10^6 to 10^8 samples per day.⁶⁸ The key and the most significant challenges lie in

developing suitable methods for coupling phenotypical traits to genotypic information compatible with the high-throughput regime. Herein, individual assessment of libraries containing millions of mutants using classical analysis methods becomes unpractical. Although selection techniques that link cell viability or growth to a desired enzymatic activity have been successfully applied for vast libraries (10^9 to 10^{12} variants)⁶⁹, they are inherently limited to detoxifying enzymes or proteins required for essential nutrients synthesis. Initial improvements were achieved with the introduction of automatization and robotization for protein engineering studies; however, state-of-the-art fully automated robotic systems are only capable of screening up to 10^4 - 10^5 mutants *per day*.⁶⁹

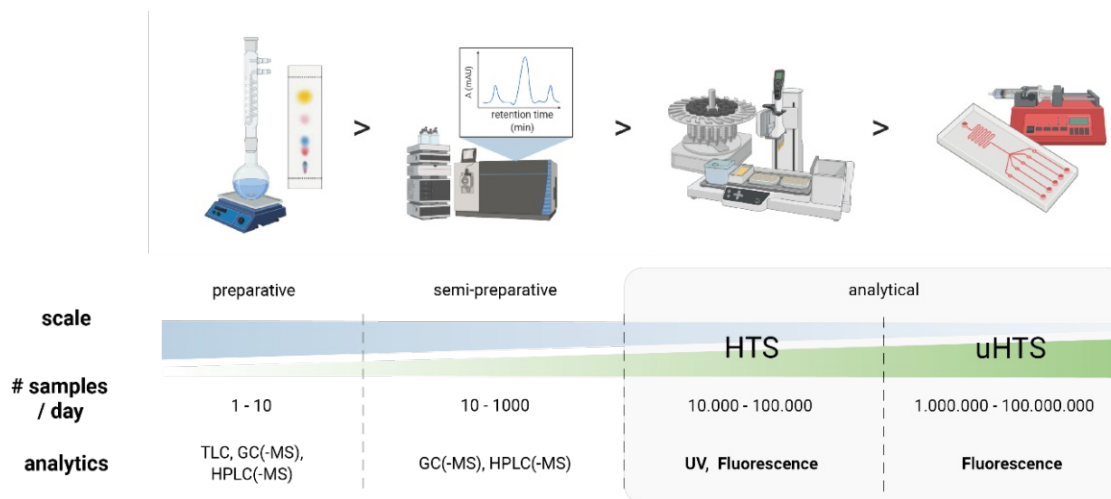


Fig. 6: Change of analytical approach depending on screening scale and mutagen library size: Increase in library size urges shift from chromatographic methods to spectroscopic detection for HTA.

A further increase in library size comes with a particular caveat as reaction volumes, and material cost cannot be simultaneously scaled.⁷⁰ In consequence, miniaturization with implications on the applied downstream analytics used for the high-throughput screenings becomes a significant factor. Chromatographic methods (GC, HPLC) forfeit their relevance to spectroscopic techniques, which become critical in the HTA field due to shorter analysis times, lower detection limits, and a higher degree of sensitivity (Fig. 6).^{33,71} Technical advances have cumulated in outstanding developments in instrumentation and lab-on-a-chip microfluidic technologies (fluorescent-activated cell sorting – FACS, fluorescence-activated droplet sorting – FADS) enabling single-cell analysis at picoliter level, thereby offering unprecedented screening throughputs.⁷²⁻⁷⁴ Methods including cell surface displays and *in vivo* or *in vitro* compartmentalization have been broadly applied to achieve the necessary spatial phenotype-genotype connection. The thereby confined enzymatic activity is coupled to UV-absorption or fluorescence emission signals as the principal outputs in uHTAs. Although MS-coupled techniques have also been implemented that were closing in onto the HTS regime⁷⁵, spectroscopic detection methods represent the largest group due to their unparalleled sensitivity and broad applicability⁷⁴. However, among these, fluorescence-based assays are the most sensitive and offer a wide range of screening options.

B III.1 Fluorescence-based assays

Typically, initial promiscuous activities in directed evolution experiments are expectably weak. Additionally, due to a dramatic decrease in analytical volumes compared to classical screening methods, uHTA must meet stringent sensitivity thresholds. Consequently, fluorescence-based detection methods, especially laser-induced fluorescence (LIF), are most commonly used due to their excellent sensitivity, highspeed response capability, and established detector systems. In a landmark publication, Colin *et al.* reported the most sensitive fluorescence readout in a uHTS FADS format to-date, measuring fluorescein in 2.5 nM concentrations corresponding to approximately 2,500 molecules in a singular 2 pL droplet. Using cleavable fluorescein esters as activity reporters for the directed evolution of new sulfate and phosphotriesters hydrolases, a library of 10^7 variants was screened in approximately 2 hours (2.5 kHz screening frequency).⁷⁶ Although these limits have been pushed to the extreme with encapsulating and detecting single GFP proteins inside fL-sized droplets, no subsequent sorting of the cellular compartments has yet been undertaken.⁷⁷ Highlighted by the sensitivity of these tools and the intrinsic variety and tunability of fluorescent chemical or biological sensors, a plethora of sensors have been developed. Therein ratiometric reaction-based or turn-over-based turn-on probes constitute the majority in the vast landscape of reporters, linking the product formation or enzymatic conversion to a proportional increase in fluorescence emission (Fig. 7).⁷⁸⁻⁸⁰

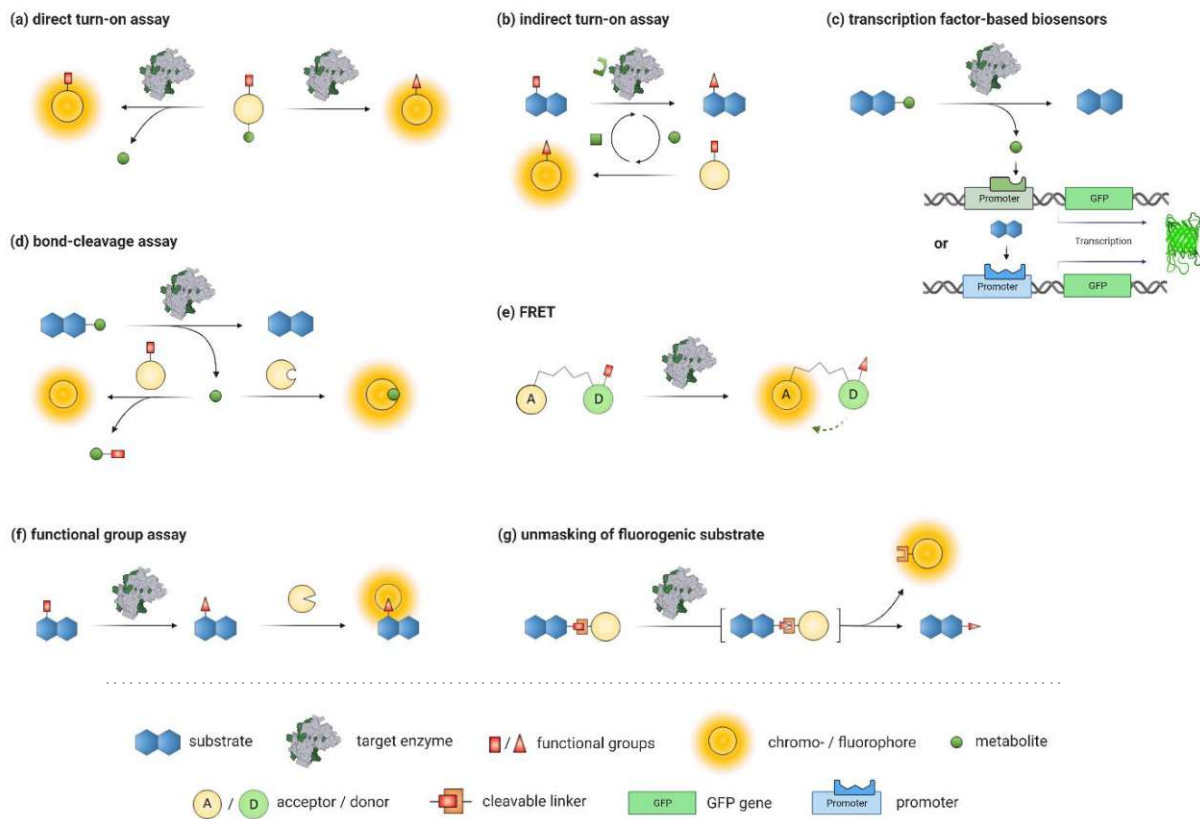


Fig. 7: Overview of several ratiometric absorptions or fluorescence turn-on strategies applied in directed enzymatic evolution in biological systems: (a) – direct detection of activity by functional group transformations or cleavage reaction of the target substrate, (b) – indirect detection of conversion **via** dye co-factor recycling with a concomitant increase in signal, (c) – triggered enhanced transcription of fluorescent biosensors, (d) – formation of dye in downstream reaction upon cleavage of metabolic reporter; detection **via** suitable recognition domain or subsequent reaction with the chromo-/fluorogenic substrate, (e) – induction of Förster resonance energy transfer (FRET), (f) – functional group transformation is detected **via** subsequent reaction with functional groups selective assay component, (g) – tandem reaction cascade of model-substrate unmasks chromo-/fluorogenic product.

The most straightforward approach for enzymatic activity screenings can be taken if the target compounds exhibit inherent fluorescent behavior (a). Among other examples⁸¹, this strategy was successfully applied to screen for improved intra- and extracellular production of fluorescent riboflavin in the fungus *Yarrowia lipolytica* using a FACS approach.⁸² Even though the biomolecular mechanism was not elucidated, the efforts led to 2.6-fold overproduction of the vitamin. Because many synthetically relevant substrates (and products) do not exhibit the desired photometrical properties, direct reaction monitoring is not generally feasible. Indirect turn-over-based approaches coupling the reaction to a by-product formation have significantly been utilized in several HTS studies summarized in several comprehensive reviews.^{78,79,83-88}

These metabolic reporters can be either directly screened in the form of depleted co-factors *via* downstream recycling coupled to a fluorogenic reaction (b) or using appropriate trapping agents (d). The former approach has been recently employed for the active site remodeling of cyclohexylamine oxidase (CHAO) from *Brevibacterium oxydans* using a FADS system, resulting in a remarkable 960-fold increase in catalytic efficiency compared to its wild-type.⁸⁹ Concomitant release of H₂O₂ was used herein as reporter system, which triggered HRP catalyzed oxidation of Amplex UltraRed to Resorufin, resulting in strong 609 nm fluorescence upon excitation.

However, the secretion of those small-molecule metabolites can also be used as direct readout, spanning pH-dependent (H⁺)⁹⁰⁻⁹³, cation or anion⁸³, H₂O₂⁹⁴⁻⁹⁷, H₂S, reactive oxygen or nitrogen species (ROS / RNS)^{84,98}, O₂⁹⁹ or formaldehyde¹⁰⁰⁻¹⁰² assays to mention a few. These assays are primarily designed as chemical reporters to trigger the desired fluorescence emission. However, natural fluorescence proteins like green or yellow fluorescent proteins (GFP/YFP) and analogs thereof can also be coupled to enzymatic activity screenings (c)¹⁰³. Secreted products or metabolites can interact with transcription factors (TFs) and trigger an increased or decreased expression by modulation of their respective promoters. Although TFs have natively evolved to respond to environmental ligands, engineering efforts have modified them to interact with a wide range of non-natural compounds of interest to biotechnology.¹⁰⁴ One application of this methodology applied in a high-throughput format was shown by the group of Soumillon, in which they used the autocatalytic capabilities of their novel activity-fed translation (AFT) approach.¹⁰⁵ They co-encapsulated two plasmids with methionine responsive TF, one encoding for GFP and the other for the target protein penicillin acylase (PAC). Hydrolysis of its substrate phenylacetyl-methionine caused secretion of the amino acid modulator, which autocatalytically enhanced the expression of both genes—this increased overall fluorescence emission, which enabled improved detection of less active mutants.

Another viable detection method uses a particular interaction between chromophores, namely the Förster resonance energy transfer (FRET). The process represents a distance-dependent transfer of electronically excited states from suitable donor to acceptor chromophores using a non-radiative dipole-dipole coupling (e). Due to the extreme sensitivity of the fluorescence emission to distance, FRET has been mostly applied to study protein interactions by tracking distinct changes in protein conformation.¹⁰⁶ Interference with either the acceptor or donor moiety can thus trigger or quench this radiative process. Enzymatic transformations of chemical probes that impose changes in their electronic structure, thus deploying them into one of the two functions, can thus be used as an optical read-out.^{107,108}

A large proportion of open literature relies on artificial substrates with build-in chromophores for the fluorometric detection of a wide range of enzymatic activities (g).¹⁰⁹ The major caveat these fluorogenic substrates entail is that they only mimic the substrate of interest, decoupling the analytical signal from the synthetically relevant product. This bears the risk of identifying biocatalysts that exhibit improvements for the chromogenic mimic but cannot replicate their enzymatic activity for the actual substrate – condensed in the saying “you get what you screen for”.¹¹⁰ Nevertheless, the methodology has been widely successful for directed evolution experiments mainly focusing on improvements of general enzymatic activity and not transformations towards defined products.^{111,112} A possible solution to the problem was highlighted in the study of Yang *et al.* for the engineering of glycosyltransferases. To avoid the identification of variants that were only active towards labeled substrates, the selection was performed by a simultaneous screening of the two differently tagged lactoses using BODIPY and coumarin fluorophores.¹¹³ Repeated FACS enabled the discovery of a variant with broader substrate tolerance than the wildtype enzyme and 300-fold higher activity. The selectivity issued can also be avoided entirely if a derived product's functionality is used as an analytical handle. These specific functional group assays (f) can act as complementary tools to reduce false positives.^{79,88} Compared to indirect methods, which can be impacted by endogenous machinery or biosensor systems which for novel systems necessarily require elaborate biosynthetic groundwork, established functional group assays represent ready-to-use systems that enable facile chemical recognition of positive variants bearing distinct functionalities.

B III.1.1 Functional group assays

Using the set of steric and electronic properties each functional group entails, the design of substrate-independent assay tools can allow for efficient discrimination of target products from substrates and cellular interferants. The general design of those probes needs to accomplish several tasks to enable their application in biological systems – sufficient chemoselectivity and reactivity, mandatory biocompatibility, and, most significantly, suitable optical properties. Crucially, high reaction rates¹¹⁴ under biological conditions and the (in optimal case quantitative) formation of a stable, fluorescent species is crucial. In addition to the chemical properties, the choice of the chromogenic platform is also essential, and knowledge about the genesis of the optical signal is necessary for the rational design of said probes. The majority of reaction-based fluorescent probes are based on a direct change of the electronic structure of the chromogenic dye.¹¹⁵ This is triggered either by changes in the degree of conjugation of the π -electron systems or the introduction or exchange of electron-donating or withdrawing groups. The thereby caused changes in absorption coefficients, quantum yields, or spectral shifts can be directly addressed if the functionality of the analyte targets those groups. Other methods employ the suppression of a photoinduced electron transfer (PET)¹¹⁶, modulate an intramolecular charge transfer (ICT)¹¹⁷, or enable an excited-state intramolecular proton transfer (ESIPT) to generate a signal. Although novel approaches using aggregation-induced emission (AIE)¹¹⁸, twisted intramolecular charge transfer (TICT)¹¹⁹, or electronic energy transfer (EET)¹¹⁹ have been reported, the latter constitute only a marginal group of reaction-based turn-on probes.

In most instances, conjugation of target products to reagent molecules is accompanied by a spectral red-shift (Fig. 8). Taking a generalized spectral profile of such functional group assay system as an example, two different wavelength shifts need to be considered during measurements – the product and Stokes shift. The former represents the shift in absorption upon conjugation with the analyte of choice, the latter the difference in red-shifted excitation and emission maxima. Problematic overlaps of the absorption spectra due to low product shifts may cause sensitivity issues as part of the incoming light is absorbed by the reagent itself. As typically low initial enzymatic activities can be expected for directed evolution studies, these probes are usually present in large excess compared to target analytes. Consequently, excitations should be performed in regions where the functional group reagents are preferentially non-absorbent. This applies particularly to fluorescent reagents, whose emission would increase background signal and thus lower the achievable S/N ratios of the overall assay.

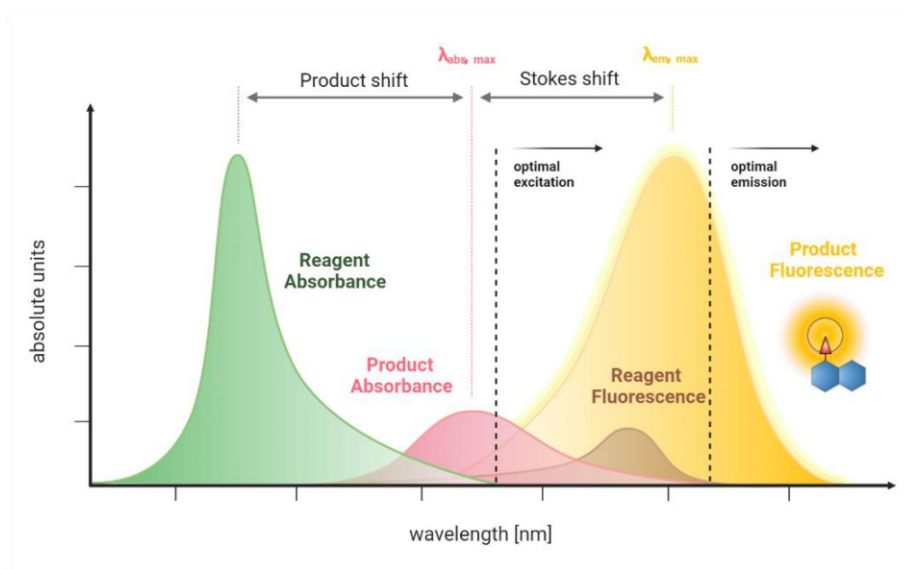


Fig. 8: Generalized spectral profile of such functional group assay system: Reagent absorbance and emission spectra are colored green and brown, product fluorophore absorbance and emission spectra are colored in red and yellow.

Similarly, the emitted light of the excited conjugates can be reabsorbed by the reporter itself. This decrease in fluorescence emission, termed the secondary inner-filter effect, is classically observed for solutions exceeding optical densities of 0.1 at given wavelengths (Fig. 9). Measurements using concentrations below this optical threshold are guaranteed to follow a linear trend. Further increases in concentration lead first to a plateauing of the signal and then to a complete loss of fluorescence emission. Thus, quantifiable spectra should always be recorded using wavelength intervals, where this phenomenon is not observed.

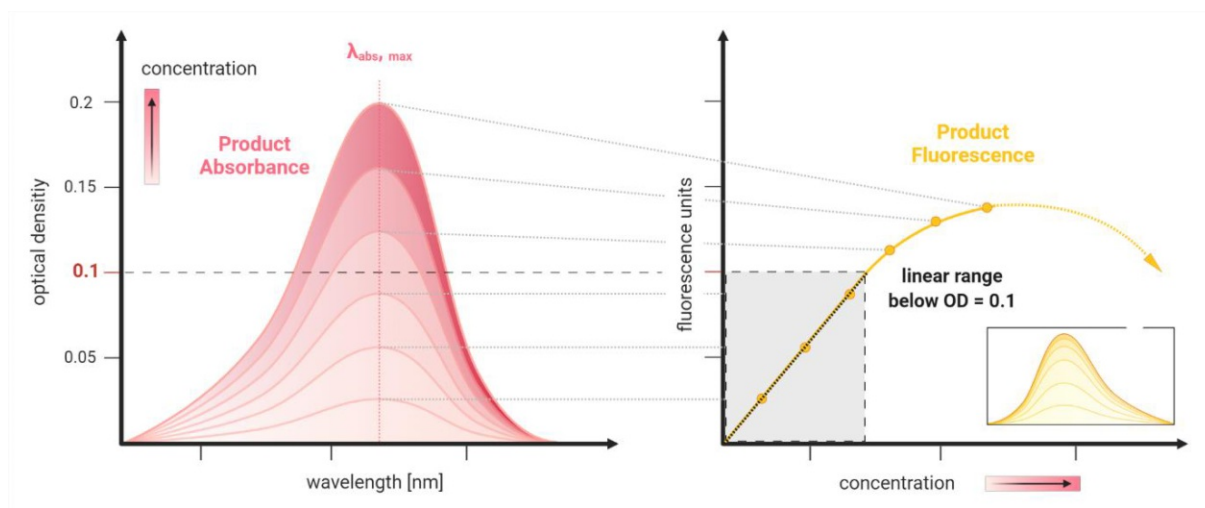
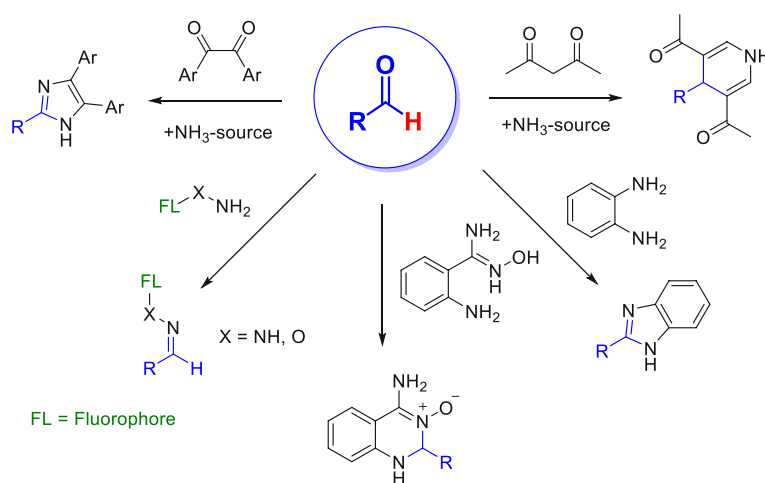


Fig. 9: Classical observations of a secondary inner-filter effect during fluorescence measurements: An increase in concentration exhibits linearity of the signal only up to solutions with an OD = 0.1 at their given wavelengths. The signal of higher concentrations gradually plateaus and starts to drop due to reabsorption effects.

Over the last decades, many functional group assays have emerged that frequently profited from the selectivity in biorthogonal conjugation chemistry and vice versa. Hence most available methods have been established to tackle amine and thiol functionalities.¹²⁰ As the enzymes of interest in this thesis represented carbonyl producers, a selection of selective assays is presented in the following chapter.

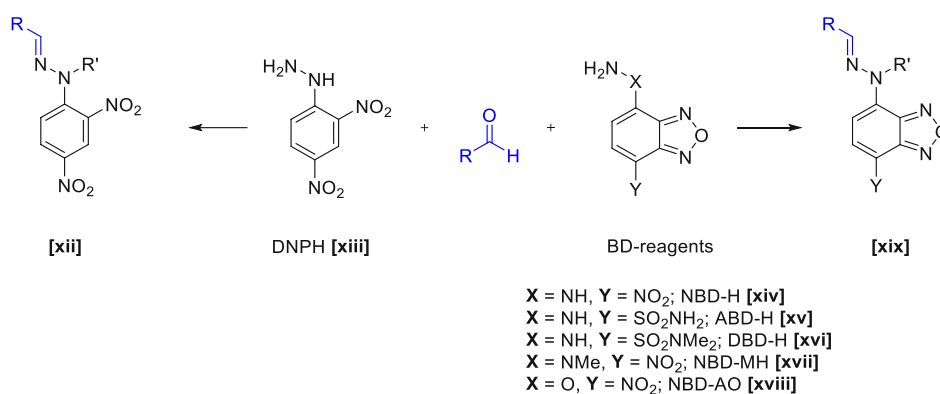
B III.1.1.1 Aldehyde selective assays

Due to the increased reactivity of aldehydes compared to other carbonyl analogs, a plethora of selective aldehyde tagging strategies have been developed, relying on its inherent electrophilicity. Classically, nitrogen-nucleophiles have been applied as trapping reagents forming hydrazones, oximes, or conjugated aliphatic and aromatic ring-systems, which exhibited the desired optical properties (Scheme 29). Although other ligation methods have been reported¹²¹, their concepts have been mainly applied to classical bioconjugations without accompanying optical read-out.



Scheme 29: Overview of aldehyde selective tagging strategies.

Most of the mentioned assay systems stem from historical findings and have unfortunately only led to a few singular reports in protein engineering studies. Due to a lack of advances in this field and thus missing variability of probes, some reagents that were discovered half a century ago are still applied in their original form, even today. As these mainly were conceptualized as off-line aldehyde reporters, applications in physiological systems were never envisioned. A majority of these reagents are thus incompatible with in- or on-line measurements of biological samples, which due to simple time restrictions, represents a necessity for uHTS applications. In some rare cases, however, further modifications of established structures have been reported, which led to applications in mutational studies. An example of such a continued evolution of a reagent used for selective carbonyl detection is dinitrophenylhydrazine DNPH [xiii].

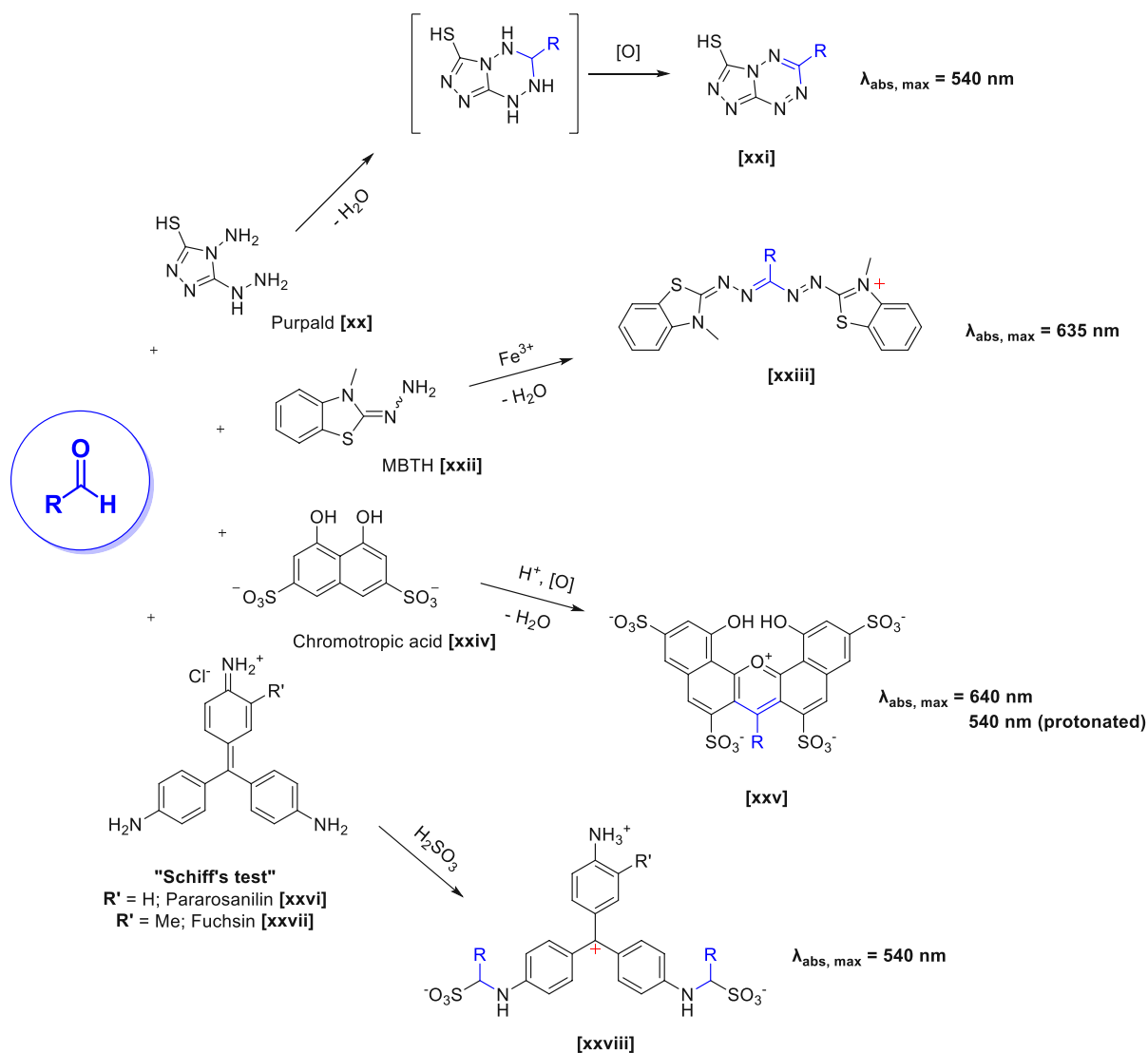


Scheme 30: Application of DNPH [xiii] or BD-derivatives for fluorogenic hydrazone formation

This orange to reddish hydrazine quickly reacts to form intensely yellow absorbing hydrazones. This conjugation has been used since its first report in 1951¹²² and has already been applied for HTS of mandelate racemase variants by chloromandelic acid detection.¹²³ As DNPH [xiii] inherently limits its application to UV-absorbance assays, its fluorescent benzoxadiazol (BD) derivatives took over and found broad use as fluorogenic reporters for aldehydes and ketones (Scheme 30).¹²⁴ By exchange of the electron-withdrawing group para to the hydrazine moiety, different spectral regions can be covered using the same scaffold (ABD-H [xv] / DBD-H [xvi]).^{125,126} Interestingly, methylation of the hydrazine (NBD-MH [xvii]) causes a dramatic increase of the previously mentioned product shift (*c.f.* Fig. 8), turning the ochre reagent deep red upon conjugation.¹²⁷ The most prominent representative of the substance class, the nitrobenzoxadiazole hydrazine (NBD-H) [xiv], has been efficiently applied to develop a HTS method for evaluating esterase activity reactions employing vinyl ester donors in organic solvents¹²⁸. The release of acetaldehyde upon esterification could be efficiently tracked using the assay system. Building upon the same BD scaffold, a novel oxime-analogue [xviii] was also proven to be applicable *in vivo* settings for the detection of sialic acid.¹²⁹ Compared to its NBD-H parent, it exhibited an approximately 6.7-fold increased intracellular staining capability.

Improvements in reactivity for hydrazone conjugations have been made thus far using aniline catalysts¹³⁰⁻¹³³, uncommon buffer systems¹³⁴, or increased salt concentrations¹³⁵, boosting especially reaction at physiological pH values. Unfortunately, similar to DNPH, most of the developed assays, which have not been illustrated in Scheme 31, exhibit just chromogenic and not fluorogenic properties. These have still found repeated uses for trace analysis of aldehydes in industrial processes, the food industry,

or the medicinal field but have been rarely employed for protein engineering efforts and even less in (u)HTS systems.



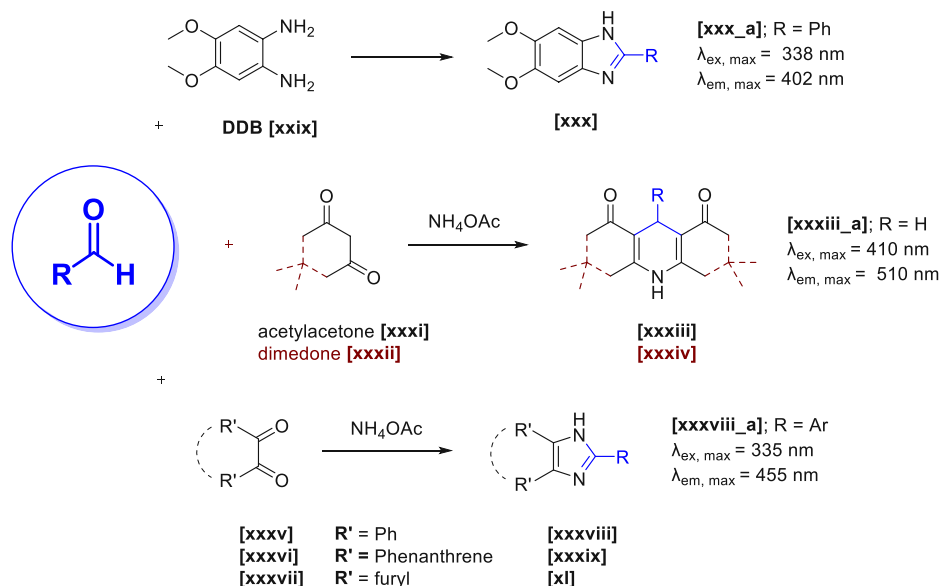
Scheme 31: Overview of historic chromogenic tools for sensitive aldehyde detection.

As one of these exceptions, mercaptotriazole purpald [xx] has been reported in a substrate-binding-guided mutagenesis experiment applied for the detection of benzaldehyde to improve the C_β -stereoselectivity of a threonine aldolase.¹³⁶ The MBTH [xxii] assay has been repeatedly used for the quantification of reducing sugars¹³⁷ and has been recently modified for off-line analysis using a HT robotic platform for accurate quantification of sugar concentrations present in the biomass hydrolysates.¹³⁸ Its need for a Fe^{3+} -oxidant, however, prohibits its use for certain buffers due to precipitations of insoluble salts (e.g., phosphate buffer). Chromotropic acid [xxiv] reacts *via* acid-catalyzed condensation to form intensely colored dibenzoxanthylum cation [xxv], which was used to quantify formaldehyde.^{139,140} *In-situ* sulfonation of either pararosaniline [xxvi] or fuchsin [xxvii] sets up these reagents for the historic Schiff's test¹⁴¹. This assay was employed in a colorimetric HTS format for the engineering of the P450 enzyme variant CYP102D1 for selective O-dealkylations. Formaldehyde

which was released upon cleavage of aromatic methoxy-groups, was detected as trapped purple salt [xxviii].¹⁴²

Advances in the field have indeed led to developments of fluorogenic probes forming (benz)imidazoles and Hantsch-ester derivatives (Scheme 32). However, these have unfortunately only been applied for HPLC-derivatization or trace analysis of environmental and physiological aldehydes.

143,144

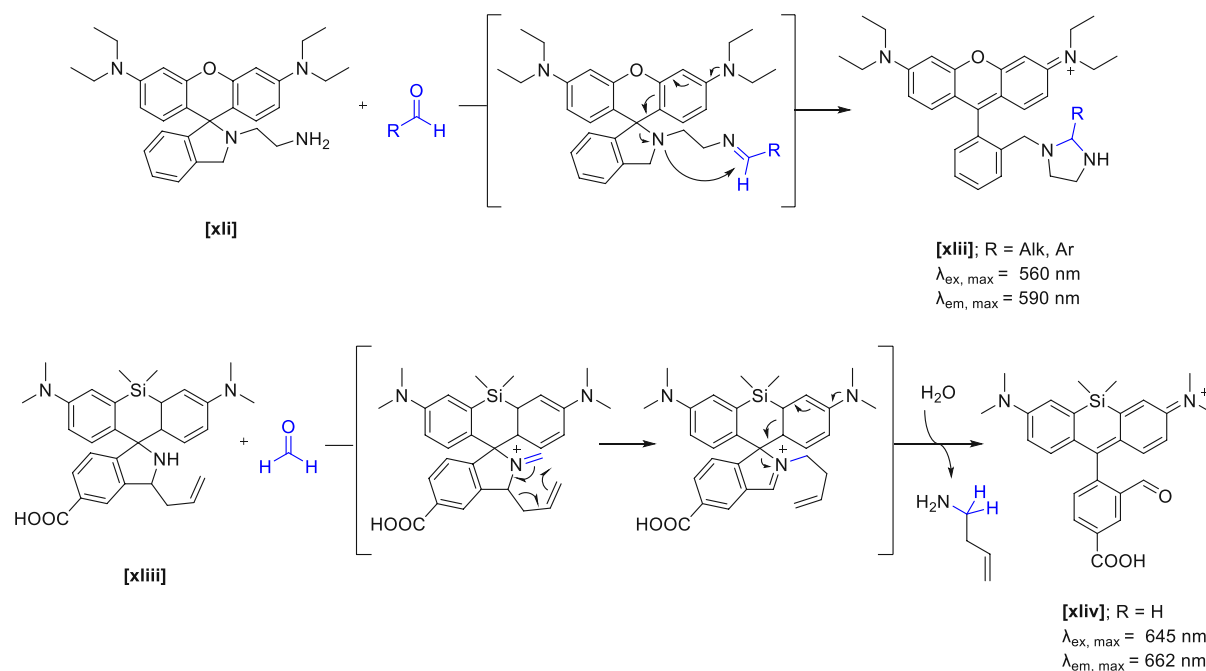


Scheme 32: Overview of fluorogenic reagents for sensitive aldehyde detection.

DDB (1,2-diamino-4,5-dimethoxybenzene) [xxix] has been reported as an efficient reagent for the fluorometric detection of aromatic aldehydes¹⁴⁵, as well as acrolein¹⁴⁶ and methylglyoxal¹⁴⁷ in blood samples in neutral or acidic conditions. Simple 1,3-diketones as acetylacetone [xxxii] or its cyclic derivative dimedone [xxxii] have been readily used for the synthesis of Hantsch esters (1,4-dihydropyridines) [xxxiii] and [xxxiv] with the addition of an ammonia source.^{148,149} These products were found to exhibit fluorescent properties and have been used for the detection of aliphatic and aromatic aldehydes in blood plasma or seawater samples.^{144,150} Lastly, also 1,2-diketones were found to selectively form imidazoles when treated with an aldehyde and ammonia. Two studied derivatives of benzil [xxxv], the phenanthrene- [xxxvi]¹⁵¹ and 2,2'-furyl derivative [xxxvii]¹⁵², were employed for the detection of aldehyde content in human sera.

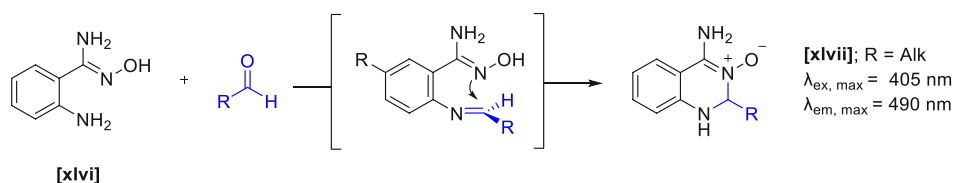
An exciting concept that has recently emerged uses the reaction with an aldehyde to trigger a targeted ring-opening of the deoxylactam moiety of rhodamine derivatives [xli] and [xlili] (Scheme 33). Cleavage of the C-N bond in such a system was known to immediately restore full conjugation and cause a rapid increase in fluorescence emission under physiological conditions. While Li *et al.* used the formation of a highly reactive Schiff's base as the trigger for the ring-opening, trapping the aldehyde inside the imidazolidine moiety [xliv]¹⁵³, the group of Chang applied an intramolecular aza-cope approach to trap the initially formed imine. The thus formed carbocation was immediately quenched by lactam opening, which was rendered irreversible by hydrolysis of the homoallylamine.¹⁵⁴ The latter approach was only reported for formaldehyde detection and was not expanded for aliphatic or aromatic

aldehydes. Both assays were proven to work under physiological conditions by staining sialic acid and formaldehyde respectively in living cells.



Scheme 33: Fluorogenic reagents targeting the deoxylactam-moiety of rhodamine derivatives for signal generation.

Another study for highly specific and rapid aldehyde conjugation was reported by Kitov *et al.* employing highly reactive 2-amino benzamidoxime reagents [xlv] (Scheme 34).¹⁵⁵ In the postulated mechanism for the assay, after an initial attack of the aniline, the intermediately formed imine is immediately and irreversibly trapped by the nitrogen of the oxime moiety. The thus formed quinazoline oxides [xlvii] exhibited a substantial shift in absorbance from 360 to 405 nm and the emergence of strong fluorescence at 490 nm.



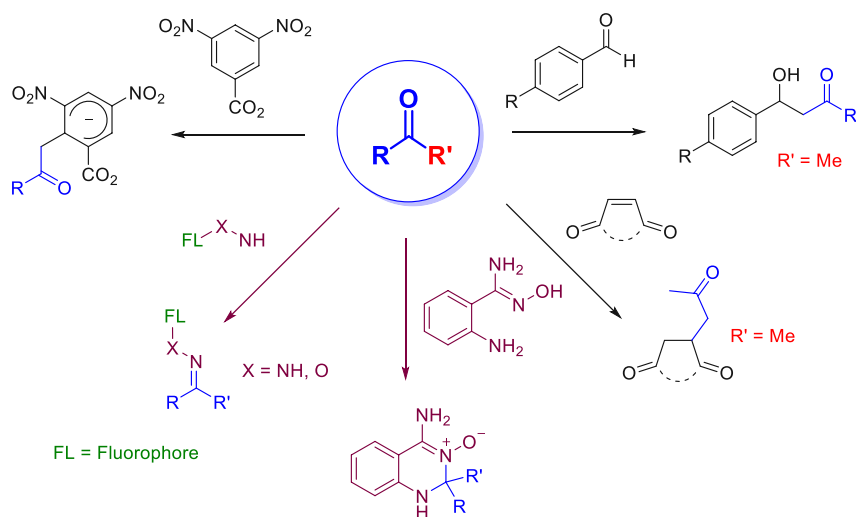
Scheme 34: Reaction of 2-amino benzamidoxime [xlv] reagents with aldehydes forming fluorescent quinazoline oxides [xlvii].

Prompted by unmatched kinetics paralleling the fastest known bio-orthogonal reactions with rates $40 \text{ M}^{-1} \cdot \text{s}^{-1}$, our group used the assay system for a systematic mutation study for CAR (*c.f.* B II.3).¹⁵⁶⁻¹⁵⁸

B III.1.1.2 Ketone selective assays

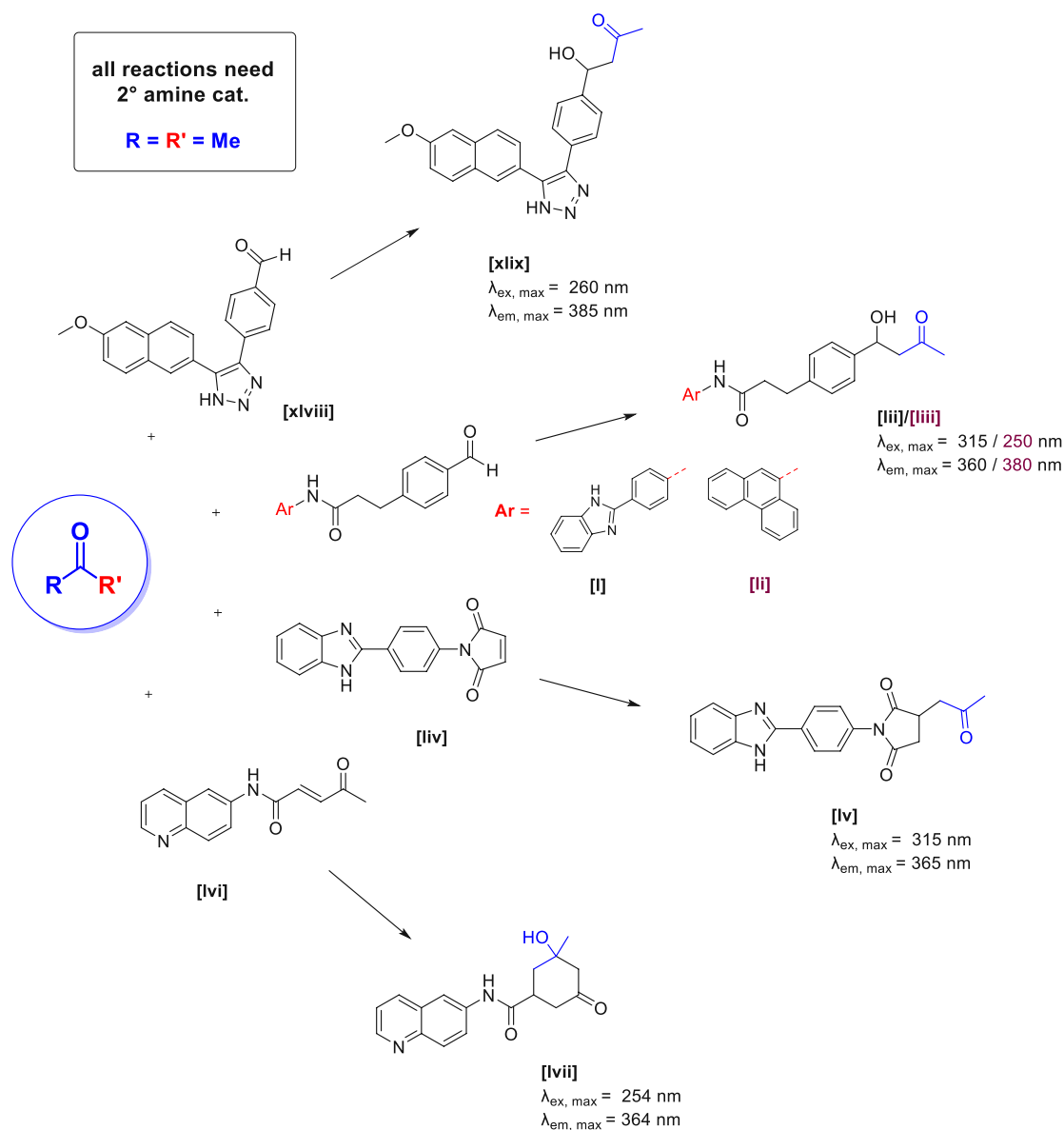
Compared to most aldehydes, ketones display a dramatically decreased reactivity due to an increase in steric bulk and diminished electrophilicity caused by the electron-donating nature of the attached alkyl groups. This inactivation renders specific targeting of keto-moieties significantly more challenging, as the necessary increase in reagent reactivity prompts a concomitant drop in selectivity. Although certain approaches have been developed for specific conjugations, they rely - for the most

part - on the identical methodology already introduced for aldehyde assays (purple reactions in Scheme 41). Nevertheless, ketones have unfortunately been proven in all literature reports to date to be very reluctant to undergo rapid conjugation at physiological conditions¹³⁰ – especially for applications where low concentrations impose an even more complex kinetical challenge.



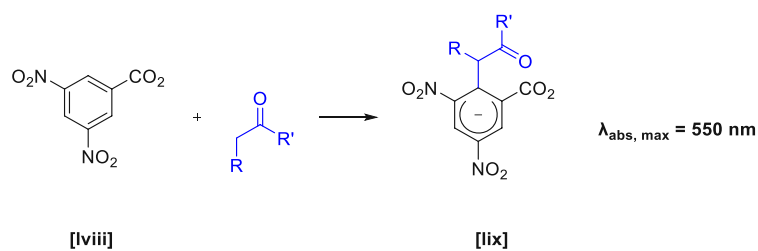
Scheme 35: Overview of ketone selective tagging strategies.

A particular strategy to circumvent this reactivity bottleneck was to use the property of ketones to enolize and thus undergo reactions observed for soft bases – aldol reactions and Michael additions. This methodology has been broadly explored by the group of Barbas III. In a series of published papers¹⁵⁹⁻¹⁶¹, multiple different designs for clever ketone traps were investigated (Scheme 37). These studies were, however, only limited to acetone as the analyte of choice and required some form of activation by enamine formation. Therefore, either pyrrolidine, certain amino acids (arginine, glycine, proline), or aldolase antibody 38C2 were used in catalytical amounts. Furthermore, a dramatic excess of the substrate was always necessary (1000x) to afford appreciable conversions. Both triazine aldehyde [xlvi], as well as the best performing phenanthrene amide-linked aldehyde [li], demonstrated similar excitation and emission properties (260 nm excitation; 380 nm emission). Although further red-shifts were enabled with an exchange of the aryl-moieties to the benzimidazole analog [I], these were proven to be detrimental to the overall sensitivity of the assay, as thereby the parent aldehydes turned to strong emitters. The Michael acceptors [liv] and [lvi] were also shown to exhibit beneficial turn-on properties¹⁶⁰ upon addition. However, a spectral overlap of the substrate-product pair of [lvii] rendered them less ideal for screening applications. Both probes additionally exhibited a similar problematic low reactivity comparable to the aldol sensors.



Scheme 36: Overview of fluorogenic reagents for sensitive ketone detection.

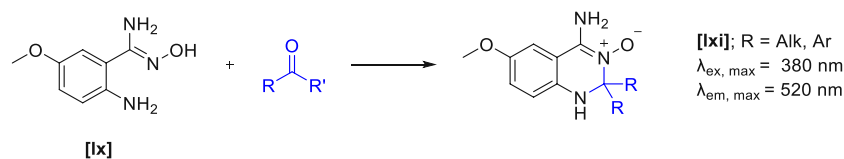
The Janovsky reaction will be mentioned for completeness, as it was used to rapidly evaluate Baeyer-Villiger monooxygenase substrates. Under basic conditions, enolizable ketones can form stable purple-colored σ -complex [lix] with 3,5-dinitrobenzoic acid [lviii]. The depletion of 11 ketones was followed by a spectroscopic assay at 550 nm (Scheme 37).¹⁶²



Scheme 37: Chromogenic Janovsky reaction for the selective detection of enolizable ketones.

Interestingly, the previously mentioned ABAO-reaction, initially suspected to be unreactive towards ketones, was proven to be an effective probe for aliphatic and aromatic ketones.¹⁶³ To combat

prolonged reaction times, the methoxy analog [Ix] was employed, which exhibited enhanced reactivity due to the mesomeric effect of the methoxy group (Scheme 39).



Scheme 38: Reaction of methoxy 2-amino benzamidoxime [Ix] with ketones forming fluorescent quinazoline oxides [Ixi].

The methodology was efficiently applied to perform enzyme mining for alcohol dehydrogenases (ADHs) and subsequent directed evolution studies.⁶⁷

B IV Fluorescence-activated droplet sorting

As previously mentioned, successful directed evolution experiments necessarily require a spatial correlation between the expressed genetic mutants and the corresponding enzymatic turn-over. In classical screenings, the cells or the proteins of interest are physically separated using microtiter multi-well plates. However, these systems cannot be indefinitely miniaturized to encompass more extensive libraries due to inherent physical barriers imposed by capillarity and increased evaporation with volumes less than 1 μL .¹⁶⁴ Here, microfluidic systems completely changed how far screening efforts can be taken with the possibility of reproducibly handling small sub- μL volumes. Initial FACS (fluorescence-activated cell sorting) systems enabled rapid assessments of millions of fluorescently labeled cells in a matter of hours compared to even automated robotic platforms, which needed days for the same endeavor.¹⁶⁵ The application of those fluorescent reporters that enabled the phenotypic read-out is, however, limited to either intracellular space or the cell's surface due to the instrumental set-up. As FACS employs cellular walls to compartmentalize, it cannot identify variants that overproduce extracellular metabolites. Although this problem has been combated with the development of w/o/w emulsions, which spatially separate extracellular matrices, these require a more complicated experimental setup.^{165,166} Furthermore, significant investments need to be accounted for a commercial FACS machine (starting from \$100.000¹). Nevertheless, several studies using this approach have already successfully proved the work-around for this methodology.¹⁶⁷⁻¹⁶⁹

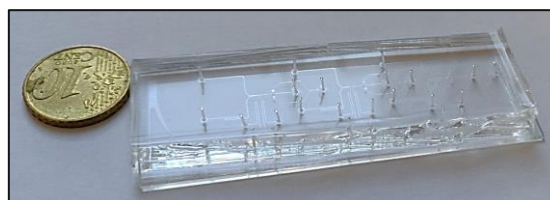


Fig. 10: Size comparison of typical microfluidic PDMS chips used for FADS.

FADS (fluorescence-activated droplet sorting) systems which have emerged since their first report in 2009 by Baret *et al.*¹⁶⁶, offer an attractive alternative. Herein, microfluidic PDMS chips (Fig. 10) with defined channel geometries allow individual cells expressing the target protein mutants to be entrapped in singular pL-sized w/o emulsions, thereby turning them into small biochemical reactors.

¹ <https://www.excedr.com/blog/how-much-does-a-flow-cytometer-cost/> (accessed September 2021)

Simultaneously encapsulated assay components react with the target of choice enabling sensitive detection *via* laser-induced fluorescence (LIF). With the use of surfactants, coalescence of the droplets is prevented, and the phenotypic readout can be directly correlated to the genetic sequence. Using this methodology, extracellular components are also trapped inside these vesicles and can be thus coupled to the enzymatic activity (*in vitro* compartmentalization).¹⁷⁰ Lysis agents are frequently added into the droplets for cell-membrane impenetrable substrates.

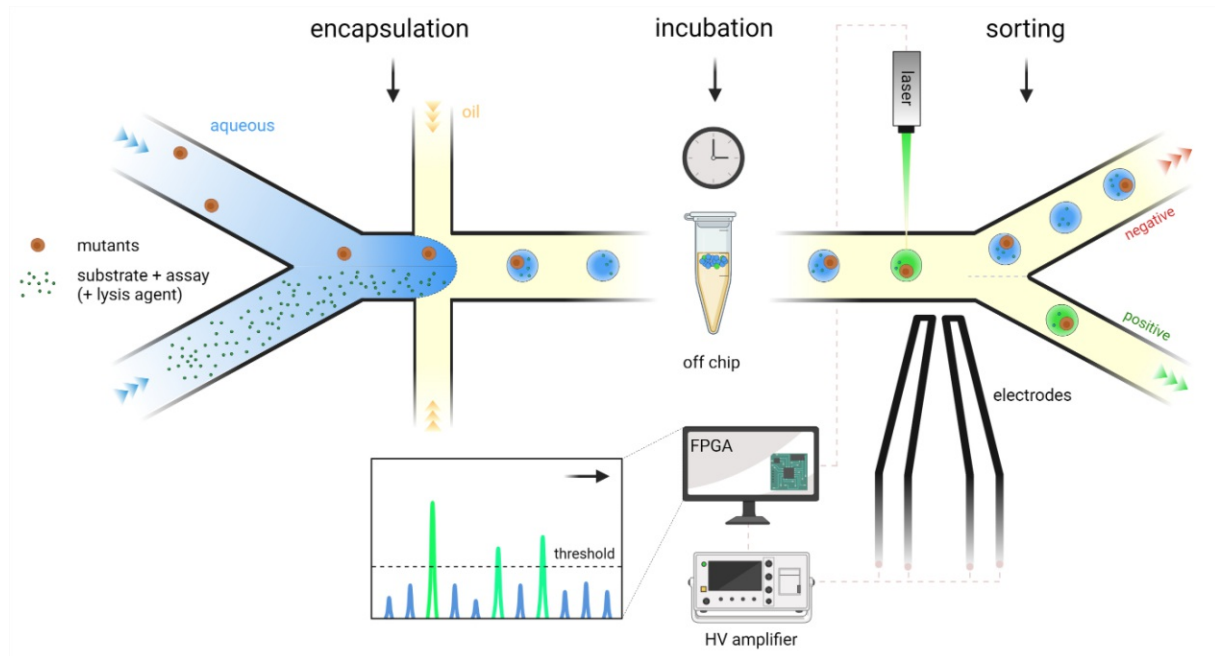


Fig. 11: Work-flow for a classical application for FADS.

The workflow of a FADS experiment is classically divided into three parts – droplet encapsulation on the droplet formation chip, incubation, and the concluding droplet sorting on a separate microfluidic chip (Fig. 11). In the first step, all aqueous components, including the cellular host expressing the evolved enzyme library, the fluorogenic sensor, and corresponding substrates, are encapsulated using a flow-focusing junction. An increased flow rate of the oil layer triggers the separation of the aqueous phase into discrete droplets (Fig. 12 left). According to a Poisson distribution model, single-occupancy of cells can be guaranteed by choosing an appropriate dilution.¹⁷¹ If necessary, the expressed proteins are liberated using either chemical, enzymatic, or heat lysis.

The thus formed droplets are typically collected off-chip in Eppendorf tubes and incubated for a set time and temperature. If active mutants have been expressed for the desired transformation, the product is formed inside the aqueous vesicles and trapped *via* appropriate fluorogenic probes or utilizing a different detection mechanism (*c.f.* B III.1). In the case of very fast processes (minutes to hours) for both the biotransformation and the signal generation, droplets can also be incubated directly on the chip using appropriately large reservoirs.¹⁷²

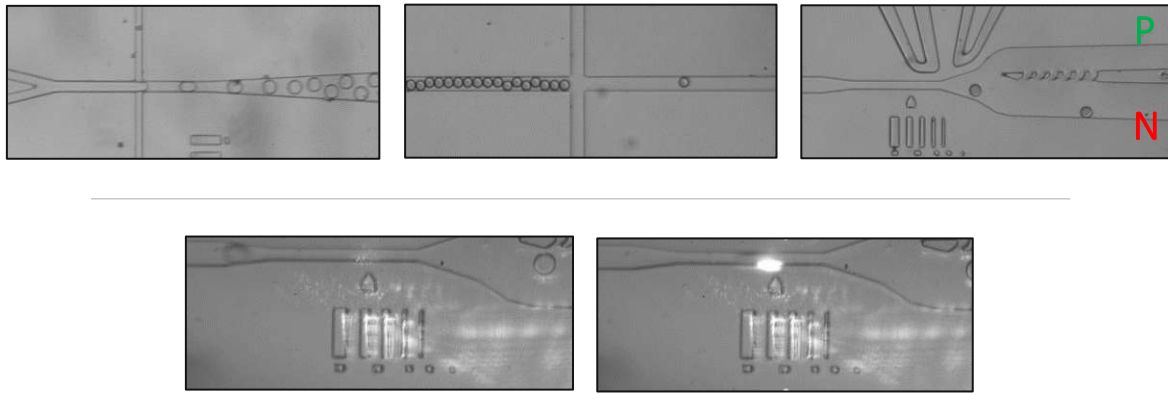


Fig. 12: Representation droplet manipulation steps needed for a FADS – **top left:** droplet encapsulation, **middle:** spacing of droplets prior to the sorting junction, **right:** droplet sorting, positive channel represented with a green P, negative channel with a red N, **bottom:** excitation of fluorophore containing droplets upon passing the laser beam.

Ultimately, the droplets are reinjected into the sorting chip and, after being initially spaced (Fig. 12 middle), are guided to the sorting junction. Excitation of the fluorophore-containing droplets using a defined laser source causes a fluorescence emission, which by exceeding a user-set intensity threshold, triggers a short high voltage sorting pulse at the junction. Due to the difference in dielectric permittivity between the aqueous phase ($\epsilon \sim 80$) and the (mostly fluorinated) continuous oil phase ($\epsilon \sim 2$), the resulting dielectrophoretic force pulls the droplets towards the positive channel (Fig. 12 right; green P). If no sorting pulse is applied, droplets exhibit a biased flow towards the negative channel (red N) created by the appropriate geometry of the sorting chip.¹⁷³ The plasmids of the thus sorted cells can be harvested and re-subjected to another iteration of (randomized) mutagenesis.

This workflow and components by themselves represent the minimal necessary structure for a FADS. However, notable developments in the field have led to an enlarged set of possible manipulations on the chip, which comprise droplet merging and splitting¹⁷⁴, piconjection¹⁷⁵ of additional material after initial droplet formation (Fig. 13), or multiplex sorting employing several sorting channels¹⁷⁶. The latter has still only been shown to work in a proof-of-concept study.

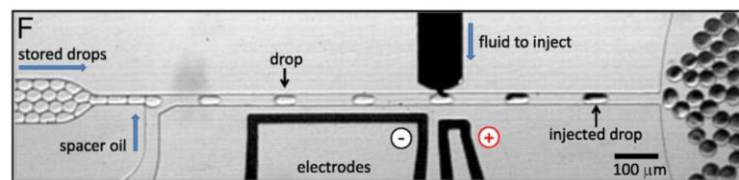


Fig. 13: Representative example of piconjection in a microfluidic experiment reported by Abate et al.¹⁷⁵

Pico-injection, on the other side, has already been applied for cases in which the fluorogenic probes were proven to be unstable under aqueous conditions and were necessarily added after the incubations period.¹⁷⁷

B IV.1 Limitations

Although FADS was shown to be complementary to the FACS methodology by expanding the HTS-field to include extracellularly located reactions, this in itself was found to entail certain limitations and challenges.

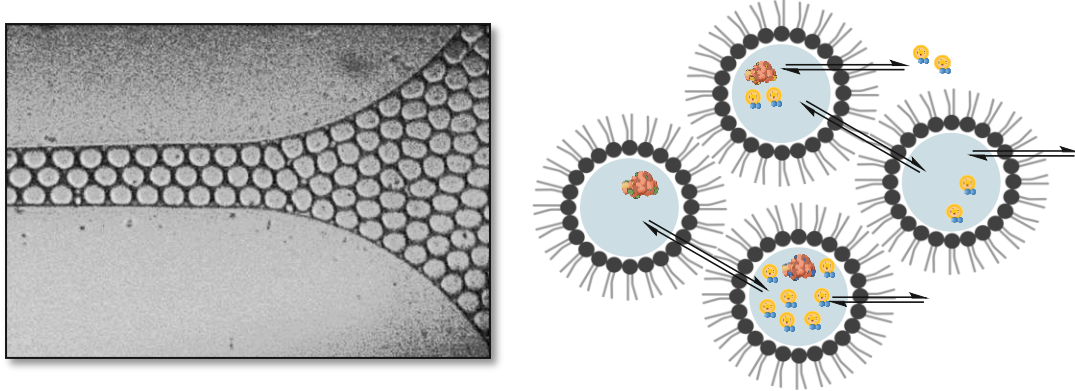


Fig. 14: Collection of droplets prior to reinjection into the sorting device: The proximity of the droplets enables rapid migration of apolar material out of or in between the droplets if certain hydrophilicity thresholds are not met.

Without cellular barriers or covalent linkages to cell membranes, all components can freely disperse inside the droplets upon encapsulation. Highly apolar molecules were in doing so found to readily migrate out of or in between the droplets. This leakage across the droplet interface is especially problematic if it affects the fluorogenic reporter, as, by this, any phenotype-genotypic linkage is lost. This was proven in a small study by Woronoff *et al.*, where a direct correlation between the LogP values of the employed fluorophores and their migration tendency was proven.¹⁷⁸ LogP values lower than -2.59 were found to sufficiently avoid any cross-talk between droplets.

The migration of fluorescent reporters across droplets can be attributed to two phenomena. Compounds can either partition and diffuse through the carrier oil or exchange between droplets through micellar transport.¹⁷⁹ This overall leakage was reduced with the use of fluorinated oils (compared to mineral oils)¹⁸⁰, which became standard for any FADS application, the addition of 5 % (w/v) bovine serum albumin (BSA)¹⁸¹, or by the reduction of surfactants concentration to limit the formation of micellar structures.¹⁸² Other recently developed systems omit surfactants entirely and instead rely on pickering emulsions using perfluorinated nanoparticles.^{183,184} However, no case studies with applications have been reported so far. Substrate modifications by incorporating highly polar (or charged) groups into the fluorogenic reporter were proven to be the most potent method to prevent leakage.^{178,185}

B IV.2 Applications in protein engineering efforts

With the establishment of the FADS technology, several outstanding studies were reported using this methodology to dramatically accelerate directed evolution experiments for various substrates and target modifications. The experiments included screenings for a general improved enzymatic activity, targeted improved enantioselectivity or enhanced fitness of organisms, and were applied for gene mining, among others. Various publications have been already mentioned in previous chapters (c.f. B III.1.1) – additional ones are highlighted below:

One of the first applications using a working FADS system was reported by Agresti *et al.* for the directed evolution of horse radish peroxidase (HRP) in yeast strain EBY100. Using a cell surface display approach, the mutagenized HRP was fused with the membrane anchoring peptide (Aga2) and screened for an activity using the catalyzed oxidation of Amplex Ultrared as the fluorogenic reporter. Already after the second screening iteration using a library of 10^7 variants, an approximately 10-fold rate increase was observed.²³ In another report following an *in vitro* compartmentalization approach, Beneyton *et al.* screened for thermostable mutants of endo- β -1,4-xylanase in *Yarrowia lipolytica* using the xylobiose-tagged coumarin as the fluorogenic probe. To increase the sensitivity of the system, singular yeast cells were grown inside the 20 pL droplets resulting in dozens of encapsulated cells per droplet. Following a heat shock at 90 °C before the encapsulation, eight clones displayed an approximately tenfold higher residual activity than the wild type.¹⁸⁶ In seminal work from Fuqiang *et al.*, the classical screening concept was expanded for the directed evolution of an enantioselective esterase from *Archaeoglobus fulgidus* using their dual-channel microfluidic droplet screening (DMDS) approach. Similar to the approach mentioned before (c.f. B III.1.1, examples for g), the group initially selected for improved activity towards both differently labeled (*S*)-ibuprofen esters (*S*)-[Ixii] / [Ixiii] to avoid a substrate bias. After 4-fold improvement of activity, the screening was turned into “biased”-mode, thereby concomitantly screening for increased reactivity towards the (*S*)-[Ixii] and decreased reactivity towards the (*R*)-[Ixii] enantiomer (Fig. 15. Two additional rounds of mutagenesis discovered a variant with 700-fold greater (*S*)-enantioselectivity, which was proven to persist for other profen-esters.¹⁸⁷

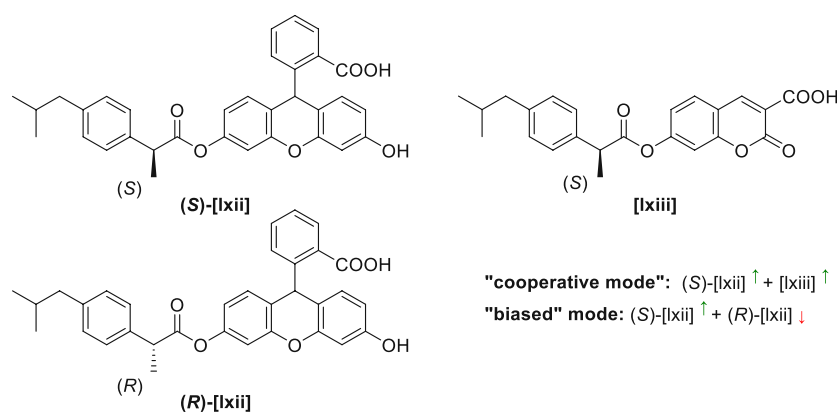


Fig. 15: Substrates applied use for screenings for enantioselectivity for the esterase from *Archaeoglobus fulgidus* in dual-channel microfluidic droplet screening (DMDS) by Fuqiang *et al.*¹⁸⁷

A very recent publication by the FADS-pioneers from the Hollfelder group reported the first successful cell-free directed evolution in an uHTS format. The incompatibility between DNA amplification and cell-free expression in compartmentalized vessels rendered the approach until then

impossible. Employing a highly controlled consecutive dual picoinjection of *in-vitro* transcription and translation (IVTT) components and substrate on their microfluidic device ultimately enabled a 5-fold improvement of a subtilisin-like protease in six evolution steps.¹⁸⁸

Advances in directed evolution methodology in the past decade have thus shown its tremendous potential for reaching new standards in protein engineering. Especially with the entry into the ultra-high-throughput field, targeted modifications to enzymatic functionality became finally identifiable. These were, however, only possible with the emergence of novel instrumentation and underlying chemical tools. Although still in its infancy, the FADS methodology represents one promising approach to harnessing nature's long yearned specificity and efficiency.

B V Objectives

Within this thesis, we aimed to improve the analytical toolsets for protein engineering of carbonyl-producing enzymes. Herein known reactions catalyzed by native and already mutated SHCs and CARs (Fig. 16) and the products thereof were chosen as starting points for the development of assays and were to be investigated from different vantage points (reactivity, applicability, optical properties). A particular focus was placed on the application in FADS format, targeting the limitations discussed in chapter B IV.1.

Due to the unfamiliarity with the SHC enzyme class, initial studies should be undertaken to achieve a general understanding of its catalytic promiscuity. This should be achieved by exploring steric and electronic limitations for the already known enzymatically catalyzed Prins reaction of citronellal [I]. Based on these findings, further applications of the particular catalytic machinery of the SHCs were to be investigated. A particular focus should be placed on the optical tracing of selected reactions, enabling a faster downstream evaluation of improved enzymatic mutants. This should be achieved by the synthesis and optical evaluation of suitable chromogenic Friedel-Crafts acylation substrates and their resulting products.

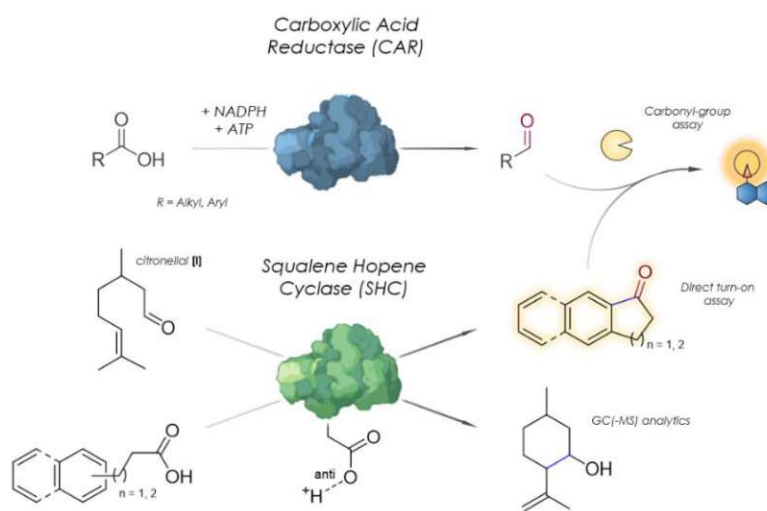


Fig. 16: Envisioned assay methodologies for the respective CAR and SHC catalyzed reactions: **top** - NADPH and ATP promoted reduction of alkyl and aryl carboxylic acids detected **via** carbonyl-selective assay; **bottom**: Prins reaction of citronellal screened using GC(-MS) analysis; Friedel-Crafts acylation of aryl propionic or butyric acids detected either **via** inherently fluorescent naphthylketones or **via** subsequent detection using the carbonyl-selective assay.

To further depart from a substrate-dependent optical read-out and broaden the applicability of these screening tools, a substrate-independent approach was sought after. Herein two distinct approaches using already established carbonyl-specific assay tools based upon NBD (7-nitro-2,1,3-benzoxadiazole)¹²⁴ and ABAO (amino benzamidoxime)¹⁵⁵ reagents were to be explored in a biocatalytic regime (Fig. 17).

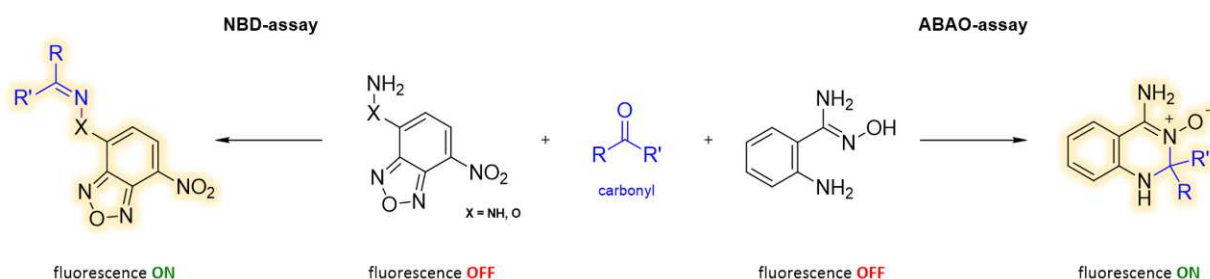


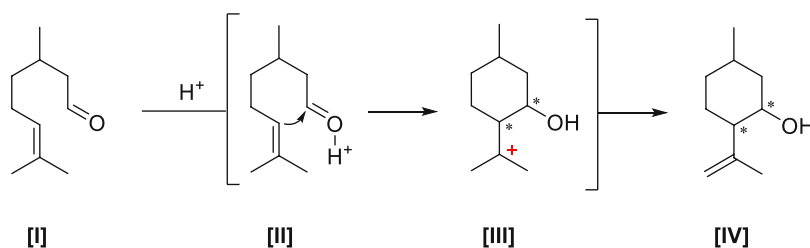
Fig. 17: Substrate-independent carbonyl-selective assays taken as starting points for assay development – left: formation of fluorescence hydrazones upon reaction with non-fluorescent 7-nitro-2,1,3-benzoxadiazole hydrazine (NBD-H) and its derivatives, right: formation of fluorescent dihydro quinazolines upon cyclization with non-fluorescent amino benzamidoximes (ABAO).

In the third part of the thesis, the assembly and testing of a novel microfluidic FADS (fluorescence-activated droplet sorting) platform for protein engineering was to be established on the TU Wien. The system should be custom-built and allow cheap, easy manipulation and exchange of all optical, optomechanical and electrical components. The production of microfluidic PDMS chips, initial droplets encapsulation, as well as droplet sorting experiments should be performed. Due to the restrictions posed by the FADS described in chapter B IV.1, modifications with the introduction of highly polar groups onto these reagents above were to be performed, facilitating their application in HTS regimes.

C Results and discussion

C I.1 Part I – SHC catalyzed Prins reaction

This chapter investigates the substrate specificity and thus promiscuity of known SHCs for the enzymatic Prins reaction of citronellal **[I]** analogs. In the reaction, protonated and thus activated aldehyde **[II]** can be similarly trapped by electron-rich double bonds to the well-known Friedel-Crafts acylation (Scheme 39). The positively charged intermediate **[III]** can then undergo exocyclic elimination to form isopulegol **[IV]**, an essential precursor for menthol synthesis. This general C-C bond-forming mechanism is termed Prins-reaction and has found many applications for the synthesis of substituted tetrahydropyrans¹⁸⁹⁻¹⁹¹, tetrahydrofurans¹⁹², 1,3-dioxanes^{193,194}, or even spirocyclic compounds by employing ketones as the carbonyl species¹⁹⁵. Many preceding investigations targeted the stereoselective control of this process by employing either Lewis acids^{196,197}, zeolites¹⁹⁸, or biocatalysts^{49,52} as sources of chirality.



Scheme 39: General mechanism for the acid-catalyzed Prins reaction of citronellal **[I]**.

This investigation aimed to elaborate on the effect of different steric and electronic motives on the reactivity and selectivity of selected SHC mutants, thereby enabling the establishment of a reactivity profile. Herein several citronellal derivatives were envisioned as substrates for the enzymatic transformation (Fig. 18).

Due to the known impact of the stereochemistry of the β -methyl group on the outcome of the enzymatic transformations⁵², (*R*)-, (*S*)- as well demethylated analogs were synthesized. Furthermore, variations of electrophiles were performed. Herein nitriles, carboxylic acids, and thioesters were considered as possibly activatable sp^2 and sp^3 centers. Secondary alcohols and mesylated analogs were envisioned as reaction partners due to their improved leaving groups' capability. To understand the requirements of the substitution pattern of the double bond and thus the stability of the intermediately formed carbocation, effects of double bond geometry were studied employing un-, mono- and disubstituted derivatives and cyclic structures.

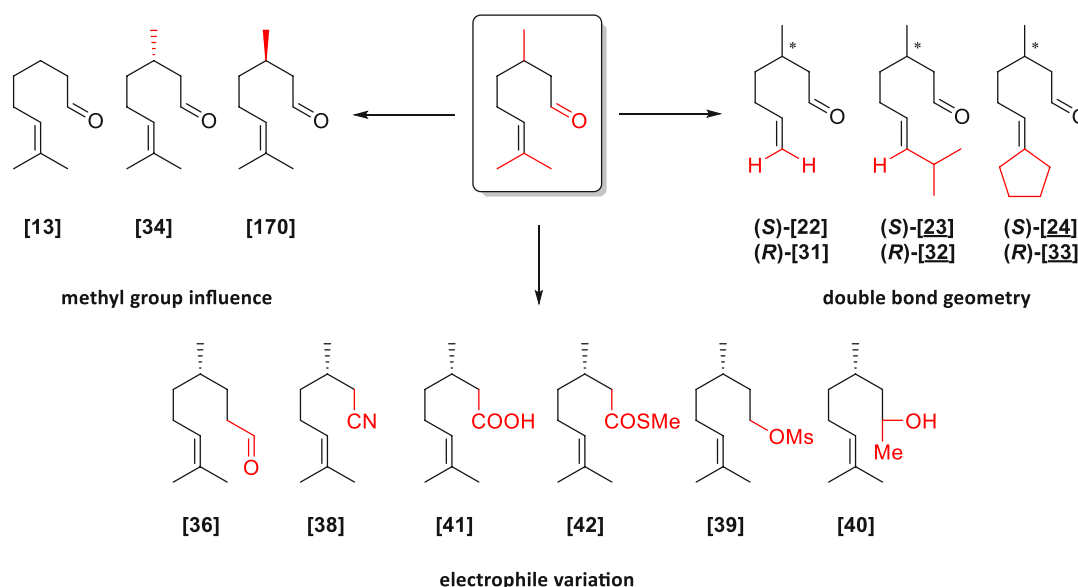
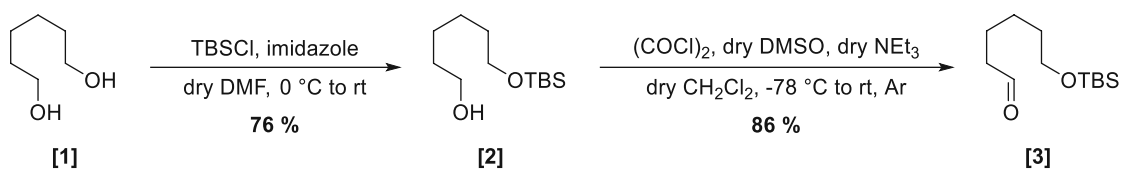


Fig. 18: Summary of citronellal analogs synthesized in this thesis.

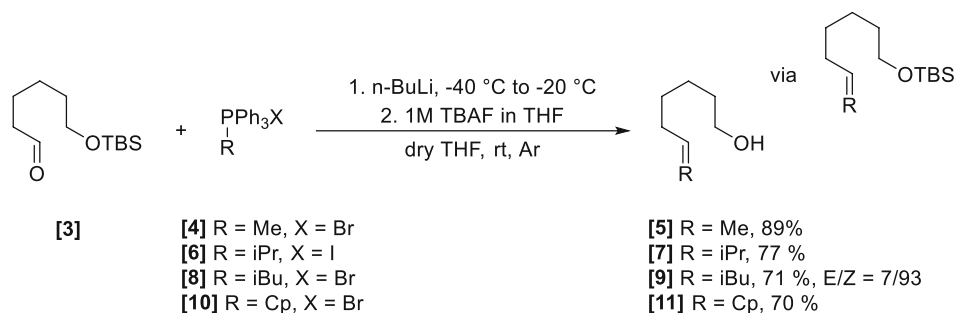
C I.1.1 Synthesis of citronellal derivatives

The synthesis for the demethylated analogs was commenced with the TBS (tert-butyldimethylsilyl) protection of 1,6-hexanediol **[1]**.¹⁹⁹ To improve the isolation of the desired monoprotected product **[2]**, TBS-Cl was used as the limiting reagent and the diol **[1]** in 10-fold excess. Unreacted diol could be easily removed with several washing steps with dH₂O. The final product needed to be purified by flash column chromatography to yield sufficient purity for the subsequent Swern oxidation (Scheme 40).²⁰⁰



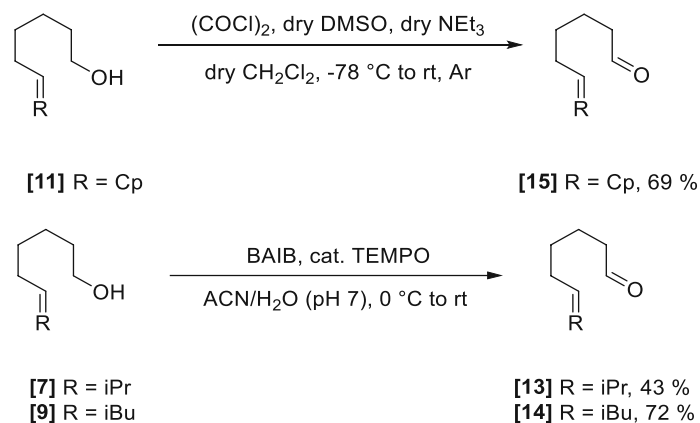
Scheme 40: Desymmetrization of hexanediol **[1]**.

The TBS-protected aldehyde **[3]** could be isolated in 86 % yield, albeit the need for careful control of the vacuum during the evaporation of the solvent, due to its highly volatile nature. All TBS-protected citronellal derivatives exhibited the same behavior. Hence any obtained products were extracted and columned exclusively in Et₂O or mixtures thereof.



Scheme 41: Introduction of different double bond residues by Wittig reaction of TBS-protected aldehyde **[3]**.

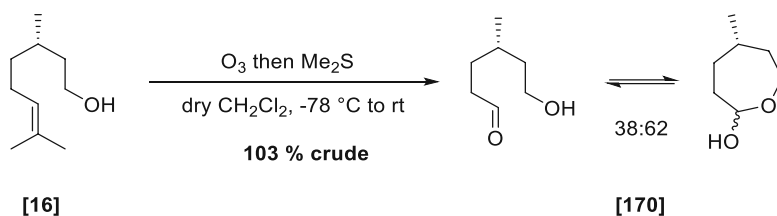
For the introduction of the double bond, classical Wittig-conditions²⁰¹ were applied using n-BuLi as base at -40 °C and the respective triphenylphosphonium bromides [4], [8], [10] or iodides [6] as alkyl donors (Scheme 41). Higher temperatures during the deprotonation step proved to be unreliable and led to unreproducible results. After the completed addition of base and aldehyde, the reaction was allowed to reach -20 °C to improve the speed of the process. Due to the aforementioned volatility of the intermediates, immediate deprotection with 1M TBAF (tetrabutylammonium fluoride) was essential to alleviate the loss of product during solvent evaporation. Especially in the case of commercial cyclopentyltriphenylphosphonium bromide [10], thorough drying of the salt was necessary to enable any formation of the phosphonium ylide due to its potential residual water content. Generally, any deprotonation of the Wittig reagents led to an immediate substantial color evolution (yellow for [4], blood red for [6], orange to red for [8] and [10]) which needed to persist throughout the addition of the aldehyde to afford any product formation. Hence prior threefold azeotropic co-evaporation with dry toluene proved to be very reliable and improved the yields of any subsequent Wittig reactions. The usual problematic removal of concomitantly formed triphenylphosphine oxide was accomplished by precipitation of the by-product with sufficient Et₂O addition to the crude reaction mixture and successive flash column chromatography. After careful bulk removal of the solvent, the deprotection could be subsequently performed without additional purification, delivering the respective unsaturated citronellol derivatives [5], [7], [9], and [11] in good to excellent yields. Final oxidation to the respective aldehydes was achieved using either classical Swern-conditions^{200,202} or the BAIB/TEMPO²⁰³ (bis(acetoxy)iodobenzene / (2,2,6,6-Tetramethylpiperidin-1-yl)oxyl) system (Scheme 42). Both approaches proved to be applicable, whereas the former proved to be the more reliable oxidation.



Scheme 42: Selective aldehyde oxidation enabled either **via** Swern oxidation conditions (**top**) or **via** a combination of the BAIB/TEMPO oxidant system (**bottom**).

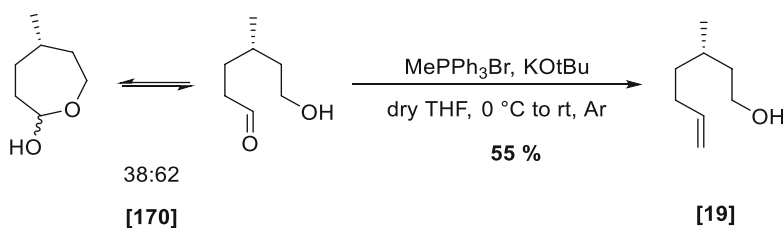
Unfortunately, both reaction conditions showed high irreproducibility due to the possible volatility and reactivity of the products, which was especially the case for [13]. To enable the unproblematic application of the purified products for the subsequent biotransformation, partial loss of product due to evaporation was accepted.

A similar strategy was applied for the synthesis of the methylated analogs. By taking advantage of the commercially available enantiopure start materials, the synthesis could be commenced with the (*R*)- and (*S*)-citronellol [16] and [25], respectively.



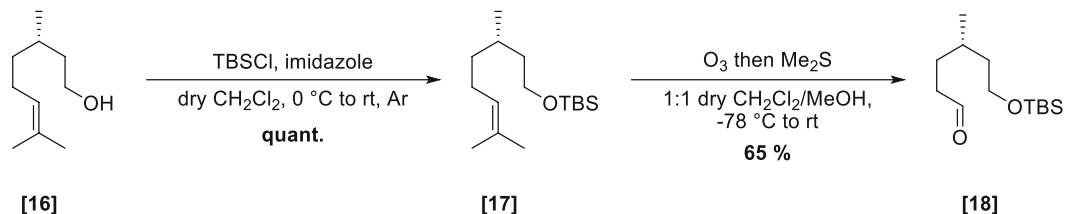
Scheme 43: Ozonolysis of unprotected (S)-citronellol **[16]**.

To elaborate the double bond functionality, an ozonolysis²⁰⁴/Wittig approach²⁰⁵ was first envisioned, which led to the formation of the aldehyde **[170]**, which could be isolated as a mixture of open and hemiacetal form (Scheme 43). Due to the fast equilibria and the unstable nature of the product, isolation of the pure compound either *via* column chromatography or distillation failed. The product showed increased decomposition after any purification attempt. Hence direct Wittig olefination was attempted with the crude mixture.



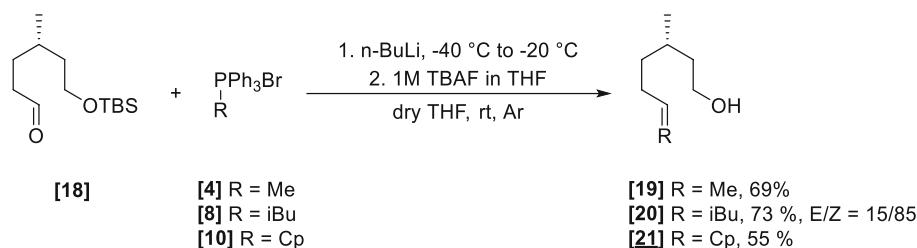
Scheme 44: Wittig reaction of the aldehyde **[170]**.

To our surprise, applying the only known literature conditions²⁰⁶ using solid KOTBu as base at 0°C , yielded 55% for the methyl-citronellal analog **[19]** in very high purity after column chromatography (Scheme 44). Unfortunately, storage of the aldehyde **[16]** in the freezer even at -20°C under argon led to evident decomposition already after several days, proven by NMR analysis. This was furthermore evident due to the beginning phase separation of the viscous mixture. Hence a similar strategy to the demethylated analog was used. Prior TBS-protection²⁰⁷ of the alcohol functionality in quantitative yield enabled a much smoother ozonolysis reaction and a more straightforward separation of triphenylphosphine oxide in subsequent Wittig reactions due to a distinct difference in polarity (Scheme 45). Albeit the persisting inexplicable instability of the protected aldehyde **[18]**, previously detrimental column chromatography of the crude could be performed to isolate the product in excellent purity.



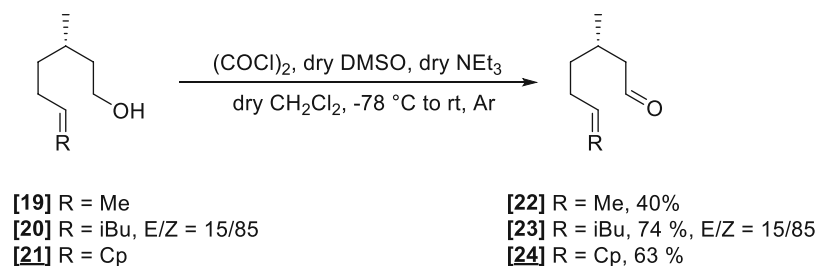
Scheme 45: Improved synthesis of Wittig precursor **[18]** by TBS protection of citronellol **[16]**.

To achieve an acceptable yield, all Wittig / deprotection sequences needed to be completed rapidly after the isolation of **[18]**. Detrimental effects to the quality could be already observed after one week of storage at -20°C under argon. The same procedure as mentioned was applied for the reaction of the demethylated analogs, and the respective citronellol derivatives **[19-21]** could be isolated after deprotection in good yields (Scheme 46).



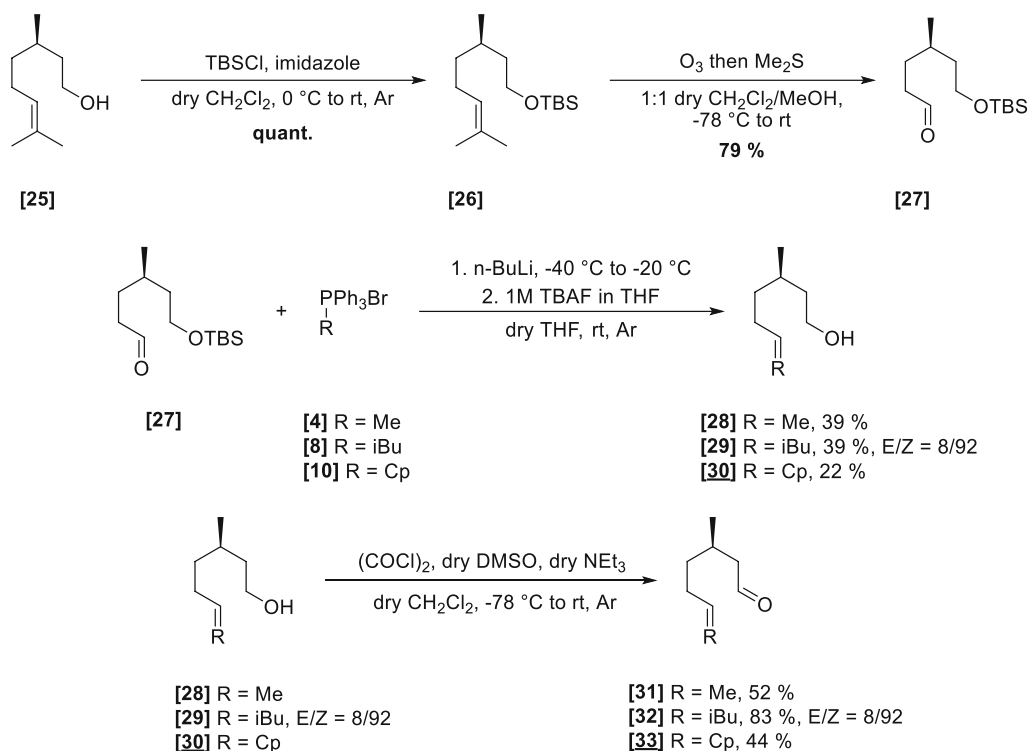
Scheme 46: Introduction of different double bond residues by Wittig reaction of TBS-protected aldehyde **[18]**.

Oxidation of the aldehydes was accomplished using conventional Swern oxidation conditions in mediocre to good yields (Scheme 47). The high volatility of the shortest carbon-chain analog proved to be yet again problematic.



Scheme 47: Swern oxidation of primary alcohols **[19-21]**.

With this established sequence in hand, the synthesis of the enantiomeric compounds was performed accordingly (Scheme 48). Unfortunately, the synthesis of **[29]** and **[30]** exhibited lower yields due to the already partly decomposed aldehyde precursor **[27]**. Nevertheless, the synthesis was carried on, and the respective (*R*)-citronellal derivatives **[31]**–**[33]** could be obtained in mediocre to good yields after column chromatography.



Scheme 48: Synthesis of (*R*)-citronellal derivatives **[31]**–**[33]** using the previously established route for the (*S*)-enantiomer citronellal analogs **[19]**–**[21]**.

With one part of the substrate scope at hand, we turned to the synthesis of the citronellal derivatives bearing different electrophilic groups. The synthesis was initially limited to the (*S*)-enantiomer due to its commercial abundance but would be expanded to the (*R*)-enantiomer if promising results were obtained. Using the set of substrates, several interesting product motifs could be envisioned using the same activation mode described for citronellal (Fig. 19).

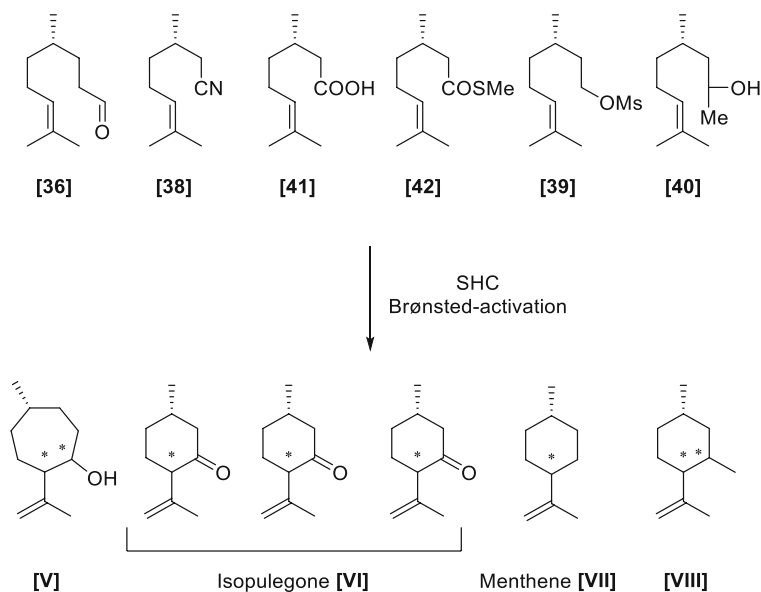
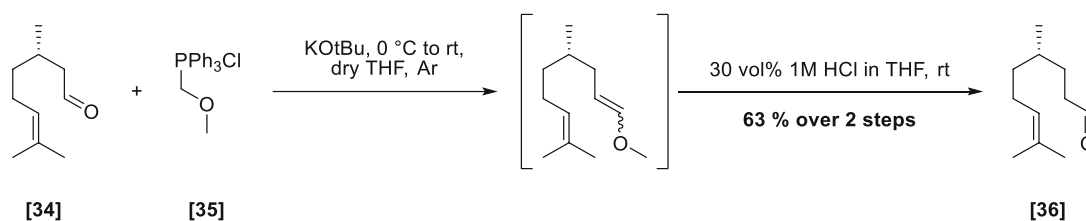


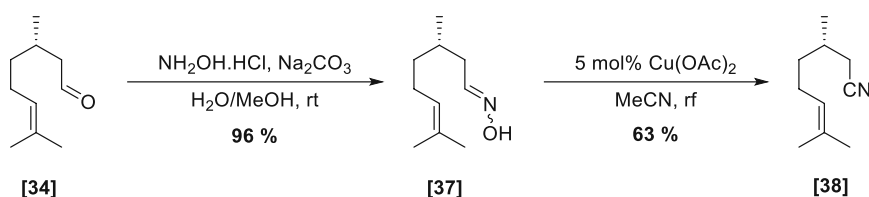
Fig. 19: Theoretically expected products upon SHC catalyzed Prins-type reactions with electrophile analogs [36-40].

To see if the enzyme would enable the synthesis of the unknown heptacycle motif [V], one of the envisioned substrates was the homologous derivative [36] which could be synthesized using a literature Wittig protocol with the (methoxymethyl)triphenylphosphonium chloride [35].²⁰⁸ Applying the same work-up mentioned for the synthesis of previously mentioned citronellol derivatives [5]-[9], the intermediately isolated enol ether could be easily deprotected using 1 M HCl in THF (Scheme 49).



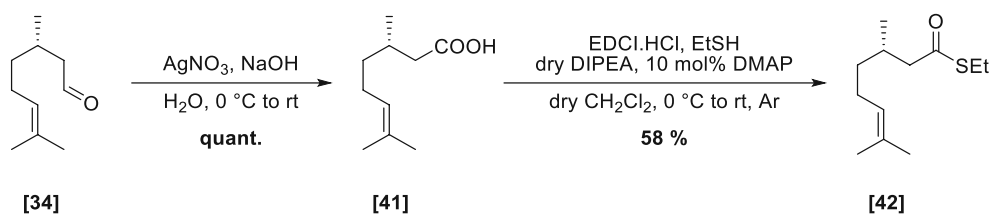
Scheme 49: Synthesis of homologous analog [36] using a Wittig reaction/hydrolysis sequence.

The corresponding nitrile [38] was synthesized using a known literature sequence²⁰⁹ via the oxime [37], which was dehydrated using catalytic amounts of copper acetate in acetonitrile in good yield (Scheme 50).



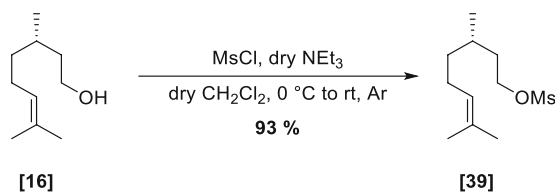
Scheme 50: Synthesis of nitrile [38].

To enable several routes to the interesting fragrance compound isopulegon [VI] carboxylic acid [41] as well as its thioethyl ester derivate [42] were also synthesized. The thiol was believed to act as the better leaving group, improving product formation during the enzymatic transformation. The synthesis was achieved using *in-situ* generated Ag_2O , which readily oxidized the aldehyde albeit two-phasic conditions.²¹⁰ Due to the instability of the formed Ag(I) particles to light, the flask was covered with aluminum foil throughout the reaction. After organic extraction and evaporation of the solvent, the product could be obtained without additional purification. The highly aromatic citronellic acid [41] was converted to the thioester using classical EDCI (1-Ethyl-3-(3-dimethylaminopropyl)carbodiimide)-coupling conditions and ethanethiol. After column chromatography, the desired thioester could be isolated in 58 % as a colorless and surprisingly odorless oil (Scheme 51).



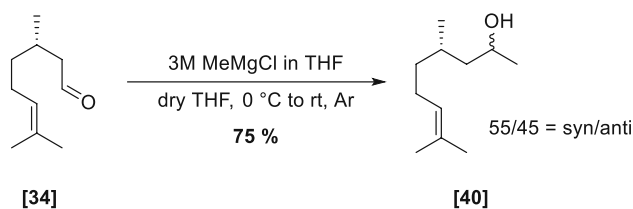
Scheme 51: Synthesis of thioethyl ester derivate [42] via citronellic acid [41].

Seeing if activation of mesylates would lead to methene [VII] formation, the corresponding mesylate [39] was also synthesized in excellent yield using mesyl chloride and (*S*)-citronellol [16] (Scheme 52).



Scheme 52: Synthesis of mesylate [39].

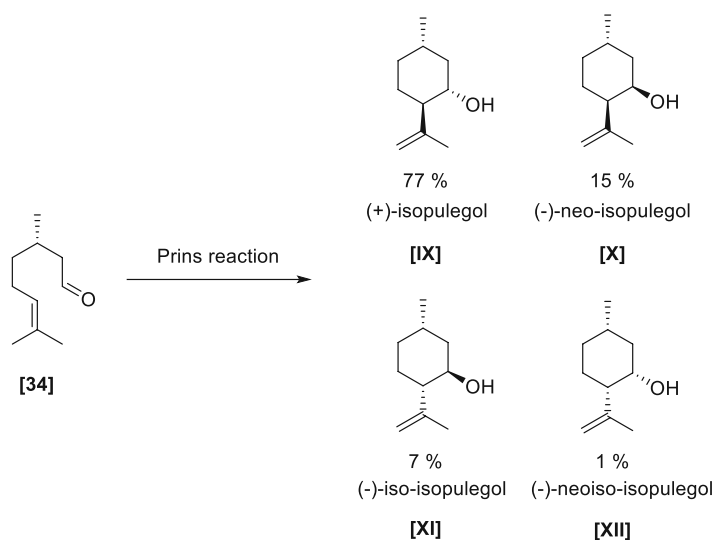
To evaluate if a possible Brønsted activation of alcohol functionalities was also feasible with the SHC, secondary alcohol [40] was also synthesized using a commercial 3M MeMgCl Grignard reagent.²¹¹ Work-up and column chromatography delivered the product as a mixture of 55/45 = syn/anti isomers (Scheme 53).



Scheme 53: Synthesis of secondary alcohol [40] as a mixture of syn/anti diastereomers.

To understand the theoretical product distribution of the unselective Prins reaction of citronellal derivatives, preliminary cyclization tests were performed with (*S*)-citronellal [34]. In an achiral environment, the relative abundance of isomers can be estimated by using the Boltzmann distribution of the relative energies of the respective carbocationic intermediates¹⁹⁸. Using these models, the predicted distribution of products could be expected to be as described in Scheme 54. An experimental

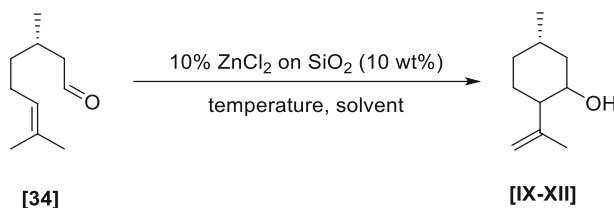
confirmation would thus enable us to conclude the subsequent selectivity of the biocatalytic process. Hence, (*S*)-citronellal [34] was cyclized using Lewis acidic ZnCl₂ adsorbed onto SiO₂ in different solvents and reaction temperatures (Table 1).



Scheme 54: Theoretically expected distribution of isopulegol-products after Prins reaction using the Boltzmann distribution of the relative energies of the respective carbocationic intermediates.¹⁹⁸

Reactions Lewis basic DMF did not lead to any product formation due to possible sequestration of ZnCl₂. Although reactions under neat conditions quickly consumed the starting material, crude TLC analysis of the product revealed definitive side reactivity. Cyclizations performed in CH₂Cl₂ or toluene revealed complete conversion after 1 hour with the least amount of formed decomposition products.

Table 1: Investigation on the ZnCl₂ on SiO₂ catalyzed Prins reaction using the influence of different temperatures and solvents. *Reactions in CH₂Cl₂ were only performed at 25 °C.



Solvents (0.78 M)	CH ₂ Cl ₂	toluene	DMF	neat
temperature	25 °C	Clean conversion, minor side product formation	n.r.	full conversion, some decomposition / side reactions
	60 °C*		n.r.	major decomposition

To achieve a cleaner conversion, the concentration was decreased from 0.78 M to 0.08 M, which produced all isopulegol isomers [IX]-[XII] cleanly in 5 hours. Enabling a simpler separation of the product from the bulk solvent, the reaction was performed in CH₂Cl₂ at room temperature.

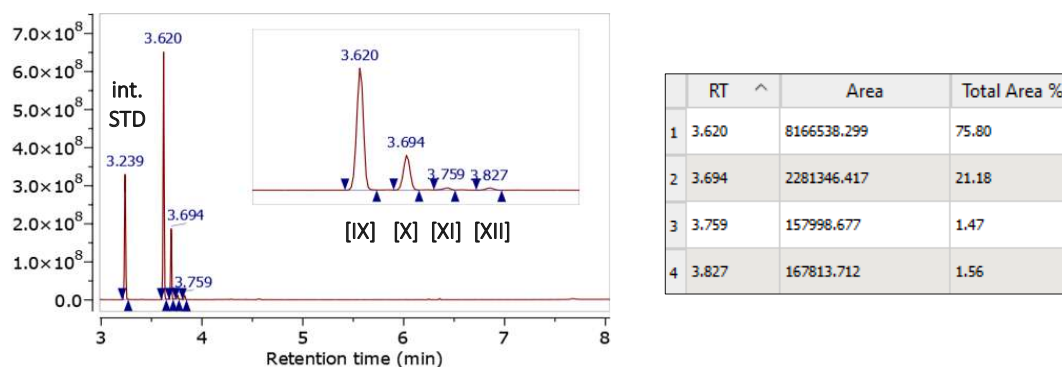


Fig. 20: GC-MS spectrum and respective peak table including the information about retention times and relative areas of formed isopulegol isomers. $^1\text{H-NMR}$ analysis confirmed peaks in descending order to correspond to (+)-isopulegol [IX], (-)-neo-isopulegol [X], (-)-iso-isopulegol [XI] and, (-)-neo-isopulegol [XII]. The peak at 3.239 corresponds to the internal standard methyl benzoate.

Due to the literature known sequence of retention times⁵², the product distribution roughly matched the theoretical calculations and enabled us to pinpoint any of the formed four diastereomers (Fig. 20). The crude $^1\text{H-NMR}$ analysis furthermore supported the structures of the two most abundant species to be the (+)-isopulegol [IX] and (-)-neo-isopulegol [X], respectively.

C I.1.2 Biotransformation with citronellal analogs

As was previously mentioned, three different SHCs families were investigated. One enzyme originated from *Alicyclobacillus acidocaldarius* (*A. acidocaldarius* - *Aac*) and two different strains of *Zymomonas mobilis* (*Z. mobilis* - *Zmo_0872* and *Zmo_1548*). These showed a distinct difference in the stability and activity of their respective wild-type enzymes. Whereas the SHC_{Aac} wild-type exhibited excellent and highly specific activity towards its eponymous substrate squalene [i], only minimal (< 1 %) activity towards truncated or elongated analogs, as well as any of the citronellal enantiomers [34] and [170], was observed.^{49,52} The SHC_{Zmo} family, on the other hand, seemed to forfeit its activity towards the triterpene but showed increased conversion for analogous compounds as homofarnesol⁵¹ or citronella⁵⁷. Interestingly in both cases, specific single-point mutations caused a dramatic change in affinity, underlining their possible application for protein engineering studies.^{49,198} The most promising candidates used for non-native transformations were found in the SHC_{Aac} class bearing the mutations A419G/Y420C/G600A and I261A, as well as muteins of the SHC_{Zmo} family with either W555Y, F438C, or F486C mutations. These exhibited activity for the native transformation but additionally showed reactivity towards the desired carbonyl functionality.

Table 2: Optimal temperature and pH for the respective SHC family

SHC family	pH	temperature
SHC _{Aac}	4.5	60 °C
SHC _{Zmo}	6.0	30 °C

Considering the optimal reaction conditions, the *Aac* family, as the name suggests (acidus, lat. = acid, caldus, lat. = warm or hot), exhibited due to its thermal origins increased stability in high temperature and acidic regimes (Table 2). This significantly impacted the purification of these integral membrane enzymes and their applicability in the Prins reaction of citronellal. Aldehydes are generally not tolerated by any organisms due to their highly reactive nature. Hence any microbial organisms commonly use reductases or oxidases to remove these species, thus limiting the theoretical yield of any citronellal biotransformations. Fortunately, due to the increased stability of the SHC_{Aac}, a thermal heat-shock at 55 - 60 °C for 25 minutes was sufficient to eliminate any undesired and retain the wanted reactivity. For *Zmo* variants, this methodology led to a complete loss of activity. Herein the other attribute of the SHC could be efficiently harvested. Due to the monotopic nature of these proteins, ultrasonic treatment of the obtained cell pellets and thorough washing led to a complete disappearance of unwanted cross-reactivity. All optimization studies towards growth, expression, and biocatalytic application of the SHCs were performed by Erna Zukic. The thereof resulting protocols are summarized in the experimental chapter E IV.2.

All mutants were expressed and checked for the known substrate conversion to confirm and validate the literature results. In these experiments, already high unselective cyclization of citronellal and the dominant formation of not reported polar side-products could be observed to this day. This was the case for any transformations employing either pH 4.5 or increased temperatures (> 30 °C).

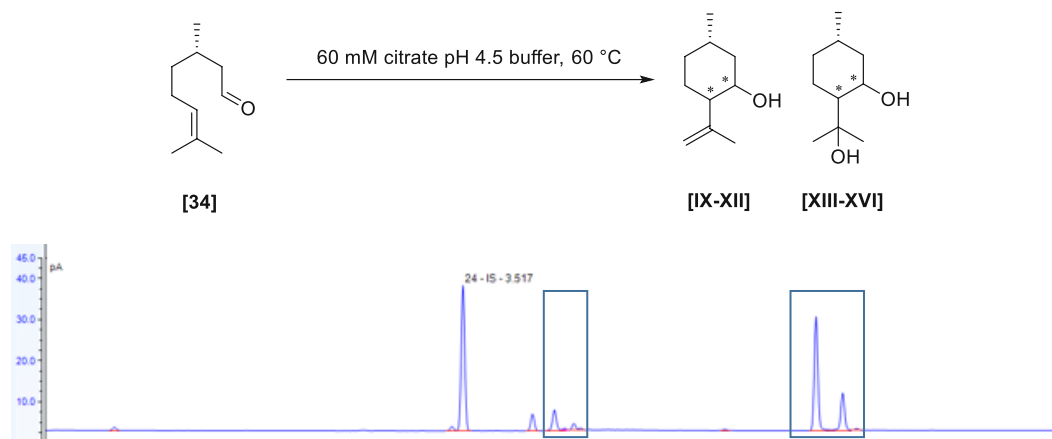


Fig. 21: Blank reaction employing (*S*)-citronellal at pH 4.5 at 60 °C. Boxes represent the two distributions of sets of products concomitantly formed during the reaction.

These were shown to be formed concomitantly to any isopulegol products [IX-XII] and seemed to follow a similar product distribution during the reaction confirmed by GC and GC-MS spectra. Blank experiments using the only buffer revealed a general independent background process (Fig. 21). ¹H-NMR analysis of crude isolated side-products revealed the formation of hydroxy-isopulegol isomers [XIII]-[XVI]. Surprisingly, this result has not once been reported in the literature dealing with the enzymatic conversion of citronellal [I], albeit the known transformation of squalene to its two products, hopene and the hydrolyzed hopanol. As clearly indicated by the proportionality of signals in the GC spectra, this background reaction had a massively detrimental impact on the yield of the desired unsaturated isopulegols and the selectivity of an enzymatic process.

Fortunately, any unspecific cyclization towards either isopulegol isomers [IX]-[XII] or their hydrolysis products [XIII]-[XVI] was shut down at pH 6.0 and 25 °C, which was proven to be still compatible with the thermophilic SHC_{Aac}. Even though cooling to 15 °C further reduced undesired background reactivity, it also drastically slowed down the overall enzymatic reaction speed.

With the optimized protocols in hand, all biotransformations were thus performed at 25 °C in pH 6.0 citrate buffer at OD₅₉₀ of 20-25 for 24 hours using 4 mM of the substrate. Control experiments were executed using (±)-citronellal [I] with SHC_{Zmo} and SHC_{Aac} mutants. Unfortunately, only substrates bearing the analogous double bond substitution to the parent compound were accepted by any mutants. All other aldehydes exhibited slow decomposition and, additionally, for short-chain aldehydes [12], [22], [31], possible volatilization of the substrate during the reaction. In the case of all electrophile variants, either no conversion or slow hydrolysis for the thioester [42] and mesylate [40] derivatives could be detected (Fig. 22).

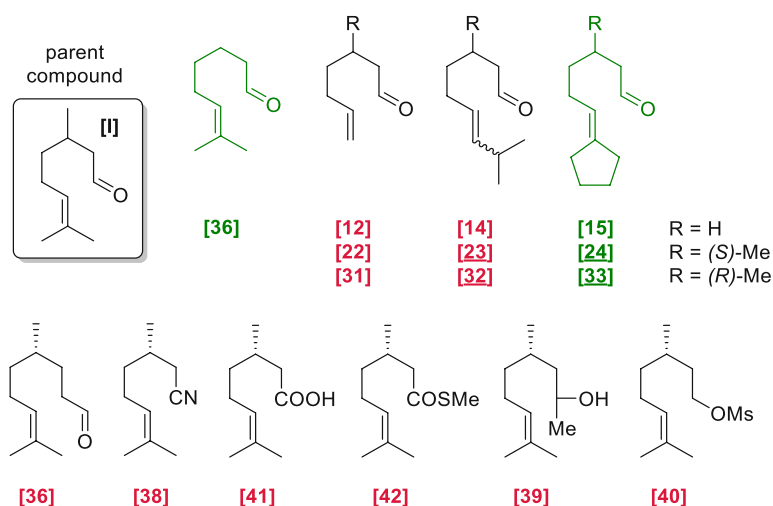
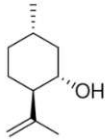
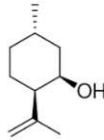
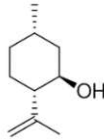
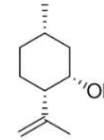


Fig. 22: Complete library of citronellal derivatives subjected to SHC catalysis at 25 °C in pH 6.0 citrate buffer at OD₅₉₀ of 20-25 for 24 hours- All substrates were subjected to all expressed SHC (SHC_{Aac}Wt, SHC_{Aac}A419G/Y420C/G600A, SHC_{Aac}I261A, SHC_{Zmo}W555Y, SHC_{Zmo}F438C or SHC_{Zmo}F486C). Red numbers represent not accepted structures by either SHC mutant. Green numbers represent structures accepted by at least one SHC variant. No conversion could be detected for any SHC_{Aac} mutant.

Fortunately, in the case of the cyclopentyl-derivatives, some of the applied enzymes showed remarkable selectivity towards one of the isopulegol stereoisomers (see. Table 3). Even though no conversion could be shown for SHCs from the *Aac*-family, a successful cyclization was confirmed with the SHC_{Zmo} mutants.

	 (+)-isopulegol [IX]	 (-)-neo-isopulegol [X]	 (-)-iso-isopulegol [XI]	 (-)-neoiso-isopulegol [XII]
retention times (min)	[IX]	[X]	[XI]	[XII]
isopulegol	3.62	3.69	3.76	3.83
cyclopentyl-isopulegol	4.95	5.02	5.07	5.11

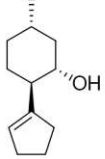
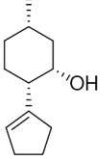
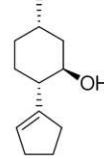
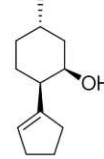
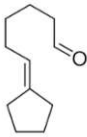
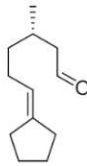
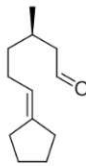
	 (+)-isopulegol [161]	 (-)-neoiso-isopulegol [XVII]	 (-)-iso-isopulegol [XVIII]	 (-)-neo-isopulegol [XIX]
retention times (min)	[161]	[XVII]	[XVIII]	[XIX]

Fig. 23: Comparison of retention times between the formed isopulegol isomers between the products of the Prins reaction resulting from (*S*)-citronellal **[34]** and its cyclopentyl derivative **[24]**. The $^1\text{H-NMR}$ analysis supported by $^1\text{H-}^1\text{H}$ NOESY correlations revealed a change in the sequence of retention times of isopulegol structures **[XVII]** and **[XIX]** (blue text). The determination of the absolute stereochemistry of the products was enabled after isolation of the in Table. X depicted enantiomers.

Due to the missing methyl group for the substrate **[15]**, only two diastereomers could be expected in the cyclization reaction due to its C_2 -symmetry, compared to four products for the methylated analogs. Interestingly, subsequent NMR analysis revealed a change in the sequence of retention times for the respective diastereomers in the Prins reaction compared to the parent citronellal cyclization. In the case of the non-methylated species **[15]**, only the F486C mutation exhibited a specific preference for the trans-isomer **[XX]**, albeit problematic product isolation due to massive side-product formation. The structure was nevertheless assigned to the trans-compound by GC-analysis, as background reactivity was known to preferentially from the less sterically hindered configuration. However, this SHC mutant showed incredible selectivity towards the methylated analogs **[24]** and **[33]**, forming the (+)-isopulegol **[161]** and (-)-neoiso-isopulegol **[162]** as almost exclusive stereoisomers. This observation confirmed the literature results, whereas the β -methyl groups had a significant impact on the selectivity of the cyclization. In the case of the W555Y mutation, exclusive formation of (-)-iso-isopulegol **[163]** from **[33]** could be observed. This exceptional selectivity was unfortunately lost if its enantiomer **[24]** was used as substrate.

Table 3: Complete set of cyclopentyl-citronellal derivatives **[15]**, **[24]** and **[33]** subjected to SHC catalysis at 25 °C in pH 6.0 citrate buffer at OD₅₉₀ of 20-25 at 4 mM substrate concentrations. Substrates were subjected to all expressed SHC mutants (SHC_{Aac}L261A, SHC_{Aac}A419G/Y420C/G600A, SHC_{Zmo}F486C, SHC_{Zmo}W555Y, and SHC_{Zmo}F438C). Products distributions were judged after 24 hours via GC-MS using methyl benzoate as internal standard; n.d. – not determined.

	 [15]	 [24]	 [33]
SHC _{Aac} L261A	-	-	-
SHC _{Aac} A419G/Y420C/G600A	-	-	-
SHC _{Zmo} ₁₅₄₈ F486C	53 % <i>trans</i> -[XX] ¹ 5 % <i>cis</i> -[XXI] ¹ 42 % other	98 % (+)-[161] 2 % neoiso-[XVII]	3 % (-)-[XXII] 96 % neoiso-[162] 1 % iso-[163]
SHC _{Zmo} ₁₅₄₈ W555Y	40 % <i>trans</i> -[XX] 60 % <i>cis</i> -[XXI]	7 % [24] 31 % (+)-[161] 11 % neoiso-[XVII] 2 % iso-[XVIII] 19 % neo-[XIX] 30% unident.*	95 % iso-[163] 5 % neo-[XIX]
SHC _{Zmo} ₀₈₇₂ F438C	68 % <i>trans</i> -[XX] 32 % <i>cis</i> -[XXI]	n.d.	n.d.

Prompted by these promising results, preparative scale experiments were performed with the most successful combinations. Herein all cyclopentyl-isopulegol derivatives **[161]-[163]** could be isolated after column chromatography in 19 - 32 % yield. The stereochemistry of the isolated structures was confirmed by ¹H-¹H NOESY NMR analysis. Important correlations are depicted in the scheme X and could be used to identify all formed products and retrospectively assign the correct stereodescriptors.

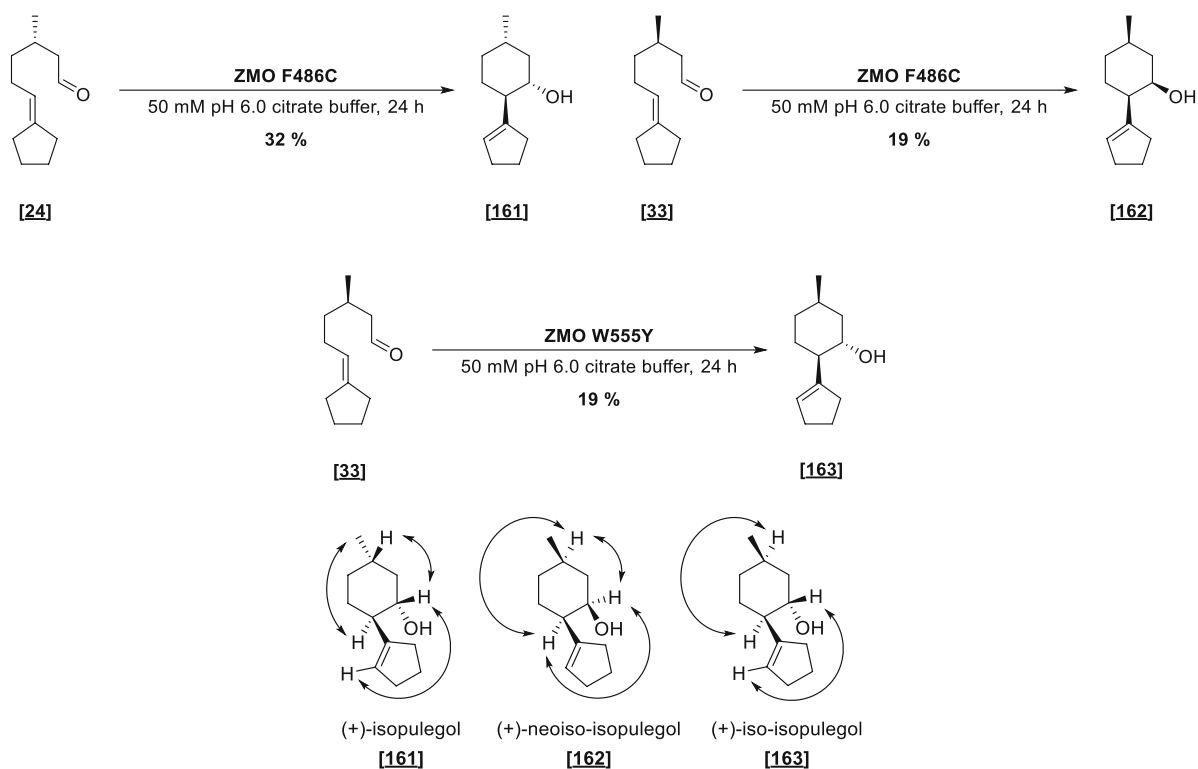
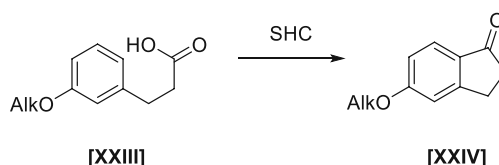


Fig. 24: Preparative scale experiments using the most selective cyclopentyl-citronellal substrate-SHC_{Zmo} mutant combinations. All products could be isolated after extraction with Et₂O and subsequent column chromatography. The absolute stereochemistry of the isolated structures was confirmed by ¹H-¹H NOESY correlations.

Within this investigation, we could thus efficiently establish SHC as selective biocatalysts in the research group and apply mutants from the *Zymomonas mobilis* family for the stereospecific Prins reaction of cyclopentyl-citronellal derivatives **[24]** and **[33]** to yield three different isopulegol derivatives.

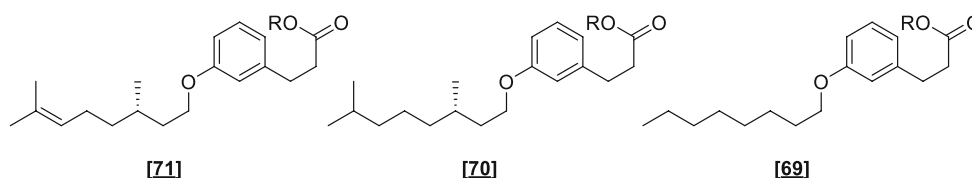
C 1.2 Part II – Friedel-Crafts reaction of alkylated 3-(3-hydroxyphenyl)propanoic acids

With the establishment of the SHC methodology in the research group, we focused our attention on the Friedel-Craft reaction. Due to the preference of the SHC for terpenoid structures we speculated, that with the incorporation of an alkyl chain as a recognition motif onto the aromatic core, a possible cyclization could be enabled with the enzymatic machinery. Hence, we envisioned the biocatalytic transformation of alkylated 3-(3-hydroxyphenyl)propanoic acids [XXIII] towards the corresponding indanone structures [XXIV] bearing this motif (Scheme 55).



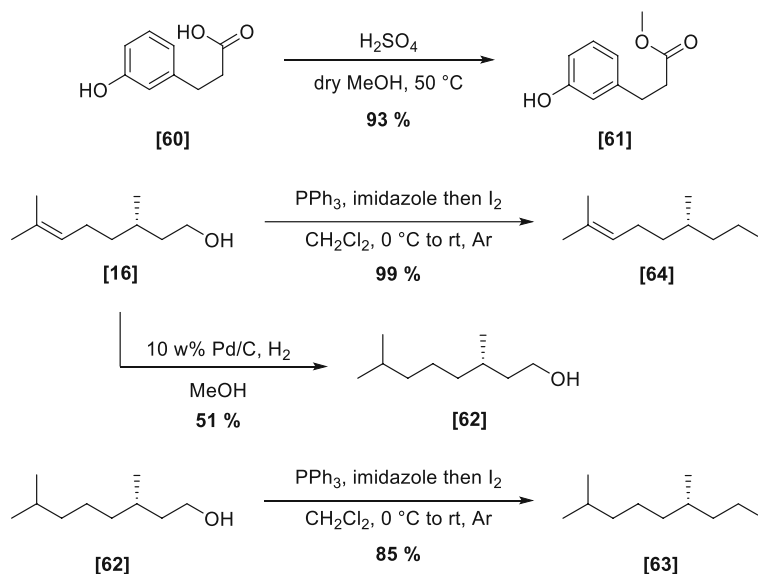
Scheme 55: Envisioned enzymatic intramolecular Friedel-Crafts acylation transforming alkylated 3-(3-hydroxyphenyl)propanoic acids [XXIII] into their corresponding cyclized indanone structures [XXIV].

To include a certain degree of structural variation, the citronellyl-[71], its dihydro-form [70] as well, as the octyl-derivate [69] was envisioned as substrates for the transformation (Scheme 56).



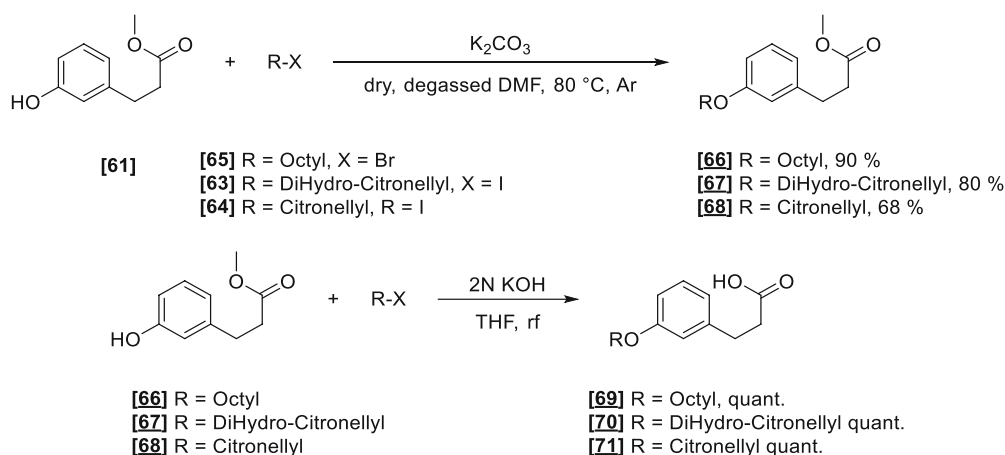
Scheme 56: Intended substrates for the SHC catalyzed Friedel-Crafts acylation.

These derivatives were synthesized from commercially available 3-(3-hydroxyphenyl)propionic acid [60]. Acid-catalyzed esterification proceeded in near quantitative yield, setting up the material for subsequent etherification (Scheme 57). For the incorporation of the citronellyl and dihydrocitronellyl-alkyl chains, (*S*)-citronellol [16] was either directly transformed into the corresponding alkyl iodide [64] applying literature Mitsunobu conditions²¹² or hydrogenated *via* H₂ and Pd on charcoal²¹¹. Although the reduction was repeated with careful monitoring, unexplainable losses of the unsaturated alcohol [62] were continuously observed for this transformation. Nevertheless, the product was further transformed using the identical Mitsunobu conditions to yield the alkyl iodide [63] in 85 % yield. Due to the highly volatile nature of the alkyl iodides application, the vacuum had to be limited to 400 mbar to prevent product losses.



Scheme 57: Synthesis of **[61]** and alkyl-donors **[64]** and **[63]**.

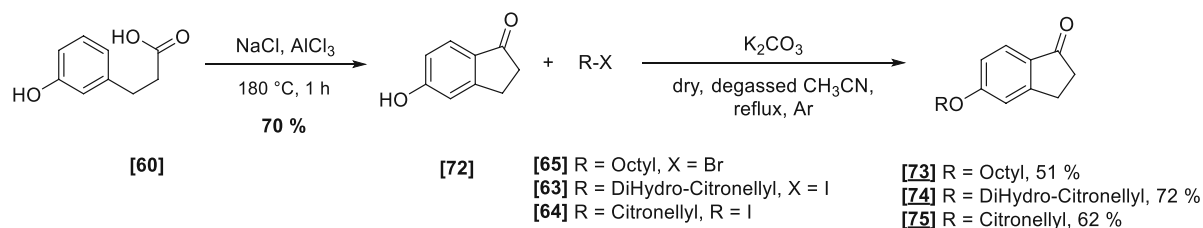
With both building blocks in hand, etherification of phenol **[61]** was enabled by classical substitution of the respective alkyl halides **[63]**-**[65]**.²¹³ Proper degassing of the solvent and the use of threefold azeotropic drying using dry toluene of **[62]** allowed for a clean transformation, albeit the necessity for another addition of the respective alkyl halide after 18 hours. The resulting ethers **[66]**-**[68]** were then cleanly hydrolyzed, resulting in the quantitative formation of the corresponding carboxylic acids **[69]**-**[71]** in quantitative yields (Scheme 58). These could be used for further experimentation without additional purification.



Scheme 58: Synthesis route to the desired alkylated 3-(3-hydroxyphenyl)propanoic acids **[69]**-**[71]**.

Synthesis of the corresponding indanones was believed to be accessible with direct chemical cyclization of the acids **[69]**-**[71]** by employing PPA at $80\text{ }^\circ\text{C}$ or *via* the corresponding acyl chlorides in a classical Friedel-Crafts acylation. Unfortunately, any cyclization attempts using PPA (polyphosphoric acid) led to complete cleavage of the ether moiety prior to any indanone formation, even at room temperature. Unfortunately, using a very mild literature protocol for Friedel-Crafts acylations²¹⁴ employing oxalyl chloride and then HFIP (hexafluoroisopropanol) for the cyclization step led to strong decomposition. Hence, to omit the problematic ether cleavage, a different approach was selected. The indanone core was thus formed first using an atypical literature approach using an $\text{AlCl}_3/\text{NaCl}$ melt in

neat conditions²¹⁵ followed by the already established etherification. This sequence led to the isolation of [72] in 70 % and the respective indanones [73]-[75] good yields (Scheme 59).

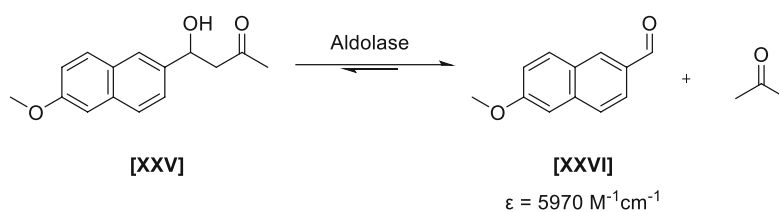


Scheme 59: Synthesis sequence for cyclized indanone products [73]-[75].

Having all components assembled, enzymatic cyclization studies were performed with all esters [66]-[68] and carboxylic acids [69]-[61] employing all to this day available SHCs in the research group. These included the SHC from *A. acidocaldarius* (*Aac*) bearing mutations A419G/Y420C/G600A or I261A and muteins of the *Z. mobilis* (*Zmo*) SHC family with W555Y, F438C, and F486C mutations. Biotransformations were performed at 25 °C in 50 mM pH 6.0 citrate buffer at OD₅₉₀ of 20-25 for 24 hours using 4 mM of the substrate. Control experiments were executed using (\pm)-citronellal [I]. Blank experiments were performed employing *Escherichia coli* (*E. coli*) cells lacking the respective genes and experiments without any cellular material. Unfortunately, none of these substrates was accepted by any of the SHCs candidates. The concentration of the starting materials remained unchanged even after prolonged reaction times. Inactivity of the mutants was ruled out due to the complete conversion of (\pm)-citronellal [I] to the respective isopulegol isomers [IX]-[XII]. Due to an unforeseen departure of our biochemical expert in the group, no further studies were undertaken to investigate the biocatalytic FCA of the alkylated 3-(3-hydroxyphenyl)propanoic acids.

C 1.3 Part III – Synthesis of fluorogenic substrates for SHC catalyzed Friedel-Crafts acylation reactions

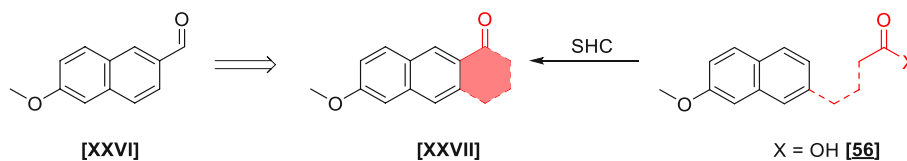
Due to the partly promising but disappointing results, we focused the synthetic efforts on synthesizing optical tools that would enable a faster screening of mutants that exhibited the desired enzymatic Friedel-Crafts acylation (FCA) functionality. Herein we built upon the fluorogenic probe from the work of Giger *et al.*²¹⁶ In their research, they employed 6-methoxy-2-naphthaldehyde [XXVI] as a fluorogenic activity reporter for the optimization of their artificial retro-aldolase RA95.5-8 (Scheme 60).



Scheme 60: Fluorescent 6-methoxy-2-naphthaldehyde [XXVI] used as retro-aldolase RA95.5-8 probe.²¹⁶ Exposition of the carbonyl functionality triggered an immediate spectroscopic signal used as an optical reporter for their FADS system.

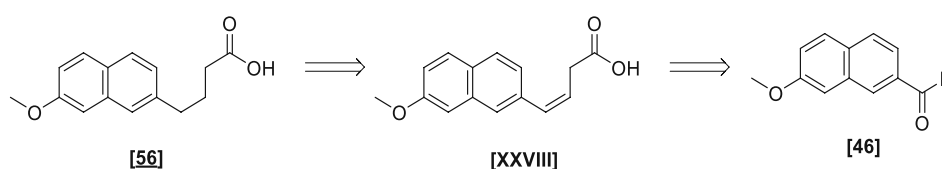
Intrigued by the strategy, we wondered if a similar method would be feasible to establish a screening platform for Friedel-Crafts acylations promoted by the SHC. Herein activation of the carbonyl functionality in a similar fashion to the Prins-reaction could trigger a cyclization event. This approach

would lead back to the 6-methoxy-2-naphthylketone [XXVII], which could be derived *via* the cyclization of carboxylic acid [56] (Scheme 61).



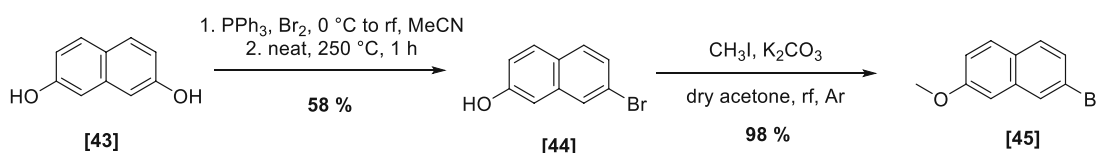
Scheme 61: Cyclization of [56] to form [XXVII] was envisioned as a similar fluorogenic readout as [XXVII], enabling screening for a possible enzymatic FCA reaction.

As the first synthetic approach, the carboxylic acid [56] itself could be synthesized from the unsaturated precursor [XXVIII] by simple hydrogenation, which would be derived by classical Wittig-reaction of 7-methoxy-2-naphthaldehyde [46] (Scheme 62).



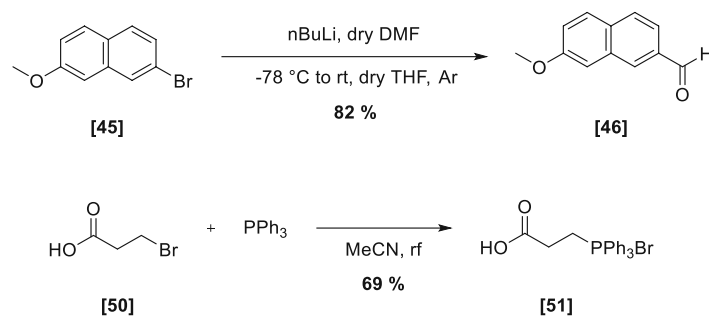
Scheme 62: Retrosynthetic analysis towards [56] using a Wittig reaction approach starting from 7-methoxy-2-naphthaldehyde [46].

As only the 6-naphthaldehyde isomer [XXVI] was commercially available, the desired compound had to be synthesized in two steps from 2,6-dihydroxynaphthalene [43] (Scheme 63). The diol was converted to the mono brominated product [44] using extremely harsh literature conditions²¹⁷.



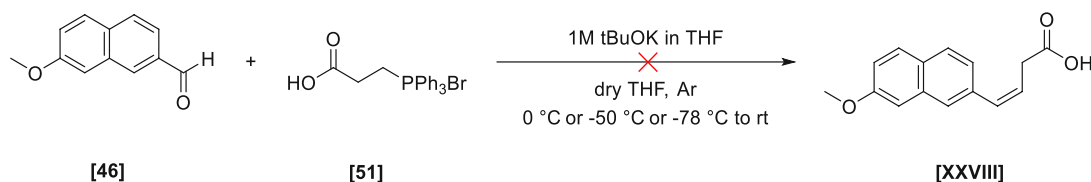
Scheme 63: Synthesis of [45].

Herein *in-situ* generated triphenylphosphine dibromide was allowed to react with the diol forming an intermediate phosphonium salt. Upon removal of the solvent, the reaction was heated to > 250 °C, thereby liberating highly corrosive HBr as a colorless vapors and a thick viscous violet mixture consisting of triphenylphosphine oxide and brominated products. The work-up of the reaction mixture proved to be dreadfully difficult, especially when larger quantities of the starting material were to be converted (15 g literature scale, crude yield 300 %). As stated in the literature, direct column chromatography of the resulting tar was impossible due to solubility and separability issues. To circumvent these problems, the bulk of highly polar side products was removed using a short silica flash chromatography using only the soluble fraction in CH₂Cl₂. The resulting residue could be dissolved and decanted in boiling ligroin, which upon evaporation of the solvent, led to a columnable mixture. Limiting the use of the diol [43] to a 3 g scale led to a dramatic improvement of general handling and enabled direct purification of [44] by column chromatography after short pass CH₂Cl₂ silica filtration in 58 % yield.



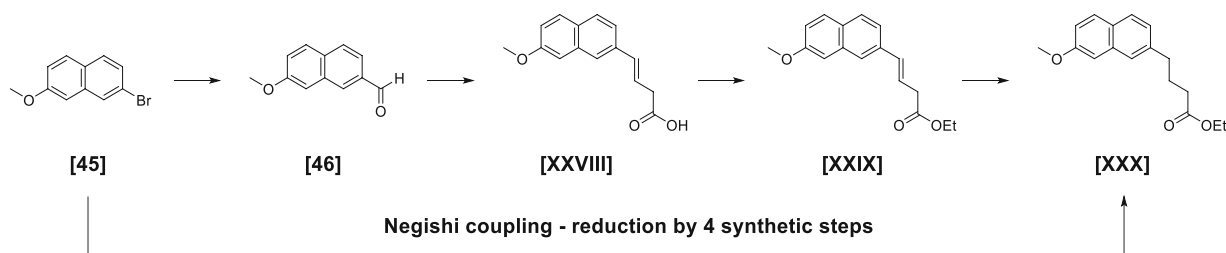
Scheme 64: Synthesis of Wittig reaction precursors [46] and [51].

Following the methylation²¹⁸, in nearly quantitative yield, the 2-bromo-7-methoxynaphthalene [45] was formylated using a lithiation / DMF addition sequence²¹⁹, which set up the resulting aldehyde [46] for the subsequent Wittig reaction. The Wittig reagent [51] was prepared by classical substitution reaction from the corresponding 3-bromopropionic acid [50] with PPh₃ (Scheme 64)²²⁰. Dissolution of the resulting salt in minimal amounts of CHCl₃ and precipitation with Et₂O at -20 °C led to unproblematic isolation of the product. Low temperatures were crucial in this step, as merely the formation of a viscous mass was observed at room temperature.



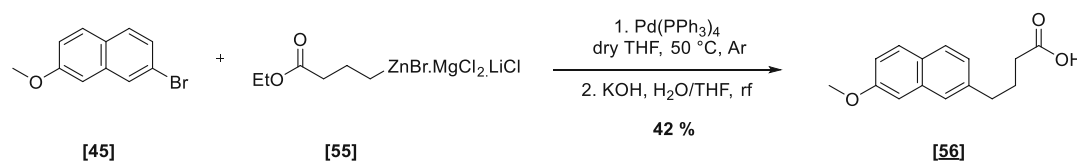
Scheme 65: Attempted Wittig reaction towards the unsaturated acid [XXVIII].

The Wittig reaction (Scheme 65) was first performed according to a modified literature protocol²²¹ at 0 °C, whereas preliminary screening showed that cooling to even lower temperatures (-50 °C or -78 °C) decreased, not determined side-product formation as judged from TLC analysis. Unfortunately, separation from the triphenylphosphine oxide proved impossible by either standard column chromatography mixtures or recrystallization from either THF, ligroin, or toluene. Although not directly stated in the literature, this problem seemed to be circumvented by direct methylation with CH₃I of the crude reaction mixture and isolation of the corresponding methyl esters in good yields.²²² Meanwhile, however, a second approach had been established, which employed a Negishi reaction to incorporate the alkyl chain (Scheme 66). This method immediately reduced the synthetic pathway by omitting four steps and enabled a more straightforward synthesis of regioisomers, if required.



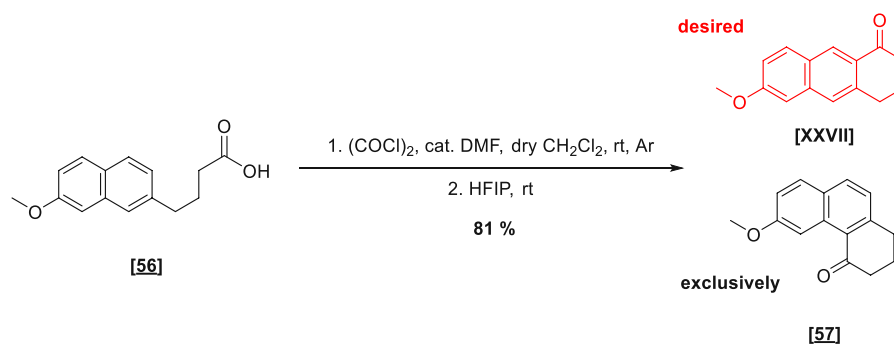
Scheme 66: Shortening of the synthetic pathway by employing a Negishi coupling approach.

Herein the bromonaphthalene [45] could be directly alkylated using freshly prepared 4-ethoxy-4-oxobutylzinc bromide [55] using $\text{Pd}(\text{PPh}_3)_4$ as catalyst (Scheme 67).²²³ In contrast to the classical synthesis of Negishi reagents, using Zn dust, LiCl, and the corresponding alkyl halides²²⁴, the formation could be conveniently performed by replacing Zn dust with magnesium turnings in the presence of ZnCl_2 and LiCl. This was shown to accelerate the synthesis of the organozinc reagents and improve their reactivity towards electron-rich aromatic systems. Despite the laborious synthesis of these organozinc reagents (*c.f.* E II.4), they were proven to form the corresponding alkylated naphthalene [56] in a straightforward manner. One downside of the reaction was presented by the formation of both homocoupled alkyl and aryl byproducts (14 % and 13 %) which prohibited direct isolation of the target. Due to the surprising similarity of the polarity of the homocoupled dialkyl species to the desired product, separation was made impossible with column chromatography using standard LP/EtOAc or $\text{CH}_2\text{Cl}_2/\text{MeOH}$ mixtures. However, direct saponification and thus the formation of the corresponding carboxylic acids enabled facile removal of the apolar diaryl and the highly polar diacid species by column chromatography.



Scheme 67: Negishi coupling employing freshly prepared 4 ethoxy 4-oxobutylzinc bromide [55] forming naphthalene butanoic acid [56].

With this approach, the one-pot synthesis of 4-(7-methoxynaphthalen-2-yl)butanoic acid [56] was possible in a 42 % yield. With the desired compound in hand, the Friedel-Crafts acylation was carried using a chlorination/cyclization-sequence with $(\text{COCl})_2$ and Brønsted acidic HFIP.²¹⁴ Analysis of the substitution pattern in the $^1\text{H-NMR}$, however, revealed the exclusive formation of the 2,8-substituted naphthalene and only traces (< 2 %) of the desired 2,6-isomer [XXVII] (Scheme 68). The cyclization proceeded yet cleanly in 81 % yield. In the case that regioisomer [57] exhibited similar fluorescence properties to the 2,6-naphthaldehyde [XXVI], it could nevertheless still serve as optical activity sensor for the biocatalytic FCA.



Scheme 68: Chemical Friedel-Crafts acylation forming the undesired 2,8-isomer [57] as dominant product.

Hence, with the first naphthyl ketone compound, initial absorption measurements were performed. These pointed to a beneficial increase in absorbance and a strong red-shift in the supra-300 nm range from 328 nm of [56] to 348 nm of [57] upon cyclization. Furthermore, due to the

rapid decay in the absorption signal of [56] above 330 nm, only minimal fluorescence quenching of the product emission would have been expected under assay conditions (Fig. 25).

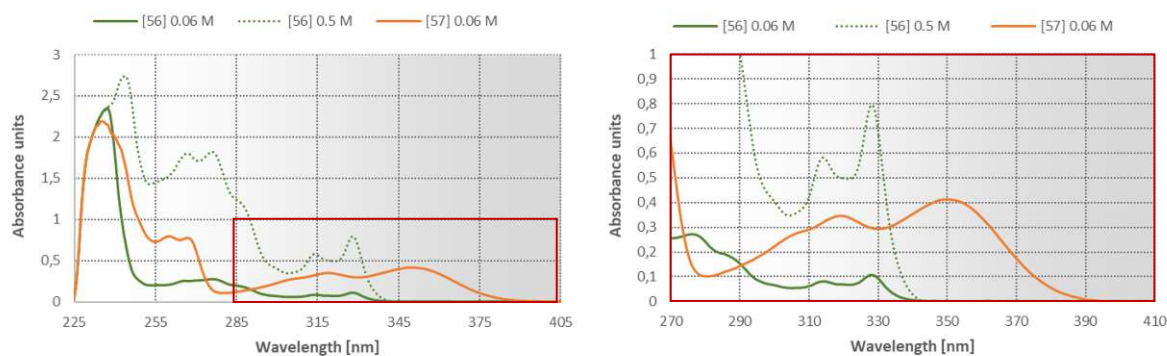


Fig. 25: Preliminary absorption measurements revealing a beneficial red-shift and a dramatic increase in absorption upon cyclization of [56]. . *left:* magnification of area outlined by a red rectangle. Measurements were performed in CH_2Cl_2 .

Regrettably, the excitation at the absorption maximum of 348 nm did not trigger any fluorescence. In fact, excitation at all absorption bands above 280 nm exhibited only negligible fluorescence of [57] exemplified by excitation at 310 nm (Fig. 26).

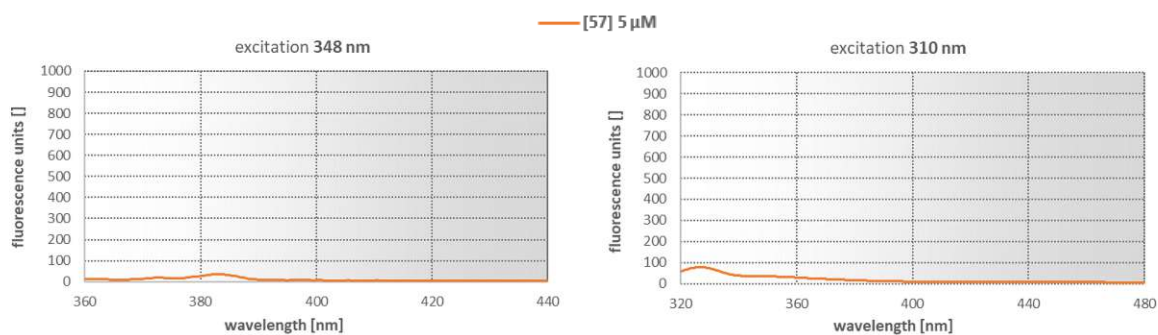


Fig. 26: Fluorescence measurements determine the cyclized product [57] to be practically non-fluorescent. Measurements were performed in CH_2Cl_2 , excitation wavelengths 348 nm and 310 nm respectively, 5.0 nm slit, 775 V gain.

To determine if the compound exhibited any practical fluorescence behavior at all, measurements at wavelengths where definitive reabsorption of the emitted signal *via* [56] would be expected were still performed. Herein excitation at 260 nm proved to be the only wavelength at which the cyclized product [57] exhibited a minimally stronger fluorescence signal compared to the corresponding carboxylic acid [56], albeit only at lower wavelengths (Fig. 27).

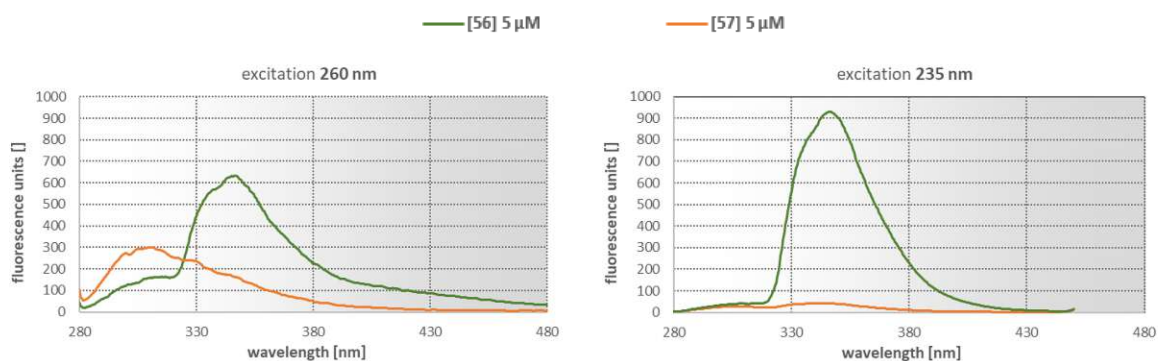
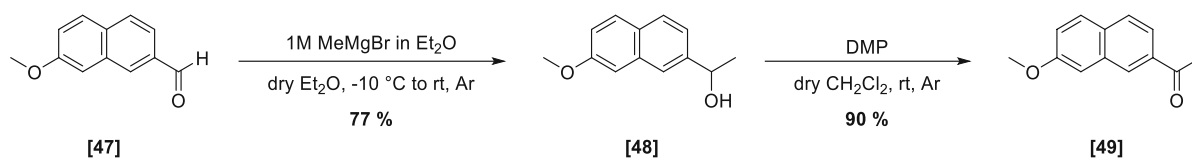


Fig. 27: Fluorescence measurements of [56] and [57] performed at excitation wavelengths in regions of strong absorbance by the uncyclized reagent [56]. Measurements were performed in CH_2Cl_2 , excitation wavelengths 260 nm and 235 nm respectively, 5.0 nm slit, 775 V gain.

This result made it clear that excitation above 280 nm only triggered fluorescence-inactive relaxations of [57]. Furthermore, precursor [56] proved to be a stronger fluorophore than its cyclized form, and therefore its application as a Friedel-Crafts activity sensor would be out of the question.

We thus wondered if the ketone-functionality had potentially fluorescence quenching effects and if this effect was general or highly dependent on the substitution pattern of the naphthalene core. Therefore, a selection of commercially available or easily accessible acetyl- and formyl- naphthalenes were checked for their fluorescence properties. The 2,7-substituted acetyl derivative could be easily synthesized in two steps using the already prepared 7-methoxy-2-naphthaldehyde [47]. The addition of methyl-Grignard in 77 % and Dess-Martin oxidation²²⁵ of the alcohol [48] gave access to the keto-derivative [49] in 90 % yield (Scheme 69). Unfortunately, the 2,8-isomer was not easily accessible and was thus not included.



Scheme 69: Synthesis of acetyl analog [49].

All fluorophores were excited at the local absorption maxima using the same excitation parameters (775 V, 5.0 slit). Interestingly, the position of the keto-group had a particular effect on the position of the absorption maxima of the fluorophores as well as their fluorescence emission intensity (see Fig. 28, comparison of commercial [XXXII] and [46]). The methoxy-functionality and the acetyl-substitution seemed to be necessary for the emergence of a second red-shifted absorption maximum, which enabled a desired supra-300 nm excitation. In the case of the isomer [49], a dramatic decrease in emission could be observed, highlighting the acetyl-position's importance. These results encouraged us to pursue the synthesis of the correctly substituted Friedel-Crafts product analogous to the acetylated product [XXXII].

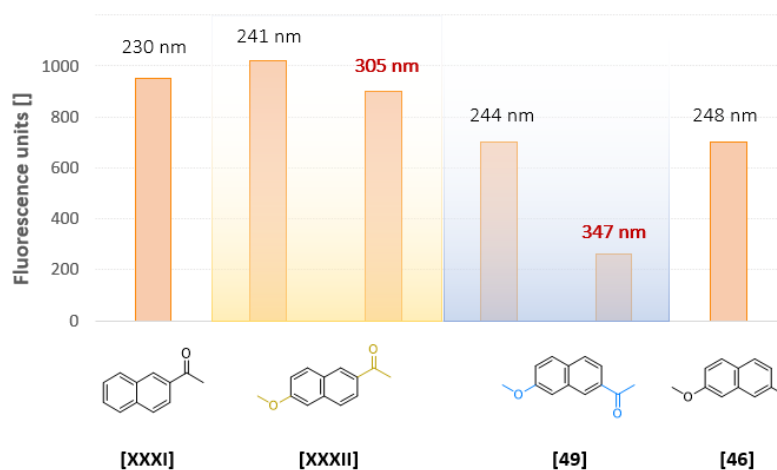
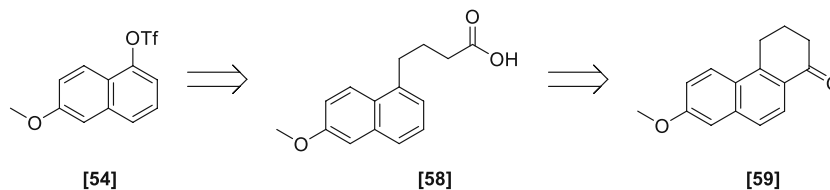


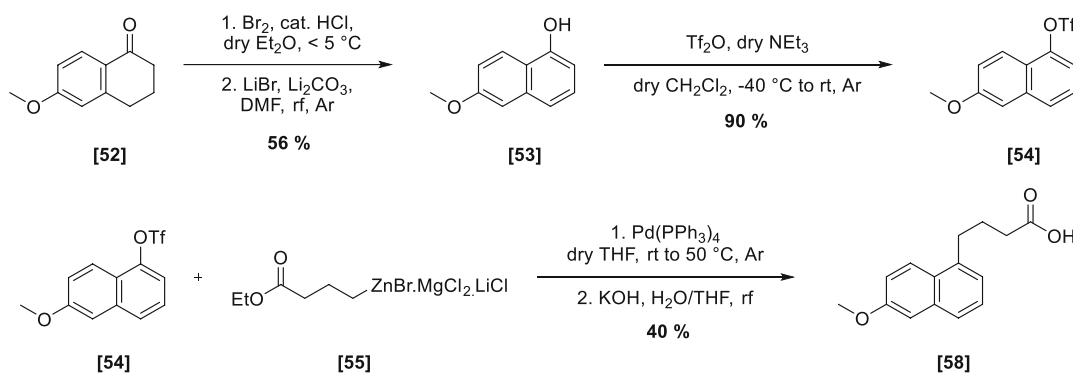
Fig. 28: Impact of the fluorescence emission maximum and fluorescence intensity depending on the position of the acetyl group. Measurements were performed in 5 μM concentration in CH_2Cl_2 . Fluorophores were excited at the local absorbance maxima, 5.0 nm slit, 775 V gain.

With the correct target in mind, the synthetic plan had to be adapted to incorporate the desired regiochemistry. Building upon the established Negishi protocol, access towards the 2,6-substituted naphthalene could be enabled *via* the 5-alkylated species [58], which could be in turn synthesized from the corresponding triflate [54] (Scheme 70).



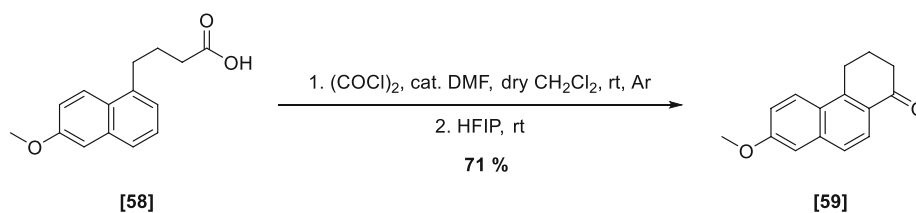
Scheme 70: Retrosynthetic pathway towards [58] using the novel Negishi approach leading back to triflate [54].

The synthesis towards the triflate commenced with the aromatization of commercial 6-methoxy-1-tetralone [52] using a literature known bromination, elimination approach²²⁶. The intermediately formed α -brominated species readily eliminated by treatment with a base under Li-Lewis acidic conditions forming the respective enone. This structure quickly tautomerized, yielding the 6-methoxynaphthalen-1-ol [53] in 56 % yield after column chromatography. Triflation set up [54] for the subsequent Negishi coupling, which gave the desired alkylated species [58] in 40 % yield after saponification (Scheme 71).



Scheme 71: Synthesis of the desired naphthalene butanoic acid regioisomer [58].

The carboxylic acid was then finally cyclized using the identical conditions for [57], forming the desired regioisomer [59] in 71 % yield (Scheme 72).



Scheme 72: Chemical cyclization of [58].

Evaluation of the absorption spectra revealed both similarities and the big difference between the optical properties of the cyclized products [57] and [59] and their precursors [56]/[58]. Whereas the shift in absorption maxima from [56] to [57] exhibited a 20 nm red-shift upon cyclization (see Fig. 25), [59] displayed its maximum below the bulk absorption of its uncyclized form [58] (Fig. 29).

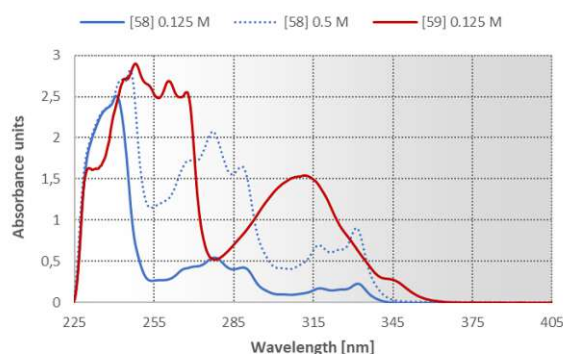
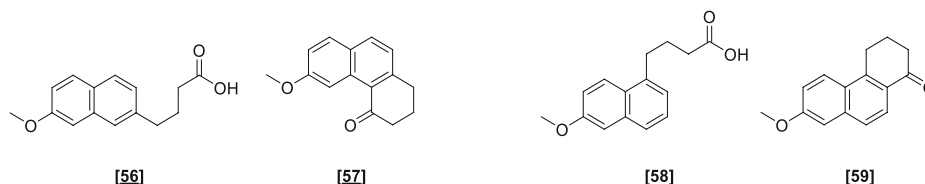


Fig. 29: Preliminary absorption measurements revealing a detrimental blue-shift albeit a substantial increase in absorption upon cyclization of [58]. Measurements were performed in CH_2Cl_2 .

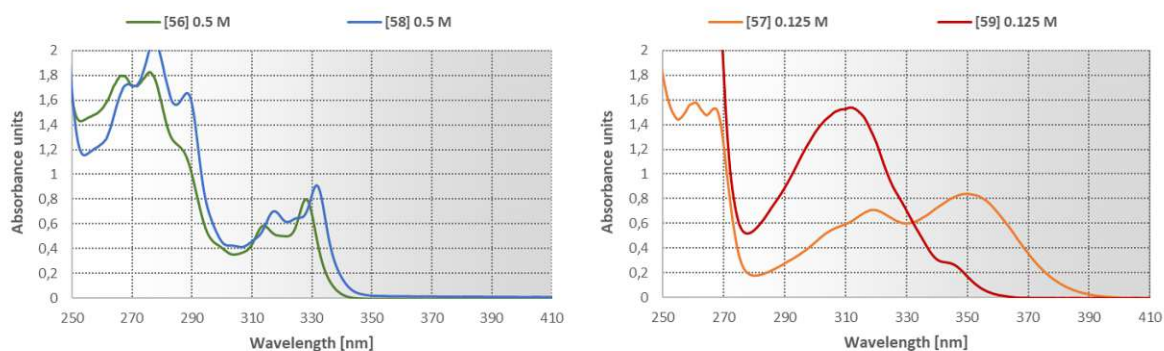


Fig. 30: Comparison of the absorption spectra of both uncyclized [56]/[58] as well as cyclized products [57]/[59], revealing an already expected strong dependency on the substitution pattern of the naphthalene core. Measurements were performed in CH_2Cl_2 .

In both cases, cyclization seemed to drastically increase the absorption coefficient of the naphthalene core, as can be judged by a direct comparison of the spectra at the same concentrations. Interestingly, the absorption spectra of the precursors seemed to be unaffected by the position of the alkyl substituent. Hence, the position of the keto group seemed to play a crucial factor (Fig. 30). Unfortunately, also [58]/[59] exhibited the same behavior as their regioisomer pair [56]/[57]. Despite the increased emission maximum at around 370 nm, [59] proved to be a much poorer fluorophore than its uncyclized precursor. The best conditions for the excitation are exemplified in Fig. 31, whereas only a minimally stronger fluorescence emission could be detected above 380 nm upon irradiation at 310 nm.

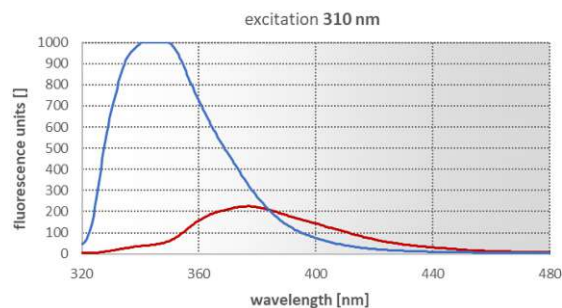


Fig. 31: Fluorescence measurements of [58] and [59] reveal a similar behavior to the regioisomer pair [56]/[57]. The cyclized product [59] proved to be practically non-fluorescent at relevant excitation wavelengths. Measurements were performed in CH_2Cl_2 , excitation wavelength 310 nm, 5.0 nm slit, 775 V gain.

Given the results, unfortunately, none of the synthesized compounds could be applied in a Friedel-Crafts assay format based upon fluorescence detection. Although the [56]/[57] pair could be used as a chromogenic sensor at 348 nm to detect an FCA activity, an application in a FADS due to higher sensitivity of fluorescence measurements was the one that was sought after.

C 1.4 Part IV – Substrate independent approach for the detection of carbonyl compounds using NBD-type reagents

Learning from the previous results in chapter C 1.3, in which minor differences in the chemical structure of the FCA assay products gave rise to significant differences in their optical properties, we envisioned a substrate-independent approach as a possible solution to this problem. Herein the products would not act as the optical reporters themselves, but a second assay component would react with the formed aryl ketones, thereby triggering an optical signal.

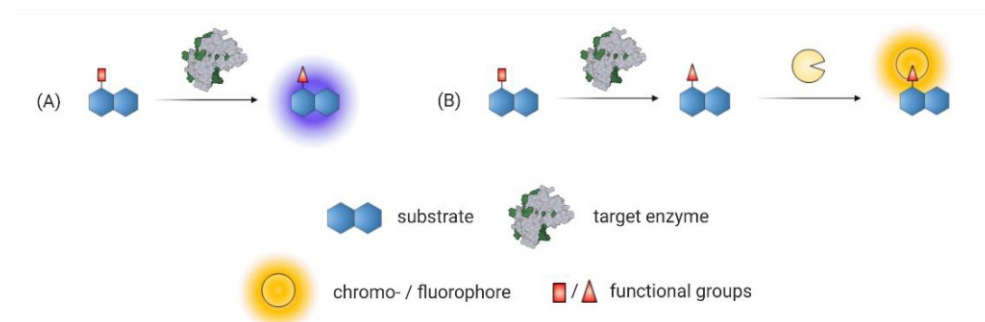
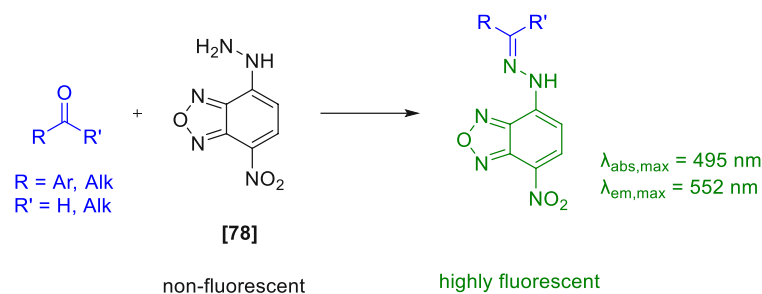


Fig. 32: Schematic comparison of direct and indirect spectroscopic reporters of the efficiency of enzymatic transformations: (A) – direct detection of enzymatic conversion by the production of a fluorogenic or chromogenic product; (B) – indirect detection *via* a substrate independent approach, the signal is emitted only upon subsequent reaction with the enzymatically transformed material.

As already touched upon in part in the introduction (*c.f.* B III.1.1), this would achieve several benefits compared to the previous approach:

- Due to the nature of the intramolecular FCA mechanism, theoretically, two different products could be formed by the cyclization of non-ortho substituted substrates. If they exhibit dramatic differences in their optical signal read-out, another unnecessary variable would be added to an already complex system. The number of theoretically possible products could further increase if an intermolecular reaction were the focus of the study.
- Screenings would not be limited to a particular substrate that would fulfill the optical prerequisites to act as a signal reporter. Hence, the protein engineering efforts could be directed at multiple structures of interest without potentially impacting the products' optical activity response factor.
- In cases where not the synthesis of a defined product but the optimization of a general reaction type would be the target of the protein engineering study, a complex matrix of substrates could be investigated simultaneously using the identical assay system to identify potentially highly promiscuous enzymes.

With this clear goal in mind, literature pointed us to nitrobenzoxadiazole hydrazine (NBD-H) [78] structures that had been heavily utilized for conjugation^{121,227}, derivatization^{124,126,228}, and diverse screenings^{127,128} of carbonyl compounds employing the formation of fluorescent hydrazones.



Scheme 73: Representation of the NBD assay – non-fluorescent nitrobenzoxadiazole-hydrazine NBD-H **[78]** reacts with an alkyl or aryl-carbonyl species forming highly fluorescent hydrazones.

As described in B III.1.1.1, these fluorogenic hydrazines have been effectively used to modify aliphatic and aromatic aldehydes, as well as aliphatic ketones^{131,133,229}. Although several studies included simple aryl ketones in their screenings, no general investigations about reactions with this substance class had been performed. The absence of biological systems and their low reactivity being the most obvious reasons.

Within this chapter, we thus wanted to focus our investigations on hydrazone or oxime conjugations with benzylic ketones and gather profound insight about their applicability as potential assaying tools. The most common reagents used for this purpose were the NBD-H **[78]** and NBD-MH **[77]** hydrazines. Despite conflicting claims about its stability in aqueous media, we also included the more recently reported NBD-AO **[86]** in our investigation (Fig. 33).^{129,227}

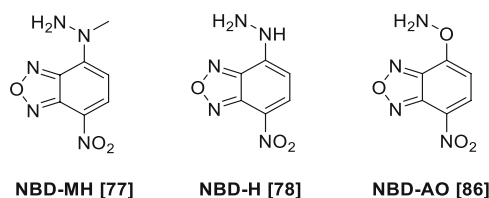
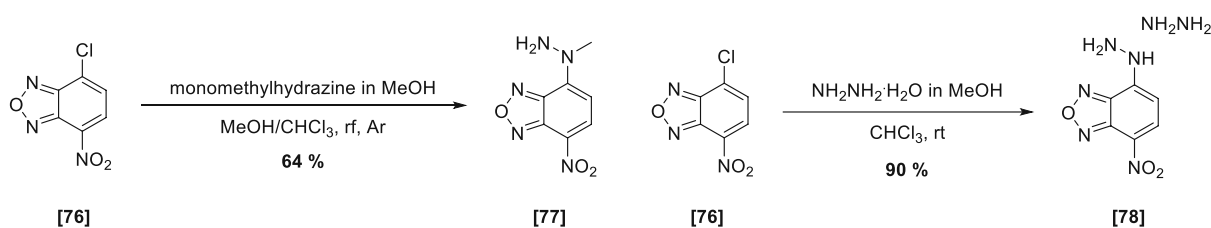


Fig. 33: NBD-H **[78]** and analogs used for carbonyl detection either employing a methyl-hydrazine **[77]** or amino-oxo **[86]** derivatives.

The synthesis of both hydrazine derivatives was done according to known literature reports in a classical nucleophilic substitution of the NBD-chloride **[76]** in 64 % and 90 %, respectively (Scheme 74).^{127,129} Due to the dramatic increase in polarity, precipitation in CHCl_3 enabled the facile isolation of the two products.



Scheme 74: Synthesis of NBD-H **[78]** and NBD-MH **[77]**.

$^1\text{H-NMR}$ analysis of these two hydrazines revealed some puzzling features, which had not been mentioned in any literature report (Fig. 34). Surprisingly, the methyl group on the proximal nitrogen had a profound influence on the H6 the $^1\text{H-NMR}$ spectrum of the hydrazines, causing a considerable inexplicable broadening of the signal. This behavior completely disappeared for the NBD-H **[78]**, additionally displaying a distinct high-field shift of both aromatic protons as well as a dramatic low-field

shift of the $-NH_2$ group from 6.1 to 8.1 ppm. A second observation reported, at least in some publications, was that the product could only be isolated as a hydrazine adduct. This was evident by a broad background peak in the spectrum of **[78]**, which could not be removed by recrystallization of the product in H_2O , MeOH, or EtOH mixtures. The only possible removal of the hydrazine was affected by silica filtration with MeOH with very poor recoverability of the product. As the assay reagent was always applied without additional purification in any literature reference, we opted for the same approach.

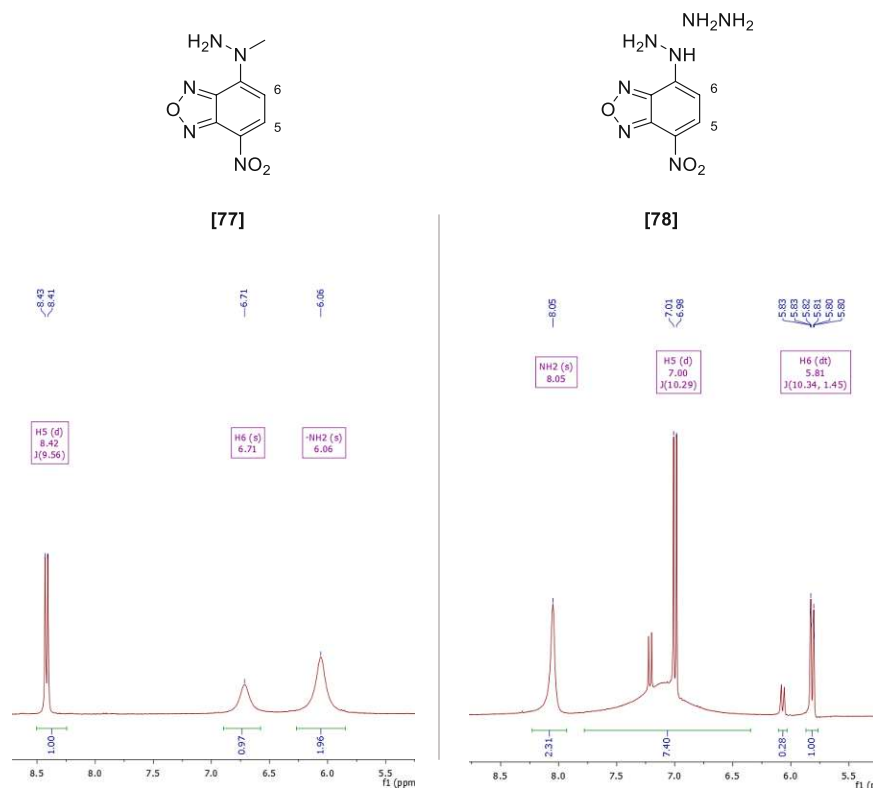


Fig. 34: 1H -NMR comparison of **[77]** and **[78]** in d^6 -DMSO – *left:* clean formation of the methyl-hydrazine, H6 of the structure showed a very strong broadening of the aromatic signal, *right:* identical reaction conditions lead to the formation of two sets of aromatic signals for NBD-H **[78]**, broad signal underlying the aromatic region was found to be an $NH_2.NH_2$ adduct, which was formed during the reaction and could be removed *via* column chromatography. H6 of **[78]** product did not exhibit the same broadening as its methylated analog.

The last peculiarity about **[78]** had missed any mention in literature. The evident formation of the second set of signals in the spectrum of NBD-H prompted the question if the compound exhibited any instability or if any inseparable side products were formed during the synthesis. As the aforementioned recrystallization and column chromatography yielded perfectly crystalline material displaying identical spectral information, the question about a possible dynamic equilibrium was raised.

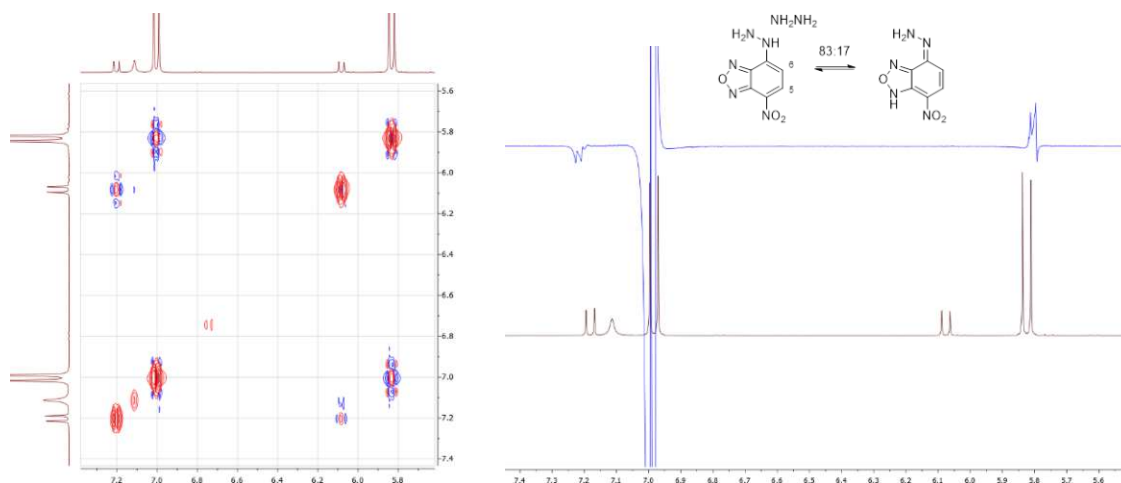


Fig. 35 *left*: 2D-TOCSY of **[78]** in d^6 -DMSO – spectrum did not reveal any correlations between the aromatic pairs and thus could not explain the observed set of signals by an equilibrium process; *right*: 1D-TOCSY (10 hours) of **[78]** in d^6 -DMSO using selective excitation at 7.0 ppm – spectrum finally revealed the dynamic, but slow equilibrium with the decrease of the signal intensity of the aromatic doublet at 7.2 ppm. Concomitant increase of the signal at 5.8 ppm also confirmed the neighborhood of H5 and H6 protons.

Unfortunately, the 2D-TOCSY spectrum remained inconclusive, showing no correlation between both sets of aromatic signals. This meant either that the present equilibrium was possibly too slow for the NMR experiment timescale or that an inseparable mixture of products had been formed. A prolonged 1D-TOCSY experiment (10h!), however, finally revealed a tiny but definite transfer of excitation of the major H5 proton onto its equilibrium equivalent. We thus postulated in Fig. 35 depicted slow equilibrium of **[78]** to cause the occurrence of secondary signals in the NMR experiments. Surprisingly, measurements in d^4 -MeOD and D_2O had no impact on the proportions of these two species. Furthermore, whereas the addition of NaOD led to complete decomposition of the material, DCl caused only a general downfield shift of all signals, which would go in line with a protonation and thus deshielding of the whole electronic structure (Fig. 36). However, only a minimal change (17 % to 13 %) of the equilibrium concentrations could be observed under acidic conditions.

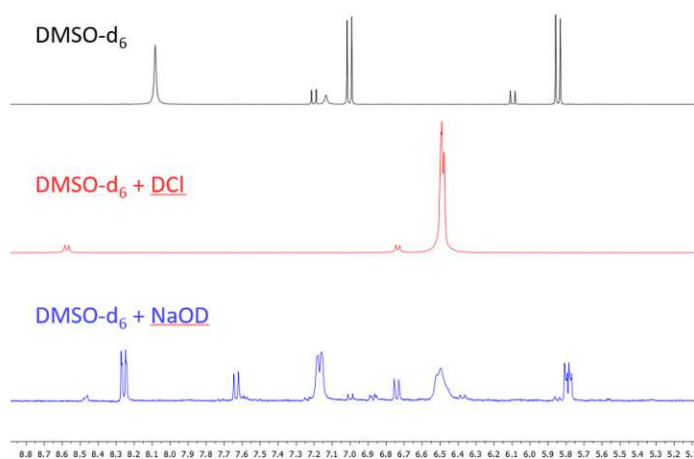
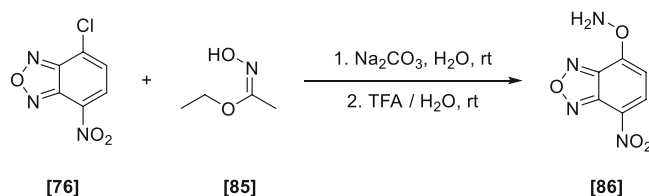


Fig. 36: 1H -NMR equilibrium study of **[78]** in d^6 -DMSO: Addition of 3 drops of conc. DCl in D_2O to the sample led to the collapse of the major set of signals and a general downfield shift. The equilibrium concentrations remained practically unchanged (13 % to 10 %). The addition of 3 drops of NaOD as 25 % solution in D_2O led to rapid decomposition of the sample.

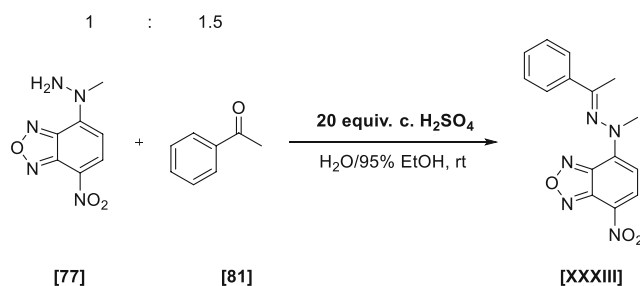
Puzzled by these results, we hoped that the equilibrium had only minimal impact on the results of the hydrazone formation, as the prevailing literature had nonetheless entirely disregarded this general behavior.



Scheme 75: Synthesis of amino-oxy analog [86].

We then turned to the synthesis of [86], which was rapidly synthesized from [76]. Nucleophilic substitution of the NBD-chloride [76] with the masked oxime donor ethyl-N-hydroxyacetimidate [85] and subsequent cleavage of ethyl acetate in aqueous TFA revealed the amino-oxy compound [86] in 66 % yield after flash column chromatography (Scheme 75).¹²⁹

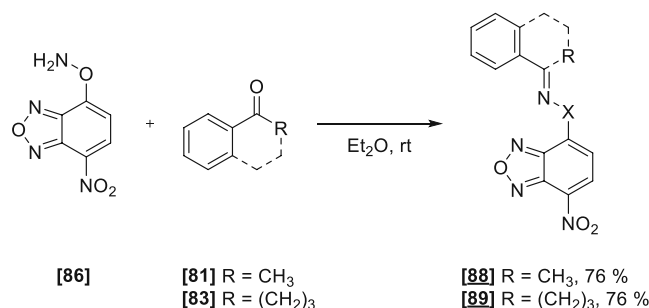
With the complete set of the desired reagents in our hands, we chose to focus the study on two benzylic ketones, acetophenone [81] and the possibly more sterically demanding tetralone [83]. The latter would represent the product from a successful intramolecular FCA and could verify the feasibility of these reagents as assay tools for this biotransformation. We opted to begin our investigations with the methylhydrazine derivative [77], which did not exhibit any potentially interfering equilibria and had already been studied for the detection of aromatic aldehydes.¹²⁷



Scheme 76: Attempted synthesis of NBD-MH acetophenone adduct [XXXIII].

Following a similar literature approach, acid catalysis was necessary to enable the formation of respective hydrazones. This became evident, as no reaction could be forced even with an excess of keto-species (> 20 equiv.) added. To enable the formation of the respective hydrazones with [77], however, very high amounts of acid were needed to solubilize the starting material and push the reaction to completion. Preliminary screenings concluded the need for at least 20 equivalents of concentrated H₂SO₄ to form the corresponding hydrazone with acetophenone [81] in 24 hours at room temperature (Scheme 76). Any heating of the reaction mixture led to evident decomposition of the material. Although the acetophenone-adduct [XXXIII] could be isolated as red solids, the product could be recovered only in impure form judged by ¹H-NMR analysis. The hydrazone formation with tetralone [83] proceeded even more sluggishly. Even with prolonged stirring only incomplete conversion was detected at any time point judged by TLC analysis. Due to the limited stability of these hydrazones on silica, isolation of products was rendered impossible using standard column chromatography. Hence, the only reliable method for isolating these compounds was the collection, and subsequent recrystallization of the during the reaction precipitated adducts. However, recrystallization in MeOH or EtOH of the tetralone-adduct [XXXIV] yielded only an impure product. Give the necessity for the highly acidic conditions for the condensation reaction. We thus tested if any appreciable conversion to the product would be detectable at biocompatible conditions (100 mM citrate buffer pH 4.5, 5 % DMSO,

1 mM NBD-MH, 50 μ M carbonyl) using colorimetric and fluorometric measurements. Regrettably, only trace conversion (< 2% change) using the acetophenone **[81]**, and no conversion for the tetralone could be observed at the presumed optimal conditions for a SHC biotransformation. Given the unsatisfactory results, we changed our focus on amino-oxy reagent **[86]**. Herein synthesis of the adducts was performed in a straightforward fashion by stirring the reagent with the respective ketone in dry Et₂O (Scheme 77).¹²⁹



Scheme 77: Synthesis of NBD-AO acetophenone **[88]** and tetralone **[89]** adducts.

The collected bright yellow precipitates yielded the respective adducts, both with excellent purity in 76 % yield. Comparison of the UV spectra of the amino-oxy reagent **[86]** and the respective adducts **[88]** / **[89]** showed a surprising similarity in their absorptive properties (Fig. 37).

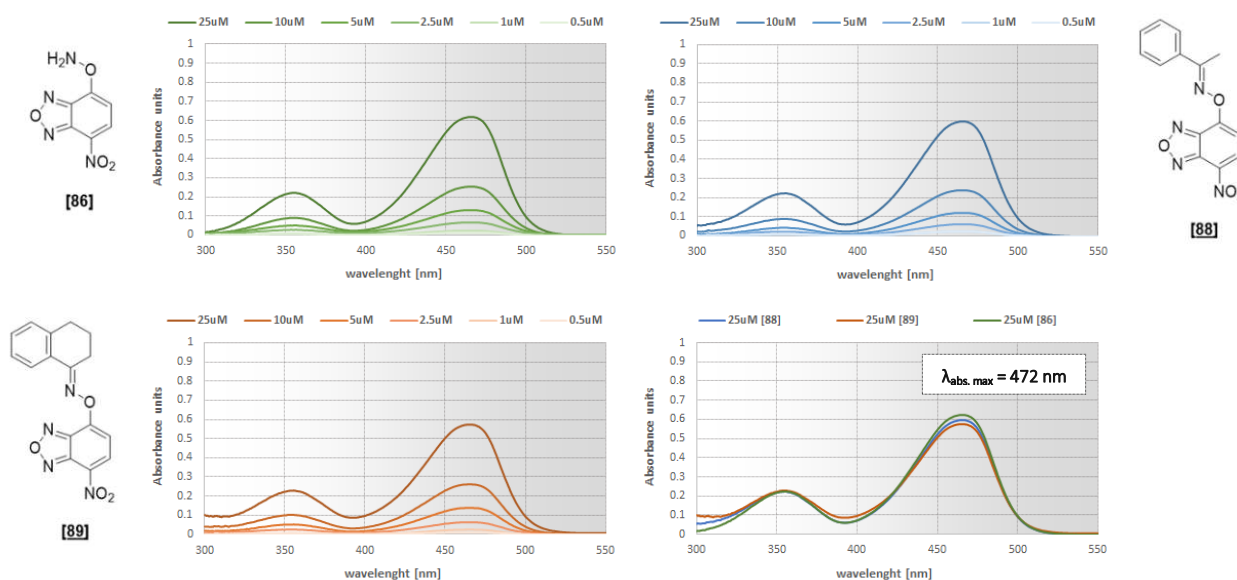


Fig. 37: UV-absorption calibrations of NBD-AO **[86]** and its acetophenone and tetralone conjugates **[88]** / **[89]**: Measurements reveal no change in absorptive properties upon conjugation. All spectra were recorded in 100 mM pH 4.5 Na-citrate buffer, 5 vol% DMSO, 0.2 vol% Triton X-100.

Puzzled by the identity of all spectrums and thus doubting the stability of the reagents under acidic, aqueous conditions, HPLC-MS data was recorded. This, however, confirmed the stability of the adducts under assay conditions, which meant, in turn, that upon conjugation, no change in absorption would be triggered. As a strong absorbance shift between the two components is essential to enable sufficient excitation of the product, this evidence would impair the general applicability of **[86]**. Regrettably, also excitation at any of the absorbance peaks yielded only minimal fluorescence emission of the adducts, as well as the amino-oxy reagent (Fig. 38).

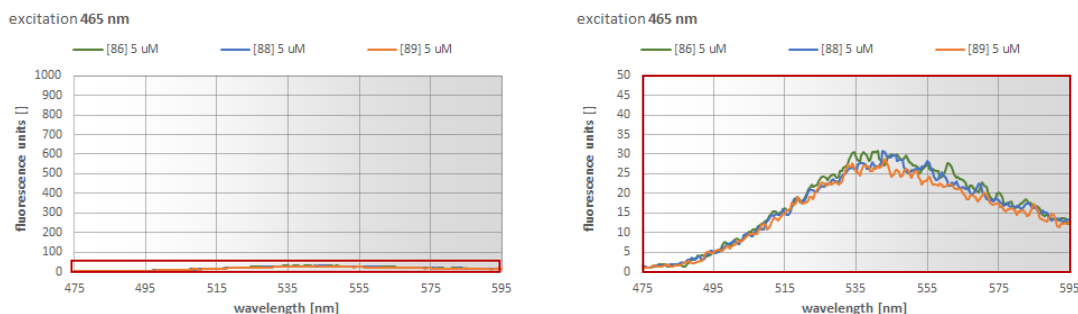
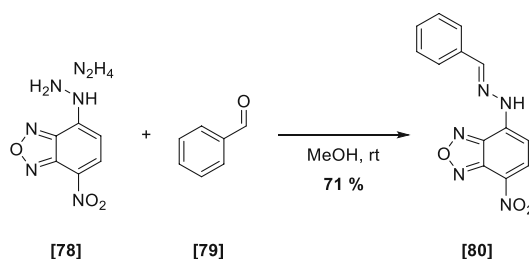


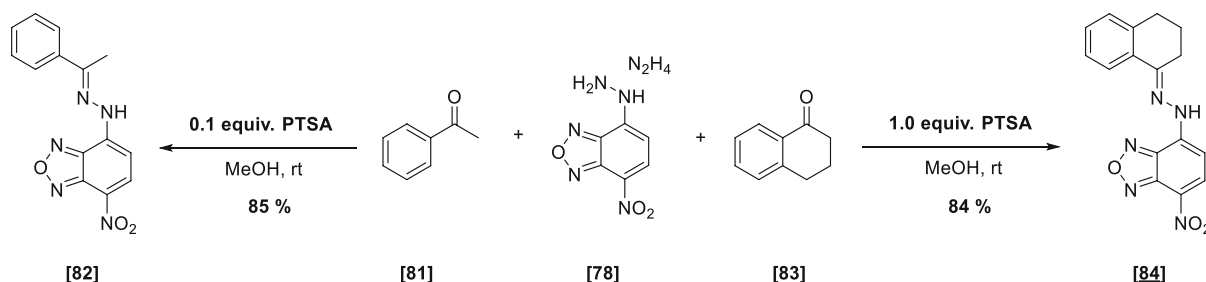
Fig. 38: Preliminary fluorescence measurements of NBD-AO **[86]** and its acetophenone and tetralone conjugates **[88]** / **[89]** at 5 μM concentrations: All compounds exhibited identical optical properties and were practically non-fluorescent. *left:* magnified area (*right*) outlined by a red rectangle. All spectra were recorded in 100 mM pH 4.5 Na-citrate buffer, 5 vol% DMSO, 0.2 vol% Triton X-100; excitation wavelength 465 nm, 5.0 nm slit, 775 V gain.

With both **[77]** and **[86]** ruled out for further studies, we continued with the synthesis of the adducts with NBD-H **[78]** using a known literature procedure for the benzaldehyde adduct. Herein addition of the carbonyl source to a methanolic suspension of the NBD-H triggered immediate conversion towards the hydrazones in the case of benzaldehyde **[79]** (Scheme 78). Despite its poor solubility in MeOH, the slow dissolution of the ochre hydrazine **[78]** could be observed over several minutes, accompanied by a deep red discoloring of the solution. Upon continued stirring, precipitation of the bright red benzaldehyde adduct **[80]** occurred, which was collected by suction filtration.



Scheme 78: Synthesis of NBD-H benzaldehyde adduct **[80]** adduct.

In the case of keto-derivatives **[82]** and **[84]**, however, a similar necessity for an acid catalyst for the hydrazone formation was observed (Scheme 79). Only negligible conversion could be detected for acetophenone **[81]** using a massive excess of the ketone (50 equiv.)—addition of catalytic amounts of conc. H_2SO_4 , Amberlyst-15, or PTSA triggered the immediate formation of the adduct visible *via* a blood-red discoloring of the suspension. Due to the poor separability of the Amberlyst resin from the precipitated products, we opted for the use of PTSA as the catalyst. Using this approach, the immediate difference in reactivity became apparent again.



Scheme 79: Synthesis of NBD-H acetophenone **[82]** and tetralone **[84]** adducts.

Whereas catalytic amounts of acid were sufficient to push the reaction to completion with acetophenone [81] in 30 minutes, equimolar addition of PTSA was necessary to fully convert tetralone [83] in a similar timeframe. Discontinued stirring after complete dissolution of the NBD-H facilitated better isolation of the products by improved filtration of the crystallized material. With this method, the synthesis of both hydrazone adducts [82]/[84] was possible in excellent yield.

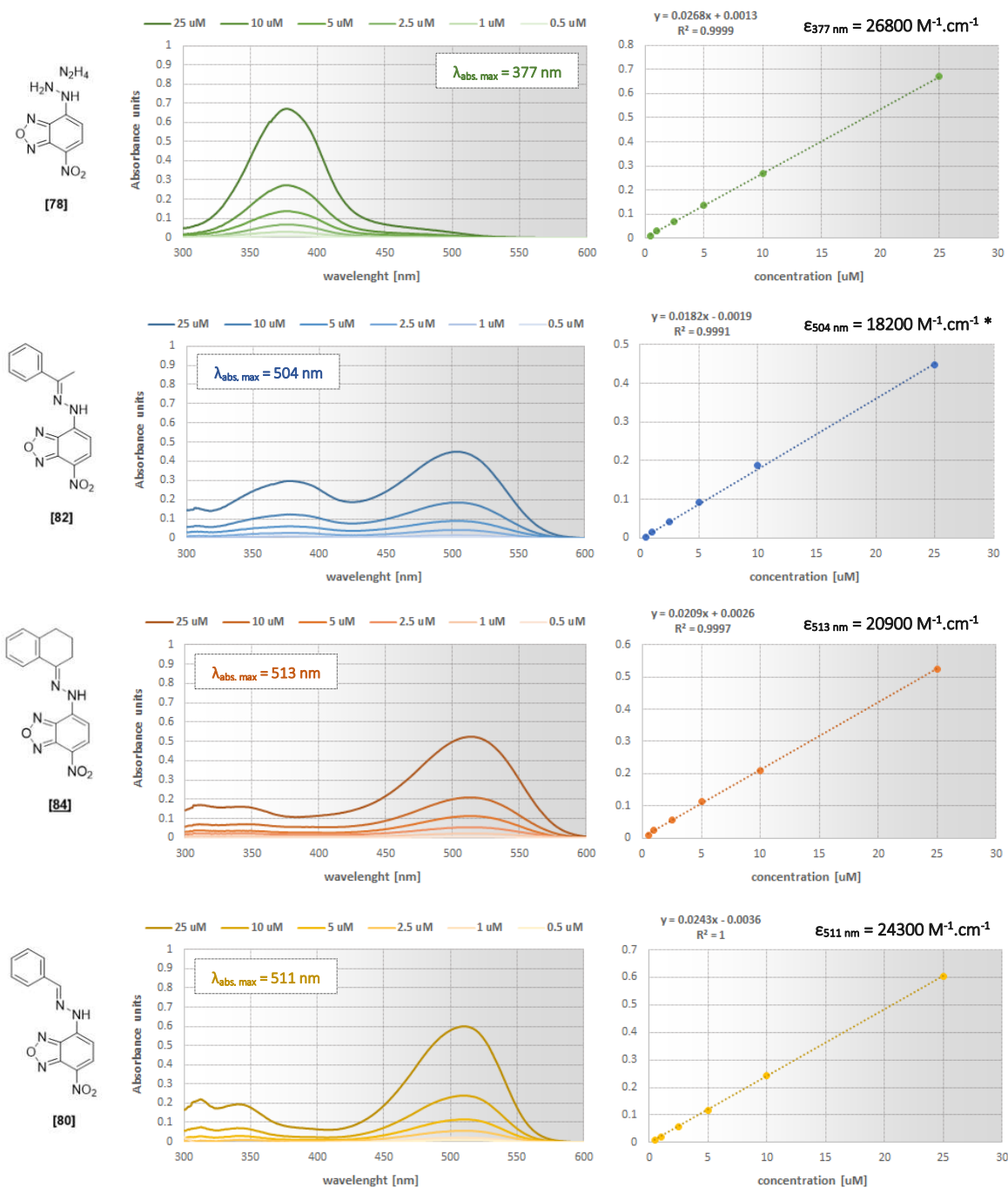


Fig. 39: UV-absorption calibrations of NBD-H [78] and its benzaldehyde, acetophenone, and tetralone conjugates [80] / [82] / [84]: Measurements reveal a strong red-shift of the absorption maximum upon conjugation from 377 nm to above 500 nm. All spectra were recorded in 100 mM pH 4.5 Na-citrate buffer, 5 vol% DMSO, 0.2 vol% Triton X-100. *absorbance coefficient might be underrepresented due to the possible fast hydrolysis of the material, which is visible by an already rising peak at 377 nm.

UV-absorbance measurements of the respective products and parent hydrazine (Fig. 39) revealed the distinct already literature-known red-shift of the absorbance maximum after adduct formation (377 nm to approx. 510 nm). This dramatic change in absorbance is generally beneficial for

an application in assay format and explains the prevalent use of these NBD-adducts for the detection of aldehydes.

During preparations for the UV measurement, a particular hydrolytic instability of the acetophenone conjugate [82] could be observed by discoloration of the red sample solutions, which could be even tracked with the naked eye.

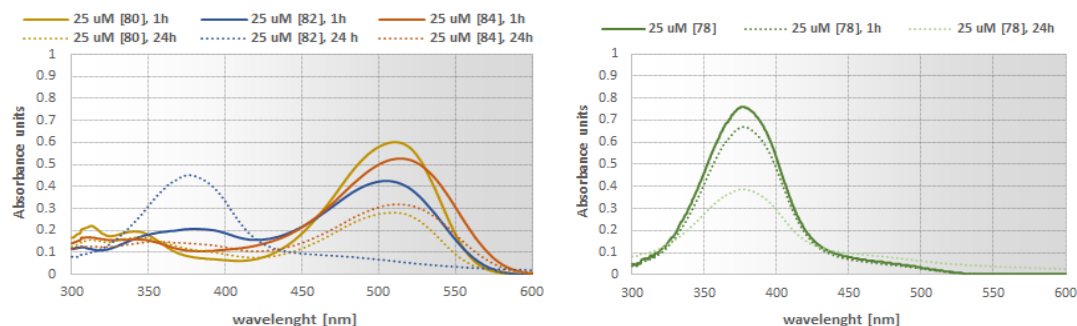


Fig. 40: Comparison stability of NBD-H [78] and its benzaldehyde, acetophenone, and tetralone conjugates [80] / [82] / [84] judged by UV-absorption measurements after 1 hour and 24 hours – *left:* Measurements reveal sufficient stability of [80] and [84], but a surprising hydrolytic instability of [82]; *right:* The NBD-H reagent [78] itself was shown to be unstable in the reaction medium and to decompose unspecifically – this presumable oxidative decomposition triggered an increase in signal above the 500 nm region. All spectra were recorded in 100 mM pH 4.5 Na-citrate buffer, 5 vol% DMSO, 0.2 vol% Triton X-100.

This phenomenon was confirmed by comparing the calibration spectra, which were measured one hour after the samples had been prepared. Whereas in the cases of benzaldehyde [80] and tetralone-adducts [84], only minimal hydrolysis to the NBD-H [78] was observed, complete hydrolysis of [82] was evident after 24 hours (Fig. 40). This surprising instability of the acetophenone adduct might explain why aryl ketones have been disregarded for hydrazone conjugations to this day. Judging from the spectral data, a general (non-hydrolytic) instability of the formed hydrazones could be shown in the reaction media. This behavior was unfortunately proven to be universal for this class of compounds as a deterioration of signal was also evident for the NBD-H reagent itself. However, prompted by sufficient stability of the theoretical FCA conjugate [84], we focused our investigation on this particular substance.

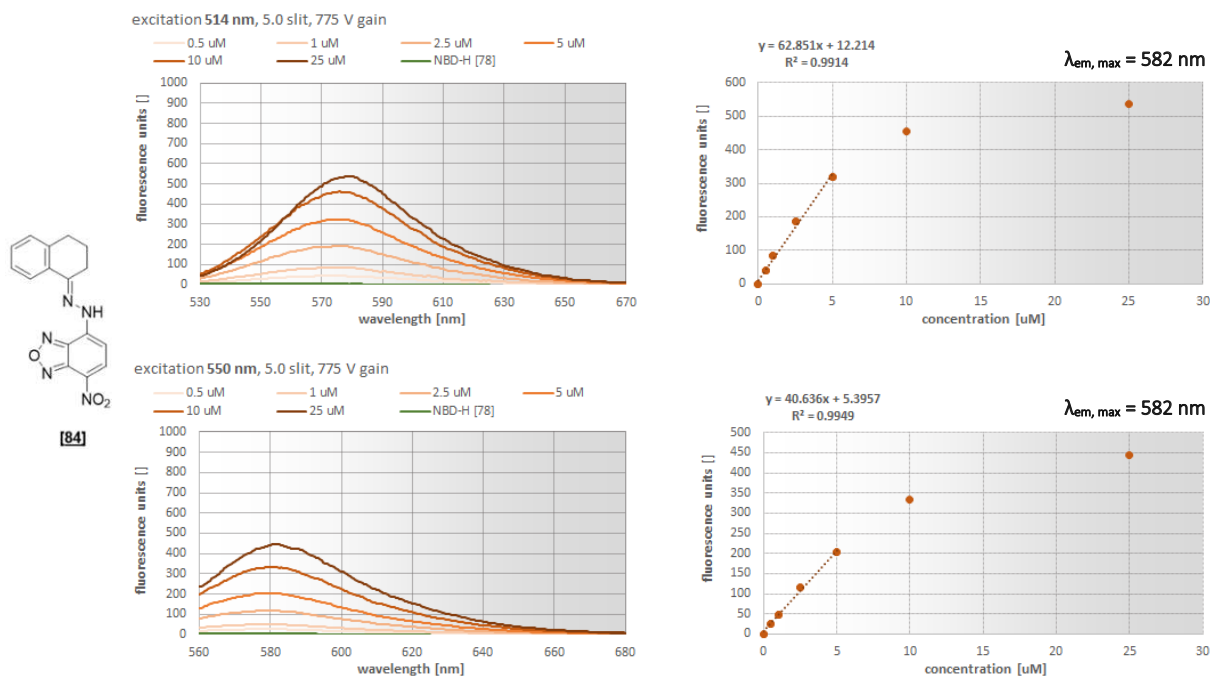


Fig. 41: Fluorescence calibrations of [84]: Excitation causes a strong fluorescence emission with a $\lambda_{em, max}$ at 582 nm. A distinct inner filter effect by reabsorption of the emitted light could be observed for excitations at the absorption maximum of 514 nm for wavelengths below 550 nm at concentrations above 5 μM . Excitation at 550 nm minimally improved the linear range of the calibration, albeit resulting in a drop of emission signal. All spectra were recorded in 100 mM pH 4.5 Na-citrate buffer, 5 vol% DMSO, 0.2 vol% Triton X-100; excitation wavelengths 514 nm and 550 nm respectively, 5.0 nm slit, 775 V gain.

Fluorescence measurements of [84] showed an emission maximum at 582 nm and linearity of the signal of up to 5 μM (Fig. 41). Above this threshold, the linear curve leveled off, which correlated well with a secondary inner filter effect (c.f. B III.1.1). As could be seen from the emission spectra at 514 nm excitation, self-quenching was evident below 570 nm for higher concentrations. To counteract the phenomenon and prevent a possible re-absorption of the excitation signal by the NBD-H, a calibration at 550 nm was also performed. A comparison of absorbance spectra of NBD-H [78] and absorbance and emission spectra of tetralone adduct [84] is depicted in Fig. 42.

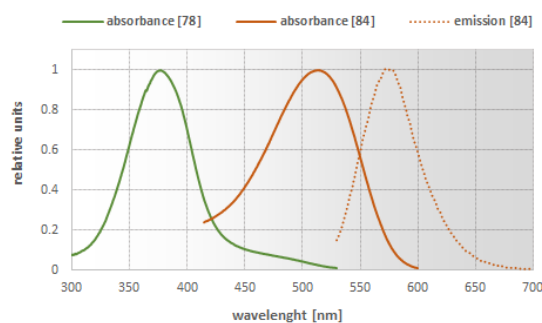


Fig. 42: Comparison of NBD-H [78] absorption ($\lambda_{abs, max} = 377 \text{ nm}$) and absorption and emission spectra of the tetralone conjugate [84] ($\lambda_{ex, max} = 514 \text{ nm}$, $\lambda_{em, max} = 582 \text{ nm}$). Absolute absorbance and emission values are normalized on their maximal values.

Subsequently, we investigated the pH dependence of the conjugate and were puzzled about the complete loss of signal, even for the already measured pH 4.5 citrate buffer system (Fig. 43). Furthermore, very fast discoloring of the red sample solutions could be observed for the more acidic pH 3.0 and 4.5 buffered systems (< 30 minutes). The fading was even faster than for the previously reported acetophenone conjugate [82]. We thus concluded that the Triton X-100 [XXXV], which was excluded in

the pH screening, had a dominant effect, not only on the fluorescence intensity but also on the stability of the adduct. The surfactant was added in biotransformation to solubilize the SHC from the cell membrane.

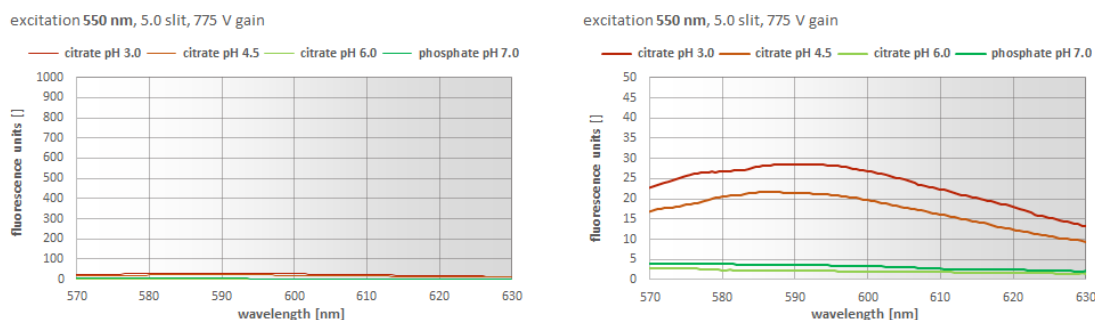
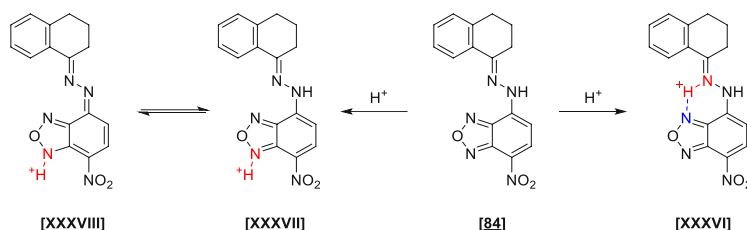


Fig. 43: pH dependency on the fluorescence emission of tetralone conjugate [84] at 5 μ M concentrations: Without the addition of Triton X-100 [XXXV], the adduct is practically non-fluorescent albeit showing minimal fluorescence at lower pH values (3.0 and 4.5). All spectra were recorded in 100 mM pH 4.5-6.0 Na-citrate buffer or pH 7.0 phosphate buffer, 5 vol% DMSO, 0.2 vol% Triton X-100; excitation wavelength 550 nm, 5.0 nm slit, 775 V gain.

The addition of 0.2 vol% of Triton X-100 [XXXV] to the buffer immediately restored the expected signal intensity. Interestingly, decreasing the pH to 3.0 caused a strong surge in fluorescence signal, whereas an increase of the pH to 6.0 and even further to pH 7.0 completely shut down any fluorescence emission. One explanation for this result could be the protonation of the hydrazone [XXXVI], which would match previous reports about these conjugates' general reactivity (Quelle). As protonation represented the first step for the hydrazone cleavage, this would also explain the hydrolytic instability of the adduct in acidic solutions (Scheme 80). The proton could be, in theory, additionally complexed by the adjacent oxadiazole ring forming a six-membered structure. If the behavior would be general, the hydrazone adducts could be theoretically applied as cation reporters. Considering the assumed equilibrium of [78], the increase in fluorescence could also be explained by the protonation of the oxadiazole-ring itself [XXXVII]. Activation of the ring could promote a shift in the equilibrium of [84], causing a possible expansion of the delocalized electron system [XXXVIII], which could impact the optical properties of the conjugate.



Scheme 80: Hypothetical protonation states of the tetralone conjugate [84]: Protonation could be either envisioned at the hydrazone nitrogen forming a potential six-membered structure [XXXVI] or at the oxadiazol moiety [XXXVII].

The presumable neutralization of the hypothesized protonated structures [XXXVI]-[XXXVIII] caused a dramatic change in the shape of the absorption spectrum and a shift of the absorption maximum from approx. 520 nm to 485 nm. Excitation at this wavelength, however, proved to be only minimally fluorescence active (not shown).

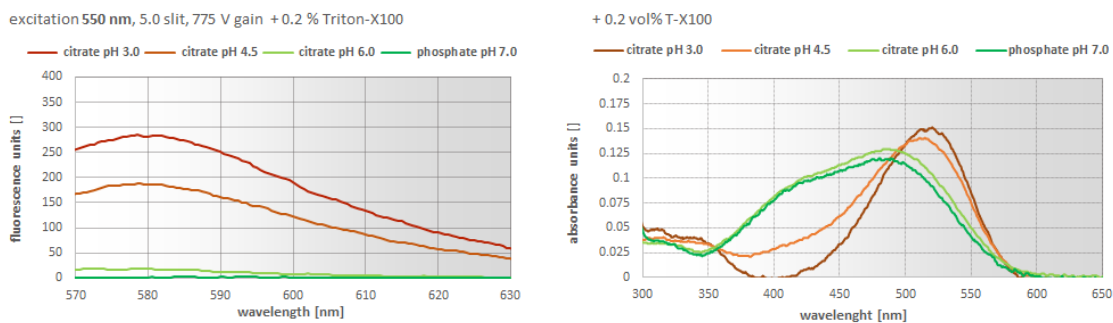


Fig. 44: pH dependency on the fluorescence emission and UV-absorption of tetralone conjugate [84] using 0.2 vol% Triton X-100 [XXXV] at 5 μ M concentration – *left:* Addition of the surfactant dramatically increases the fluorescence emission for pH 3.0 and 4.5; *right:* The increase in pH caused a dramatic change in the absorption spectrum which could be possibly correlated to the pK_A of the hydrazone (calculated 4.7 – ChemAxon® Chemicalize pK_A calculator). All spectra were recorded in 100 mM pH 4.5-6.0 Na-citrate buffer or pH 7.0 phosphate buffer, 5 vol% DMSO, 0.2 vol% Triton X-100; excitation wavelength 550 nm, 5.0 nm slit, 775 V gain.

Working under acidic conditions was thus essential for the assay. Additionally, the use of Triton X-100 [XXXV] was necessary for two reasons – as a stabilization agent and as a signal amplifier. This serendipitous finding would have probably never been discovered if the target of the study had not been a membrane protein, with a pH optimum at 4.5. We thus set out to elaborate if this effect could be rationalized. Four different commonly with the SHC applied non-ionic surfactants (Triton X-100 [XXXV], Tween 20 [XXXIX], Tween 80 [XL], Pluronic 68 [XLI]) were chosen and measured at pH 4.5 (Fig. 45).

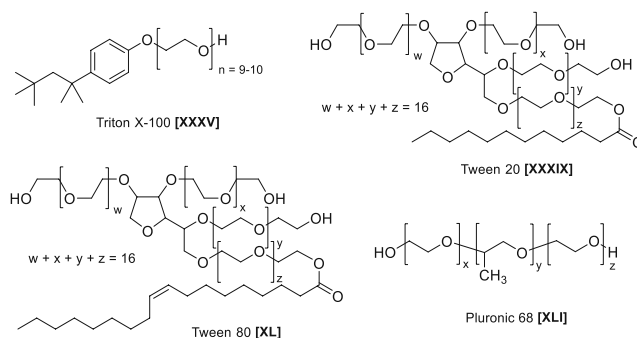


Fig. 45: Set of non-ionic surfactants applied for fluorescence screening of [84].

Increasing the concentration of three out of the four surfactants caused an immediate rise in fluorescence signal up to a certain plateau (Fig. 46). Interestingly, the most significant leap in signal was observed above their respective cmc (critical micelle concentration).

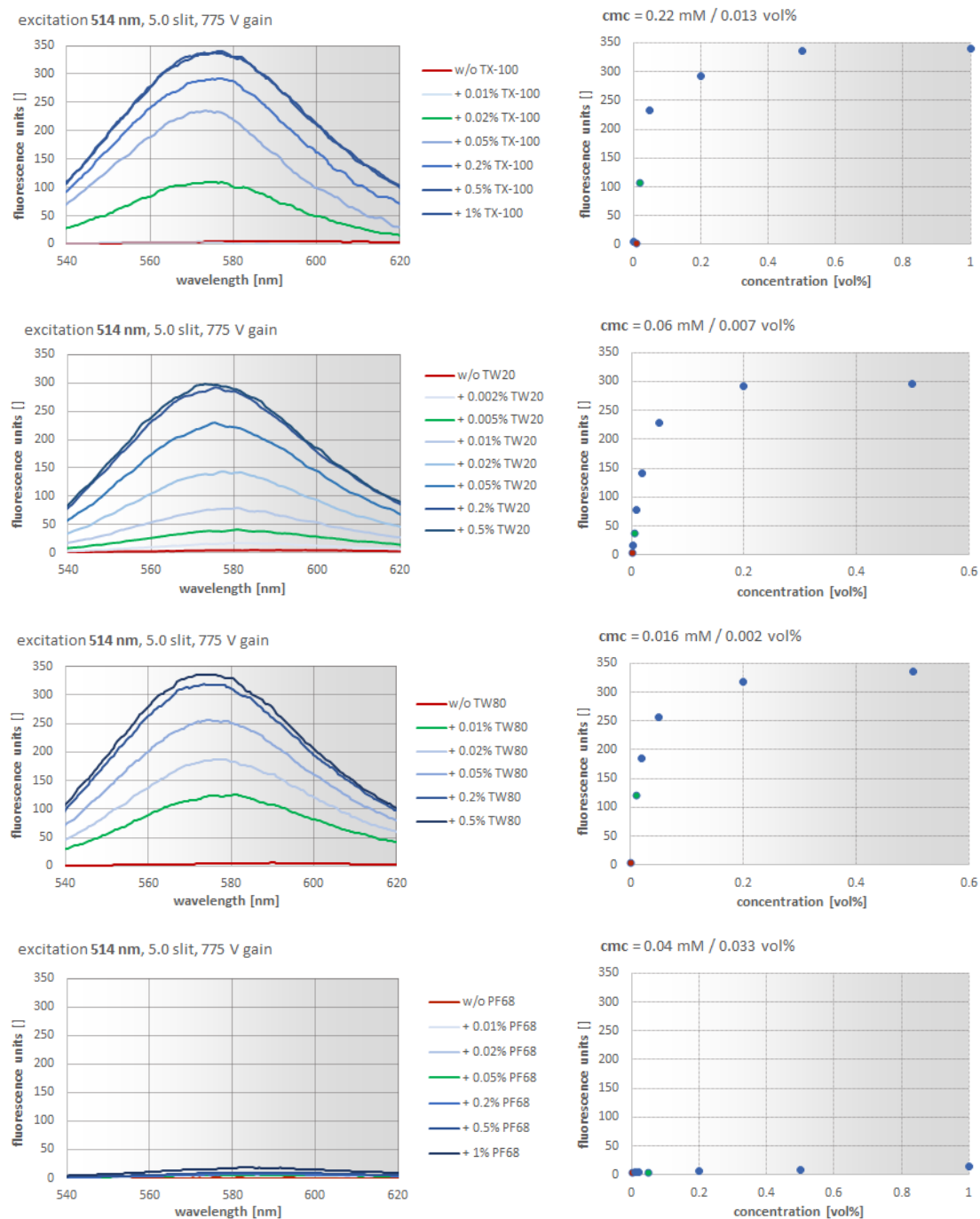


Fig. 46: Dependency on the non-ionic surfactant concentration on the fluorescence emission of [84] at 5 μM concentrations – used surfactants depicted in Fig. 45: In all cases except for Pluoronic 68 [XLI], an increase of surfactant concentration above the known cmc (critical micelle concentration) values depicted by the green line caused a dramatic surge in fluorescence signal. Further addition of surfactants led to a plateauing of the signal. All spectra were recorded in 100 mM pH 4.5 Na-citrate buffer, 5 vol% DMSO, respective surfactant concentration; excitation wavelength 514 nm, 5.0 nm slit, 775 V gain.

As NBD-H adducts are known to be stronger fluorophores in apolar media (Quelle), the use of surfactants above their cmc might create zones of decreased polarity inside the formed micelles. If the adducts are preferably located inside these structures, then this would also explain the increased tolerance against hydrolysis. Surprisingly, PF68 did not exhibit the same behavior, which might be explained by the absence of a large hydrophobic tail that could impair sufficient aggregation. All remaining surfactants were very close in their signal amplifying behavior, albeit Triton X-100 showing a distinct fluorescent background emission with a maximum of around 600 nm (Fig. 47). This effect was

avoided if excitation was performed at higher wavelengths (e.g., 550 nm) or higher concentrations (> 5 μM) of any hydrazine or hydrazine-adduct were dissolved in the buffer solutions. Triton X-100 had already been successfully applied in trial SHC biotransformation, so we opted for this surfactant for further testing.

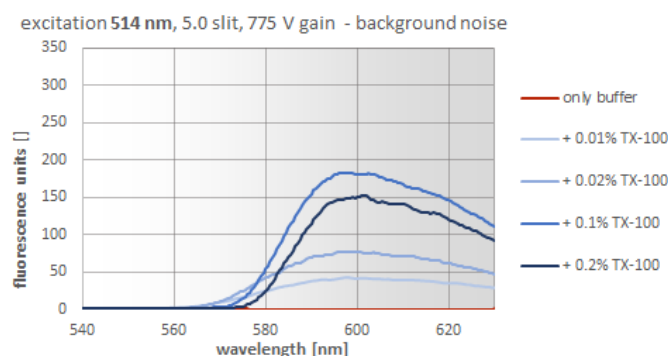


Fig. 47: Background signal of Triton X-100 [XXXV] upon excitation at 514 nm, which triggered fluorescence with an emission maximum at 593 nm. All spectra were recorded in 100 mM pH 4.5 Na-citrate buffer, 5 vol% DMSO, and respective surfactant concentration; excitation wavelength 514 nm, 5.0 nm slit, 775 V gain.

Having the rudimentary conditions for the assay established, we conducted initial kinetical studies. Due to the already reported general low reactivity of aromatic ketones^{130,133}, we opted for an experiment employing concentrations that would theoretically surpass the optical density of 0.1 even at minimal conversions (*c.f.* Fig. 39 & Fig. 41: 5-10 μM concentrations). This meant that reliable concentration values in the linear range for the inline measurements could only be obtained for adduct formations in the range of 1-2 % at 500 μM using 550 nm excitation. Additionally, above a certain threshold, a possible decline in signal could be expected due to the prevalent inner-filter effect of the product.

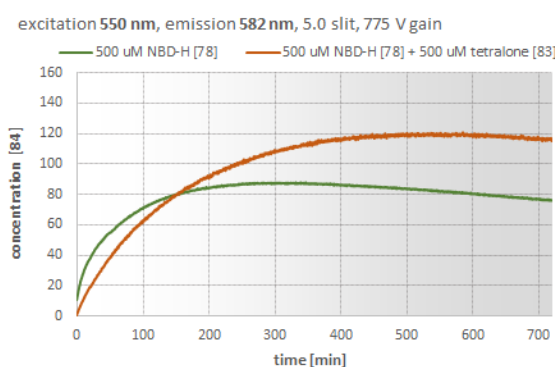
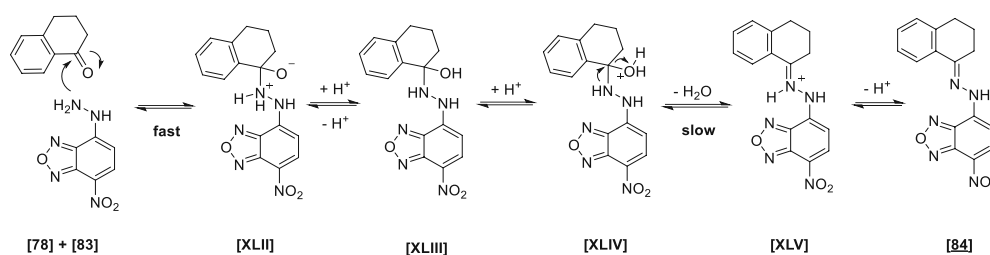


Fig. 48: Fluorescence stability measurements of NBD-H [78] and initial kinetic studies for the formation of the tetralone conjugate [84] at 500 μM . Kinetics were recorded in 100 mM pH 4.5 Na-citrate buffer, 5 vol% DMSO and 0.2 vol% Triton X-100; excitation wavelength 514 nm, emission wavelength 582 nm, 5.0 nm slit, 775 V gain, 1-minute intervals.

Looking at the results, this was, in fact, the case after approx. 540 minutes, upon which a slight decrease in signal could be observed (Fig. 48). Multiple dilution steps of the sample (not shown) were needed to re-enter the linear signal range (> 10 μM), confirming the inner filter effect to be causing the plateau in the fluorescence signal. However, the maximal signal intensity of 120 fluorescence units did not match the previously established calibration (*c.f.* Fig. 41), where the maximum would be expected well above 400-500. This meant that absorption *via* the NBD-H reagent itself had to be causing the loss in signal and needed to be taken into account. This effect was also supported by the comparison of the

spectra of the hydrazine at 0 and 24 hours. The presumable decomposition of the material caused an increase in the absorption at 550 nm, which added to the inner filter effect of the probe itself (Fig. 40 right). This instability of the NBD-H [78] furthermore triggered a substantial increase in background emission that was unfortunately at a similar magnitude compared to the product signal (Fig. 48). Surprisingly, the addition of tetralone to the NBD-H solution seemed to mitigate this effect as the initial increase in fluorescence signal was dampened. As tetralone [83] was proven to not affect the fluorescence in the reaction buffer or solutions of [84] (not shown), a possible non-fluorogenic reaction could explain the possibly increased stability. Hydrazone formation, as was previously reported by Stachissini *et al.*²³⁰, depends on several equilibria (Scheme 81). Whereas acid-catalyzed formation of the hemiaminal [XLIII] was proven to be rate-determining under neutral conditions, an increase in acidity to pH 4-5 rendered the dehydration of [XLIV] limiting. If part of the hydrazine was thus trapped as presumably non-fluorescent [XLIII], this effect could explain the observed kinetic profile. In how far this equilibrium was present and needed to be accounted for could, however, not be determined from these measurements.



Scheme 81: Dynamic equilibria during hydrazone formation of NBD-H [78] and tetralone [83]: Dehydration of the intermediately formed hemiaminal was found to be rate-determining under acidic conditions. Hence, the bulk of the hydrazine and the carbonyl species could be funneled into presumably non-fluorescent and stable intermediate [XLIII], which is subsequently transformed into the product [84].

As in-house equipment did not allow for parallel measurements at the desired wavelengths and the reaction proved to be sufficiently slow, we opted for 24 hours experiments with different concentrations of tetralone [83] and NBD-H [78]. They were investigated in a range from 25 to 500 μM and NBD-H concentrations from 50 to 5000 μM , respectively (see Table 4). To eliminate any effects stemming from the background decomposition of NBD-H (see Fig. 48), calibrations were performed after the same time using blank “decomposed” NBD-H spectra as background (Fig. 49).

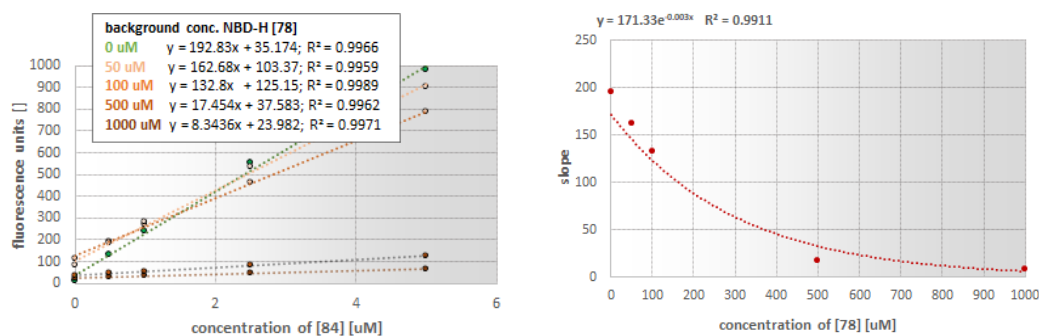


Fig. 49: Fluorescence calibrations of the tetralone adduct [84] after 24 hours using untreated NBD-H [78] solutions as blank – **left:** Due to the increased optical density of the NBD-H [78] itself, a decrease in the response factor for each calibration could be observed with the increase in NBD-H concentration; **right:** The loss in signal-to-noise (S/N) could be plotted as exponential decay. 5 mM calibration was omitted due to a complete loss of signal. All spectra were recorded in 100 mM pH 4.5 Na-citrate buffer, 5 vol% DMSO, 0.2 vol% Triton X-100; excitation wavelength 550 nm respectively, 5.0 nm slit, 775 V gain.

As shown in Fig. 50, the concentration of NBD-H [78] had dramatic effects on the final signal intensity of the adduct. Whereas minimal signal penalty was observed for concentrations until 100 μM , increasing the concentration of the NBD-H to 500 μM led to approx. 80% loss of fluorescence intensity. Interestingly, plotting the slope of the calibration curves against the background concentration of [78] led to an excellent exponential correlation which described how far the sensitivity of the system was corrupted by increased reagent concentration.

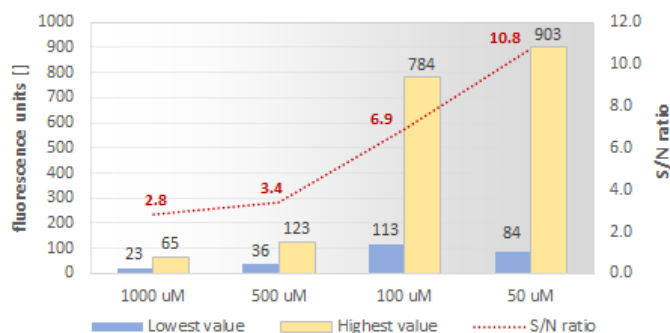


Fig. 50: Numerical values of the fluorescence calibrations, including the lowest and highest measured values, as well as the resulting S/N ratio.

This experiment also showed the general capabilities of the assays systems to discriminate between background and product signal (Fig. 50). Whereas the 50 μM system allowed for a theoretical S/N ratio of 10.8, using 1 mM of reagent only enabled a S/N of 2.8. Applying the established calibrations, the results for the screening are summarized as determined concentrations of [84] and as theoretical yields corrected for the limiting components in Table 4.

Table 4: Resulting final concentrations [μM] and yields [%] for NBD-H-tetralone conjugation using different hydrazine and ketone concentrations. Final yields and concentrations were assigned for the limiting component and were determined with the calibrations established in Fig. 49. Reactions performed with 500 μM [78] and 250 / 500 μM [83] were necessarily 1:10 diluted due to values outside of the linear range and judged with calibration corresponding to the 50 μM [78] calibration. Red marked entries exemplify the system's limits for high concentrations of NBD-H and low concentrations of tetralone, whereas correlations were completely lost due to unselective background processes.

final conc. [84], [μM]	NBD-H [78], [μM]				yield / limiting component [%]	NBD-H [78], [μM]			
	50	100	500	1000		tetralone [83], [μM]	50	100	500
tetralone [83], [μM]	50	100	500	1000	tetralone [83], [μM]	50	100	500	1000
25	0.1	0.2	1.0	-1.1	25	0.4%	0.8%	3.8%	-4.3%
50	0.2	0.5	2.4	-0.4	50	0.4%	0.9%	4.8%	-0.7%
250	1.3	2.2	12.1*	5.6	250	2.5%	2.2%	4.8%*	2.3%
500	2.0	3.6	13.4*	8.8	500	4.0%	3.6%	2.7%*	1.8%

Regrettably, only a maximum 5 % of conversion could be detected for any screened combinations after 24 h. Using a higher concentration of NBD-H indeed increases the yield for adduct formation, however with the already mentioned decline in S/N. The loss in signal was even more evident by looking at the values for the 1 mM case, where especially for low concentrations of tetralone, no correlation could be established. Although experiments using 5 mM of [78] were performed, these led to a complete loss in signal and were thus excluded. Nevertheless, as was already expected, both an increase in NBD-H and tetralone concentration led to improved conversions. Moreover, using higher amounts of the reagent compared to the tetralone is recommended, as equimolar concentration led to even more insufficient conversions.

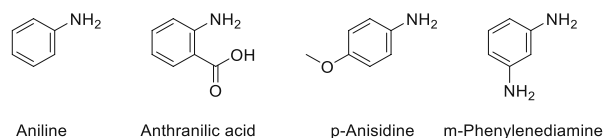
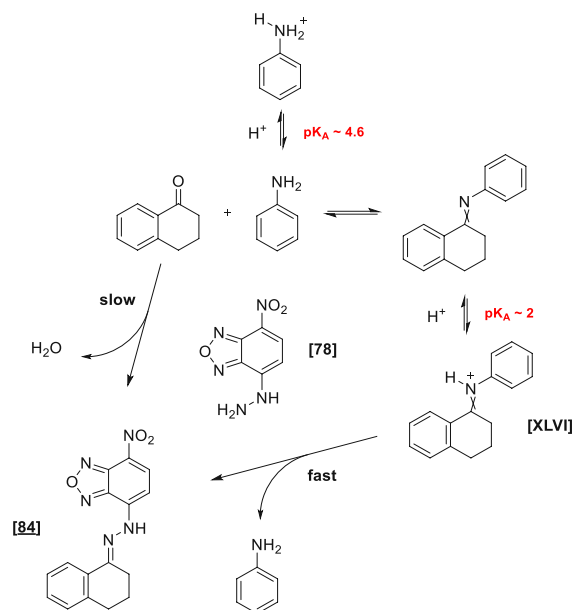


Fig. 51: Set of catalysts known for their beneficial effects for hydrazone conjugations.

Before abandoning the project, we decided to give it one last try using aniline and aniline derivatives that are used since the report from Jencks²³¹ as catalysts for these types of linkages (Fig. 51).^{130,131,134} Due to their low pK_a values, these can still act as nucleophiles (compared to alkyl amines), activating the carbonyl functionality with the intermediate formation of the iminium species [XLVI], which represents a much stronger electrophile compared to the naked ketone and is thus trapped faster by the alpha nucleophilic hydrazine reagent (Scheme 82). The aniline also represents a better leaving group in the substitution reaction, omitting the necessity for the subsequent slow dehydration step, which was proven to be rate-determining under acidic conditions. Although some groups reported only minimal benefits using these catalysts for aryl ketone substrates attributed to their steric bulk¹³⁰, we still decided to test these systems for the NBD-H – tetralone system.



Scheme 82: Uncatalyzed and aniline-catalyzed pathway towards hydrazone formation.

Due to the complicated screening using the fluorescence methodology, we opted to switch to further screenings to UV-spectroscopy and, in the case of positive hits, subsequently validate the experiments with the fluorometer. As 500 μM NBD-H reagent represented a good starting point for the screenings, we tried to confirm the results from the fluorescence experiments (Fig. 52). Surprisingly using the same reaction set-up as in the fluorometer and the already established calibrations, the 500 μM / 500 μM case exhibited approximately double the amount of [84] formation. Repeated measurements, however, confirmed the slightly improved yields. Due to the low conversions, the signal intensities were typically highly unstable. Especially measurements using lower amounts of tetralone [83] (< 100 μM) exhibited massive fluctuations in signal – therefore also the 50 μM case was not included. Additional attempts to improve the experimental precision were not undertaken, as the kinetics were insufficient for further applications.

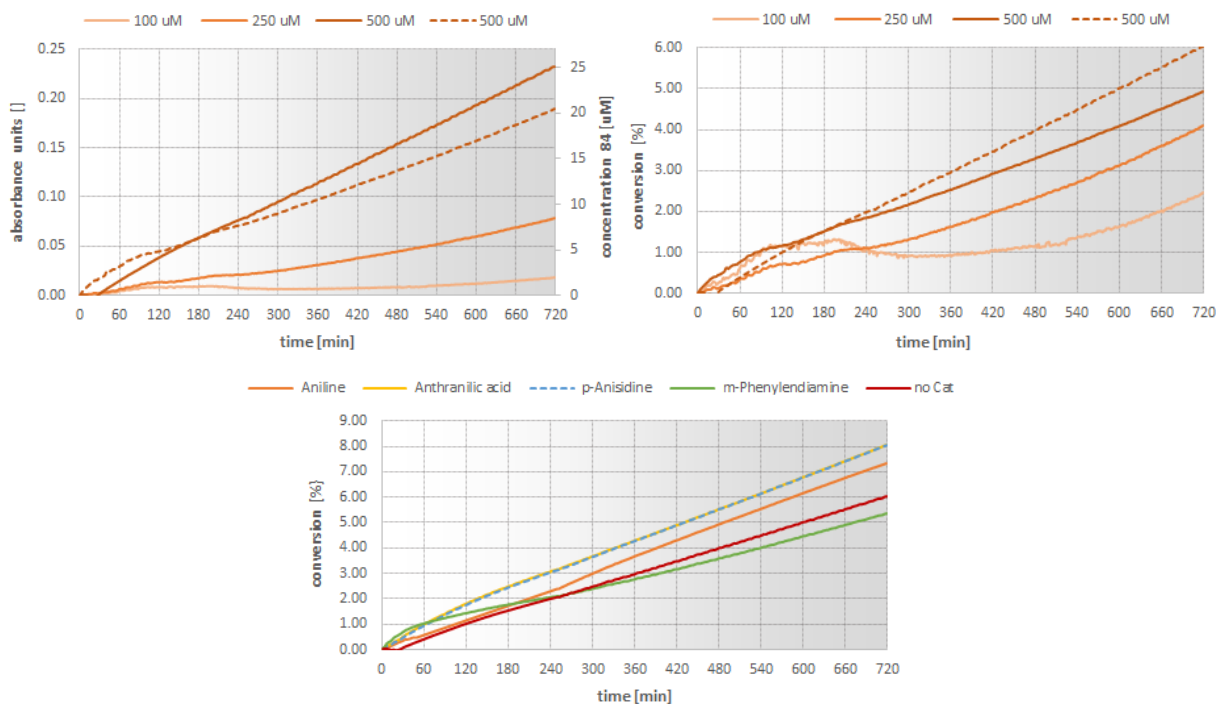


Fig. 52: UV-absorption kinetic studies of the formation of the tetralone conjugate [84] using 500 μM NBD-H [78] and 100-500 μM tetralone [83] concentrations at 560 nm absorption – *left*: Increase of absorbance units over time; *right*: Calculated conversions over time using the in Fig. 39 determined calibrations at 560 nm; *bottom*: Addition of 500 μM catalysts prior to the initiation of the reaction with the addition of tetralone. Kinetics were recorded in 100 mM pH 4.5 Na-citrate buffer, 5 vol% DMSO, 0.2 vol% Triton X-100, 1-minute intervals. Spectra are corrected for 500 μM NBD-H [78] blank.

Employing the aforementioned “catalysts” in equimolar amounts, which are generally used in overstoichiometric amounts for bioconjugations²²⁹, however, did not substantially improve the conversion of tetralone to the NBD-H adduct [84] (Fig. 52 bottom). All yields for the hydrazone formation were consistently below 10 % in a 12 h timeframe. Being faced with these kinetic hurdles, we judged that no application in an assay format would be possible for the detection of tetralone-type substrates using the NBD-H reagent. However, having the optimal conditions for the assay established – especially the massive improvement in fluorescence yield - we still opted to check its reactivity towards benzaldehyde and determine its optical properties (Fig. 53).

Herein a massive difference in initial velocities of the two carbonyl sources could be observed, as benzaldehyde reacted faster by a factor of 126.

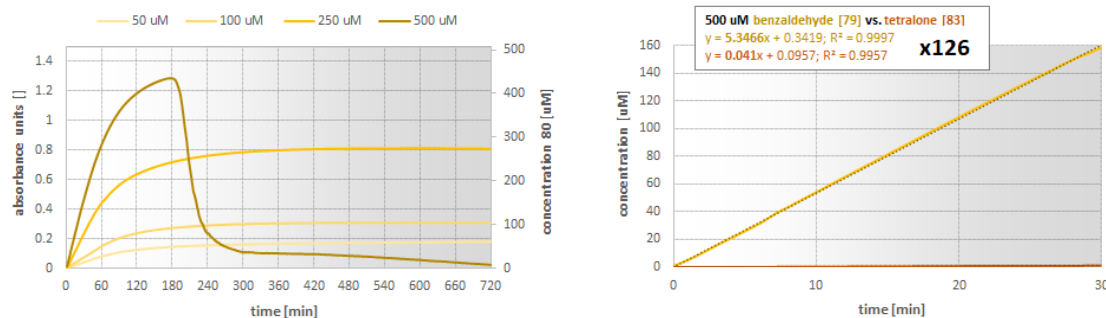
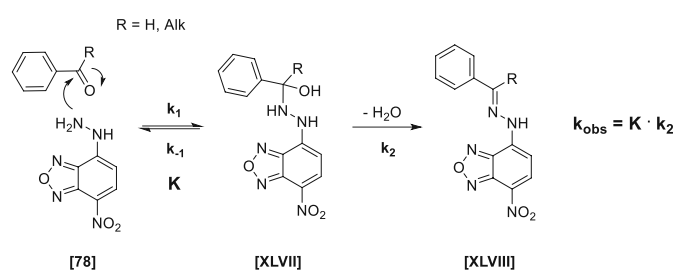


Fig. 53 - left: UV-absorption kinetic studies of the formation of the benzaldehyde conjugate [80] using 500 μM NBD-H [78] and 50-500 μM benzaldehyde [79] concentrations at 560 nm absorption. Precipitation of the conjugate in the 500 μM reaction caused a decrease in signal intensity after approx. 180 min; *right*: Comparison of initial kinetics of the 500 μM benzaldehyde [79] and tetralone [83] conjugations using the first 30 minutes of reaction time – respective concentration values were calculated using the in Fig. 39 determined calibrations at 560 nm. Assessment of the slopes revealed an approx. 126-fold increase in conjugation. Kinetics were recorded in 100 mM pH 4.5 Na-citrate buffer, 5 vol% DMSO, 0.2 vol% Triton X-100, 1-minute intervals.

Furthermore, the reaction towards the benzaldehyde adduct [80] seemed to exhibit first-order kinetics (see Fig. 54). Using the initial 20 minutes of the reaction for calculations at different aldehyde concentrations, a rate constant of $k = 1.6 \times 10^{-4} \pm 2.3 \times 10^{-5} \text{ s}^{-1}$ could be determined. This independence of carbonyl concentration would match the reports for the aforementioned acid-catalyzed hydrazone formations. Although not as conclusive, these findings seemed to be also supported by the fluorescence screenings with tetralone [83] in cases where hydrazone was used in dramatic excess. This effect would also affirm the assumptions that a large part of the carbonyl species was trapped as hemiaminal, thus superficially increasing the NBD-H reagent's stability. The concentration of the carbonyl source could, however, slightly affect the kinetics if the rate constant k_{-1} for the back-reaction of the equilibrium for the hemiaminal formation would be larger than k_1 (Scheme 83). As the equilibrium constant of the NBD-H [78] with either benzaldehyde [79] as well as tetralone [83] were unknown under these conditions, only an absolute rate could be theoretically determined.



Scheme 83: Kinetic profile for the hydrazone formation of NBD-H [78] with carbonyl species in acidic media ($k_1 \gg k_2$). k_1 represents the second-order rate constant for the formation of the hemiaminal [XLVII], k_{-1} represents the rate constant for the elimination of the hydrazine liberating the carbonyl species, k_2 represents the dehydration forming the final hydrazone product [XLVIII]. The observed rate constant k_{obs} correspond to the product of the equilibrium constant K and the first-order rate constant k_2 .

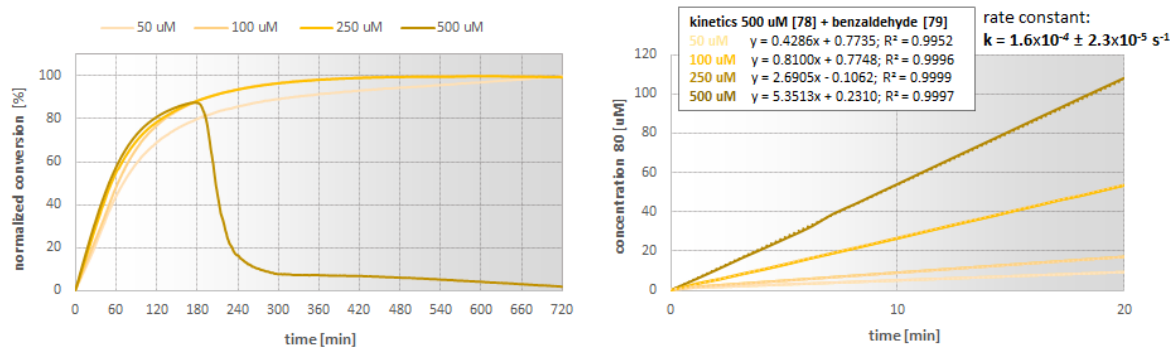


Fig. 54 - left: UV-absorption kinetic studies of the formation of the benzaldehyde conjugate [80] using 500 μM NBD-H [78] and 50-500 μM benzaldehyde [79] concentrations at 560 nm absorption normalized by the final absorbance values. **right** – initial change of concentrations of benzaldehyde adduct formation – first-order rate constant was calculated to be $1.6 \times 10^{-4} \pm 2.3 \times 10^{-5} \text{ s}^{-1}$. Kinetics were recorded in 100 mM pH 4.5 Na-citrate buffer, 5 vol% DMSO, 0.2 vol% Triton X-100, 1-minute intervals.

The substantial decline in signal for the 500 μM experiment could be explained by precipitation of the benzaldehyde adduct above 400 μM . Seeing if these results could be reproduced using fluorescence spectroscopy, calibrations with the benzaldehyde adduct [80] were performed. Surprisingly, the fluorescence yield of the adducts seemed to be 3-times larger than its corresponding tetralone counterpart (Fig. 55).

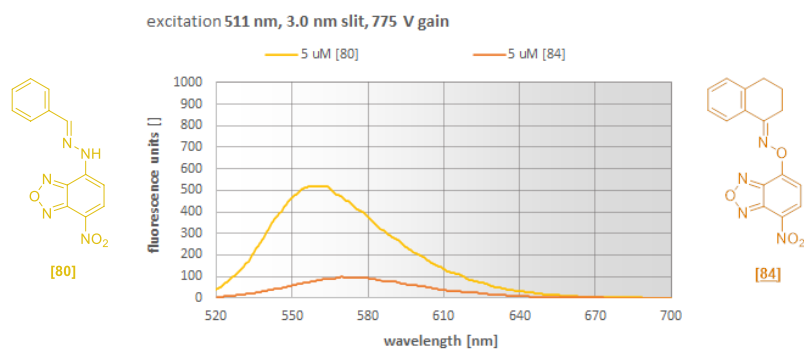


Fig. 55: Comparison of the fluorescence spectra of the benzaldehyde [80] and tetralone conjugate [84] at 5 μM: The aldehyde adduct exhibited approx. 3-fold increase in fluorescence yield (see **Table 5**). Compared to [84], the emission maximum of [80] was minimally less red-shifted to 560 nm (vs. 582 nm). All spectra were recorded in 100 mM pH 4.5 Na-citrate buffer, 5 vol% DMSO, 0.2 vol% Triton X-100; excitation wavelengths 511 nm, 3.0 nm slit, 775 V gain.

Given the slightly stronger absorbance coefficient of the benzaldehyde adduct (*c.f.* Fig. 39), calibrations at the optimal wavelength exhibited only sufficient linearity up to 2.5 μM concentration. To omit the effect, calibrations were also redone at 550 nm, which allowed to sidestep the strong inner-filter effect (Fig. 56).

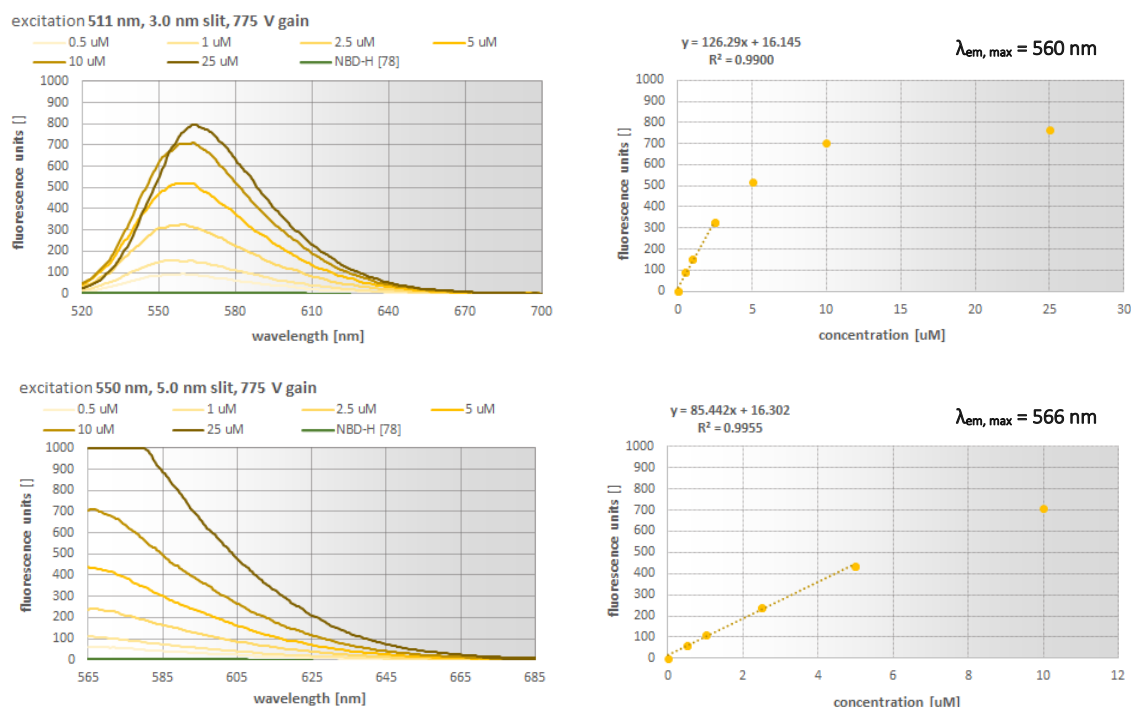


Fig. 56: Fluorescence calibrations of [80]: Excitation causes a strong fluorescence emission with a $\lambda_{em,max}$ at 560 nm. A distinct inner filter effect by reabsorption of the emitted light could be observed for excitations at the absorption maximum of 511 nm for wavelengths below 560 nm. Excitation at 550 nm improved the linear range and caused a slight red-shift of the emission maximum. All spectra were recorded in 100 mM pH 4.5 Na-citrate buffer, 5 vol% DMSO, 0.2 vol% Triton X-100; excitation wavelengths 511 nm, 3.0 nm slit, 775 V gain, and 550 nm, 5.0 nm slit, 775 V gain, respectively.

Preliminary fluorescence experiments confirmed the apprehension that prolonged kinetic measurements should be only limited to UV spectroscopy at relevant concentrations due to the strong inner filter effect of the adducts. This behavior is exemplified in Fig. 57, which results in a substantial decline in signal after approximately 30 minutes of reaction for the benzaldehyde adduct formation. Furthermore, as reported for the tetralone reaction, the stabilization *via* the respective hemiaminals caused a dramatic difference in background signal (*c.f.* Fig. 48). Due to this dynamic equilibrium, the

fluorescence readouts would thus be always flawed with an underlying uncertainty - especially for low carbonyl concentrations. Hence, extended kinetic measurements could only be qualitatively evaluated if the studied reactions proved to be rapid enough to plateau in the screened timeframe (see. Fig. 57).

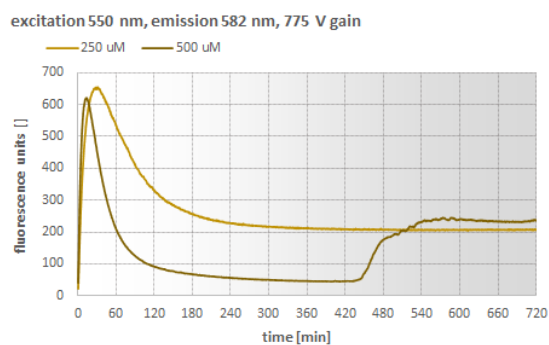


Fig. 57: Fluorescopic kinetic studies of the formation of the benzaldehyde conjugate [80] using 500 μM NBD-H [78] and 250 / 500 μM benzaldehyde [79] concentrations. Due to the inner-filter effect of the product, the emission signal showed a sharp decline after approx. 30 minutes. Similar to the UV absorption studies, precipitation of the 500 μM product was observed after a certain time. Kinetics were recorded in 1-minute intervals in 100 mM pH 4.5 Na-citrate buffer, 5 vol% DMSO, 0.2 vol% Triton X-100 using the excitation wavelength 550 nm, emission wavelength 582 nm, 5.0 nm slit, 775 V gain.

Initial kinetic investigations could still be performed under circumstances where background fluorescence and inner filter effect could be neglected. This would be true in the latter case for either fast kinetics or if the theoretical background signal remained insignificant compared to the fluorescent adducts. The inner-filter effect would, however, impose a time restriction on the screenings, as at some point, a linear signal correlation would be abandoned. This was observed already after 4 minutes for the benzaldehyde adduct formation, in which reactions employing higher concentrations of benzaldehyde would depart from the linear trend (Fig. 58).

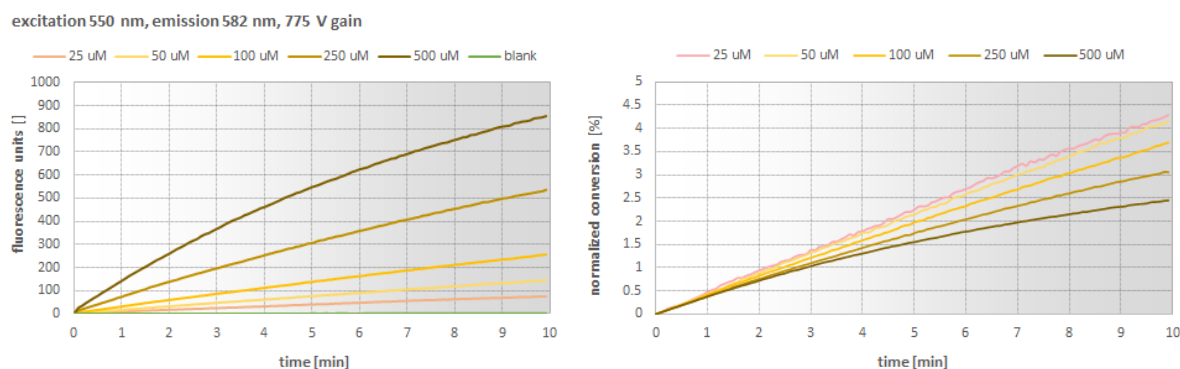
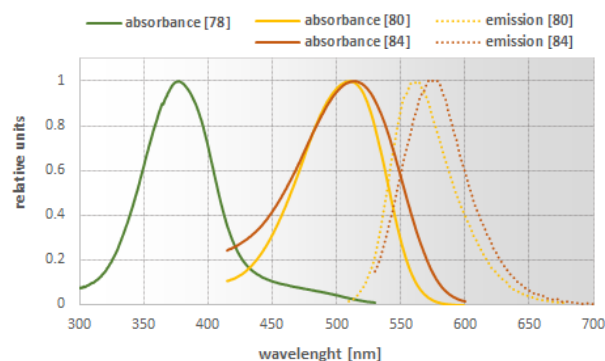


Fig. 58: Fluorescopic kinetic studies of the formation of the benzaldehyde conjugate [80] using 500 μM NBD-H [78] and 25-500 μM benzaldehyde [79] concentrations. Due to the inner filter effect, reactions were tracked only for 10 minutes – *left*: Increase of fluorescence units over time; *right*: calculated normalized conversions over time using the in Fig. 56 determined calibrations at 582 nm. Kinetics were recorded in 1-minute intervals in 100 mM pH 4.5 Na-citrate buffer, 5 vol% DMSO and 0.2 vol% Triton X-100; excitation wavelength 550 nm, emission wavelength 582 nm, 5.0 nm slit, 775 V gain.

One possibility to overcome the limitation would be to excite at higher wavelengths and thus theoretically measure at lower optical densities. This approach would always come with a tradeoff for a general loss in signal and a decrease in S/N ratio as the excitation would be performed at suboptimal wavelengths. Nevertheless, these limits were not explored for the benzaldehyde adduct [80]. All the results of the evaluation for the NBD-H adducts are summarized in Table 5.

Table 5: Summary of structural and optical properties of the substances used in this study. n.a. – not available, n.d. – not determined. Comparison of NBD-H [78] absorption and benzaldehyde [80] tetralone conjugate [84] product and Stokes shifts. Absolute absorbance and emission values are normalized on their maximal values.

	M [g·mol ⁻¹]	$\lambda_{\text{abs, max}}$ [nm]	ϵ [cm ⁻¹ ·M ⁻¹]	$\lambda_{\text{em, max}}$ [nm]	Φ_F (rhodamine B)	brightness
NBD-H.NH ₂ -NH ₂ [78]	227.18	377	26800	n.a.	n.a.	n.a.
benzaldehyde-NBD-H [80]	283.25	511	24300	560	0.055	1337
acetophenone-NBD-H [82]	279.27	504	18200	571	n.d.	n.d.
tetralone-NBD-H [84]	323.31	514	20900	582	0.016	334

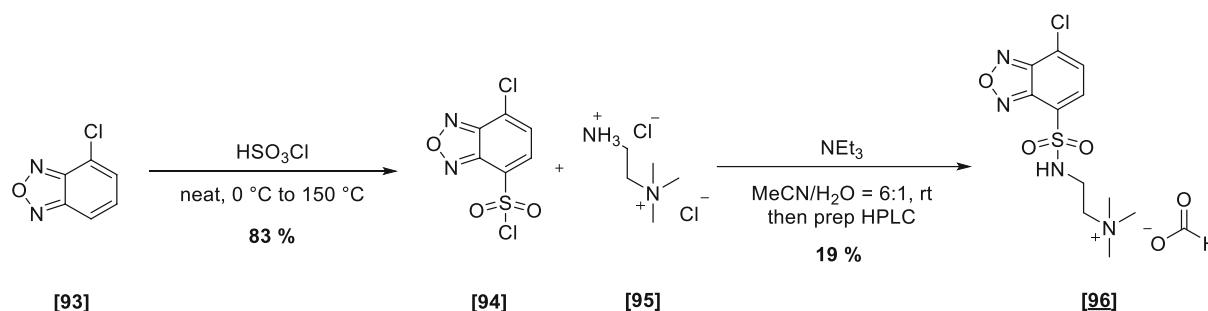


At this point, the project's focus started to shift towards the use of the NBD-H reagent in a fluorescence-activated droplet sorting format for the detection of aldehydes. As mentioned in B IV.1, to enable their application in this microfluidic setup, an essential prerequisite of these assay compounds was excellent water solubility. Due to the observed precipitation of [83] at higher concentrations, this property was not given for these adducts. This assumption was also supported by computational logD calculation using the online tool ChemAxon®. Herein the logD_{4.5} values for the benzaldehyde [80] and tetralone [84] adducts were determined to be + 2.63 and + 3.63, respectively, which put them far in the hydrophobic region. To limit the migration of the assay compounds between the droplets, a logD value between approx. - 1.5 to - 2.0 was estimated by Woronoff *et al.*¹⁷⁸ With this clear target in mind, we departed on the synthesis of water-soluble NBD-H analogs.

C I.5 Part V – Improving the water solubility of assay compounds for carbonyl detection

C I.5.1 Nitrobenzoxadiazole (NBD) reagents

Several groups already incorporated modifications into the NBD core to either improve its stability, change its optical properties, or affects its reactivity^{124,232-234}. Although some efforts were undertaken to improve its water solubility²³⁵, these were used for the corresponding thiol-sensing aryl chloride **[96]** isolated as TFA salt after preparative HPLC purification. As this structure represented a possible intermediate for the corresponding hydrazine **[111]** applying a similar synthetic methodology as in C I.4, we opted to follow up on their strategy. In their study, the introduction of quaternary ammonium salts was enabled using a sulfonamide bridge that was incorporated *via* the respective sulfonyl chloride (Scheme 84).

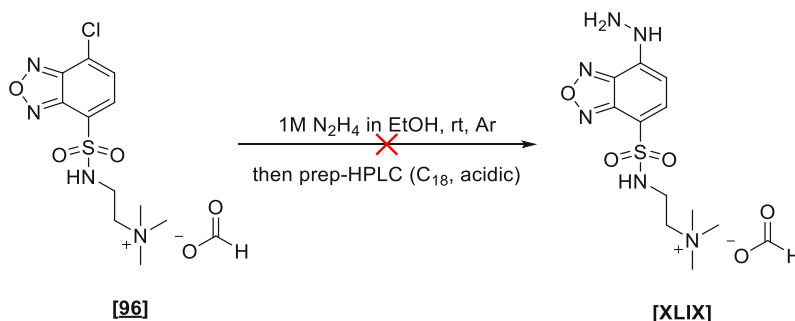


Scheme 84: Identical synthetic approach from Masuda *et al.* for the synthesis of aryl-chloride **[96]**.²³⁵

The synthesis of the NBD-sulfonyl chloride **[94]** was performed *via* an electrophilic aromatic substitution using chlorosulfonic acid as a reagent and solvent. This method enabled the synthesis of the product, albeit its electron deficiency, in 83 % yield as a single regioisomer. The sulfonyl chloride could be isolated without additional purification after extraction in excellent purity. The introduction of the quaternary ammonium salt was first envisioned *via* (2-aminoethyl)trimethylammonium chloride hydrochloride **[95]** in a simple condensation reaction described in the abovementioned literature²³⁵. As the water was necessarily used as a co-solvent to achieve substantial dissolution of the ammonium salt, a copious amount of sulfonic acid hydrolysis (> 50 %) product was always observed. The side-product proved to be impossible to be removed *via* standard column chromatography or recrystallization. Only after tedious optimization using the in-house preparative HPLC system a sufficient separation was enabled on a C_{18} column resulting in a mediocre yield of 19 %. Any attempts to exclude water for this transformation by employing different solvents led either to no conversions (dioxan, MeNO_2) or complete decompositions (DMSO, DMF, DMA, pyridine). Although experiments to limit the amount of water was performed, a decrease, unfortunately, scaled with the speed of the reaction, making the elimination of water impractical.

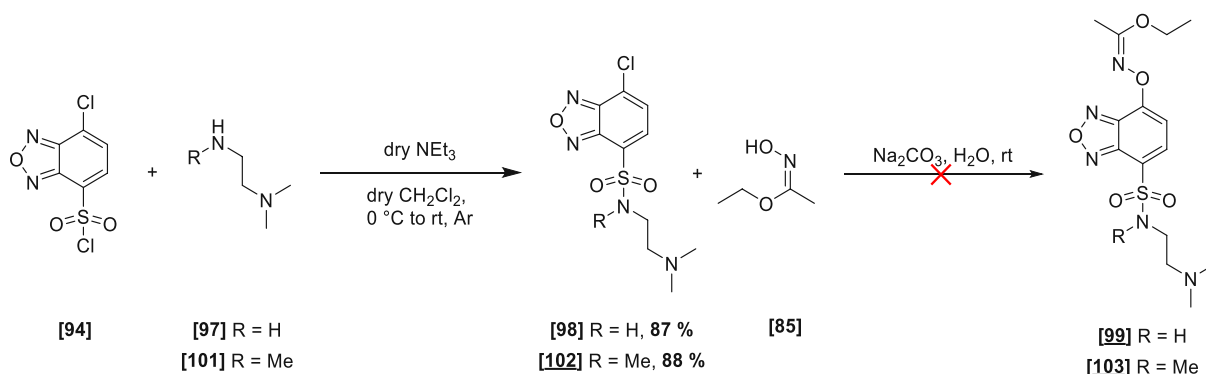
With the quaternary ammonium salt in hand, hydrazine formation was attempted employing the same conditions as for the NBD-H **[78]** case using hydrazine hydrate. Due to the low solubility of the starting material in apolar solvents, reactions employing $\text{MeOH}/\text{CHCl}_3$ mixtures were too slow. Omitting any co-solvent and performing the reactions in pure MeOH led to complete conversion overnight, albeit

with a dramatic loss in product signal over the course of the reaction observed *via* the HPLC-MS. Interestingly in these reactions also hydrolysis to the sulfonic acid could be observed. Removal of the solvent *in vacuo* and purification of the target mass *via* preparative HPLC (C₁₈, acidic conditions; compound eluted in the injection peak) only led to the recovery of highly decomposed material. HPLC-MS traces additionally indicated further decomposition during the removal of the solvent. We thus opted to perform the reaction in 1 M ethanolic N₂H₄ under inert conditions, which drastically improved the performance and cleanness of the reaction (Scheme 85). Complete conversion towards [XLIX] was confirmed by HPLC-MS overnight.



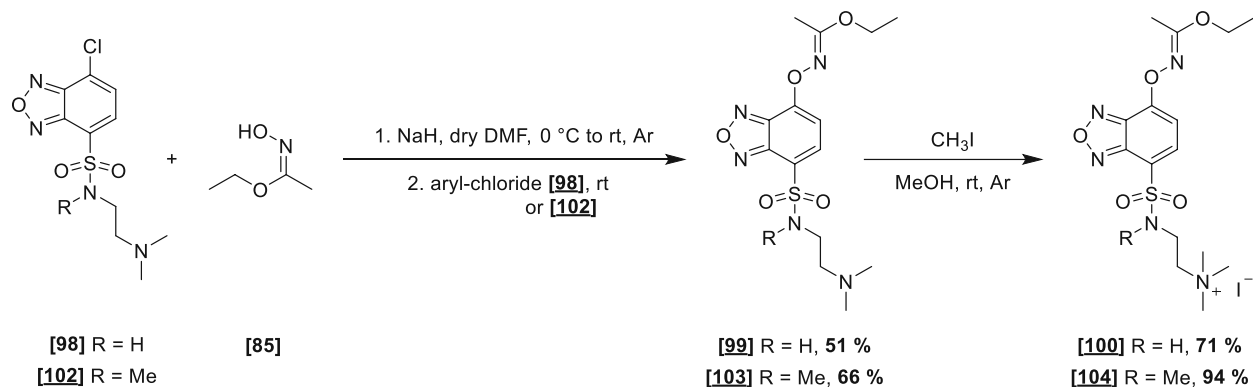
Scheme 85: Failed synthesis of [XLIX] due to its increased instability detected during preparative HPLC runs.

However, any attempts at purification of the product *via* preparative HPLC pointed to the high instability of the product as repeated injections of the fully converted material yielded continuously less signal in the chromatogram traces. Furthermore, NMR spectra of the pooled fractions after removal of MeOH at the rotavap and lyophilization of bulk water revealed complete decomposition of the product. Further literature search prompted us to believe that a possible photochemical instability of the furazan ring resulted in the rapid decomposition of these compounds. This would also align with the previously mentioned instability of the NBD-H reagent [78] (see Fig. 40). Replacement of the oxygen in the ring by sulfur or selenium was believed to improve the stability of the assay compounds.²³⁴ However, as this instability was only evident for the to-date synthesized hydrazines [78] and [XLIX] and could not generally be traced back to the furazan moiety, we still pursued the synthesis of the quaternary ammonium amine-oxy derivative [L] (see below) as the optical properties of this derivative were still unknown. Due to the problematic direct introduction of the quaternary ammonium functionality, we adapted the synthesis to a stepwise approach. Herein the sulfonyl chloride [94] was first trapped by the respective amines [97] / [101] and only ultimately methylated with methyl iodide. This method allowed for the intermediate introduction of the amino-oxy functionality and omitted any problems resulting from the purification of ionic intermediates.



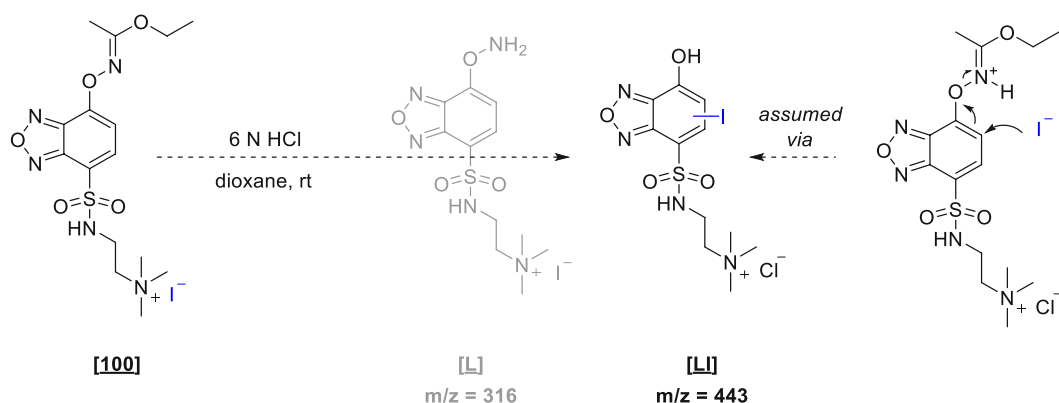
Scheme 86: Synthesis of the sulfonamide bridge by classical nucleophilic substitution. Further incorporation of the amino-oxy handle failed.

As these aryl-chlorides readily react with nucleophiles *via* aromatic substitution, the addition of the amines [97] / [101] was performed at 0 °C with minimal excess (Scheme 86). Both a primary and secondary amines were chosen to study their impact on the respective sulfonamide stability. Luckily facile isolation of these products [98] and [102] was rendered possible due to their precipitation in CH₂Cl₂. Using the identical conditions for the formation of the protected amino-oxy products as used before (*c.f.* [86]), however, did not lead to any noticeable conversion of starting material. Hence a different literature approach²³⁶ was employed where ethyl-N-hydroxyacetimidate [85] was initially deprotonated with NaH followed by the subsequent addition of the aryl chlorides (Scheme 87).



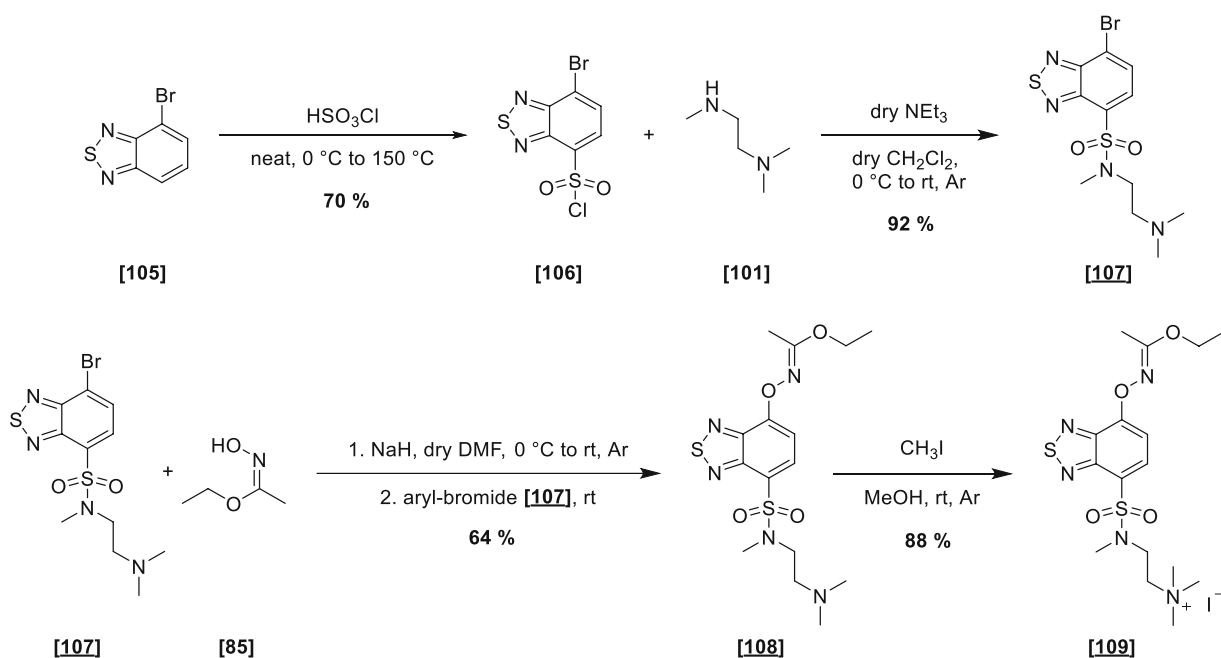
Scheme 87: Synthesis of acetimidates [100] and [104]. Methylated sulfonamide analogs [103] and [104] generally showed cleaner transformations than their non-methylated analog.

As the sulfonamide functionality of [98] was readily deprotonated under these conditions, 2.5 equivalents of the amine-oxy donor had to be used for this step. Extractive workup and column chromatography delivered both protected products in 51 % and 66 %, respectively. Herein methylated compound [103] proved to be formed much cleaner as judged from crude TLC analysis. Before the final deprotection, the acetimidates [99] and [103] were methylated employing methyl iodide in MeOH.²³⁷ Immediate precipitation of the ionic compounds and collection by suction filtration yielded the products [100] and [104] in 71 % and 94 % (Scheme 87). Likewise, during this step, improved yields were observed for the methylated product. Subsequent deprotection of [100] was attempted employing 6 N HCl in dioxane according to a literature report²³⁸ which caused immediate very clean peak to peak transformation towards an unidentified, unexpectedly heavier side-product (Scheme 88). A premature belief that the product was the desired target [L] with unidentifiable adduct formation during the UHPLC-MS runs was quickly abandoned. Isolation of the side-product was made possible by employing the preparative HPLC and was ultimately identified as the iodinated phenol [LI]. ¹H-NMR further confirmed the surprising iodination by the counterion as one of the aromatic proton signals disappeared, and the heavy atom effect of the iodide became evident. Unfortunately, exact determination of the substitution position of the iodide could not be established with the NMR analytics, but an acid-catalyzed ortho-attack as depicted in Scheme 88 seemed plausible. Due to the advanced state of the synthesis of the benzothiadiazole derivate (see below) at that time, further deprotection studies were only performed on the sulfur analog [109].



Scheme 88: Failed deprotection of acetimidate **[100]** by treatment with 6 N HCl. The reaction caused immediate transformation to the iodo-phenol species **[LI]** by presumable nucleophilic attack of the counterion with concomitant cleavage of the acetimidate and subsequent re-aromatization.

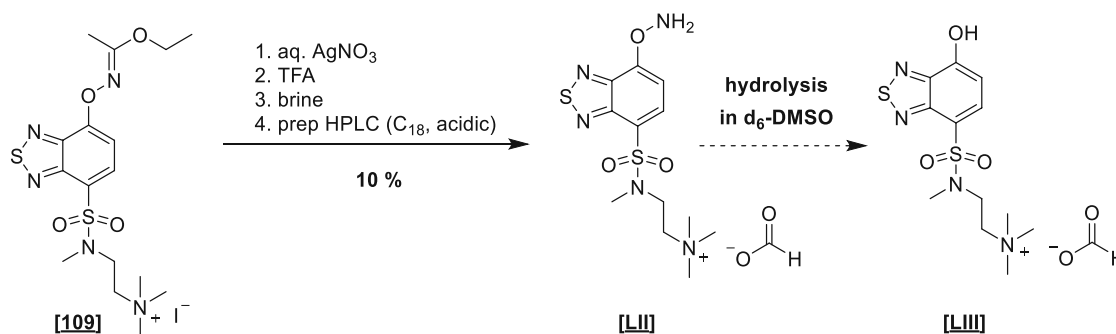
The synthesis of benzothiadiazole hydrazine and the amino-oxy assay compounds was commenced similarly from the commercially available 4-bromo-2,1,3-benzothiadiazole **[105]**. All further steps were performed in accordance with the benzoxadiazole series (*c.f.* C I.4), starting with the chlorosulfonation yielding the product **[106]** in 70 % yield. Due to the previous experience with the amine linker, only the methylated analog **[107]** using **[101]** was synthesized. Subsequent installation of the amino-oxy donor and methylation yielded the sulfur analog **[109]** (Scheme 89).



Scheme 89: Synthetic route towards sulfur-acetimidate analog **[109]**.

Due to the now known interference of the iodide counterion, several attempts to hinder its attack were undertaken. In the case of intermediately formed iodine caused the side-reaction, all further procedures were performed in brown-glass vials and under an inert atmosphere which had no impact on the outcome of the reaction. Interestingly switching from HCl to 50 % TFA (1:1) improved the conversion towards the desired product, albeit showing additional signs of hydrolysis. After 10 minutes upon fast addition of the TFA to the aqueous solution, HPLC-MS showed nearly complete consumption of the starting material with minimal iodide species formation. However, removal of the bulk TFA on the

rotavap in the dark triggered immediate iodination and several unidentified side reactions. With this finding, the formation of the iodide was found to be irrespective of the progress of the cleavage reaction and had to be suppressed from the beginning. This was achieved with the use of 2 equivalents of aqueous AgNO_3 prior to any addition of acid. Here the iodide was immediately trapped as insoluble silver salt and could therefore not participate as a nucleophile. Subsequent addition of 50 equivalents of TFA cleanly converted the product to the corresponding amino-oxy compound overnight at room temperature. In several cases where the reaction proceeded very slowly, NMP was added as a co-solvent. Upon confirmation of complete conversion, the precipitated AgI was removed by syringe filtration, and the reaction was lyophilized. The lyophilization proved to be unfortunately detrimental as again strong decomposition and formation of several unidentified masses were evident. We thus opted to purify the reaction mixture with the preparative HPLC system immediately. To limit contamination of the mass spectrometer with Ag-salts, the excess Ag^+ was precipitated with 2 equivalents of sat. NaCl after the complete conversion had been confirmed by HPLC-MS. The resulting suspension was syringe filtered and subjected to the preparative column chromatography using the C_{18} column with acidic conditions.



Scheme 90: Synthetic strategy to overcome the nucleophilic iodide attack on the aromatic ring. Iodide was trapped as insoluble AgI and was thus removed as reactive species. Subsequent cleavage was triggered by TFA. Removal of residual Ag^+ to limit contaminations of the preparative HPLC was enabled by precipitation with brine and subsequent syringe filtration. Amine-oxy compound [LII] showed dramatic hydrolytic instability, as complete cleavage of the reactive group was evident in the NMR tube overnight.

Gratifyingly, collection of product fractions and subsequent lyophilization yielded 10 % pure product [LII] judged by ^1H -NMR-analysis. (Scheme 90) Additional NMR experiments on the following day, however, revealed a substantial shift in the aromatic region. Furthermore, the signal corresponding to the NH_2 -group had completely disappeared, which meant that the amino-oxy group had been seemingly cleaved, forming phenol [LIII]. HPLC-MS confirmed the complete hydrolysis of the product in deuterated d_6 -DMSO (Fig. 59). Puzzled by these results we speculated, that neutral conditions might be already sufficient enough to cleave the reactive handle. Due to these complications, we opted not to invest any more time to elaborate the limits of this compound [109].

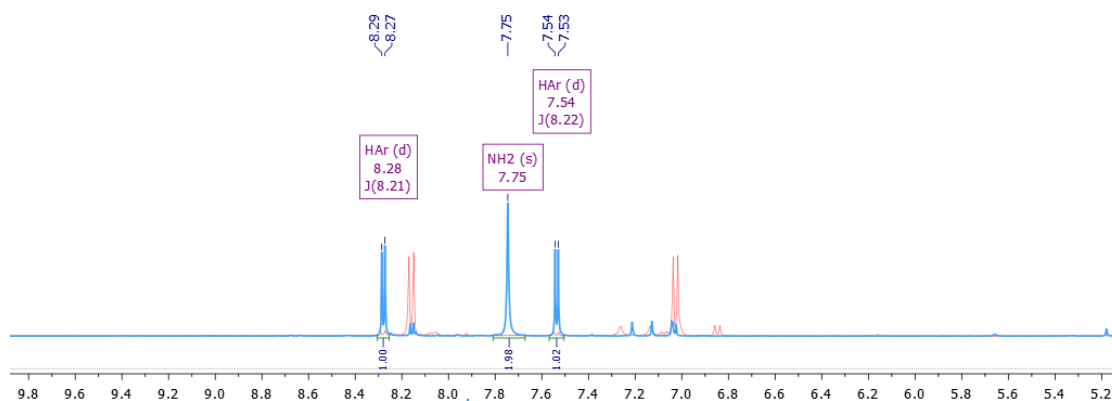
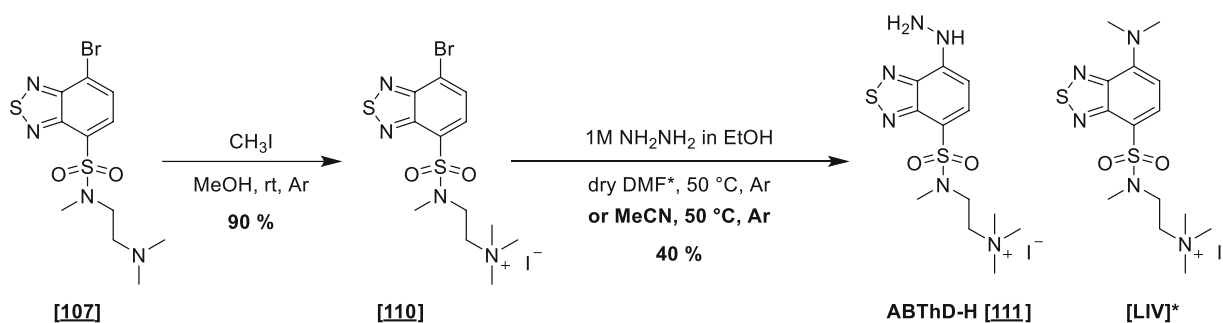


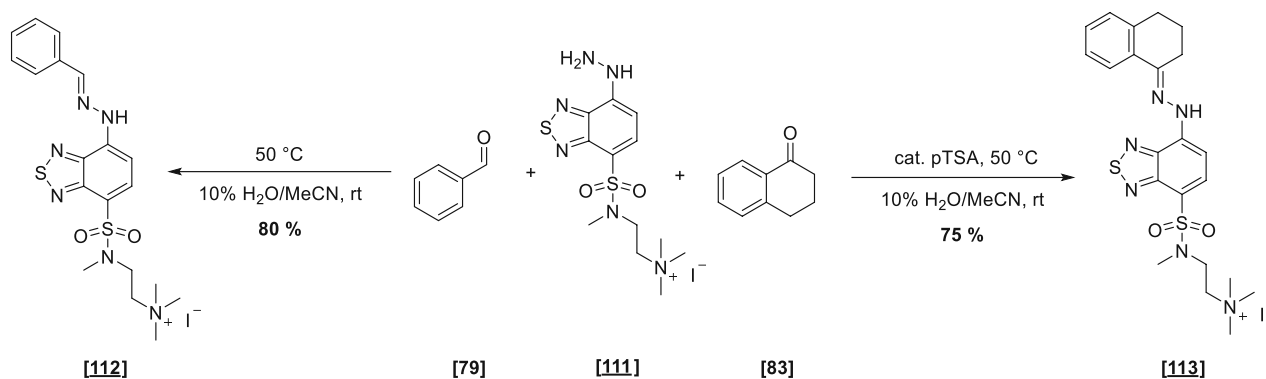
Fig. 59: $^1\text{H-NMR}$ comparison of the aromatic region of **[LII]** in $d_6\text{-DMSO}$ immediately upon isolation (blue) and upon storage in the NMR tube overnight (red): Loss of NH_2 signal, as well a shift of aromatic signals, confirmed the cleavage of the amino-oxy group.

As the corresponding hydrazine was the original target of this investigation, the synthesis was retraced back a few steps to the tertiary amine **[107]**, which was reacted with methyl iodide. The collected yellow ammonium salt **[110]** was subsequently treated with 1M ethanolic NH_2NH_2 (Scheme 91). However, due to the insolubility of the compound in alcoholic solvents, the addition of DMF and a minimal increase in temperature were needed to sufficiently solubilize all components. HPLC-MS confirmed clean conversion to the product overnight, but also the formation of a dimethylamine adduct **[LIV]**. The side-product resulted from residual dimethylamine originating from DMF production, which was immediately trapped by the aryl bromide **[110]**. These compounds have been readily studied as amine and thiol probes and exhibit an increased reactivity towards strong nucleophiles. Repetition of the synthesis in MeCN eliminated any side-product formation and cleanly delivered the hydrazine. Cooling of the reaction solution in the $-20\text{ }^\circ\text{C}$ freezer overnight caused crystallization of deep orange crystals, which yielded the hydrazine **[111]** in 40 % yield upon filtration. Interestingly the dynamic equilibrium observed for the NBD-H **[78]** was not present here anymore.



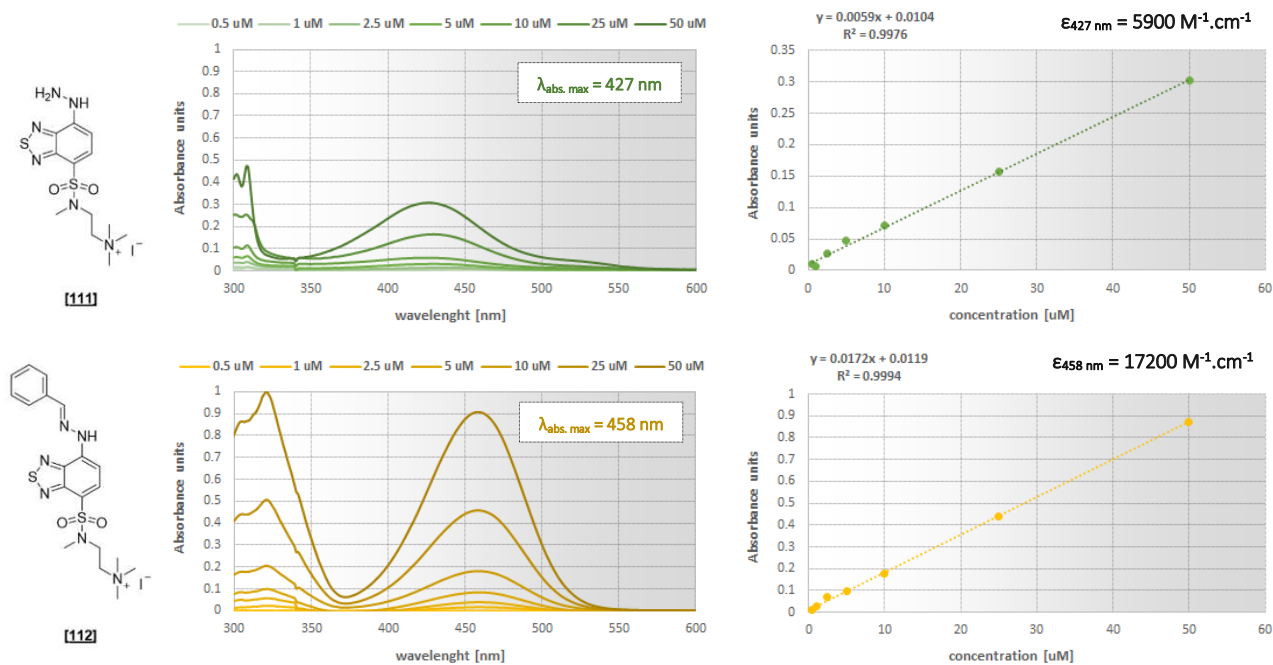
Scheme 91: Synthesis route towards **[111]**. *Nucleophilic substitution in DMF caused the formation of **[LIV]** by trapping of residual dimethylamine contained in all commercial DMF samples (not isolated).

With the desired hydrazine **[111]** in hands, adduct formations with benzaldehyde **[79]** and tetralone **[83]** were performed in MeCN (Scheme 92). Due to the highly polar, ionic character of the reactants, small amounts of water were necessary to solubilize the reaction mixture. A minimal increase in temperature facilitated a clean formation of the respective hydrazones in below one hour. Similar to the NBD-H adduct formations with aryl-ketones, catalytic amounts of PTSA were added to accelerate the reaction in the tetralone reaction. Precipitation of products in Et_2O enabled unproblematic isolation of the desired adducts **[112]** and **[113]** in 80 % and 75 %, respectively.



Scheme 92: Synthesis of ABThD-conjugates **[112]** and **[113]**.

UV spectra of the ammonium salts (ABThD – ammonium benzothiazdiazoles) revealed some differences compared to the parent NBD-H compounds. Whereas the unreacted hydrazine **[111]** exhibited a 50 nm red-shift of the absorption maximum compared to the parent NBD-H **[78]** (*c.f.* Fig. 39 and Fig. 60, 427 nm vs. 377 nm) and was shown to be about 4.5x less absorbent, the adducts, unfortunately, did not share this shift in the absorbance spectra. Both adducts were about 50 nm less red-shifted than their respective NBD-adduct analogs (*c.f.* Fig. 39 and Fig. 60, 510 nm vs. 460 nm). While a decrease in the spectral shift between the unreacted and condensed form generally negatively impacted a possible application in an assay format, the concomitant reduction of the absorption coefficient of **[111]** proved to be advantageous due to lesser reabsorption of the signal by the unreacted reagent.



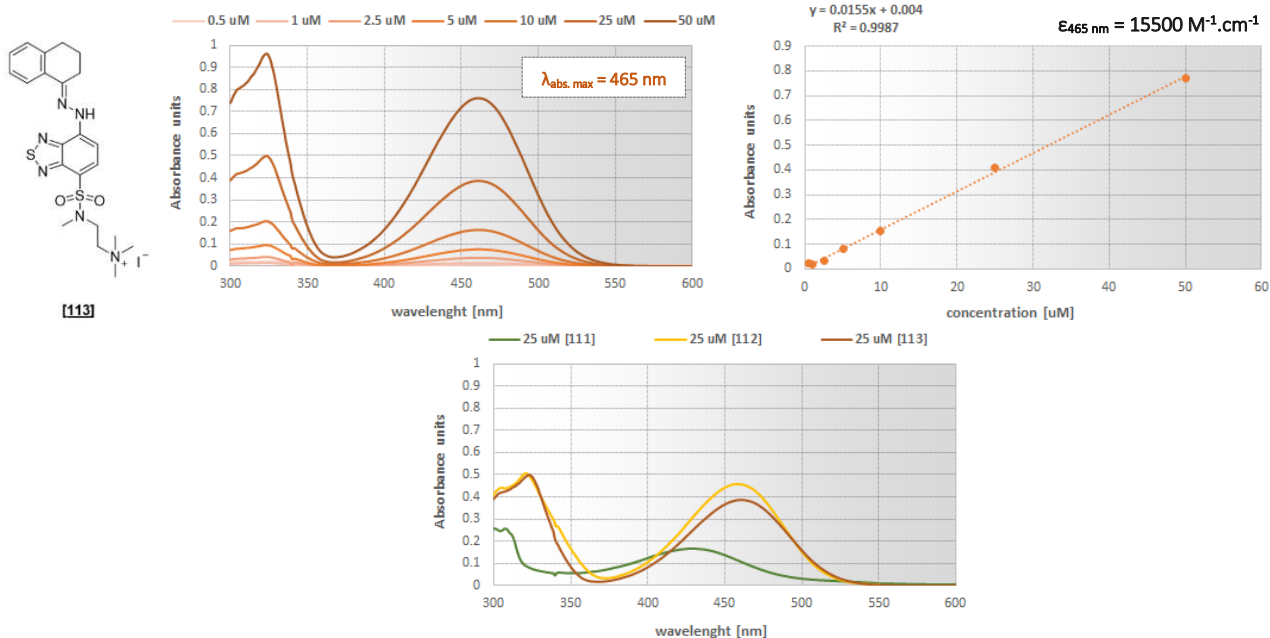


Fig. 60: UV-absorption calibrations of ABThD-H [111] and its benzaldehyde and tetralone conjugates [112] / [113]: Measurements reveal a small red-shift of the absorption max. from 427 nm to approx. 460 nm upon conjugation. ABThD-H [111] was shown to be less absorptive by a factor of 3 compared to its conjugates. All spectra were recorded in 100 mM pH 4.5 Na-citrate buffer, 5 vol% DMSO, 0.2 vol% Triton X-100.

Due to a similarly beneficial impact of the surfactants (not shown) on the ABThD-adduct fluorescence and for the sake of comparability, all fluorescence spectra were measured in the identical medium as for the NBD case (Fig. 61). Interestingly for the benzaldehyde adduct [112], the excitation maximum did not match the absorption maximum and was approx. 20 nm red-shifted from 458 to 480 nm. Hence a slightly broader linear range could be measured due to the reduced inner-filter effect than the tetralone adduct [113].

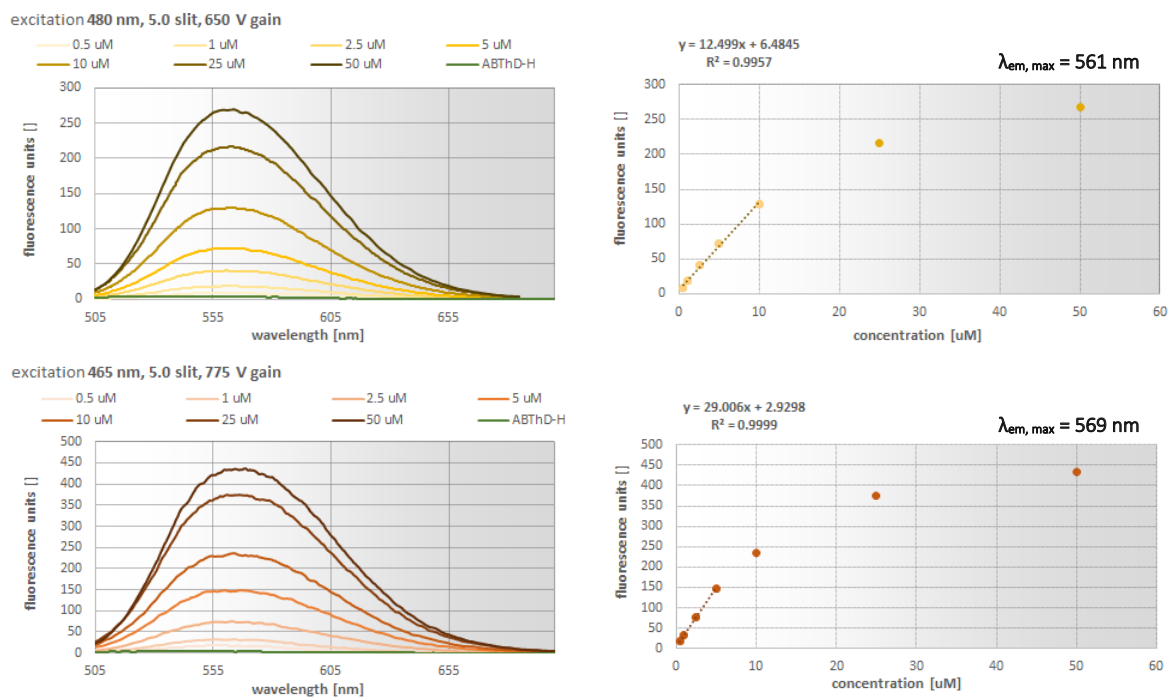
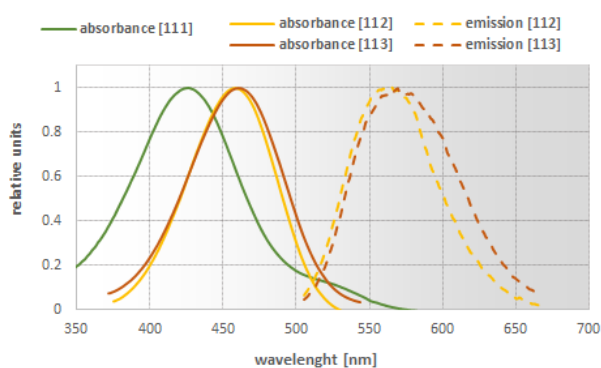


Fig. 61: Fluorescence calibrations of [112] and [113]: Excitations at either 480 nm and 465 nm caused a strong fluorescence emission with a $\lambda_{\text{em, max}}$ at 561 nm and 569 nm, respectively. Both adducts exhibited linear ranges up to 5 μM , whereas benzaldehyde conjugate [112] could expand its linearity due to a red-shift excitation maximum (compared to its absorption maximum at 458 nm). All spectra were recorded in 100 mM pH 4.5 Na-citrate buffer, 5 vol% DMSO, 0.2 vol% Triton X-100; excitation wavelengths 480 nm, 5.0 nm slit, 650 V gain, and 465 nm 5.0 nm slit, 775 V gain, respectively.

Similar to [80], the benzaldehyde-adduct [112] proved to be several factors brighter than its tetralone conjugate (Table 6). Furthermore, both ABThD-adducts exhibited similar fluorescence properties with their emission maxima at 561 nm and 569 nm, respectively, compared to their NBD-H counterparts at 560 and 582 nm. Most notably was the unchanged non-fluorescent nature of the ABThD-H [111] itself, which only exhibited a dramatic increase in fluorescence upon carbonyl conjugation. Hence, the substitution of the strong electron-withdrawing nitro-group by the sulfonamide bridge kept its properties intact. Unfortunately, this exchange was accompanied by a slight loss of fluorescence yield and brightness (see. Table 6).

Table 6: Summary of structural and optical properties of the substances used in this study. Comparison of ABThD-H [111] absorption and benzaldehyde [112] tetralone conjugate [113] product and Stokes shifts. Absolute absorbance and emission values are normalized on their maximal values. n.a. – not available.

	M [g.mol ⁻¹]	$\lambda_{\text{abs, max}}$ [nm]	ϵ [cm ⁻¹ .M ⁻¹]	$\lambda_{\text{em, max}}$ [nm]	ϕ_f (rhodamine B)	brightness
ABThD-H [111]	472.36	427	5900	n.a.	n.a.	n.a.
benzaldehyde-ABThD-H [112]	560.47	458	17200	561	0.031	533
tetralone-ABThD-H [113]	600.54	465	15500	569	0.012	186



With the general features for the system established, stability experiments were performed and revealed the envisioned increased instability, as the absorbance spectrum remained practically unchanged over the course of 24 hours (Fig. 62). Only a minimal change could be detected in the first 60 minutes upon dissolution in the buffer system. This effect was also observed for its fluorescence spectra, where after a distinct rapid increase in fluorescence emission, the signal plateaued out. As the fluorescence signal remained steady after this initial surge, we speculated that the already for the NBD-H [78] assumed equilibrium could be responsible for this effect but that the reagent remained stable over prolonged periods of time.

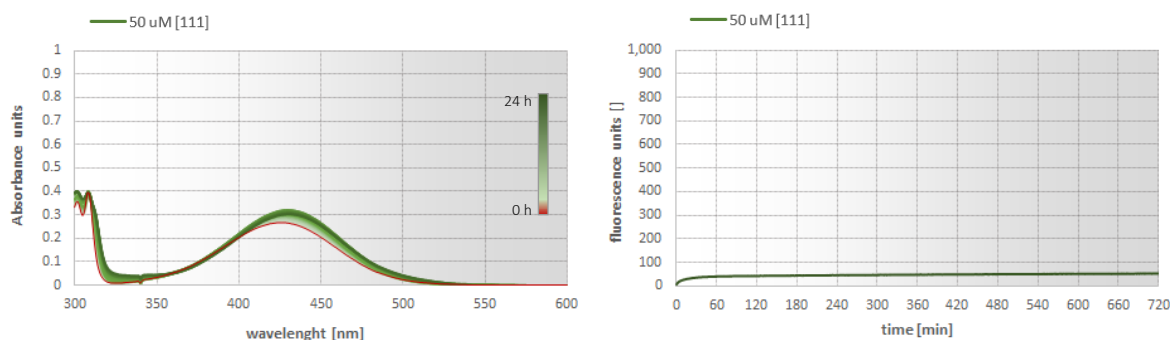


Fig. 62: UV-absorbance and fluorescence stability evaluation of ABThD-H [111] at 50 μM concentration. Both measurements revealed a minimal change of its optical properties in the first 60 minutes, detectable by a slight increase in absorption and emission upon dissolution. Subsequent plateauing of the signal confirmed the indefinite stability of the reagent in the tested conditions. Kinetics were recorded in pH 4.5 Na-citrate buffer, 5 vol% DMSO and 0.2 vol% Triton X-100. UV measurements were performed in 10-minute intervals. Fluorescence spectra were recorded using an excitation wavelength of 480 nm, emission wavelength of 560 nm, 5.0 nm slit, 775 V gain, 1-minute intervals.

With these promising stability results, we turned to the kinetic measurements employing these two substrates (Fig. 63). To decrease a possible spectral overlap between ABThD-H [111] and its products, all measurements were performed at 515 nm and not at their respective absorption maxima using once again 500 μM of the reagent. Due to the slow nature of the reaction employing tetralone [83], the abovementioned initial rise in signal had a dramatic effect on the kinetic data. Subtraction of the blank from the target reactions showed an interesting feature of the adduct formation. Herein a complete decoupling from the tetralone concentration could be observed, which was in contrast to the NBD-H reagent [78] (at least for the tetralone conjugation).

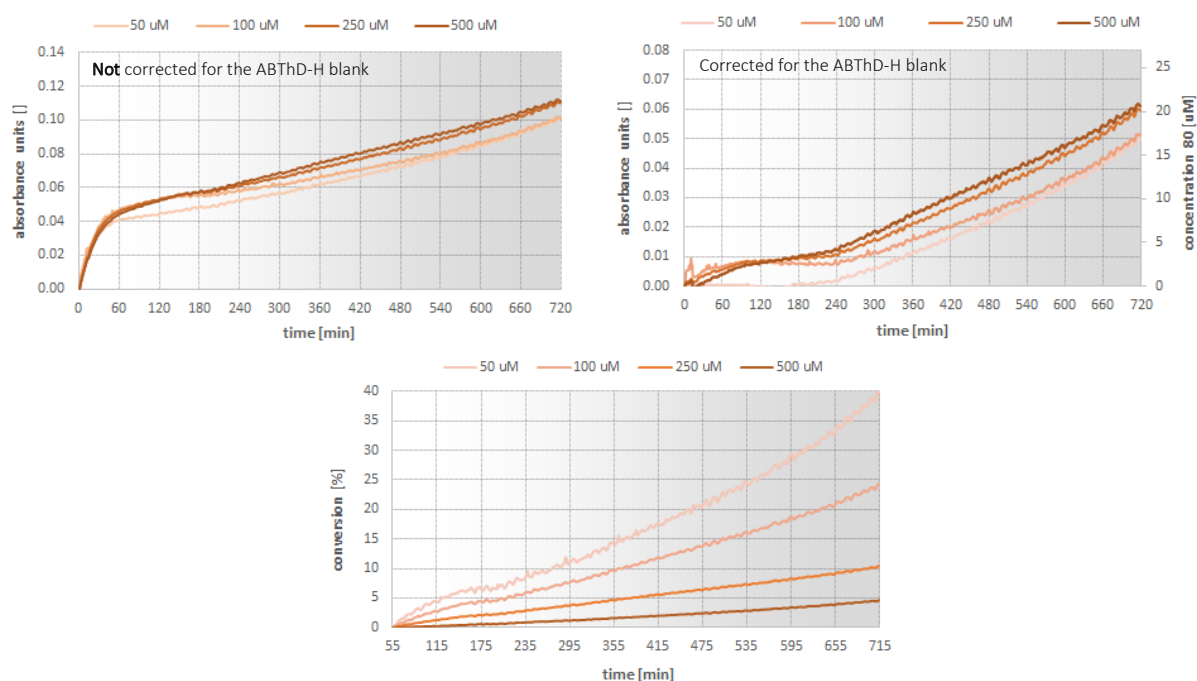


Fig. 63: UV-absorption kinetic studies of the formation of the tetralone conjugate [113] using 500 μM ABThD-H [111] and 50-500 μM tetralone [83] concentrations at 515 nm absorption – *left*: Increase of absorbance units over time – blank was not subtracted to show the steep increase of absorbance in the first 60 minutes; *right*: Corrected values for the absorbance units over time depicting a linear increase of signal over time; *bottom*: Calculated conversions over time using the in Fig. 60 determined calibrations at 515 nm. To enable a better comparison, the initial 55 minutes of the reaction were excluded, and all traces were aligned. Kinetics were recorded in 100 mM pH 4.5 Na-citrate buffer, 5 vol% DMSO, 0.2 vol% Triton X-100, 1-minute intervals. Left and bottom kinetics were corrected for 500 μM ABThD-H [111] blank.

This observation suggested that for small tetralone concentrations, higher percentual conversions to the adduct would be reached in a faster timeframe. For comparison reasons, if the first 55 minutes of the reaction were excluded and all traces were aligned, the total conversion of tetralone

for the 50 μM case would reach approx. 40 % after 12 hours. This would represent a dramatic increase in reaction kinetics for the aryl-ketone adduct formation. Looking at the 500 μM case, however, only a minimal difference could be detected in comparison to the NBD-H case as for both reactions, the yield did not increase past the 5-10 % mark after 12 hours. As these results still did not classify for acceptable use in an assay format, no further investigations were performed for the tetralone conjugation. These results could, however, represent a possible starting point for further investigations with the employment of aniline catalysts and other auxiliaries (different buffer, increased salt concentration that might proliferate the reaction (*c.f.* B III.1.1.1). These studies are still ongoing research within the group.

Due to the growing interest in the group for aldehyde-selective assays, the application for the screening with benzaldehyde was given greater importance. Similarly, for the NBD-H reactions, a dramatic increase in reactivity towards benzaldehyde was immediately evident. A direct comparison of the tetralone and benzaldehyde reactions at 500 μM ABThD-H concentration resulted in a dramatic 1000x fold increase in reaction speed for the initial kinetics (Fig. 64).

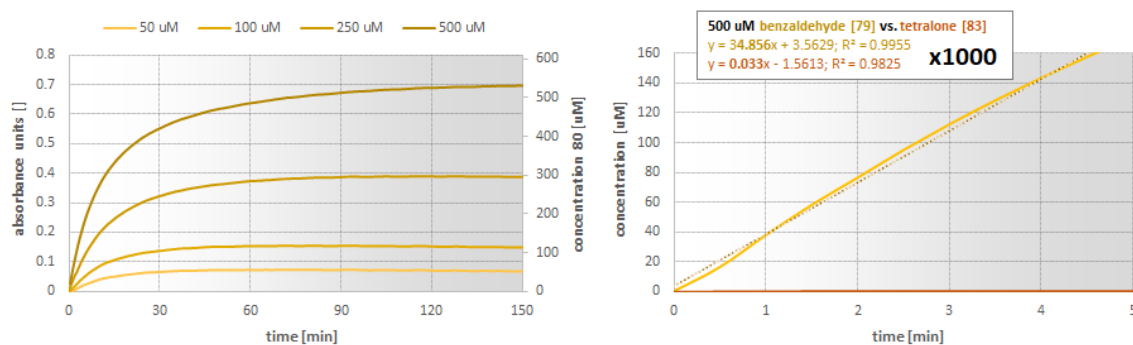


Fig. 64 - left: UV-absorption kinetic studies of the formation of the benzaldehyde conjugate [112] using 500 μM ABThD-H [111] and 50-500 μM benzaldehyde [79] concentrations at 515 nm absorption; **right:** Comparison of initial kinetics of the 500 μM benzaldehyde [79] and tetralone [83] conjugations using the first 5 minutes of reaction time – respective concentration values were calculated using the in Fig. 60 determined calibrations at 515 nm. Assessment of the slopes revealed an approx. 1000-fold increase in conjugation. Kinetics were recorded in 100 mM pH 4.5 Na-citrate buffer, 5 vol% DMSO, 0.2 vol% Triton X-100, 1-minute intervals.

Additionally, no precipitation occurred even at higher concentrations, which was expected, as the compound exhibited excellent water solubility. Similar to the NBD-H case, the adduct formation was found to strictly follow first-order kinetics, representing an immediate addition, followed by slow rate-determining dehydration (Fig. 65).

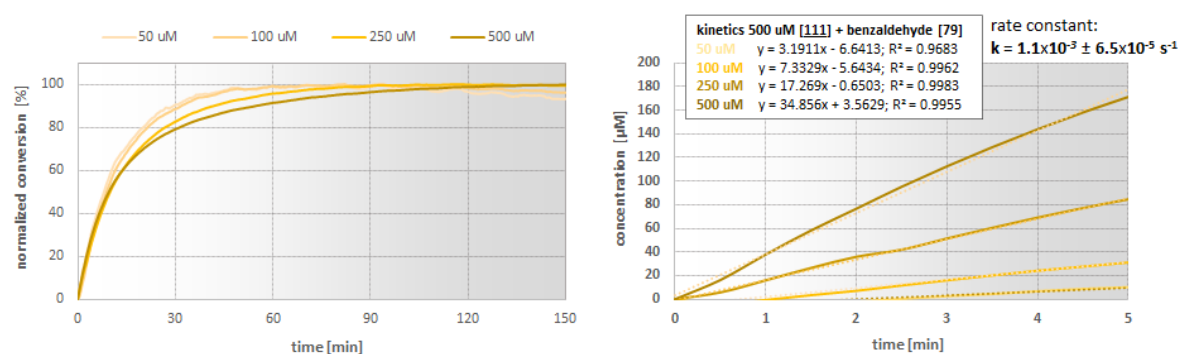


Fig. 65 - left: UV-absorption kinetic studies of the formation of the benzaldehyde conjugate [112] using 500 μM ABThD-H [111] and 50-500 μM benzaldehyde [79] concentrations at 515 nm absorption normalized by the final absorbance values; **right** – initial change of concentrations of benzaldehyde adduct formation – first-order rate constant was calculated to be $1.1 \times 10^{-3} \pm 6.5 \times 10^{-5} \text{ s}^{-1}$. Kinetics were recorded in 100 mM pH 4.5 Na-citrate buffer, 5 vol% DMSO, 0.2 vol% Triton X-100, 1-minute intervals.

Direct comparison of the reaction of benzaldehyde with the NBD-H [78], as well as the ABThD-H [111] reagent, revealed a substantial increase in reactivity for the latter (Fig. 66). The first-order rate constant was determined to be $1.1 \times 10^{-3} \pm 6.5 \times 10^{-5} \text{ s}^{-1}$ representing an approximately 6-fold increase compared to the NBD-H adduct formation. A direct comparison for the tetralone conjugation could not be made, as the kinetical profile did not seem to follow the same pattern. However, looking at the tetralone reactions (*c.f.* Fig. 52 and Fig. 63), the ABThD-H reagent outperformed the NBD-H, especially at low concentrations.

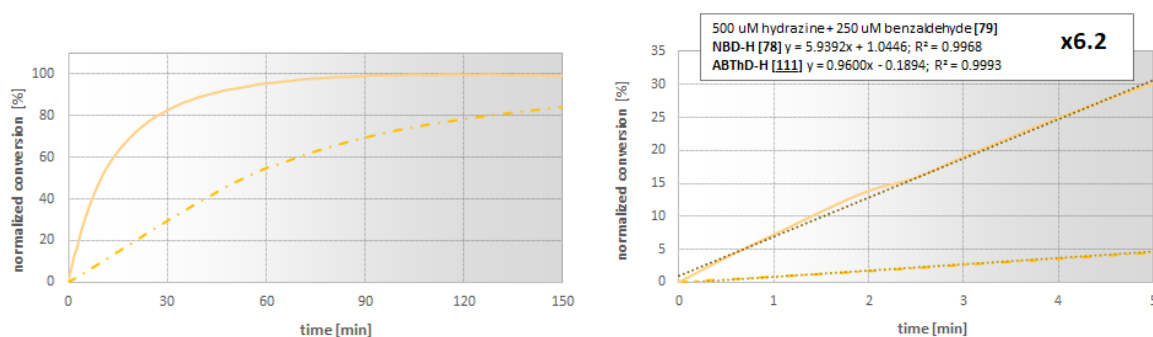


Fig. 66 - left: Comparison of UV-absorption kinetic studies of the formation of the benzaldehyde conjugate [80] (dashed line) / [112] (solid line) using either 500 μM NBD-H [78] or ABThD-H [111] and 250 μM benzaldehyde [79]. Absorbance measurements were performed using either 560 nm or 515 nm and were normalized by the final absorbance values; **right:** Comparison of initial kinetics of the conjugations using the first 5 minutes of the reaction revealed an approx. 6-fold increase in conjugation efficiency of the ABThD-H [111] compared to its NBD-H [78] parent. Kinetics were recorded in 100 mM pH 4.5 Na-citrate buffer, 5 vol% DMSO, 0.2 vol% Triton X-100, 1-minute intervals.

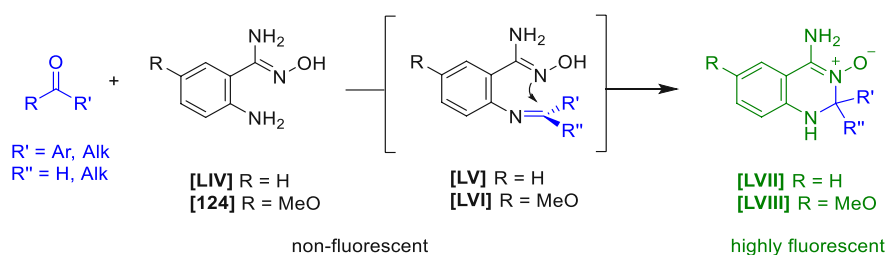
As no further in-depth studies had been performed during this Ph.D., further investigations are needed to elaborate the system's limits. Nevertheless, several improvements could already be achieved during these initial investigations. Firstly, the widely applied NBD-H reagent was transformed into the water-soluble ABThD-H [111] equivalent without dramatic consequences for its fluorogenic behavior. The synthesis was achieved by a simple 4-step cascade, whereas if the initial expendable extraction of the sulfonyl chloride [94] was even omitted, all intermediates could be isolated by precipitation and subsequent suction filtration with an overall yield of 35 % starting from commercial 4-bromo-2,1,3-benzothiadiazole [105]. This simple access to the compound might enable broad accessibility even for the untrained synthetic chemist. Although the original strong absorption red-shift upon conjugation had been lost, the reduced spectral difference only exhibited a limited detrimental impact on the use of the compound in an assay format. Enhancing its stability by incorporating sulfur into the aromatic system further improved its general applicability in long-term experiments.

Moreover, due to the performed modifications of the fluorophore structure, a surprising 6-fold increase in reactivity was enabled, which was typically only achieved with the use of auxiliary catalysts or specific buffer systems. As an additional finding during the exploration of these reagents for carbonyl detection, the use of surfactants (Triton X-100, Tween 20/80) was found to dramatically increase the fluorescence yields of this class of compounds due to the possible formation of micellar systems. One big downside represented their sensitivity of the fluorescence signal to pH. Whereas an increase in the acidity of the buffer system above a certain pH - which was speculated to correlate with the pK_a of the hydrazone - caused a surge in signal, any use in the neutral pH range rendered these reagents practically non-fluorescent. Also, an application of the hydrazone conjugation for the targeted aryl-ketones was unfortunately not made possible, as these carbonyl species were simply too unreactive for rapid

hydrazone conjugations. However, if the limits of these systems were further explored, the general applicability of this tool for the detection of aryl and alkyl-aldehydes could be manifested. Ultimately, however, a major target of this investigation, to enable an application of this hydrazone assay in a FADS format, was achieved.

C 1.5.2 Amino benzamidoxime (ABAO) reagents

The second class of reagents investigated in our research group for selective detection of carbonyl compounds were the so-called ABAO reagents [LV]/[124]. In the postulated mechanism for the assay after an initial attack of the aniline-moiety, the intermediately formed imine is trapped by the nitrogen of the oxime (Scheme 93).¹⁵⁵ The thus formed quinazoline oxides [LVII]/[LVIII] exhibited a substantial shift in absorbance from 360 to 405 nm, as well as the emergence of strong fluorescence at 490 nm.



Scheme 93: Representation of the NBD assay – non-fluorescent amino benzamidoxime ABAO [LV] reacts with an alkyl or aryl-carbonyl species forming highly fluorescent quinazoline oxides.

Kitov and al.¹⁵⁵ were the first to report an in-depth analysis of these detections systems and found an LFER (linear free energy relationship) with the pK_a of the respective anilinium species (Fig. 67). Whereas para-nitro substitution led to a dramatic loss of activity, incorporation of a para-methoxy group dramatically enhanced the conjugation speed. As no accumulation of the resulting Schiff's base [LV] could be found in their NMR experiments, they postulated the formation of the Schiffs-base to represent the rate-determining step.

The ABAO [LV] as well as its methoxy variant [124] had been extensively used in our research group for the detection of the open-chain content of aldoses²³⁹ as well as for preliminary mutational studies for the evolution of carboxylic acid reductases.^{62,67} However, both approaches were based upon an absorbance assay employing either well-plate systems or sophisticated robotic platforms. Due to the interest for further applications in a fluorescence-activated droplet sorting format, we speculated if any modifications to the ABAO structure were possible that would increase its water solubility and concomitantly would not interfere with its native activity.

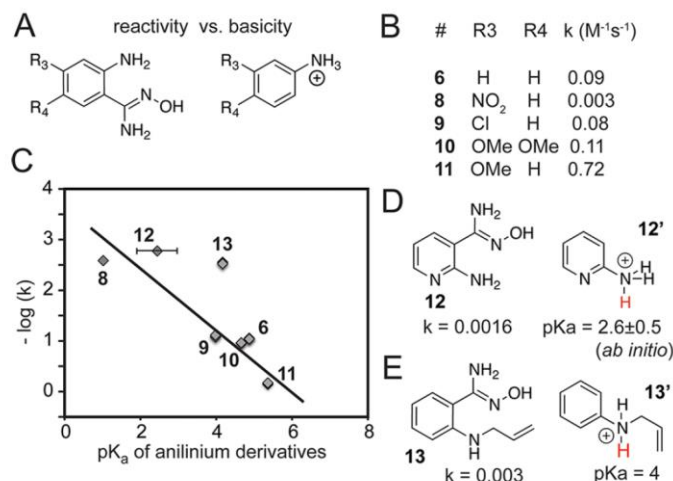


Fig. 67 - LFER (linear free energy relationship) established by Kitov and al.¹⁵⁵ highlighting the importance of electron-donating functionality para to the amino group of the respective ABAO-reagents. (Quelle)

As the MeO-ABAO **[124]** showed a dramatic increase in reactivity compared to its parent compound, we opted to focus our synthetic efforts on its derivatives. To limit any steric impact on the conjugation, a single position of the aromatic core was deemed accessible for modifications. As already mentioned, LogP/D values below -1.50 were deemed to be compatible with a FADS assay by impairing the transport out of the droplets.

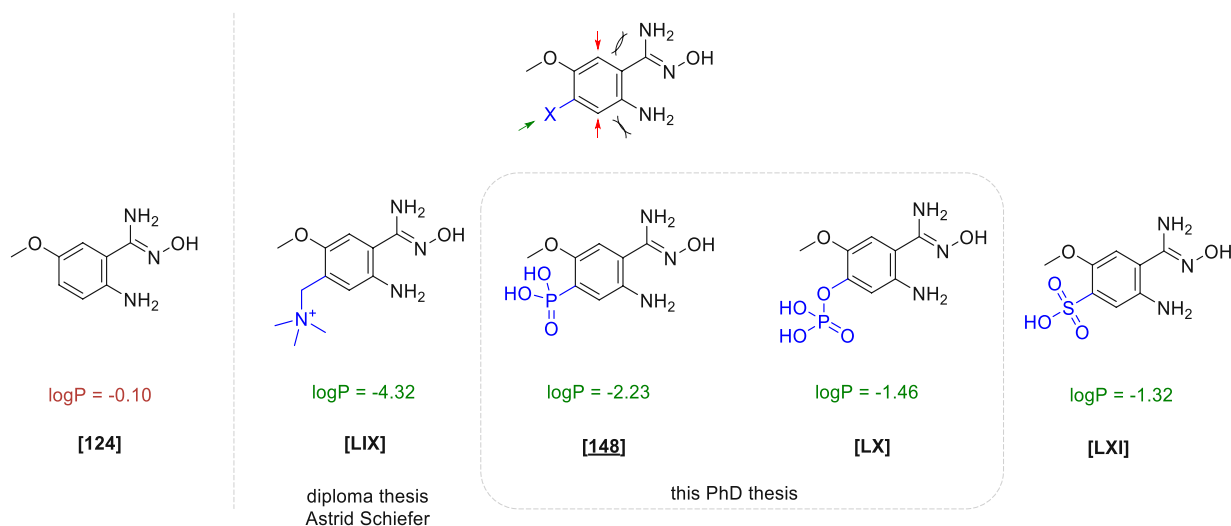
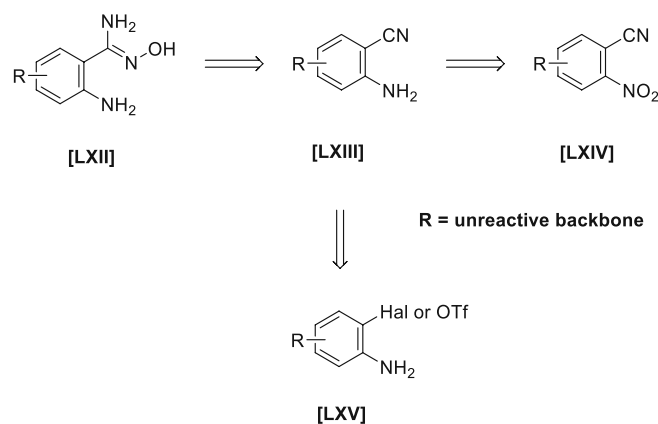


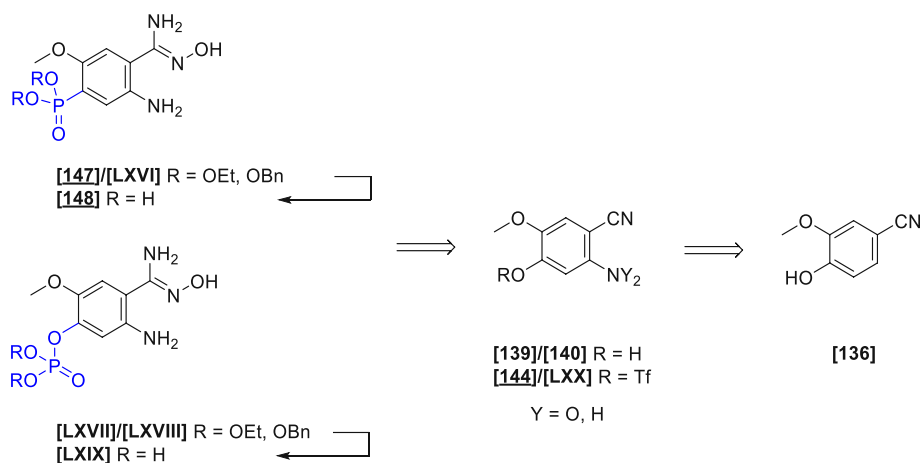
Fig. 68 - Comparison of the calculated LogP values of the parent MeO-ABAO **[LVI]** and several highly water-soluble analogs substituted at the desired position (green arrow) to limit the possible sterical impact of the hydrophilic handle with the ABAO moiety (red arrows). Synthesis of quaternary ammonium analog **[LX]** was attempted in the diploma thesis of Astrid Schiefer. In this work, the focus was placed on the remaining phosphonic and phosphoric acid analogs **[148]** and **[LXI]**. logP values were calculated using the ChemAxon® Chemicalize logP calculator.

With the comparison of the calculated LogP value for several analogs using the online-tool Chemicalize from ChemAxon®, we opted to pursue the synthesis of the more hydrophilic phosphorous analogs **[148]** and **[LX]** and the quaternary ammonium compound **[LIX]** (Fig. 68). The synthetic efforts towards the latter are discussed in the diploma thesis of Astrid Schiefer. The following chapter will focus exclusively on the synthesis and spectroscopic investigation of phosphor-containing ABAO derivatives. Herein all synthetic steps will be discussed prior to any optical analysis.



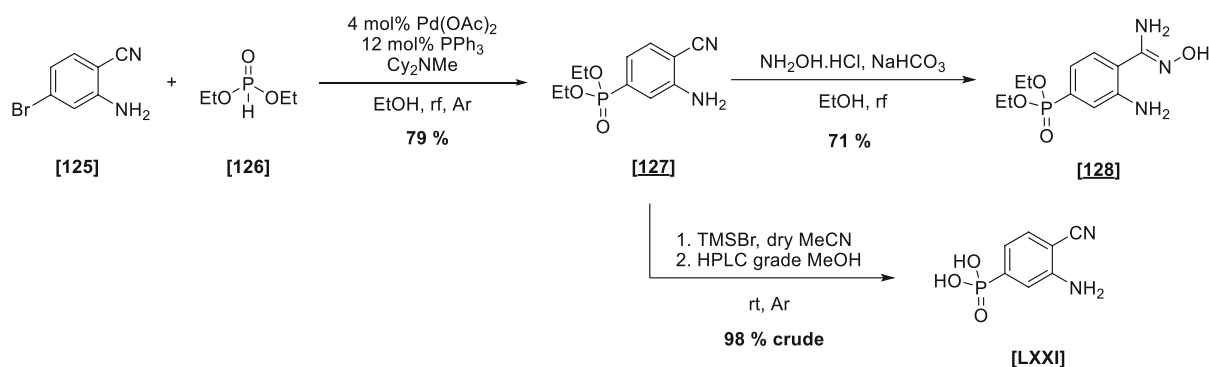
Scheme 94: Retrosynthetic strategy towards ABAO compounds.

Looking at the classic synthetic strategy towards ABAO assay compounds, the amidoxime as the reactive handle was always installed last using a nucleophilic addition of hydroxylamine onto the nitrile [LXIII].⁶² The intermediate [LXIII] could be either derived by a palladium-catalyzed nitrile-coupling²⁴⁰ from [LXV] or by reduction from the corresponding nitro-derivative²⁴¹ [LXIV] (Scheme 94). All these steps were needed to be compatible with either the already installed backbone or the synthetic strategy for the backbone introduction needed to account for the electronic changes of the aromatic core during the respective transformations.



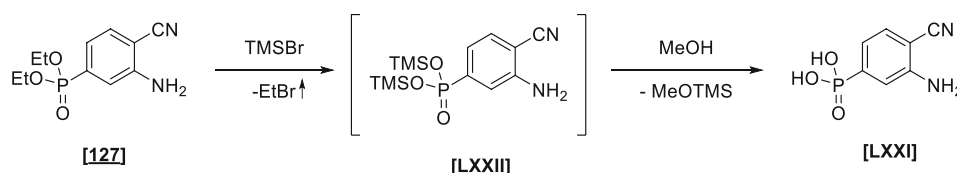
Scheme 95: Retrosynthetic strategy for incorporating phosphinic or phosphoric acid moiety onto the ABAO core leading back to 4-hydroxy-3-methoxybenzonitrile [136].

We thus speculated that both possible products could be traced back to the phenol [136]. A direct introduction of the phosphate, as well as the phosphonic acid group, was envisioned *via* literature known substitution²⁴² or applying a Pd-catalyzed P-C coupling protocol^{243,244} using the triflates [144] or [LXX] (Scheme 95). As the incorporation of these groups was broadly performed in its protected, alkylated forms, subsequent deprotection to the respective acids had to be also investigated. It became quite clear at the beginning that determination of the order of synthetic events would pose the biggest challenge in this study. In this regard also the influence or interference of the oxidation stage of the nitrogen had to be investigated.



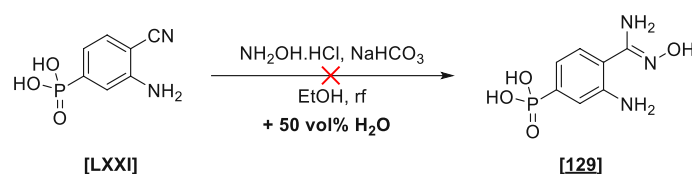
Scheme 96: Synthetic route towards [128] and [LXXI] to elaborate synthetic feasibility of the retrosynthetic strategy.

To understand if the introduction of the phosphonic group exhibited any influence on the subsequent installation of the reactive ABAO-handle, we began our investigation with a commercial substrate [125]. The compound had the presumably more challenging amine functionality already present (Scheme 96). Using known Pd-coupling conditions²⁴⁵, the coupling proceeded without any trouble in 79% yield after column chromatography, albeit the product being contaminated with small amounts of triphenylphosphine oxide (6%), which presumably resulted from oxidation of the ligand during the coupling reaction. We nevertheless proceeded with trial amidoxime [128] formation of the phosphonate employing NH₂OH·HCl in EtOH, which resulted in the isolation of the product in 78% yield. Also, classical deprotection of [127] using TMSBr^{246,247} led to the unproblematic isolation of corresponding acid [LXXI]. The acid was isolated in sufficient purity for subsequent trials.



Scheme 97: Mechanism for the TMSBr induced cleavage of diethyl phosphonate ester by transesterification and subsequent methanolysis.

The mechanism for the latter proceeded *via* the formation of the TMS-phosphinic acid ester [LXXII]²⁴⁶, which was readily cleaved by stirring in methanol (Scheme 97). The thus formed MeOTMS could be removed directly on the rotavap delivering the product in a very clean process. Intermediate removal of excess TMSBr omitted the formation of HBr, which could possibly interfere with the product formation by amine-salt formation.



Scheme 98: Failed attempt at the synthesis of 4-P-ABAO [129] by final amid oxime formation.

Interestingly, performing the amidoxime formation after the deprotection was problematic (Scheme 98). Due to the dramatically increased polarity of the phosphonic acid [LXXI], the addition of H₂O was necessary to enable any dissolution of the starting material. Even though complete consumption could be observed overnight, the ³¹P-NMR analysis revealed a triple of unidentifiable products. The similarity of NMR shifts in the spectrum (10.7, 10.2, 9.4 ppm) prompted the assumption that all peaks

corresponded to phosphinic acid structures. Unfortunately, no difference in retention time could be detected in any UHPLC-MS measurements. All presumable product peaks eluted in the C_{18} and C_4 columns in the injection peak – HILIC chromatograms remained highly inconclusive as no defined, narrow peaks were observed. Due to the amphiphilic nature of the compound, this behavior was partly expected. However, as minor apolar components were still identified in the chromatograms, preparative HPLC purification using the C_{18} column was attempted to see if any purification was possible. Collection of the immediately eluted material regrettably only confirmed further decomposition of the material (six ^{31}P -NMR spots). This also hinted at the instability of the material, which was also observed by purification attempts using recrystallization.

As cleavage of the esters disabled any further purification attempts using classical normal phase chromatographic methods, we opted to perform the deprotection as the last step for all further studies. Having the amidoxime **[128]** obtained in perfect purity after column chromatography and factoring in the messy deprotection, we opted to directly investigate the reaction in a time-resolved ^{31}P -NMR experiment using CD_3CN and H_3PO_4 (0 ppm) as standard (Fig. 69). The process was easily trackable and revealed a clean conversion of the diethyl ester to the double TMS-protected derivative after 2.5 hours. Following the evaporation of the solvent and excess TMSBr , the resulting off-white solid crude was dissolved in HPLC grade MeOH . Interestingly redissolving of the solids in CD_3CN was not possible anymore. The reaction in MeOH was concentrated after 30 minutes resulting in an off-white product. The ^{31}P -NMR analysis confirmed > 90 % purity. Additional washing steps with pure EtOH or $\text{MeOH}/\text{CH}_2\text{Cl}_2$ mixtures further removed residual impurities and enabled isolation of the first pure phosphorus-ABAO derivative (4-P-ABAO **[129]**), albeit with slightly diminished yield.

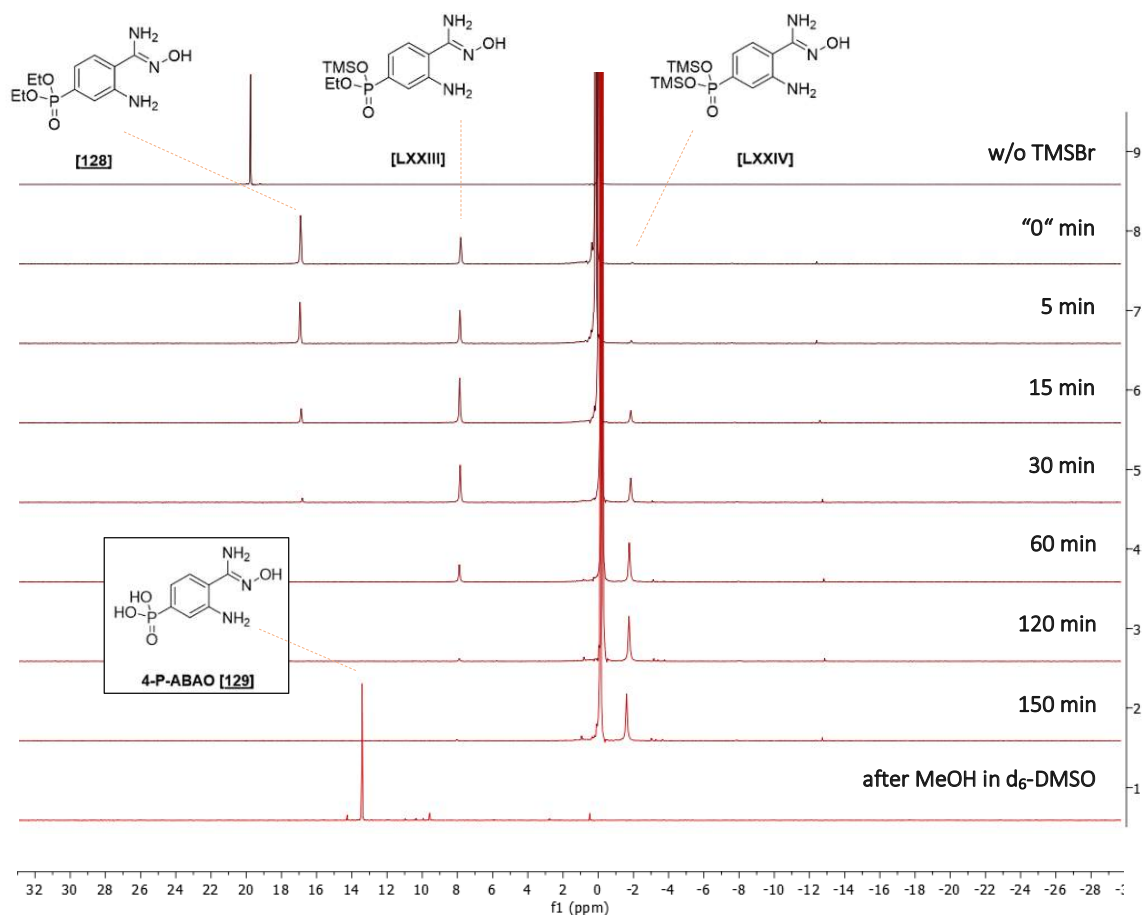
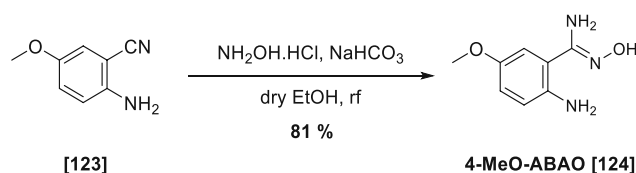


Fig. 69: Time-resolved ^{31}P -NMR study for the cleavage of diethyl phosphonate **[128]** via stepwise transesterification of the ethyl esters by TMSBr in CD_3CN : The experiment was started with the addition of 10 equiv. of TMSBr to the NMR tube. During the first 15 minutes, a gradual decrease of the signal of **[128]** (16.9 ppm), with a concomitant increase of **[LXXIII]**-signal (7.9 ppm) could be observed which subsequently shifted towards the disubstituted TMS-product **[LXXIV]** (-1.8 ppm). Complete conversion could be detected after 2.5 hours of reaction at room temperature. Final evaporation of bulk TMSBr and methanolysis revealed the phosphonic acid of 4-P-ABAO **[129]**, bearing a shift of 13.8 ppm in d_6 -DMSO.

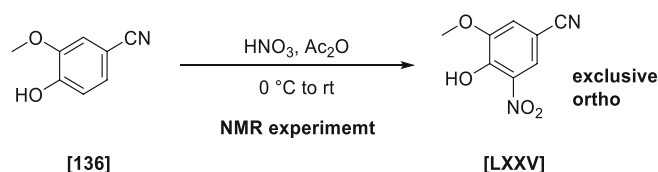
With the compound in hand, preliminary kinetic studies were performed using octanal as aldehyde of choice in an already reported buffer medium (Quelle). Herein reactions employing ABAO **[LIV]** and MeO-ABAO **[124]** were compared with the novel 4-P-ABAO **[129]**. Verena Scheibelreiter thankfully prepared the ABAO. 4-MeO-ABAO **[124]** was synthesized from commercial 2-amino-5-methoxybenzonitrile **[123]** in 81 % yield (Scheme 99).



Scheme 99: Synthesis of 4-MeO-ABAO **[124]**.

An apparent loss in reactivity towards the substrate could be immediately observed. Also, the dramatic increase in reaction kinetics by the employment of the methoxy-variant became evident (see Fig. 71). Nevertheless, the respective phosphorous compound was proven to exhibit the wanted reactivity towards aldehydes. We thus hypothesized that incorporation of the methoxy-group into the 4-P-ABAO structure would possibly lead to a restoration of the kinetic profile.

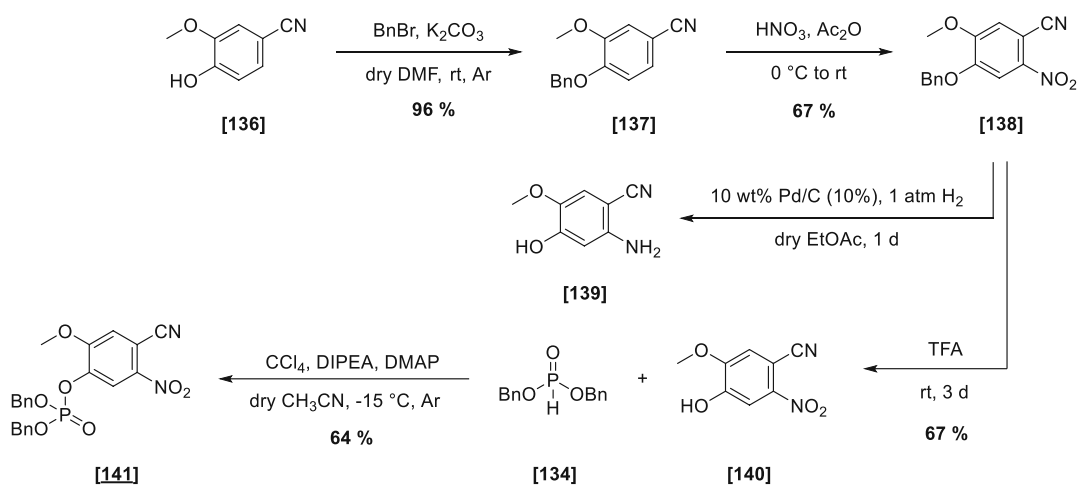
We now focused on targets [148] and [LX] and followed up on the previously mentioned synthetic strategy. Looking at literature-known examples, the introduction of the nitro-group in the desired position was unfortunately not possible with the naked phenol [136]. This result was also confirmed by performing classical nitration that resulted exclusively in the ortho-nitrated product [LXXV] (Scheme 100).



Scheme 100: Nitration of 4-hydroxy-3-methoxybenzonitrile [136] yielded the exclusive formation of the undesired ortho-nitro-product [LXXV].

Concealing the reactive group etherification with subsequent deprotection was considered as the initial approach (Scheme 101). To limit the number of necessary steps, the benzyl-ether group was chosen strategically as deprotection, and reduction of the nitro-compound [138] could be performed simultaneously employing Pd/C and H₂. Yields for the etherification and nitration could be reproduced using literature reference procedures resulting in 96 % of [137] and 67 % of [138], respectively.²⁴⁸ The simultaneous deprotection and reduction to form [139], however, were problematic. Due to the increased polarity of the nitro compound, only incomplete dissolutions could be achieved in either MeOH or EtOAc. As literature examples pointed to increased yields in reactions performed in EtOAc, we still opted for this solvent system.

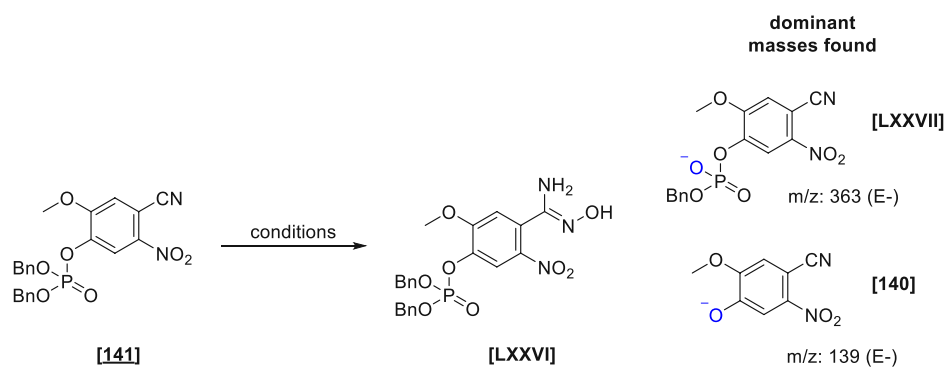
During the reaction, slow dissolution of the starting material and final precipitation of product could be observed. Several additions of MeOH were needed to solubilize the product and enable separation from the Pd/C. However, during the filtrate collection, immediate rapid darkening could be observed, which was later confirmed to arise from the oxidation of the product [139]. As electron-rich anisidine structures generally show a tendency for rapid oxidations, we tried to limit the exposition to light and air in several subsequent attempts, especially during the filtration process – unfortunately, without success. Quick evaporation of solvent only enabled the isolation of highly contaminated products. Attempted column chromatography of the crude was possible but just marginally increased the quality of the product.



Scheme 101: Synthetic route towards dibenzyl phosphoric acid [141].

We attempted phosphorylation using a known literature procedure that employed dibenzyl phosphite and carbon tetrachloride.²⁴² Similarly to the etherification, the phosphate benzyl ester **[134]** was chosen to limit the number of necessary steps by enabling simultaneous hydrogenative cleavage of any reducible groups. However, due to the high instability of the starting material, no appreciable amounts of product could be isolated. Hence, we opted to keep the nitro group intact and only reduce it after the installation of the phosphate group. The benzyl-ether **[138]** was thus deprotected by stirring in TFA for 3 days²⁴⁹ forming **[140]** and followed up by the phosphorylation²⁴² yielding **[141]** in 67 % and 64 %, respectively (Scheme 101). Knowing about the troubles of purification of the deprotected phosphinic acid **[129]**, this step was again envisioned last.

Table 7: Attempted installation of the amidoxime functionality.

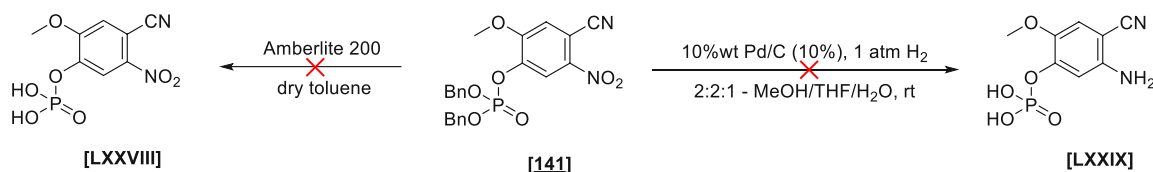


entry	conditions	yield
1	NH ₂ OH.HCl, NaHCO ₃ , 25 % H ₂ O/EtOH, rt to reflux	decomp.
2	50 wt% NH ₂ OH in H ₂ O, MeCN, rt	decomp.
3	NH ₂ OH.HCl, dry NEt ₃ , dry MeCN, rt	decomp.

Hence amidoxime formation was attempted (Table 7), initially using the already established procedure in H₂O/EtOH mixtures (see Scheme 98). Herein insufficient dissolution of the starting material and, moreover, predominant phosphate cleavage rendered the reaction unusable (entry 1). We thus switched to MeCN, which immediately improved the solubility and attempted the reaction in both aqueous (entry 2) and anhydrous conditions (entry 3). Surprisingly, in both cases, monodebenzylation **[LXXVII]**, as well as complete phosphate cleavage **[140]** (higher amount under aqueous conditions), were the dominant products. No fully deprotected phosphate product could be detected during any attempt. Additionally, only minimal amidoxime formation was observed *via* HPLC-MS measurements – albeit none in products still bearing the fully protected phosphate group. In every reaction, the immediate formation of a distinct yellow color pointed to the formation of a typically yellow-colored nitro-phenolate species²⁵⁰, which was an immediate indicator for a failed reaction.

We thus speculated if initial deprotection of the phosphoric acid might improve the stability of the linkage and attempted to either cleave the phosphate esters using reductive conditions or by applying acid resin Amberlite 200²⁵¹ (Scheme 102). The strongly acidic resin again caused slow conversion to the monobenzylated product **[LXXVII]**, which was then presumably further converted to phenol **[140]**. Again, no target mass of the phosphoric acid could be detected in the spectra. Applying hydrogenative conditions caused clean transformation to a distinct mass

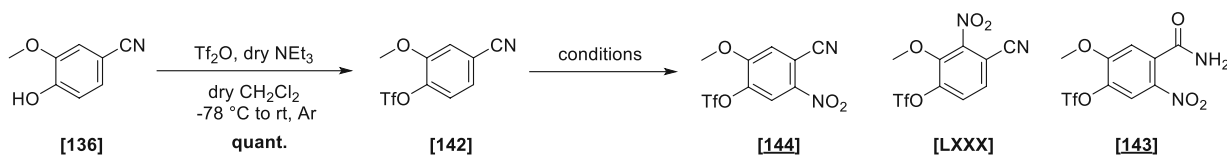
($m/z = 232$, C_{18} , acidic, E+) which eluted in the injection peak and could not be assigned to any structure. Attempted isolation of this product using the preparative HPLC yielded only fully decomposed material after lyophilization as no defined aromatic signals in $^1\text{H-NMR}$ analysis. Given the absence of product mass in any of the spectra, we concluded that the phosphoric acid **[141]** might be too unstable in its free form and thus did not pursue the synthesis any further.



Scheme 102: Attempted cleavage of benzyl esters of **[141]** using acid catalysis or employing hydrogenolytic Pd/C cleavage.

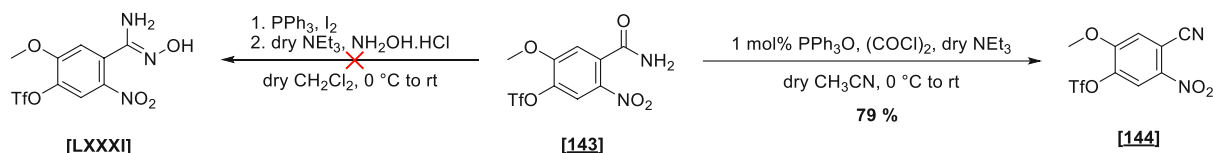
However, having the methodology towards the P-C coupled product established for the 4-P-ABAO **[129]**, we now focused on its methoxy variant. Due to the known compatibility of triflates for the Pd-catalyzed phosphite coupling²⁴⁴, we started with known triflation of the phenol **[136]**, forming the triflate **[142]** in quantitative yield.²⁵² As phenol substitution had a proven effect on the regioselectivity of the nitration, we were initially skeptical that the nitro-group would be introduced at the correct position and if the triflate would survive harsh conditions. Using classical nitration conditions, spot-to-spot conversion of **[142]** was observed, which was, however, unfortunately, exclusively converted to the amide **[143]** in 77% (Table 8 entry 1). As the hydrolysis was already observed during the reaction by TLC analysis and not during aqueous work-up other activators were initially employed to prohibit the undesired reactivity. Acetic anhydride and glacial AcOH did not exhibit any reaction even at elevated temperatures (entries 2 & 3). Attempts employing the more acidic perchloric acid, which was believed to hinder any attack of water by extensive protonation, prevented any amide formation but caused the formation of 30 % of the 'wrong' regio-isomer **[LXXX]** (entry 4). Reduction of the equivalents did not lead to any improvements (entry 5). We thus reattempted the nitration using sulfuric acid and lower temperatures. As complete consumption of the starting material was already observed after 10 minutes, immediate quenching using an ice / solid Na_2CO_3 mixture finally facilitated the direct isolation of the nitrile in 46 %, albeit concomitant formation of 29 % of amide (entry 6).

Table 8: Screening of nitration conditions for **[142]** by variations of activators and HNO_3 equivalents.



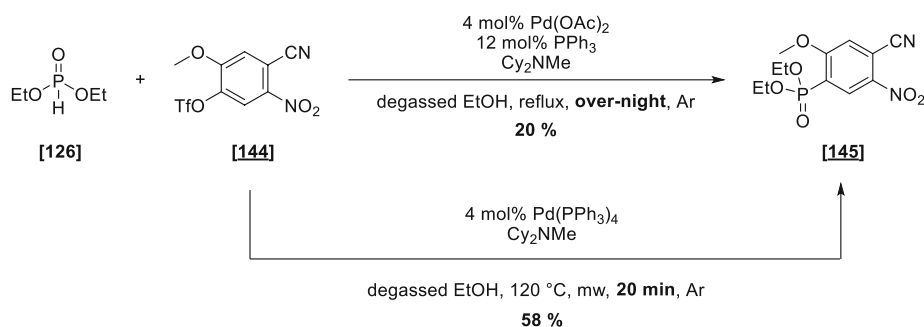
entry	conditions	yield - [144] / [LXXX] / [143]
1	100 % $\text{HNO}_3/\text{H}_2\text{SO}_4$, rt	0/0/77
2	100 % $\text{HNO}_3/\text{Ac}_2\text{O}$, 0 °C to 50 °C	No reaction
3	100 % $\text{HNO}_3/\text{glacial AcOH}$, 0 °C to 50 °C	No reaction
4	4.5 eq. 100 % $\text{HNO}_3/70$ % HClO_4 , 0 °C	70/30/0
5	2.0 eq. 100 % $\text{HNO}_3/70$ % HClO_4 , 0 °C	70/30/0
6	100 % $\text{HNO}_3/\text{H}_2\text{SO}_4$, -5 °C	46/0/29

Due to the undesired amide formation, the compound was attempted to be salvaged by direct amidoxime formation using the only known literature procedure²⁵³ for this transformation (Scheme 103). Herein the amide could be theoretically transformed into the corresponding iodo-amide, which could be presumably trapped by hydroxylamine forming the product [LXXXI]. Unfortunately, any attempts employing this methodology only led to the complete decomposition of the material.



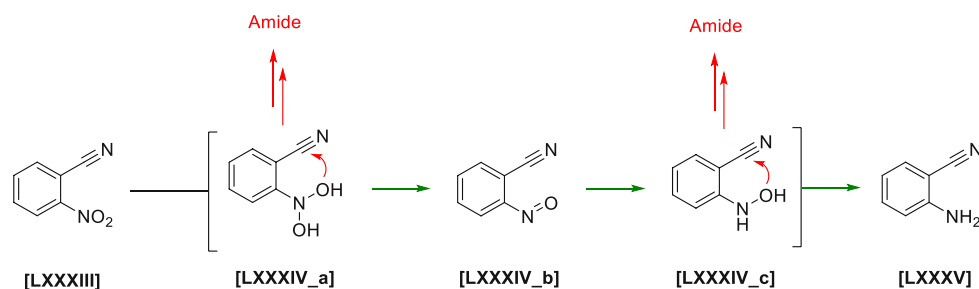
Scheme 103: Attempts to salvage the undesired amide [143] via direct amidoxime formation or dehydration to the nitrile [144].

However, a regeneration of the amide was made possible by using a known dehydration procedure for aryl amides employing a catalytic Appel reaction²⁵¹. Herein the desired nitrile [144] could be isolated after slight variations of reaction temperature – by cooling from 0 °C to -15 °C – in 79 % yield after column flash column chromatography. With the desired compound in hand, we turned to the coupling reaction, whereas replicating the identical conditions led to the immediate isolation of the phosphate ester [145], albeit in only 20 % yield (Scheme 104). Direct employment of freshly prepared Pd(PPh₃)₄ and the use of microwave irradiation dramatically improved the yield to 58 % and decreased the necessary reaction time for this transformation.



Scheme 104: P-C coupling of [144] employing in-situ generated Pd(PPh₃)₄ with conventional heating and the improved synthetic approach using microwave irradiation and freshly prepared Pd-catalyst.

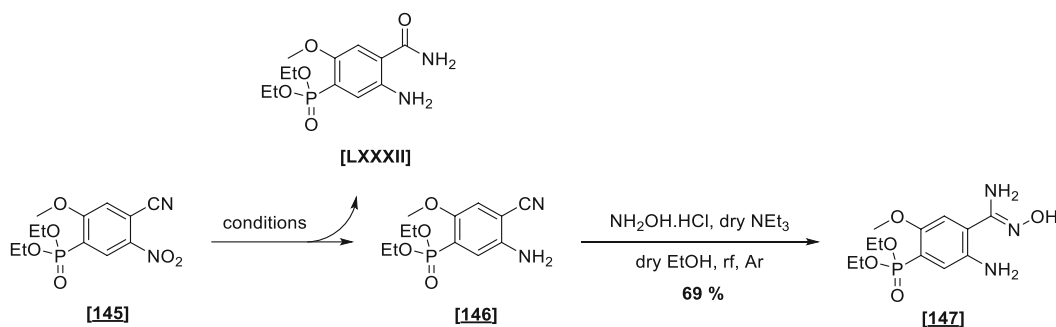
The reduction of the nitro-group (Table 9) was subsequently investigated using initially classical hydrogenative reduction conditions in HPLC grade MeOH. However, reaction control *via* HPLC-MS revealed substantial amounts of nitrile hydrolysis (entry 1) forming [LXXXII]. Changing to anhydrous conditions and even adding 3Å MS even worsened the outcome (entry 2). Switching to aprotic conditions employing dry EtOAc only yielded the same amount of hydrolysis (entry 3). The reason for this outcome was rationalized by the mechanism for the reduction (Scheme 105). Due to the proximity of the intermediately formed di- or monohydroxyl amines [LXXXIV_a] or [LXXXIV_c], a nucleophilic attack onto the ortho-nitrile was possible if subsequent dehydration would be too slow.²⁵⁴



Scheme 105: Known intermediates for the reduction of nitro-groups: The stepwise reductive and dehydrative process leads over di- and monohydroxyl amines [LXXXIV_a] / [LXXXIV_c], which due to the ortho-position of the nitrile group can lead to an addition onto the triple bond even under anhydrous conditions. Subsequent proton-shifts lead to the formation of the undesired amide side-product.

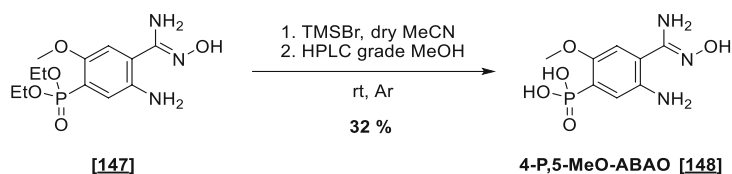
Using iron as the reductant in acetic conditions⁶² (entry 4) facilitated a clean transformation to the amine with minimal hydrolysis. The addition of acid could have also improved the hydrogenolytic reduction but was not tested. Interestingly both products bearing the amine exhibited strong light-blue fluorescence, which could even be used to separate those compounds during column chromatography. In further studies, a strong dependence on the applied iron source could be pinpointed for this transformation. The 87 % yield for the reduction represented the most optimal case, although yields as low as 50 % could be reported in several reactions. The results for these screenings are discussed in detail in the diploma thesis of Astrid Schiefer. Powdered iron acquired from Sigma Aldrich (#209309, 97 %, 325 mesh) had been found to produce the amine with the least amount of concomitant hydrolysis.

Table 9: Screening of reductive conditions for the nitro compound [145]. ^aDetermined *via* UHPLC-MS; ^bisolated yield.



entry	conditions	yield
1	10 wt% Pd/C, 1 atm H ₂ , HPLC grade MeOH	65 % hydrolysis [143] ^a
2	10 wt% Pd/C, 1 atm H ₂ , dry MeOH + 3 Å MS	80 % hydrolysis [143] ^a
3	10 wt% Pd/C, 1 atm H ₂ , dry EtOAc + 3 Å MS	65 % hydrolysis [143] ^a + MeO cleavage
4	Fe, AcOH, dry MeOH reflux	50-87 % [147] ^b

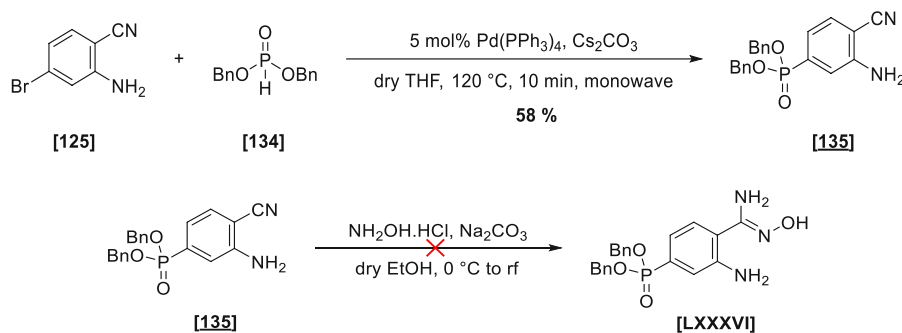
The isolated amine was transformed to the amidoxime [147] in 69 % yield using the already applied reaction conditions. With the time frame for the TMSBr induced deprotection established, the reaction was performed using identical conditions for [129] (Scheme 106). HPLC-MS measurements furthermore confirmed complete deprotection with the disappearance of the mono-protected mass.



Scheme 106: Synthesis of 4-P,5-MeO-ABAO **[148]**.

The resulting yellow solids after treatment with MeOH and removal of solvent were shown to have 80 % purity judged by ^{31}P -NMR and could be used directly for any preliminary ABAO-adduct formations and spectroscopic measurements. Trituration of the crude solids in EtOH proved to be very beneficial to the quality of fluorescence measurements. The treatment removed any yellow discoloring which predominantly accumulated in the EtOH layer and evidently improved the background signal of the 4-P,5-MeO-ABAO **[148]**. The success of this washing step heavily depended on the cleanness of the deprotection, as increased side-product formation was proven to interfere with the downstream separation. The absence of light was shown to be crucial, as the methoxy-variant exhibited evident instability under ambient and UV light conditions. This behavior could be especially shown in UV and fluorescence measurements, where prolonged irradiation led to a dramatic increase in unspecific background emission. Hence, all subsequent deprotection was performed in brown-glass vials and under argon. However, despite multiple repetitions using the same procedures, the outcome of the reaction proved to be highly unreproducible. The reason for this behavior was elucidated in subsequent studies by Astrid Schiefer and could be traced back to the water content of the MeCN. Complete exclusion of water was proven to be detrimental to the overall product quality. Reactions performed in CD_3CN in which the water content was determined to be 317 ppm by Karl-Fischer titration proved to cleanly transform the respective phosphonate ester. With the product in hand, preliminary kinetic studies were performed with octanal, depicted in Fig. 70.

However, due to troublesome ethyl phosphonate ester deprotection at the time, the corresponding benzyl phosphonate esters were also investigated for the synthesis of P-C coupled products. These could be theoretically deprotected using hydrogenolytic conditions. Herein again, the 4-P-ABAO precursor **[125]** was used as the trial compound. A different literature procedure (Quelle) was taken as a starting point, as dibenzyl phosphite **[134]** was also included as a coupling substrate in the study. Although the same catalyst system was used, THF was judged herein to be the solvent of choice and either Cs_2CO_3 or NEt_3 as the base. Attempted reactions employing conventional heating did not lead to any product formation. The dibenzyl phosphite was shown to rapidly decompose at increased temperatures ($> 80\text{ }^\circ\text{C}$). As temperatures at or above $120\text{ }^\circ\text{C}$ were found to be essential for product formation, conventional heating was too slow to cross the necessary temperature barrier in due time. Due to possible explosion hazards known for the Biotage[®] microwave reactor using heterogeneous mixtures, the reaction was attempted using the Anton Paar[®] Monowave applying literature conditions. The increased temperature ramp enabled with the device facilitated the formation of the wanted phosphonate ester **[135]** in 58 % yield (Scheme 107), albeit the need for slightly increased phosphite equivalents (0.9 to 1.1).

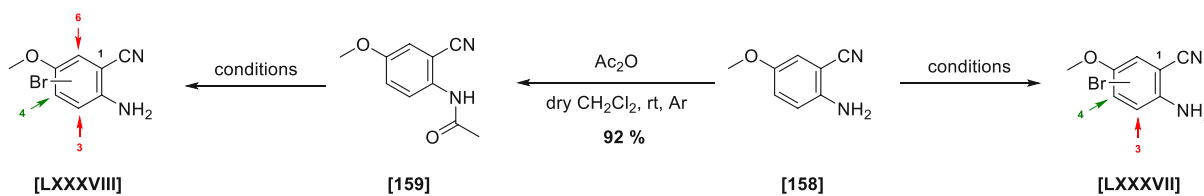


Scheme 107: Synthesis of dibenzyl phosphonate derivative **[135]**, which was shown to be unstable under amidoxime formation conditions.

Unfortunately, subsequent attempts at the installation of the amidoxime reactive handle using very mild, anhydrous conditions (dry EtOH, 0 °C) immediately led to complete decomposition of the material as six evenly distributed P-species could be detected in the crude NMR spectra. With this result and the previous experience with the instability of dibenzyl esters, we did not pursue the synthesis of these analogs any further.

On the other hand, we tried to shorten the synthetic approach by starting from commercial 2-amino-5-methoxybenzonitrile **[158]**, which was used as start material for the MeO-ABAO **[124]** (Table 10). Envisioned bromination at the 4-position would set up the compound for immediate phosphite coupling. However, as was already observed for the nitration of the phenol **[136]**, aromatic compounds as **[158]** bearing unprotected strong electron donors force the bromination into the *ortho*-position (entries 1 & 2). Deactivation of the ring by acetylation and reattempted bromination using NBS in CH₂Cl₂ only slowly brominated the starting material, albeit still only in the 3-position (entry 3). TFA as solvent promoted the reaction but again also seemed to force bromination in the 3-position. Prolonged stirring using more equivalents of NBS showed additional substitution at the 6-position (entry 4). With these results, we concluded that the desired 4-position was not selectively activatable, and no further efforts were undertaken to synthesize 4-P,5-MeO-ABAO **[148]** *via* this route.

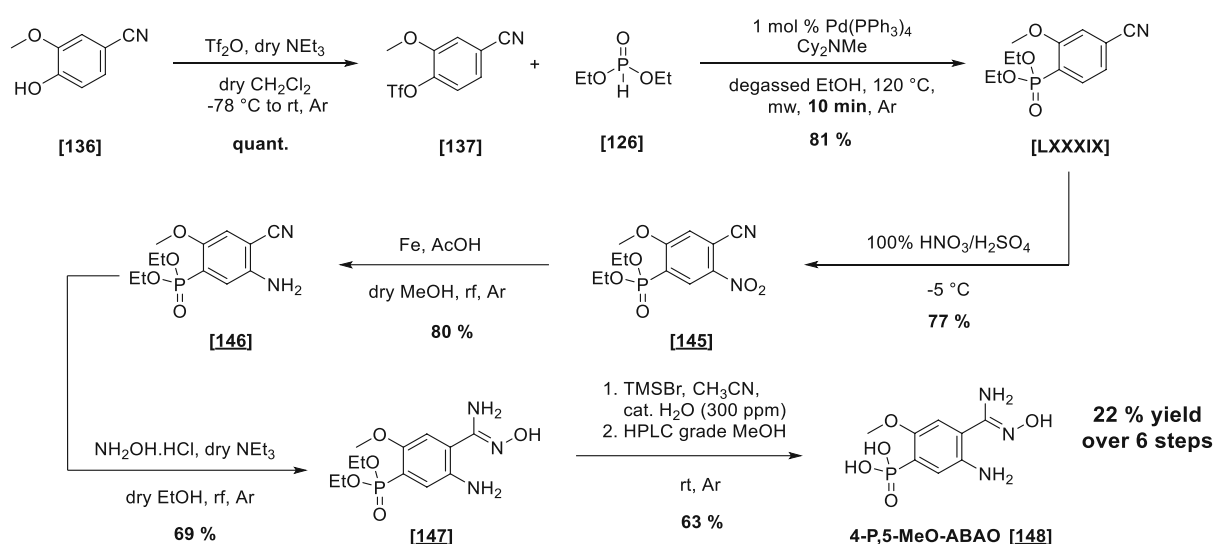
Table 10: Attempts at introducing bromide into the 4-position of the aromatic system by electrophilic brominations of **[158]** and **[159]**.



entry	starting material	conditions	outcome
1	[158]	NBS, dry CH ₂ Cl ₂ , 0 °C to rt, Ar	exclusive 3
2	[158]	TBCA, TFA, 0 °C to rt, Ar	exclusive 3
3	[159]	NBS, dry CH ₂ Cl ₂ , 0 °C to rt, Ar	exclusive 3 (slow)
4	[159]	NBS, TFA, 0 °C to rt, Ar	exclusive 3 then 6

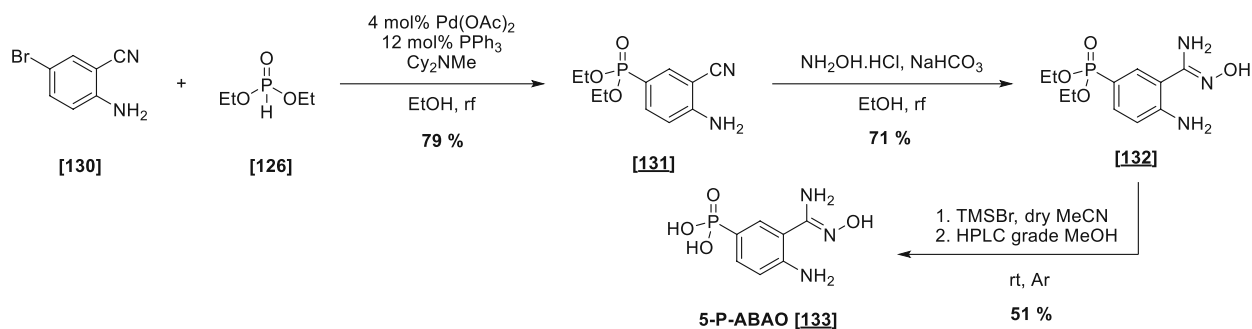
However, as can be judged from the general synthesis of **[148]**, several of these steps still needed further optimization as low yields and side-product formations rendered the whole procedure

impractical. These investigations were undertaken by Astrid Schiefer and can be read about in her diploma thesis. The summary of the synthesis can be seen in Scheme 108, whereas three modifications had been implemented. By performing the coupling reaction first and nitration second, not only could the yield of the P-C coupling be raised from 58 to 81 %, the phosphonate enabled the clean introduction of the nitro-group without concurrent hydrolysis. Herein a reduction in both catalyst loading and reaction time seemed to be beneficial for the coupling yield. As was also mentioned before, a clean phosphonate deprotection was indispensable for good isolation of the 4-P,5-MeO-ABAO [148]. As mentioned, the use of MeCN with increased water content that was determined to be around 300 pm (present in CD₃CN – determined by Karl Fischer titration²⁵⁵) led to much cleaner alkyl-cleavage than the use of its anhydrous form. After methanolic treatment of the TMS-esters, the target product could be readily isolated by EtOH trituration in high purity. The increased water content also improved the reproducibility of the deprotection, enabling straightforward isolation of the 4-P,5-MeO-ABAO [148].



Scheme 108: Improved synthetic route towards 4-P,5-MeO-ABAO [148] by Astrid Schiefer.

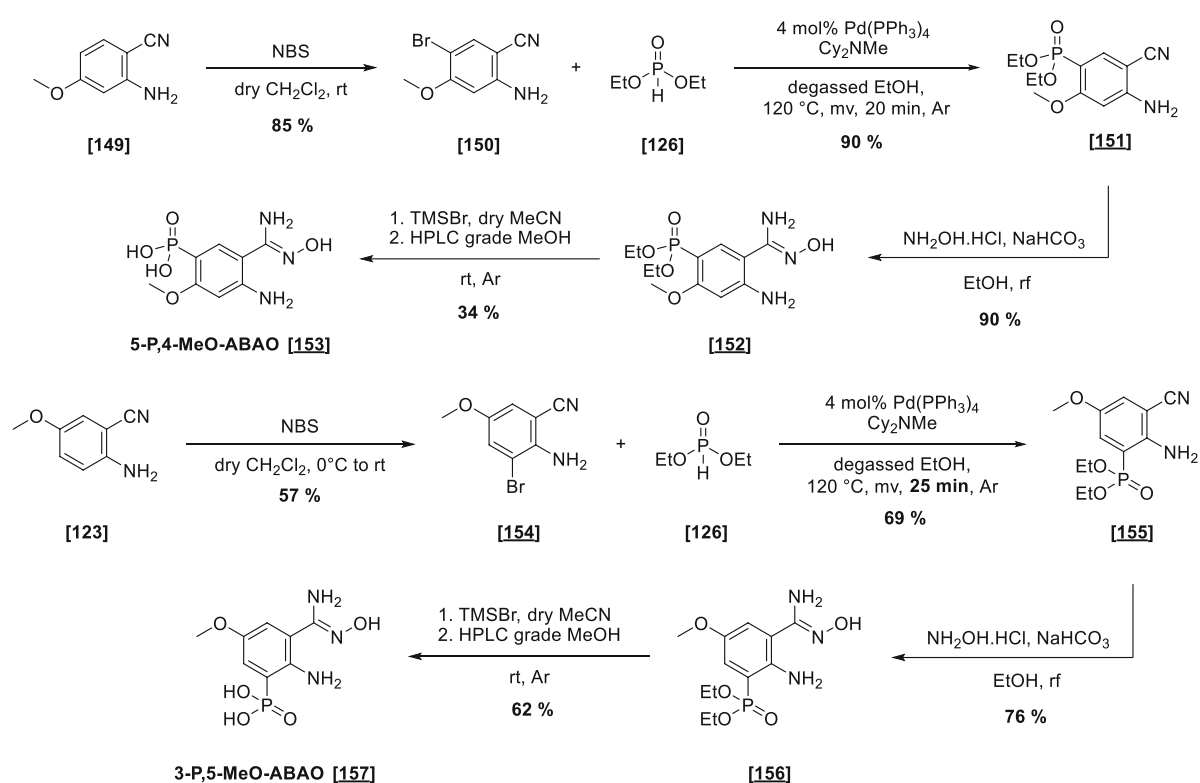
All these modifications were unfortunately only determined after completing all synthetic efforts undertaken during this Ph.D. and have thus not been implemented in the synthetic procedures. To enable a more rational approach in the design of future (P-)ABAO derivatives, we also applied this synthetic methodology for the synthesis of several analogs, namely 5-P-ABAO [133], 5-P,4-MeO-ABAO [153], and 3-P,5-MeO-ABAO [157].



Scheme 109: Synthesis of analog 5-P-ABAO [133].

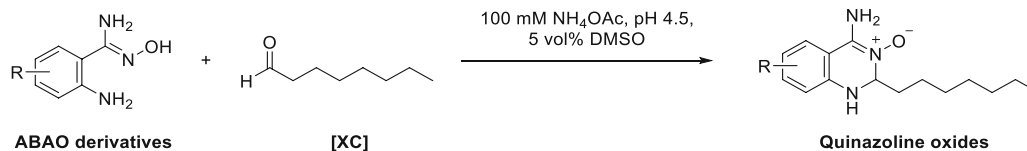
The 5-P-ABAO variant was synthesized in the same format as its 4-substituted analog [129]. After phosphite coupling of the readily available 2-amino-5-bromobenzonitrile [130] to yield [131] in 79 %, and amidoxime formation in 71 %, the phosphonate ester [132] was deprotected using TMSBr to give the desired 5-P-ABAO [133] (Scheme 109).

For the synthesis of the methoxy-derivatives, luckily, the readily available amino-methoxybenzonitriles [149] and [123] rendered their synthesis relatively straightforward. Herein, the introduction of the bromo-handle necessary for the phosphine coupling could be easily performed, as the most electron-rich, non-substituted aromatic position was always targeted. Upon bromination, the already established synthetic protocol could be applied for the synthesis of the respective P-MeO-ABAO derivatives (Scheme 110).

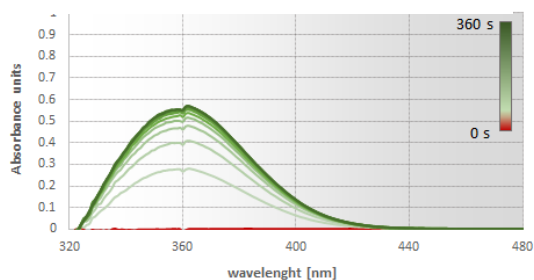


Scheme 110: Incorporation of the phosphinic acid handle onto the aromatic core and follow-up.

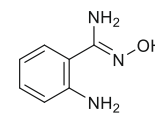
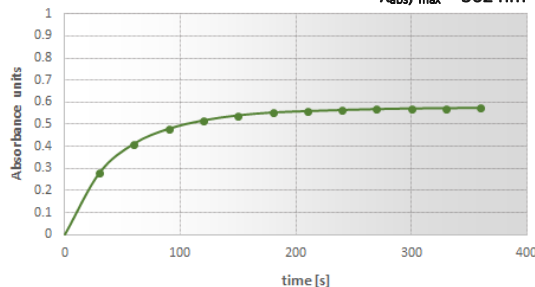
With all compounds in hand, adduct formation was studied with octanal [XC] to find the most suitable candidate for in-depth investigations (Fig. 71). Octanal [XC] was chosen as a target due to a shift of interest towards aliphatic aldehydes as substrates, their availability, and sufficient low volatility for this class of compounds. Based on previous in-house reports from Rössmann *et al.*⁶², the aldehyde was reacted with a 5x excess of the respective ABAO-compounds in NH₄OAc pH 4.5 buffer, and the kinetics of the adduct formation were compared. Similar to the NBD-H studies, UV-spectroscopy was used as a more straightforward tool for this analytic purpose. All samples were blanked against the free ABAO-reagents.



2.5 mM ABAO [LIV] + 0.5 mM octanal [XC]

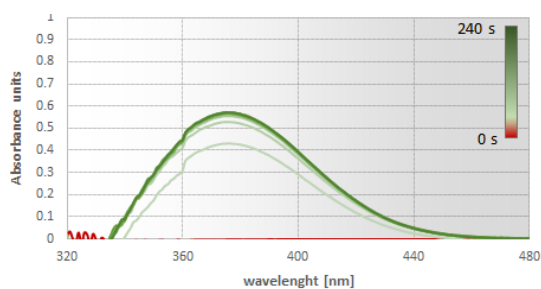


$\lambda_{\text{abs, max}} = 362 \text{ nm}$

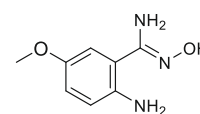
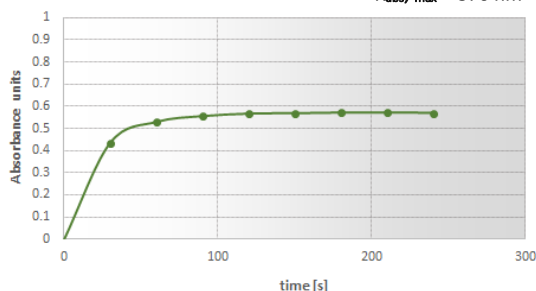


ABAO [LIV]

2.5 mM 5-MeO-ABAO [126] + 0.5 mM octanal [XC]

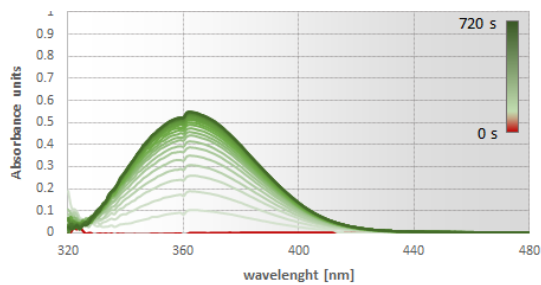


$\lambda_{\text{abs, max}} = 376 \text{ nm}$

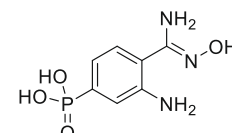
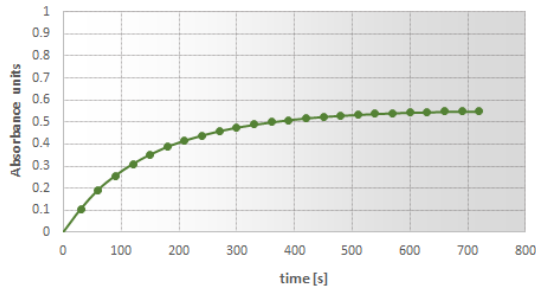


5-MeO-ABAO [126]

2.5 mM 4-P-ABAO [129] + 0.5 mM octanal [XC]

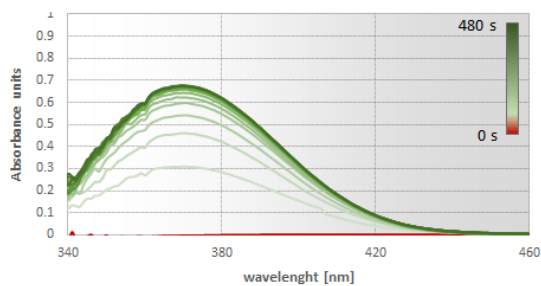


$\lambda_{\text{abs, max}} = 362 \text{ nm}$

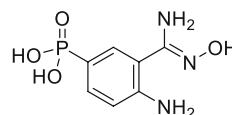
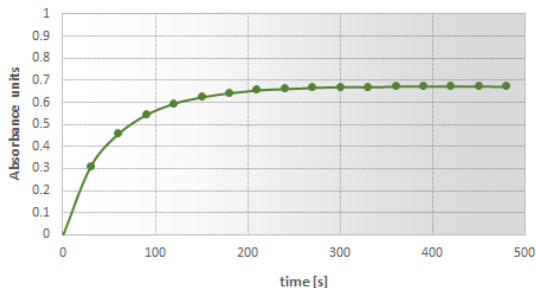


4-P-ABAO [129]

2.5 mM 5-P-ABAO [133] + 0.5 mM octanal [XC]



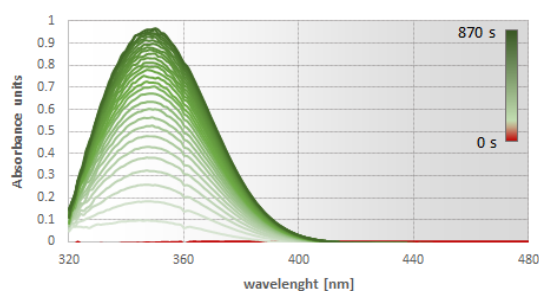
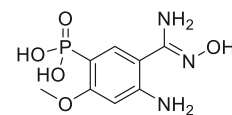
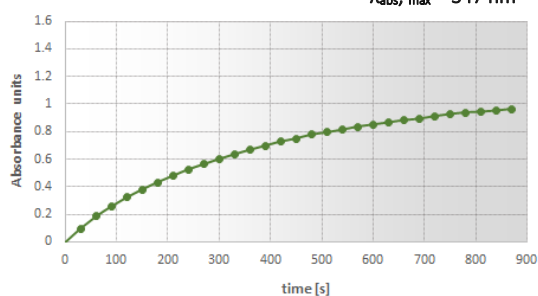
$\lambda_{\text{abs, max}} = 370 \text{ nm}$



5-P-ABAO [133]

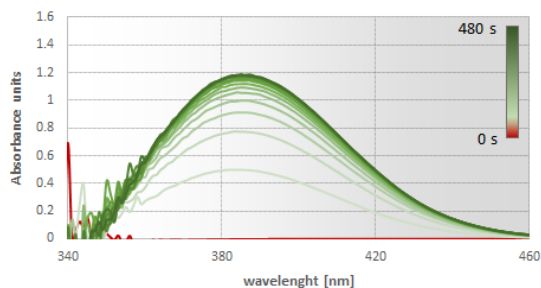
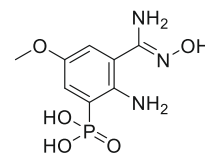
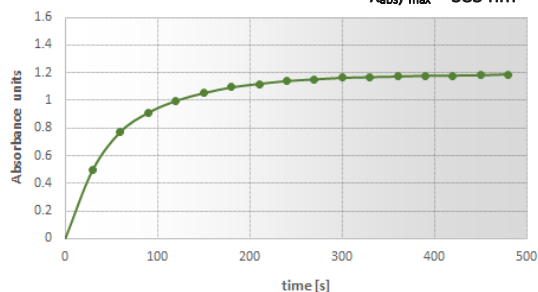
Fig. 70: UV-absorbance kinetic evaluation of all synthesized P-ABAO derivatives: All analogs were reacted with 500 μM octanal [XC] in 5-fold excess. Kinetics were recorded by interval measurements of the complete spectral information in pH 4.5 NaAc buffer, 5 vol% DMSO in 30-second intervals blanked with the respective P-ABAO derivative. The screening revealed the 4-P,5-MeO-ABAO [148] candidate to exhibit the fastest kinetics being on par with the parent 5-MeO-P-ABAO [126] reagent.

2.5 mM 5-P,4-MeO-ABAO [153] + 0.5 mM octanal [XC]


 $\lambda_{\text{abs, max}} = 347 \text{ nm}$


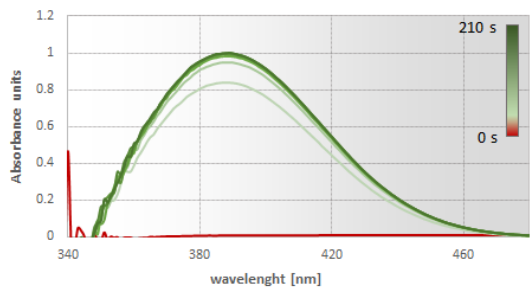
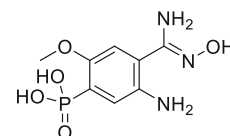
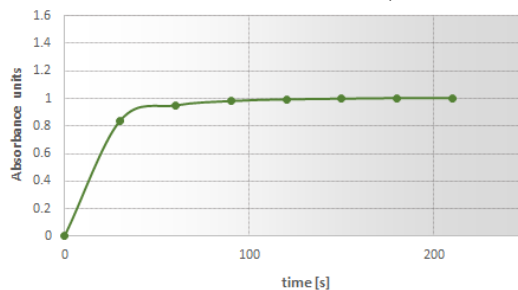
5-P,4-MeO-ABAO [153]

2.5 mM 3-P,5-MeO-ABAO [157] + 0.5 mM octanal [XC]


 $\lambda_{\text{abs, max}} = 385 \text{ nm}$


3-P,5-MeO-ABAO [157]

2.5 mM 4-P,5-MeO-ABAO [148] + 0.5 mM octanal [XC]


 $\lambda_{\text{abs, max}} = 387 \text{ nm}$


4-P,5-MeO-ABAO [148]

Fig. 70 cont: UV-absorbance kinetic evaluation of all synthesized P-ABAO derivatives.

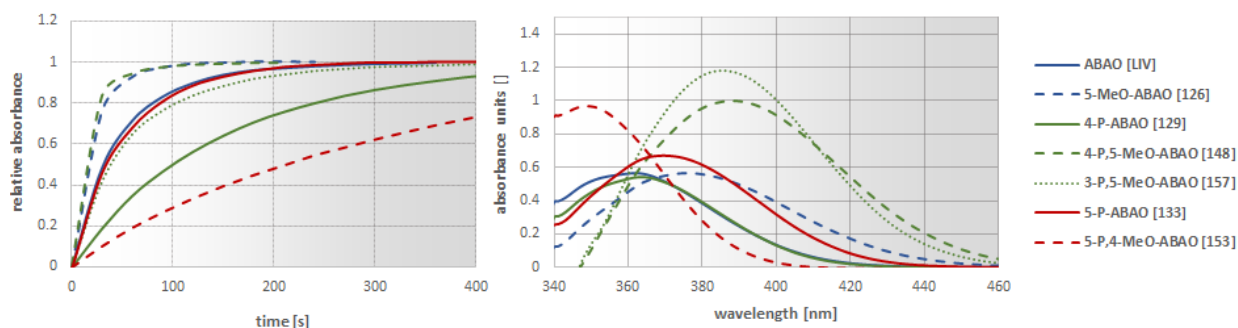


Fig. 71: Comparison of kinetic and spectral data of all tested P-ABAO analogs; blue lines represent the parent AB AO compounds, green lines represent reagents bearing a 4-P or 3-P substitution, red lines represent a 5-P substitution – **left:** Normalized absorbance values over time – kinetics were recorded by intervalled measurements of the complete spectral information in pH 4.5 NaAc buffer, 5 vol% DMSO in 30-second intervals blanked with the respective P-ABAO derivative. The comparison revealed a necessary balance between the electron-donating functionality of the methoxy-group and the electron-withdrawing characteristic of the phosphonate ester. Reagents bearing a 5-MeO functionality were generally shown to be dramatically more reactive than their non-methylated analogs; **right:** Comparison of UV-absorption spectra upon complete conversion of octanal [XC] – combinations bearing a methoxy and phosphonate ester substitution were shown to exhibit higher absorption values. 5-MeO was shown to cause a 20-30 nm red-shift to the non-methylated analogs.

Supporting the findings of Kitov *et al.* (Quelle), the placement of the electron-donating methoxy-group para to the amine moiety at position 5, was beneficial for the reactivity of the 5-MeO-ABAO [126] compared to their parent compounds (5-MeO-ABAO [126], 4-P,5-MeO-ABAO [148]). Although the

introduction of the phosphinic acid moiety at the envisioned 4-position impaired the activity of the 4-P-ABAO [129] – dropping it even below the undecorated ABAO [LVI] - concomitant placement of the methoxy-group restored its fast kinetic profile. Interestingly, the introduction of phosphinic acid at the 5-position had no adverse effect on the kinetics. This behavior was surprising, as its electron-withdrawing functionality was believed to be detrimental. Even more surprising was the observed deceleration with the addition of the 4-methoxy group. The 5-P,4-MeO-ABAO [148] represented the slowest ABAO tested in this study. As expected, changing the position of the acid to a possibly sterically more congested 3-position for the 3-P,5-MeO-ABAO [157] also negatively impacted the reaction. Looking at the absorption spectra for the conjugates, a clear red-shift for all reagents could be observed if a 5-methoxy functionality was present. Herein the 4-P,5-MeO-ABAO [148] and the 3-P,5-MeO-ABAO [157] exhibited the strongest absorption spectra, making them the most sensitive compounds. Herein again, a clear outlier was found to be the 5-P,4-MeO-ABAO [148], which showed a slight blue shift compared to even its parent ABAO [LVI].

With these results, the clear candidate for further studies was evident to be the 4-P,5-MeO-ABAO [148]. Not only did it exhibit the fastest adduct formation, comparable to the 5-MeO-ABAO [126], but secondly showed one of the highest absorption coefficients among the tested variants.

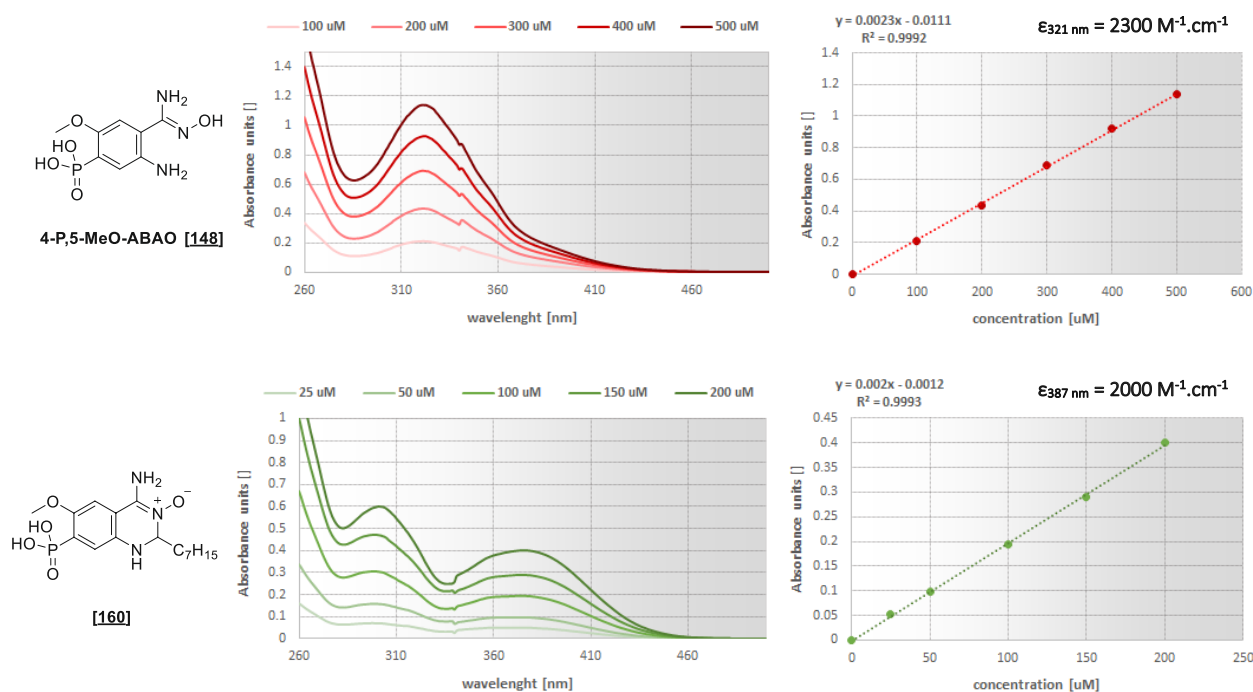


Fig. 72: UV-absorption calibrations of 4-P,5-MeO-ABAO [148] and its octanal conjugate [160]: Measurements reveal a strong red-shift of the absorption maximum upon conjugation from 321 nm to above 387 nm. All spectra were recorded in 100 mM pH 4.5 NaAc buffer, 5 vol% DMSO. [160] calibrations were performed by in-situ formation of the adduct due to isolation problems of pure conjugation product.

Similar to the already reported ABAO [LVI] and 5-MeO-ABAO [126] systems, a strongly desired red-shift of the local absorption maximum from 321 nm to 387 nm upon conjugation could be observed (Fig. 72). Compared to the NBD-H analogs, the ABAO-chromophores were generally one magnitude less sensitive by comparison of the absorption coefficients (20.000 vs. 2.000 $M^{-1}\cdot cm^{-1}$). We also checked its stability in the desired acidic buffer systems and found the 4-P,5-MeO-ABAO [148] to be indefinitely stable (Fig. 73).

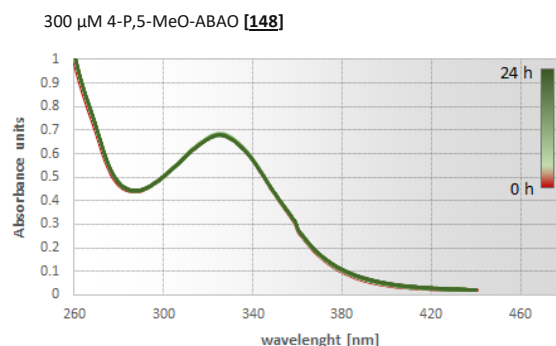


Fig. 73: UV-absorbance stability evaluation of 4-P,5-MeO-ABAO [148] at 300 μM concentration. Measurements confirmed the indefinite stability of the reagent in the tested buffer. Kinetics were recorded in 100 mM pH 4.5 NaAc buffer, 5 vol% DMSO in 30-minute intervals.

Hence we turned to investigate its fluorescence behavior. Calibrations with the parent 4-P,5-MeO-ABAO [148] and its product with octanal [XC] revealed the desired fluorogenic behavior of the system upon adduct formation (Fig. 74). Although the adduct exhibited the maximal absorption at 387 nm, due to the spectral overlap of its free form, the optimal excitation wavelength was found to be 415 nm. Measurements at this wavelength additionally enabled to counteract the inner-filter effect, and thus, linearity was observed up to 200 μM . Similar to its absorptive properties, the conjugate was several orders less sensitive than the hydrazone-systems, as could be seen by the 10 μM emission representing the lowest detectable value. This concentration represented the upper boundary for the ABThD-H [111] assay system. Hence both assay systems complemented their detection regions.

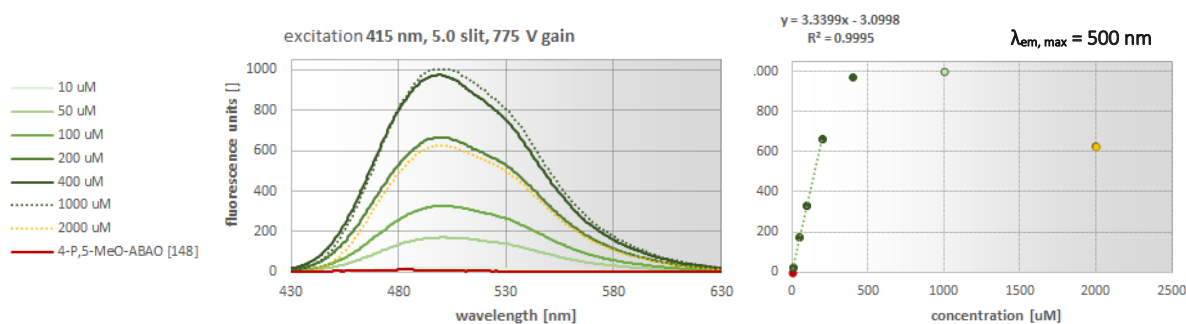
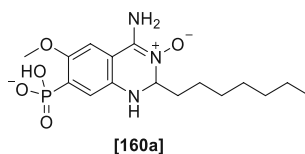


Fig. 74: Fluorescence calibrations of 4-P,5-MeO-ABAO octanal adduct [160]: Conjugation with octanal [XC] caused strong turn-on fluorescence. Excitations at 415 nm triggered emission with a $\lambda_{\text{em, max}}$ at 500 nm, which exhibited a linear dependency of signal up to 200 μM – evident inner filter effect caused a dramatic decline in emission above 1 mM concentrations. All spectra were recorded in 100 mM pH 4.5 NaAc buffer, 5 vol% DMSO, excitation wavelength 415 nm, 5.0 nm slit, 775 V gain.

In-depth investigations about the water-solubility and the pH dependence of the conjugation and its consequence for the signal intensity can be found in the diploma thesis of Astrid Schiefer – however, a general trend towards faster reaction speeds was found by decreasing the pH of the buffer (from 7 to 4.5). On the other hand, the maximal fluorescence emission was observed at a pH of 5.0-5.5, which correlated well with the expected calculated predominant deprotonated state of 4-P,5-MeO-ABAO octanal adduct [160a] at this pH (Scheme 111).



Scheme 111: Calculated protonation state of 4-P,5-MeO-ABAO octanal adduct [160] at pH 4.5 using ChemAxon® software Chemicalize.

Determinations of the LogP and LogD values in the optimal buffer systems were done by employing the stir-flask method²⁵⁶ in n-octanol/water or n-octanol/buffer systems. The studies confirmed an improvement of the water solubility of the 4-P,5-MeO-ABAO [148] of up to three orders of magnitude compared to the parent ABAO [LVI] as well as the kinetically faster 5-MeO-ABAO [126].

Table 11: Comparison of determined LogD and LogP values of parent ABAO compounds and the newly synthesized 4-P,5-MeO-ABAO [148].

entry	LogD (pH 5.5)	LogP (pH 7.4)
ABAO [LVI]	-0.02 ± 0.01	0.03 ± 0.01
4-MeO-ABAO [126]	-0.57 ± 0.05	-0.19 ± 0.04
4-P,5-MeO-ABAO [148]	-2.18 ± 0.18	-2.83 ± 0.19

During our search for the optimal wavelength for the application in the fluorescence-activated droplet sorting system, a presumed instability of these species in ambient light, as well as UV, was detected (see Fig. 76). Measurements of samples placed inside the UV chamber (254 nm) for 15 minutes revealed a strong red-shift in fluorescence emission. This increase in greenish emission at the solution's surface could even be seen with the naked eye. To understand the supposed decomposition process, time-dependant ¹H-NMR studies were conducted, whereas the ABAO was mixed with octanal [XC] in a NMR tube and placed in the UV chamber (Fig. 75).

Several changes in the spectrum immediately pointed to oxidation of the conjugate [160], forming the quinazoline product [XCI]. The disappearance of the most characteristic signal at 5 ppm, which corresponded to the trapped carbonyl-H (red proton), was the most indicative proof for this transformation. Also, the distinct change in the aromatic region (blue protons) and the emergence of the low-field shifted triplet of the β-CH₂ group at 2.8 ppm (orange protons) supported this hypothesis. As this oxidation was not only causing a beneficial strong red-shift in fluorescence emission but additionally an increase in the response signal, we envisioned a possible subsequent light-induced oxidation of the conjugate. Regrettably, using any form of light as the promoter did not only lead to the desired oxidation but, as was already previously mentioned, to a certain degree of 4-P,5-MeO-ABAO [148] decomposition. The increase in background signal caused by this irradiation, unfortunately, exceeded the gain in product emission (Fig. 76), making the whole system less sensitive (lower S/N).

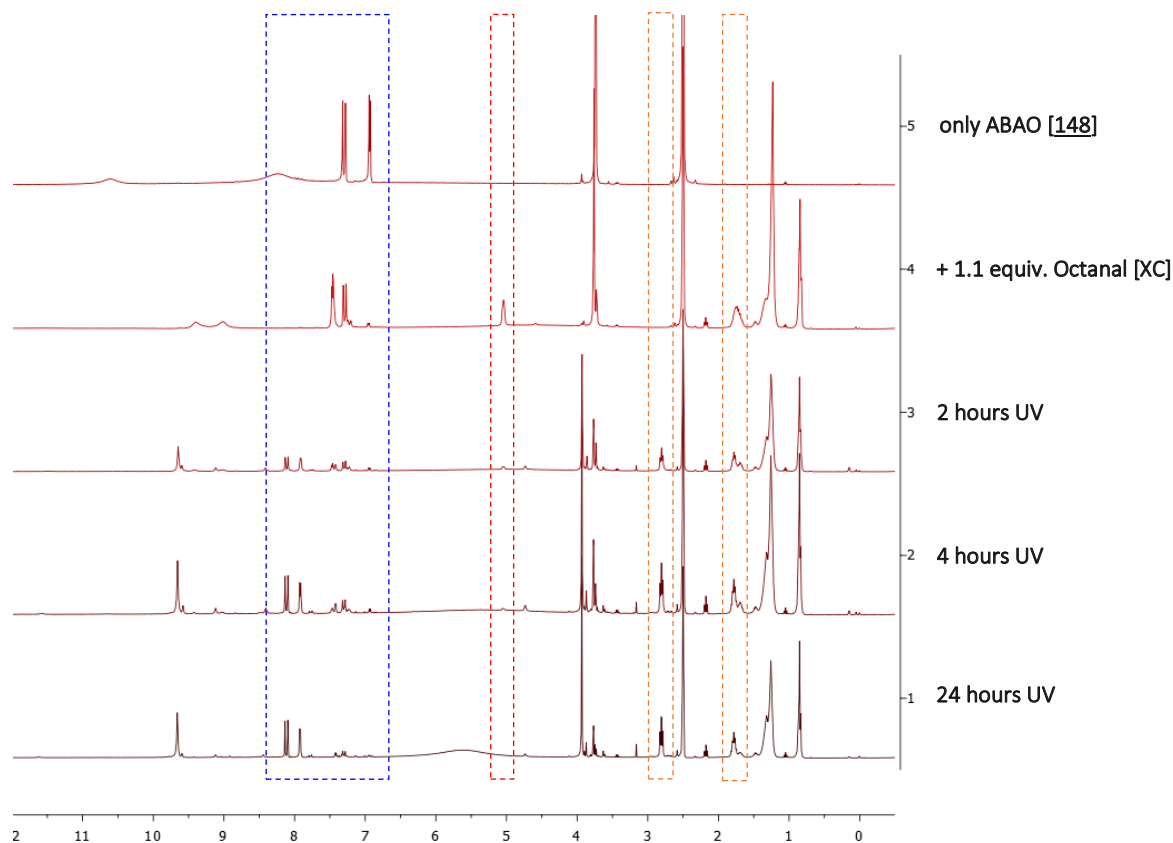
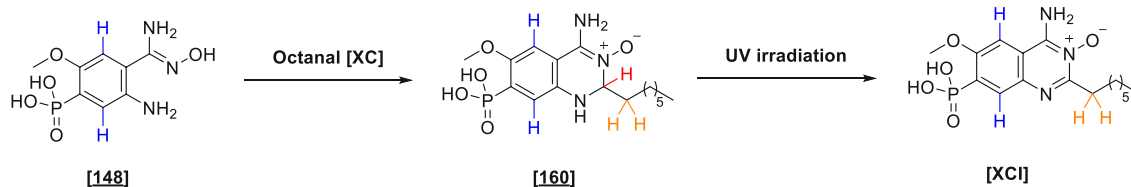


Fig. 75: Time-resolved ^1H -NMR study for the oxidation of octanal conjugate **[160]** triggered by UV-irradiation in d_6 -DMSO: Experiment was performed using in-situ formed adduct with the addition of 1.1 equiv. of octanal **[XC]** to a dissolved sample of **[148]**. Irradiation of the NMR tube in a UV-chamber (distance 15 cm) caused gradual disappearance of the characteristic trapped carbonyl-H (5.1 ppm, red) as well as the appearance of benzylic triplet signals (2.8 ppm, orange) over 24 hours. Additionally, a definitive change in the aromatic region (blue) pointed to the formation of a fully aromatized structure **[XC]**.

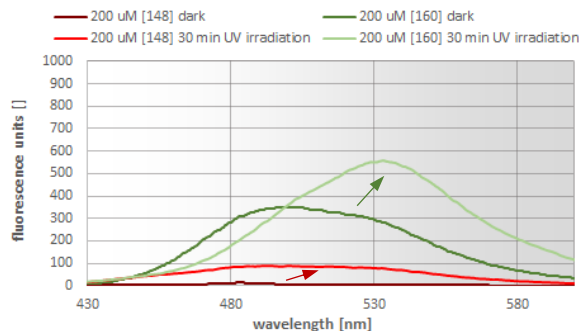


Fig. 76: Change of fluorescence emission caused by UV-irradiation of cuvettes containing 200 μM solutions of **[148]** and **[160]** respectively: Exposition of the samples to UV light for 30 minutes caused strong background emission of the practically non-fluorescent 4-P,5-MeO-ABAO **[148]**, as well as an increase in fluorescence emission due to full aromatization of the octanal conjugate **[160]**. The detrimental rise in background emission dramatically lowered the theoretical S/N ratio of the assay system, which made the handling of all samples in the dark necessary. All spectra were recorded in 100 mM pH 4.5 NaAc buffer, 5 vol% DMSO, excitation wavelength 415 nm, 5.0 nm slit, 775 V gain.

To achieve any form of selectivity for this oxidation, we turned to known chemical reagents for classical aromatic oxidation, as well as a presumably more specific photosensitizer-systems using blue LEDs and transition metal catalysts (Table 12). These experiments were performed in the already

mentioned buffer systems in closed 8 mL glass vials. All samples were first reacted with 1.1 equivalents of octanal [XC] and then treated with the chosen oxidation method. Samples were then checked in 10-minute intervals in the fluorometer for the reaction progress. The unreacted 4-P,5-MeO-ABAO [148] was always treated in the same fashion, and the background and product emissions were compared to see if any selectivity towards the octanal adduct [160] could be observed.

Table 12: Set of used conditions and chemical tools to trigger selective oxidation of [160].

entry	conditions	outcome	selectivity?
1	UV chamber (10 cm distance)	20 minutes full conversion	no
2	Ambient light (bench)	2-3 hours till complete conversion	no
3	Halogen lamp (150 W, 10 cm distance) no additive	30 minutes full conversion	no
4	Halogen lamp (150 W, 10 cm distance) 1 mol% Ru(bpy) ₃ Cl ₂	30 minutes full conversion (no difference)	no
5	Blue LEDs (462 nm, 45 W, 5 cm distance) no additive	10 minutes till complete conversion	no
6	Blue LEDs (462 nm, 45 W, 5 cm distance) 1 mol% Ru(bpy) ₃ Cl ₂	10 minutes till full conversion (no difference)	no
7	Blue LEDs (462 nm, 45 W, 5 cm distance) 10 mol% Ru(bpy) ₃ Cl ₂	10 minutes till full conversion (no difference)*	no
8	1 equiv. DDQ	Immediate oxidation to an unknown product	yes
9	1 equiv. BQ	No reaction	-
10	1 equiv. chloranil	No reaction	-
11	1 equiv. Na ₂ S ₂ O ₈	No reaction	-
12	1 equiv. TEMPO	No reaction	-
13	1 equiv. TEMPO + 1 equiv. Cu(OAc) ₂	No reaction	-
14	20 mol% TEMPO + 200 U Laccase	No reaction	-

Light as the source of excitation caused in any of the cases full transformation to the oxidized product. While placing the reaction vessel in the UV chamber completed the reaction in 20 minutes, using the in-house blue-LED irradiation system (Quelle David Schönbauer) was even quicker to trigger a full transformation. Leaving the sample standing on the bench prolonged the needed time to around 3 hours. The addition of the known photosensitizer Ru(bpy)₃Cl₂ for blue LED systems in the commonly used concentration of 1 mol% did not influence the reaction time or selectivity. Also, increasing the amount of photosensitizer to 10 mol % did not show any change - herein, sampling was even reduced to 1-minute intervals due to the fast reaction. In all of these cases, decomposition of the unreacted ABAO was always more prominent than the signal gain by the light-induced quinazoline oxidation. Employing any chemical means for the oxidation revealed a surprising behavior. The addition of one equivalent of either benzoquinone (BQ), chloranil, Na₂S₂O₈, TEMPO, as well as TEMPO-Cu(OAc)₂ or TEMPO-Laccase combinations did not show any change in the fluorescence spectrum and were thus not interacting with the adduct even after prolonged reaction times. The use of DDQ (2,3-dichloro-5,6-dicyano-1,4-benzoquinone), however, caused an immediate transformation of the adduct to a singular species, which was also supported by ¹H-NMR / ³¹P-NMR evidence (Fig. 77).

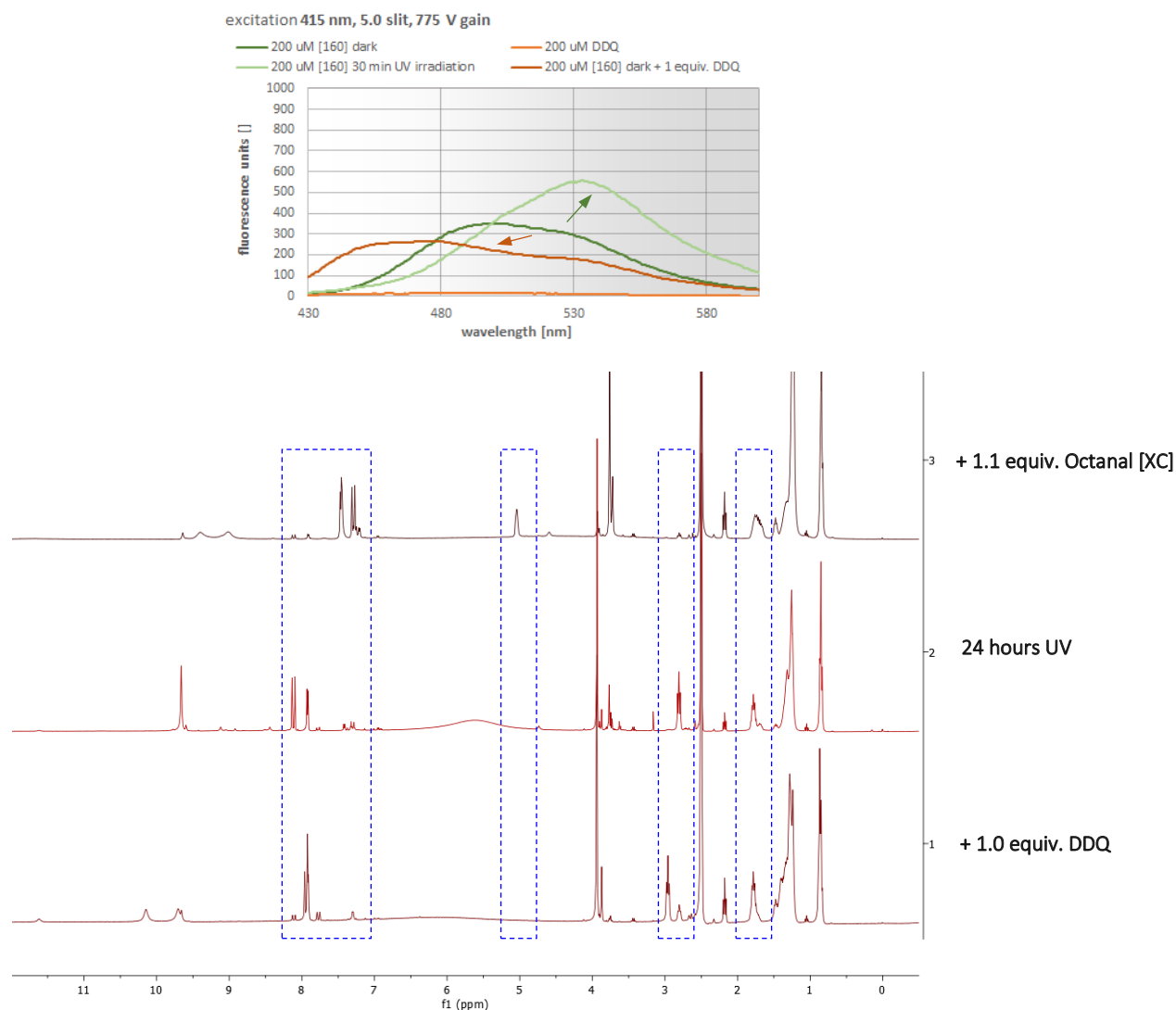


Fig. 77: Fluorescence and ^1H -NMR comparison of [160] oxidations employing either UV light or DDQ – **top:** Addition of 1 equivalent of the chemical oxidant to [160] solutions triggered immediate blue-shift of the fluorescence spectrum and emergence of a fluorescence emission maximum at 480 nm which was proven to derive from the chemical oxidation. Spectra were recorded in 100 mM pH 4.5 NaAc buffer, 5 vol% DMSO, excitation wavelength 415 nm, 5.0 nm slit, 775 V gain.; **bottom:** Treatment of the conjugate in d_6 -DMSO with DDQ caused the emergence of a similar oxidation peak pattern as UV induced aromatization, albeit with distinct differences in blue highlighted peak areas.

Although some similarities to the UV-oxidized species were found by comparison of the emerging or disappearing peaks (blue boxes – *c.f.* Fig. 75), no definitive structure could be ascribed to the product. The most dominant mass in the HPLC-MS spectrum pointed to similar oxidation with the loss of two 2 protons, albeit demonstrably having a different structure as seen from the NMR evidence as well as the changes in the fluorescence spectrum. As this DDQ-oxidation was proven to be detrimental for the fluorescence signal, no in depth-investigations were performed, further elucidating the exact structure. To see if the light-induced process was general for the ABAO-conjugates, further irradiations were performed with adducts of benzaldehyde [79] as well as cinnamaldehyde [164] (Fig. 78). Whereas both substrates showed a clean transformation to the dihydro quinazoline products, the benzaldehyde adduct furthermore showed clean oxidation to [XCII] by UV-excitation overnight. On the other hand, evident decomposition was observed for the oxidized cinnamaldehyde adduct [XCIII]. Especially the loss of the olefinic region below 7 ppm (blue box) could point to a vulnerability in the structure. Simple aliphatic, as well as aromatic aldehyde conjugates, might be thus oxidized to stable quinazolines using this method.

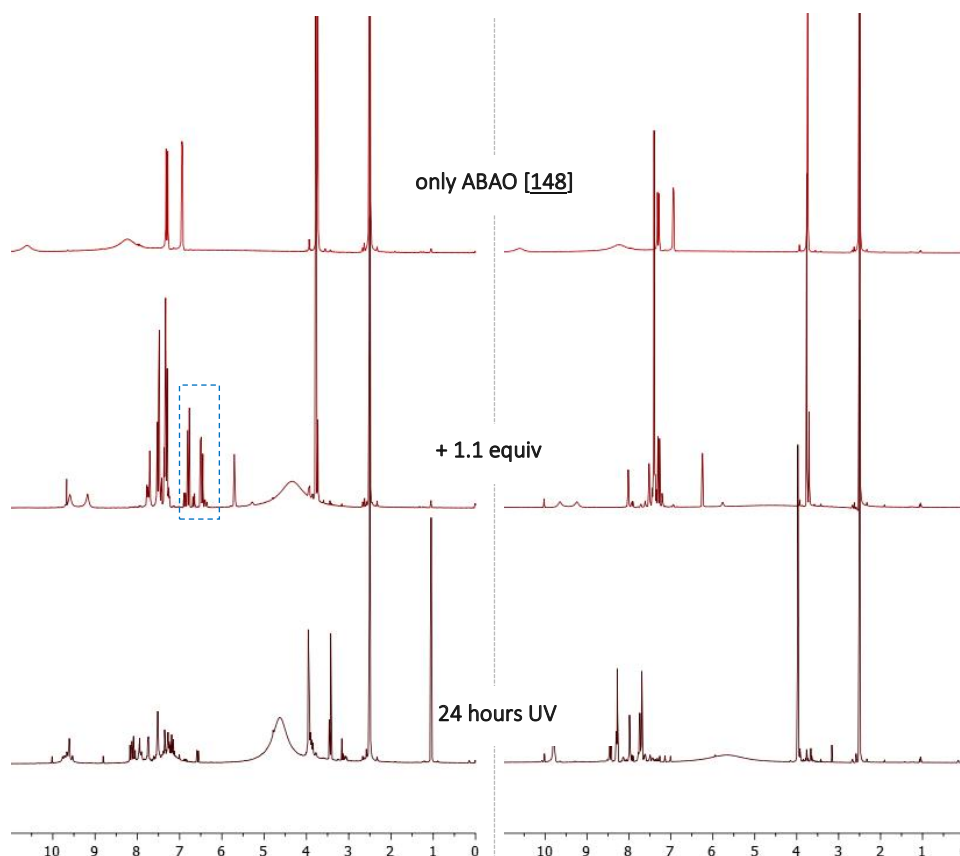
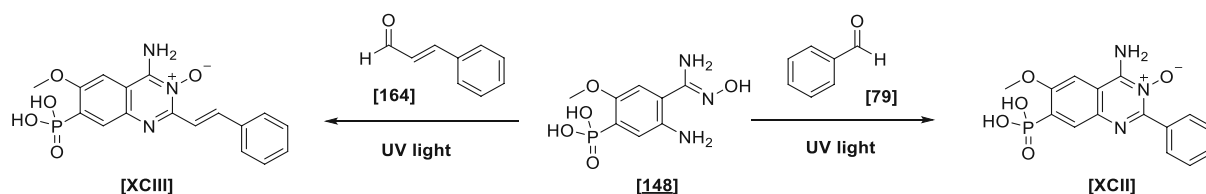


Fig. 78: ¹H-NMR comparison of UV-light induced oxidations of [148]-conjugates with cinnamaldehyde [164] (left) benzaldehyde [79] (right): Irradiation of the benzaldehyde adduct triggered clean conversion towards the quinazoline product [XCII], similar treatment of the cinnamaldehyde adduct caused complete decomposition of the material, evident with the disappearance of the signals corresponding to the double bond (blue box).

By comparison of all synthesized P-ABAO structures, the 4-P,5-MeO-ABAO [148] proved to be the ideal contender for the application in the FADS by having the fastest kinetics, the highest overall red-shift of the candidates, and comparably one of the highest absorptions coefficients (Fig. 71). Due to the instability of the free ABAO and a chemically inaccessible selective oxidation of the adduct, we decided to perform the sorting trials in the unoxidized state. As mentioned, although excitation closer to the absorption maximum below 400 nm improved the overall fluorescence emission, the spectral overlap with the free ABAO at these wavelengths caused troublesome background fluorescence emission. Hence excitation at higher wavelengths (410-440 nm) proved to be more optimal for the overall sensitivity of the system and would allow detection of lower enzymatic conversions due to higher S/N ratios. Tolerable pH ranges for an adequate fluorescence signal, as well as sufficient reaction kinetics, were found to be between 4,5-5,5 (Schiefer). Further increase in pH caused the reaction even with fast aliphatic aldehyde octanal [XC] to become sluggish (> 30 min). Due to the limited availability of laser irradiations sources (Roither), we thus opted to buy the 415 blue-violet laser diode from CNI for the final application in the FADS.

C I.1 Part VI – Fluorescence-activated droplet sorting

Having no previous experience in the group with either microfluidics, photolithography, PDMS chip manufacturing, complicated optical assemblies, high voltage manipulation, or LabView® programming, extensive literature search pointed us to several essential literature sources as well as introductory material from National Instruments® (LabView®) which are summarized in Table 13.

Table 13: Summary of used literature sources used for the assembly of the FADS system

subject	main literature	further sources
Compendium	171	257, 258, 187, 259, 260
PDMS chip manufacturing & Photolithography	261	171, 2
Microfluidics	262	171, 260
Optical assembly	263	171
LabView FPGA programming	National Instruments Learning Centre https://learn.ni.com/	-

Herein the nature protocol by Mazutis *et al.*¹⁷¹ proved to be the most reliable source for many steps needed for the assembly. Not only did the paper describe a step-by-step procedure for the establishment of a fluorescence-activated droplet sorting system, but it also provided a list of necessary components and their associated suppliers. Although several connections between these singular units of the system were not explained or in sparing detail, the script provided many reference points. Additional insightful explanations about the intricacies of the assembly could be found in sources from Qiao *et al.*²⁶⁴ and Abate *et al.*¹⁷⁵ As final results regarding the fluorogenic investigations of the 4-P,5-MeO-ABAO [148] assay system were performed before the finalization of the results for the ABThD-H [111], the whole FADS assembly was planned according to its fluorescence excitation and emission.

Hence, the goal for this thesis can be formulated as follows: The target of this study was the establishment of a working FADS system on the TU Wien and proof of concept by the application of the 4-P,5-MeO-ABAO [148] assay system for the detection of carbonyl compounds. Consequently, an aqueous solution containing the 4-P,5-MeO-ABAO-octanal adduct [160] should be encapsulated inside aqueous droplets and sorted according to a set voltage threshold. Proof should be delivered by the separation of a defined population of fluorophore-filled and empty droplets and analysis of sorted populations. The focus of the system was placed on future flexibility of the assembly to enable facile replacements of any parts and economic aspects. Hence, more expensive components were bought as refurbished products (high voltage amplifier, national instruments FPGA card). The following chapters will deal with the assembly of the whole system as well as the stepwise achievement of stretch goals towards the final sorting process.

² https://www.microresist.de/en/?jet_download=6869, accessed September 2021.

C I.1.1 Optical assembly

Most established FADS systems were built around a commercial bright-field inverse microscope from Nikon or Olympus.²⁶⁴⁻²⁶⁶ These fully decorated platforms allow for an easy and exact operation of the pre-installed optical components (excitation and emission source orientation, camera mount, optical table manipulation, magnification settings). However, modern systems start to be priced at around 10.000 € (in used conditions) and are generally constructed as rigid boxes, where subsequent alterations (incorporation of multiple laser sources, changes to the optical system) are rendered impossible. Certain groups have overcome this issue by installing a separate unit adjacent to the microscope with a notable effort by constructing intricate 3D-printed housings. However, these modifications were not described in overwhelming detail, which complicated any replication attempts. We thus opted to collect the most beneficial information out of all sources available and build our own system. Details about the assembly were summarized in the experimental section FADS (E V).

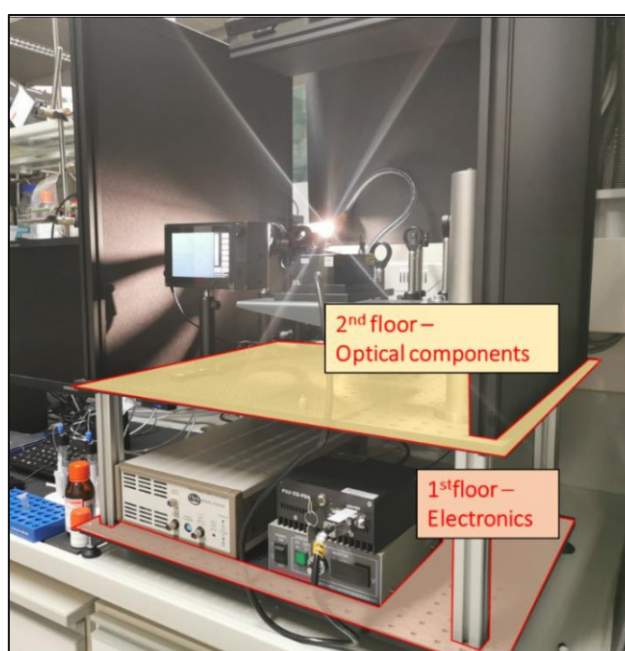


Fig. 79: Front view of the FADS showing the two-storied assembly.

As depicted in Fig. 79, we envisioned the system encased in a cubical structure to limit exposition of the analytic hardware as well as the fluorophores to stray light and thus limit any background signal. In the first version, we constructed the system as single-level construction but quickly realized that a second floor was beneficial for handling reasons due to space restrictions. We finally decided to split the assembly and move all the optical assembly onto a 2nd floor, which massively improved the manipulation of movable parts and subsequent adjustments of the optical system.

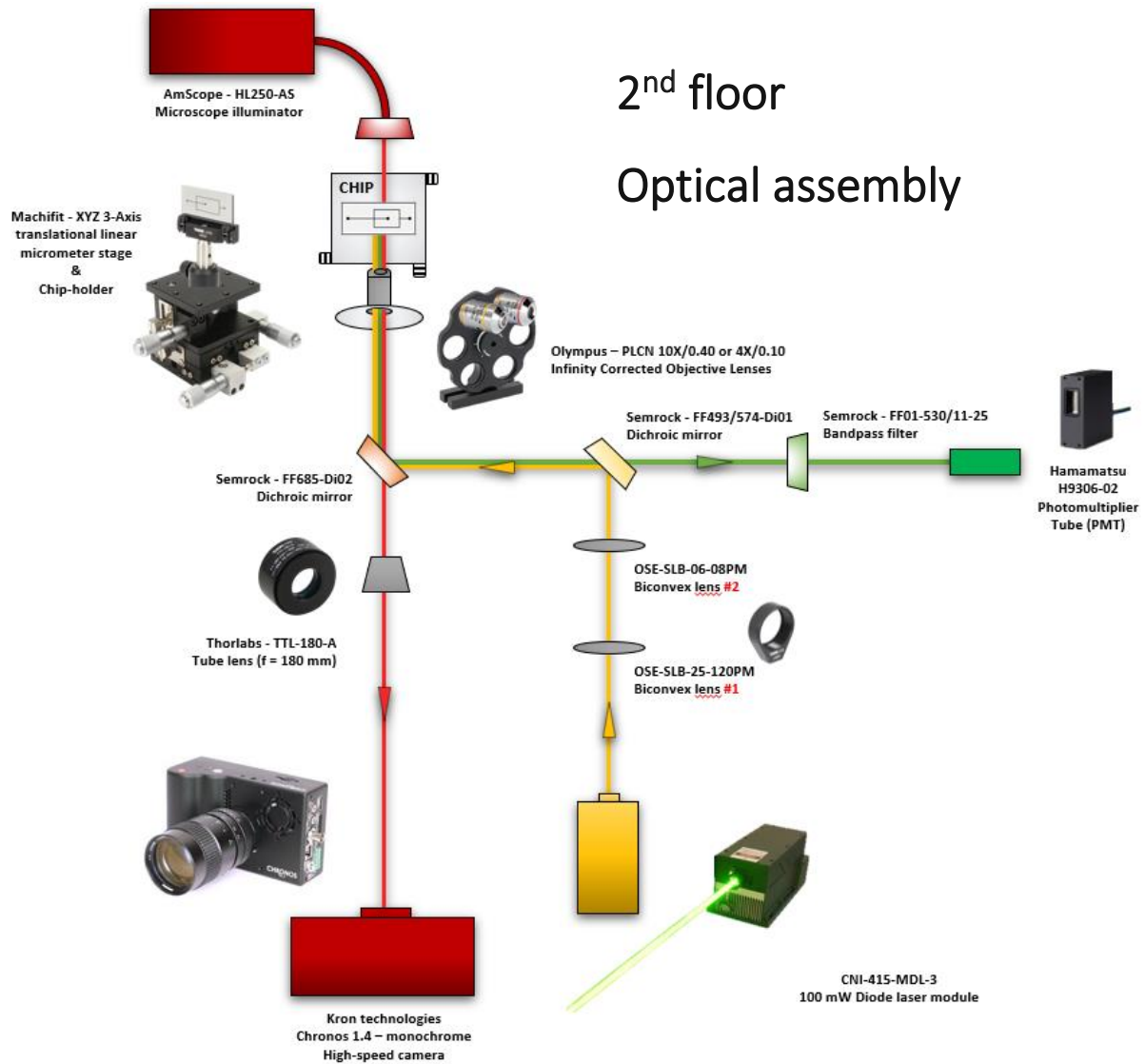


Fig. 80: Schematic overview of the optical assembly of the FADS. Light paths of the different emission sources are marked in different colors. The red path illustrates the backlight illumination of the chip with the halogen lamp and thus enables visual control of droplet manipulations; The yellow path describes the optical train of the laser beam through the optical set-up; The green path describes the route of the emitted fluorescence signal to the photomultiplier tube

On this floor, we thus incorporated several interplaying optical components. As simultaneous fluorescence excitation, emission measurements, and visual tracking of the sorting process were desired, the optical assembly was needed to accomplish that.

The final design is depicted in Fig. 80. Three different optical pathways could be drawn and followed – the yellow path represented the fluorescence excitation by the CNI-415 MDL-3 blue-violet laser diode. In the final configuration, the emitted laser light was guided through a combination of the OSE-SLB-25-120PM and OSE-SLB-06-08PM biconvex lenses. The thus magnified laser beam was reflected off the Semrock FF493/574-Di01-25x36 and Semrock FF685-Di02-22x29 dichroic mirrors and projected through a microscope lens onto the chip. Using the Olympus PLCN 10X/0.20 lens, a total 150-fold magnification of the laser beam (approx. 2.5 mm) was possible, creating an approx. 16 μm spot on the microfluidic chip. By appropriate substitution of the biconvex lenses (see

Table 14) and thus necessary adjustment of their spacing (representing the sum of their focal lengths), scaling of the laser beam could be prior to the different the laser width achieved final

biconvex lens #1	biconvex lens #2	spacing	magnification
OSE-SLB-25-120PM	OSE-SLB-06-06PM	12.6 cm	20x
OSE-SLB-25-120PM	OSE-SLB-06-08PM	12.8 cm	15x
OSE-SLB-25-120PM	OSE-SLB-06-10PM	13 cm	12x
OSE-SLB-25-90P	OSE-SLB-06-10PM	10 cm	9x
OSE-SLB-25-60P	OSE-SLB-06-10PM	7 cm	6x
OSE-SLB-25-120PM	OSE-SLB-25-30P	15 cm	4x

magnification using the respective microscope lenses (see equation 1). This allowed for flexible adjustment of the laser beam diameter without impacting the optical system for visual read-out of the camera (red path).

Table 14: Set of different lens combinations enabling different biconvex lens magnifications of the laser beam (2.5 mM diameter) prior to passing the microscope lens onto the chip.

biconvex lens #1	biconvex lens #2	spacing	magnification
OSE-SLB-25-120PM	OSE-SLB-06-06PM	12.6 cm	20x
OSE-SLB-25-120PM	OSE-SLB-06-08PM	12.8 cm	15x
OSE-SLB-25-120PM	OSE-SLB-06-10PM	13 cm	12x
OSE-SLB-25-90P	OSE-SLB-06-10PM	10 cm	9x
OSE-SLB-25-60P	OSE-SLB-06-10PM	7 cm	6x
OSE-SLB-25-120PM	OSE-SLB-25-30P	15 cm	4x

$$\text{Final magnification} = \text{biconvex magnification} \times \text{microscope lens magnification} \quad (1)$$

The green path represented the emitted fluorescence signal reflected off the Semrock FF685-Di02-22x29 nm longpass mirror, passed through the Semrock FF01-530/11-25 and Semrock FF493/574-Di01-25x36 bandpass filters, and was finally picked up by the Hamamatsu H9306-2 photomultiplier tube. Concomitant observation of the chip was enabled by a custom-built infinity-corrected microscope using a combination of infinity-corrected microscope lenses (see Experimental Table 18), a Thorlabs TTL-180-A tube lens, and a Kron technologies Chronos 1.4 – high-speed monochrome camera as the optical sensor. The exact placement of all optical components using an optical rail (red path) was necessary to enable a correct read-out (Fig. 81). The nature of the thus created parallel infinity space enabled any subsequent manipulations (deflection, reflections) of the light within the space between the tube lens and the microscope lens without impacting the signal. This feature was used to couple the visual read-out of the camera with the laser emission/fluorescence detection.

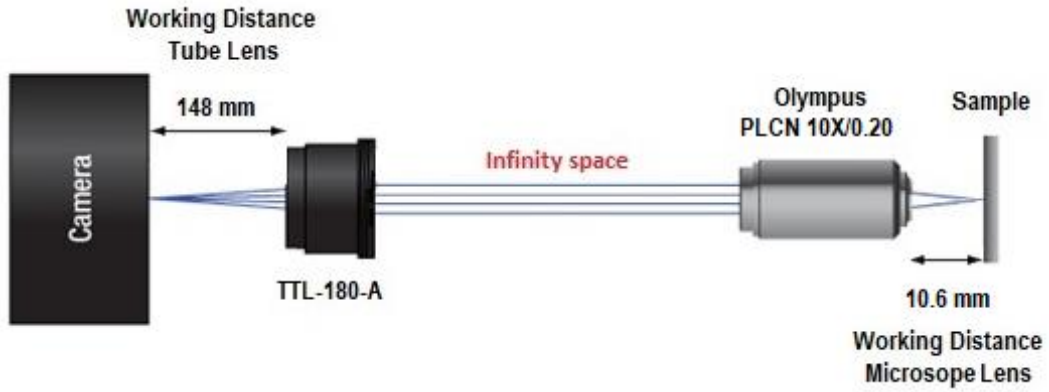


Fig. 81: Spatial alignment of the infinity-corrected microscope – section between the tube lens and the microscope lens represents the infinity space which provides a path of parallel light rays into which complex optical components can be placed without distortion of the visual readout. The represented illustration represents the actually equipped setup for a droplet sorting experiment (not to scale).

Due to the limited exposure time in high-speed recordings, a strong illumination of the chip using an AmScope HL250-AS microscope illuminator was necessary (Fig. 109). The flexible goose-neck of the lamp was equipped with a Thorlabs FELH0700 – 700 nm longpass filter, which prohibited undesired excitation of the fluorophores and stray light interference with the PMT measurements. The top view of the assembled second floor of the FADS can be seen in Fig. 82.

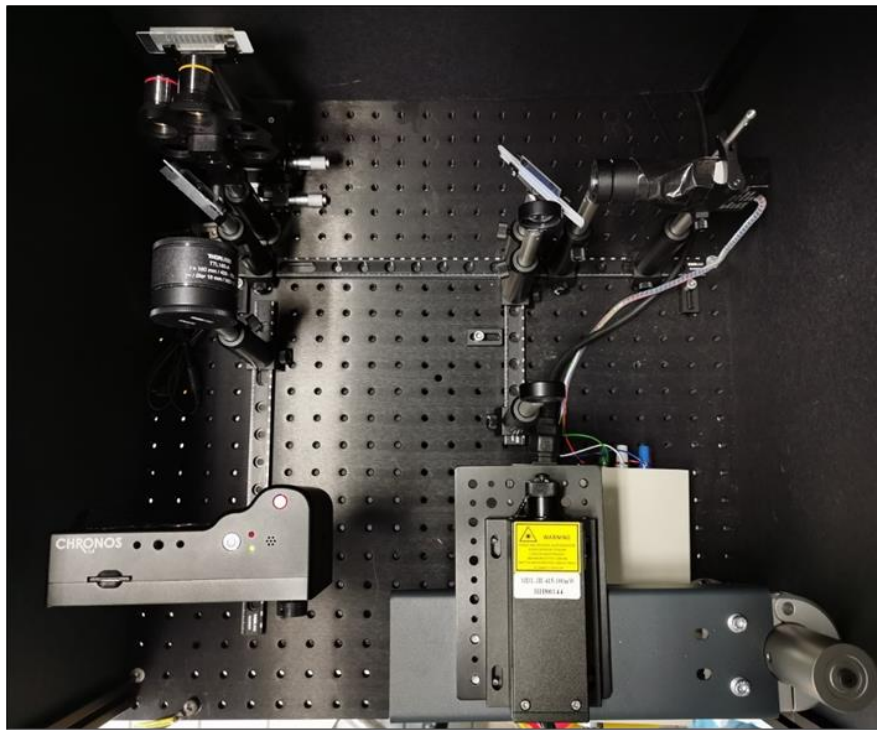


Fig. 82: Top view of the optical assembly, including all mounted optical components.

Using this configuration and switching the set of microscope lenses using the rotatable microscope lens holder, three different magnifications could be set on the chip (Fig. 83).

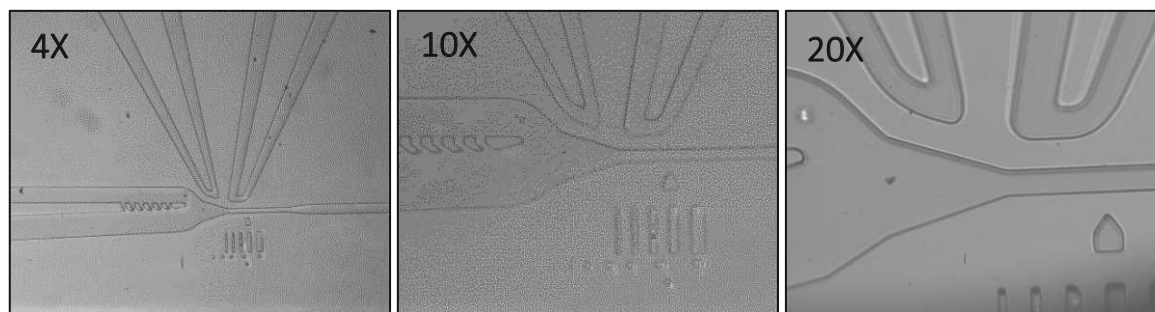


Fig. 83: Three different magnifications of the visual read-out enabled by the set of microscope lenses summarized in *Table 18* are selectable by rotation of the microscope lens holder.

Due to a difference in working distances for each of the respective lenses, a final fine adjustment of the Z-coordinate of the micrometer stage was needed for a sharp image. The most optimal lens for appropriate laser beam magnification and concomitant visual control of the droplet manipulation was found to be the Olympus PLCN 10X/0.20. Both the 4X/0.10 as well as the 20X/0.40 magnification caused either a too strong broadening of the laser beam or did not allow for appropriate tracking of the sorting process. If no beam excitation was required, the 4X/0.10 magnification enabled the best overview of any operations (Fig. 83). The precise alignment of the laser beam, as well as the positioning of the dichroic mirrors, was described in E V.1.1. Proof for a correct assembly of all optical components could be made by following the excitation of the droplets on camera (Experimental Fig. 126 top) and by the simultaneous recording of the PMT voltage data represented in Fig. 126 bottom.

C I.1.2 Manufacturing of microfluidic PDMS chips

A crucial step for the operation of a FADS platform at the TU Wien was the manufacturing of microfluidic devices. Herein the TU Wien research group of Prof. Ertl gratefully offered their help and facilities for the production of the PDMS chips. Due to the expected slow nature of unoptimized enzymatic systems, prolonged incubation of the encapsulated drops for periods up to 1-2 days was envisaged. Hence the system was planned in accordance with the previously mentioned nature protocol of Mazutis *et al.*¹⁷¹ in two separate parts – one microfluidic chip for droplet encapsulation and one for droplet sorting. The details about the constitution of those structures are explained in later chapters. (C I.1.3 & C I.1.4) These designs were freely accessible and represented, albeit having a different application, a similar use-case.¹⁷¹ The AutoCAD designs (*c.f.* Fig. 114) were printed on a chrome-based photomask by Jena Compugraphics (Fig. 84). These photomasks were used as negatives for the soft-lithography process described in detail in chapter E V.2.

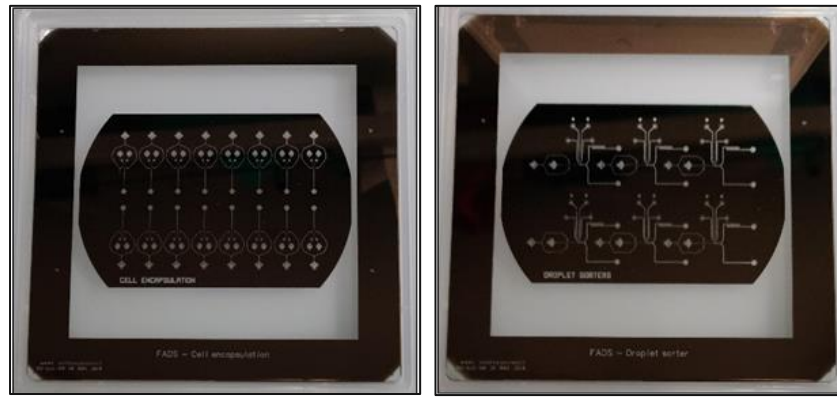


Fig. 84: Printed chrome-based photomasks by Jena Compugraphics with imprinted microfluidic AutoCAD designs representing the droplet encapsulation (*left*) and droplet sorting devices (*right*).

The procedure was primarily based on the instructions described by the technical data sheet³ of the manufacturer of the SU-2025 photoresist (Kayaku Advanced Materials) with slight alterations implemented by the members of the Ertl research group. Herein baking times and temperatures were slightly adjusted to fit the already preset (and proven well-performing) instrument settings in the lab. A summary of the process steps needed to manufacture the silicone master molds has been summarized in Table 15. All baking steps were performed on commercial hot plates with built-in temperature sensors.

Table 15: Summary of all tasks necessary to manufacture silicium master molds with respective times and temperatures/settings.

task	time	temperature / settings
Dehydration of wafers on the hot plate	15-20 minutes	145 °C
Plasma-treatment of wafers using the <i>Harrick Plasma - PDF-002-CE plasma cleaner</i>	5 minutes	high
Spin-coating of wafers with SU-2025 using the <i>Laurel WS-650MZ-23NPPB</i>	10 seconds @ 500 rpm, then 30 seconds @ 3000 rpm	-
Soft-bake of coated wafers	5-6 minutes	90 °C
UV light exposition using the <i>UV-KUB 2 masking system</i>	7 seconds	23.8 mW/cm ² (50% intensity)
Post-exposure bake	5-6 minutes	90 °C
Development of the photoresist using the <i>mr-Dev 600 SU-8 developer</i>	5 minutes swirling in the developer bath	-
HPLC grade iPrOH rinse of the wafers	-	-
Hard-bake of the developed wafer	30 minutes	200 °C
Silanization in the vacuum desiccator using <i>trichloro(1H, 1H, 2H, 2H-perfluorooctyl)silane</i>	5 minutes	-
Final bake of the finished master mold	30 minutes	90 °C

Two adjustments were necessarily made during the manufacture of the molds. As the research group predominantly prepared microfluidic chips bearing much wider channels geometries than those used in this thesis, dust contaminations were not as impactful for their applications. However, the widths of the channels for the FADS system were already similar in size to smaller dust particles. As

³ https://www.microresist.de/en/?jet_download=6869 – accessed September 2021.

these facilities were not equipped as clean-rooms, dust contaminants were prevalent and detrimental to the overall quality of the master molds. Hence the handling in between the spin-coating and the soft-bake of the viscous photoresist was crucial. Fast transfer of the freshly spin-coated wafers onto the hot plate and immediately cover with a large glass petri dish during the baking process limited the exposition to particulates. Secondly, due to the large size of the gratuitously supplied 6" wafers of *Infineon*, these, unfortunately, did not fit into the UV exposer, which was designed to irradiate 4" wafer sizes. Hence all soft-baked molds had to be cut to the appropriate size using a glass cutter. To identify the falsely produced chip molds after the final baking step, visual checks under the microscope were always performed prior the any PDMS casting. This adapted procedure made reproducible production of master molds bearing the wanted motifs as patterned silicon wafers possible (Fig. 85).

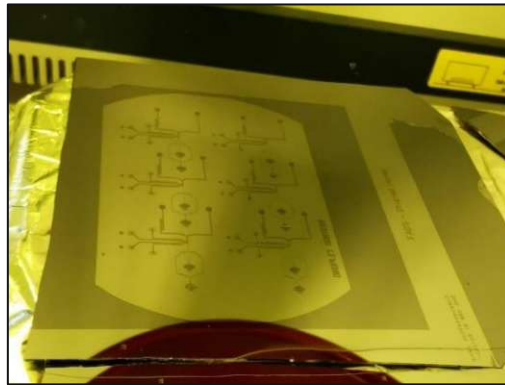


Fig. 85: Finished master mold with the structures visible to the naked eye.

To enable simultaneous casting (Fig. 86) of a larger number of chips, several master molds for droplet encapsulation and droplet sorting were produced. The PDMS chips were formed using a commercial mixture of Sylgard 184 pre-polymer and curing agent 10:1 (v/v), which after removal of any suspended bubbles was cured in the oven at 80 °C for 2 hours.

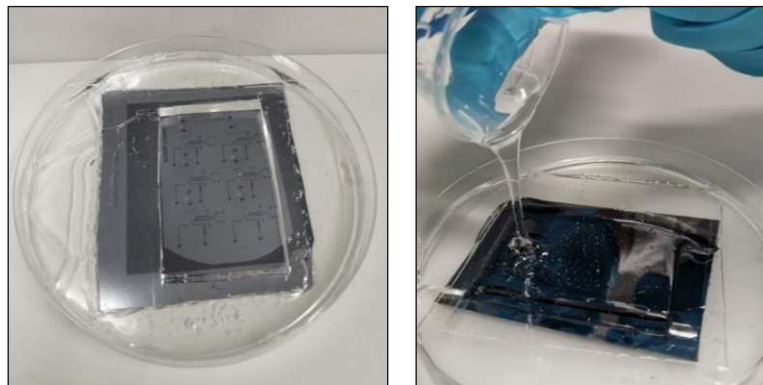


Fig. 86: Pouring freshly degassed PDMS onto a master mold into a pre-cut cavity resulting from previous castings.

The hardened PDMS slabs were carefully peeled from the silicon wafers, cut to size and inlet, as well as outlet holes for tubing, and electrodes were punched using a WPI biopsy puncher ($\varnothing = 0.75$ mm). Non-coated glass slides for droplet encapsulation or ITO (indium-tin-oxide) coated ones for droplet sorting (!) were thoroughly cleaned and activated by plasma treatment. The ITO coating enabled the necessary grounding of the chip, which prevented undesired coalescence of the droplets in the voltage-driven sorting process. The glass slides were subsequently contact bonded to the PDMS slab by initial plasma treatment of the surfaces and subsequent compression at 80 °C in the oven over two days. In

preliminary attempts, this was realized by clamping of the chip using strong spring clamps, but this approach was found to be detrimental due to a collapse of wider microfluidic channels (Fig. 87, left). Careful cleaning of both substrates using HPLC grade iPrOH, careful drying in the oven, blow-drying with pressurized N₂, and a final treatment with scotch tape was vital for sufficient activation of both surfaces. This process enabled facile bonding by gently applying pressure using just finger strength and subsequent thermal treatment. If the removal of the PDMS slab was easily possible (Fig. 87, right), both substrates had to be cleaned and re-bonded. In cases where the adhesion was insufficient immediate leaking upon introducing liquids into the microfluidic channels was evident. Chips should generally withstand pressures up to 2000 mbar without any lifting of the PDMS layer.

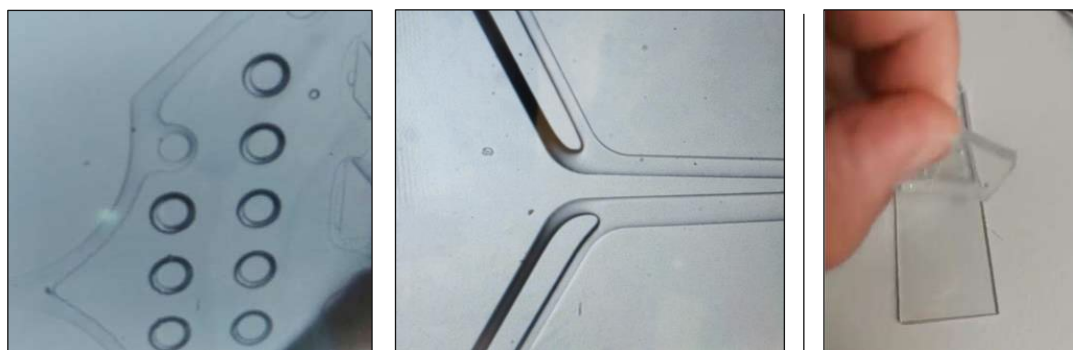


Fig. 87: Strong compression of the PDMS chips during plasma bonding caused the collapse of broader microfluidic channels, especially at the droplet inlet (**left**) and after the sorting junction (**middle**) of the droplet sorting devices. Insufficient bonding enabled facile detachment of the PDMS slab (**right**).

After recovery of the chips from the oven, the microfluidic channels were treated with a syringe-filtered 1 vol% tridecafluoro-1,1,2,2-tetrahydrooctyl)trichlorosilane solution in HFE-7500 using the Elveflow OB1 flow controller at 1000 mbar (see. Fig. 124, left). The silanization dramatically decreased the hydrophilicity of the PDMS and was needed to stabilize the aqueous droplets.



Fig. 88: Inexplicable darkening of the PDMS chips surrounding the microfluidic channels by prolonged treatment with 1 vol% tridecafluoro-1,1,2,2-tetrahydrooctyl)trichlorosilane solution (**left**). Limiting the reaction to maximum 5 minutes prevented this effect (**right**).

The solution was initially passed through the channels with constant pressure for 30 - 60 minutes and subsequently flushed with fresh HFE-7500. These prolonged times caused an inexplicable blackening of the channel walls, which impaired any visual control (Fig. 88). Limiting the treatment to 5 minutes immediately improved the optical conditions without impairing droplet stability. The channels were then cleared with fresh solvent and then with air, delivering ready-to-use

microfluidic devices. These were wrapped in scotch tape to prohibit any further contaminations (Fig. 89).



Fig. 89: Mass production of chips enabled by the manufacture of multiple master molds.

C I.1.3 Droplet encapsulation

With the finished microfluidic devices in hand and the optical system established, we turned to droplet encapsulation experiments. The device for the droplet formation consisted of three inlets – one for the oil / continuous phase and two for the aqueous phases (Fig. 90). Collision of the layers at the flow-focusing junction (Fig. 91) triggered the formation of the aqueous droplets, which were typically collected in a pre-drilled Eppendorf tube connected *via* the outlet tubing. Each of the channels was equipped with a filter (Fig. 120) to block larger debris from entering the microfluidic system and a fluid resistor to dampen fluctuations resulting from the elasticity of the PDMS chip. The flow-focusing junction geometry was designed to apply similar sums of pressures of the oil and aqueous channels for the droplet encapsulation.

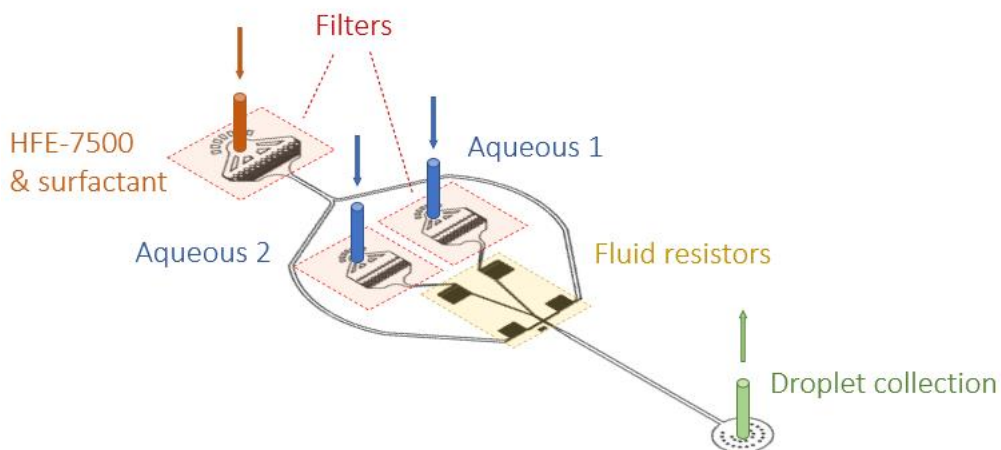


Fig. 90: Schematic of the droplet encapsulation chip - inlets should be connected to the respective XS reservoir tanks *via* 0.012" ID x 0.030" OD PTFE tubing. The outlet should be connected to a separate black pre-drilled Eppendorf tube. All solutions entering the chip initially pass filters, limiting a possible blockage of the chip.

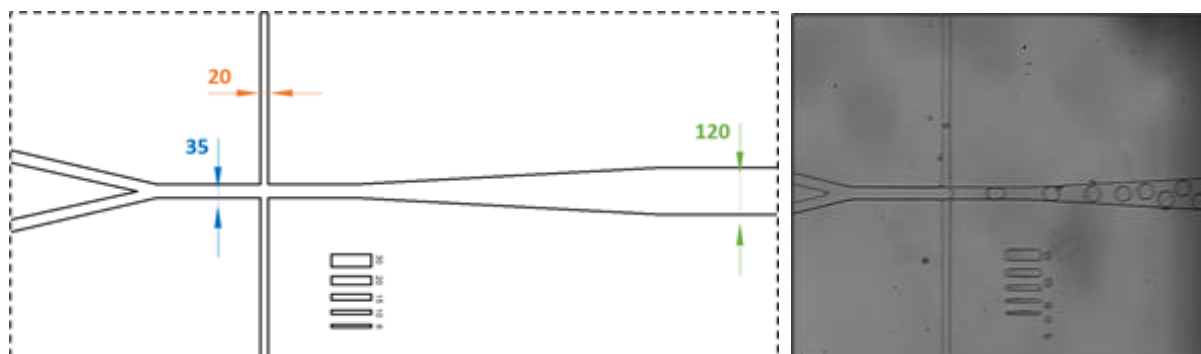


Fig. 91 - left: AutoCAD design of the flow-focusing junction of the droplet encapsulation device with respective channel widths (in μm); right: Snapshot of the droplet encapsulation event at the same location.

The inlets and outlets were connected according to Fig. 90, and the chip was placed in the chip holder in front of the objective (Fig. 92). The Elveflow[®] microfluidic control software (Fig. 124, left) was used to adjust the pressures on every channel. The best results were obtained when all pressures were set in parallel, and no backflow into any of the non-pressurized channels was possible.

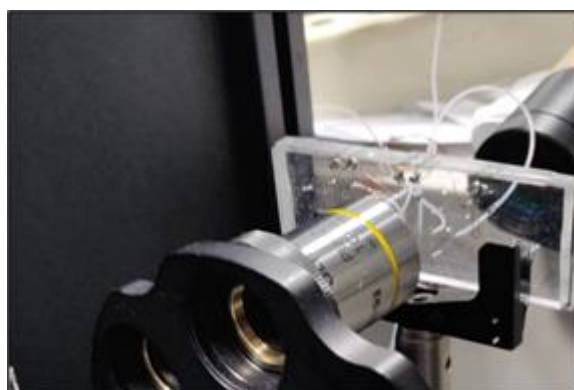


Fig. 92: Fully connected microfluidic chip in front of the 10X/0.20 microscope lens.

Assuming a spherical geometry of the droplets, their volumes were approximated using the diameter of the recordings and known channel widths. Droplets between 35-50 μm diameters could be translated to 25-65 μL volumes. Selected rates of droplet formation, the required pressures, and resulting droplet volumes are summarized in Experimental Table 19. However, due to minor differences in the chip geometries and possible channel constrictions, pressures for each experiment had to be individually adjusted. The continuous phase always consisted of a 2 wt% solution of RAN Biotechnology 008-FluoroSurfactant in HFE-7500. The aqueous phases were varied according to the desired experiment.

Preliminary trials proved the droplet formation to be, in fact, a very robust process as droplets were formed very consistently and reproducibly at constant pressures. We, however quickly realized, that the microfluidic channels, although being cleanly handled, were quickly blocked by small particulates (Fig. 93). Several steps were taken to avoid this issue. All tubes inserted into the chip were freshly cut using a tube-cutter and flushed with the respective solutions for several seconds. Furthermore, all liquids injected into the droplet encapsulation chip, including the perfluorination solution, had to be syringe filtered. Lastly, all reservoir containers were freshly cleaned with EtOH and dried prior to their use. With this droplet, the formation could be carried out for hours (max. 12 hours attempted) without any drop in quality.

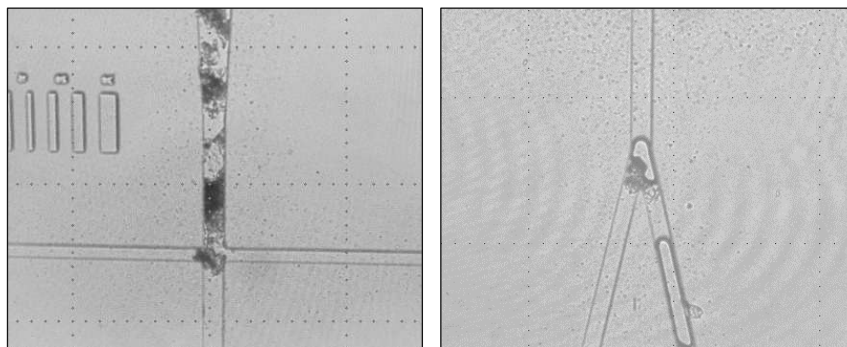


Fig. 93: Typical blockages by small debris or dust particulates that entered the microfluidic chips.

The initial droplet forming process was checked using a strongly red-colored solution of Safranin-O [XCIV] as the second aqueous source. Due to the microfluidic regime, the laminar and thus immiscible flow was observed even upon the first contact of the fluids. Only upon reaching the flow-focusing junction, the turbulence in the droplets caused rapid mixing (Fig. 94).

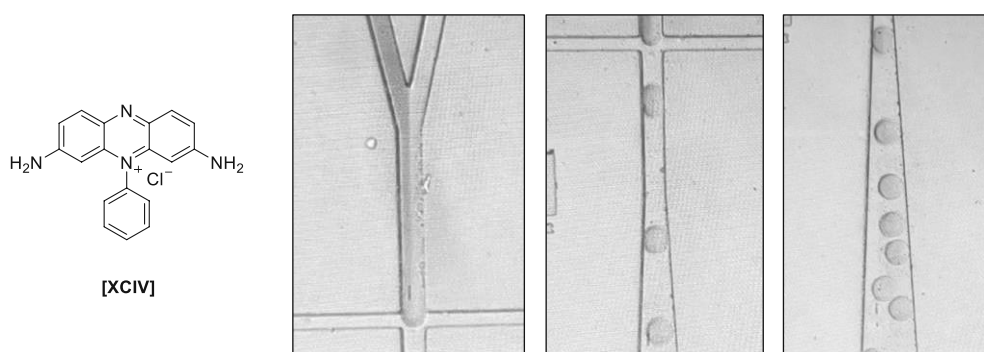


Fig. 94: Illustration of the laminar flow regime prior to the flow-focusing junction. The deep red-colored Safranin-O [XCIV] aqueous solution showed only mixing after the encapsulation event. Due to the monochrome character of the camera, the red color was only picked up as a dark grey solution.

This property was desired, as any enzymatic and assay reactions should only proceed upon successful encapsulation. The collection of the formed droplets should always be performed into an Eppendorf pre-filled with surfactant-containing HFE-7500 solution to prevent any evaporation and coalescence of droplets. The accumulated droplets were typically stored for up to two days at room temperature as increasing coalescence prevented any subsequent sorting experiments. Ideally, the sorting experiments were done immediately after the encapsulation (or after the incubation period).

C 1.1.4 Droplet sorting

The device for the droplet sorting consisted of two inlets – the reinjection port for the incubated droplets and one inlet for the carrier oil (Fig. 96). Sufficiently spaced droplets (Fig. 95) were guided to the sorting junction where they crossed the excitation laser beam, which was focused onto the channel above the red arrow (see Fig. 97).

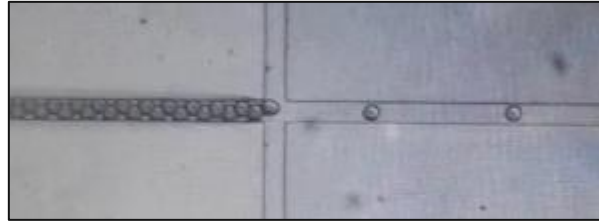


Fig. 95: Snapshot of the reinjected droplets at the spacing junction.

If the thus emitted fluorescence exceeded a user-set threshold defined by the GUI in the custom-written LabView program (see. Fig. 102), an electric sorting field was turned on by passing a high voltage pulse through the electrodes. Due to the difference in dielectric permittivity between the aqueous phase ($\epsilon \sim 80$) and the fluorinated oil ($\epsilon \sim 2$), the resulting dielectrophoretic force pulled the droplets towards the positive channel. In the case no voltage was applied, the geometry of the channels created a biased flow towards the broader and shorter negative channel.

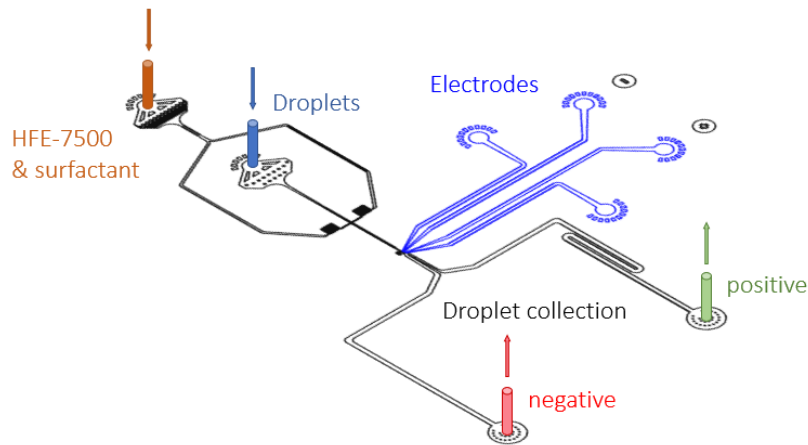


Fig. 96: Schematic of the droplet sorting chip - inlets should be connected to the respective XS reservoir tanks via 0.012" ID x 0.030" OD PTFE tubing. The outlets should be connected to separate Eppendorf tubes.

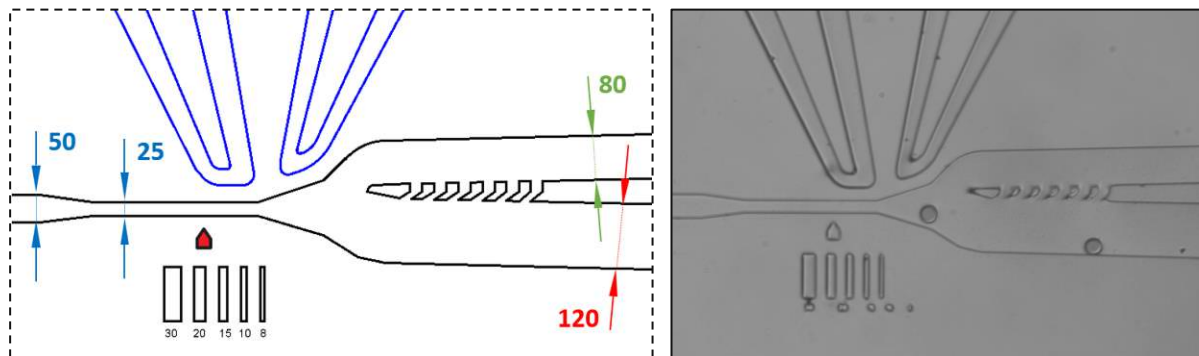


Fig. 97 - left: AutoCAD design of the sorting junction of the droplet sorting device with respective channel widths (in μm) – broader red channel presents a biased flow of droplets due to the increased channel width and channel geometry; **right:** Snapshot of the droplet sorting event at the same location.

The devices were manufactured and prepared identically to the droplet encapsulation, albeit with two differences. As previously mentioned, the glass substrates for these chips were ITO coated to prevent the merging of droplets upon prolonged exposition to high voltage pulses. Additionally, conductive material had to be inserted into the electrode channels (blue color), enabling the sorting process. Several possibilities were reported using low melting solders, liquified metals, or concentrated aqueous salt solutions. However, the most applied systems consisted of electrodes made from Field's

metal (32.5% Bi, 51% In, 16.5%, melting point 62 °C) introduced into the preheated chip by the inherent capillary forces of the channels. Herein the microfluidic device was generally placed on a 90 °C hot plate for approx. 10 minutes before any further manipulations. Due to the size of the electrode inlets, a thin wire (\varnothing 0,020 mM) had to be used for this purpose which, albeit having a generally cheap price tag for the alloy (approx. 100-200 € / 100 g), was considerably more expensive as a wire (930 € / 100 g). Although several attempts to introduce the liquified bulk metal were attempted *via* pre-heated syringes and the manufacture of self-made wires using Teflon tubing as casting molds, the metal quickly lost connectivity after cooling the chip. We speculated that the removal of the syringes or the overly bulky wires from the chip (both from hot or cold chips) resulted either in a deformation of the PDMS or a suction effect that disrupted the integrity of the electrodes. Using the commercial wire, the introduction of the metal was easily possible just by insertion of approx. 1 cm of the metal into the electrode channels of the preheated microfluidic device. If an outflow of metal was observed at the opposite end of the electrode, the wire was slightly bent, which caused the facile disconnection. Finally, thin copper wires were inserted into the molten metal, and the chip was allowed to cool on the slowly switched-off hotplate (Fig. 98). To prohibit any short circuit of the metal, the connections were covered with cyanoacrylate adhesive. This was especially important as undesired contact potentially led to irreversible damage of the high voltage amplifier. With this, the chip was ready to use and could be connected to the reservoir and the high-voltage amplifier. For a successful injection of the droplets, the tubing in the reservoir / Eppendorf tube was necessarily submerged at the lowest height of the milky droplet layer (Fig. 124, middle).

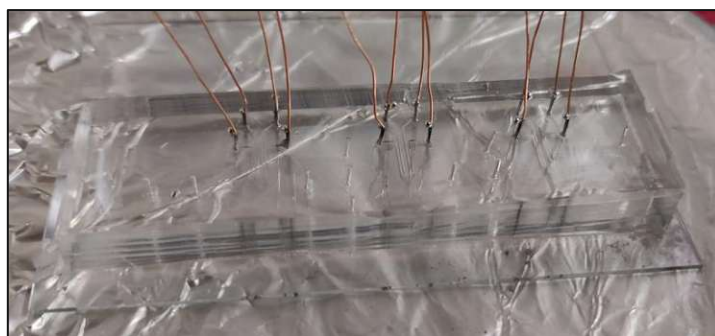


Fig. 98: Droplet sorting chip with connected copper electrodes.

The whole analysis software for the sorting process was custom-written and based on the National Instruments LabView FPGA (field-programmable gate array) programming language. As FPGA cards contain an array of programmable logic blocks (Quelle) that are wired together on a hardware level, they exclude any CPU from the host computer to participate in the calculations. This leads to a dramatic decrease in the execution time of the code and enables high-throughput signal processing. All analysis components were thus coded in such a way that allowed for sorting speeds of several kHz. The programming was necessarily divided into two parts: Firstly, the code that ran directly on the FPGA hardware and was responsible for the analysis of the PMT voltage, evaluation of thresholds, and immediate triggering of the sorting pulses, and secondly, the code on the host computer, which was responsible for the GUI (graphical user interface) and graphical representation of the voltage signals and pulses and data storage. Due to a limited amount of hardware resources (logic blocks, memory units), the code for the FPGA card had to be as concise as possible (Fig. 99).²⁶⁷

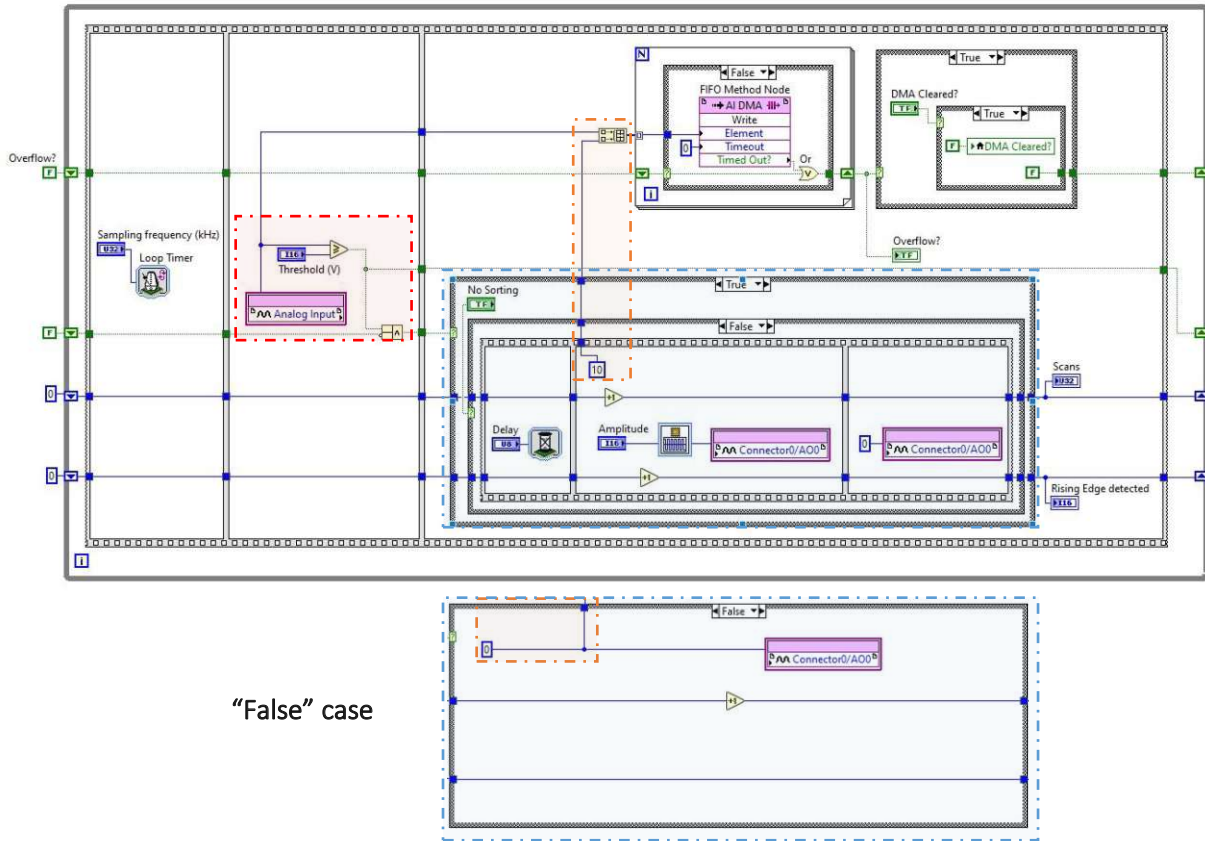


Fig. 99: LabView block diagram of the FPGA VI (virtual instrument) – false case (no rising edge detected during one sampling cycle) immediately set the output voltage to 0 (bottom).

The whole code was placed inside a while loop which ran until terminated by the user. The loop was executed in intervals set by the loop timer corresponding to the sampling frequency f_s . The voltage signal V_{PMT} which was acquired *via* the 16-bit analog input of the SCB-68A connector pane (see. Fig. 122), was checked if it surpassed a user-defined threshold ($V_{PMT} \geq V_T$). If this was the case and a rising edge of the signal was detected – standing for a low-to-high transition of the threshold voltage (red box), only then was the case structure (blue box) was set to true. Subsequently, the voltage pulse was prompted using the square-wave generator VI (50 kHz, 50 % duty cycle, 60 μ s) after a set delay that corresponded to the droplets' travel time from the laser spot to the sorting junction. The analog voltage output (Connector0/AO0) voltage signal was increased 200-fold using the Trek PZD700 high-voltage amplifier, which was passed onto the chip. Following the pulse, the voltage was set back to 0 V. The signal V_{PMT} corresponding to each time point, as well as the information about corresponding high-voltage triggers (orange boxes; 10 = pulse triggered, 0 = no pulse), were combined into a 1D-array in consecutive pairs and forwarded to the FPGA FIFO (first-in-first-out) buffer. Using the DMA (direct memory access) system of the FPGA, the buffered information was transferred to the host computer with a set transfer rate of T representing the number of measuring points that were simultaneously transmitted. Flexible assignment of this value allowed to prevent either over- or under-sampling. In the case an overflow of the FPGA FIFO (TRUE value of “Time Out?” on the FIFO method node) was detected, a warning was sent to the GUI, the DMA data on the host was flushed into a separate memory and immediately cleared – the program was not halted.

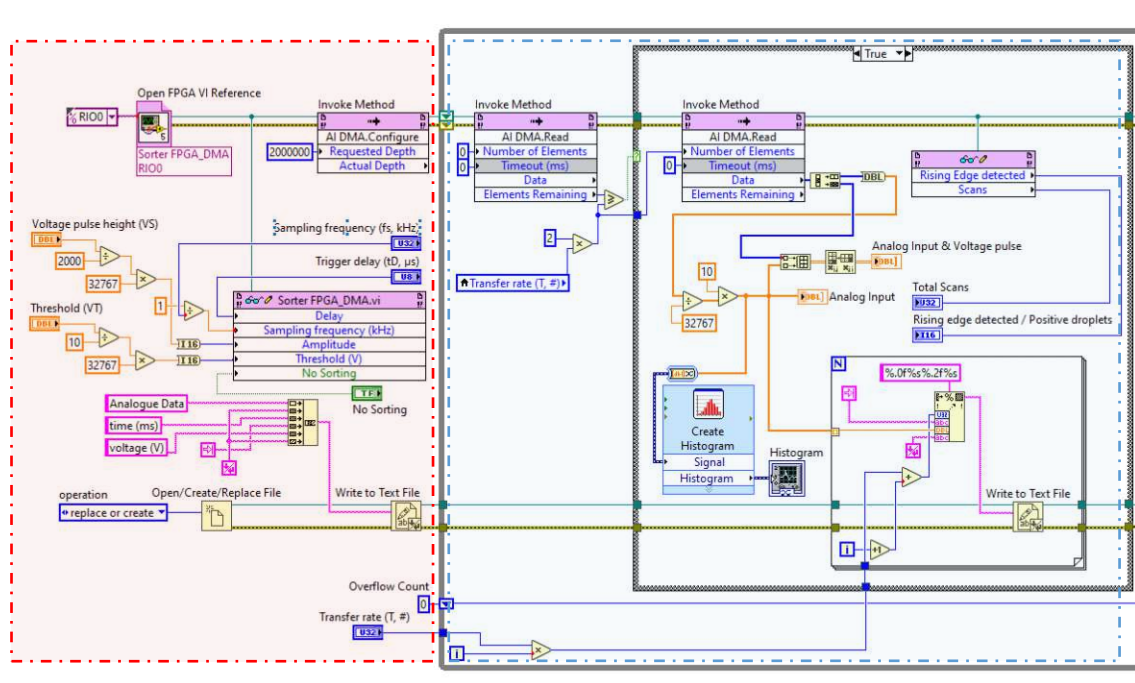


Fig. 100: LabView block diagram running of host VI (virtual instrument) – left part representing the initialization and data acquisition domain.

The code on the host computer could be split into three different parts (Fig. 100 & Fig. 101). The red box represented the initialization of the whole system. This included the input of the FPGA reference information (card and code) and the settings for all initial values (sampling frequency f_s , threshold voltage V_T , trigger delay t_D , transfer rate T , and voltage pulse height V_S corresponding to the voltage of the high-voltage pulse). Furthermore, specifications for the file containing the voltage data were set, and the filename was inquired. Due to the 16-bit analog signals, conversions of the voltage inputs had to be accounted for. As depicted in the blue box, the signal acquired from the FPGA was pulled using the DMA read node using the set transfer rate T . As the data was read out as a 1D-array, in which the analog voltage of the PMT V_{PMT} was alternating with the pulse information (0 or 10), the data had to be split into two different 1D arrays coupling the time information with each separate data point. This was achieved using the decimate 1D array function. The 16-bit analog readout was again converted into voltage data and either represented as a histogram or a time-dependent voltage chart (see. GUI). To accomplish a concomitant presentation of voltage information, which included the time-points where rising edges were detected, the split 1D arrays were combined into a 2D array using the build array function. After transposition of the array, the data could be correctly displayed as a chart on the GUI (Fig X - Analog input & Voltage pulse). As voltages were read out in batches from the FPGA corresponding to the predefined transfer rate T , singular data points had to be extracted for the data file. Due to the characteristics of LabView while loops, every element of an array could be addressed by each iteration if the array was wired into the loop. Using this method, each time point was extracted, matching the iteration the loop was running. The index corresponding to each time point was necessarily adjusted for the number of prior DMA transfers to obtain the correct time-stamps. The data file was thus filled with voltage and pulse information for each execution of the FPGA code.

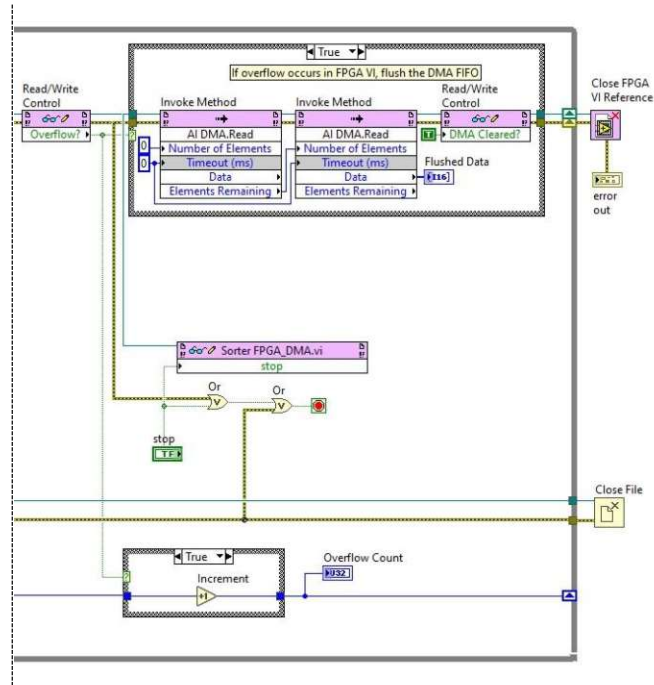


Fig. 101: LabView block diagram running of host VI (virtual instrument) – right part representing the overflow and shut down domain.

The last part of the code running on the host factored in the case an overflow of data was observed. As previously mentioned, if no further data points could be buffered onto the FPGA FIFO memory, the read method was invoked on the host to flush all data into a separate 1D array. Upon clearance of the memory, the acquisition process was immediately continued. The program was only halted if an error message was recorded or by user intervention. Upon termination of the host program, both the FPGA program was terminated and the data file saved. The document was saved in .txt-format with all voltage-time points successively logged. Due to a large number of data points, the resulting files sizes reached sizes of several gigabytes already after 10 minutes of runtime, depending on the sampling frequency.

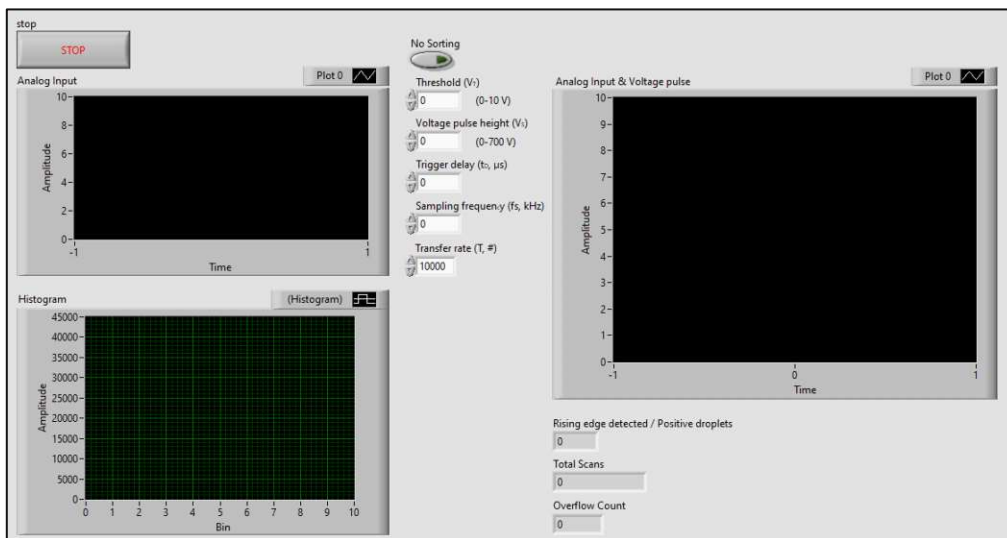


Fig. 102: LabView GUI on the host computer depicting the actual signal, histogram, and voltage pulses during the sorting experiment, as well as all controls for the droplet sorting settings.

Before any actual sorting, the system was allowed to equilibrate without switching on the laser diode, PMT controller, and high voltage amplifier. If a stable flow of droplets was visually confirmed, all optoelectronics were turned on, and the LabView FPGA program was launched. Initially, the program was run with the “No sorting” box ticked (see. Fig. 102). This prevented any sorting events as the laser beam had to be still aligned, and the optimal PMT controller voltage had to be set.

Whereas correct positioning of the laser was determined by the appearance of defined droplet signal peaks in analog input windows of the GUI (see. Fig. 102), the PMT voltage was used to adjust the overall peak amplitude of the system. Ideally, the maximum voltage of 9-10 V should be attained with the droplets containing the highest concentration of ABAO-octanal adduct [160]. To determine this value, the system was always run for up to 10 minutes with constant pressures (set *via* the Elveflow software) with a droplet frequency of approx. 100 Hz. Although an increase in pressures and thus flowrates resulted in quicker sorting speeds and sharper peaks, it also caused a drop in the overall S/N-ratio due to partial loss of signal intensity. Adjustments of the oil and thus carrier flowrate had the most significant impact on the sorting frequency. The droplet emulsion flow rate had to be mostly adjusted only to prevent backflow into the reservoirs. However, as the actual sorting speeds depended on the volume of the droplets and the quality of the chip, these settings had to be set for each individual experiment. As a general recommendation, although the FADS system being enclosed, all sorting experiments should be performed in the dark, as this was found to be beneficial for the background signal.

All settings for sorting on the GUI had to be set prior to any sorting experiment (Fig. 102) and could not be changed during each run. Each time a run was aborted and restarted, a separate acquisition file was generated.

Threshold voltage (V_T ; 1 - 10 V): Voltage compared to the fluorescence-dependent voltage output of the PMT (V_{PMT}). Detection of a rising edge (condition: $V_{PMT} > V_T$) triggers the sorting event.

Voltage pulse height (V_s ; 0 – 700 V): Corresponds to the high voltage pulse applied on the electrodes in the microfluidic chips – values match the output if the multiplier of the high voltage amplifier is set to 200 V/V.

Trigger delay (t_D , μs): Delay of the sorting pulse in μs after the rising edge has been detected.

Sampling frequency (f_s , kHz): Sampling frequency of the FPGA – reciprocal value corresponds to an entire data acquisition cycle equivalent to a singular data point.

Transfer rate (T, #): Number of data points stored on the FPGA FIFO (first-in-first-out storage unit) that are transferred in one package from the FPGA to the host. Too low or too high numbers cause over- or undersampling errors and can lead to loss of data.

The voltage threshold V_T represented the minimal voltage upon which a sorting event was triggered. As empty droplets exhibited minor fluorescence due to the background emission of the unreacted 4-P,5-MeO-ABAO [148], these peaks were quickly identified as the “negative” droplets. The minimal threshold for sorting should be set at least 1 V above the maximal signal intensity of those negatives. The voltage pulse height V_s and sampling frequency f_s represented crucial values essential for the sorting events. Whereas the voltage pulse height V_s needed to be adjusted to higher values for faster flow rates and larger droplets, the sampling frequency f_s represented the minimal time for one acquisition cycle and could thus be translated to a theoretical maximal voltage triggering frequency. To enable a sufficient analytical separation between two droplet peaks, this frequency was set at least two orders of magnitude higher than the actual frequency of droplets passing the sorting fork. Giving that in real sorting scenarios, only a fraction (approx. 10 % for monocellular sorting) of droplets would contain cells that would potentially exhibit any measurable fluorescence signal, the necessary triggering of high-voltage pulses would be anyhow significantly reduced. Nonetheless, this system was planned to accommodate even larger numbers of cells to be sorted in reasonable timeframes. Exploration of the achievable boundaries of the system concerning droplet characteristics and sorting settings were planned in the following studies and were not performed in this thesis.

C I.1.4.1 Proof of concept (unsuccessful at the point of writing)

As a final trial with the current status of the setup as described in E V.5, two different populations of droplets filled with either 20 mM 4-P,5-MeO-ABAO-octanal adduct [160] or unreacted 20 mM 4-P,5-MeO-ABAO [148] were created using the droplet encapsulation device. For this effort, approximately ten million droplets of the respective species were formed at approx. 2000 Hz in approx. 2 hours running time and collected in 0.5 mL Eppendorf tubes. The two populations were mixed by carefully transferring the milky droplet layer with a plastic pipette (glass pipettes are detrimental to droplet stability) into a new Eppendorf tube and reinjected into the manufactured droplet sorting device. The copper wires (Fig. 121) were connected to the high voltage amplifier using electrode clamps, and upon alignment of the laser beam, the flow equilibration was started. Upon verification of steady droplet flow *via* the GUI and the high-speed camera, the sorting of the droplets was attempted. Unfortunately, any combinations of settings of voltage pulse height (V_s , 300 to 700 V – 100 V steps), trigger delay (t_D , 1 to 100 μ s – 2 μ s steps), at a sufficiently high sampling frequency f_s (100 kHz) combined with different droplet flow rates (10-200 Hz – 20 Hz steps) did not lead to any deflection of the droplets inside the channels. Although the sorting was attempted using several freshly prepared sorting chips, no effect was observed in any of these cases.

At the time of writing, the current hardware setup could unfortunately not verify if the applied voltage pulses (0.5 μ s in length) were correctly forwarded to the electrodes on the chip as no high-speed oscilloscope (with enhanced tolerance for high voltages) had been installed. Also, simply due to a lack of time and thus experience with the sorting device, many possible error sources could have remained undetected, which in the end prevented successful sorting. Hence regrettably, no successful sorting experiment could be reported for the novel established FADS system. Nevertheless, every other component of the assembly was proven to be working. As of this, it should not be long before a successful experiment is recorded.

D Conclusion and Outlook

Three different projects and subject areas had been tackled in this thesis with a common goal of laying a foundation for directed evolution studies of carbonyl-producing enzymatic systems. The first chapter focused on challenging a novel enzymatic Brønsted catalyst in the group, namely the SHC (Squalene hopene cyclase) with non-native substrates, to elaborate its catalytic promiscuity. Based on its recently discovered carbonyl activation mode, differently modified citronellal analogs were synthesized and subjected to several already known SHCs mutants known to exhibit a broader catalytic profile in the enzymatic Prins reaction (SHC_{Aac} bearing A419G/Y420C/G600A or I261A and the SHC_{Zmo} variants with W555Y, F438C or F486C single point mutations). Unfortunately, only the substrates bearing a similar double bond geometry and thus stabilizing the carbocationic intermediate showed any novel activity towards cyclization. Any changes of the electrophile were proven to be not accepted. However, the orientation of β -methyl was shown to play a defining role as transformations of the cyclopentyl-enantiomers [24]/[33] were shown to proceed highly selective towards one of the possible four diastereomers depending on the applied SHC variant. Using the SHC_{Zmo_1548}F486C mutant, exclusively access towards cyclopentyl derivatives (+)-isopulegol [161] and (-)-neoiso-isopulegol [162] was possible. Application of the SHC_{Zmo_1548}W555Y mutant enabled isolation of (-)-iso-isopulegol [163]. All products could be isolated and characterized in good yields in preparative scale experiments.

With the general SHC methodology established, the enzymatic catalysts were applied for initial Friedel Crafts cyclization trial experiments. For this purpose, differently alkylated 3-(3-hydroxyphenyl)propanoic acids or methyl esters, as well as their corresponding Friedel Crafts indanone products, were synthesized. Incorporation of octyl or citronellyl-alkyl chains onto the aromatic core was believed to act as apolar recognition motifs and thus improve acceptance of the substrates. Regrettably, none of the SHC mutants exhibited any Friedel Crafts cyclization activity. As an enzymatic FCA was still sought after, a toolset for the evolution of these enzymes was required.

The second part of the thesis thus dealt with the establishment of assays that would enable facile recognition of enzymatic activity upon formation of Friedel-Crafts carbonyl products using rapid screening methodology. Initially, this was attempted by building upon the fluorogenic retroaldolase probe 6-methoxy-2-naphthaldehyde [XXVI] from the work of Giger *et al.*²¹⁶, which triggered fluorescence emission upon exposure of the carbonyl group. Therefore, differently substituted methoxy-naphthalene butanoic acid substrates and their dihydrophenanthrenone cyclization products were prepared. An improved Negishi approach helped herein with the facile construction of several analogs. Surprisingly, all cyclizations, albeit causing a desired red-shift of the absorption spectra, were detrimental to the fluorescence emission, and the products were thus unusable as assaying tools. A change in strategy thus prompted us to pursue a different class of assay compounds, namely nitrobenzoxadiazole-hydrazines [78] (NBD-H) and its derivatives. This reagent selectively reacts with carbonyl functionalities forming fluorescence hydrazones independent of the underlying structure. As this conjugation had not yet been studied in detail for presumed aryl ketone-FCA products, initial evaluation about its reactivity in the required medium for SHC reactions revealed several serendipitous discoveries. All NBD-H products showed a dramatic increase (approx. x100) in fluorescence emission

upon addition of non-ionic surfactants above their cmc (critical micelle concentration), which were needed to solubilize the monotopic enzyme. Furthermore, these surfactants increased the apparent stability of the hydrazone conjugates due to a presumed formation of micellar systems, which were hypothesized to shield the reaction center in an apolar cavity and cause both beneficial effects.

Additionally, performing reactions in the necessarily acidic buffer (> pH 6.0) further increased the fluorescence response of the assay. The phenomenon was ascribed to be coupled with the pK_A of the newly formed hydrazone. Although a fluorometric tracing of the reaction progress with tetralone [83] was made possible in aqueous systems under these conditions, the reagent remained too slow for an appreciable application in an assay format. Preliminary tests with benzaldehyde [79] confirmed the already well-known dramatic increase of reactivity towards aryl aldehydes (x126) but also exemplified the boundaries of the system, which exhibited precipitation of the benzaldehyde adduct [80] above 500 μ M due to its low hydrophilicity. Still, the NBD-H assay displayed remarkable sensitivity using fluorescence spectroscopy in a cuvette format, with a LOQ of approx. 1 μ M for both the tetralone adduct [84] and benzaldehyde adduct [80], respectively. Necessarily a strong turn-on upon conjugation could be observed, as the unreacted NBD-H remained practically non-fluorescent.

With the emerging interest in a FADS (fluorescence-activated droplet sorting) system in the research group and a shift away from aryl ketone substrates, the final part of the thesis dealt with the establishment of the device as well as the development of suitable assays. Due to an unavoidable requirement for strongly hydrophilic assay tools applied in the FADS, the NBD-H [78] reagent had to be adapted to incorporate highly polar groups. Attachment of a quaternary ammonium group *via* an alkyl sulfonamide bridge enabled the synthesis of the water-soluble analog ABThD-H [111] in four steps without the need for column chromatography starting from commercial 4-bromo-2,1,3-benzothiadiazole [105]. Although the reagent did not exhibit a similar strong red-shift of the absorption and fluorescence emission upon conjugation compared to its NBD-H counterpart, it proved to be kinetically faster in the benzaldehyde adduct [112] formation by a factor of 6. Unfortunately, this increase in reactivity could not be translated to the tetralone conjugation, which remained impractically slow. The sensitivity, LOD value, and turn-on properties remained, however, practically unchanged. Furthermore, the replacement of the oxygen for sulfur in the aromatic ring system dramatically enhanced its stability and was thus beneficial for long-term experiments.

In addition to the NBD-H reagent, the already established amino benzamidoxime (ABAO) carbonyl assay, which had been previously applied in the group for directed evolution studies of CARs⁶⁷ and well as the determination of open-chain content of reducing sugars²³⁹, was also further developed. As reference compounds, the undecorated ABAO [LIV] and its kinetically faster 5-MeO variant [126] were used. Herein introduction of a phosphonic acid functionality by a Pd-catalyzed P-H coupling gave facile access to highly polar ABAO derivatives. Several differently substituted aromatic motifs were thus synthesized, whereas the 4-P,5-MeO-ABAO [148] derivative was found to be the ideal candidate for the application in the FADS. The reagent could be synthesized in six steps from commercial 4-hydroxy-3-methoxybenzotrile [136] and exhibited a similar kinetic behavior comparable to the fast 5-MeO-ABAO [126], as well as a beneficial red-shift and increase insensitivity. Applying this reagent, full conjugation with the reference aldehyde octanal [160] could be achieved in approx. 2 minutes using a 5-fold excess of 4-P,5-MeO-ABAO in μ M concentrations. Similar turn-on behavior was observed to the ABThD-H [111]

reagent. The principal difference between the probes was manifested in their difference in LOD values. Whereas ABThD-H [111] conjugation allowed for tracing conversions in the μM range, 4-P,5-MeO-ABAO [148] adduct formations could be used in the mM range. The former could be thus applied to pursue novel activities of enzymes better expressed as the search for the “needle in the haystack”. Optimizations of already established enzymatic systems would be only achievable using the 4-P,5-MeO-ABAO [148] reagent. However, both assays were limited to an application in an acidic ($\text{pH} < 6$, optimal $\text{pH} < 5$) environment due to either loss of fluorescence signal or detrimental kinetic properties. As final results for the spectroscopic investigations and logP determination of the 4-P,5-MeO-ABAO [148] assay were obtained prior to the finalization of the results for the ABThD-H [111] system, the whole FADS assembly was planned according to its fluorescence excitation and emission.

The custom-built FADS system was constructed using nature protocols by Mazutis *et al.*¹⁷¹ as the most important reference. Therein included designs for the microfluidic devices were employed for the manufacture of both encapsulation and sorting chips. An essential focus of the hardware assembly was placed on future flexibility and interchangeability of components and an economic aspect. The total cost for the assembly was estimated to be approx. 40.000 €, compared to the commercial top-of-the-line FACS devices pricing between \$100.000 and \$500.000². The assembly included the complete structural and optomechanical framework, the microfluidic flow controller installation, the manufacture of microfluidic PDMS chips, and the LabView code for the final sorting process. Partial proof of concept was delivered with the encapsulation of 4-P,5-MeO-ABAO [148] containing aqueous droplets and droplets containing its octanal adduct [160]. Both populations were mixed and reinjected into the sorting chip. Due to inexplicable effects, regrettably, no sorting was made possible by applying any changes to the sorting settings. Nevertheless, several steps towards the final goal with the establishment of the whole platform, tackling the hardware as well as the software side, were already accomplished.

The outcome of the thesis could be thus summarized to lay foundations that would be used for further studies in protein engineering of organisms expressing carbonyl-producing enzymes. Although proofs of concept for both water-soluble assays were delivered, a holistic investigation about a spectral and kinetic dependency on different types of substrate structures (alkyl- and aryl aldehydes as well as ketones) was under progress. Especially the determination of the logP values for the ABThD-H [111] conjugates was still ongoing. Similarly, while the assembly of the FADS was completed and its functionality proven, no investigation about its practical limits was undertaken. Adaptation of the system to include the ABThD-H [111] assay system, with the exchange of the mirror optics and the laser excitation source, were also pending at the moment of writing. However, with the introduction of the more sensitive assay, directed evolution experiments could finally be undertaken with selected enzymes.

⁴ <https://www.akadeum.com/technology/cost-comparison-of-cell-separation-methods/> - accessed September 2021.

E Experimental part

E I Materials and methods – chemical synthesis

Unless noted otherwise, all substrates and reagents were purchased from commercial suppliers and used without further purification. The purity of the reported compounds is > 95% according to NMR.

HPLC grade solvents (methanol, water, acetonitrile) were received from VWR. Anhydrous dichloromethane, tetrahydrofuran, methanol, diethyl ether, 1,4-dioxane, and acetonitrile were pre-dried using an Innovative Technologies PureSolv system or retrieved for small scale experiments (< 10 mL) from Acros (*AcroSeal Dry Solvents*). Anhydrous ethanol was used from (Chem Lab). Dry triethylamine was prepared by refluxing over CaH₂ for 2 hours and subsequent bulb-to-bulb distillation. The reagent was further stored over BaO and used for several months. All other non-specified chemicals were retrieved from the chemical storage of TU Wien and freshly distilled or recrystallized.

Ozone enriched oxygen was generated using a Triogen LAB2B Ozone generator.

Microwave reactions were performed on a Biotage Initiator Sixty™ microwave unit.

Moisture and air-sensitive reactions were carried out in flame-dried glass vessels under an argon atmosphere using Schlenk techniques. All reactions were stirred magnetically unless otherwise stated.

E I.1 Chromatographic methods

TLC-analysis for general reaction control and column chromatography was performed on precoated aluminum-backed plates (Silica gel 60 F254, Merck). Visualization was enabled by UV irradiation (254 nm) or, if necessary, by staining the plates with anisaldehyde solution (180 mL EtOH, 10 mL anisaldehyde, 10 mL H₂SO₄ conc., 2 mL AcOH), potassium permanganate solution (3.0 g KMnO₄, 20.0 g K₂CO₃, 250 mg KOH, 300 mL H₂O) or cerium molybdate solution (“Mostain”, 21 g (NH₄)₆Mo₇O₂₄·4 H₂O, 1 g Ce(SO₄)₂ 31 mL H₂SO₄ conc., 500 mL H₂O).

Chromatographic isolation of products was performed with glass columns and silica gel from Merck (43-60 μm). Unless otherwise noted, all products were purified using a compound to silica weight ratio of 1:100. Eluent mixtures and the applied gradients are given as volume ratios in the respective experiments.

HPLC preparative chromatography was carried out with an Autopurification system of Waters using an ACQUITY QDa Detector in combination with a 2998 Photodiode Array Detector. Analytical runs were conducted using the Waters XSelect CSH C18 5 μm (4.6 x 150 mm) column. Preparative separation was performed using the Waters XSelect CSH Prep C18 5 μm OBD (30 x 150 mm) column. HPLC grade methanol and HPLC grade water containing 0.1 vol% formic acid were used as solvents. Eluent mixtures and the applied gradients are given as volume ratios in the respective experiments.

GC analysis for reaction control of biotransformations was performed on a Thermo Scientific Trace 1300 Dual GC, equipped with a TR-5MS column (15 m, 0.25 mm ID, film thickness 1.0 μm) and an FID detector using the following temperature program:

Carrier gas: helium, column flow: 1.5 mL/min, 1 minute at 80 °C, 60°C/min until 280 °C, 5 minutes at 280 °C – run time 10 minutes

GC–MS analysis was performed on a Thermo Finnigan Focus GC/DSQ II with a standard capillary column BGB5 column (30 m, 0.25 mm ID, film thickness 0.25 μm) coupled to a Voyager Quadrupole mass spectrometer (electron ionization, 70 eV) using standardized temperature programs:

Carrier gas: helium, column flow: 2.0 mL/min

"Method A" (2 minutes at 100 °C, 35 °C/min until 300 °C, 2 minutes at 300 °C) – run time 10 minutes

"Method B" (2 minutes at 100 °C, 35 °C/min until 300 °C, 4 minutes at 300 °C) – run time 12 minutes

"Method C" (2 minutes at 100 °C, 35 °C/min until 300 °C, 6 minutes at 300 °C) – run time 14 minutes

HPLC-MS analysis was performed on a Nexera X2 UHPLC system (Shimadzu) comprised of LC-30AD pumps, SIL-30AC autosampler, CTO-20AC column oven, and DGU-20A5/3degasser module. Detection was done using an SPD-M20A photo diode array and an LCMS-2020 mass spectrometer (ESI/APCI). If not stated otherwise, all separations were performed using a Waters XSelect CSH C18 2,5 μm (3.0 x 50 mm) column XP at 40 °C, and a flowrate of 1.7 mL/min. Gradient elution was performed using mixtures of HPLC grade MeCN and HPLC grade water with either 0.1 vol% formic acid (acidic separation) or as 50 mM pH NH_4HCO_2 solution (basic separation).

E 1.2 NMR spectroscopy

NMR spectra were recorded at 297 K in the solvent indicated with a Bruker Avance UltraShield 400 and an Avance III HD 600 spectrometer and processed with MestReNova. Chemical shifts are given in parts per million (ppm) and were calibrated with internal standards of deuterium-labeled solvents. Annotations of unknown structures were confirmed by ^1H - ^1H COSY, ^1H - ^{13}C , HSQC, and ^1H - ^{13}C , HMBC, and by comparison to predicted spectra. Signal multiplicities are denoted by the following abbreviations: s (singlet), d (doublet), t (triplet), q (quartet), p (quintet), hex (hextet), hept (heptet), m (multiplet), b (broad signal) or combinations thereof. Coupling constants (J) are presented in Hz (Hertz). Carbon multiplicities (in H-decoupled ^{13}C NMR experiments) are denoted by theoretically expected C-H couplings as s (singlet), d (doublet), t (triplet), and q (quartet). In the case of fluoro- or phosphorus substituents, the coupling constant is denoted as xy, $^2J_{\text{C-X}} = \# \text{ Hz}$, whereas x represents the multiplicity of the CH coupling, y the multiplicity of the C-X heteroatom coupling, and z the order of spin-spin coupling.

E 1.3 UV-Vis & Fluorescence spectroscopy

UV-Vis measurements were conducted on a Shimadzu UV-1800 UV-Vis spectrophotometer in Hellma Analytics QS quartz cuvettes (1 cm light path) using a volume of 2 mL.

For the recording of general spectral information, 0.2 - 1.0 mM stock solutions of the respective fluorogenic reagents and adducts were prepared in DMSO and appropriately diluted with NH₄OAc buffer (100 mM, pH = 4.5) to obtain concentrations between 0.02 mM and 0.5 mM with a final concentration of 5% DMSO. Spectra were recorded in a range from 260 nm to 600 nm with incremental steps of 1 nm and fast scanning settings. Buffer blanks spiked to 5 % DMSO were recorded prior to the spectral measurements and automatically subtracted.

For kinetic measurements of ABAO reagents, 50 µL of 8-40 mM ABAO derivative in DMSO was dissolved in 1.9 mL NH₄OAc buffer (100 mM, pH = 4.5). To start the reaction, 50 µL of 8 mM carbonyl species in DMSO was added, and the solution was thoroughly mixed using the pipette tip. Reactions were either followed by recording the full spectral information from 265 to 600 nm in fixed timed increments or using the kinetic method of the UVProbe software (instrument's software) at the respective absorption maximum. Buffer blanks spiked to 5 % DMSO were recorded prior to the spectral measurements and automatically subtracted.

Fluorescence spectra were recorded on a Perkin Elmer LS 55 Fluorescence spectrometer using Hellma Analytics QS quartz cuvettes (1 cm light path) using a volume of 2 mL. Spectral information was collected by exciting the respective fluorogenic reagents and adducts at the maximum wavelength for the highest fluorescence emission (not necessarily absorption maximum). Spectra were generally recorded using 5.0/5.0 nm emission and excitation slits with medium PMT gain. If too high or too low emission was observed, settings were corrected by a first widening of the spectral window and then adjustment of the gain (generally 300-700 intensity units recommended).

Kinetic measurements were performed at a specific emission/excitation wavelength combination yielding the highest signal/noise ratio and intensity. For this, emission spectra of the ABAO reagent and the adduct were recorded and compared at the same excitation wavelength. 50 µL of 8-40 mM ABAO derivative in DMSO was dissolved in 1.9 mL NH₄OAc buffer (100 mM, pH = 4.5). To start the reaction, 50 µL of 8 mM carbonyl species in DMSO was added, and the solution was thoroughly mixed using the pipette tip.

E 1.4 Specific rotation

Specific rotation values $[\alpha]_D^{20}$ (10^{-1} deg cm⁻² g⁻¹) were determined using an MCP 500 polarimeter from Anton-Paar with dichloromethane, chloroform, or ethanol as solvent.

E 1.5 Melting point

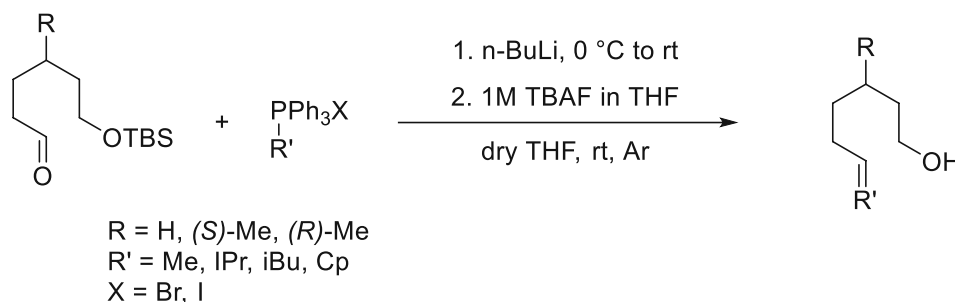
Melting points were determined by a Büchi Melting Point B-545 or by an SRS OptiMelt Automated Melting Point System and are uncorrected.

E I.6 HR-MS

HR-MS analysis was carried out from MECN solutions (concentration: 10 μ M) using an Agilent 6230 LC TOFMS mass spectrometer equipped with an Agilent Dual AJS ESI-Source. The mass spectrometer was connected to a liquid chromatography system of the 1100/1200 series from Agilent Technologies, Palo Alto, CA, USA. The system consisted of a 1200SL binary gradient pump, a degasser, a column thermostat, and an HTC PAL autosampler (CTC Analytics AG, Zwingen, Switzerland). A silica-based Phenomenex C-18 Security Guard Cartridge was used as a stationary phase. Data evaluation was performed using Agilent MassHunter Qualitative Analysis B.07.00. Identification was based on peaks obtained from extracted ion chromatograms (extraction width \pm 20 ppm).

E II General procedures

E II.1 General procedure A: Wittig reaction and deprotection of citronelloid derivative precursors



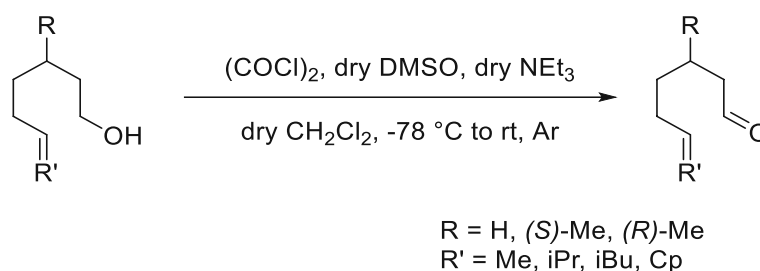
The product was synthesized according to a modified literature procedure²⁰¹.

Procedure: A flame-dried 25 mL screw-cap vial was charged with the respective triphenylphosphonium bromide or iodides [4], [8], [10] or [6] (2.60 mmol, 1.30 equiv.) which was azeotropically dried by suspending it 3 times in dry toluene (5 mL) and evaporating to dryness *in vacuo*. Under argon atmosphere, dry THF (7 mL, 0.2 M) was added, and the vial was cooled down to -40 °C by using a liquid N₂/acetone bath. With strong stirring, n-BuLi (2.5 M in hexanes, 1.06 mL, 2.6 mmol, 1.30 equiv.) was added dropwise over the wall of the vial upon which a strong color change (R' = Me – yellow, R' = rest – orange to red) with concomitant precipitation of colorless solids was observed. After 30 minutes, TBS-protected aldehyde [3], [18] or [27] (2.00 mmol, 1.00 equiv.) dissolved in dry THF (2 mL, 1 M) was added. The reaction was held at -40 °C for 1 h, then allowed to warm to -20 °C. TLC confirmed the end of the reaction after 1-3 hours. To precipitate formed triphenylphosphonium oxide, the reaction was diluted with Et₂O (20 mL) and immediately flashed over silica (30 g) with Et₂O until TLC confirmed finished product elution. After evaporation of the solvent (max. 300 mbar – intermediates are highly volatile!),

the oily crude was dissolved in THF (9.5 mL, 0.2 M). TBAF solution (1 M in THF, 2.60 mL, 2.60 mmol, 1.30 equiv.) was added at 0 °C and stirred for 1 hour, then warmed to room temperature.

Work-up: Upon confirmation of full conversion after 2-3 hours *via* TLC, the reaction was diluted with dH₂O (50 mL). The aqueous phase was extracted three times with CH₂Cl₂ (3 x 50 mL). The combined organic phases were washed with brine (100 mL), dried over Na₂SO₄, and concentrated. For the final purification, the crude was columned over silica eluting with 1:1 LP/Et₂O (improved product recovery due to lower boiling point of solvent) or 4:1 LP/EtOAc to yield the respective citronellol derivatives as a colorless oils with generally fruity-earthly odors.

E II.2 General procedure B: Swern oxidation of citronellol derivatives

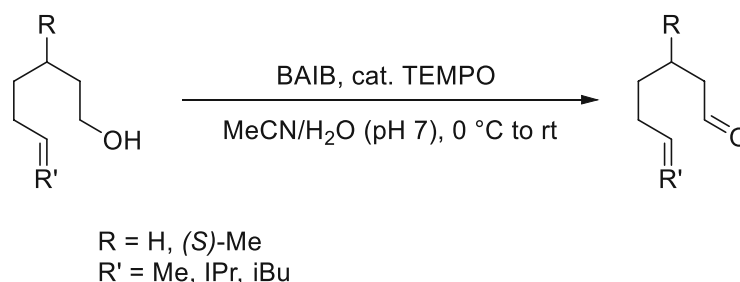


The product was synthesized according to a literature procedure²⁰⁰.

Procedure: A flame-dried 8 mL screw cap vial was charged with dry DMSO (86 μL , 94 mg, 1.21 mmol, 2.60 equiv.) and dry CH₂Cl₂ (2.6 mL, 1 M) under argon using standard Schlenk techniques. The solution was cooled to < -80 °C using a liquid N₂/acetone bath (external temperature measurement) following the dropwise addition of oxalyl chloride (52 μL , 77 mg, 0.60 mmol, 1.30 equiv.). The mixture was held below -80 °C for 2 hours, upon which gas conversion had ceased. The citronellol derivative (0.46 mmol, 1.00 equiv.) dissolved in dry CH₂Cl₂ (0.6 mL, 0.75 M) was added dropwise over a period of 2-3 minutes, causing immediate turbidity of the solution. Subsequently, dry triethylamine (280 μL , 202 mg, 1.99 mmol, 4.30 equiv.) was added, and the reaction mixture was below -80 °C for 1 hour, then allowed to warm to room temperature by removing it from the cooling bath.

Work-up: Upon confirmation of full conversion, the reaction was quenched with the addition of dH₂O (3 mL). The aqueous layer was extracted two times with CH₂Cl₂ (2 x 3 mL), and the combined organic phases were washed with brine (10 mL), dried over Na₂SO₄, and concentrated. For the final purification, the crude was columned over silica eluting with 40:1 LP/Et₂O to yield the respective citronellal derivatives as a colorless oils with very distinct odors.

E II.3 General procedure C: BAIB/TEMPO oxidation of citronellol derivatives

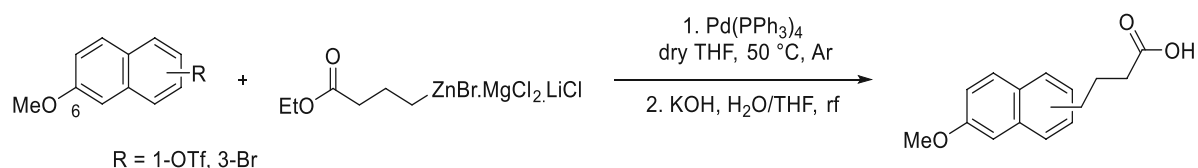


The product was synthesized according to a literature procedure²⁰³.

Procedure: An 8 mL screw cap vial was charged with citronellol derivative (0.63 mmol, 1.00 equiv.) and MeCN (2.30 mL, 0.20 M). 1 M pH 7.0 Phosphate buffer solution (0.60 mL, 1 M) was added, and the reaction mixture was cooled to 0 °C using an ice/water bath. After subsequent addition of BAIB (0.22 g, 0.69 mmol, 1.10 equiv.) and TEMPO (9.8 mg, 0.06 mmol, 0.10 equiv.), the resulting reddish suspension was stirred for 1.5 h during which the BAIB had dissolved entirely, and TLC indicated full conversion.

Work-up: The reaction was quenched with a 1:1 mixture of saturated Na₂SO₃/NaHCO₃ solution (6 mL). The aqueous layer was extracted three times with Et₂O (3 x 10 mL), and the combined organic layers were washed with brine (40 mL), dried over Na₂SO₄, and concentrated. For the final purification, the crude orange oil was columned over silica eluting with LP/CH₂Cl₂ 1:1 to yield the respective citronellal derivatives as a colorless oils with very distinct odors.

E II.4 General procedure D: Negishi coupling of naphthyl derivatives with activated 4-ethoxy-4-oxobutylzinc bromide



The product was synthesized according to a modified literature procedure²²³.

Preparation of Negishi-reagent: LiCl and ZnCl₂ were dried at 150 °C at 10 mbar for 24 hours. For 20 mL of an approx. 0.3-0.5 M solution, a flame-dried Schlenk-tube was charged with LiCl (0.64 g, 15.00 mmol) and ZnCl₂ (0.64 g, 11.00 mmol) under argon. The solids were then stirred in dry THF (10 mL), accompanied by strong exothermicity. After 2-3 hours, almost complete dissolution of all particulates could be observed. The solution was transferred by syringe filtration into a second flame-dried Schlenk-tube containing Mg-filings (478 mg, 20 mmol) to remove the residual suspended particles. Subsequently, freshly distilled ethyl 4-bromobutanoate (1.43 mL, 1.95 g, 10.00 mmol) was added, and the reaction was heated to 45 °C for 3 hours, completely darkening the solution. To remove unreacted Mg, another syringe filtration was performed, which prolonged the shelf life of the reagent. To determine the final concentration of the 4-ethoxy-4-oxobutylzinc bromide [55], a titration with I₂ was performed. For this purpose, a 0.25 M I₂ solution in 0.5 M LiCl in dry THF (127 mg I₂ in 2 mL 0.5 M LiCl THF-solution) was prepared, and the Negishi reagent was added at 0 °C. The endpoint was reached with the discoloration of the deep yellow solution. Approximately 1.25 mL were needed for a concentration of 0.4 M. The reagent was stored under argon atmosphere, but for not longer than two weeks.

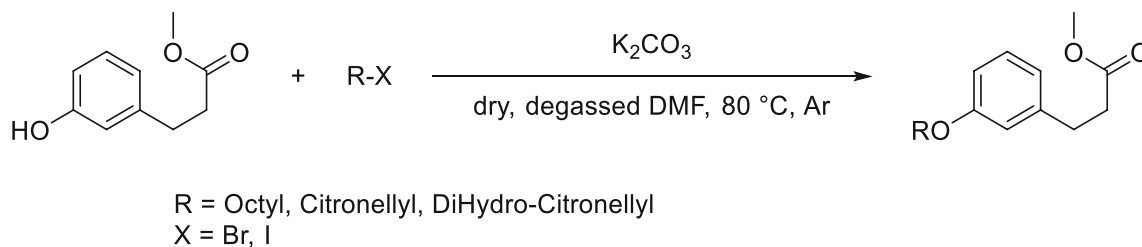
Procedure 1: A flame-dried 50 mL Schlenk tube was charged with naphthyl reagent [45] or [54] (1.26 mmol, 1.00 equiv.), Pd(PPh₃)₄ (29 mg, 0.03 mmol, 0.02 equiv.) and dry THF (1.1 mL, 1.1 M) under argon. The freshly prepared 4-ethoxy-4-oxobutylzinc bromide [55] (1.20 equiv.) was then added dropwise in 1-2 minutes, and the reaction was heated to 50 °C for 4 hours, upon which TLC indicated full conversion.

Work-up 1: The mixture was quenched with sat. NH₄Cl (50 mL) and the aqueous phase was extracted three times with CH₂Cl₂ (3 x 50 mL). The combined organic layers were washed with brine (100 mL), dried over Na₂SO₄, and concentrated.

Procedure 2: Due to the inseparability of the target from homo-coupled by-products (alkyl and aryl), the crude was immediately taken up in a 1:1 mixture of 4 N aqueous KOH / THF (9 mL) and heated to reflux for 3 hours.

Work-up 2: The reaction was then further diluted with 2 N NaOH (20 mL) and washed three times with Et₂O (3x 30 mL) – effecting the removal of the aryl-homocoupled product. The organic layers were extracted once with 2 N NaOH (20 mL) and combined. Subsequent acidification with c. HCl (pH 1-2) triggered the precipitation of colorless solids. The aqueous phase was once again extracted with Et₂O (3 x 50 mL). The combined organic layers were washed with brine (100 mL), dried over Na₂SO₄, and concentrated. For the final purification, the crude was columned over silica (1:30) with 9:1 CHCl₃/MeOH to yield the naphthalene propionic acids [56] or [58] as a colorless solids.

E II.5 General procedure E: Alkylation of phenylpropionic acid, methyl esters

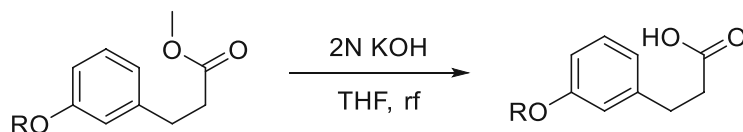


The product was synthesized according to a literature procedure²¹³.

Procedure: A flame-dried 25 mL screw-cap vial was charged with finely ground and dried K_2CO_3 (0.61 g, 4.44 mmol, 2.00 equiv.) and dry DMF (10 mL, 0.44 M). The solution was degassed for 30 minutes at 40 °C by bubbling argon through it. Subsequently, 3-(3-hydroxyphenyl)propionic acid, methyl ester (2.22 mmol, 1.00 equiv.), which was azeotropically dried with toluene (5 mL), was added to the solution with gentle argon counterflow. After complete dissolution, the respective side-chain bromide or iodide [63]-[65] (2.33 mmol, 1.05 equiv.) was added, and the temperature was raised to 80 °C. Another portion of the alkyl donor (0.46 mmol, 0.20 equiv.) was needed after 18 hours to promote reaction progress. Totalling 24 hours, reaction TLC confirmed the full conversion of starting material.

Work-up: The reaction mixture was poured onto ice-cold dH_2O (100 mL) and was extracted four times with EtOAc (4 x 15 mL). The combined organic layers were washed with brine (50 mL), dried over Na_2SO_4 , and concentrated. The crude product was further purified *via* column chromatography (LP/EtOAc 40:1) to yield to the respective ethers as a colorless oils.

E II.6 General procedure F: Saponification of alkylated phenylpropionic acid, methyl esters

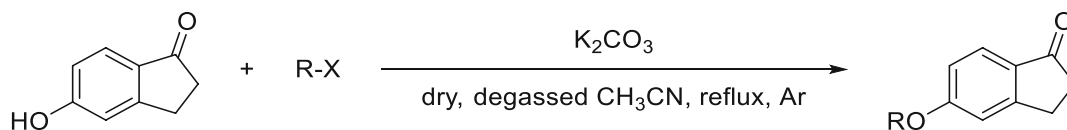


R = Octyl, Citronellyl, DiHydro-Citronellyl

Procedure: A 8 mL screw cap vial was charged the respectively alkylated phenylpropionic acid, methyl ester [66]-[68] (0.85 mmol, 1.00 equiv.), which was dissolved in a 1:1 mixture of THF / 2 N KOH (3 mL, 0.28 M). The reaction was stirred at 60 °C for 3 hours, upon which TLC indicated full conversion.

Work-up: The reaction was quenched with the addition of sat. NH_4Cl (20 mL). The aqueous phase was extracted four times with EtOAc (4 x 15 mL). The combined organic layers were washed with brine (50 mL), dried over Na_2SO_4 , and concentrated. The products [69]-[71] could be used for further experimentation without additional purification.

E II.7 General procedure G: Alkylation of 5-hydroxy-1-indanones

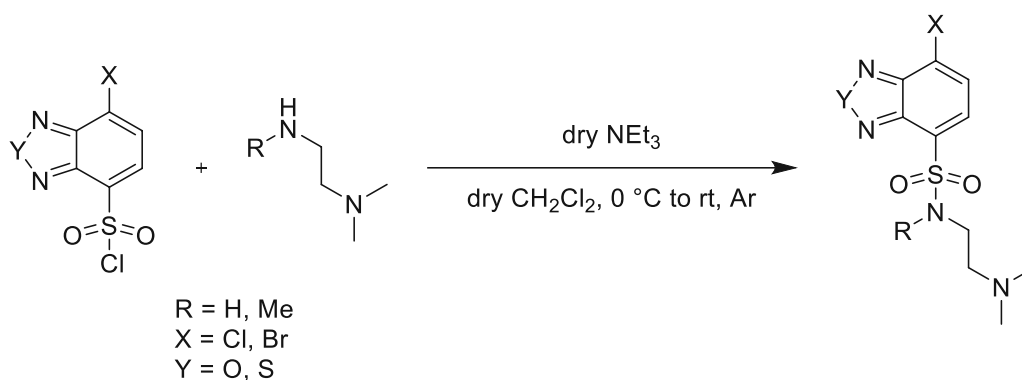
R = Octyl, Citronellyl, DiHydro-Citronellyl
X = Br, I

The product was synthesized according to a literature procedure²¹³.

Procedure: A flame-dried 8 mL screw cap vial was charged with the 5-hydroxy-2,3-dihydro-1H-indanone [72] (50 mg, 0.34 mmol, 1.00 equiv.), finely ground and dried K_2CO_3 (93 mg, 0.67 mmol, 2.00 equiv.) and dry MeCN (1.2 mL, 0.3 M). The solution was degassed for 30 minutes at 40 °C by bubbling argon through it. Subsequently, the respective side-chain bromide or iodide [63]-[65] (0.44 mmol, 1.30 equiv.) was added, and the reaction was refluxed for 24 hours, upon which TLC indicated full conversion.

Work-up: The reaction mixture was poured on dH_2O (20 mL) and was extracted four times with EtOAc (4 x 10 mL). The combined organic layers were washed with brine (50 mL), dried over Na_2SO_4 , and concentrated. The crude product was further purified *via* column chromatography (LP/EtOAc 10:1) to yield to the respective indanone ethers [73]-[75] as yellow oils.

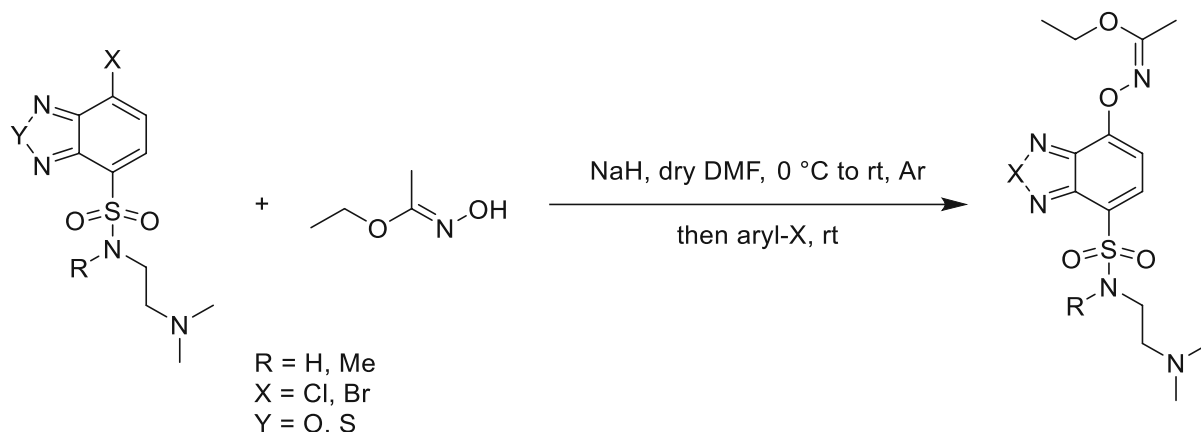
E II.8 General procedure H: Sulfonamidations of [1,2,5]-benzoxa- / benzthiadiazole sulfonyl chlorides.



Procedure: A flame-dried 25 mL screw-cap vial was charged with the respective sulfonyl chloride [94]-[106] (4.78 mmol, 1.00 equiv.) and then evacuated and backfilled with argon using standard Schlenk techniques. The solids were dissolved in dry CH_2Cl_2 (9.6 mL, 0.5 M) and cooled to 0 °C with an ice/water bath. In cases where precipitation of starting material was observed, additional CH_2Cl_2 was added until the full dissolution of solids was achieved. The respective diethylene amine [97] or [101] (5.26 mmol, 1.10 equiv.) was added dropwise at 0 °C, which caused immediate yellowing of the solution and precipitation of colorless solids. In certain cases, the complete addition of the amine solidified the reaction mixture. Subsequently, dry triethylamine (5.26 mmol, 1.10 equiv.) was added the mixture was warmed to room temperature. The reaction was stirred for additional 30 minutes, upon which TLC indicated full conversion.

Work-up: The reaction was diluted with CH_2Cl_2 (50 mL) and washed with sat. NaHCO_3 (100 mL). The aqueous phase was extracted twice with CH_2Cl_2 (2 x 30 mL), and the combined organic layers were washed with brine (100 mL), dried over Na_2SO_4 , and concentrated. The resulting solids were dried *in vacuo* to yield the respective sulfonamides as deep yellow solids.

E II.9 General procedure I: Nucleophilic aromatic substitution of sulfonamide aryl chloride and bromides with ethyl N-hydroxyacetimidate

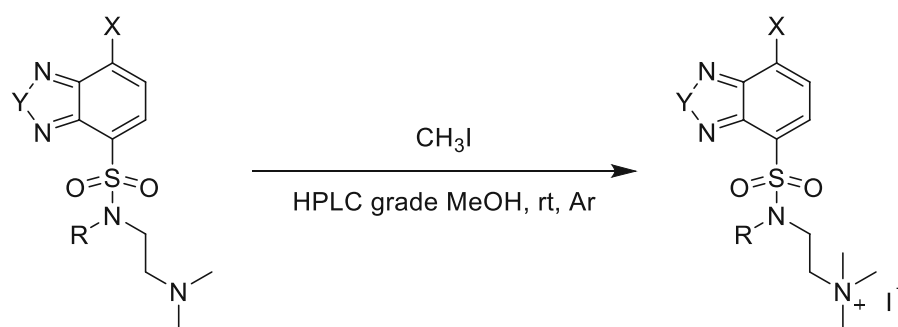


The product was synthesized according to a modified literature procedure²³⁶.

Procedure: A solution of ethyl N-hydroxyacetimidate [85] (R = Me, 2.07 mmol, 1.10 equiv.; R = H, 4.70 mmol, 2.50 equiv.) in dry DMF (11 mL, 0.16 M) was cooled to 0 °C under argon and was treated with the equimolar amounts of NaH (R = Me, 2.07 mmol, 1.10 equiv.; R = H, 4.70 mmol, 2.50 equiv., 60 % dispersion in mineral oil). Immediate strong bubbling (H₂ evolution, pressure equalization needed!) was observed, typically accompanied by a slight brown or red discoloring of the solution. The mixture was allowed to warm to room temperature over 30 minutes under vigorous stirring. Subsequently, the respective sulfonamide halide (1.88 mmol, 1.00 equiv.) was added in one portion, which triggered an immediate yellow color change. In some cases, precipitation of solids prohibited further stirring – here, quick, strong manual shaking recovered homogeneity of the solution. The reaction was stirred at room temperature for 5 hours, upon which TLC indicated full conversion.

Work-up: The reaction was diluted with EtOAc (50 mL) and washed twice with sat. NH₄Cl (2 x 100 mL). The combined aqueous phases were extracted twice with fresh EtOAc (2x 100 mL), and the combined organic layers were washed with brine (100 mL), dried over Na₂SO₄, and concentrated. The crude product was further purified *via* column chromatography (CH₂Cl₂/MeOH 20:1). Due to the highly viscous nature of the wet product, a frothing during the evaporation of the solvent mixture was observed and omitted with the use of a disproportionately larger RBF. The resulting imidates were isolated as yellow oils that crystallized upon standing.

E II.10 General procedure J: Quaternarizations of sulfonamide derivatives



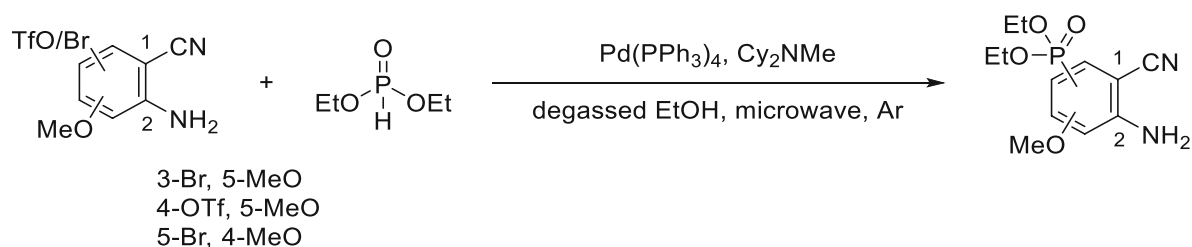
R = H, Me
X = Br, ethyl N-hydroxyacetimidate
Y = O, S

The product was synthesized according to a modified literature procedure²³⁷.

Procedure: An 8 mL screw cap vial was charged with the respective sulfonamide (1.72 mmol, 1.00 equiv.), which was dissolved in HPLC grade MeOH (17 mL, 0.11 M). Subsequently, methyl iodide (5.16 mmol, 3.00 equiv.) was added in one portion, and the yellow solution was stirred for 16 hours. Generally, complete precipitation of products as yellow solids could be observed at this point. This phenomenon furthermore pushed the product formation to completion. If this was not the case refrigerating of the solution without additional stirring for an additional day forced crystallization and thus complete conversion of products which was confirmed *via* TLC analysis.

Work-up: The product was collected by suction filtration and was thoroughly washed with -20 °C HPLC grade MeOH (2 x 5 mL) and Et₂O (3 x 10 mL). The resulting solids were dried *in vacuo* to yield the respective quaternary ammonium salts as yellow solids.

E II.11 General procedure K: Palladium-catalyzed phosphine-Carbon coupling of decorated ABAO precursors

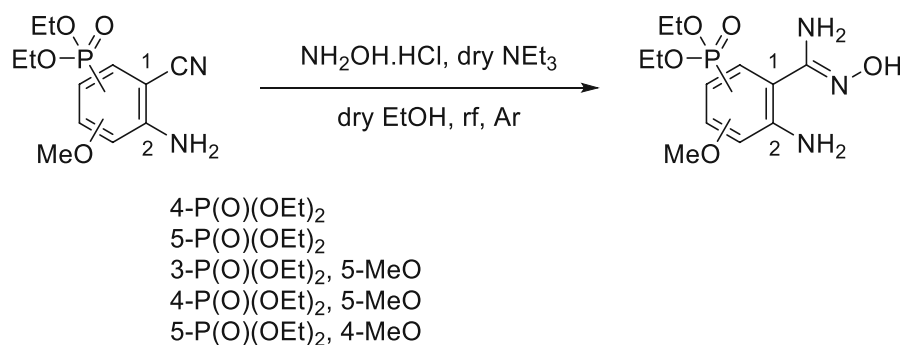


The product was synthesized according to a modified literature procedure^{243,244}.

Procedure: A 20 mL microwave vial was charged with aryl reagent (4.27 mmol, 1.00 equiv.) and bright yellow Pd(PPh₃)₄ (51 mg, 0.044 mmol, 0.01 equiv.). The vial was crimped and then evacuated and backfilled with argon using standard Schlenk techniques. Degassed EtOH (16 mL, 0.27 M), freshly distilled N,N-dicyclohexylmethylamine (1.70 mL, 1.50 g, 7.90 mmol, 1.80 equiv.), and freshly distilled diethyl phosphite (0.90 mL, 0.96 g, 6.97 mmol, 1.60 equiv.) were added consecutively. The vial was transferred into the Biotage microwave auto-sampler and heated with the following temperature program: 120 °C for 10 min; 1 minute pre-stirring; absorbance: high. For certain batches, prolonged microwave irradiation (20 - 30 minutes total) was needed to achieve full conversion. In these cases, multiple runs with the same conditions were performed until TLC confirmed the full conversion of the starting material. A deep yellow solution was generally indicative of a successful reaction; ochre or colorless reaction mixtures pointed to an early decomposition of the catalyst. Further purification of the starting material or repeated washing of the catalyst with MeOH and then Et₂O typically solved all issues.

Work-up: The solvent was removed *in vacuo*, and the resulting oily residue was taken up in EtOAc (100 mL) and washed with twice 1N HCl (2 x 100 mL). The aqueous phase was re-extracted twice with EtOAc (2 x 50 mL). The combined organic layers were washed with brine (200 mL), dried over Na₂SO₄, and concentrated. The crude product was further purified *via* column chromatography (pure EtOAc or CH₂Cl₂/MeOH – 20:1) to yield to the respective phosphonates as a colorless crystalline solids. In cases where the product started to crystallize after evaporation of the solvent, repeated washing steps with -20 °C Et₂O were sufficient for the isolation of 95% pure product.

E II.12 General procedure L: 2-Amino benzamidoxime (ABAO) synthesis by nucleophilic addition

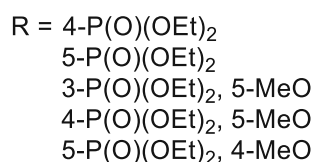
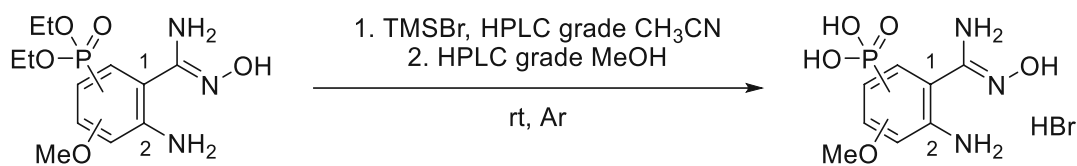


The product was synthesized according to a modified literature procedure⁶².

Procedure: A flame-dried 25 mL screw-cap vial was charged with the respective aryl-nitrile (3.52 mmol, 1.00 equiv.) and hydroxylamine hydrochloride (0.52 g, 7.41 mmol, 2.10 equiv.). The atmosphere was exchanged for argon using standard Schlenk-techniques, and subsequently, dry EtOH (8 mL, 0.44 M) and dry triethylamine (1.20 mL, 0.87 g, 8.62 mmol, 2.40 equiv.) were added immediately, triggering strong gas evolution. The yellow suspension was heated at 80 °C for 12 hours, upon which TLC indicated full conversion.

Work-up: The reaction was immediately concentrated to dryness. The remaining yellow oil was taken up in a minimal amount of 5-10 % MeOH in EtOAc and directly adsorbed onto Celite (10-20 g). The adsorbed product was then purified *via* column chromatography (EtOAc/MeOH – 20:1 to 10:1) to yield to the respective 2-amino benzamidoxime as a colorless crystalline solids.

E II.13 General procedure M: Lewis-acid promoted phosphonate deprotection of P-ABAO derivates



The product was synthesized according to a modified literature procedure²⁴⁶.

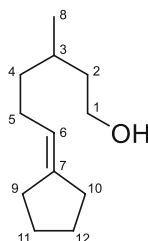
All of the following steps should be performed preferably in the dark or with minimal contact with light sources. Coverage of the vessels with aluminum foil during work-up processes increased reproducibility and recovery of product.

Procedure: A flame-dried, 8 mL brown-glass screw-cap vial was charged with the respective phosphonate (1.09 mmol, 1.00 equiv.), which was suspended in HPLC grade MECN (2.3 mL, 0.47 M) under argon. The solution was subsequently cooled with an ice/water bath to 0 °C, and TMSBr (1.41 mL, 1.67 g, 10.87 mmol, 10.00 equiv.) was added dropwise in 1 minute. This strong exothermic process triggered the complete dissolution of all particulates and yellowing of the reaction mixture. The reaction was then allowed to stir at room temperature for 1-3 hours. Careful tracking of the reaction progress *via* HPLC-MS (C₁₈, acidic) and crude NMR measurements were needed to reduce side product formation due to prolonged reaction times. In certain cases, minimal precipitation of colorless solids or the formation of a fine dispersion could be observed. Methoxy-substituents were shown to accelerate the reaction – therefore, sampling should be performed at 30-minute timepoints. Upon confirmation of full conversion, the reaction was concentrated to complete dryness by rotary evaporation at room temperature (full removal of TMSBr!). The resulting yellow solids were re-dissolved in HPLC grade MeOH (2.3 mL) and stirred for 30 minutes at room temperature. In certain cases, incomplete dissolution but only the formation of a cloudy suspension was observed.

Work-up: The reaction was subsequently concentrated to leave bright yellow solids. In certain cases, NMR analysis of the obtained product confirmed excellent purity at this point, and the crude was used for further experimentation. If ³¹P-NMR analysis indicated increased side-product formation, the solids were suspended in -20 °C dry EtOH (2-3 mL). Deep yellow-colored side-products preferably dissolved in EtOH, enabling the isolation of the product either by suction filtration or centrifugation (5000 rpm). Repeated washing steps improved the quality of the following fluorescence measurements by decreasing the background signal, albeit diminishing the overall yield. The resulting off-white solids were dried *in vacuo* to give the respective phosphonic acids.

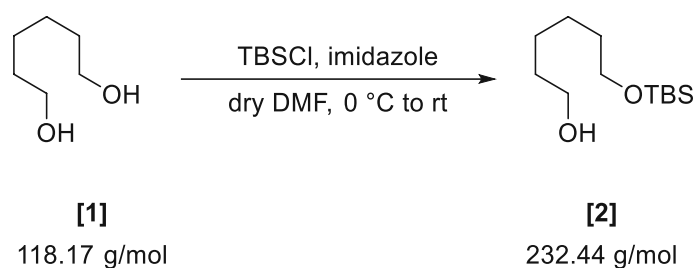
E III Chemical Synthesis

E III.1 Part I – Synthesis of citronellal analogs for SHC catalyzed Prins-reactions



NMR assignments of core structures in this chapter were given according to the following example.

E III.1.1 6-((Tert-butyl dimethylsilyl)oxy)hexan-1-ol [2]



The product was synthesized according to a literature procedure¹⁹⁹.

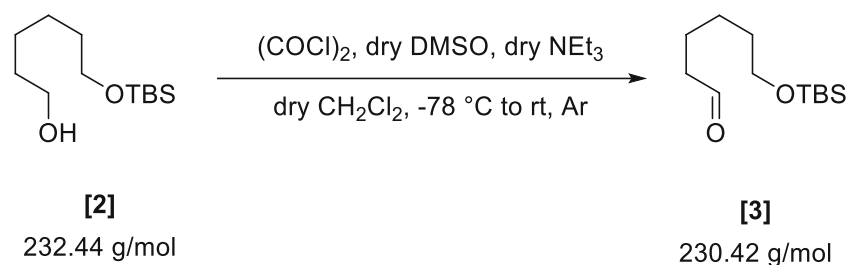
Procedure: TBSCl (5.00 g, 33.17 mmol, 1.00 equiv.) dissolved in dry DMF (40 mL) was added to 1,6-hexanediol **[1]** (39.21 g, 331.74 mmol, 10.00 equiv.) and imidazole (2.71 g, 39.81 mmol, 1.20 equiv.) in dry DMF (70 mL) at 0 °C over a period of 60 minutes. The cooling bath was removed, and the light-yellow mixture was allowed to stir at room temperature overnight at room temperature.

Work-up: The reaction was diluted with 5% LiCl solution (300 mL) and was extracted with Et₂O (3 x 100 mL). The combined Et₂O layers were washed with dH₂O (200 mL), 5% LiCl solution (200 mL), brine (200 mL), then dried over Na₂SO₄, and concentrated. For the final purification, the crude was columned over silica (200 g, 1:30) with 4:1 to 1:1 LP/EtOAc to yield 5.84 g (76 %) of **[2]** as a colorless oil.

Yield	5.84 g (76 %)
Appearance	colorless oil
TLC	R _f (LP/EtOAc - 3/1) = 0.42 (anisaldehyde)

Reaction scale	5.00 g (33.17 mmol)
Substrate concentration	0.30 M
Purification	column chromatography (silica) LP/EtOAc 4:1 to 1:1
Sum formula, m.w.	C ₁₂ H ₂₈ O ₂ Si, 232.44 g/mol
¹ H-NMR (400 MHz, DMSO- <i>d</i> ₆)	δ 0.04 (s, 6H, -Si(CH ₃) ₂), 0.89 (s, 9H, -Si-C(CH ₃) ₃), 1.33 – 1.40 (m, 4H, H3, H4), 1.48 – 1.62 (m, 4H, H2, H5), 1.84 (s, 1H, -OH), 3.60 (t, <i>J</i> = 6.5 Hz, 2H, H1), 3.64 (t, <i>J</i> = 6.7 Hz, 2H, H6).
¹³ C-NMR (151 MHz, DMSO- <i>d</i> ₆)	δ 18.5 (s, -Si-C(CH ₃) ₃), 25.7 (t, C3 or C4), 25.7 (t, C3 or C4), 26.1 (q, 3C, -Si-C(CH ₃) ₃), 32.9 (t, C2 or C5), 32.9 (t, C2 or C5), 63.1 (t, C6), 63.3 (t, C1).

E III.1.2 6-((Tert-butyldimethylsilyloxy)hexanal [3]



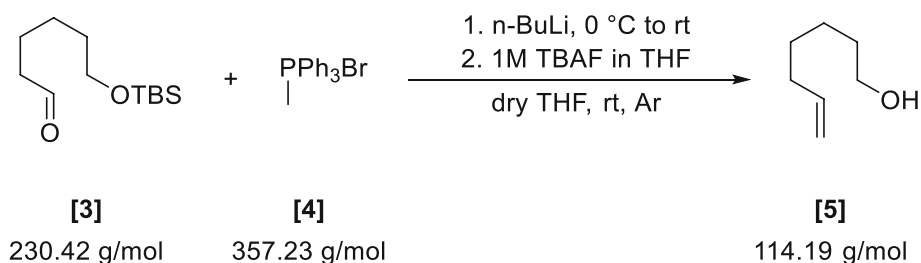
The product was synthesized according to a literature procedure²⁰⁰.

Procedure: A flame-dried 500 mL three-necked was charged with dry DMSO (4.81 g, 4.37 mL, 61.52 mmol, 2.60 equiv.) and dry CH₂Cl₂ (200 mL) under argon atmosphere. The solution was cooled to -78 °C *via* acetone/N₂ bath, and a bubbler was installed. Oxalyl chloride (3.90 g, 2.64 mL, 30.76 mmol, 1.30 equiv.) was added dropwise over a period of 5 minutes leading to evident gas evolution. The solution was stirred for 30 minutes, then [2] (5.50 g, 23.66 mmol, 1.00 equiv.) dissolved in dry CH₂Cl₂ (50 mL) was added over a period of 1 hour. Subsequent addition of dry triethylamine (13.38 g, 18.33 mL, 132.27 mmol, 4.30 equiv.) in 30 minutes caused minor turbidity of the solution. The reaction mixture was stirred at -78 °C for 1.5 hours, then warmed to room temperature by removal of the cooling bath.

Work-up: The reaction was quenched with the addition of dH₂O (150 mL). The phases were separated, and the aqueous phase was extracted twice with CH₂Cl₂ (2 x 100 mL). The combined organic layers were washed with dH₂O (150 mL), brine (150 mL), dried over Na₂SO₄, and concentrated. The resulting suspension was taken up in Et₂O (20 mL), and the residual solids were removed by filtration over a pad of Celite. For final purification, the crude yellow oil was columned over silica (150 g) with 10:1 to 5:1 (Et₂O:LP) to yield 4.68 g (86 %) of [3] as a colorless oil which was immediately stored at -20 °C under argon.

Yield	4.68 g (86 %)
Appearance	colorless oil
TLC	R_f (LP/EtOAc - 10/1) = 0.33 (anisaldehyde)
Reaction scale	5.50 g (23.66 mmol)
Substrate concentration	0.1 M
Purification	column chromatography (silica) LP/Et ₂ O 10:1 to 5:1
Sum formula, m.w.	C ₁₂ H ₂₆ O ₂ Si, 230.42 g/mol
¹ H-NMR (400 MHz, CDCl ₃)	δ 0.04 (s, 6H, -Si(CH ₃) ₂), 0.89 (s, 9H, -Si-C(CH ₃) ₃), 1.32 – 1.44 (m, 2H, H3), 1.49 – 1.58 (m, 2H, H2), 1.65 (p, J = 7.4 Hz, 2H, H4), 2.43 (td, J = 1.8, 7.4 Hz, 2H, H5), 3.60 (t, J = 6.4 Hz, 2H, H1), 9.76 (t, J = 1.8 Hz, 1H, H6).
¹³ C-NMR (151 MHz, CDCl ₃)	δ 18.5 (s, -Si-C(CH ₃) ₃), 22.1 (t, C4), 25.6 (t, C3), 26.1 (q, 3C, -Si-C(CH ₃) ₃), 32.7 (t, C2), 44.1 (t, C5), 63.0 (t, C1), 202.9 (d, C6).

E III.1.3 Hept-6-en-1-ol [5]

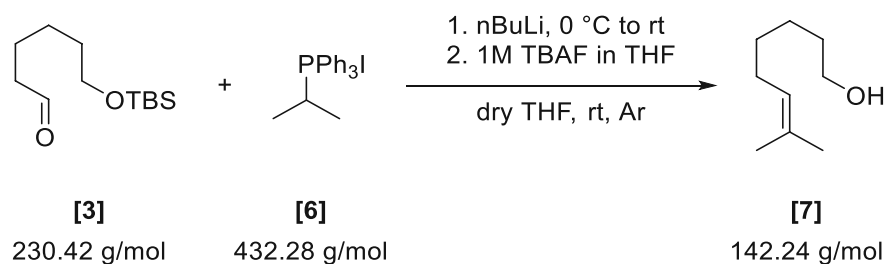


Hept-6-en-1-ol [5] was synthesized according to general procedure A using 6-((tert-butyldimethylsilyloxy)hexanal [3] (0.50 g, 2.17 mmol) and methyltriphenylphosphonium bromide [4] (1.09 g, 2.82 mmol).

Yield	0.22 g (89 %)
Appearance	colorless oil
TLC	R_f (LP/EtOAc - 3/1) = 0.37 (anisaldehyde)
Reaction scale	0.50 g (2.17 mmol)
Substrate concentration	0.23 M
Purification	column chromatography (silica) LP/Et ₂ O 1:1
Sum formula, m.w.	C ₇ H ₁₄ O, 114.19 g/mol

$^1\text{H-NMR}$ (400 MHz, CDCl_3)	δ 1.09 – 1.39 (m, 4H, H3, H4), 1.48 (p, $J = 6.8$ Hz, 2H, H2), 1.70 (br s, 1H, -OH), 1.89 – 2.02 (m, 2H, H5), 3.55 (t, $J = 6.6$ Hz, 2H, H1), 4.81 – 4.96 (m, 2H, H7), 5.72 (ddt, $J = 6.7, 10.2, 16.9$ Hz, 1H, H6).
$^{13}\text{C-NMR}$ (151 MHz, CDCl_3)	δ 25.4 (t, C3), 28.8 (t, C4), 32.7 (t, C2), 33.8 (t, C5), 63.1 (t, C1), 114.5 (t, C7), 139.0 (d, C6).

E III.1.4 7-Methyloct-6-en-1-ol [7]

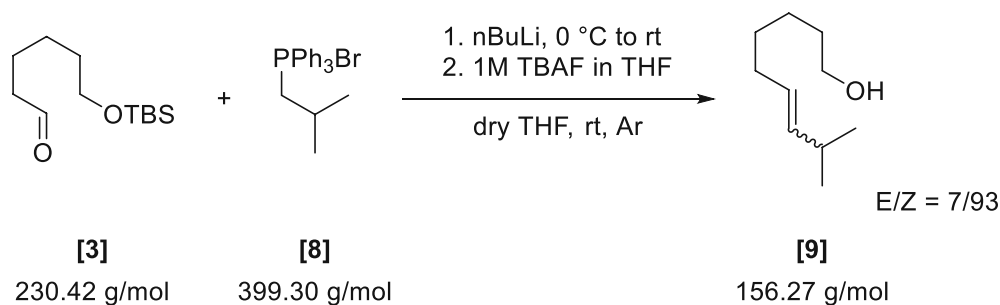


7-methyloct-6-en-1-ol [7] was synthesized according to general procedure A using 6-((tert-butyldimethylsilyloxy)hexanal [3] (0.50 g, 2.17 mmol) and isopropyltriphenylphosphonium iodide [6] (1.22 g, 2.82 mmol).

Yield	0.24 g (77 %)
Appearance	colorless oil
TLC	R_f (LP/EtOAc - 3/1) = 0.45 (anisaldehyde)
Reaction scale	0.50 g (2.17 mmol)
Substrate concentration	0.23 M
Purification	column chromatography (silica) LP/EtOAc 5:1
Sum formula, m.w.	$\text{C}_9\text{H}_{18}\text{O}$, 142.24 g/mol

$^1\text{H-NMR}$ (400 MHz, CDCl_3)	δ 1.31 – 1.38 (m, 4H, H3, H4), 1.51 – 1.60 (m, 2H, H2), 1.59 (s, 4H, H10), 1.68 (s, 3H, H9), 1.98 (q, $J = 6.6$ Hz, 2H, H5), 3.63 (t, $J = 6.6$ Hz, 2H, H1), 5.11 (dddd, $J = 1.5, 2.9, 7.1, 8.7$ Hz, 1H, H6).
$^{13}\text{C-NMR}$ (151 MHz, CDCl_3)	δ 17.8 (q, C10), 25.5 (t, C3), 25.9 (q, C9), 28.1 (t, C5), 29.8 (t, C4), 32.9 (t, C2), 63.2 (t, C1), 124.7 (d, C6), 131.6 (s, C7).

E III.1.5 8-Methylnon-6-en-1-ol [9]



8-methylnon-6-en-1-ol [9] was synthesized according to general procedure **A** using 6-((tert-butyldimethylsilyloxy)hexanal [3] (0.50 g, 2.17 mmol) and isobutyltriphenylphosphonium bromide [8] (1.04 g, 2.60 mmol). Product is isolated as a mixture of inseparable *E/Z* = 7/93 isomers.

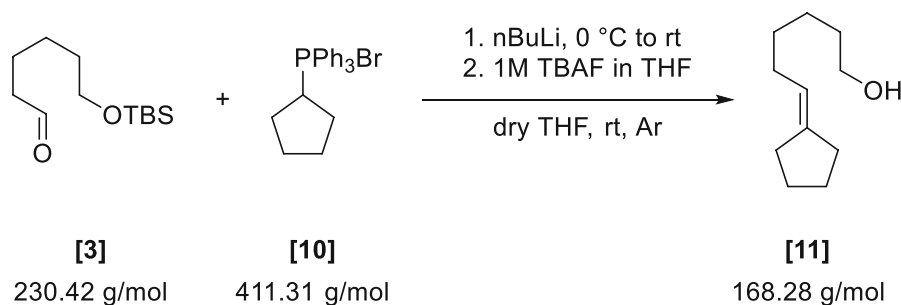
Yield 0.24 g (71 %)
Appearance colorless oil
TLC R_f (LP/EtOAc - 3/1) = 0.47 (anisaldehyde)

Reaction scale 0.50 g (2.17 mmol)
Substrate concentration 0.23 M
Purification column chromatography (silica) LP/EtOAc 4:1
Sum formula, m.w. $C_{10}H_{20}O$, 156.27 g/mol

1H -NMR (400 MHz, $CDCl_3$) δ 0.84 – 1.04 (m, 6H, *E*-H10, *Z*-H10, *E*-H11, *Z*-H11), 1.37 (p, J = 3.6 Hz, 4H, *E*-H3, *Z*-H3, *E*-H4, *Z*-H4), 1.47 – 1.77 (m, 3H, *E*-H2, *Z*-H2, -OH), 1.93 – 2.12 (m, 2H, *Z*-H5), 2.16 – 2.28 (m, 2H, *E*-H9), 2.58 (ddt, J = 6.6, 8.3, 13.2 Hz, 1H, *Z*-H9), 3.64 (td, J = 2.0, 6.6 Hz, 2H, *E*-H1, *Z*-H1), 5.12 – 5.27 (m, 2H, *Z*-H6, *Z*-H7), 5.30 – 5.43 (m, 2H, *E*-H6, *E*-H7).

^{13}C -NMR (151 MHz, $CDCl_3$) δ 22.8 (q, *E*-C10, *E*-C11), 23.4 (q, *Z*-C10, *Z*-C11), 25.4 (t, *E*-C3), 25.5 (t, *Z*-C3), 26.6 (d, *Z*-C9), 27.4 (t, *Z*-C5), 29.6 (t, *E*-C4), 29.8 (t, *Z*-C4), 31.1 (d, *E*-C9), 32.6 (t, *E*-C5), 32.8 (t, *E*-C2), 32.8 (t, *Z*-C2), 63.1 (t, *Z*-C1), 63.2 (t, *E*-C1), 127.0 (d, *E*-C6), 127.3 (d, *Z*-C6), 137.9 (d, *Z*-C7), 137.9 (d, *E*-C7).

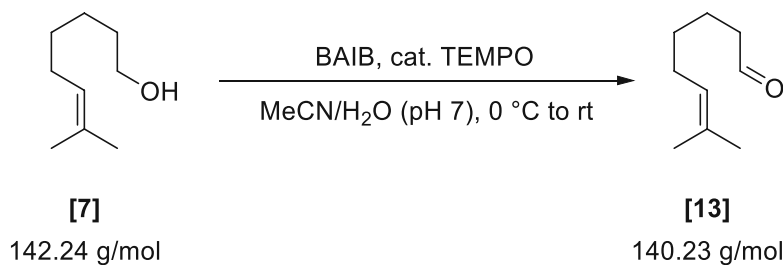
E III.1.6 6-Cyclopentylidenehexan-1-ol [11]



6-cyclopentylidenehexan-1-ol [11] was synthesized according to general procedure **A** using 6-((tert-butyldimethylsilyloxy)hexanal [3] (0.50 g, 2.17 mmol) and cyclopentyltriphenylphosphonium bromide [10] (1.16 g, 2.82 mmol).

Yield	0.24 g (70 %)
Appearance	colorless oil
TLC	R_f (LP/EtOAc - 3/1) = 0.47 (anisaldehyde)
Reaction scale	0.50 g (2.17 mmol)
Substrate concentration	0.23 M
Purification	column chromatography (silica) LP/Et ₂ O 1:1
Sum formula, m.w.	C ₁₁ H ₂₀ O, 168.28 g/mol
¹H-NMR (400 MHz, CDCl₃)	δ 1.29 (s, 1H, -OH), 1.32 – 1.39 (m, 4H, H3, H4), 1.54 – 1.61 (m, 4H, H2, H11), 1.65 (p, J = 6.7 Hz, 2H, H12), 1.83 – 2.05 (m, 2H, H5), 2.16 (tdt, J = 1.3, 2.6, 7.1 Hz, 2H, H9), 2.21 (ddt, J = 1.7, 5.4, 7.0 Hz, 2H, H10), 3.64 (t, J = 6.7 Hz, 2H, H1), 5.19 – 5.26 (m, 1H, H6).
¹³C-NMR (151 MHz, CDCl₃)	δ 25.6 (t, C3), 26.5 (t, C12), 26.6 (t, C11), 28.7 (t, C9), 29.6 (t, C4), 29.7 (t, C5), 32.9 (t, C2), 33.7 (t, C10), 63.2 (t, C1), 120.1 (d, C6), 143.4 (s, C7).

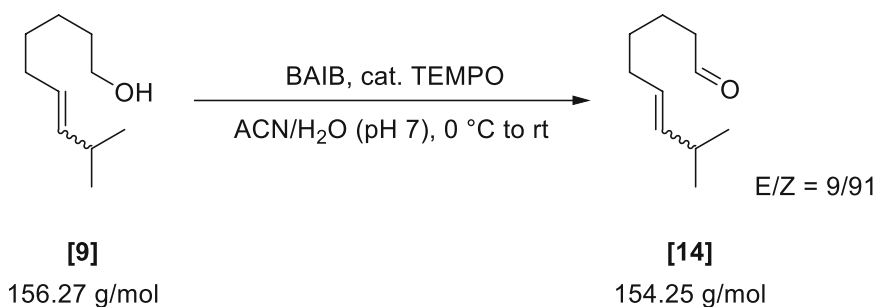
E III.1.7 7-Methyloct-6-enal [13]



7-methyloct-6-enal [13] was synthesized according to general procedure C using 7-methyloct-6-en-1-ol [7] (100 mg, 0.63 mmol), BAIB (222 mg, 0.69 mmol) and TEMPO (9.8 mg, 0.06 mmol).

Yield	38 mg (43 %)
Appearance	colorless oil
TLC	R_f (LP/CH ₂ Cl ₂ - 1/1) = 0.32 (anisaldehyde)
Reaction scale	100 mg (0.63 mmol)
Substrate concentration	0.22 M
Purification	column chromatography (silica) LP/Et ₂ O 1:1
Sum formula, m.w.	C ₉ H ₁₆ O, 140.23 g/mol
¹H-NMR (400 MHz, CDCl₃)	δ 1.31 – 1.43 (m, 2H, H4), 1.60 (s, 3H, H10), 1.61 – 1.66 (m, 2H, H3), 1.66 – 1.71 (m, 4H, H9), 1.99 (q, <i>J</i> = 7.4 Hz, 2H, H5), 2.42 (td, <i>J</i> = 1.9, 7.4 Hz, 2H, H2), 5.05 – 5.14 (m, 1H, H6), 9.76 (t, <i>J</i> = 1.9 Hz, 1H, H1).
¹³C-NMR (151 MHz, CDCl₃)	δ 17.8 (q, C10), 21.9 (t, C3), 25.8 (q, C9), 27.8 (t, C5), 29.5 (t, C4), 44.0 (t, C2), 124.1 (d, C6), 132.1 (s, C7), 203.0 (d, C1).
GC-MS (method B)	t_R = 3.05 minutes, main fragments 140 (6, M+), 122 (11), 107 (23), 81 (55), 69 (100)

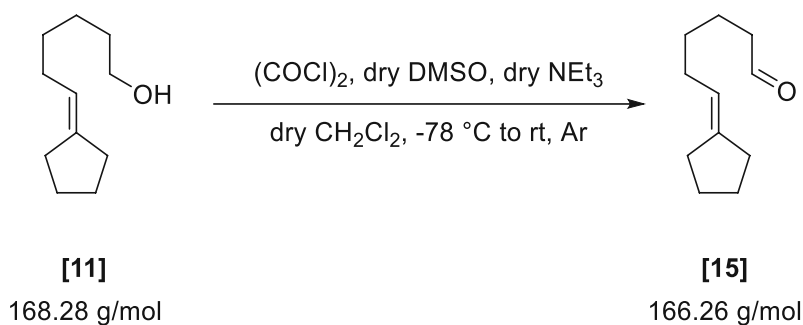
E III.1.8 8-Methylnon-6-enal [14]



8-methylnon-6-enal [14] was synthesized according to general procedure C using 8-methylnon-6-en-1-ol [9] (100 mg, 0.64 mmol), BAIB (227 mg, 0.70 mmol) and TEMPO (10 mg, 0.06 mmol). Product is isolated as a mixture of inseparable *E/Z* = 9/91 isomers.

Yield	71 mg (72 %)
Appearance	colorless oil
TLC	R_f (LP/CH ₂ Cl ₂ - 1/1) = 0.35 (anisaldehyde)
Reaction scale	100 mg (0.64 mmol)
Substrate concentration	0.20 M
Purification	column chromatography (silica) LP/Et ₂ O 1:1
Sum formula, m.w.	C ₁₀ H ₁₈ O, 154.25 g/mol
¹H-NMR (400 MHz, CDCl₃)	δ 0.94 (d, <i>J</i> = 6.7 Hz, 6H, <i>E</i> -H10, <i>Z</i> -H10, <i>E</i> -H11, <i>Z</i> -H11), 1.39 (tt, <i>J</i> = 6.5, 10.0 Hz, 2H, <i>Z</i> -H4, <i>E</i> -H4), 1.55 – 1.71 (m, 2H, <i>E</i> -H3, <i>Z</i> -H3), 1.99 (q, <i>J</i> = 6.9 Hz, 2H, <i>E</i> -H5), 2.01 – 2.11 (m, 2H, <i>Z</i> -H5), 2.21 (tt, <i>J</i> = 6.5, 12.4 Hz, 1H, <i>E</i> -H9), 2.43 (td, <i>J</i> = 1.9, 7.3 Hz, 2H, <i>E</i> -H2, <i>Z</i> -H2), 2.57 (dp, <i>J</i> = 6.6, 8.2 Hz, 1H, <i>Z</i> -H9), 5.14 – 5.26 (m, 2H, <i>Z</i> -H6, <i>Z</i> -H7), 5.26 – 5.43 (m, 2H, <i>E</i> -H6, <i>E</i> -H7), 9.76 (t, <i>J</i> = 1.8 Hz, 1H, <i>E</i> -H1, <i>Z</i> -H1).
¹³C-NMR (151 MHz, CDCl₃)	δ 21.7 (t, <i>E</i> -C3), 21.8 (t, <i>Z</i> -C3), 22.8 (q, <i>E</i> -C9, <i>E</i> -C10), 23.3 (q, <i>Z</i> -C9, <i>Z</i> -C10), 26.6 (d, <i>Z</i> -C9), 27.1 (t, <i>Z</i> -C5), 29.2 (t, <i>E</i> -C4), 29.5 (t, <i>Z</i> -C4), 31.1 (d, <i>E</i> -C9), 32.3 (t, <i>E</i> -C5), 43.9 (t, <i>E</i> -C2, <i>Z</i> -C2), 126.4 (d, <i>E</i> -C6), 126.7 (d, <i>Z</i> -C6), 138.3 (d, <i>Z</i> -C7), 138.4 (d, <i>E</i> -C7), 202.8 (d, <i>Z</i> -C1), 203.0 (d, <i>E</i> -C1).
GC-MS (method B)	t_R = 3.35 minutes (<i>Z</i>) / 3.39 minutes (<i>E</i>), main fragments 136 (21), 121 (23), 95 (35), 69 (99), 55 (100)

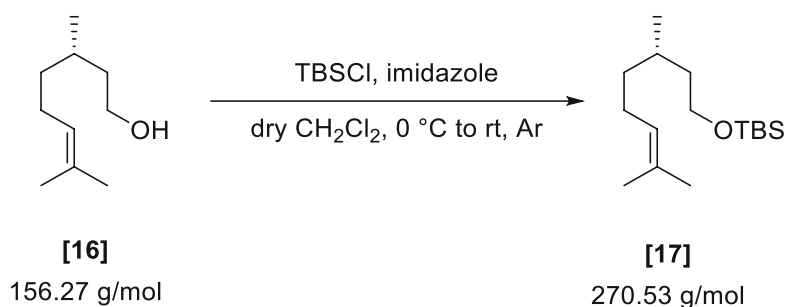
E III.1.9 6-Cyclopentylidenehexanal [15]



6-cyclopentylidenehexanal [15] was synthesized according to general procedure **B** using 6-cyclopentylidenehexan-1-ol [11] (200 mg, 1.19 mmol).

Yield	140 mg (69 %)
Appearance	colorless oil
TLC	R_f (LP/Et ₂ O – 40:1) = 0.28 (anisaldehyde)
Reaction scale	200 mg (1.19 mmol)
Substrate concentration	0.15 M
Purification	column chromatography (silica) LP/Et ₂ O 40:1
Sum formula, m.w.	C ₁₁ H ₁₈ O, 166.26 g/mol
¹H-NMR (400 MHz, CDCl₃)	δ 1.32 – 1.46 (m, 2H, H4), 1.55 – 1.61 (m, 3H, H11), 1.62 – 1.68 (m, 5H, H3, H12), 1.98 (td, $J = 1.5, 7.3$ Hz, 2H, H5), 2.15 (tdt, $J = 1.3, 2.7, 7.1$ Hz, 2H, H9), 2.21 (tdt, $J = 1.7, 5.2, 8.8$ Hz, 2H, H10), 2.42 (td, $J = 1.9, 7.4$ Hz, 2H, H2), 5.21 (tp, $J = 2.3, 7.1$ Hz, 1H, H6), 9.76 (t, $J = 1.9$ Hz, 1H, H1).
¹³C-NMR (151 MHz, CDCl₃)	δ 21.9 (t, C3), 26.5 (t, C11), 26.6 (t, C12), 28.8 (d, C9), 29.3 (t, C4), 29.4 (t, C5), 33.7 (t, C10), 44.0 (d, C2), 119.5 (d, C6), 143.9 (s, C7), 203.1 (d, C1).
GC-MS (method B)	$t_R = 4.67$ minutes, main fragments 166 (1, M ⁺), 148 (19), 95 (42), 79 (38), 67 (100)

E III.1.10 (S)-Tert-butyl((3,7-dimethyloct-6-en-1-yl)oxy)dimethylsilane [17]



Procedure: A three-necked round bottom flask was charged with (S)-citronellol [16] (4.00 g, 25.6 mmol, 1.00 equiv.) dry CH₂Cl₂ (40 mL). Imidazole (3.49 g, 51.2 mmol, 2.00 equiv.) was added, and the reaction mixture was cooled to 0 °C under argon atmosphere using an ice/water bath. TBS-Cl (4.24 g, 28.2 mmol, 1.10 equiv.) was added in several portions, which caused the immediate formation of a white suspension. The ice/water bath was removed, and the suspension was stirred for 1 hour until the end of the reaction was confirmed *via* TLC.

Work-up: The reaction was quenched with the addition of MeOH (1 mL) to remove any unreacted silylchlorid species. After stirring for an additional 30 minutes, sat. NaHCO₃ (40 mL) was added. The aqueous phase was extracted with CH₂Cl₂ (3 x 40 mL). The combined organic phases were washed with brine (100 mL), dried over Na₂SO₄, and concentrated to yield 6.92 g (quant.) of (S)-tert-butyl((3,7-dimethyloct-6-en-1-yl)oxy)dimethylsilane [17] as a colorless oil. The resulting material could be used directly for the next step without further purification.

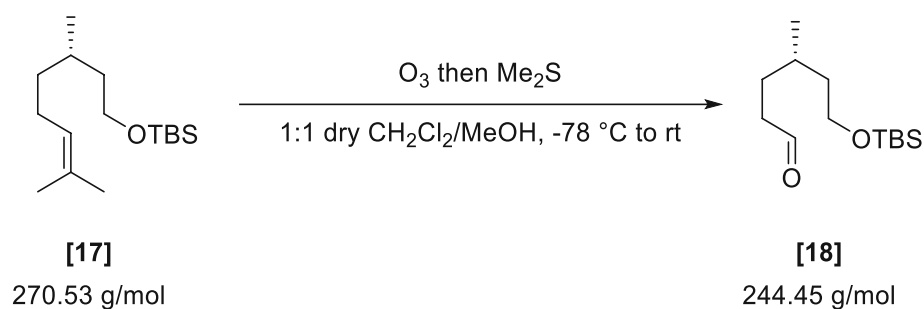
Yield	6.92 g (quant.)
Appearance	colorless oil
TLC	R _f (LP/EtOAc - 5/1) = 0.95 (anisaldehyde)

Reaction scale	5.50 g (23.66 mmol)
Substrate concentration	0.60 M
Purification	pure after work-up
Sum formula, m.w.	C ₁₆ H ₃₄ OSi, 270.53 g/mol
Optical rotation	[α] _D ²⁰ = -1.1 (c = 0.58, CHCl ₃)

¹H-NMR (400 MHz, CDCl₃) δ 0.05 (s, 6H, -Si(CH₃)₂), 0.86 – 0.93 (m, 12H, H8, -Si-C(CH₃)₃), 1.09 – 1.21 (m, 1H, H4), 1.24 – 1.41 (m, 2H, H2, H4'), 1.49 – 1.58 (m, 2H, H2', H3), 1.60 (s, 3H, H10), 1.68 (d, J = 1.4 Hz, 3H, H9), 1.85 – 2.10 (m, 2H, H5), 3.58 – 3.69 (m, 2H, H1), 5.07 – 5.13 (m, 1H, H6).

¹³C-NMR (151 MHz, CDCl₃) δ 17.8 (q, C10), 18.5 (s, -Si-C(CH₃)₃), 19.8 (q, C8), 25.6 (t, C5), 25.9 (q, C9), 26.1 (q, -Si-C(CH₃)₃), 29.3 (d, C3), 37.4 (t, C4), 40.1 (t, C2), 61.6 (t, C1), 125.1 (d, C6), 131.2 (s, C7).

E III.1.11 (S)-6-((Tert-butyl dimethylsilyl)oxy)-4-methylhexanal [18]



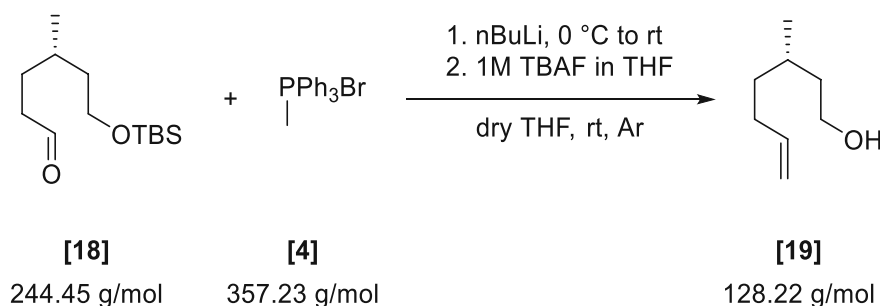
Procedure: A flame-dried 500 mL three-necked round bottom flask was charged with (S)-tert-butyl((3,7-dimethyloct-6-en-1-yl)oxy)dimethylsilane [17] (3.00 g, 11.09 mmol, 1.00 equiv.) and dissolved in a 1:1 mixture of MeOH and dry CH₂Cl₂ (20 mL). Under argon atmosphere, the solution was cooled to -78 °C using a liquid N₂/acetone bath. The ozone generator was connected to an O₂ gas cylinder and the reaction flask *via* an empty drechsel bottle in such a manner, that suck-back into the generator is prevented. The outlet of the flask was connected to two drechsel bottles. The second bottle was filled with an aqueous 10 w/w% KI solution (200 mL) to neutralize excess O₃; the first bottle was empty to prevent suck-back into the reaction vessel. Ozone was bubbled through the solution at a rate of 4 L/min at -78 °C until a blue color persisted. Subsequently, the solution was flushed with argon to remove excess O₃ indicated by the disappearance of color. Dimethyl sulfide (6.92 mL, 5.86 g, 94.26 mmol, 8.50 equiv.) was then added dropwise in 1 h, after which the mixture was allowed to warm to room temperature by stirring in the cooling bath overnight. The complete reduction of all reactive peroxide species was confirmed with peroxide test strips by taking a sample of the solution and dispersing it in the same volume of dH₂O.

Work-up: The crude was diluted with dH₂O (50 mL) and was extracted twice with CH₂Cl₂ (2 x 100 mL). The combined organic phases were washed with brine (100 mL), dried over Na₂SO₄, and concentrated. For final purification, the crude was flashed over silica (150 g) with 10:1 (LP:EtOAc) and again concentrated. To further remove the strong dimethyl sulfide smell, n-pentane (30 mL) was added, and the sulfide species was removed by azeotropic distillation. 1.76 g (65 %) of (S)-6-((tert-butyl dimethylsilyl)oxy)-4-methylhexanal [18] was isolated as a colorless, odorless oil which was stored at -20 °C under argon.

Yield	1.76 g (65 %)
Appearance	colorless viscous oil
TLC	R _f (LP/EtOAc - 10/1) = 0.54 (anisaldehyde)
Reaction scale	3.00 g (11.09 mmol)
Substrate concentration	0.55 M
Purification	flash chromatography (silica) LP/EtOAc 10:1 + azeotropic distillation (n-pentane)

Sum formula, m.w.	C ₁₃ H ₂₈ OSi, 244.45 g/mol
Optical rotation	[α] _D ²⁰ = -1.4 (c = 0.44, CH ₂ Cl ₂)
¹ H-NMR (400 MHz, CDCl ₃)	δ 0.04 (s, 6H, -Si(CH ₃) ₂), 0.88 (s, 9H, -Si-C(CH ₃) ₃), 0.90 (d, J = 6.5 Hz, 3H, H8), 1.35 (dddd, J = 5.8, 6.6, 7.8, 13.5 Hz, 1H, H2'), 1.47 (dddd, J = 6.1, 7.5, 9.2, 13.5 Hz, 1H, H4'), 1.55 (ddd, J = 5.3, 6.8, 13.9 Hz, 1H, H3), 1.56 – 1.65 (m, 1H, H2), 1.67 (dddd, J = 5.5, 6.3, 9.1, 13.4 Hz, 1H, H4), 2.36 – 2.50 (m, 2H, H5), 3.59 – 3.70 (m, 2H, H1), 9.77 (t, J = 1.8 Hz, 1H, H6).
¹³ C-NMR (151 MHz, CDCl ₃)	δ -5.2 (q, 2C, -Si(CH ₃) ₂), 18.5 (s, -Si-C(CH ₃) ₃), 19.5 (q, C8), 26.1 (q, 3C, -Si-C(CH ₃) ₃), 29.1 (t, C4), 29.3 (d, C3), 39.7 (t, C2), 41.8 (t, C5), 61.2 (t, C1), 203.0 (d, C6).

E III.1.12 (S)-3-Methylhept-6-en-1-ol [19]



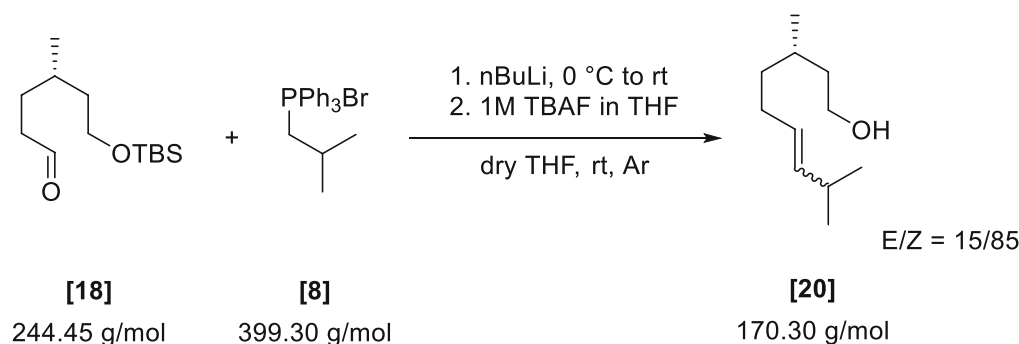
(S)-3-methylhept-6-en-1-ol [19] was synthesized according to general procedure A using (S)-6-((tert-butyldimethylsilyloxy)-4-methylhexanal [18] (0.70 g, 2.86 mmol) and methyltriphenylphosphonium bromide [4] (1.43 g, 4.01 mmol).

Yield	0.26 g (69 %)
Appearance	colorless oil
TLC	R _f (LP/EtOAc – 3:1) = 0.23 (anisaldehyde)
Reaction scale	0.70 g (2.86 mmol)
Substrate concentration	0.22 M
Purification	column chromatography (silica) LP/EtOAc 4:1
Sum formula, m.w.	C ₈ H ₁₆ O, 128.22 g/mol
Optical rotation	[α] _D ²⁰ = -2.3 (c = 0.51, CHCl ₃)

$^1\text{H-NMR}$ (400 MHz, CDCl_3) δ 0.91 (d, $J = 6.6$ Hz, 3H, -H8), 1.24 (dddd, $J = 5.7, 7.7, 9.7, 13.4$ Hz, 1H, H4'), 1.34 – 1.46 (m, 3H, H2', H4, OH), 1.54 – 1.66 (m, 2H, H2, H3), 1.98 – 2.15 (m, 2H, H5), 3.62 – 3.74 (m, 2H, H1), 4.93 (ddt, $J = 1.2, 2.3, 10.1$ Hz, 1H, cis-H7), 5.00 (dq, $J = 1.7, 17.1$ Hz, 1H, trans-H7), 5.80 (ddt, $J = 6.6, 10.2, 16.9$ Hz, 1H, H6).

$^{13}\text{C-NMR}$ (151 MHz, CDCl_3) δ 19.6 (q, C8), 29.1 (d, C3), 31.4 (t, C5), 36.4 (t, C4), 40.0 (t, C2), 61.3 (t, C1), 114.4 (t, C7), 139.2 (d, C6).

E III.1.13 (S)-3,8-Dimethylnon-6-en-1-ol [20]



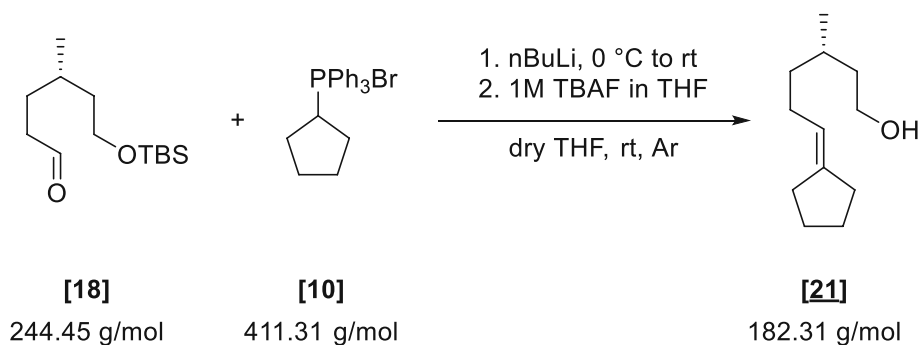
(S)-3,8-dimethylnon-6-en-1-ol [20] was synthesized according to general procedure A using (S)-6-((tert-butyl(dimethyl)silyloxy)-4-methylhexanal [18] (0.70 g, 2.86 mmol) isobutyltriphenylphosphonium bromide [8] (1.06 g, 2.66 mmol). Product is isolated as a mixture of inseparable $E/Z = 15/85$ isomers.

Yield	0.26 g (73 %)
Appearance	colorless oil
TLC	R_f (LP/EtOAc – 3:1) = 0.46 (anisaldehyde)
Reaction scale	0.50 g (2.05 mmol)
Substrate concentration	0.23 M
Purification	column chromatography (silica) LP/EtOAc 5:1
Sum formula, m.w.	$\text{C}_{11}\text{H}_{22}\text{O}$, 170.30 g/mol
Optical rotation	$[\alpha]_D^{20} = -2.6$ ($c = 0.51, \text{CHCl}_3$)

$^1\text{H-NMR}$ (400 MHz, CDCl_3) δ 0.9 (dd, $J = 1.2, 6.6$ Hz, 12H, E -H10, Z -H10, E -H11, Z -H11), 1.0 (d, $J = 6.7$ Hz, 6H, E -H8, Z -H8), 1.2 – 1.3 (m, 2H, E -H4', Z -H4'), 1.3 – 1.5 (m, 2H, E -H4, Z -H4), 1.9 – 2.0 (m, 2H, E -H5), 1.9 – 2.1 (m, 4H, E -H3, Z -H3, Z -H5), 2.2 (ddd, $J = 2.6, 8.0, 16.1$ Hz, 2H, E -H2', Z -H2'), 2.4 (ddd, $J = 2.1, 5.6, 16.1$ Hz, 3H, E -H2, Z -H2, E -H9), 2.6 (dhept, 1H, Z -H9), 5.1 – 5.2 (m, 2H, Z -H6, Z -H7), 5.3 – 5.4 (m, 2H, E -H6, E -H7), 9.7 – 9.8 (m, 2H, E -C1, Z -C1).

^{13}C -NMR (151 MHz, CDCl_3) δ 19.6 (Z-C8), 19.7 (E-C8), 22.8 (E-C10 or E-C11), 22.8 (E-C10 or E-C11), 23.4 (Z-C10, Z-C11), 24.9 (Z-C5), 26.6 (Z-C9), 29.2 (E-C3), 29.3 (Z-C3), 30.1 (E-C5), 31.1 (E-C9), 37.2 (E-C4), 37.5 (Z-C4), 40.0 (E-C2, Z-C2), 61.3 (Z-C1), 61.3 (E-C1), 127.2 (E-C6), 127.4 (Z-C6), 137.7 (Z-C7), 137.8 (E-C7).

E III.1.14 (S)-6-Cyclopentylidene-3-methylhexan-1-ol [21]



(S)-3,8-dimethylnon-6-en-1-ol [21] was synthesized according to general procedure A using (S)-6-((tert-butyl(dimethyl)silyloxy)-4-methylhexanal [18] (0.70 g, 2.86 mmol) and cyclopentyltriphenylphosphonium bromide [10] (1.65 g, 4.01 mmol).

Yield 0.29 g (55 %)
Appearance colorless oil
TLC R_f (LP/EtOAc – 4:1) = 0.43 (anisaldehyde)

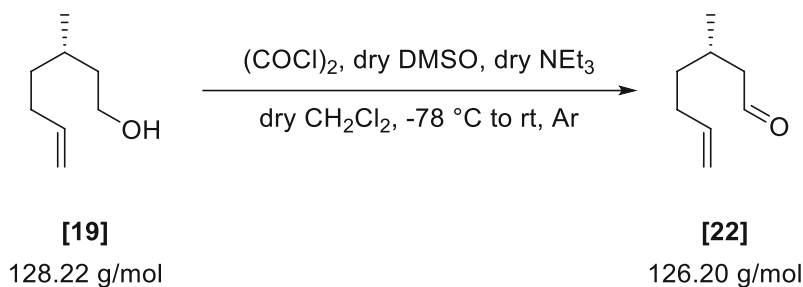
Reaction scale 0.70 g (2.86 mmol)
Substrate concentration 0.23 M
Purification column chromatography (silica) LP/EtOAc 4:1
Sum formula, m.w. $\text{C}_{12}\text{H}_{22}\text{O}$, 182.31 g/mol
Optical rotation $[\alpha]_D^{20} = -2.9$ (c = 0.52, CHCl_3)

^1H -NMR (400 MHz, CDCl_3) δ 0.90 (d, $J = 6.5$ Hz, 3H, H8), 1.11 – 1.28 (m, 1H, H4), 1.30 – 1.45 (m, 2H, H2, H4'), 1.62 (dtd, $J = 5.9, 7.4, 22.2$ Hz, 7H, H2', H3, H11, H12, OH), 1.89 – 2.06 (m, 2H, H5), 2.12 – 2.25 (m, 4H, H9, H10), 3.61 – 3.76 (m, 2H, H1), 5.18 – 5.25 (m, 1H, H6).

^{13}C -NMR (151 MHz, CDCl_3) δ 19.7 (q, C8), 26.5 (t, C11 or C12), 26.6 (t, C11 or C12), 27.2 (t, C5), 28.7 (t, C9), 29.3 (d, C3), 33.7 (t, C10), 37.2 (t, C4), 40.1 (t, C2), 61.4 (t, C1), 120.2 (d, C6), 143.2 (s, C7).

HRMS (ESI) not found.

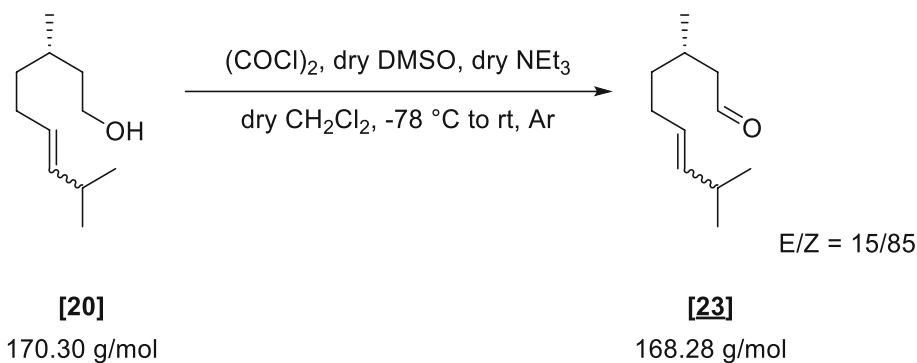
E III.1.15 (S)-3-Methylhept-6-enal [22]



(S)-3-methylhept-6-enal [22] was synthesized according to general procedure B using (S)-3-methylhept-6-en-1-ol [19] (115 mg, 0.90 mmol).

Yield	45 mg (40 %)
Appearance	colorless oil
TLC	R_f (LP/Et ₂ O– 40:1) = 0.28 (anisaldehyde)
Reaction scale	115 mg (0.90 mmol)
Substrate concentration	0.14 M
Purification	column chromatography (silica) LP/Et ₂ O 40:1
Sum formula, m.w.	C ₈ H ₁₄ O, 126.20 g/mol
Optical rotation	$[\alpha]_D^{20} = -2.3$ (c = 0.51, CHCl ₃)
¹H-NMR (400 MHz, CDCl₃)	δ 0.97 (d, $J = 6.7$ Hz, 3H, H8), 1.33 (ddt, $J = 5.9, 7.8, 9.4, 13.6$ Hz, 1H, H4'), 1.44 (ddt, $J = 6.1, 9.5, 13.6$ Hz, 1H, H4), 2.01 – 2.15 (m, 3H, H3, H5), 2.24 (ddd, $J = 2.6, 7.9, 16.1$ Hz, 1H, H2'), 2.41 (ddd, $J = 2.0, 5.7, 16.1$ Hz, 1H, H2''), 4.96 (ddt, $J = 1.3, 2.3, 10.2$ Hz, 1H, cis-H7), 5.02 (ddt, $J = 1.7, 17.2$ Hz, 1H, trans-H7), 5.79 (ddt, $J = 6.6, 10.2, 16.9$ Hz, 1H, H6), 9.75 (t, $J = 2.3$ Hz, 1H, CHO).
¹³C-NMR (151 MHz, CDCl₃)	δ 19.9 (q, C8), 27.7 (d, C3), 31.3 (t, C5), 36.1 (t, C4), 51.1 (t, C2), 114.9 (t, C7), 138.5 (d, C6), 203.0 (d, C1).

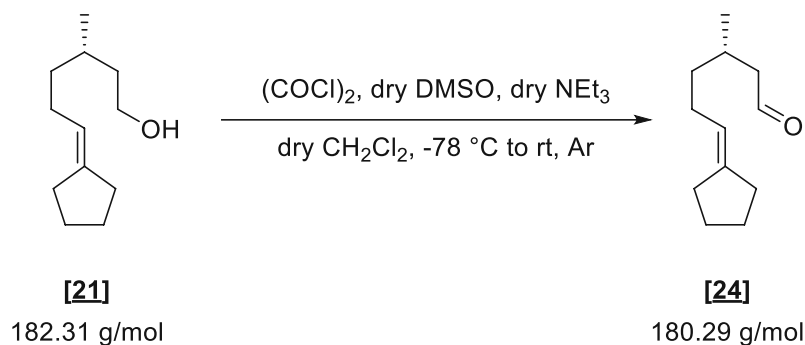
E III.1.16 (S)-3,8-Dimethylnon-6-enal [23]



(S)-3,8-dimethylnon-6-enal [23] was synthesized according to general procedure B using (S)-3,8-dimethylnon-6-en-1-ol [20] (79 mg, 0.46 mmol). Product is isolated as a mixture of inseparable E/Z = 15/85 isomers.

Yield	58 mg (74 %)
Appearance	colorless oil
TLC	R_f (LP/Et ₂ O– 40:1) = 0.24 (anisaldehyde)
Reaction scale	79 mg (0.46 mmol)
Substrate concentration	0.14 M
Purification	column chromatography (silica) LP/Et ₂ O 40:1
Sum formula, m.w.	C ₁₁ H ₂₀ O, 168.28 g/mol
Optical rotation	$[\alpha]_D^{20} = -8.3$ (c = 0.53, CHCl ₃)
¹H-NMR (400 MHz, CDCl₃)	δ 0.94 (dd, $J = 1.2, 6.6$ Hz, 6H, <i>E</i> -H10, <i>Z</i> -H10, <i>E</i> -H11, <i>Z</i> -H11), 0.97 (d, $J = 6.7$ Hz, 3H, <i>E</i> -H8, <i>Z</i> -H8), 1.17 – 1.33 (m, 1H, <i>E</i> -H4', <i>Z</i> -H4'), 1.34 – 1.47 (m, 1H, <i>E</i> -H4, <i>Z</i> -H4), 1.94 – 2.03 (m, 2H, <i>E</i> -H5), 1.92 – 2.14 (m, 3H, <i>E</i> -H3, <i>Z</i> -H3, <i>Z</i> -H5), 2.24 (ddd, $J = 2.6, 8.0, 16.1$ Hz, 1H, <i>E</i> -H2', <i>Z</i> -H2'), 2.41 (ddd, $J = 2.1, 5.6, 16.1$ Hz, 2H, <i>E</i> -H2, <i>Z</i> -H2, <i>E</i> -H9), 2.57 (dhept, 1H, <i>Z</i> -H9), 5.15 – 5.23 (m, 2H, <i>Z</i> -H6, <i>Z</i> -H7), 5.28 – 5.41 (m, 2H, <i>E</i> -H6, <i>E</i> -H7), 9.75 – 9.76 (m, 1H, <i>E</i> -C1, <i>Z</i> -C1).
¹³C-NMR (151 MHz, CDCl₃)	δ 20.0 (q, <i>Z</i> -C8), 20.0 (q, <i>E</i> -C8), 22.8 (q, <i>E</i> -C10 or <i>E</i> -C11), 22.8 (q, <i>E</i> -C10 or <i>E</i> -C11), 23.3 (q, <i>Z</i> -C10, <i>Z</i> -C11), 24.8 (t, <i>Z</i> -C5), 26.7 (d, <i>Z</i> -C9), 27.8 (d, <i>E</i> -C3), 27.9 (d, <i>Z</i> -C3), 30.0 (t, <i>E</i> -C5), 31.1 (d, <i>E</i> -C9), 36.9 (t, <i>E</i> -C4), 37.2 (t, <i>Z</i> -C4), 51.1 (t, <i>E</i> -C2), 51.1 (t, <i>Z</i> -C2), 126.6 (d, <i>E</i> -C6), 126.7 (d, <i>Z</i> -C6), 138.2 (d, <i>Z</i> -C7), 138.2 (d, <i>E</i> -C7), 203.1 (d, <i>Z</i> -C1), 203.2 (d, <i>E</i> -C1).
HRMS (ESI)	not found.
GC-MS (method B)	$t_R = 3.67$ minutes (<i>Z</i>) / 3.74 minutes (<i>E</i>), main fragments 150 (15), 135 (14), 107 (30), 95 (49), 81 (46), 69 (93), 55 (100)

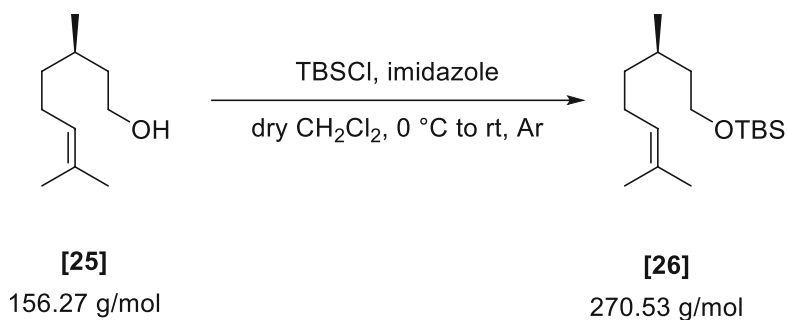
E III.1.17 (S)-6-Cyclopentylidene-3-methylhexanal [24]



(S)-6-cyclopentylidene-3-methylhexanal [24] was synthesized according to general procedure B using (S)-6-cyclopentylidene-3-methylhexan-1-ol [21] (120 mg, 0.66 mmol).

Yield	75 mg (63 %)
Appearance	colorless oil
TLC	R_f (LP/Et ₂ O– 40:1) = 0.26 (anisaldehyde)
Reaction scale	120 mg (0.66 mmol)
Substrate concentration	0.13 M
Purification	column chromatography (silica) LP/Et ₂ O 40:1
Sum formula, m.w.	C ₁₂ H ₂₀ O, 180.29 g/mol
Optical rotation	$[\alpha]_D^{20} = -15.3$ (c = 0.64, CHCl ₃)
¹H-NMR (400 MHz, CDCl₃)	δ 0.97 (d, <i>J</i> = 6.7 Hz, 3H, H8), 1.29 (dddd, <i>J</i> = 6.2, 7.7, 9.1, 13.6 Hz, 1H, H4'), 1.34 – 1.42 (m, 1H, H4), 1.55 – 1.62 (m, 2H, H12), 1.62 – 1.70 (m, 2H, H11), 1.92 – 2.04 (m, 2H, H5), 2.04 – 2.11 (m, 1H, H3), 2.16 (dddq, <i>J</i> = 1.4, 2.6, 5.3, 9.3 Hz, 2H, H10), 2.21 (dq, <i>J</i> = 1.3, 3.1, 6.8 Hz, 2H, H9), 2.21 – 2.28 (m, 1H, H2'), 2.41 (ddd, <i>J</i> = 2.1, 5.6, 16.0 Hz, 1H, H2), 5.20 (tp, <i>J</i> = 2.3, 7.0 Hz, 1H, H6), 9.75 (dd, <i>J</i> = 2.0, 2.7 Hz, 1H, H1).
¹³C-NMR (151 MHz, CDCl₃)	δ 20.0 (q, C8), 26.5 (t, C11), 26.6 (t, C12), 27.1 (t, C5), 28.0 (d, C3), 28.7 (t, C9), 33.7 (t, C10), 36.9 (t, C4), 51.2 (t, C2), 119.6 (s, C7), 143.7 (d, C6), 203.3 (d, C1).
HRMS (ESI)	not found.
GC-MS (method B)	t_R = 4.91 minute, main fragments 180 (1, M ⁺), 162 (21), 95 (52), 79 (45), 67 (100)

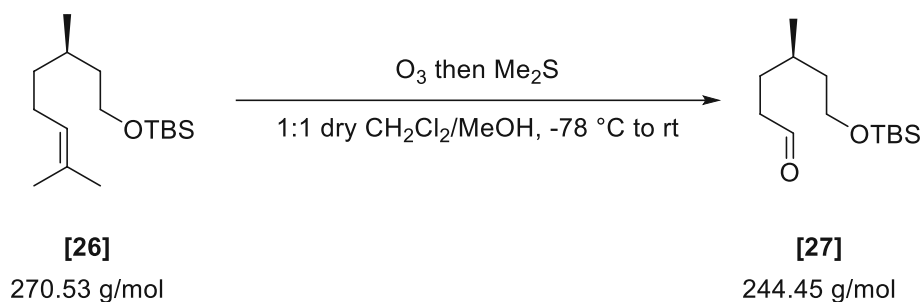
E III.1.18 (R)-Tert-butyl((3,7-dimethyloct-6-en-1-yl)oxy)dimethylsilane [26]



(R)-tert-butyl((3,7-dimethyloct-6-en-1-yl)oxy)dimethylsilane [26] was synthesized applying the same conditions for the synthesis of its enantiomer using (R)-citronellol [25] (3.26 g, 20.86 mmol), TBS-Cl (3.46 g, 22.95 mmol) and imidazole (2.84 g, 41.72 mmol).

Yield	5.68 g (quant.)
Appearance	colorless oil
TLC	R_f (LP/EtOAc– 5:1) = 0.95 (anisaldehyde)
Reaction scale	3.26 g (20.86 mmol)
Substrate concentration	0.52 M
Purification	pure after work-up
Sum formula, m.w.	$C_{16}H_{34}OSi$, 270.53 g/mol
Optical rotation	$[\alpha]_D^{20} = +1.8$ (c = 0.71, $CHCl_3$)
1H-NMR (400 MHz, $CDCl_3$)	spectral data in accordance with its enantiomer (S)-tert-butyl((3,7-dimethyloct-6-en-1-yl)oxy)dimethylsilane
^{13}C-NMR (151 MHz, $CDCl_3$)	spectral data in accordance with its enantiomer (S)-tert-butyl((3,7-dimethyloct-6-en-1-yl)oxy)dimethylsilane

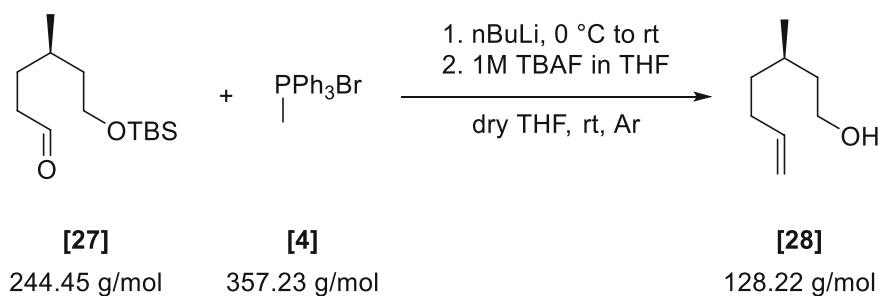
E III.1.19 (R)-6-((Tert-butyldimethylsilyl)oxy)-4-methylhexanal [27]



(R)-6-((tert-butyldimethylsilyl)oxy)-4-methylhexanal [27] was synthesized applying the same conditions for the synthesis of its enantiomer using (R)-tert-butyl((3,7-dimethyloct-6-en-1-yl)oxy)dimethylsilane [26] (5.68 g, 20.99 mmol) and dimethyl sulfide (11.09 g, 178.46 mmol).

Yield	4.06 g (79 %)
Appearance	colorless viscous oil
TLC	R_f (LP/EtOAc - 10/1) = 0.54 (anisaldehyde)
Reaction scale	5.68 g (20.99 mmol)
Substrate concentration	0.55 M
Purification	flash chromatography (silica) LP/EtOAc 10:1 + azeotropic distillation (n-pentane)
Sum formula, m.w.	$C_{13}H_{28}O_2Si$, 244.45 g/mol
Optical rotation	$[\alpha]_D^{20} = +0.8$ (c = 0.65, CH_2Cl_2)
1H-NMR (400 MHz, $CDCl_3$)	spectral data in accordance with its enantiomer (S)-6-((tert-butyldimethylsilyl)oxy)-4-methylhexanal
^{13}C-NMR (151 MHz, $CDCl_3$)	spectral data in accordance with its enantiomer (S)-6-((tert-butyldimethylsilyl)oxy)-4-methylhexanal

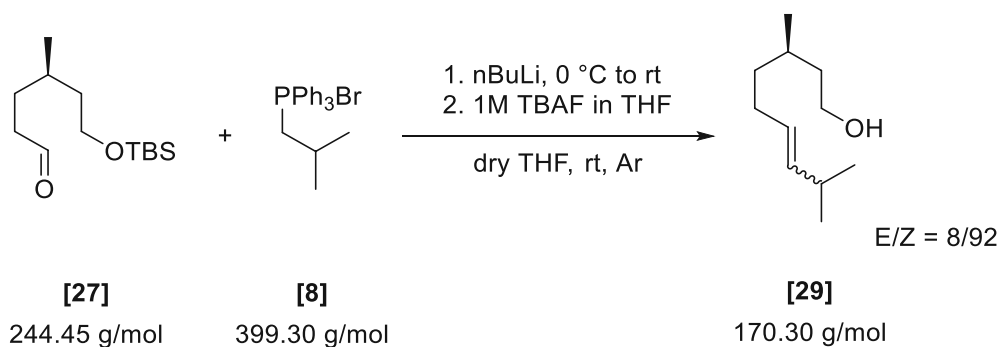
E III.1.20 (R)-3-Methylhept-6-en-1-ol [28]



(R)-3-methylhept-6-en-1-ol [28] was synthesized according to general procedure **A** using (R)-6-((tert-butyldimethylsilyloxy)-4-methylhexanal [27] (0.70 g, 2.86 mmol) and methyltriphenylphosphonium bromide [4] (1.43 g, 4.01 mmol).

Yield	0.15 g (39 %)
Appearance	colorless oil
TLC	R_f (LP/EtOAc – 3:1) = 0.49 (anisaldehyde)
Reaction scale	0.70 g, (2.86 mmol)
Substrate concentration	0.23 M
Purification	column chromatography (silica) LP/Et ₂ O 2.5:1
Sum formula, m.w.	C ₈ H ₁₆ O, 128.22 g/mol
Optical rotation	$[\alpha]_D^{20} = +2.0$ (c = 0.57, CHCl ₃)
¹H-NMR (400 MHz, CDCl₃)	spectral data in accordance with its enantiomer (S)-3-methylhept-6-en-1-ol
¹³C-NMR (151 MHz, CDCl₃)	spectral data in accordance with its enantiomer (S)-3-methylhept-6-en-1-ol

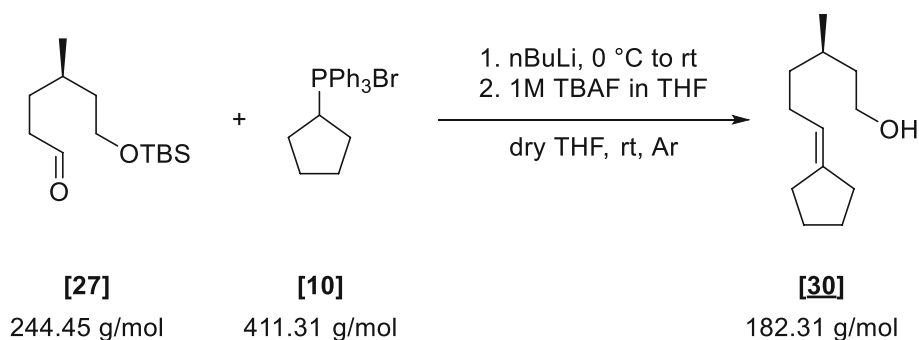
E III.1.21 (R)-3,8-Dimethylnon-6-en-1-ol [29]



(R)-3,8-dimethylnon-6-en-1-ol [29] was synthesized according to general procedure **A** using (R)-6-((tert-butyldimethylsilyloxy)-4-methylhexanal [27] (0.50 g, 2.45 mmol) and isobutyltriphenylphosphonium bromide [8] (0.98 g, 2.45 mmol). Product is isolated as a mixture of inseparable E/Z = 8/92 isomers.

Yield	0.14 g (39 %)
Appearance	colorless oil
TLC	R_f (LP/EtOAc – 3:1) = 0.51 (anisaldehyde)
Reaction scale	0.50 g, (2.45 mmol)
Substrate concentration	0.23 M
Purification	column chromatography (silica) LP/EtOAc 7:1 to 5:1
Sum formula, m.w.	$C_{11}H_{22}O$, 170.30 g/mol
Optical rotation	$[\alpha]_D^{20} = +2.5$ (c = 0.50, $CHCl_3$)
1H-NMR (400 MHz, $CDCl_3$)	spectral data in accordance with its enantiomer (R)-3,8-dimethylnon-6-en-1-ol
^{13}C-NMR (151 MHz, $CDCl_3$)	spectral data in accordance with its enantiomer (R)-3,8-dimethylnon-6-en-1-ol

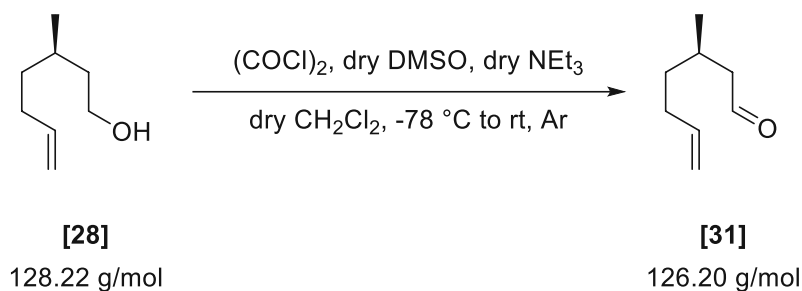
E III.1.22 (R)-6-Cyclopentylidene-3-methylhexan-1-ol [30]



(R)-6-cyclopentylidene-3-methylhexan-1-ol [30] was synthesized according to general procedure A using (R)-6-((tert-butyl(dimethylsilyloxy)-4-methylhexanal [27] (0.70 g, 2.86 mmol) and cyclopentyltriphenylphosphonium bromide [10] (1.65 g, 4.01 mmol).

Yield	0.11 g (22 %)
Appearance	colorless oil
TLC	R_f (LP/EtOAc – 3:1) = 0.51 (anisaldehyde)
Reaction scale	0.70 g, (2.86 mmol)
Substrate concentration	0.23 M
Purification	column chromatography (silica) LP/Et ₂ O 2.5:1
Sum formula, m.w.	C ₁₂ H ₂₂ O, 182.31 g/mol
Optical rotation	$[\alpha]_D^{20} = +3.0$ (c = 0.44, CHCl ₃)
¹ H-NMR (400 MHz, CDCl ₃)	spectral data in accordance with its enantiomer (R)-3,8-dimethylnon-6-en-1-ol
¹³ C-NMR (151 MHz, CDCl ₃)	spectral data in accordance with its enantiomer (R)-3,8-dimethylnon-6-en-1-ol

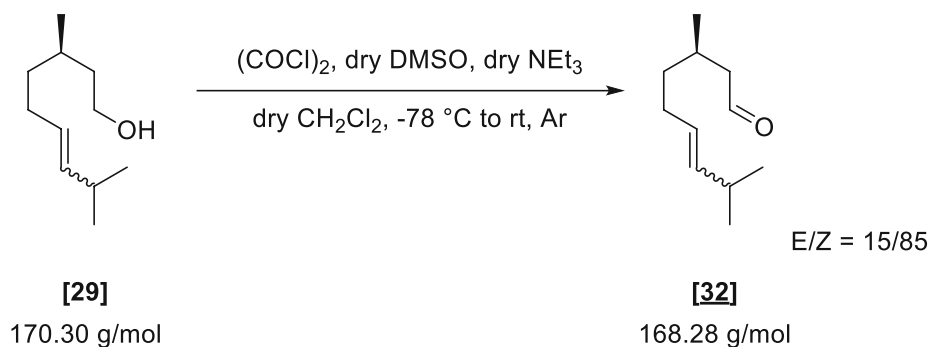
E III.1.23 (R)-3-Methylhept-6-enal [31]



(R)-3-methylhept-6-enal [31] was synthesized according to general procedure B using (R)-3-methylhept-6-en-1-ol [28] (144 mg, 1.12 mmol).

Yield	74 mg (52 %)
Appearance	colorless oil
TLC	R _f (LP/EtOAc – 10:1) = 0.35 (anisaldehyde)
Reaction scale	144 mg (1.12 mmol)
Substrate concentration	0.15 M
Purification	column chromatography (silica) LP/Et ₂ O 40:1
Sum formula, m.w.	C ₈ H ₁₄ O, 126.20 g/mol
Optical rotation	[α] _D ²⁰ = +3.5 (c = 0.65, CHCl ₃)
¹H-NMR (400 MHz, CDCl₃)	spectral data in accordance with its enantiomer (S)-3-methylhept-6-enal
¹³C-NMR (151 MHz, CDCl₃)	spectral data in accordance with its enantiomer (S)-3-methylhept-6-enal
GC-MS (method B)	spectral data in accordance with its enantiomer (S)-3,8-dimethylnon-6-enal

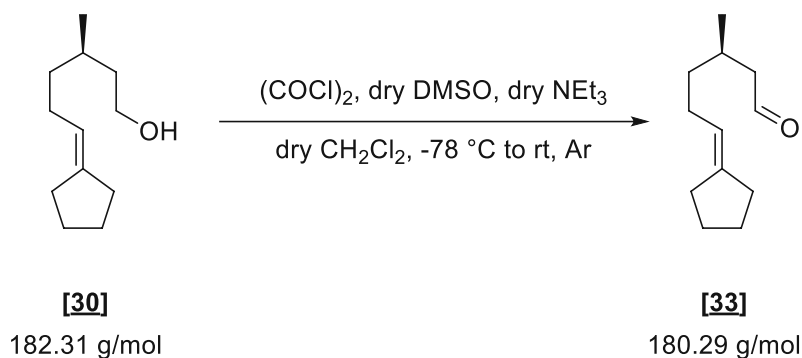
E III.1.24 (R)-3,8-Dimethylnon-6-enal [32]



(R)-3,8-dimethylnon-6-enal [32] was synthesized according to general procedure B using (R)-3,8--dimethylnon-6-en-1-ol [29] (110 mg, 0.65 mmol). Product is isolated as a mixture of inseparable E/Z = 8/92 isomers.

Yield	90 mg (83 %)
Appearance	colorless oil
TLC	R_f (LP/Et ₂ O – 30:1) = 0.33 (anisaldehyde)
Reaction scale	110 mg (0.65 mmol)
Substrate concentration	0.15 M
Purification	column chromatography (silica) LP/Et ₂ O 40:1
Sum formula, m.w.	C ₁₁ H ₂₀ O, 168.28 g/mol
Optical rotation	$[\alpha]_D^{20} = +9.7$ (c = 0.58, CHCl ₃)
¹H-NMR (400 MHz, CDCl₃)	spectral data in accordance with its enantiomer (S)-3,8-dimethylnon-6-enal
¹³C-NMR (151 MHz, CDCl₃)	spectral data in accordance with its enantiomer (S)-3,8-dimethylnon-6-enal
HRMS (ESI)	not found.
GC-MS (method B)	spectral data in accordance with its enantiomer (S)-3,8-dimethylnon-6-enal

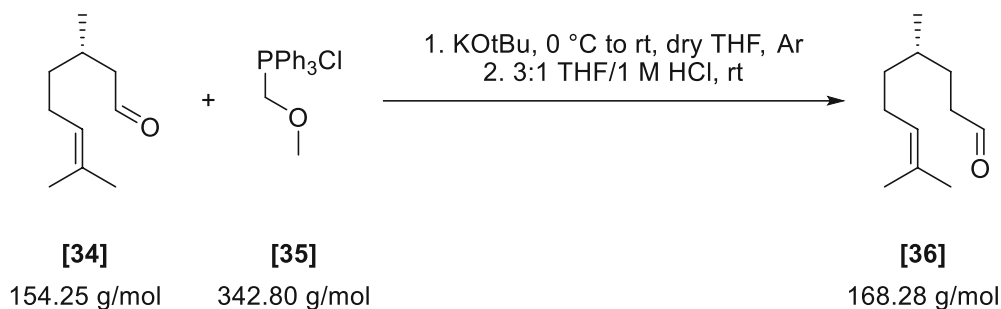
E III.1.25 (R)-6-Cyclopentylidene-3-methylhexanal [33]



(R)-6-cyclopentylidene-3-methylhexanal [33] was synthesized according to general procedure B using (R)-6-cyclopentylidene-3-methylhexan-1-ol [30] (97 mg, 0.53 mmol).

Yield	42 mg (44 %)
Appearance	colorless oil
TLC	R_f (LP/Et ₂ O – 40:1) = 0.48 (anisaldehyde)
Reaction scale	110 mg (0.65 mmol)
Substrate concentration	0.11 M
Purification	column chromatography (silica) LP/Et ₂ O 40:1
Sum formula, m.w.	C ₁₂ H ₂₀ O, 180.29 g/mol
Optical rotation	$[\alpha]_D^{20} = +14.4$ (c = 0.45, CHCl ₃)
¹H-NMR (400 MHz, CDCl₃)	spectral data in accordance with its enantiomer (S)-6-cyclopentylidene-3-methylhexanal
¹³C-NMR (151 MHz, CDCl₃)	spectral data in accordance with its enantiomer (S)-6-cyclopentylidene-3-methylhexanal
HRMS (ESI)	not found.
GC-MS (method B)	spectral data in accordance with its enantiomer (S)-3,8-dimethylnon-6-enal

E III.1.26 (S)-4,8-Dimethylnon-7-enal [36]



The product was synthesized according to a literature procedure²⁰⁸.

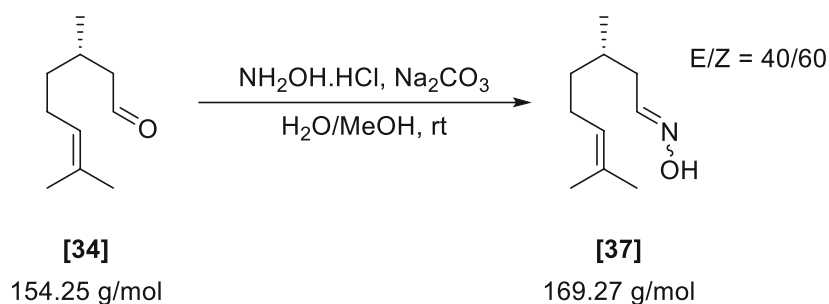
Procedure: The first part of the reaction was performed according to general procedure **A** using (S)-citronellal [34] (0.50 g, 3.24 mmol) and (methoxymethyl)triphenylphosphonium chloride (1.44 g, 4.21 mmol). For the deprotection of the enol, the crude was dissolved in THF (23 mL), and 1 M HCl (30 mL, 10 equiv.) was added, and the reaction was stirred under argon overnight.

Work-up: The reaction was quenched with the addition of sat. NaHCO₃ (100 mL) and the aqueous phase was extracted three times with CH₂Cl₂ (3 x 100 mL). The combined organic layers were washed with brine (100 mL), dried over Na₂SO₄, and concentrated. For the final purification, the crude was columned over silica eluting with 40:1 LP/Et₂O to yield the respective (S)-4,8-dimethylnon-7-enal [36] as a colorless oil with a distinct odor.

Yield	0.35 g (63 %)
Appearance	colorless oil
TLC	R _f (LP/Et ₂ O – 40:1) = 0.50 (anisaldehyde)
Reaction scale	0.50 g (3.24 mmol)
Substrate concentration	Wittig: 0.22 M, Deprotection: 0.14 M
Purification	column chromatography (silica) LP/Et ₂ O 40:1
Sum formula, m.w.	C ₁₁ H ₂₀ O, 168.28 g/mol

¹H-NMR (400 MHz, CDCl₃)	δ 0.86 – 0.93 (m, 3H, H8), 1.11 – 1.27 (m, 1H, H4'), 1.27 – 1.43 (m, 1H, H4), 1.39 – 1.52 (m, 2H, H2', H3), 1.60 (s, 3H, H10), 1.63 – 1.72 (m, 1H, H2), 1.68 (s, 3H, H9), 1.98 (dp, J = 7.7, 24.0 Hz, 2H, H5), 2.33 – 2.52 (m, 2H, H1), 5.08 (ddp, J = 1.5, 5.7, 8.6 Hz, 1H, H6), 9.77 (t, J = 1.8 Hz, 1H, H _{homolog}).
¹³C-NMR (151 MHz, CDCl₃)	δ 17.8 (q, C8), 19.4 (q, C10), 25.6 (t, C5), 25.9 (q, C9), 29.0 (t, C2), 32.2 (d, C3), 36.9 (t, C4), 41.8 (t, C1), 124.7 (d, C6), 131.6 (s, C7), 203.1 (d, C _{homolog}).

E III.1.27 (S)-3,7-Dimethyloct-6-enal oxime [37]



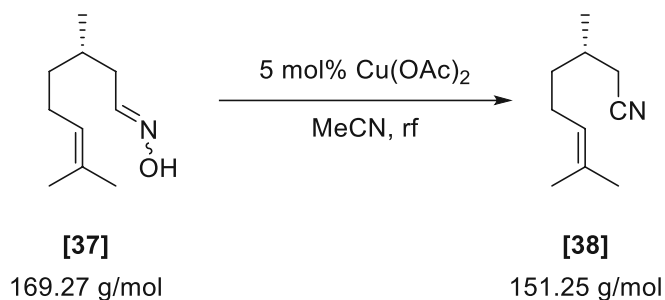
The product was synthesized according to a literature procedure²⁰⁹.

Procedure: A 8 mL screw cap vial was charged with hydroxylamine hydrochloride (0.34 g, 4.86 mmol, 1.50 equiv.), dissolved in dH₂O (3 mL). Sodium carbonate (0.52 g, 4.86, 1.50 equiv.) was added in one portion leading to strong gas evolution. Subsequently, MeOH (2 mL) and (S)-citronellal **[34]** (0.50 g, 3.24 mmol, 1.00 equiv.) were added, and the reaction was stirred at room temperature for 5 hours, upon which TLC indicated full conversion.

Work-up: The aqueous phase was extracted three times with CH₂Cl₂ (3 x 10 mL), and the combined organic layers were washed with brine (10 mL), dried over Na₂SO₄, and concentrated. 0.53 g (96%) of (S)-3,7-dimethyloct-6-enal oxime **[37]** was isolated as colorless oil in a mixture of E/Z = 40/60 isomers and was used for further experimentation without further purification.

Yield	0.53 g (96 %), mixture of isomers – E/Z = 40/60
Appearance	colorless oil
TLC	R _f (LP/EtOAc – 5:1) = 0.37 / 0.45 (both isomers, anisaldehyde)
Reaction scale	0.50 g (3.24 mmol)
Substrate concentration	0.65 M
Purification	-
Sum formula, m.w.	C ₁₀ H ₁₉ NO, 169.27 g/mol
¹H-NMR (400 MHz, CDCl₃)	δ 0.95 (dd, J = 6.7, 7.4 Hz, 8H, H8), 1.15 – 1.44 (m, 7H, H4), 1.60 (s, 5H, H10), 1.68 (s, 6H, H9), 1.63 – 1.77 (m, 2H, H3), 1.91 – 2.10 (m, 7H, E-H2', H5), 2.15 – 2.43 (m, 5H, Z-H2, Z-H2', E-H2), 5.09 (tdp, J = 1.4, 2.9, 7.2 Hz, 3H, H6), 6.74 (t, J = 5.5 Hz, 2H, Z-H1), 7.42 (t, J = 6.5 Hz, 1H, E-H1), 7.70 (s, 1H, E-OH), 8.07 (s, 2H, Z-OH).
¹³C-NMR (151 MHz, CDCl₃)	δ 17.8 (q, C10), 19.6 (q, E-C8), 19.9 (q, Z-C8), 25.6 (t, E-C5), 25.6 (t, Z-C5), 25.9 (q, C9), 30.7 (d, Z-C3), 31.1 (d, E-C3), 32.0 (t, Z-C2), 36.6 (t, E-C2), 36.8 (t, E-C4), 37.0 (t, Z-C4), 124.4 (d, Z-C6), 124.5 (d, E-C6), 131.7 (s, C7), 151.8 (d, E-C1), 152.3 (d, Z-C1).

E III.1.28 (S)-3,7-Dimethyloct-6-enenitrile [38]



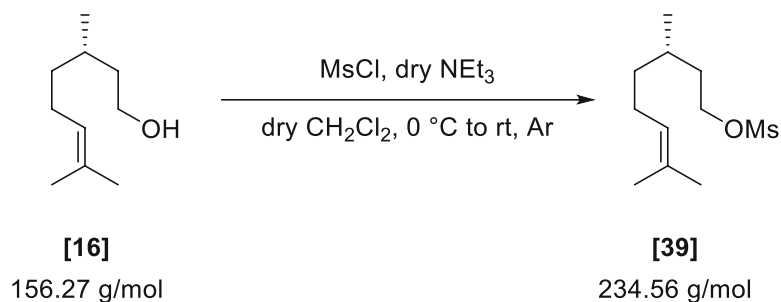
The product was synthesized according to a literature procedure²⁰⁹.

Procedure: A 8 mL screw cap vial was charged with the isomeric mixture of (S)-3,7-dimethyloct-6-enal oximes **[37]** (0.51 g, 3.01 mmol, 1.00 equiv.), which was dissolved in HPLC MeCN (3 mL). Cu(OAc)₂ (27 mg, 0.15 mmol, 0.05 equiv.) was added, and the reaction was heated to reflux for 4 hours, upon which TLC indicated full conversion.

Work-up: The solution was concentrated, directly adsorbed onto Celite, and columned over silica (50 g) eluting with 25:1 LP/EtOAc to yield 0.29 g (63%) of (S)-3,7-dimethyloct-6-enenitrile **[38]** as a colorless oil with a distinct odor.

Yield	0.29 g (63 %)
Appearance	colorless oil
TLC	R _f (LP/EtOAc – 5:1) = 0.67 (anisaldehyde)
Reaction scale	0.51 g (3.01 mmol)
Substrate concentration	1.00 M
Purification	column chromatography (silica) LP/EtOAc 25:1
Sum formula, m.w.	C ₁₀ H ₁₇ N, 151.25 g/mol
Optical rotation	[α] _D ²⁰ = +11.5 (c = 0.95, EtOH)
¹H-NMR (400 MHz, CDCl₃)	δ 1.07 (d, J = 6.7 Hz, 3H, H8), 1.23 – 1.41 (m, 1H, H4'), 1.39 – 1.53 (m, 1H, H4), 1.61 (s, 3H, H10), 1.69 (q, J = 1.3 Hz, 3H, H9), 1.80 – 1.93 (m, 1H, H3), 1.94 – 2.08 (m, 2H, H5), 2.23 (dd, J = 6.9, 16.7 Hz, 1H, H2'), 2.32 (dd, J = 5.6, 16.7 Hz, 1H, H2), 5.07 (ddq, J = 1.4, 5.7, 8.6 Hz, 1H, H6).
¹³C-NMR (151 MHz, CDCl₃)	δ 17.8 (q, C10), 19.5 (q, C8), 24.6 (t, C2), 25.4 (t, C5), 25.8 (q, C9), 30.1 (d, C3), 36.0 (t, C4), 119.0 (s, -CN), 123.6 (d, C6), 132.4 (s, C7).

E III.1.29 (S)-3,7-Dimethyloct-6-en-1-yl methanesulfonate [39]



Procedure: A 8 mL screw cap vial was charged with the (*S*)-citronellol **[16]** (0.50 g, 3.20 mmol, 1.00 equiv.), which was dissolved in dry CH₂Cl₂ (8 mL). Dry triethylamine (0.89 mL, 0.65 g, 6.40 mmol, 2.00 equiv.) was added, and the solution was cooled to 0 °C with a water/ice bath. Mesylchloride (0.30 mL, 0.44 g, 3.84 mmol, 1.20 equiv.) was then added dropwise, which led to the immediate formation of a voluminous colorless precipitate. The reaction was stirred at 0 °C for 30 minutes and then warmed to room temperature. The suspension was stirred for 2.5 hours, upon which TLC indicated full conversion.

Work-up: The reaction was quenched with the addition of sat. NaHCO₃ (10 mL). The aqueous phase was extracted twice with CH₂Cl₂ (2 x 10 mL), and the combined organic layers were washed with brine (10 mL), dried over Na₂SO₄, and concentrated. For the final purification, the crude was flashed over silica eluting with pure CH₂Cl₂ to yield 0.70 g (93 %) of the (*S*)-3,7-dimethyloct-6-en-1-yl methanesulfonate **[39]** as a colorless oil.

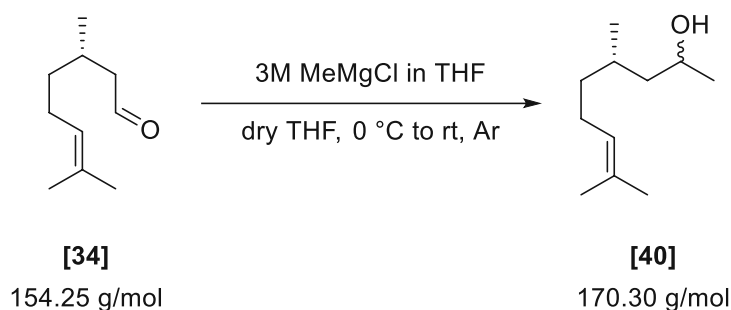
Yield	0.70 g (93 %)
Appearance	colorless oil
TLC	R _f (CH ₂ Cl ₂) = 0.65 (anisaldehyde)

Reaction scale	0.50 g (3.20 mmol)
Substrate concentration	0.40 M
Purification	flash chromatography (silica) CH ₂ Cl ₂
Sum formula, m.w.	C ₁₁ H ₂₂ O ₃ S, 234.56 g/mol
Optical rotation	[α] _D ²⁰ = -2.4 (c = 1.02, CHCl ₃)

¹H-NMR (400 MHz, CDCl₃) δ 0.93 (d, *J* = 6.5 Hz, 3H, H₈), 1.20 (dddd, *J* = 6.1, 7.7, 9.3, 13.6 Hz, 1H, H_{4'}), 1.35 (dddd, *J* = 5.2, 6.6, 9.4, 13.4 Hz, 1H, H₄), 1.50 – 1.66 (m, 2H, H₂, H₃), 1.60 (s, 3H, H₁₀), 1.68 (q, *J* = 1.3 Hz, 3H, H₉), 1.80 (dtd, *J* = 4.7, 7.1, 13.4 Hz, 1H, H₂), 1.88 – 2.09 (m, 2H, H₅), 3.00 (s, 3H, -SO₃CH₃), 4.19 – 4.33 (m, 2H, H₁), 5.08 (tdt, *J* = 1.5, 2.8, 7.1 Hz, 1H, H₆).

$^{13}\text{C-NMR}$ (151 MHz, CDCl_3) δ 17.8 (q, C10), 19.3 (q, C8), 25.4 (t, C5), 25.8 (q, C9), 29.1 (d, C3), 36.1 (t, C2), 36.9 (t, C4), 37.5 (q, $-\text{SO}_3\text{CH}_3$), 68.7 (t, C1), 124.4 (d, C6), 131.8 (s, C7).

E III.1.30 (4*S*)-4,8-Dimethylnon-7-en-2-ol [40]



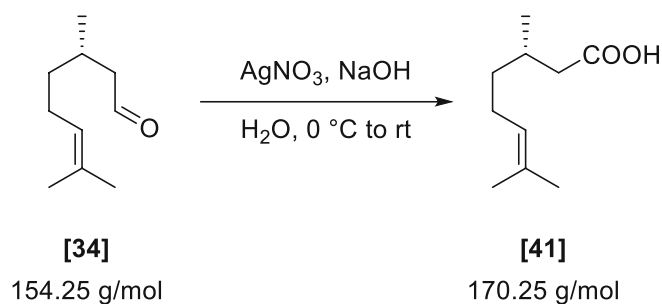
The product was synthesized according to a literature procedure²¹¹.

Procedure: To a solution of (*S*)-citronellal [34] (0.29 mL, 0.25 g, 1.62 mmol, 1.00 equiv.) in THF (2 mL) under argon atmosphere was added MeMgCl (3 M in THF, 0.76 mL, 2.27 mmol, 1.40 equiv.) at 0 °C. The mixture was allowed to warm to room temperature and was stirred for 12 h upon which TLC indicated full conversion.

Work-up: The reaction was quenched with the addition of $\text{d.H}_2\text{O}$ (5 mL), and the aqueous phase was extracted twice with Et_2O (2 x 5 mL). The combined organic layers were washed with brine (10 mL), dried over Na_2SO_4 , and concentrated. For the final purification, the crude was columned over silica eluting with 3:1 LP/EtOAc to yield 0.21 g (75 %) of *rac*-(4*S*)-4,8-dimethylnon-7-en-2-ol [40] as a colorless oil as a mixture of syn/anti = 55/45 isomers.

Yield	0.21 g (75 %)
Appearance	colorless oil
TLC	R_f (LP/EtOAc – 3:1) = 0.41 (anisaldehyde)
Reaction scale	0.25 g (1.62 mmol)
Substrate concentration	0.81 M
Purification	column chromatography (silica) LP/EtOAc 3:1
Sum formula, m.w.	$\text{C}_{11}\text{H}_{20}\text{O}$, 170.30 g/mol

- $^1\text{H-NMR}$ (400 MHz, CDCl_3)** δ 0.91 (dt, $J = 1.4, 6.7$ Hz, 3H, syn-H8, anti-H8), 1.17 (d, $J = 7.6$ Hz, 3H, syn- CH_3 or anti- CH_3), 1.10 – 1.24 (m, 1H, syn-H4', anti-H4'), 1.19 (d, $J = 6.3$ Hz, 3H, syn- CH_3 or anti- CH_3), 1.24 – 1.42 (m, 4H, syn-H2, syn-H2', anti-H2', syn-H4, anti-H4), 1.44 – 1.65 (m, 1H, syn-H3, anti-H3, anti-H2), 1.60 (s, 3H, syn-H10, anti-H10), 1.68 (s, 3H, syn-H9, anti-H9), 1.99 (qq, $J = 7.6, 14.4$ Hz, 2H, syn-H5, anti-H5), 3.83 – 3.96 (m, 1H, syn-H1, anti-H1), 5.10 (tq, $J = 1.5, 7.1$ Hz, 1H, syn-H6, anti-H6).
- $^{13}\text{C-NMR}$ (151 MHz, CDCl_3)** δ 17.8 (q, syn-C10, anti-C10), 19.4 (q, syn-C8 or anti-C8), 20.2 (q, syn-C8 or anti-C8), 23.8 (q, syn- CH_3 or anti- CH_3), 24.5 (q, syn- CH_3 or anti- CH_3), 25.5 (t, syn-C5 or anti-C5), 25.6 (t, syn-C5 or anti-C5), 25.9 (q, syn-C9, anti-C9), 29.2 (d, syn-C3 or anti-C3), 29.7 (d, syn-C3 or anti-C3), 37.1 (t, syn-C4 or anti-C4), 37.9 (t, syn-C4 or anti-C4), 46.9 (t, syn-C2 or anti-C2), 47.1 (t, syn-C2 or anti-C2), 66.0 (d, syn-C1 or anti-C1), 66.4 (d, syn-C1 or anti-C1), 124.9 (d, syn-C6, anti-C6), 131.4 (syn-C7 or anti-C7), 131.4 (syn-C7 or anti-C7).

E III.1.31 (S)-3,7-Dimethyloct-6-enoic acid [41]

The product was synthesized according to a literature procedure.²¹⁰

Procedure: A freshly prepared AgNO_3 solution (1.26 g dissolved in 13 mL d H_2O , 7.45 mmol, 2.30 equiv.) was added dropwise to a NaOH solution (0.64 g dissolved in 13 mL d H_2O , 15.88, 4.90 equiv.) at 0 °C to form finely dispersed AgO . The reaction vessel was covered in aluminum foil and stirred for 30 minutes. Subsequently, (S)-citronellal **[34]** (0.50 g, 3.24 mmol, 1.00 equiv.) was added in one portion, and the solution was allowed to warm to room temperature by stirring in the cooling bath overnight upon which TLC indicated full conversion.

Work-up: The suspension was filtered over a pad of Celite and acidified with conc. HCl . The aqueous phase was extracted three times with CH_2Cl_2 (3 x 10 mL). The combined organic layers were washed with brine (10 mL), dried over Na_2SO_4 , and concentrated to yield 0.55 g (quant.) of (S)-3,7-dimethyloct-6-enoic acid **[41]** as a colorless oil.

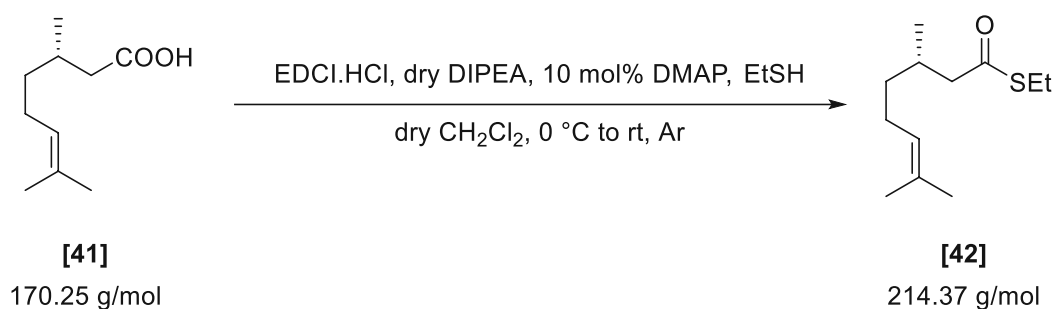
Yield 0.55 g (quant.)
Appearance colorless oil
TLC R_f (LP/EtOAc – 5:1) = 0.07 (KMnO₄)

Reaction scale 0.50 g (3.24 mmol)
Substrate concentration 0.12 M
Purification -
Sum formula, m.w. C₁₀H₁₈O₂, 170.25 g/mol
Optical rotation $[\alpha]_D^{20} = -2.2$ (c = 1.01, CHCl₃)

¹H-NMR (400 MHz, CDCl₃) δ 0.98 (d, *J* = 6.6 Hz, 3H, H8), 1.25 (dddd, *J* = 6.2, 7.7, 9.2, 13.6 Hz, 1H, H4'), 1.38 (dddd, *J* = 5.8, 6.6, 9.3, 13.4 Hz, 1H, H4), 1.60 (s, 3H, H10), 1.68 (q, *J* = 1.1 Hz, 3H, H9), 1.89 – 2.10 (m, 3H, H3, H5), 2.15 (dd, *J* = 8.2, 15.0 Hz, 1H, H2'), 2.37 (dd, *J* = 5.8, 15.0 Hz, 1H, H2), 5.09 (tdq, *J* = 1.4, 2.8, 7.0 Hz, 1H, H6).

¹³C-NMR (151 MHz, CDCl₃) δ 17.8 (q, C10), 19.7 (q, C8), 25.5 (t, C5), 25.8 (q, C9), 30.0 (d, C3), 36.8 (t, C4), 41.6 (t, C2), 124.3 (d, C6), 131.8 (s, C7), 179.4 (s, C1).

E III.1.32 S-Ethyl (S)-3,7-dimethyloct-6-enethioate [42]

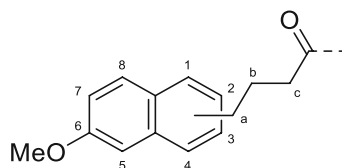


Procedure: A 25 mL screw-cap vial was charged with (S)-3,7-dimethyloct-6-enoic acid **[41]** (0.25 g, 1.47 mmol, 1.00 equiv.), which was dissolved in CH₂Cl₂ (10 mL). Subsequently, dry DIPEA (0.28 mL, 0.21 g, 1.10 equiv.), DMAP (18 mg, 0.15 mmol, 0.10 equiv.) and ethanethiol (0.32 mL, 0.27 g, 4.41 mmol, 3.00 equiv.) were added, and the solution was cooled to 0 °C with an ice/water-bath following the addition of EDCI.HCl (0.34 g, 1.76 mmol, 1.20 equiv.). The reaction was allowed to warm to room temperature by stirring in the cooling bath overnight, upon which TLC indicated full conversion.

Work-up: The reaction was quenched with the addition of sat. NaHCO_3 (10 mL). The aqueous phase was extracted twice with CH_2Cl_2 (2 x 10 mL), and the combined organic layers were washed with brine (10 mL), dried over Na_2SO_4 , and concentrated. For the final purification, the crude was columned over silica eluting with 25:1 LP/EtOAc to yield 0.18 g (58 %) of S-ethyl (S)-3,7-dimethyloct-6-enethioate [42] as a colorless oil.

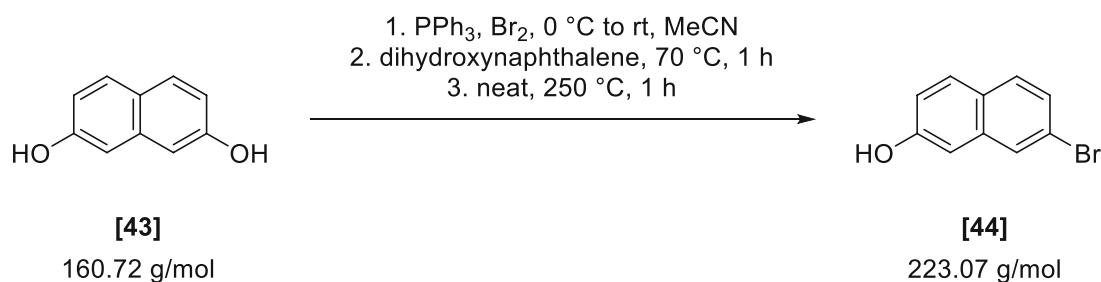
Yield	0.18 g (58 %)
Appearance	colorless oil
TLC	R_f (LP/EtOAc – 25:1) = 0.42 (KMnO_4)
Reaction scale	0.25 g (1.47 mmol)
Substrate concentration	0.15 M
Purification	column chromatography (silica) LP/EtOAc 25:1
Sum formula, m.w.	$\text{C}_{12}\text{H}_{22}\text{OS}$, 214.37 g/mol
Optical rotation	$[\alpha]_D^{20} = -3.5$ (c = 0.91, CHCl_3)
$^1\text{H-NMR}$ (400 MHz, CDCl_3)	δ 0.94 (d, $J = 6.7$ Hz, 3H, H8), 1.15 – 1.27 (m, 1H, H4'), 1.24 (t, $J = 7.4$ Hz, 3H, -S- CH_2 - CH_3), 1.36 (dddd, $J = 5.8, 6.6, 9.4, 13.4$ Hz, 1H, H4), 1.60 (s, 3H, H10), 1.68 (q, $J = 1.3$ Hz, 3H, H9), 1.88 – 2.11 (m, 3H, H3, H5), 2.34 (dd, $J = 8.2, 14.4$ Hz, 1H, H2'), 2.54 (dd, $J = 5.9, 14.4$ Hz, 1H, H2), 2.87 (q, $J = 7.4$ Hz, 2H, -S- CH_2 - CH_3), 5.08 (tdt, $J = 1.4, 2.9, 7.1$ Hz, 1H, H6).
$^{13}\text{C-NMR}$ (151 MHz, CDCl_3)	δ 15.0 (q, -S- CH_2 - CH_3), 17.8 (q, C10), 19.6 (q, C8), 23.4 (t, -S- CH_2 - CH_3), 25.5 (t, C5), 25.9 (q, C9), 30.9 (d, C3), 36.8 (t, C4), 51.5 (t, C2), 124.3 (d, C6), 131.8 (s, C7), 199.4 (s, -COS-).

E III.2 Part II – Synthesis of fluorogenic substrates for SHC catalyzed Friedel-Crafts reactions



NMR assignments of core structures in this chapter were given according to the following example.

E III.2.1 7-Bromonaphthalen-2-ol [44]



The product was synthesized according to a literature procedure²¹⁷.

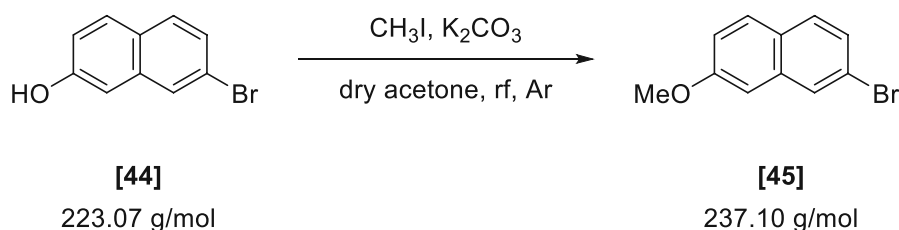
Procedure: Bromine (1.15 mL, 3.59 g, 22.48 mmol, 1.20 equiv.) was added dropwise to a suspension of triphenylphosphine (5.90 g, 22.48 mmol, 1.20 equiv.) in MeCN (9 mL) at 0 °C. The first drops of bromine were immediately consumed, and the solution was immediately discolored. Upon complete addition, the orange reaction mixture was allowed to warm to room temperature, and then 2,7-dihydroxynaphthalene [43] (3.00 g, 18.73 mmol, 1.00 equiv.) was added in several portions. The clumpy suspension was heated to 70 °C for 1 hour, causing complete dissolution of all solids. Subsequently, the solvent was removed *in vacuo*, and the vessel was connected to a gas trap filled with 4 N NaOH in such a way that suck-back into the reaction flask was prevented. The ochre crude was heated at 220-250 °C with a heating mantle (maximum setting; oil bath was not sufficient!) for 1 hour, causing strong colorless vapor evolution and blackening of the product.

Work-Up: After cooling to room temperature, the mixture was dissolved in CH₂Cl₂ (200 mL), flashed over a pad of silica, and concentrated. If massive side product formation was evident, decanting of solubilized product in boiling ligroin improved the isolation. For the final purification, the crude was columned over silica eluting with 1:1 LP/CH₂Cl₂ to yield 2.44 g (58 %) of 7-bromonaphthalen-2-ol [44] as beige solid.

Yield	2.44 g (58 %)
Appearance	beige solid
TLC	R _f (LP/CH ₂ Cl ₂ - 1/1) = 0.34

Reaction scale	3.00 g (18.73 mmol)
Substrate concentration	2.00 M
Purification	column chromatography (silica) LP/CH ₂ Cl ₂ 1:1
Sum formula, m.w.	C ₁₀ H ₇ BrO, 223.07 g/mol
M.p.	130 – 132 °C
¹ H-NMR (400 MHz, CDCl ₃)	δ 5.03 (s, 1H, -OH), 7.05 (dd, <i>J</i> = 0.6, 2.5 Hz, 1H, H5), 7.10 (dd, <i>J</i> = 2.5, 8.8 Hz, 1H, H7), 7.40 (dd, <i>J</i> = 1.9, 8.7 Hz, 1H, H2), 7.63 (dd, <i>J</i> = 0.7, 8.7 Hz, 1H, H1), 7.71 (dd, <i>J</i> = 0.7, 8.8 Hz, 1H, H8), 7.84 (dd, <i>J</i> = 0.7, 1.9 Hz, 1H, H4).
¹³ C-NMR (151 MHz, CDCl ₃)	δ 108.8 (d, C5), 118.3 (d, C7), 120.9 (s, C3), 127.2 (d, C2), 127.5 (s, C8a), 128.5 (d, C4), 129.5 (d, C1), 130.0 (d, C8), 135.9 (s, C4a), 154.3 (s, C6).

E III.2.2 2-Bromo-7-methoxynaphthalene [45]



The product was synthesized according to a literature procedure²¹⁸.

Procedure: A 250 mL 3-neck RBF was charged with a mixture of 7-bromonaphthalen-2-ol **[44]** (2.44 g, 10.94 mmol, 1.00 equiv) and potassium carbonate (4.54 g, 32.82 mmol, 3.00 equiv.) suspended in acetone (40 mL). Iodomethane (3.40 mL, 7.76 g, 54.69 mmol, 5.00 equiv.) was added, and the reaction mixture was refluxed under argon for 18 hours.

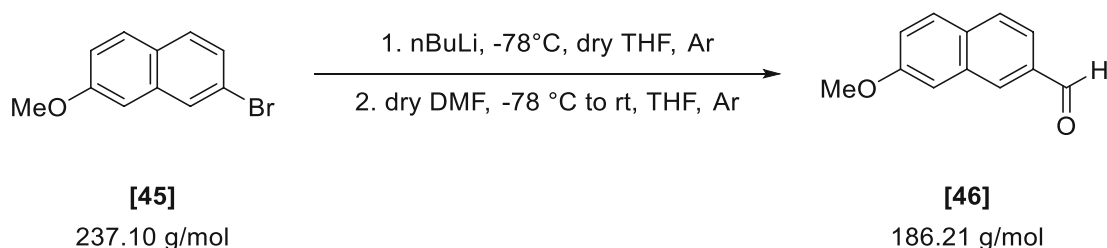
Work-Up: After cooling to room temperature, the suspension was filtered through a sintered funnel, and the filtrate was concentrated. For the final purification, the crude was columned over silica (1:30), eluting with 25:1 LP/EtOAc to yield 2.72 g (98 %) of 2-bromo-7-methoxynaphthalene **[45]** as a colorless solid.

Yield	2.72 g (98 %)
Appearance	colorless solid
TLC	R _f (LP/EtOAc - 10/1) = 0.66

Reaction scale	2.44 g (10.94 mmol)
Substrate concentration	0.21 M
Purification	column chromatography (silica) LP/EtOAc 25:1
Sum formula, m.w.	C ₁₁ H ₉ BrO, 237.10 g/mol
M.p.	91 - 92.5 °C (lit. ²⁶⁸ 97.5 – 98 °C)

$^1\text{H-NMR}$ (400 MHz, CDCl_3)	δ 3.92 (s, 3H, $-\text{OCH}_3$), 7.03 (d, $J = 2.5$ Hz, 1H, H8), 7.15 (dd, $J = 2.5, 8.9$ Hz, 1H, H7), 7.40 (dd, $J = 2.0, 8.7$ Hz, 1H, H2), 7.62 (d, $J = 8.6$ Hz, 1H, H4), 7.70 (d, $J = 9.0$ Hz, 1H, H5), 7.90 (d, $J = 2.0$ Hz, 1H, H1).
$^{13}\text{C-NMR}$ (151 MHz, CDCl_3)	δ 55.5 (q, $-\text{OCH}_3$), 105.1 (d, C5), 119.3 (d, C7), 120.7 (s, C3), 127.0 (d, C2), 127.5 (s, C4a), 128.9 (d, C8), 129.4 (d, C4), 129.5 (d, C1), 136.0 (s, C8a), 158.5 (s, C6).

E III.2.3 7-Methoxy-2-naphthaldehyde [46]



The product was synthesized according to a literature procedure²¹⁹.

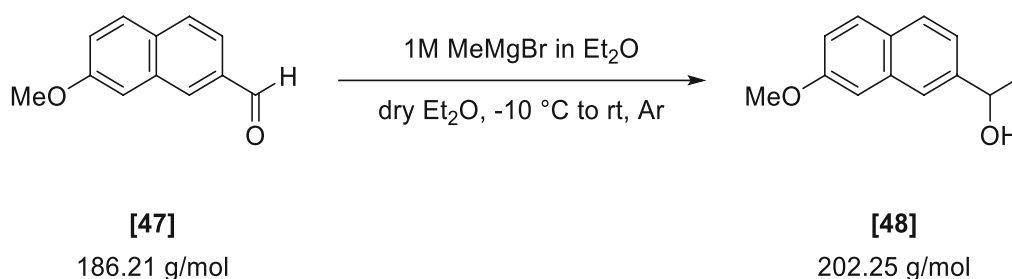
Procedure: A 25 mL 3-neck RBF was charged with 2-bromo-7-methoxynaphthalene **[45]** (0.50 g, 2.11 mmol, 1.00 equiv), which was dissolved in dry THF (7 mL) under argon. The solution was cooled to < -75 °C using an acetone / liquid N_2 bath, and nBuLi (2.5 M in hexanes, 0.93 mL, 2.32 mmol, 1.10 equiv.) was added slowly in 2-3 minutes, turning the solution deep yellow. The reaction was stirred for 30 minutes at this temperature, following the addition of dry DMF (0.18 mL, 0.17 g, 2.32 mmol, 1.10 equiv.) directly into the solution (freezes on the wall of the flask!). The reaction was warmed to room temperature by removal of the cooling bath and stirred for 1 hour, upon which TLC indicated full conversion.

Work-Up: The reaction was quenched with the addition of sat. NH_4Cl (10 mL). The aqueous phase was extracted three times with CH_2Cl_2 (3 x 10 mL), and the combined organic layers were washed with brine (10 mL), dried over Na_2SO_4 , and concentrated. For the final purification, the crude was columned over silica eluting with 15:1 to 7:1 LP/EtOAc to yield 0.32 g (82 %) of 7-methoxy-2-naphthaldehyde **[46]** as a colorless solid.

Yield	0.32 g (82 %)
Appearance	colorless solid
TLC	R_f (LP/EtOAc - 10/1) = 0.32
Reaction scale	0.50 g (2.11 mmol)
Substrate concentration	0.30 M
Purification	column chromatography (silica) LP/EtOAc 15:1 to 7:1
Sum formula, m.w.	$\text{C}_{12}\text{H}_{10}\text{O}_2$, 186.21 g/mol
M.p.	55 – 57 °C

$^1\text{H-NMR}$ (400 MHz, CDCl_3)	δ 3.96 (s, 3H, $-\text{OCH}_3$), 7.28 (d, $J = 2.5$ Hz, 1H, H5), 7.30 (dd, $J = 2.5, 8.8$ Hz, 1H, H7), 7.80 (d, $J = 8.8$ Hz, 1H, H8), 7.81 (dd, $J = 1.6, 8.4$ Hz, 1H, H2), 7.87 (d, $J = 8.4$ Hz, 1H, H1), 8.24 (dd, $J = 0.7, 1.5$ Hz, 1H, H4), 10.14 (d, $J = 0.6$ Hz, 1H, $-\text{CHO}$).
$^{13}\text{C-NMR}$ (151 MHz, CDCl_3)	δ 55.6 (q, $-\text{OCH}_3$), 107.3 (d, C5), 121.0 (d, C2), 122.1 (d, C7), 128.9 (d, C1), 129.6 (d, C8), 132.1 (s, C4a), 133.1 (d, C4), 134.1 (s, C8a), 134.7 (s, C3), 158.6 (s, C6), 192.6 (d, $-\text{CHO}$).

E III.2.4 1-(7-Methoxynaphthalen-2-yl)ethan-1-ol [48]



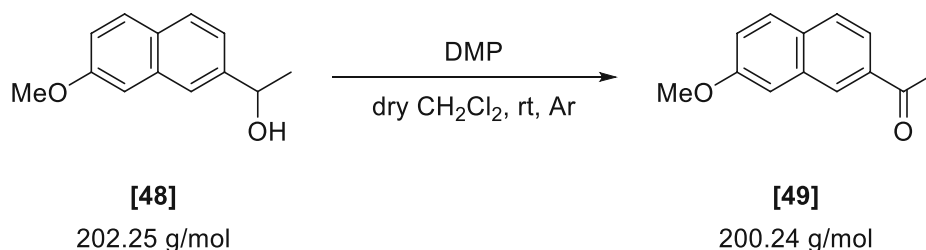
Procedure: A 8 mL screw-cap vial was charged with 7-methoxy-2-naphthaldehyde [47] (0.42 g, 2.27 mmol, 1.00 equiv.), which was dissolved in dry Et_2O (2 mL) under argon. The solution was cooled with a water/ice bath to 5°C , and then MeMgBr (1.1 M in Et_2O , 3.10 mL, 3.42 mmol, 1.50 equiv.) was added dropwise over a period of 2 minutes. Precipitation and continuous dissolution of colorless solids were observed during the addition. The reaction was allowed to warm to room temperature and was stirred for 1 hour, upon which TLC indicated full conversion.

Work-Up: The reaction was poured into ice-cold sat. NH_4Cl followed with the addition of 2 N HCl (100 mL). The aqueous phase was extracted three times with CH_2Cl_2 (3 x 30 mL), and the combined organic layers were washed with brine (100 mL) and dried over Na_2SO_4 . Due to the solution's persisting cloudiness, the crude was filtered over a pad of Celite and concentrated. For the final purification, the ochre solids were recrystallized from ligroin (20 mL) to yield 0.36 g (77 %) of 1-(7-methoxynaphthalen-2-yl)ethan-1-ol [48] as colorless crystals.

Yield	0.36 g (77 %)
Appearance	colorless crystals
TLC	R_f (LP/EtOAc - 2/1) = 0.36
Reaction scale	0.42 g (2.11 mmol)
Substrate concentration	1.10 M

Purification	recrystallization from ligroin
Sum formula, m.w.	C ₁₃ H ₁₄ O ₂ , 202.25 g/mol
M.p.	83 – 85 °C
¹ H-NMR (400 MHz, CDCl ₃)	δ 1.58 (d, <i>J</i> = 6.5 Hz, 3H, -CH-CH ₃), 1.88 – 1.95 (m, 1H, -OH), 3.92 (s, 3H, -OCH ₃), 5.05 (qd, <i>J</i> = 2.6, 6.3 Hz, 1H, -CH-OH), 7.09 – 7.17 (m, 2H, H7, H5), 7.36 (dd, <i>J</i> = 1.5, 8.4 Hz, 1H, H2), 7.69 – 7.80 (m, 2H, H1, H4), 7.76 (d, <i>J</i> = 8.4 Hz, 1H, H8).
¹³ C-NMR (151 MHz, CDCl ₃)	δ 25.3 (-CH-CH ₃), 55.4 (-OCH ₃), 70.8 (-CH-OH), 106.1 (s, C5), 118.7 (d, C7), 121.7 (d, C2), 122.9 (d, C4), 128.2 (d, C1), 128.5 (s, C8a), 129.3 (d, C8), 134.7 (s, C4a), 143.9 (s, C3), 158.0 (s, C6).

E III.2.5 1-(7-Methoxynaphthalen-2-yl)ethan-1-one [49]



The product was synthesized according to a literature procedure²²⁵.

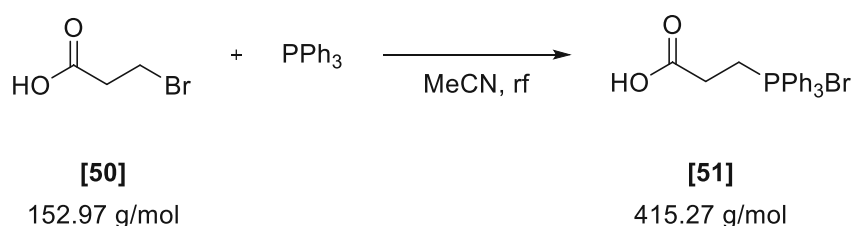
Procedure: A 8 mL screw-cap vial was charged 1-(7-methoxynaphthalen-2-yl)ethan-1-ol **[48]** (50 mg, 0.25 mmol, 1.00 equiv.), which was dissolved in dry CH₂Cl₂ (1.5 mL) under argon. Dess-Martin periodinane (157 mg, 0.37 mmol, 1.50 equiv.) was then added in one portion, and the reaction was stirred for 30 minutes at room temperature, upon which TLC indicated full conversion.

Work-Up: The formed precipitate was removed by filtration over a cotton plug. The reaction was further diluted with CH₂Cl₂ (5 mL) and washed twice with dH₂O (2 x 10 mL). The aqueous phase was extracted twice with CH₂Cl₂ (2 x 10 mL), and the combined organic layers were washed with brine (30 mL), dried over Na₂SO₄, and concentrated. For the final purification, the crude was columned over silica (pipette column, 2 g) eluting with 5:1 LP/EtOAc to yield 45 mg (90 %) of 1-(7-methoxynaphthalen-2-yl)ethan-1-one **[49]** as a colorless oil that crystallized upon standing.

Yield	45 mg (90 %)
Appearance	colorless crystals
TLC	R _f (LP/EtOAc - 5/1) = 0.31 (anisaldehyde)
Reaction scale	50 mg (0.25 mmol)
Substrate concentration	0.16 M

Purification	column chromatography (silica) LP/EtOAc 5:1
Sum formula, m.w.	C ₁₃ H ₁₂ O ₂ , 200.24 g/mol
M.p.	62 – 64 °C (lit. ²⁶⁹ 82 – 83 °C, ²⁷⁰ 95.5 – 96 °C)
¹ H-NMR (400 MHz, CDCl ₃)	δ 2.73 (s, 3H, -CH ₃), 3.96 (s, 3H, -OCH ₃), 7.24 – 7.31 (m, 2H, H7, H5), 7.78 (d, <i>J</i> = 8.6 Hz, 1H, H8), 7.83 (d, <i>J</i> = 8.6 Hz, 1H, H1), 7.90 (dd, <i>J</i> = 1.6, 8.5 Hz, 1H, H2), 8.38 (s, 1H, H4).
¹³ C-NMR (151 MHz, CDCl ₃)	δ 26.9 (q, -CH ₃), 55.5 (q, -OCH ₃), 107.2 (d, C5), 121.5 (d, C7), 122.0 (d, C2), 128.2 (d, C1), 128.9 (d, C4), 129.3 (d, C8), 131.3 (s, C8a), 133.9 (s, C4a), 135.1 (s, C3), 158.3 (s, C6), 198.4 (s, -CO-).

E III.2.6 (2-Carboxyethyl)triphenylphosphonium bromide [51]



The product was synthesized according to a literature procedure²²⁰.

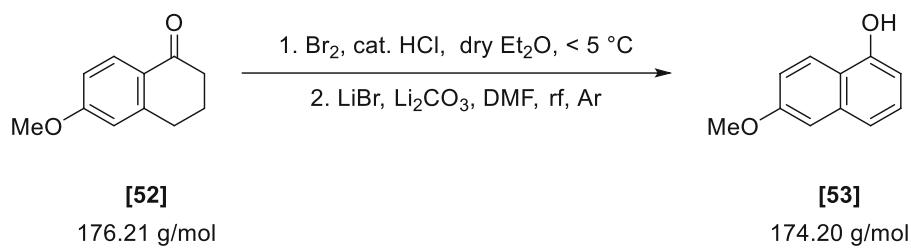
Procedure: A 50 mL 3-neck RBF was charged with 3-bromopropionic acid **[50]** (5.00 g, 32.77 mmol, 1.00 equiv.), which was dissolved in HPLC grade MeCN (12.5 mL). Following the addition of triphenylphosphine (8.60 g, 32.77 mmol, 1.00 equiv.), the reaction was refluxed for 24 hours.

Work-Up: The solvent was removed under reduced pressure by careful control of the vacuum. Due to the highly viscous nature of the wet product, a frothing can be expected. The crude was dissolved in a minimal amount of CHCl₃ and crashed out with the addition of Et₂O. Further precipitation was enabled by placing the suspension in the freezer. To enable unproblematic isolation of the solids, the sintered funnel was cooled to -20 °C as warming typically led to clogging of the filter due to dissolution and softening of the product. The product was further dried *in vacuo* and stored in a desiccator due to its hygroscopic nature. 9.50 g of 3 (2-carboxyethyl)triphenylphosphonium bromide **[51]** could be isolated as colorless crystals.

Yield	9.50 g (69 %)
Appearance	colorless crystals
TLC	-
Reaction scale	5.00 g (32.77 mmol)
Substrate concentration	2.62 M

Purification	column chromatography (silica) LP/EtOAc 5:1
Sum formula, m.w.	C ₂₁ H ₂₀ O ₂ PBr, 415.27 g/mol
M.p.	195 – 196 °C (lit. ²⁷¹ 196 °C)
¹ H-NMR (400 MHz, CDCl ₃)	δ 3.00 – 3.12 (m, 2H, COOH-CH ₂ -), 3.69 – 3.81 (m, 2H, -CH ₂ -Ph3P), 7.64 – 7.85 (m, 15H, ArH), 8.62 (s, 1H, COOH).
¹³ C-NMR (151 MHz, CDCl ₃)	δ 19.2 (td, ¹ J _{C-P} = 55.1 Hz, -CH ₂ -Ph3P), 28.4 (td, ² J _{C-P} = 2.7 Hz, COOH-CH ₂ -), 117.5 (d, ¹ J _{C-P} = 86.8 Hz, 3C, C1), 130.8 (dd, ² J _{C-P} = 12.7 Hz, 6C, C2, C6), 133.8 (dd, ³ J _{C-P} = 10.1 Hz, 6C, C3, C5), 135.5 (dd, ⁴ J _{C-P} = 2.8 Hz, 3C, C4), 171.3 (d, ³ J _{C-P} = 14.1 Hz, -COOH).
³¹ P NMR (243 MHz, CDCl ₃)	δ 24.7 (-PPh ₃).

E III.2.7 6-Methoxynaphthalen-1-ol [53]



The product was synthesized according to a literature procedure²²⁶.

Procedure 1: A 500 mL 3-neck RBF was charged with 6-methoxy-1-tetralone [52] (7.00 g, 39.72 mmol, 1.00 equiv.), which was dissolved in dry Et₂O (200 mL) containing catalytic amounts of ethereal HCl (1M, 2 mL). The solution was cooled to 0 °C with a water/ice bath. Subsequently, bromine (2.06 mL, 6.41 g, 40.12 mmol, 1.01 equiv.) was added dissolved in a 10:1 mixture of CCl₄ and Et₂O (22 mL) while maintaining a temperature < 5 °C. The reaction was stirred with cooling for 30 minutes, upon which TLC indicated full conversion.

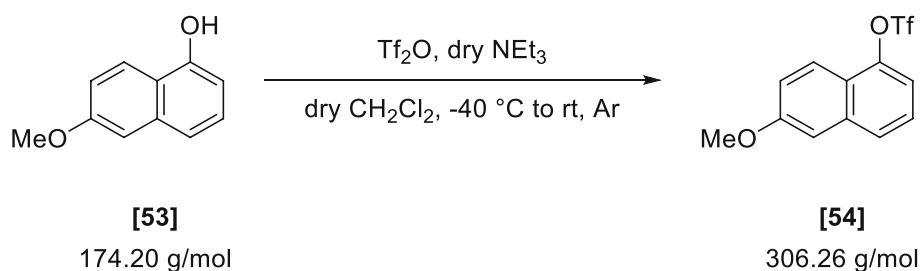
Work-Up 1: The organic phase was directly washed twice with dH₂O (2 x 200 mL), dried over Na₂SO₄, and concentrated, leaving 9.91 g of the alpha-bromo intermediate as a viscous brown oil.

Procedure 2: A solution of the crude product in DMF (200 mL) containing LiBr (7.85, 90.42 mmol, 2.33 equiv.) and Li₂CO₃ (5.88, 79.55 mmol, 2.05 equiv.) was refluxed for 3 hours under argon upon which TLC indicated full conversion.

Work-Up 2: The solvent was removed *in vacuo*, and the resulting oil was first suspended with dH₂O (100 mL), then 2 N HCl (100 mL). The emulsion was then taken up in Et₂O (200 mL) and washed with dH₂O (200 mL), brine (200 mL), dried over Na₂SO₄, and concentrated. For the final purification, the crude was flashed over silica (150 g), eluting with 3:1 LP/EtOAc to yield 5.15 g (76 % over two steps) of 6-methoxynaphthalen-1-ol [53] as ochre solid.

Yield	5.15 g (76 %)
Appearance	ochre solid
TLC	R_f (LP/EtOAc - 3/1) = 0.32 (anisaldehyde)
Reaction scale	7.00 g (39.72 mmol)
Substrate concentration	1 step: 0.20 M 2. step: 0.19 M
Purification	flash chromatography (silica) LP/EtOAc 3:1
Sum formula, m.w.	$C_{11}H_{10}O_2$, 174.20 g/mol
M.p.	85 – 86 °C (lit. ²⁷² 83 – 84 °C)
¹ H-NMR (400 MHz, CDCl ₃)	δ = 3.93 (s, 3H, -OCH ₃), 5.27 (s, 1H, -OH), 6.63 – 6.72 (m, 1H, H ₂), 7.12 (d, J = 2.3 Hz, 1H, H ₅), 7.15 (dd, J = 9.1, 2.5 Hz, 1H, H ₇), 7.27 (t, J = 7.8 Hz, 1H, H ₃), 7.34 (d, J = 8.2 Hz, 1H, H ₄), 8.10 (d, J = 9.1 Hz, 1H, H ₈) ppm.
¹³ C-NMR (151 MHz, CDCl ₃)	δ = 55.4 (q, -OCH ₃), 105.9 (d, C ₅), 106.8 (d, C ₂), 117.9 (d, C ₇), 119.7 (d, C ₄), 119.8 (s, C _{8a}), 123.5 (d, C ₈), 126.8 (d, C ₃), 136.4 (s, C _{4a}), 151.7 (s, C ₁), 158.2 (s, C ₆) ppm.

E III.2.8 6-Methoxynaphthalen-1-yl trifluoromethanesulfonate [54]



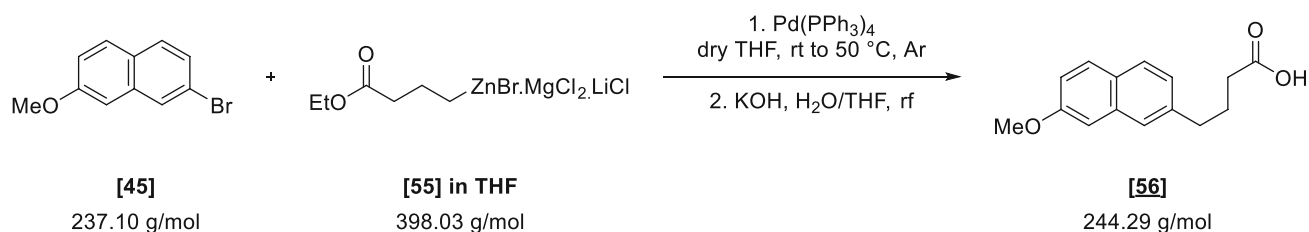
Procedure A 100 mL three-necked RBF was charged with 6-methoxy-1-naphthol **[53]** (2.00 g, 11.5 mmol, 1.00 equiv.), which was dissolved in dry CH_2Cl_2 (40 mL). The solution was cooled to $-40^\circ C$ *via* acetone/liquid N_2 bath followed by the addition of dry triethylamine (3.20 mL, 3.89 g, 22.9 mmol, 2.00 equiv.). After 15 minutes trifluoromethanesulfonyl anhydride (3.20 mL, 2.32 g, 13.8 mmol, 1.20 equiv.) was added dropwise, and the reaction mixture was warmed to $-10^\circ C$ and stirred at this temperature for 2 h upon which TLC indicated full conversion.

Work-up: The reaction mixture was quenched with the addition of sat. $NaHCO_3$ (50 mL). The aqueous phase was extracted twice with CH_2Cl_2 (2 x 100 mL), and the combined organic layers were washed with brine (100 mL), dried over Na_2SO_4 , and concentrated. For the final purification, the crude was columned over silica eluting with 10:1 LP/EtOAc to yield 3.17 g (90 %) of 6-methoxynaphthalen-1-yl trifluoromethanesulfonate **[54]** as a colorless oil.

Yield	3.17 g (90 %)
Appearance	colorless oil
TLC	R_f (LP/EtOAc - 4/1) = 0.60 (anisaldehyde)
Reaction scale	2.00 g (11.5 mmol)
Substrate concentration	0.29 M
Purification	column chromatography (silica) LP/EtOAc 10:1
Sum formula, m.w.	$C_{12}H_9F_3O_4S$, 306.26 g/mol

1H -NMR (400 MHz, $CDCl_3$)	δ = 3.94 (s, 3H, -OCH ₃), 7.19 (d, J = 2.3 Hz, 1H, H5), 7.28 – 7.32 (m, 2H, H2, H7), 7.44 (t, J = 8.0 Hz, 1H, H3), 7.75 (d, J = 8.3 Hz, 1H, H4), 7.98 (d, J = 9.2 Hz, 1H, H8) ppm.
^{13}C -NMR (101 MHz, $CDCl_3$)	δ = 55.6 (q, -OCH ₃), 106.1 (d, C5), 115.5 (d, C2), 118.9 (q, $^1J_{C-F}$ = 320.5 Hz, -CF ₃), 120.9 (d, C7), 121.8 (s, C8a), 122.6 (d, C8), 126.0 (d, C3), 127.3 (d, C4), 136.7 (s, C4a), 146.0 (s, C1), 158.8 (s, C6) ppm.
^{19}F NMR (376 MHz, $CDCl_3$)	δ -73.4 (-CF ₃).

E III.2.9 4-(7-Methoxynaphthalen-2-yl)butanoic acid [56]

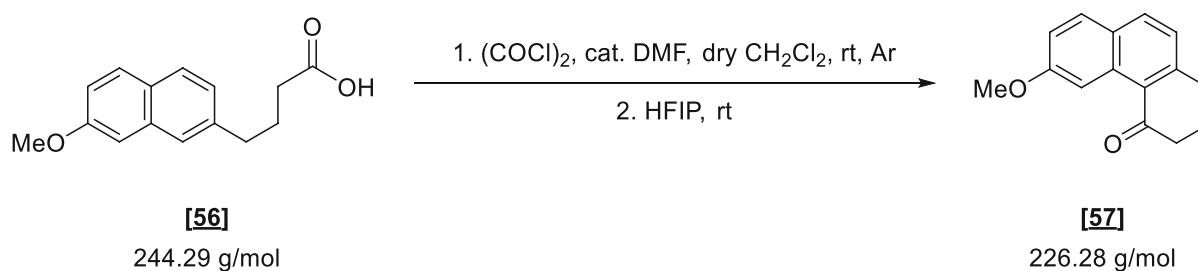


4-(7-methoxynaphthalen-2-yl)butanoic acid [56] was synthesized according to general procedure D using 2-bromo-7-methoxynaphthalene [45] (1.50 g, 6.33 mmol).

Yield	650 mg (42 % over two steps)
Appearance	colorless solid
TLC	R_f ($CHCl_3$ /MeOH – 20:1) = 0.30 (anisaldehyde)
Reaction scale	1.50 g (6.33 mmol)
Substrate concentration	1. step: 1.15 M, 2. step: 0.37 M
Purification	column chromatography (silica) $CHCl_3$ /MeOH 20:1
Sum formula, m.w.	$C_{15}H_{16}O_3$, 244.29 g/mol
M.p.	131 – 132 °C

$^1\text{H-NMR}$ (400 MHz, CDCl_3)	δ 2.07 (p, $J = 7.5$ Hz, 2H, Hb), 2.43 (t, $J = 7.4$ Hz, 2H, Hc), 2.83 (t, $J = 7.5$ Hz, (t, $J = 7.5$ Hz, 2H, Ha), 3.92 (s, 3H, $-\text{OCH}_3$), 7.08 – 7.15 (m, 2H, H5, H7), 7.20 (dd, $J = 1.7, 8.4$ Hz, 1H, H2), 7.54 (s, 1H, H4), 7.71 (d, $J = 8.3$ Hz, 2H, H1, H8), 10.74 (s, 1H, $-\text{COOH}$).
$^{13}\text{C-NMR}$ (151 MHz, CDCl_3)	δ 26.2 (t, Cb), 33.5 (t, Cc), 35.3 (t, Ca), 55.4 (q, $-\text{OCH}_3$), 105.6 (d, C5), 118.2 (d, C7), 125.0 (d, C2), 125.8 (d, C4), 127.7 (s, C8a), 127.9 (d, C1), 129.2 (d, C8), 134.9 (s, C4a), 139.4 (s, C3), 157.9 (s, C6), 180.1 (s, $-\text{COOH}$).
HRMS (ESI)	not found

E III.2.10 6-Methoxy-2,3-dihydrophenanthren-4(1H)-one [57]



The product was synthesized according to a literature procedure²¹⁴.

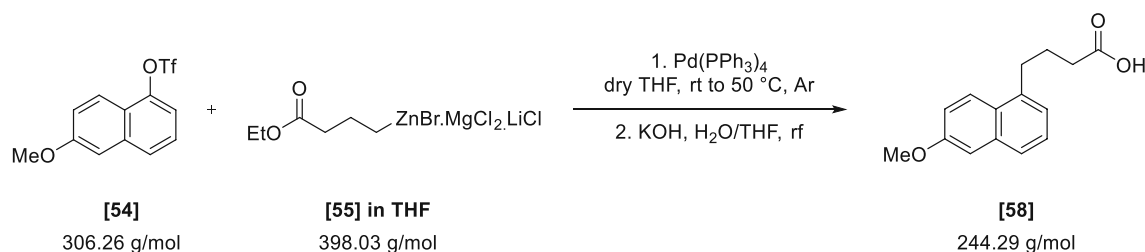
Procedure A GC-MS vial was charged with 4-(7-methoxynaphthalen-2-yl)butanoic acid [56] (40 mg, 0.16 mmol, 1.00 equiv.) and was crimped tightly. The vial was evacuated and backfilled with argon using standard Schlenk techniques followed with the subsequent addition of dry CH_2Cl_2 (0.8 mL), catalytical dry DMF (2 μL), and finally oxalyl chloride (28 μL , 42 mg, 0.33 mmol, 2.00 equiv.). The dropwise addition caused immediate strong gas evolution. The reaction was stirred for 30 minutes at room temperature and was then concentrated on the rotary evaporator (7 mbar, 10 minutes) by piercing the septum with a 30-gauge needle. After the addition of HFIP (0.4 mL), the reaction was stirred for 30 minutes, upon which TLC indicated full conversion.

Work-up: The solvent was removed *in vacuo*, and the crude was immediately columned over silica (pipette column, 2 g) eluting with pure CH_2Cl_2 to yield 30 mg (81 %) of 6-methoxy-2,3-dihydrophenanthren-4(1H)-one [57] as light-yellow oil that crystallized upon standing.

Yield	30 mg (81 %)
Appearance	light-yellow solid
TLC	R_f (LP/EtOAc – 3/1) = 0.49 (anisaldehyde)

Reaction scale	40 mg (0.16 mmol)
Substrate concentration	chlorination: 0.20 M, Friedel-Crafts acylation: 0.41 M
Purification	column chromatography (silica) CH ₂ Cl ₂
Sum formula, m.w.	C ₁₅ H ₁₄ O ₂ , 226.28 g/mol
M.p.	74 – 76 °C
¹ H-NMR (400 MHz, CDCl ₃)	δ 2.18 (p, <i>J</i> = 6.5 Hz, 2H, H _b), 2.74 – 2.82 (m, 2H, H _c), 3.12 (t, <i>J</i> = 6.1 Hz, (t, <i>J</i> = 6.1 Hz, 2H, H _a), 3.98 (s, 3H, -OCH ₃), 7.15 (dd, <i>J</i> = 2.6, 8.9 Hz, 1H, H ₇), 7.18 (d, <i>J</i> = 8.3 Hz, 1H, H ₂), 7.69 (d, <i>J</i> = 8.9 Hz, 1H, H ₈), 7.85 (d, <i>J</i> = 8.2 Hz, 1H, H ₁), 9.02 (d, <i>J</i> = 2.5 Hz, 1H, H ₅).
¹³ C-NMR (151 MHz, CDCl ₃)	δ 23.2 (t, C _b), 32.0 (t, C _a), 41.4 (t, C _c), 55.5 (q, -OCH ₃), 105.5 (d, C ₅), 118.5 (d, C ₇), 124.7 (d, C ₂), 126.1 (s, C ₄), 128.4 (s, C _{8a}), 129.8 (d, C ₈), 133.3 (s, C _{4a}), 134.2 (d, C ₁), 147.7 (s, C ₃), 160.6 (s, C ₆), 200.9 (s, -CO-).
HRMS (ESI)	calc. for C ₁₅ H ₁₅ O ₂ ⁺ [M+H] ⁺ 227.1067, found 227.0991 – Δ = -33.46 ppm.

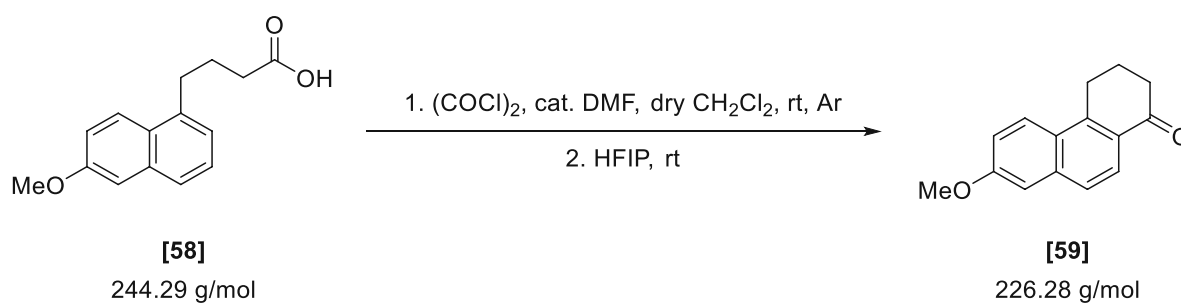
E III.2.11 4-(6-Methoxynaphthalen-1-yl)butanoic acid [58]



4-(6-methoxynaphthalen-1-yl)butanoic acid [58] was synthesized according to general procedure D using 6-methoxynaphthalen-1-yl trifluoromethanesulfonate [54] (0.26 g, 0.83 mmol).

Yield	82 mg (40 % over two steps)
Appearance	colorless solid
TLC	R _f (CHCl ₃ /MeOH – 20:1) = 0.30 (anisaldehyde)
Reaction scale	0.26 (0.83 mmol)
Substrate concentration	1. step: 0.83 M, 2. step: 0.42 M
Purification	column chromatography (silica) CHCl ₃ /MeOH 20:1
Sum formula, m.w.	C ₁₅ H ₁₆ O ₃ , 244.29 g/mol
M.p.	151 – 152 °C (lit. ²⁷³ 151.5 – 152 °C)

- ¹H-NMR (400 MHz, CDCl₃)** δ = 2.09 (p, J = 7.4 Hz, 2H, Hb), 2.46 (t, J = 7.3 Hz, 2H, Hc), 3.06 – 3.16 (m, (t, J = 7.3 Hz, 2H, Ha), 3.93 (s, 3H, -OCH₃), 7.13 – 7.22 (m, 3H, H2, H5, H7), 7.36 (t, J = 7.6 Hz, 1H, H3), 7.62 (d, J = 8.2 Hz, 1H, H4), 7.96 (d, J = 9.1 Hz, 1H, H8), 10.96 (s, 1H, -COOH) ppm.
- ¹³C-NMR (151 MHz, CDCl₃)** δ = 25.7 (t, Cb), 32.4 (t, Ca), 33.6 (t, Cc), 55.4 (q, -OCH₃), 106.9 (d, C5), 118.6 (d, C7), 124.3 (d, C2), 125.5 (d, C8), 125.9 (d, C4), 126.3 (d, C3), 127.4 (s, C8a), 135.4 (s, C4a), 137.5 (s, C1), 157.4 (s, C6), 179.1 (s, -COOH) ppm.

E III.2.12 7-Methoxy-3,4-dihydrophenanthren-1(2H)-one [59]

The product was synthesized according to a literature procedure²¹⁴.

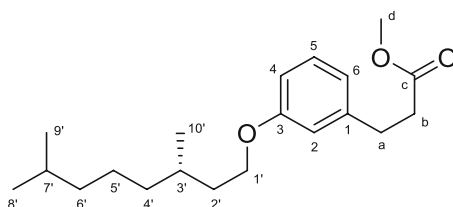
Procedure A GC-MS vial was charged with 4-(6-methoxynaphthalen-1-yl)butanoic acid **[58]** (40 mg, 0.16 mmol, 1.00 equiv.) and was crimped tightly. The vial was evacuated and backfilled with argon using standard Schlenk techniques followed with the subsequent addition of dry CH₂Cl₂ (0.8 mL), catalytical dry DMF (2 μ L), and finally oxalyl chloride (28 μ L, 42 mg, 0.33 mmol, 2.00 equiv.). The dropwise addition caused immediate strong gas evolution. The reaction was stirred for 30 minutes at room temperature and was then concentrated on the rotary evaporator (7 mbar, 10 minutes) by piercing the septum with a 30-gauge needle. After the addition of HFIP (0.4 mL), the reaction was stirred for 30 minutes, upon which TLC indicated full conversion.

Work-up: The solvent was removed *in vacuo*, and the crude was immediately columned over silica (pipette column, 2 g) eluting with pure CH₂Cl₂ to yield 27 mg (73 %) of 7-methoxy-3,4-dihydrophenanthren-1(2H)-one **[59]** as light-yellow solid.

Yield	27 mg (73 %)
Appearance	light-yellow solid
TLC	R _f (LP/EtOAc – 3/1) = 0.49 (anisaldehyde)
Reaction scale	40 mg (0.16 mmol)
Substrate concentration	chlorination: 0.20 M, Friedel-Crafts acylation: 0.41 M

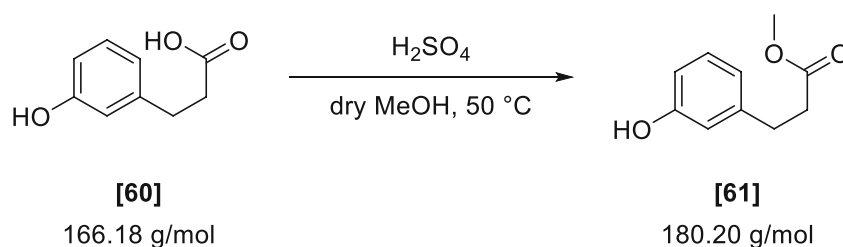
Purification	column chromatography (silica) CH ₂ Cl ₂
Sum formula, m.w.	C ₁₅ H ₁₄ O ₂ , 226.28 g/mol
M.p.	100 – 101 °C (lit. ²⁷³ 99 – 100 °C)
¹ H-NMR (400 MHz, CDCl ₃)	δ 2.28 (p, <i>J</i> = 6.4 Hz, 2H, Hb), 2.68 – 2.75 (m, 2H, Hc), 3.34 (t, <i>J</i> = 6.0 Hz, (t, <i>J</i> = 6.0 Hz, 2H, Ha), 3.95 (s, 3H, -OCH ₃), 7.15 (d, <i>J</i> = 2.2 Hz, 1H, H5), 7.22 (dd, <i>J</i> = 2.6, 9.2 Hz, 1H, H7), 7.63 (d, <i>J</i> = 8.7 Hz, 1H, H4), 8.03 (d, <i>J</i> = 9.2 Hz, 1H, H8), 8.08 (d, <i>J</i> = 8.7 Hz, 1H, H3).
¹³ C-NMR (151 MHz, CDCl ₃)	δ 22.9 (t, Cb), 25.8 (t, Ca), 38.4 (t, Cc), 55.6 (q, -OCH ₃), 107.1 (d, C5), 119.2 (d, C7), 123.7 (d, C3), 125.9 (d, C4), 126.5 (s, C8a), 126.7 (d, C8), 128.5 (s, C2), 137.7 (s, C4a), 143.1 (s, C1), 159.7 (s, C6), 198.5 (s, -CO-).

E III.3 Part III – Synthesis of alkylated 3-(3-hydroxyphenyl)propanoic acids for SHC catalyzed Friedel-Crafts acylation



NMR assignments of core structures in this chapter were given according to the following example.

E III.3.1 Methyl 3-(3-hydroxyphenyl)propanoate [61]



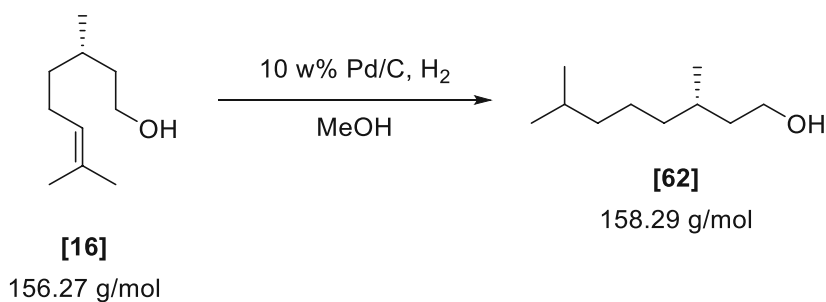
Procedure: A flame-dried 100 mL three-necked RBF was charged with 3-(3-hydroxyphenyl)propionic acid [60] (4.50 g, 27.08 mmol, 1.00 equiv.), which was dissolved in dry MeOH (55 mL). Following the addition of conc. H₂SO₄ (0.14 mL, 0.27 g, 2.71 mmol, 0.10 equiv.) the reaction was stirred at 50 °C for 6 hours, upon which TLC indicated full conversion.

Work-up: The reaction was quenched sat. NaHCO₃ solution (10 mL) and the bulk of the solvent was removed *in vacuo*. The crude was taken up in EtOAc (50 mL) and washed with sat. NaHCO₃ (20 mL) and brine (50 mL). The organic layer was then dried over Na₂SO₄ and concentrated to yield 4.54 g (93 %) of

3-(3-hydroxyphenyl)propanoate **[61]** as yellowish oil. The resulting material could be used directly for the next step without further purification.

Yield	4.54 g (93 %)
Appearance	light-yellow oil
TLC	R_f (CH ₂ Cl ₂ /MeOH - 10/1) = 0.90 (anisaldehyde)
Reaction scale	4.50 g (27.08 mmol)
Substrate concentration	0.50 M
Purification	pure after work-up
Sum formula, m.w.	C ₁₀ H ₁₂ O ₃ , 180.20 g/mol
¹H-NMR (600 MHz, CDCl₃)	δ 2.63 (t, <i>J</i> = 7.8 Hz, 2H, H _b), 2.91 (t, <i>J</i> = 7.8 Hz, 2H, H _a), 3.68 (s, 3H, H _d), 6.66–6.71 (m, 2H, H ₂ , H ₄), 6.76 (d, <i>J</i> = 7.6 Hz, 1H, H ₆), 7.15 (dd, <i>J</i> = 7.6, 8.8 Hz, 1H, H ₅).
¹³C-NMR (151 MHz, CDCl₃)	δ 30.9 (t, C _a), 35.7 (t, C _b), 51.9 (q, C _d), 113.4 (d, C ₄), 115.4 (d, C ₂), 120.7 (d, C ₆), 129.9 (d, C ₅), 142.5 (s, C ₁), 155.9 (s, C ₃), 173.7 (s, C _c).

E III.3.2 (S)-3,7-Dimethyloctan-1-ol **[62]**



The product was synthesized according to a literature procedure²¹¹.

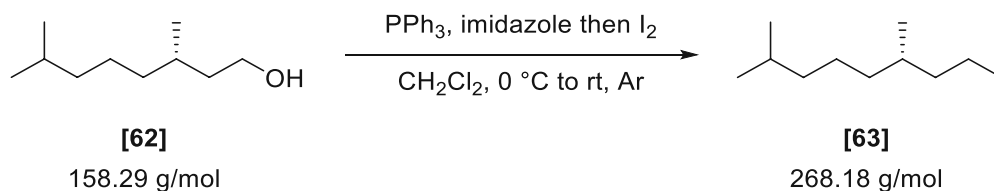
Procedure: A flame-dried 25 mL three-necked RBF was charged with (*S*)-citronellol **[16]** (1.25 g, 8.00 mmol, 1.00 equiv.), which was dissolved in dry MeOH (8 mL). The atmosphere was exchanged for argon using standard Schlenk-techniques, and then 10 % Pd/C (85 mg, 27 mg, 0.27 mmol, 0.10 equiv.) was added with argon counterflow. The vessel was then purged three times with hydrogen (3 cycles of alternating hydrogen purge and application of vacuum) and sealed. The mixture was reacted at room temperature with strong stirring for 24 hours, upon which TLC indicated full conversion.

Work-up: The reaction was filtered over a pad of Celite, and the solvent was removed by application of low vacuum (max. 150 mbar, 40 °C) on the rotary evaporator. The crude product was further purified *via* flash chromatography (*n*-pentane) over a small pad of silica and concentrated to yield 0.65 g (51 %) of (*S*)-3,7-dimethyloctan-1-ol **[62]** as a colorless oil.

Yield	0.65 g (51 %)
Appearance	colorless oil
TLC	R_f (LP/EtOAc - 10/1) = 0.58 (anisaldehyde)
Reaction scale	1.25 g (8.00 mmol)
Substrate concentration	1 M
Purification	column chromatography (silica) n-pentane
Sum formula, m.w.	$C_{10}H_{22}O$, 158.29 g/mol
Optical rotation	$[\alpha]_D^{20} = -4.9$ (c = 0.49, CH_2Cl_2)

1H -NMR (600 MHz, $CDCl_3$)	δ 0.86 (d, $J = 1.1, 6.6$ Hz, 6H, H8, H9), 0.89 (d, $J = 6.6$ Hz, 3H, H10), 1.08 – 1.18 (m, 3H, H4', H6), 1.21 – 1.34 (m, 4H, H4, H5, -OH), 1.38 (dtd, $J = 5.8, 7.5, 13.1$ Hz, 1H, H2'), 1.54 (ddt, $J = 6.6, 13.3, 22.9$ Hz, 2H, H3, H7), 1.57 – 1.63 (m, 1H, H2), 3.64 – 3.73 (m, 2H, H1).
^{13}C -NMR (151 MHz, $CDCl_3$)	δ 19.8 (q, C10), 22.7 (q, C8 or C9), 22.8 (q, C8 or C9), 24.8 (t, C5), 28.1 (d, C7), 29.6 (d, C3), 37.5 (t, C4), 39.4 (t, C6), 40.1 (t, C2), 61.4 (t, C1).

E III.3.3 (S)-1-Iodo-3,7-dimethyloctane [63]



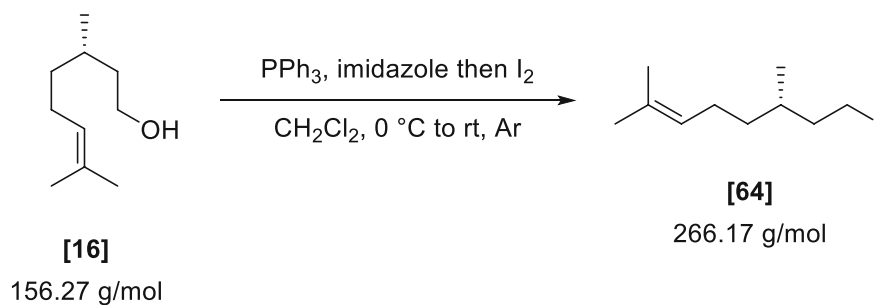
The product was synthesized according to a literature procedure.²¹²

Procedure: A flame-dried 50 mL three-necked RBF was charged with (S)-3,7-dimethyloctan-1-ol [62] (0.50 g, 3.16 mmol, 1.00 equiv.), which was dissolved in CH_2Cl_2 (17 mL). Following the addition of PPh_3 (1.04 g, 3.95 mmol, 1.25 equiv.) and imidazole (0.47 g, 6.95 mmol, 2.20 equiv.), the reaction was cooled to 0 °C with an ice/water bath under argon. Subsequently, I_2 (1.20 g, 4.74 mmol, 1.50 equiv.) was added in several portions with argon counterflow effecting a bright red discoloring of the solution. After complete addition, the reaction mixture was stirred at 0 °C for an additional 30 minutes and was then warmed to room temperature. The mixture was stirred for 24 hours, upon which TLC indicated full conversion.

Work-up: The reaction was quenched with a sat. $\text{Na}_2\text{S}_2\text{O}_3$ solution (20 mL), which turned the solution almost colorless. The aqueous phase was extracted four times with CH_2Cl_2 (4 x 15 mL). The combined organic layers were washed with brine (100 mL), dried over Na_2SO_4 , and the solvent was removed by applying a low vacuum (max. 400 mbar, 40 °C). To remove residual triphenylphosphine oxide, n-pentane was added to the residue resulting in the precipitation of colorless solids. The mixture was then filtered over a pad of silica. Removal of the solvent under reduced pressure (250 mbar, 40 °C) yielded 0.72 g (85 %) of (S)-1-iodo-3,7-dimethyloctane **[63]** as a colorless oil.

Yield	0.72 g (85 %)
Appearance	colorless oil
TLC	R_f (LP/EtOAc – 25/1) = 0.92 (KMnO_4)
Reaction scale	0.50 g (3.16 mmol)
Substrate concentration	0.19 M
Purification	filtration (silica) n-pentane
Sum formula, m.w.	$\text{C}_{10}\text{H}_{21}\text{I}$, 268.18 g/mol
Optical rotation	$[\alpha]_D^{20} = +8.9$ (c = 0.63, CH_2Cl_2)
$^1\text{H-NMR}$ (600 MHz, CDCl_3)	δ 0.87 (d, 9H, H8, H9, H10), 1.08 – 1.18 (m, 3H, H4', H6), 1.21 – 1.34 (m, 3H, H4, H5), 1.46 – 1.59 (m, 2H, H3, H7), 1.60 – 1.69 (m, 1H, H2'), 1.83 – 1.92 (m, 1H, H2), 3.13 – 3.20 (m, 1H, H1'), 3.22 – 3.29 (m, 1H, H1).
$^{13}\text{C-NMR}$ (151 MHz, CDCl_3)	δ 5.6 (t, C1), 18.9 (q, C10), 22.7 (q, C8 or C9), 22.8 (q, C8 or C9), 24.7 (d, C5), 28.1 (d, C7), 34.0 (d, C3), 36.6 (t, C4), 39.3 (t, C6), 41.1 (t, C2).

E III.3.4 (S)-8-Iodo-2,6-dimethyloct-2-ene [64]



The product was synthesized according to a literature procedure.²¹²

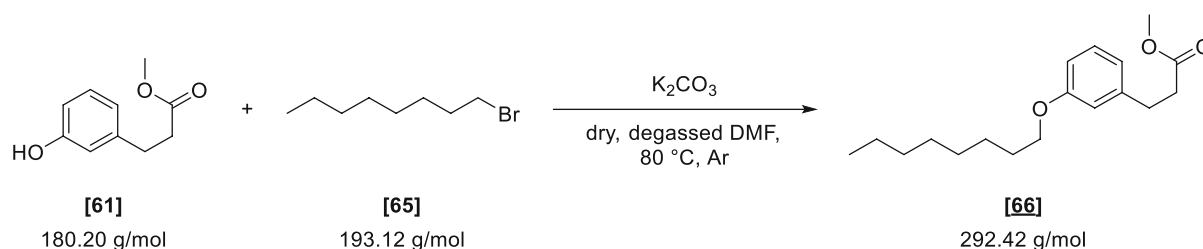
Procedure: A flame-dried 100 mL three-necked RBF was charged with (S)-citronellol **[16]** (2.00 g, 12.80 mmol, 1.00 equiv.), which was dissolved in CH₂Cl₂ (60 mL). Following the addition of PPh₃ (4.20 g, 16.00 mmol, 1.25 equiv.) and imidazole (1.92 g, 28.16 mmol, 2.20 equiv.), the reaction was cooled to 0 °C with an ice/water bath under argon. Subsequently, I₂ (4.87 g, 19.20 mmol, 1.50 equiv.) was added in several portions with argon counterflow effecting a bright red discoloring of the solution. After complete addition, the reaction mixture was stirred at 0 °C for an additional 30 minutes and was then warmed to room temperature. The mixture was stirred for 24 hours, upon which TLC indicated full conversion.

Work-up: The reaction was quenched with a sat. Na₂S₂O₃ solution (80 mL) turning the solution almost colorless. The aqueous phase was extracted four times with CH₂Cl₂ (4 x 50 mL). The combined organic layers were washed with brine (200 mL), dried over Na₂SO₄, and the solvent was removed by applying a low vacuum (max. 400 mbar, 40 °C). To remove residual triphenylphosphine oxide, n-pentane was added to the residue resulting in the precipitation of colorless solids. The mixture was then filtered over a pad of silica. Removal of the solvent under reduced pressure (250 mbar, 40 °C) yielded 3.38 g (99 %) of (S)-8-iodo-2,6-dimethyloct-2-ene **[64]** as a colorless oil.

Yield	3.38 g (99 %)
Appearance	colorless oil
TLC	R _f (LP/EtOAc – 10/1) = 0.95 (KMnO ₄)
Reaction scale	2.00 g (12.80 mmol)
Substrate concentration	0.19 M
Purification	filtration (silica) n-pentane
Sum formula, m.w.	C ₁₀ H ₁₉ I, 266.17 g/mol
Optical rotation	[α] _D ²⁰ = +10.8 (c = 0.47, CH ₂ Cl ₂)

$^1\text{H-NMR}$ (600 MHz, CDCl_3)	δ 0.89 (d, $J = 6.6$ Hz, 3H, H10), 1.11 – 1.22 (m, 1H, H4'), 1.31 – 1.38 (m, 1H, H4), 1.53 – 1.57 (m, 1H, H3), 1.61 (s, 3H, H9), 1.62 – 1.68 (m, 1H, H2'), 1.69 (s, 3H, H8), 1.88 (dddd, $J = 5.3, 7.1, 8.6, 13.9$ Hz, 1H, H2), 1.92 – 2.04 (m, 2H, H5), 3.14 – 3.19 (m, 1H, H1'), 3.22 – 3.28 (m, 1H, H1), 5.09 (dqt, $J = 1.5, 2.9, 7.1$ Hz, 1H, H6).
$^{13}\text{C-NMR}$ (151 MHz, CDCl_3)	δ 5.3 (t, C1), 17.8 (q, C9), 18.8 (q, C10), 25.5 (t, C5), 25.9 (q, C8), 33.7 (d, C3), 36.5 (t, C4), 41.0 (t, C2), 124.6 (d, C6), 131.6 (s, C7).

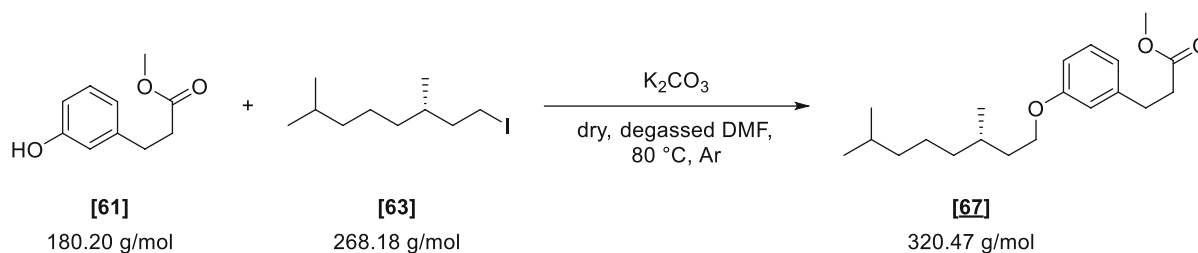
E III.3.5 Methyl 3-(3-(octyloxy)phenyl)propanoate [66]



Methyl 3-(3-(octyloxy)phenyl)propanoate [66] was synthesized according to general procedure E using methyl 3-(3-hydroxyphenyl)propanoate [61] (0.50 g, 2.77 mmol) and octyl bromide [65] (0.56 + 0.11 g, 2.91 + 0.56 mmol).

Yield	0.72 g (90 %)
Appearance	colorless oil
TLC	R_f (LP/EtOAc – 10:1) = 0.60 (anisaldehyde)
Reaction scale	0.50 g (2.77 mmol)
Substrate concentration	0.28 M
Purification	column chromatography (silica) LP/EtOAc 10:1
Sum formula, m.w.	$\text{C}_{18}\text{H}_{28}\text{O}_3$, 292.42 g/mol

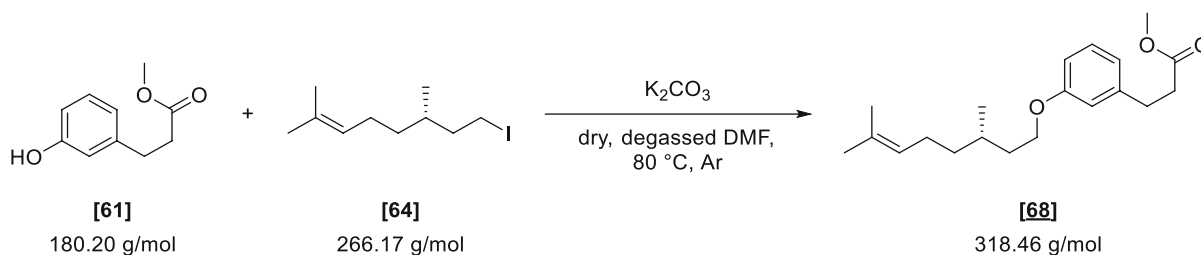
$^1\text{H-NMR}$ (600 MHz, CDCl_3)	δ 0.87 – 0.91 (m, 3H, H8'), 1.23 – 1.38 (m, 8H, H4', H5', H6', H7'), 1.42 – 1.48 (m, 2H, H3'), 1.77 (p, 2H, H2'), 2.63 (t, $J = 7.3, 8.6$ Hz, 2H, Hb), 2.92 (t, 2H, Ha), 3.68 (s, 3H, Hd), 3.93 (t, $J = 6.6$ Hz, 2H, H1'), 6.72 – 6.75 (m, 2H, H4, H6), 6.75 – 6.79 (m, 1H, H2), 7.16 – 7.21 (m, 1H, H5).
$^{13}\text{C-NMR}$ (151 MHz, CDCl_3)	δ 14.2 (q, C8'), 22.8 (t, C7'), 26.2 (t, C3'), 29.4 (t, C2' or C4' or C5'), 29.5 (t, C2' or C4' or C5'), 29.5 (t, C2' or C4' or C5'), 31.1 (t, Ca), 32.0 (t, C6'), 35.8 (t, Cb), 51.8 (q, Cd), 68.0 (t, C1'), 112.3 (d, Ca), 114.8 (d, C6), 120.5 (d, C2), 129.6 (d, C5), 142.2 (s, C1), 159.4 (s, C3), 173.5 (s, Cc).
HRMS (ESI)	not found

E III.3.6 Methyl (*S*)-3-(3-((3,7-dimethyloctyl)oxy)phenyl)propanoate [67]

Methyl (*S*)-3-(3-((3,7-dimethyloctyl)oxy)phenyl)propanoate [67] was synthesized according to general procedure E using methyl 3-(3-hydroxyphenyl)propanoate [61] (0.40 g, 2.22 mmol) and (*S*)-1-iodo-3,7-dimethyloctane [63] (0.63 + 0.11 g, 2.33 + 0.44 mmol).

Yield	0.57 g (80 %)
Appearance	colorless oil
TLC	R_f (LP/EtOAc – 15:1) = 0.57 (anisaldehyde)
Reaction scale	0.40 g (2.22 mmol)
Substrate concentration	0.28 M
Purification	column chromatography (silica) LP/EtOAc 40:1 to 25:1
Sum formula, m.w.	$\text{C}_{20}\text{H}_{32}\text{O}_3$, 320.47 g/mol
Optical rotation	$[\alpha]_D^{20} = -3.5$ ($c = 0.62$, CH_2Cl_2)
$^1\text{H-NMR}$ (600 MHz, CDCl_3)	δ 0.87 (d, $J = 0.9$, 6.6 Hz, 6H, H8', H9'), 0.94 (d, $J = 6.6$ Hz, 3H, H10'), 1.09 – 1.21 (m, 3H, (H4')', H6''), 1.22 – 1.37 (m, 3H, H4', H5'), 1.47 – 1.62 (m, 2H, (H2')', H7), 1.63 – 1.71 (m, 1H, H3'), 1.77 – 1.86 (m, 1H, H2'), 2.63 (t, $J = 7.2$, 8.6 Hz, 2H, Hb), 2.92 (t, $J = 6.7$, 9.1 Hz, 2H, Ha), 3.68 (s, 3H, Hd), 3.92 – 4.02 (m, 2H, H1'), 6.72 – 6.76 (m, 2H, H2, H4), 6.76 – 6.79 (m, 1H, H6), 7.17 – 7.21 (m, 1H, H5).
$^{13}\text{C-NMR}$ (151 MHz, CDCl_3)	δ 19.8 (q, C10'), 22.8 (q, C8' or C9'), 22.9 (q, C8' or C9'), 24.8 (t, C5'), 28.1 (d, C7'), 30.0 (d, C3'), 31.1 (t, Ca), 35.8 (t, Cb), 36.4 (t, C2'), 37.4 (t, C4'), 39.4 (t, C6'), 51.8 (q, Cd), 66.3 (t, C1'), 112.3 (d, C4), 114.8 (d, C2), 120.5 (d, C6), 129.6 (d, C5), 142.2 (s, C1), 159.4 (s, C3), 173.5 (s, Cc).
HRMS (ESI)	calc. for $\text{C}_{20}\text{H}_{33}\text{O}_3^+$ $[\text{M}+\text{H}]^+$ 321.2424, found 321.2419 – $\Delta = -1.55$ ppm.

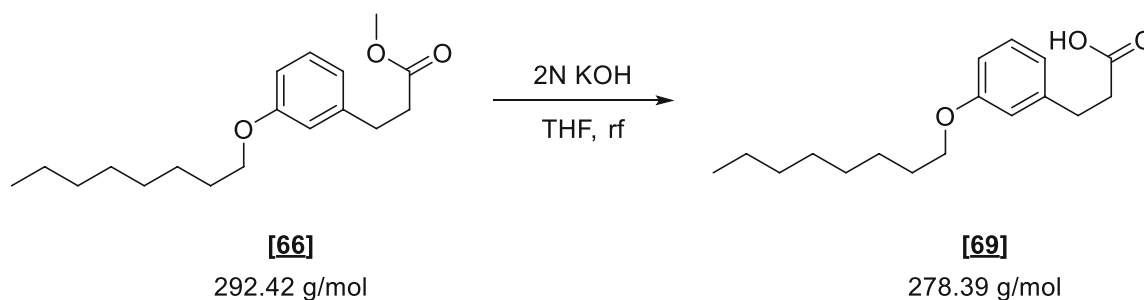
E III.3.7 Methyl (S)-3-(3-((3,7-dimethyloct-6-en-1-yl)oxy)phenyl)propanoate [68]



Methyl (S)-3-(3-((3,7-dimethyloct-6-en-1-yl)oxy)phenyl)propanoate [68] was synthesized according to general procedure E using methyl 3-(3-hydroxyphenyl)propanoate [61] (0.40 g, 2.22 mmol) and (S)-8-iodo-2,6-dimethyloct-2-ene [64] (0.62 + 0.12 g, 2.33 + 0.44 mmol).

Yield	0.55 g (78 %)
Appearance	colorless oil
TLC	R_f (LP/EtOAc – 15:1) = 0.57 (anisaldehyde)
Reaction scale	0.40 g (2.22 mmol)
Substrate concentration	0.28 M
Purification	column chromatography (silica) LP/EtOAc 40:1 to 25:1
Sum formula, m.w.	$\text{C}_{20}\text{H}_{30}\text{O}_3$, 318.46 g/mol
Optical rotation	$[\alpha]_D^{20} = +3.89$ (c = 0.47, CH_2Cl_2)
$^1\text{H-NMR}$ (600 MHz, CDCl_3)	δ 0.95 (d, $J = 6.7$ Hz, 3H, H_{10}'), 1.19 – 1.26 (m, 1H, ($\text{H}_{4'}'$)), 1.36 – 1.44 (m, 1H, H_{4}'), 1.56 – 1.60 (m, 1H, ($\text{H}_{2'}'$)), 1.61 (s, 3H, H_9'), 1.65 – 1.72 (m, 1H, H_{3}'), 1.69 (q, $J = 1.2$ Hz, 3H, H_{8}'), 1.83 (dtd, $J = 5.3, 7.1, 12.5$ Hz, 1H, H_{2}'), 1.94 – 2.09 (m, 2H, H_{5}'), 2.63 (t, $J = 7.2, 8.6$ Hz, 2H, H_b), 2.92 (t, 2H, H_a), 3.68 (s, 3H, H_d), 3.93 – 4.02 (m, 2H, H_{11}'), 5.11 (dq, $J = 1.5, 7.1$ Hz, 1H, H_{6}'), 6.72 – 6.77 (m, 2H, H_4, H_6), 6.76 – 6.79 (m, 1H, H_2), 7.17 – 7.21 (m, 1H, H_5).
$^{13}\text{C-NMR}$ (151 MHz, CDCl_3)	δ 17.8 (q, C_{9}'), 19.7 (q, C_{10}'), 25.6 (q, C_{8}'), 25.9 (t, C_{5}'), 29.7 (d, C_{3}'), 31.1 (t, C_a), 35.8 (t, C_b), 36.3 (t, C_{2}'), 37.3 (t, C_{4}'), 51.8 (q, C_d), 66.3 (t, C_{1}'), 112.3 (d, C_4), 114.8 (d, C_6), 120.5 (d, C_2), 124.8 (d, C_{6}'), 129.6 (t, C_5), 131.4 (s, C_{7}'), 142.2 (s, C_1), 159.4 (s, C_3), 173.5 (s, C_c).
HRMS (ESI)	calc. for $\text{C}_{20}\text{H}_{31}\text{O}_3^+$ $[\text{M}+\text{H}]^+$ 319.2268, found 319.2269 – $\Delta = 0.31$ ppm.

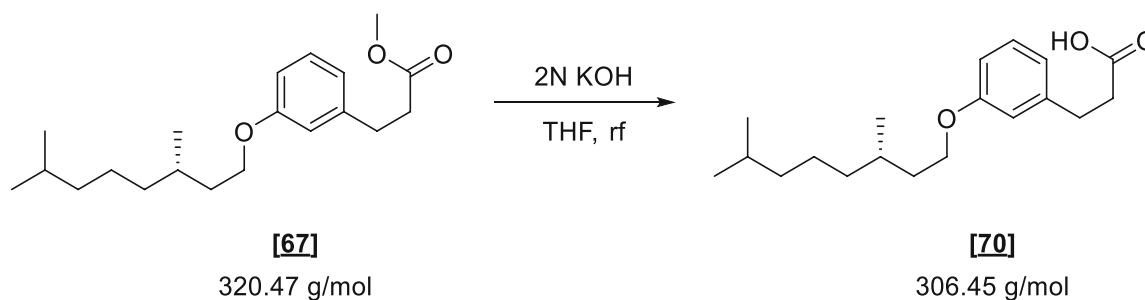
E III.3.8 3-(3-(Octyloxy)phenyl)propanoic acid [69]



3-(3-(Octyloxy)phenyl)propanoic acid [69] was synthesized according to general procedure F using methyl methyl 3-(3-(octyloxy)phenyl)propanoate [66] (0.25 g, 0.85 mmol). The product could be used for further experimentation without additional purification.

Yield	0.23 g (quant.)
Appearance	colorless solid
TLC	R_f (LP/EtOAc – 5:1) = 0.25 (anisaldehyde)
M.p.	60.9 – 61.3 °C
Reaction scale	0.25 g (0.85 mmol)
Substrate concentration	0.28 M
Purification	pure after work-up
Sum formula, m.w.	$C_{17}H_{26}O_3$, 278.39 g/mol
$^1\text{H-NMR}$ (600 MHz, DMSO-d_6)	δ 0.84 – 0.90 (m, 3H, H8'), 1.23 – 1.34 (m, 8H, H4', H5', H6', H7'), 1.37 – 1.44 (m, 2H, H3'), 1.65 – 1.73 (m, 2H, H2'), 2.52 – 2.53 (m, 2H, Hb), 2.78 (t, J = 7.7 Hz, 2H, Ha), 3.92 (t, J = 6.5 Hz, 2H, H1'), 6.72 – 6.75 (m, 1H, H4), 6.76 – 6.79 (m, 2H, H2, H6), 7.16 (t, J = 7.8 Hz, 1H, H5).
$^{13}\text{C-NMR}$ (151 MHz, DMSO-d_6)	δ 14.0 (q, C8'), 22.1 (t, C7'), 25.6 (t, C3'), 28.7 (t, C4' or C5'), 28.7 (t, C2'), 28.8 (t, C4' or C5'), 30.4 (t, Ca), 31.2 (t, C6'), 35.3 (t, Cb), 67.2 (t, C1'), 111.8 (d, C4), 114.4 (d, C2), 120.3 (d, C6), 129.3 (d, C5), 142.5 (s, C1), 158.7 (s, C3), 173.8 (s, Cc).
HRMS (ESI)	not found, pos. mode.

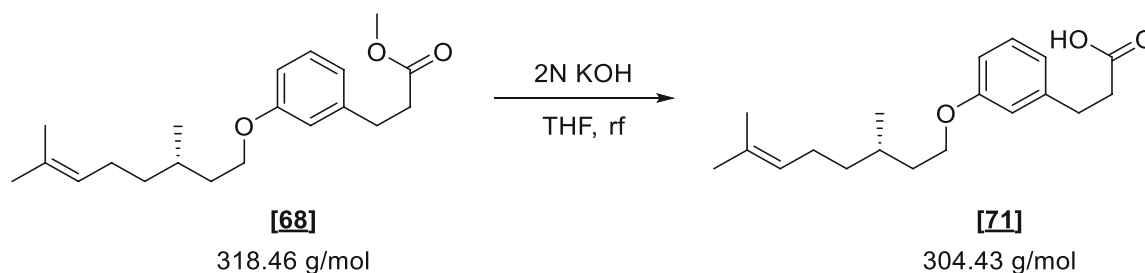
E III.3.9 (S)-3-(3-((3,7-Dimethyloctyl)oxy)phenyl)propanoic acid [70]



(S)-3-(3-((3,7-Dimethyloctyl)oxy)phenyl)propanoic acid [70] was synthesized according to general procedure F using methyl methyl (S)-3-(3-((3,7-dimethyloctyl)oxy)phenyl)propanoate [67] (0.25 g, 0.78 mmol). The product could be used for further experimentation without additional purification.

Yield	0.23 g (quant.)
Appearance	colorless oil
TLC	R_f (LP/EtOAc – 5:1) = 0.25 (anisaldehyde)
Reaction scale	0.25 g (0.75 mmol)
Substrate concentration	0.28 M
Purification	pure after work-up
Sum formula, m.w.	$C_{19}H_{30}O_3$, 306.45 g/mol
Optical rotation	$[\alpha]_D^{20} = -2.7$ ($c = 1.00$, $CHCl_3$)
1H-NMR (600 MHz, DMSO-d_6)	δ 0.86 (d, $J = 6.6$ Hz, 6H, H8', H9'), 0.91 (d, $J = 6.7$ Hz, 3H, H10'), 1.10 – 1.20 (m, 3H, (H4')', H6'), 1.23 – 1.27 (m, 1H, (H5')'), 1.28 – 1.36 (m, 2H, H4', H5'), 1.47 – 1.56 (m, 2H, (H2')', H7'), 1.60 – 1.66 (m, 1H, H3'), 1.69 – 1.77 (m, 1H, H2'), 2.52 – 2.54 (m, 2H, Hb), 2.78 (t, $J = 7.7$ Hz, 2H, Ha), 3.92 – 4.01 (m, 2H, H1'), 6.74 (dd, $J = 2.5, 8.1$ Hz, 1H, H4), 6.76 – 6.80 (m, 2H, H2, H6), 7.16 (t, $J = 7.8$ Hz, 1H, H5).
^{13}C-NMR (151 MHz, DMSO-d_6)	δ 19.5 (q, C10'), 22.5 (q, C8' or C9'), 22.6 (q, C8' or C9'), 24.1 (t, C5'), 27.4 (d, C7'), 29.3 (d, C3'), 30.4 (t, Ca), 35.2 (t, Cb), 35.7 (t, C2'), 36.6 (t, C4'), 38.7 (t, C6'), 65.5 (s, C1'), 111.9 (d, C4), 114.4 (d, C2), 120.3 (d, C6), 129.3 (d, C5), 142.5 (s, C1), 158.7 (s, C3), 173.8 (s, Cc).
HRMS (ESI)	not found, pos. mode.

E III.3.10 (S)-3-(3-((3,7-Dimethyloct-6-en-1-yl)oxy)phenyl)propanoic acid [71]



(S)-3-(3-((3,7-Dimethyloct-6-en-1-yl)oxy)phenyl)propanoic acid [71] was synthesized according to general procedure F using methyl (S)-3-(3-((3,7-dimethyloct-6-en-1-yl)oxy)phenyl)propanoate [68] (0.25 g, 0.78 mmol). The product could be used for further experimentation without additional purification.

Yield 0.23 g (quant.)
Appearance colorless oil
TLC R_f (LP/EtOAc – 5:1) = 0.25 (anisaldehyde)

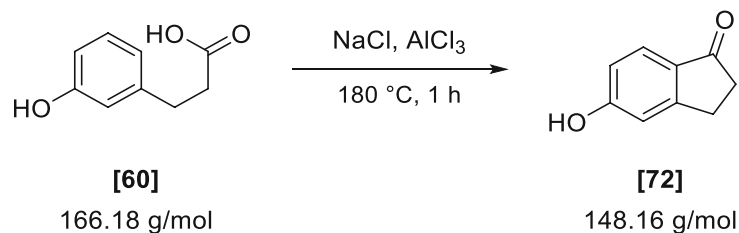
Reaction scale 0.25 g (0.75 mmol)
Substrate concentration 0.28 M
Purification pure after work-up
Sum formula, m.w. $C_{19}H_{28}O_3$, 304.43 g/mol
Optical rotation $[\alpha]_D^{20} = -3.6$ (c = 1.00, $CHCl_3$)

1H -NMR (600 MHz, DMSO- d_6) δ 0.92 (d, $J = 6.6$ Hz, 3H, H10'), 1.15 – 1.22 (m, 1H, (H4')'), 1.33 – 1.40 (m, 1H, H4'), 1.49 – 1.55 (m, 1H, (H2')'), 1.57 (s, 3H, H9'), 1.60 – 1.68 (m, 1H, H3'), 1.65 (s, 3H, H8'), 1.71 – 1.78 (m, 1H, H2'), 1.91 – 2.04 (m, 2H, H5'), 2.52 – 2.56 (m, 2H, Hb), 2.78 (t, $J = 7.7$ Hz, 2H, Ha), 3.92 – 4.00 (m, 2H, H1'), 5.10 (tq, $J = 1.4, 7.0$ Hz, 1H, H6'), 6.74 (dd, $J = 2.5, 8.2$ Hz, 1H, H4), 6.76 – 6.80 (m, 2H, H2, H6), 7.16 (t, $J = 7.8$ Hz, 1H, H5).

^{13}C -NMR (151 MHz, DMSO- d_6) δ 17.5 (q, C9'), 19.3 (q, C10'), 24.9 (t, C5'), 25.5 (q, C8'), 29.0 (d, C3'), 30.4 (t, Ca), 35.2 (t, Cb), 35.6 (t, C2'), 36.6 (t, C4'), 65.5 (t, C1'), 111.9 (d, C4), 114.4 (d, C2), 120.3 (d, C6), 124.6 (d, C6'), 129.3 (d, C5), 130.5 (s, C7'), 142.5 (s, C1), 158.7 (d, C3), 173.8 (s, Cc).

HRMS (ESI) not found, pos. mode.

E III.3.11 5-Hydroxy-2,3-dihydro-1H-indanone [72]



The product was synthesized according to a literature procedure²¹⁵.

Procedure: NaCl (84,4 mg, 1.44 mmol, 1.20 equiv.) and AlCl₃ (802 mg, 6.02 mmol, 5.00 equiv.) were homogenized and filled into a 25 mL flame-dried Schlenk flask. The vessel was evacuated and backfilled with argon using standard Schlenk techniques. Subsequently, the mixture was heated to 180 °C *via* an oil bath which caused the melting of all solids. The flask was removed from the heating bath, allowing the viscous mixture to cool and solidify. Under gentle argon counter-flow, 3-(3-hydroxyphenyl)propionic acid [60] (0.20 g, 1.20 mmol, 1.00 equiv.) was added on top of the solid, and the reaction was heated back to 180 °C. The mixture was stirred for 1 hour, during which gas evolution was observed. After the formation of gas had ceased, the reaction vessel was first slowly cooled to room temperature and then placed into an ice bath.

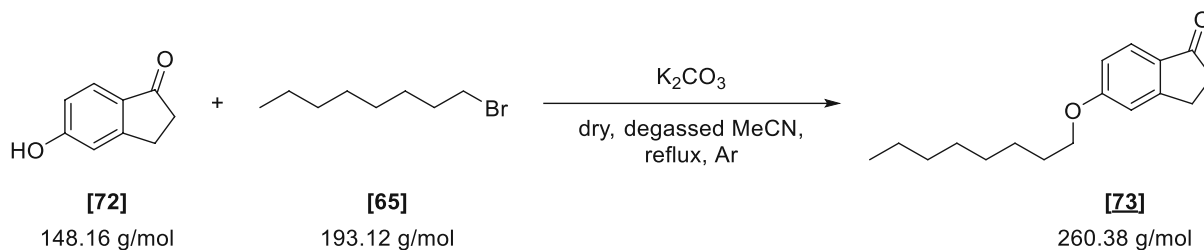
Work-up: The reaction was quenched with the addition of solid ice (10 g), which caused a strongly exothermic reaction. The solution was diluted with 1N HCl (20 mL), and the aqueous phase was extracted four times with EtOAc (4 x 10 mL). The combined organics were dried over Na₂SO₄ and concentrated. Upon removal of the solvent, 0.12 g (70 %) of 5-hydroxy-2,3-dihydro-1H-indanone [72] was obtained as light-yellow oil that crystallized upon standing. The resulting material could be used directly for the next step without further purification.

Yield	0.12 g (70 %)
Appearance	light yellow crystals
TLC	R _f (EtOAc) = 0.63 (anisaldehyde)
M.p.	179.5 – 182.6 °C (lit. ²⁷⁴ 183 – 185 °C)
Reaction scale	0.20 g (1.20 mmol)
Substrate concentration	-
Purification	pure after work-up
Sum formula, m.w.	C ₉ H ₈ O ₂ , 148.16 g/mol

¹H-NMR (600 MHz, MeOD-*d*₄) δ 2.64 (t, *J* = 5.9 Hz, 2H, Ha), 3.07 (t, *J* = 5.9 Hz, 2H, Hb), 6.81 – 6.84 (m, 1H, H5), 6.87 (d, *J* = 2.1 Hz, 1H, H2), 7.58 (d, *J* = 8.4 Hz, 1H, H5).

¹³C-NMR (151 MHz, MeOD-*d*₄) δ 26.5 (t, Cb), 37.3 (t, Ca), 113.0 (d, C2), 117.1 (d, C4), 126.5 (d, C5), 129.9 (s, C6), 160.8 (s, C1), 165.9 (s, C3), 208.3 (s, Cc).

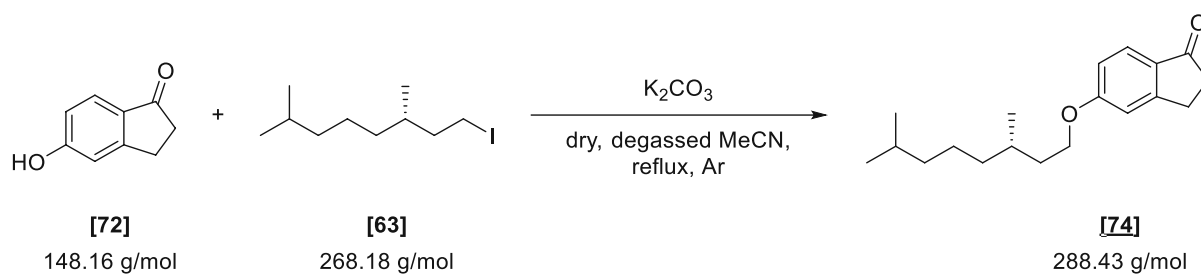
E III.3.12 5-(Octyloxy)-2,3-dihydro-1H-inden-1-one [73]



5-(Octyloxy)-2,3-dihydro-1H-inden-1-one [73] was synthesized according to general procedure g using methyl 5-hydroxy-2,3-dihydro-1H-inden-1-one [72] (50 mg, 0.34 mmol).

Yield	45 mg (51 %)
Appearance	yellow oil
TLC	R_f (LP/EtOAc – 3:1) = 0.82 (anisaldehyde)
Reaction scale	50 mg (0.34 mmol)
Substrate concentration	0.28 M
Purification	column chromatography (silica) LP/EtOAc 10:1
Sum formula, m.w.	$C_{17}H_{24}O_2$, 260.38 g/mol
$^1\text{H-NMR}$ (600 MHz, CDCl_3)	δ 0.89 (t, J = 6.8 Hz, 3H, H8'), 1.22 – 1.40 (m, 8H, H4', H5', H6', H7'), 1.46 (p, J = 6.0, 8.0, 15.0 Hz, 2H, H3'), 1.77 – 1.85 (m, 2H, H2'), 2.62 – 2.69 (m, 2H, Hb), 3.08 (t, J = 5.7 Hz, 2H, Ha), 4.02 (t, J = 6.5 Hz, 2H, H1'), 6.86 – 6.91 (m, 2H, H2, H4), 7.68 (d, J = 8.9 Hz, 1H, H5).
$^{13}\text{C-NMR}$ (151 MHz, CDCl_3)	δ 14.2 (q, C8'), 22.8 (t, C7'), 26.0 (t, Ca), 26.1 (t, C3'), 29.2 (t, C2'), 29.4 (t, C4' or C5'), 29.4 (t, C4' or C5'), 31.9 (t, C6'), 36.6 (t, Cb), 68.6 (t, C1'), 110.4 (d, C2), 115.8 (d, C4), 125.5 (d, C5), 130.3 (s, C6), 158.3 (s, C1), 165.0 (s, C3), 205.4 (s, Cc).
HRMS (ESI)	calc. for $C_{17}H_{25}O_2^+$ [M+H] $^+$ 261.1849, found 261.1800 – Δ = -18.76 ppm.

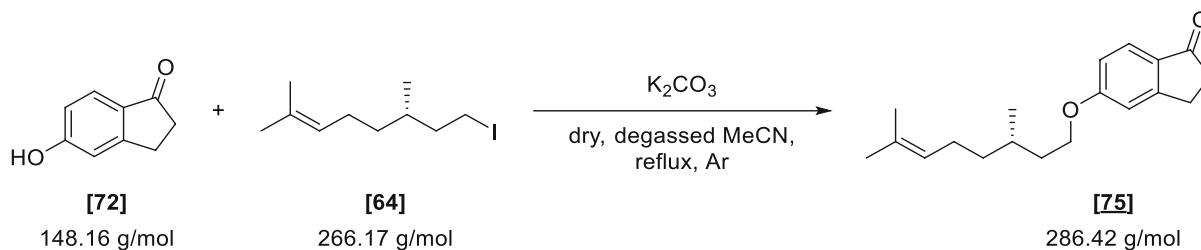
E III.3.13 (S)-5-((3,7-Dimethyloctyl)oxy)-2,3-dihydro-1H-inden-1-one [74]



(S)-5-((3,7-Dimethyloctyl)oxy)-2,3-dihydro-1H-inden-1-one [74] was synthesized according to general procedure g using methyl 5-hydroxy-2,3-dihydro-1H-inden-1-one [72] (35 mg, 0.24 mmol).

Yield	45 mg (72 %)
Appearance	yellow oil
TLC	R_f (LP/EtOAc – 3:1) = 0.80 (anisaldehyde)
Reaction scale	35 mg (0.24 mmol)
Substrate concentration	0.28 M
Purification	column chromatography (silica) LP/EtOAc 10:1
Sum formula, m.w.	$C_{19}H_{28}O_2$, 288.43 g/mol
Optical rotation	$[\alpha]_D^{20} = -3.3$ (c = 0.50, $CHCl_3$)
1H-NMR (600 MHz, $CDCl_3$)	δ 0.88 (d, $J = 6.6$ Hz, 6H, H8', H9'), 0.95 (d, $J = 6.6$ Hz, 3H, H10'), 1.13 – 1.21 (m, 3H, (H4')', H6), 1.23 – 1.40 (m, 3H, H4', H5'), 1.47 – 1.58 (m, 1H, H7'), 1.57 – 1.68 (m, 1H, (H2')'), 1.65 – 1.72 (m, 1H, H3'), 1.81 – 1.90 (m, 1H, H2'), 2.62 – 2.69 (m, 2H, Hb), 3.08 (t, $J = 5.8$ Hz, 2H, Ha), 4.02 – 4.13 (m, 2H, H1'), 6.86 – 6.91 (m, 2H, H2, H4), 7.68 (d, $J = 9.4$ Hz, 1H, H5).
^{13}C-NMR (151 MHz, $CDCl_3$)	δ 19.8 (q, C10'), 22.7 (q, C8' or C9'), 22.8 (q, C8' or C9'), 24.8 (t, C5'), 26.0 (t, Ca), 28.1 (d, C7'), 30.0 (d, C3'), 36.1 (t, C2'), 36.6 (t, Cb), 37.4 (t, C4'), 39.4 (t, C6'), 67.0 (t, C1'), 110.4 (d, C4), 115.8 (d, C2), 125.5 (d, C5), 130.4 (s, C6), 158.3 (s, C1), 165.0 (s, C3), 205.5 (s, Cc).
HRMS (ESI)	calc. for $C_{19}H_{29}O_2^+$ $[M+H]^+$ 289.2162, found 289.2134 – $\Delta = -9.68$ ppm.

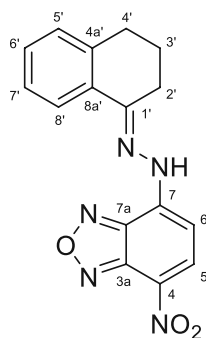
E III.3.14 (S)-5-((3,7-Dimethyloct-6-en-1-yl)oxy)-2,3-dihydro-1H-inden-1-one [75]



(S)-5-((3,7-Dimethyloct-6-en-1-yl)oxy)-2,3-dihydro-1H-inden-1-one [75] was synthesized according to general procedure g using methyl 5-hydroxy-2,3-dihydro-1H-inden-1-one [72] (35 mg, 0.24 mmol).

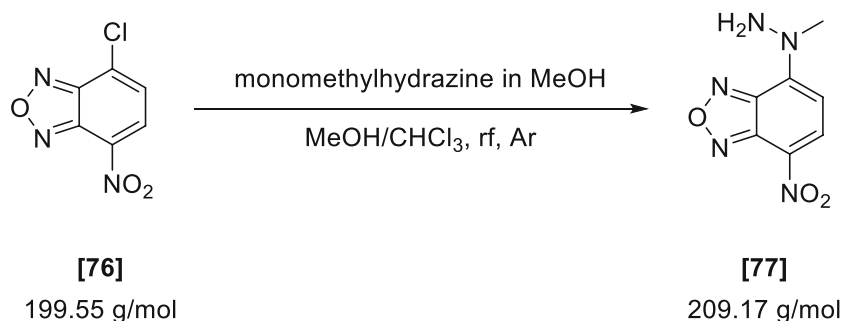
Yield	42 mg (62 %)
Appearance	yellow oil
TLC	R_f (LP/EtOAc – 3:1) = 0.82 (anisaldehyde)
Reaction scale	35 mg (0.24 mmol)
Substrate concentration	0.28 M
Purification	column chromatography (silica) LP/EtOAc 10:1
Sum formula, m.w.	$C_{19}H_{26}O_2$, 286.42 g/mol
Optical rotation	$[\alpha]_D^{20} = -4.2$ (c = 0.50, $CHCl_3$)
1H-NMR (600 MHz, $CDCl_3$)	δ 0.97 (d, $J = 6.6$ Hz, 3H, H10'), 1.24 (dddd, $J = 5.9, 7.7, 9.5, 13.5$ Hz, 1H, (H4')'), 1.34 – 1.45 (m, 1H, H4'), 1.61 (d, $J = 1.2$ Hz, 3H, H9'), 1.59 – 1.67 (m, 1H, (H2')'), 1.69 (q, $J = 1.3$ Hz, 3H, H8'), 1.67 – 1.74 (m, 1H, H3'), 1.86 (dtd, $J = 5.2, 7.0, 14.0$ Hz, 1H, H2'), 1.92 – 2.09 (m, 2H, H5'), 2.62 – 2.69 (m, 2H, Hb), 3.07 (t, $J = 6.0$ Hz, 2H, Ha), 4.01 – 4.13 (m, 2H, H1'), 5.10 (tdq, $J = 1.3, 2.8, 7.1$ Hz, 1H, H6'), 6.86 – 6.91 (m, 2H, H2, H4), 7.68 (d, $J = 9.1$ Hz, 1H, H5).
^{13}C-NMR (151 MHz, $CDCl_3$)	δ 17.8 (q, C9'), 19.7 (q, C10'), 25.6 (t, C5'), 25.9 (q, C8'), 26.0 (t, Ca), 29.6 (d, C3'), 36.1 (t, C2'), 36.6 (t, Cb), 37.2 (t, C4'), 66.9 (t, C1'), 110.4 (d, C2), 115.8 (d, C4), 124.7 (d, C6'), 125.5 (d, C5), 130.4 (s, C6), 131.6 (s, C7'), 158.3 (s, C1), 165.0 (s, C3), 205.5 (s, Cc).
HRMS (ESI)	calc. for $C_{19}H_{27}O_2^+$ [M+H] $^+$ 287.2006, found 287.1981 – $\Delta = -8.70$ ppm.

E III.4 Part IV – Studies towards the synthesis and evaluation of fluorogenic adducts with NBD-H-type reagents



NMR assignments of core structures in this chapter were given according to the following example.

E III.4.1 4-(1-Methylhydrazineyl)-7-nitrobenzo[c][1,2,5]oxadiazole (NBD-MH) [77]

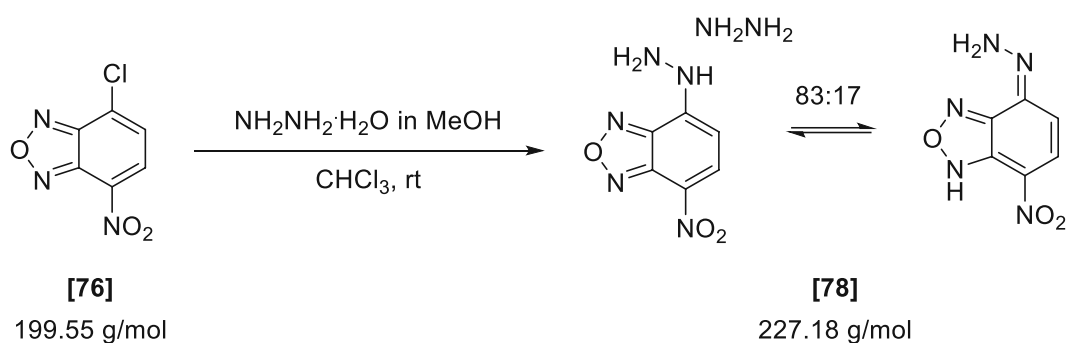


The product was synthesized according to a literature procedure¹²⁹.

Procedure: A 250 mL 3-neck RBF was charged with 4-chloro-7-nitrobenzo[2,1,3-d]oxadiazole [76] (1.00 g, 5.01 mmol, 1.00 equiv.), which was dissolved in CHCl₃ (80 mL). Subsequently, a solution of monomethylhydrazine (2.10 mL, 1.85 g, 40.08 mmol, 8.00 equiv.) in MeOH (100 mL) was added, and the reaction was refluxed for 30 minutes. Upon cooling, the product precipitated as deep red crystalline material. The solids were collected and thoroughly washed with fresh HPLC grade MeOH (3 x 5 mL) to yield 0.65 g (64 %) of 4-(1-methylhydrazineyl)-7-nitrobenzo[c][1,2,5]oxadiazole (NBD-MH) [77] as red crystals.

Yield 0.65 g (64 %)
Appearance red crystals

Reaction scale	1.00 g (5.01 mmol)
Substrate concentration	0.03 M
Purification	-
Sum formula, m.w.	C ₇ H ₇ N ₅ O ₃ , 209.17 g/mol
M.p.	decomp. > 130 °C
¹ H-NMR (400 MHz, DMSO- <i>d</i> ₆)	δ 3.93 (s, 3H, -NCH ₃), 6.06 (s, 2H, -NH ₂), 6.71 (s, 1H, H6), 8.42 (d, <i>J</i> = 9.6 Hz, 1H, H5).
¹³ C-NMR (101 MHz, DMSO- <i>d</i> ₆)	δ = 46.5 (q, -NCH ₃), 102.3 (d, C6), 118.7 (s, C7), 136.5 (d, C5), 144.2 (s, C4 or C7a), 145.5 (s, C3a), 145.8 (s, C4 or C7a).

E III.4.2 4-Hydrazineyl-7-nitrobenzo[*c*][1,2,5]oxadiazole hydrazine adduct (NBD-H) [78]

The product was synthesized according to a literature procedure^{127,129}.

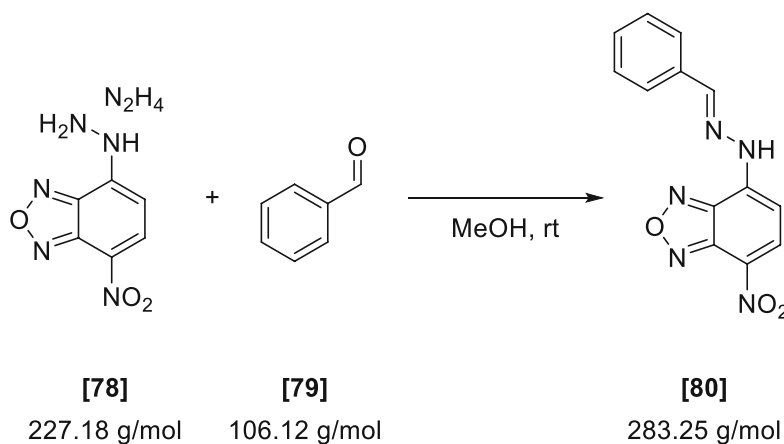
Procedure: A 2 L was charged with 4-chloro-7-nitrobenzo[2,1,3-*d*]oxadiazole [76] (1.00 g, 5.01 mmol, 1.00 equiv.), which was dissolved in CHCl₃ (500 mL) under argon. Subsequently, a solution of 65% hydrazine monohydrate (7.70 mL, 5.23 g, 104 mmol, 20.0 equiv.) in MeOH (500 mL) was added in 1 hour under vigorous stirring. Already after a few minutes, the formation of a yellow precipitant could be observed. Following the completed addition, the reaction mixture was stirred for 3 hours at room temperature. The product was isolated by suction filtration and was washed with minimal amounts of MeOH (2 x 5 mL) and then thoroughly with CH₂Cl₂ (2 x 30 mL). 1.03 g (90 %) of 4-hydrazineyl-7-nitrobenzo[*c*][1,2,5]oxadiazole (NBD-H) [78] was isolated as ochre solid as known 1:1 adduct with hydrazine and was used for further experimentation without further purification. NMR measurements exposed a slow equilibrium between two different tautomers.

Yield	1.03 g (90 %)
Appearance	ochre solid

Reaction scale	1.00 g (5.01 mmol)
Substrate concentration	0.01 M
Purification	-
Sum formula, m.w.	C ₆ H ₉ N ₇ O ₃ (hydrazine adduct), 227.18 g/mol
M.p.	185 – 188 °C

¹ H-NMR (400 MHz, DMSO- <i>d</i> ₆)	δ 5.84 (d, J = 10.3 Hz, 1H, H6 _(major)), 6.09 (d, J = 10.5 Hz, 1H, H6 _(minor)), 7.00 (d, J = 10.3 Hz, 1H, H5 _(major)), 7.13 (s, 2H, -NH ₂ _(major)), 7.19 (d, J = 10.5 Hz, 1H, H5 _(minor)), 8.07 (s, 2H, -NH ₂ _(minor)).
¹³ C-NMR (101 MHz, DMSO- <i>d</i> ₆)	δ 101.9 (d, C6 _(minor)), 108.5 (C4 _(major)), 109.5 (C4 _(minor)), 113.1 (d, C6 _(major)), 120.9 (d, C5 _(major)), 124.9 (d, C5 _(minor)), 128.6 (C7 _(major)), 131.0 (C7 _(minor)), 144.8 (C7a _(major)), 146.8 (C7a _(minor)), 147.5 (C3a _(major)), 148.9 (C3a _(minor)).

E III.4.3 (E)-4-(2-Benzylidenehydrazineyl)-7-nitrobenzo[c][1,2,5]oxadiazole [80]



Procedure: A 50 mL RBF was charged with NBD-H **[78]** (90 mg, 0.39 mmol, 1.00 equiv.), which was suspended in MeOH (30 mL). Subsequently, freshly distilled benzaldehyde **[79]** (0.40 mL, 0.42 g, 3.96 mmol, 10.00 equiv.) was added to the ochre suspension, immediately turning the reaction deep red. A slow dissolution of the starting material with concomitant precipitation of the hydrazone was observed. The reaction was thus stirred for 30 minutes at room temperature and then cooled to 0 °C to facilitate crystallization. The product was isolated by suction filtration and was washed with MeOH (3 x 2 mL) and then thoroughly with Et₂O (3 x 5 mL). The solids were dried *in vacuo* to yield 80 mg (71 %) of (E)-4-(2-benzylidenehydrazineyl)-7-nitrobenzo[c][1,2,5]oxadiazole **[80]** as a deep red solid. The product was used for further experimentation without further purification.

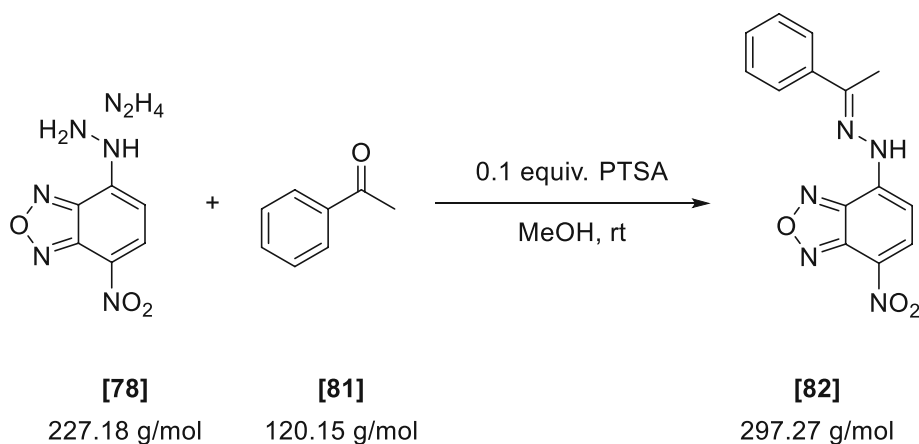
Yield	80 mg (71 %)
Appearance	deep red solid

Reaction scale	90 mg (0.39 mmol)
Substrate concentration	0.01 M
Purification	-
Sum formula, m.w.	C ₁₃ H ₉ N ₅ O ₃ , 283.25 g/mol
M.p.	218 – 223 °C

¹H-NMR (400 MHz, DMSO-*d*₆) δ 7.17 (br s, 1H, H6), 7.51 (s, 3H, H3', H4', H5'), 7.84 (br s, 2H, H2', H6'), 8.31 – 8.72 (m, 2H, H5, -N=CH-), 12.98 (s, 1H, -NH-).

¹³C-NMR (101 MHz, DMSO-*d*₆) δ 102.4 (d, C6), 123.8 (s, C4), 128.0 (d, 2C, C2', C6'), 129.5 (d, 2C, C3', C5'), 131.3 (d, C4'), 134.1 (s, C1'), 137.5 (d, C5), 141.1 (s, C3a or C7), 143.6 (s, C7a), 144.7 (s, C3a or C7), 150.3 (d, -N=CH-).

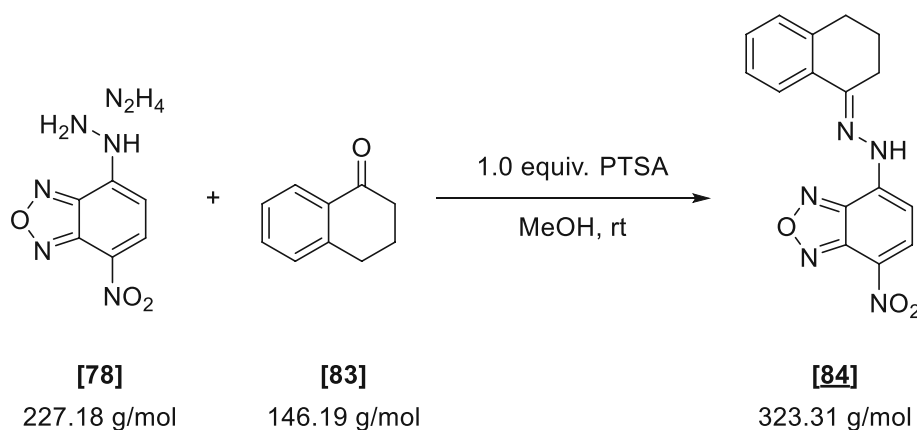
E III.4.4 (E)-4-Nitro-7-(2-(1-phenylethylidene)hydrazineyl)benzo[c][1,2,5]oxadiazole [82]



Procedure: A 50 mL RBF was charged with NBD-H [78] (90 mg, 0.39 mmol, 1.00 equiv.), which was suspended in MeOH (30 mL). Subsequently, acetophenone [81] (0.46 mL, 0.48 g, 3.96 mmol, 10.00 equiv.) was added to the ochre suspension. To force the reaction addition of PTSA (7 mg, 0.04 mmol, 0.10 equiv.) was needed, instantly turning the reaction deep red. A slow dissolution of the starting material with concomitant precipitation of the hydrazone was observed. The reaction was thus stirred for 30 minutes at room temperature and then cooled to 0 °C to facilitate crystallization. The product was isolated by suction filtration and was washed thoroughly with MeOH (3 x 5 mL) and then with Et₂O (3 x 5 mL). The solids were dried *in vacuo* to yield 100 mg (85 %) of ((E)-4-nitro-7-(2-(1-phenylethylidene)hydrazineyl)benzo[c][1,2,5]oxadiazole [82] as bright red solid. The product was used for further experimentation without further purification.

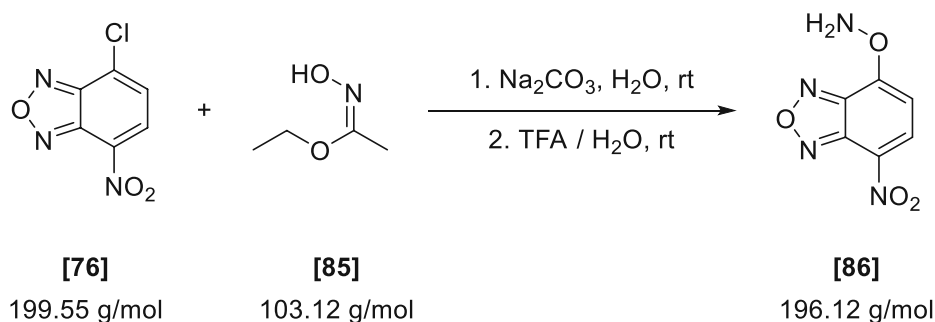
Yield	100 mg (85 %)
Appearance	bright red solid
Reaction scale	90 mg (0.39 mmol)
Substrate concentration	0.02 M
Purification	-
Sum formula, m.w.	C ₁₄ H ₁₁ N ₅ O ₃ , 297.27 g/mol
M.p.	200 – 202 °C
¹H-NMR (400 MHz, DMSO-<i>d</i>₆)	δ 2.52 (s, 3H, -CH ₃), 7.11 (d, <i>J</i> = 8.9 Hz, 1H, H ₆), 7.49 (dd, <i>J</i> = 5.1, 2.0 Hz, 3H, H _{3'} , H _{4'} , H _{5'}), 8.00 (dd, <i>J</i> = 6.7, 3.0 Hz, 2H, H _{2'} , H _{6'}), 8.60 (d, <i>J</i> = 8.9 Hz, 1H, H ₅), 11.75 (s, 1H, -NH-).
¹³C-NMR (101 MHz, DMSO-<i>d</i>₆)	δ 14.7 (-CH ₃), 103.1 (d, C ₆), 123.4 (s, C ₄), 126.7 (d, C _{2'} , C _{5'}), 128.6 (d, C _{3'} , C _{5'}), 130.1 (s, C _{4'}), 136.6 (d, C ₅), 137.3 (s, C _{1'}), 141.8 (s, C _{3a} or C ₇), 143.3 (s, C _{7a}), 144.4 (s, C _{3a} or C ₇).

E III.4.5 **(*E*)-4-(2-(3,4-Dihydronaphthalen-1(2H)-ylidene)hydrazineyl)-7-nitrobenzo[*c*][1,2,5]oxadiazole [84]**



Procedure: A 50 mL RBF was charged with NBD-H [78] (100 mg, 0.44 mmol, 1.00 equiv.), which was suspended in MeOH (30 mL). Subsequently, alpha-tetralone [83] (0.58 mL, 0.64 g, 4.40 mmol, 10.00 equiv.) and PTSA (84 mg, 0.44 mmol, 1.00 equiv.) were added, immediately dissolving all particulates, and turning the reaction deep red. After 5 minutes, slow precipitation of red solids could be observed. The stirring was immediately stopped to allow improved crystallization of the product, and the solution was left standing overnight. The bright red suspension was filtered directly through a mini-Por. 3 glass sinter funnel and washed thoroughly with fresh MeOH (4 x 2 mL) and Et₂O (3x, approx. 6 mL). The solids were dried *in vacuo* to yield 120 mg (84%) of (*E*)-4-(2-(3,4-dihydronaphthalen-1(2H)-ylidene)hydrazineyl)-7-nitrobenzo[*c*][1,2,5]oxadiazole [84] as deep green crystals. The product was used for further experimentation without further purification.

Yield	120 mg (84 %)
Appearance	deep green crystals
Reaction scale	100 mg (0.44 mmol)
Substrate concentration	0.01 M
Purification	-
Sum formula, m.w.	C ₁₆ H ₁₃ N ₅ O ₃ , 323.31 g/mol
M.p.	204 – 206 °C
¹ H-NMR (400 MHz, DMSO- <i>d</i> ₆)	δ 1.91 (p, <i>J</i> = 6.2 Hz, 2H, -CH ₂ - (H3')), 2.82 (t, <i>J</i> = 6.0 Hz, 2H, Ar-CH ₂ (H4')), 2.92 (t, <i>J</i> = 6.4 Hz, 2H, -CH ₂ -C=N (H2')), 7.09 (d, <i>J</i> = 8.9 Hz, 1H, H5), 7.24 (d, <i>J</i> = 7.4 Hz, 1H, H5'), 7.28 – 7.40 (m, 2H, H6', H7'), 8.26 (d, <i>J</i> = 8.7 Hz, 1H, H8'), 8.58 (d, <i>J</i> = 8.9 Hz, 1H, H6), 11.70 (s, 1H, -NH-).
¹³ C-NMR (101 MHz, DMSO- <i>d</i> ₆)	δ 21.4 (t, -CH ₂ - (C3')), 26.4 (t, -CH ₂ -C=N (C2')), 28.8 (t, Ar-CH ₂ (C4')), 102.9 (d, C6), 123.2 (s, C4), 125.0 (d, C8'), 126.4 (d, C7'), 128.8 (d, C5'), 130.0 (d, C6'), 131.7 (s, C8a), 136.6 (d, C5), 140.6 (s, C4a'), 141.8 (s, C3a or C7), 143.3 (s, C7a), 144.5 (s, C3a or C7).
HRMS (ESI)	calc. for C ₁₆ H ₁₄ N ₅ O ₃ ⁺ [M+H] ⁺ 324.1091, found 324.1090 – Δ = -0.46 ppm.

E III.4.6 O-(7-Nitrobenzo[*c*][1,2,5]oxadiazol-4-yl)hydroxylamine [86]

The product was synthesized according to a modified literature procedure^{127,129}.

Procedure: A 50 mL RBF was charged with ethyl N-hydroxyacetimidate **[85]** (1.55 g, 15.03 mmol, 3.00 equiv.), which was suspended in dH₂O (30 mL). Following the addition of sodium carbonate (3.98 g, 37.58 mmol, 7.50 equiv.), the mixture was stirred for 10 minutes. Subsequently, 4-chloro-7-nitrobenzo[2,1,3-d]-oxadiazole **[76]** (1.00 g, 5.01 mmol, 1.00 equiv.) was added, and the reaction was stirred for 30 minutes at room temperature. The resulting brown-yellow precipitate was isolated by suction filtration and thoroughly washed with d.H₂O (2 x 10 mL). The solids were then transferred into a 250 mL RBF and dissolved in a 1:1 mixture of TFA/water (100 mL). The reaction was stirred for 3 hours, upon which TLC indicated full conversion.

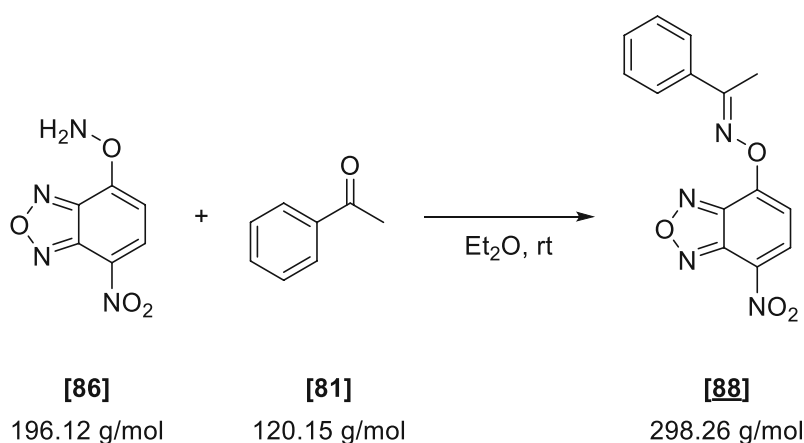
Work-up: The TFA was removed in vacuo, and the resulting aqueous solution was concentrated by lyophilization. The crude product was further purified *via* flash chromatography (CH₂Cl₂) over silica to yield 0.65 g (66 %) of O-(7-nitrobenzo[c][1,2,5]oxadiazol-4-yl)hydroxylamine (NBD-AO) **[86]** as ochre solid.

Yield	0.65 g (66 %)
Appearance	ochre solid
Reaction scale	1.00 g (5.01 mmol)
Substrate concentration	1. step: 0.17 M 2. step: 0.05 M
Purification	flash chromatography (silica) CH ₂ Cl ₂
Sum formula, m.w.	C ₆ H ₄ N ₄ O ₄ , 196.12 g/mol
M.p.	decomp. > 90 °C

¹H-NMR (400 MHz, DMSO-*d*₆) δ 5.84 (d, *J* = 9.7 Hz, 1H, H6), 8.27 (d, *J* = 9.7 Hz, 1H, H5).

¹³C-NMR (101 MHz, DMSO-*d*₆) δ 110.8 (d, C6), 113.1 (s, C4), 137.8 (d, C5), 146.5 (s, C3a), 148.0 (s, C7a), 171.6 (s, C7).

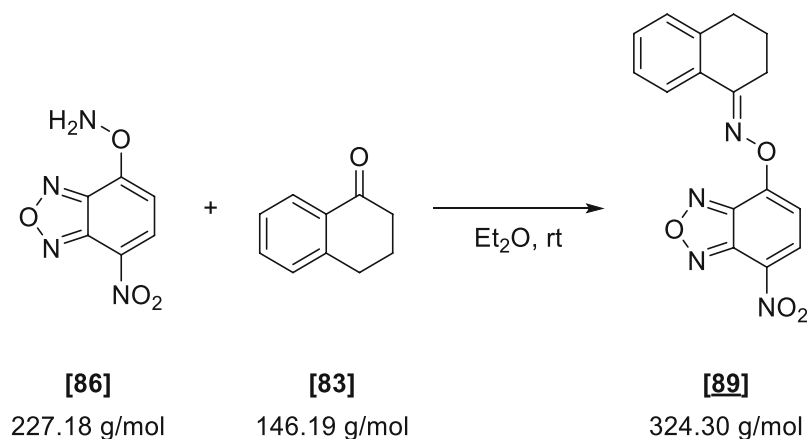
E III.4.7 (*E*)-1-Phenylethan-1-one O-(7-nitrobenzo[c][1,2,5]oxadiazol-4-yl) oxime **[88]**



Procedure: A 50 mL RBF was charged with NBD-AO **[86]** (50 mg, 0.26 mmol, 1.00 equiv.), which was dissolved in Et₂O (15 mL). Subsequently, acetophenone **[81]** (0.16 mL, 0.16 g, 1.53 mmol, 10.00 equiv.) was added immediately, turning the solution deep yellow. After 5 minutes, slow precipitation of yellow solids could be observed. The reaction was stirred for 30 minutes at room temperature and then cooled to 0 °C to facilitate crystallization. The product was isolated by suction filtration and was washed with small amounts of Et₂O (3 x 5 mL). The solids were dried *in vacuo* to yield 59 mg (76 %) of (*E*)-benzaldehyde O-(7-nitrobenzo[c][1,2,5]oxadiazol-4-yl) oxime **[88]** as yellow solid. The product was used for further experimentation without further purification.

Yield	58 mg (76 %)
Appearance	yellow solid
Reaction scale	50 mg (0.26 mmol)
Substrate concentration	0.02 M
Purification	-
Sum formula, m.w.	C ₁₄ H ₁₀ N ₄ O ₄ , 298.26 g/mol
M.p.	decomp. > 120 °C
¹ H-NMR (400 MHz, DMSO- <i>d</i> ₆)	δ 2.63 (s, 3H, -CH ₃), 7.43 – 7.66 (m, 4H, H ₆ , H _{3'} , H _{4'} , H _{5'}), 7.83 – 8.01 (m, 2H, H _{2'} , H _{6'}), 8.75 (d, <i>J</i> = 8.4 Hz, 1H, H ₅).
¹³ C-NMR (101 MHz, DMSO- <i>d</i> ₆)	δ 14.6 (q, -CH ₃), 108.6 (d, C ₆), 127.6 (d, C _{2'} , C _{6'}), 129.4 (d, C _{3'} , C _{5'}), 130.4 (s, C ₄), 131.8 (d, C _{4'}), 134.1 (s, C _{1'}), 136.4 (d, C ₅), 144.3 (s, C _{7a}), 144.7 (s, C _{3a}), 153.2 (s, C ₇), 164.9 (s, -C=N-).
HRMS (ESI)	not found.

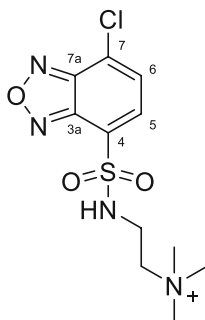
E III.4.8 (E)-3,4-Dihydronaphthalen-1(2H)-one O-(7-nitrobenzo[c][1,2,5]oxadiazol-4-yl) oxime [89]



Procedure: A 50 mL RBF was charged with NBD-AO [86] (50 mg, 0.26 mmol, 1.00 equiv.), which was dissolved in Et₂O (15 mL). Subsequently, alpha-tetralone [83] (0.34 mL, 0.37 g, 2.55 mmol, 10.00 equiv.) was added immediately, turning the solution deep yellow. After 5 minutes, slow precipitation of yellow solids could be observed. The reaction was stirred for 30 minutes at room temperature and then cooled to 0 °C to facilitate crystallization. The product was isolated by suction filtration and was washed with small amounts of Et₂O (3 x 5 mL). The solids were dried *in vacuo* to yield 58 mg (70 %) of (E)-3,4-dihydronaphthalen-1(2H)-one O-(7-nitrobenzo[c][1,2,5]oxadiazol-4-yl) oxime [89] as bright yellow solid. The product was used for further experimentation without further purification.

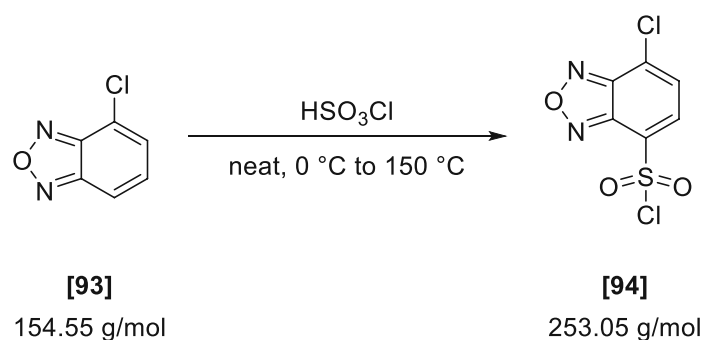
Yield	58 mg (76 %)
Appearance	bright yellow solid
Reaction scale	50 mg (0.26 mmol)
Substrate concentration	0.02 M
Purification	-
Sum formula, m.w.	C ₁₆ H ₁₂ N ₄ O ₄ , 324.30 g/mol
M.p.	decomp. > 160 °C
¹ H-NMR (400 MHz, DMSO- <i>d</i> ₆)	δ 1.91 (p, <i>J</i> = 6.2 Hz, 2H, -CH ₂ - (H3')), 2.78 – 2.90 (m, 2H, Ar-CH ₂ - (H4')), 3.11 (t, <i>J</i> = 6.5 Hz, 2H, -CH ₂ -C=N (H2')), 7.35 (t, <i>J</i> = 8.3 Hz, 2H, H5', H7'), 7.48 (t, <i>J</i> = 7.3 Hz, 1H, H6'), 7.62 (d, <i>J</i> = 8.4 Hz, 1H, H6), 8.15 (d, <i>J</i> = 7.8 Hz, 1H, H8'), 8.76 (d, <i>J</i> = 8.4 Hz, 1H, H5).
¹³ C-NMR (101 MHz, DMSO- <i>d</i> ₆)	δ 21.3 (t, -CH ₂ - (C3')), 25.5 (t, -CH ₂ -C=N (C2')), 29.1 (t, Ar-CH ₂ - (C4')), 108.5 (d, C6), 125.3 (d, C8'), 127.1 (d, C7'), 128.1 (s, C8a'), 129.7 (d, C5'), 130.2 (s, C4), 131.9 (d, C6'), 136.4 (d, C5), 142.2 (s, C4a'), 144.3 (s, C7a), 144.7 (s, C3a), 153.4 (s, C7), 163.3 (s, -C=N-).
HRMS (ESI)	not found.

E III.5 Part V – Improving water solubility of NBD-H /-HA reagents



NMR assignments of core structures in this chapter were given according to the following carbon skeleton.

E III.5.1 7-Chlorobenzo[c][1,2,5]oxadiazole-4-sulfonyl chloride [94]



The product was synthesized according to a literature procedure²³⁵.

Procedure: A flame-dried 10 mL RBF was charged with 4-chloro-2,1,3-benzoxadiazole [93] (1.00 g, 6.47 mmol, 1.00 equiv.) and then evacuated and backfilled with argon using standard Schlenk techniques. The vessel was submerged in an ice-water bath for 5 minutes, and then chlorosulfonic acid (3.00 mL, 5.28 g, 45.29 mmol, 7.00 equiv.) was added dropwise with strong stirring. The addition should be performed < 2 minutes, as the strong corrosiveness of the acid readily attacks the syringe. After the addition of approx. 1 mL of acid, all particulates had dissolved. The deep yellow solution was heated to 150 °C for 4 hours, upon which TLC indicated full conversion. Refrain from the usage of septa, as they can be trashed afterward.

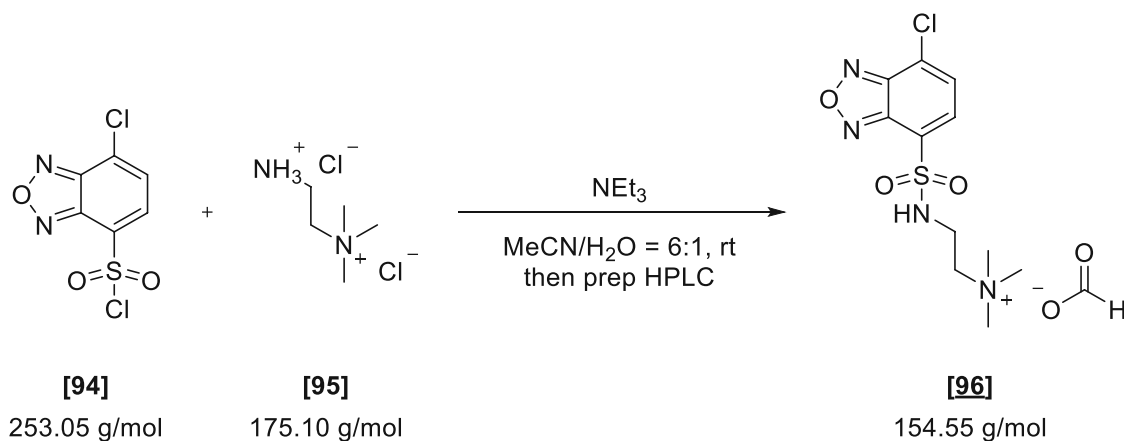
Work-up: The reaction was cooled to room temperature and was directly poured onto solid ice (a strong exothermic reaction!), causing immediate precipitation of ochre solids. The solids were dissolved with the addition of CH₂Cl₂ (100 mL). The phases were separated, and the aqueous layer was extracted twice with CH₂Cl₂ (2 x 50 mL). The combined organics were washed with brine (50 mL), dried over Na₂SO₄, and concentrated. The resulting brown oil crystallized upon standing to yield 1.36 g (83 %) of 7-chlorobenzo[c][1,2,5]oxadiazole-4-sulfonyl chloride [94] as ochre solid. The product could be used for further experimentation without additional purification.

Yield 1.36 g (83 %)
 Appearance ochre solid
 TLC R_f (LP/EtOAc – 10:1) = 0.31 (anisaldehyde)

Reaction scale 1.00 g (6.47 mmol)
 Substrate concentration neat
 Purification pure after work-up
 Sum formula, m.w. $C_6H_2Cl_2N_2O_3S$, 253.05 g/mol
 M.p. 86 – 88 °C (lit.²⁷⁵ 87 – 88 °C)

1H -NMR (600 MHz, $CDCl_3$) δ 7.68 (d, J = 7.4 Hz, 1H, H6), 8.19 (d, J = 7.5 Hz, 1H, H5).
 ^{13}C -NMR (151 MHz, $CDCl_3$) δ 128.7 (d, C6), 130.6 (s, C4), 132.0 (s, C7), 134.8 (d, C5), 143.8 (s, C3a), 149.1 (s, C7a).

E III.5.2 2-((7-Chlorobenzo[c][1,2,5]oxadiazole)-4-sulfonamido)-N,N,N-trimethylethan-1-aminium formiate [96]



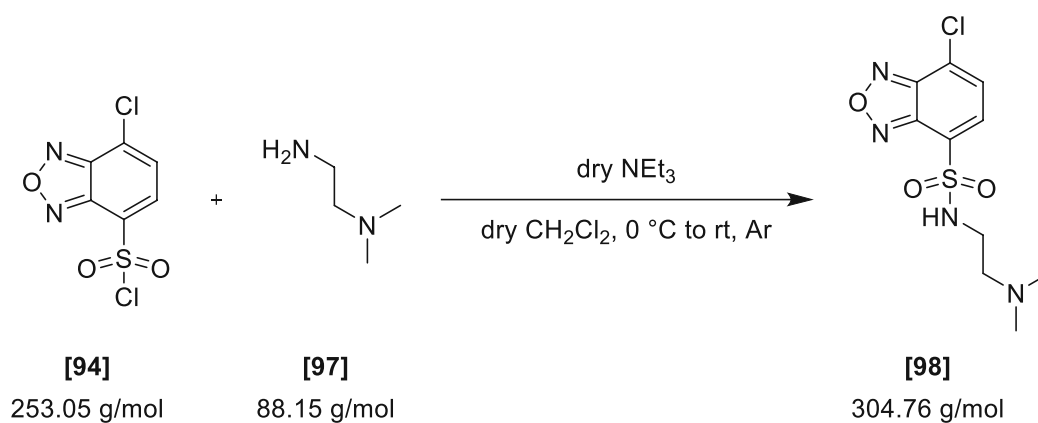
The product was synthesized according to a literature procedure²³⁵.

Procedure: To a solution of 7-chlorobenzo[c][1,2,5]oxadiazole-4-sulfonyl chloride [94] (0.60 g, 2.37 mmol, 1.00 equiv.) in HPLC grade MeCN (20 mL) was added (2-aminoethyl)trimethylammonium chloride hydrochloride [95] (0.33 g, 1.89 mmol, 0.80 equiv.) in 2 mL dH_2O . Following the addition of triethylamine (0.66 mL, 0.48 g, 4.74 mmol, 2.00 equiv.), the solution was stirred at room temperature, gradually turning the reaction deep brown. Complete darkening of the mixture was observed after 24 hours, upon which TLC and HPLC-MS (C_{18} , acidic) confirmed the full conversion of starting material.

Work-up: The solvent was removed *in vacuo*, and the remaining brown oily suspension was taken up in minimal amounts of DMSO. The crude product was further purified *via* preparative HPLC (C_{18} , acidic) to yield 0.12 g (14 %) of 2-((7-chlorobenzo[c][1,2,5]oxadiazole)-4-sulfonamido)-N,N,N-trimethylethan-1-aminium formiate [96] as brown oil. 0.13 g of hydrolyzed sulfonic acid was isolated as the second product.

Yield	0.13 g (19 %)
Appearance	brown oil
TLC	-
Reaction scale	0.60 g (2.37 mmol)
Substrate concentration	0.12 M
Purification	preparative HPLC (C_{18} , acidic)
Sum formula, m.w.	$C_{12}H_{17}ClN_4O_5S$, 364.06 g/mol
1H-NMR (600 MHz, $CDCl_3$)	δ 7.68 (d, $J = 7.4$ Hz, 1H, H6), 8.19 (d, $J = 7.5$ Hz, 1H, H5).
^{13}C-NMR (151 MHz, $CDCl_3$)	δ 128.7 (d, C6), 130.6 (s, C4), 132.0 (s, C7), 134.8 (d, C5), 143.8 (s, C3a), 149.1 (s, C7a).
HRMS (ESI)	calc. for $C_{11}H_{16}ClN_4O_3S^+$ [M-FA] $^+$ 319.0626, found 319.0622 – $\Delta = -1.35$ ppm.

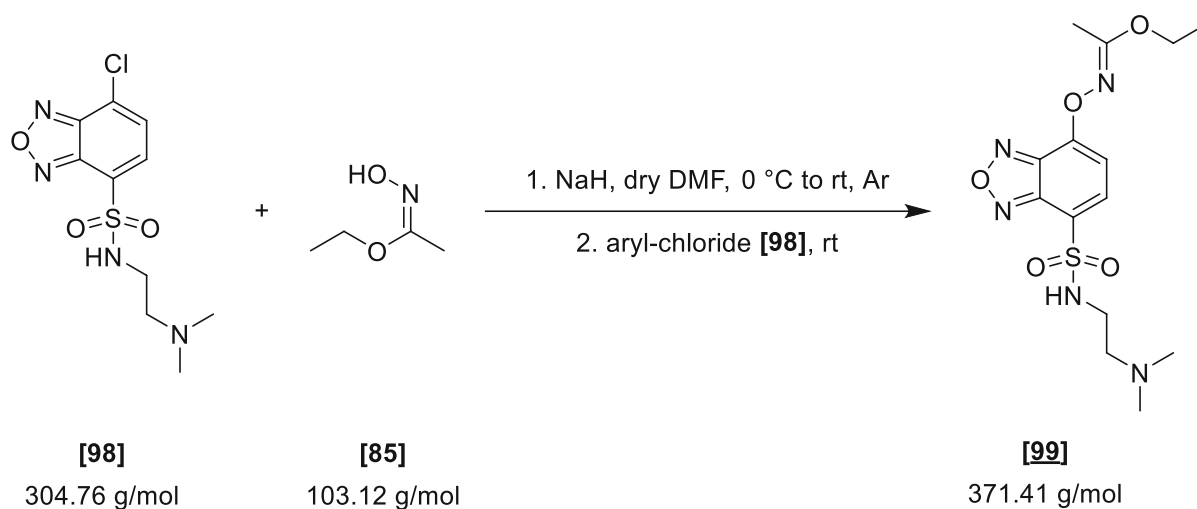
E III.5.3 7-Chloro-N-(2-(dimethylamino)ethyl)benzo[c][1,2,5]oxadiazole-4-sulfonamide [98]



7-chloro-N-(2-(dimethylamino)ethyl)benzo[c][1,2,5]oxadiazole-4-sulfonamide [98] was synthesized according to general procedure H using methyl 7-chlorobenzo[c][1,2,5]oxadiazole-4-sulfonyl chloride [94] (2.00 g, 7.80 mmol) and N,N-dimethylethylenediamine [97] (0.97 mL, 0.78 g, 8.70 mmol). The product could be used for further experimentation without additional purification.

Yield	2.11 g (87 %)
Appearance	yellow solid
Reaction scale	2.00 g (7.80 mmol)
Substrate concentration	0.52 M
Purification	pure after work-up
Sum formula, m.w.	C ₁₀ H ₁₃ ClN ₄ O ₃ S, 304.76 g/mol
M.p.	101 - 104 °C (lit. ²⁷⁶ 102 – 103 °C)
¹ H-NMR (400 MHz, CDCl ₃)	δ 2.03 (s, 6H, 2x -NCH ₃), 2.19 – 2.43 (m, 2H, -CH ₂ -N(CH ₃) ₂), 2.99 – 3.29 (m, 2H, -NH-CH ₂ -), 5.44 (s, 1H, -NH-), 7.54 (d, <i>J</i> = 7.3 Hz, 1H, H6), 7.98 (d, <i>J</i> = 7.3 Hz, 1H, H5).
¹³ C-NMR (101 MHz, CDCl ₃)	δ 40.6 (t, -NH-CH ₂ -), 44.8 (q, 2C, -NCH ₃), 57.3 (t, -CH ₂ -N(CH ₃) ₂), 127.6 (s, C7), 128.3 (s, C4), 129.3 (d, C6), 133.4 (d, C5), 145.2 (s, C3a), 148.9 (s, C7a).

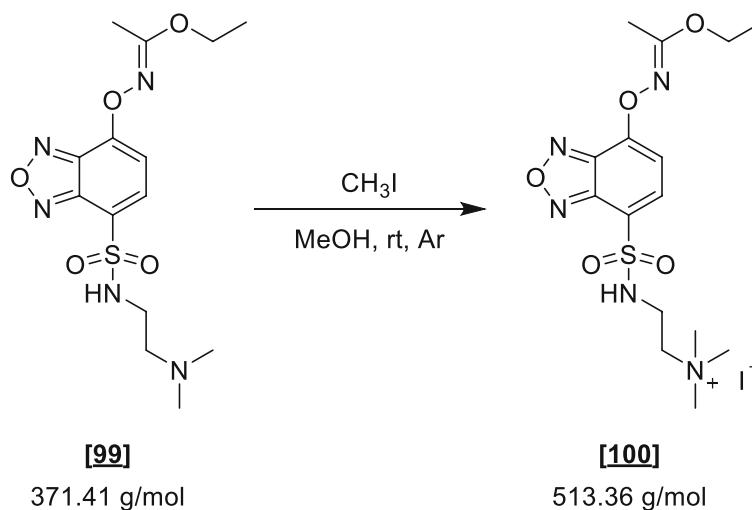
E III.5.4 Ethyl (*E*)-N-((7-(N-(2-(dimethylamino)ethyl)sulfamoyl)benzo[*c*][1,2,5]oxadiazol-4-yl)oxy)acetimidate [99]



Ethyl (*E*)-N-((7-(N-(2-(dimethylamino)ethyl)sulfamoyl)benzo[*c*][1,2,5]oxadiazol-4-yl)oxy)acetimidate [99] was synthesized according to general procedure I using 7-chloro-N-(2-(dimethylamino)ethyl)benzo[*c*][1,2,5]oxadiazole-4-sulfonamide [98] (0.50 g, 1.64 mmol) and ethyl-N-hydroxyacetimidate [85] (0.45 g, 4.10 mmol).

Yield	0.31 g (51 %)
Appearance	yellow solid
Reaction scale	0.50 g (1.64 mmol)
Substrate concentration	0.16 M
Purification	column chromatography (silica) CH ₂ Cl ₂ /MeOH 20:1
Sum formula, m.w.	C ₁₄ H ₂₁ N ₅ O ₅ S, 371.41 g/mol
M.p.	104 – 107 °C
¹ H-NMR (400 MHz, CDCl ₃)	δ 1.39 (t, <i>J</i> = 7.1 Hz, 3H, -CH ₂ -CH ₃), 2.10 (s, 6H, -N(CH ₃) ₂), 2.26 (s, 3H, -CH ₃), 2.38 – 2.47 (m, 2H, -CH ₂ -N(CH ₃) ₂), 3.06 – 3.20 (m, 2H, -NH-CH ₂ -), 4.24 (q, <i>J</i> = 7.1 Hz, 2H, -O-CH ₂ -), 7.16 (d, <i>J</i> = 7.8 Hz, 1H, H ₆), 8.01 (d, <i>J</i> = 7.9 Hz, 1H, H ₅).
¹³ C-NMR (101 MHz, CDCl ₃)	δ 14.4 (q, -CH ₂ -CH ₃), 15.0 (q, -CH ₃), 40.3 (t, -NH-CH ₂ -), 44.6 (q, 2C, -N(CH ₃) ₂), 57.4 (t, -CH ₂ -N(CH ₃) ₂), 64.0 (t, -O-CH ₂ -), 106.6 (d, C ₆), 119.7 (s, C ₄), 136.9 (d, C ₅), 143.5 (s, C _{7a}), 146.0 (s, C _{3a}), 151.5 (s, C ₇), 169.3 (s, -C=N-).

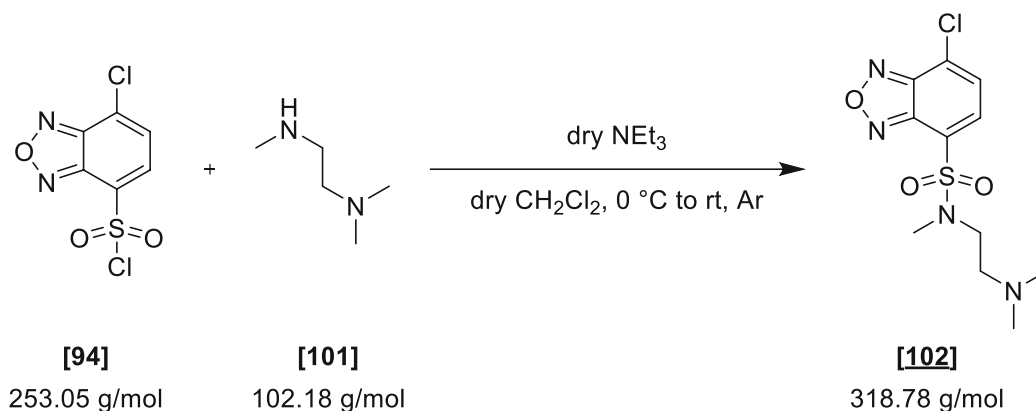
E III.5.5 (*E*)-2-((7-(((1-Ethoxyethylidene)amino)oxy)benzo[c][1,2,5]oxadiazole)-4-sulfonamido)-N,N,N-trimethylethan-1-aminium iodide **[100]**



(*E*)-2-((7-(((1-Ethoxyethylidene)amino)oxy)benzo[c][1,2,5]oxadiazole)-4-sulfonamido)-N,N,N-trimethylethan-1-aminium iodide **[100]** was synthesized according to general procedure J using ethyl (*E*)-N-((7-(N-(2-(dimethylamino)ethyl)sulfamoyl)benzo[c][1,2,5]oxadiazol-4-yl)oxy)acetimidate **[99]** (0.15 g, 0.40 mmol). The product could be used for further experimentation without additional purification.

Yield	0.16 g (76 %)
Appearance	yellow solid
Reaction scale	0.15 g (0.40 mmol)
Substrate concentration	0.11 M
Purification	pure after work-up
Sum formula, m.w.	C ₁₅ H ₂₄ IN ₅ O ₅ S, 513.36 g/mol
M.p.	159 – 161 °C
¹ H-NMR (400 MHz, DMSO- <i>d</i> ₆)	δ 1.35 (t, <i>J</i> = 7.0 Hz, 3H, -CH ₂ -CH ₃), 2.23 (s, 3H, -CH ₃), 3.07 (s, 9H, -N(CH ₃) ₃), 3.29 – 3.38 (m, 4H, -NH-CH ₂ -, -CH ₂ -N(CH ₃) ₃), 4.26 (q, <i>J</i> = 7.0 Hz, 2H, -O-CH ₂ -), 7.33 (d, <i>J</i> = 7.9 Hz, 1H, H ₆), 8.10 (d, <i>J</i> = 7.9 Hz, 1H, H ₅), 8.39 (s, 1H, -NH-).
¹³ C-NMR (101 MHz, DMSO- <i>d</i> ₆)	δ 14.2 (q, -CH ₂ -CH ₃), 14.7 (q, -CH ₃), 36.7 (t, -NH-CH ₂ -), 52.9 (q, 3C, -N(CH ₃) ₃), 63.9 (t, -O-CH ₂ -), 64.1 (t, -CH ₂ -N(CH ₃) ₃), 107.5 (d, C ₆), 119.1 (s, C ₄), 138.0 (d, C ₅), 143.5 (s, C _{7a}), 145.8 (s, C _{3a}), 150.6 (s, C ₇), 169.5 (s, -C=N-).
HRMS (ESI)	calc. for C ₁₅ H ₂₄ N ₅ O ₅ S ⁺ [M-I] ⁺ 386.1493, found 386.1519 – Δ = 6.83 ppm.

E III.5.6 7-Chloro-N-(2-(dimethylamino)ethyl)-N-methylbenzo[c][1,2,5]oxadiazole-4-sulfonamide **[102]**

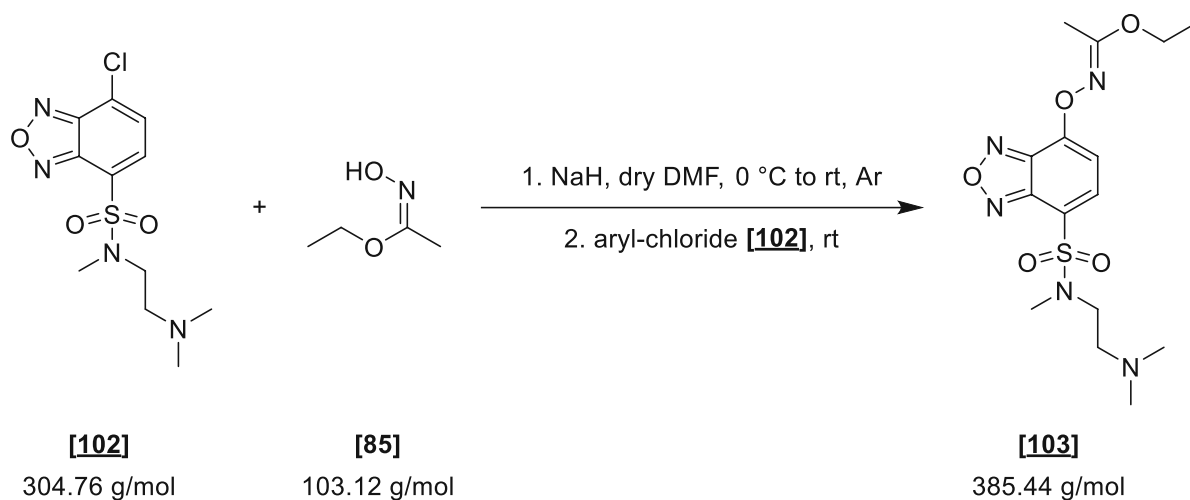


7-Chloro-N-(2-(dimethylamino)ethyl)-N-methylbenzo[c][1,2,5]oxadiazole-4-sulfonamide **[102]** was synthesized according to general procedure H using methyl 7-chlorobenzo[c][1,2,5]oxadiazole-4-sulfonyl chloride **[94]** (1.03 g, 4.07 mmol) and N,N'-trimethylethylenediamine **[101]** (0.59 mL, 0.46 g, 4.48 mmol). The product could be used for further experimentation without additional purification.

Yield	1.13 g (88 %)
Appearance	yellow solid

Reaction scale	1.03 g (4.07 mmol)
Substrate concentration	0.52 M
Purification	pure after work-up
Sum formula, m.w.	C ₁₁ H ₁₅ ClN ₄ O ₃ S, 318.78 g/mol
M.p.	84 – 85 °C
¹ H-NMR (400 MHz, CDCl ₃)	δ 2.12 (s, 6H, -N(CH ₃) ₂), 2.46 (t, <i>J</i> = 6.7 Hz, 2H, -CH ₂ -N(CH ₃) ₂), 3.04 (s, 3H, -NCH ₃), 3.37 (t, <i>J</i> = 6.7 Hz, 2H, -SO ₂ N-CH ₂ -), 7.52 (d, <i>J</i> = 7.3 Hz, 1H, H6), 7.96 (d, <i>J</i> = 7.4 Hz, 1H, H5).
¹³ C-NMR (101 MHz, CDCl ₃)	δ 35.6 (q, -NCH ₃), 45.5 (q, -N(CH ₃) ₂), 48.4 (t, -SO ₂ N-CH ₂ -), 57.5 (t, -CH ₂ -N(CH ₃) ₂), 127.4 (C4 or C7), 127.7 (C4 or C7), 129.3 (s, C6), 133.8 (s, C5), 145.7 (s, C3a), 149.0 (s, C7a).
HRMS (ESI)	calc. for C ₁₁ H ₁₆ ClN ₄ O ₃ S ⁺ [M+H] ⁺ 319.0626, found 319.0623 – Δ = -0.98 ppm.

E III.5.7 Ethyl (*E*)-N-((7-(N-(2-(dimethylamino)ethyl)-N-methylsulfamoyl)benzo[*c*][1,2,5]oxadiazol-4-yl)oxy)acetimidate **[103]**

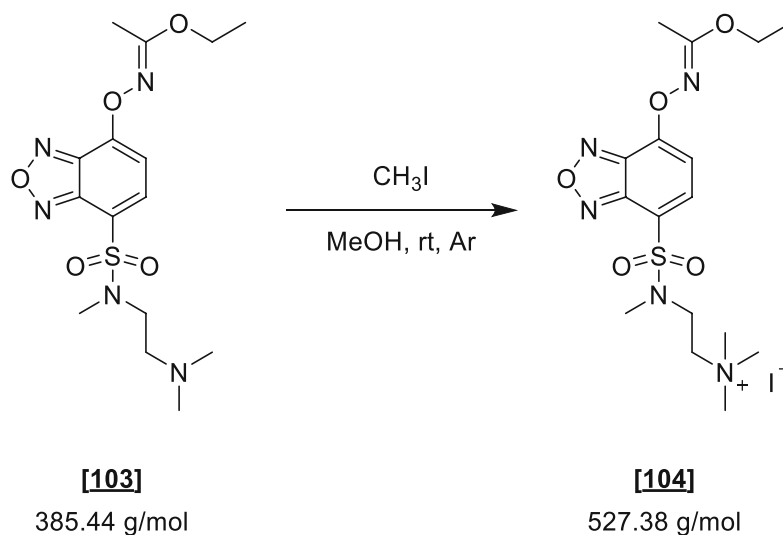


Ethyl (*E*)-N-((7-(N-(2-(dimethylamino)ethyl)-N-methylsulfamoyl)benzo[*c*][1,2,5]oxadiazol-4-yl)oxy)acetimidate **[103]** was synthesized according to general procedure I using 7-chloro-N-(2-(dimethylamino)ethyl)-N-methylbenzo[*c*][1,2,5]oxadiazole-4-sulfonamide **[102]** (0.60 g, 1.88 mmol) and ethyl-N-hydroxyacetimidate **[85]** (0.25 g, 2.26 mmol).

Yield	0.45 g (63 %)
Appearance	yellow solid

Reaction scale	0.50 g (1.64 mmol)
Substrate concentration	0.16 M
Purification	column chromatography (silica) CH ₂ Cl ₂ /MeOH 20:1
Sum formula, m.w.	C ₁₅ H ₂₃ N ₅ O ₅ S 385.44 g/mol
M.p.	58 - 60 °C
¹ H-NMR (400 MHz, CDCl ₃)	δ 1.40 (t, <i>J</i> = 7.1 Hz, 3H, -CH ₂ -CH ₃), 2.21 (s, 6H, -N(CH ₃) ₂), 2.27 (s, 3H, -CH ₃), 2.51 (t, <i>J</i> = 7.0 Hz, 2H, -CH ₂ -N(CH ₃) ₂), 2.98 (s, 3H, -NCH ₃), 3.36 (t, <i>J</i> = 7.0 Hz, 2H, -NH-CH ₂ -), 4.25 (q, <i>J</i> = 7.1 Hz, 2H, -O-CH ₂ -), 7.16 (d, <i>J</i> = 7.9 Hz, 1H, H6), 8.00 (d, <i>J</i> = 7.9 Hz, 1H, H5).
¹³ C-NMR (101 MHz, CDCl ₃)	δ 14.4 (q, -CH ₂ -CH ₃), 15.0 (q, -CH ₃), 35.6 (q, -NCH ₃), 45.6 (q, 2C, -N(CH ₃) ₂), 48.4 (t, -NH-CH ₂ -), 57.7 (t, -CH ₂ -N(CH ₃) ₂), 64.0 (t, -O-CH ₂ -), 106.6 (d, C6), 119.0 (s, C4), 137.5 (d, C5), 143.6 (s, C7a), 146.5 (s, C3a), 151.4 (s, C7), 169.2 (s, -C=N-).
HRMS (ESI)	calc. for C ₁₅ H ₂₄ N ₅ O ₅ S ⁺ [M+H] ⁺ 386.1493, found 386.1524 – Δ = 8.02 ppm.

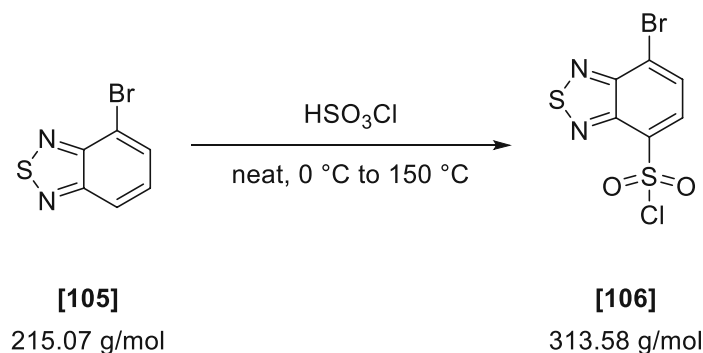
E III.5.8 (E)-2-((7-(((1-Ethoxyethylidene)amino)oxy)-N-methylbenzo[c][1,2,5]oxadiazole)-4-sulfonamido)-N,N,N-trimethylethan-1-aminium iodide **[104]**



(E)-2-((7-(((1-ethoxyethylidene)amino)oxy)-N-methylbenzo[c][1,2,5]oxadiazole)-4-sulfonamido)-N,N,N-trimethylethan-1-aminium iodide **[104]** was synthesized according to general procedure J using ethyl (E)-N-((7-(N-(2-(dimethylamino)ethyl)-N-methylsulfamoyl)benzo[c][1,2,5]oxadiazol-4-yl)oxy)acetimidate **[103]** (0.20 g, 0.52 mmol). The product could be used for further experimentation without additional purification.

Yield	0.26 g (94 %)
Appearance	yellow solid
Reaction scale	0.20 g (0.52 mmol)
Substrate concentration	0.11 M
Purification	pure after work-up
Sum formula, m.w.	C ₁₆ H ₂₆ IN ₅ O ₅ S, 527.38 g/mol
M.p.	133.5 – 134 °C
¹ H-NMR (400 MHz, CDCl ₃)	δ 1.40 (t, <i>J</i> = 7.1 Hz, 3H, -CH ₂ -CH ₃), 2.27 (s, 3H, -CH ₃), 3.02 (s, 3H, -NCH ₃), 3.59 (s, 9H, -N(CH ₃) ₃), 3.93 (t, <i>J</i> = 5.9 Hz, 2H, -NH-CH ₂ -), 4.24 (t, <i>J</i> = 5.6 Hz, 2H, -CH ₂ -N(CH ₃) ₃), 4.26 (t, <i>J</i> = 7.1 Hz, 2H, -O-CH ₂ -), 7.23 (d, <i>J</i> = 7.9 Hz, 1H, H6), 8.07 (d, <i>J</i> = 8.0 Hz, 1H, H5).
¹³ C-NMR (101 MHz, CDCl ₃)	δ 14.4 (q, -CH ₂ -CH ₃), 15.1 (q, -CH ₃), 36.2 (q, -NCH ₃), 45.8 (t, -NH-CH ₂ -), 54.7 (q, 3C, -N(CH ₃) ₃), 62.9 (t, -CH ₂ -N(CH ₃) ₃), 64.1 (t, -O-CH ₂ -), 106.9 (d, C6), 115.8 (s, C4), 139.6 (d, C5), 143.6 (s, C7a), 146.4 (s, C3a), 152.4 (s, C7), 169.6 (s, -C=N-).
HRMS (ESI)	calc. for C ₁₆ H ₂₆ N ₅ O ₅ S ⁺ [M-I] ⁺ 400.1649, found 400.1677 – Δ = 6.90 ppm.

E III.5.9 7-Bromobenzo[c][1,2,5]thiadiazole-4-sulfonyl chloride [106]



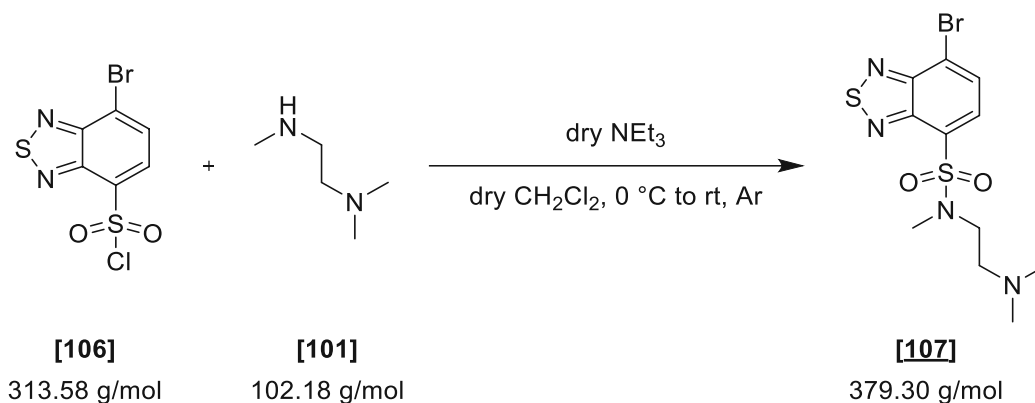
The product was synthesized according to a modified literature procedure²³⁵.

Procedure: A flame-dried 25 screw-cap vial was charged with 4-bromo-2,1,3-benzothiadiazole [105] (2.49 g, 11.60 mmol, 1.00 equiv.) and then evacuated and backfilled with argon using standard Schlenk techniques. The vessel was submerged in an ice-water bath for 5 minutes, and then chlorosulfonic acid (5.50 mL, 9.60 g, 82.40 mmol, 7.00 equiv.) was added dropwise with strong stirring. The addition should be performed <2 minutes, as the strong corrosiveness of the acid readily attacks the syringe. After the addition of approx. 1 mL of acid, all particulates had dissolved. The deep yellow solution was heated to 150 °C for 4 hours, upon which TLC indicated full conversion. Refrain from the usage of septa, as they can be trashed afterward.

Work-up: The reaction was cooled to room temperature and was directly poured onto solid ice (a strong exothermic reaction!), causing immediate precipitation of ochre solids. The solids were dissolved with the addition of CH_2Cl_2 (200 mL). The phases were separated, and the aqueous layer was extracted twice with CH_2Cl_2 (2 x 100 mL). The combined organics were washed with brine (100 mL), dried over Na_2SO_4 , and concentrated. The resulting brown oil crystallized upon standing to yield 2.54 g (70 %) of 7-bromobenzo[c][1,2,5]thiadiazole-4-sulfonyl chloride **[106]** as ochre solid. The product could be used for further experimentation without additional purification.

Yield	2.54 g (70 %)
Appearance	ochre solid
TLC	R_f (LP/EtOAc – 10:1) = 0.42 (anisaldehyde)
Reaction scale	2.49 g (11.60 mmol)
Substrate concentration	neat
Purification	pure after work-up
Sum formula, m.w.	$\text{C}_6\text{H}_2\text{BrClN}_2\text{O}_2\text{S}_2$, 313.58 g/mol
M.p.	126 – 130 °C (lit. ²⁷⁷ 141– 142 °C)
$^1\text{H-NMR}$ (600 MHz, CDCl_3)	δ 8.06 (d, J = 7.8 Hz, 1H, H6), 8.27 (d, J = 7.7 Hz, 1H, H5).
$^{13}\text{C-NMR}$ (151 MHz, CDCl_3)	δ 124.6 (s, C7), 130.5 (d, C6), 131.8 (d, C5), 134.0 (s, C4), 147.5 (s, C3a), 154.4 (s, C7a).

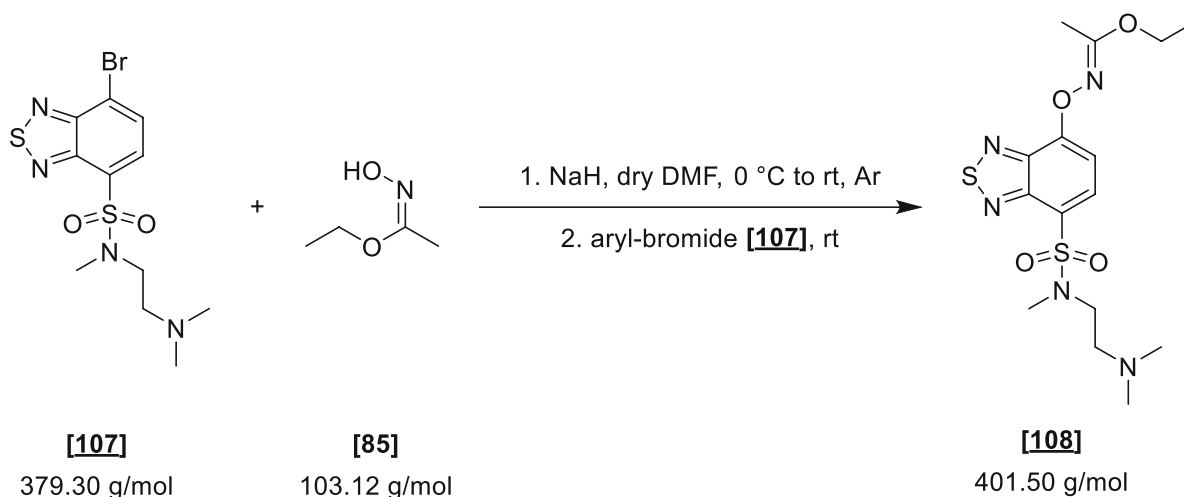
E III.5.10 7-Bromo-N-(2-(dimethylamino)ethyl)-N-methylbenzo[c][1,2,5]thiadiazole-4-sulfonamide **[107]**



7-Bromo-N-(2-(dimethylamino)ethyl)-N-methylbenzo[c][1,2,5]thiadiazole-4-sulfonamide **[107]** was synthesized according to general procedure **H** using methyl 7-bromobenzo[c][1,2,5]thiadiazole-4-sulfonyl chloride **[106]** (1.50 g, 4.78 mmol) and N,N,N'-Trimethylethylenediamine **[101]** (0.69 mL, 0.54 g, 5.26 mmol). The product could be used for further experimentation without additional purification.

Yield	1.66 g (92 %)
Appearance	yellow oil (minimal crystallization after several weeks)
Reaction scale	1.50 g (4.78 mmol)
Substrate concentration	0.52 M
Purification	pure after work-up
Sum formula, m.w.	C ₁₁ H ₁₅ BrN ₄ O ₂ S ₂ , 379.30 g/mol
¹ H-NMR (400 MHz, CDCl ₃)	δ 2.17 (s, 6H, -N(CH ₃) ₂), 2.48 (t, <i>J</i> = 7.0 Hz, 2H, -CH ₂ -N(CH ₃) ₂), 3.01 (s, 3H, -NCH ₃), 3.40 (t, <i>J</i> = 7.0 Hz, 2H, -SO ₂ N-CH ₂ -), 7.93 (d, <i>J</i> = 7.6 Hz, 1H, H6), 8.12 (d, <i>J</i> = 7.6 Hz, 1H, H5).
¹³ C-NMR (101 MHz, CDCl ₃)	δ 35.7 (q, -NCH ₃), 45.7 (q, 2C, -N(CH ₃) ₂), 48.6 (t, -CH ₂ -N(CH ₃) ₂), 57.9 (t, -SO ₂ N-CH ₂ -), 120.1 (s, C4), 131.0 (d, C6), 131.3 (s, C7), 132.3 (d, C5), 149.4 (s, C3a), 154.2 (s, C7a).
HRMS (ESI)	calc. for C ₁₁ H ₁₆ BrN ₄ O ₂ S ₂ ⁺ [M-H] ⁺ 378.9893, found 378.9918 – Δ = 6.63 ppm.

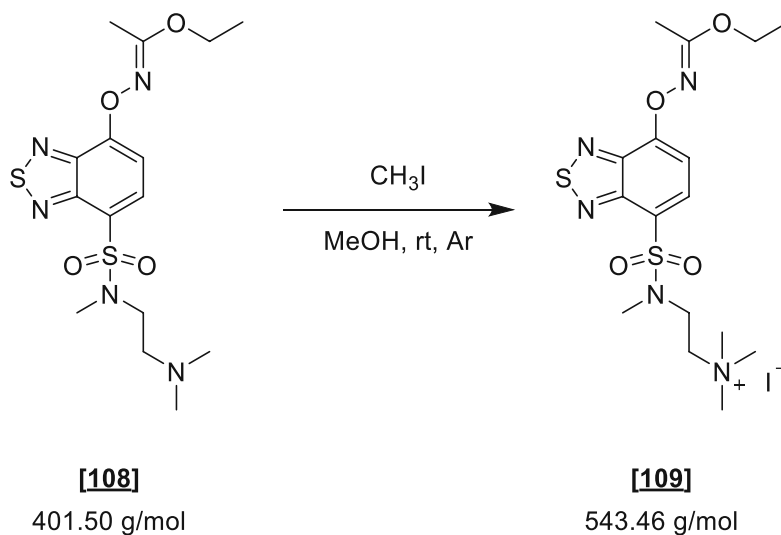
E III.5.11 Ethyl (*E*)-N-((7-(N-(2-(dimethylamino)ethyl)-N-methylsulfamoyl)benzo[c][1,2,5]thiadiazol-4-yl)oxy)acetimidate [108]



Ethyl (*E*)-N-((7-(N-(2-(dimethylamino)ethyl)-N-methylsulfamoyl)benzo[c][1,2,5]thiadiazol-4-yl)oxy)acetimidate [108] was synthesized according to general procedure I using 7-bromo-N-(2-(dimethylamino)ethyl)-N-methylbenzo[c][1,2,5]thiadiazole-4-sulfonamide [107] (0.88 g, 2.32 mmol) and ethyl-N-hydroxyacetimidate [85] (0.28 g, 2.55 mmol, 1.10 equiv.).

Yield	0.60 g (64 %)
Appearance	yellow oil
Reaction scale	0.88 g (2.32 mmol)
Substrate concentration	0.16 M
Purification	column chromatography (silica) CH ₂ Cl ₂ /MeOH 20:1
Sum formula, m.w.	C ₁₅ H ₂₃ N ₅ O ₄ S ₂ 401.50 g/mol
¹ H-NMR (400 MHz, CDCl ₃)	δ 1.41 (t, <i>J</i> = 7.1 Hz, 3H, -CH ₂ -CH ₃), 2.21 (s, 6H, -N(CH ₃) ₂), 2.30 (s, 3H, -CH ₃), 2.45 – 2.55 (m, 2H, -CH ₂ -N(CH ₃) ₂), 2.96 (s, 3H, -NCH ₃), 3.29 – 3.41 (m, 2H, -SO ₂ N-CH ₂ -), 4.28 (q, <i>J</i> = 7.1 Hz, 2H, -O-CH ₂ -), 7.39 (d, <i>J</i> = 8.1 Hz, 1H, H ₆), 8.23 (d, <i>J</i> = 8.1 Hz, 1H, H ₅).
¹³ C-NMR (101 MHz, CDCl ₃)	δ 14.4 (q, -CH ₂ -CH ₃), 15.0 (q, -CH ₃), 35.7 (q, -NCH ₃), 45.7 (q, 2C, -N(CH ₃) ₂), 48.6 (t, -SO ₂ N-CH ₂ -), 58.0 (t, -CH ₂ -N(CH ₃) ₂), 63.8 (t, -O-CH ₂ -), 106.5 (d, C ₆), 122.8 (s, C ₄), 135.2 (d, C ₅), 146.7 (s, C _{7a}), 151.3 (s, C _{3a}), 154.2 (s, C ₇), 168.7 (s, -C=N-).
HRMS (ESI)	calc. for C ₁₅ H ₂₄ N ₅ O ₄ S ₂ ⁺ [M-H] ⁺ 402.1264, found 402.1298 – Δ = 8.37 ppm.

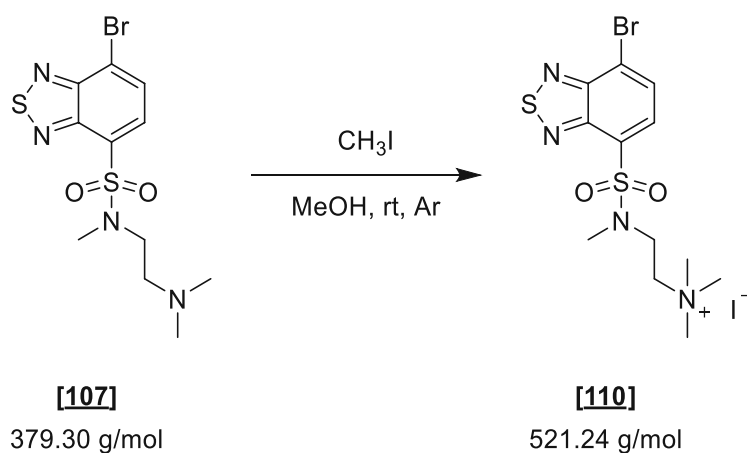
E III.5.12 (E)-2-((7-(((1-Ethoxyethylidene)amino)oxy)-N-methylbenzo[c][1,2,5]thiadiazole)-4-sulfonamido)-N,N,N-trimethylethan-1-aminium iodide **[109]**



(E)-2-((7-(((1-Ethoxyethylidene)amino)oxy)-N-methylbenzo[c][1,2,5]thiadiazole)-4-sulfonamido)-N,N,N-trimethylethan-1-aminium iodide **[109]** was synthesized according to general procedure J using ethyl (E)-N-((7-(N-(2-(dimethylamino)ethyl)-N-methylsulfamoyl)benzo[c][1,2,5]thiadiazol-4-yl)oxy)acetimidate **[108]** (0.58 g, 1.44 mmol). The product could be used for further experimentation without additional purification.

Yield	0.69 g (88 %)
Appearance	yellow solid
Reaction scale	0.58 g (1.44 mmol)
Substrate concentration	0.11 M
Purification	pure after work-up
Sum formula, m.w.	C ₁₆ H ₂₆ IN ₅ O ₄ S ₂ , 543.45 g/mol
M.p.	196 – 198 °C
¹ H-NMR (400 MHz, DMSO- <i>d</i> ₆)	δ 1.36 (t, <i>J</i> = 7.0 Hz, 3H, -CH ₂ -CH ₃), 2.25 (s, 3H, -CH ₃), 2.83 (s, 3H, -NCH ₃), 3.17 (s, 9H, -N(CH ₃) ₃), 3.62 (t, <i>J</i> = 6.6 Hz, 2H, -CH ₂ -N(CH ₃) ₃), 3.72 (t, <i>J</i> = 6.7 Hz, 2H, -SO ₂ N-CH ₂ -), 4.28 (q, <i>J</i> = 7.0 Hz, 2H, -O-CH ₂ -), 7.52 (d, <i>J</i> = 8.2 Hz, 1H, H ₆), 8.26 (d, <i>J</i> = 8.2 Hz, 1H, H ₅).
¹³ C-NMR (101 MHz, DMSO- <i>d</i> ₆)	δ 14.1 (q, -CH ₂ -CH ₃), 14.5 (q, -CH ₃), 35.0 (q, -NCH ₃), 44.4 (t, -SO ₂ N-CH ₂ -), 52.6 (q, 3C, -N(CH ₃) ₃), 61.6 (t, -CH ₂ -N(CH ₃) ₃), 63.6 (t, -O-CH ₂ -), 106.5 (d, C ₆), 120.5 (s, C ₄), 135.6 (d, C ₅), 145.7 (s, C _{7a}), 150.5 (s, C _{3a}), 153.7 (s, C ₇), 168.7 (s, -C=N-).
HRMS (ESI)	calc. for C ₁₆ H ₂₆ N ₅ O ₄ S ₂ ⁺ [M-I] ⁺ 416.1421, found 416.1460 – Δ = 9.37 ppm.

E III.5.13 2-((7-Bromo-N-methylbenzo[c][1,2,5]thiadiazole)-4-sulfonamido)-N,N,N-trimethylethan-1-aminium iodide **[110]**

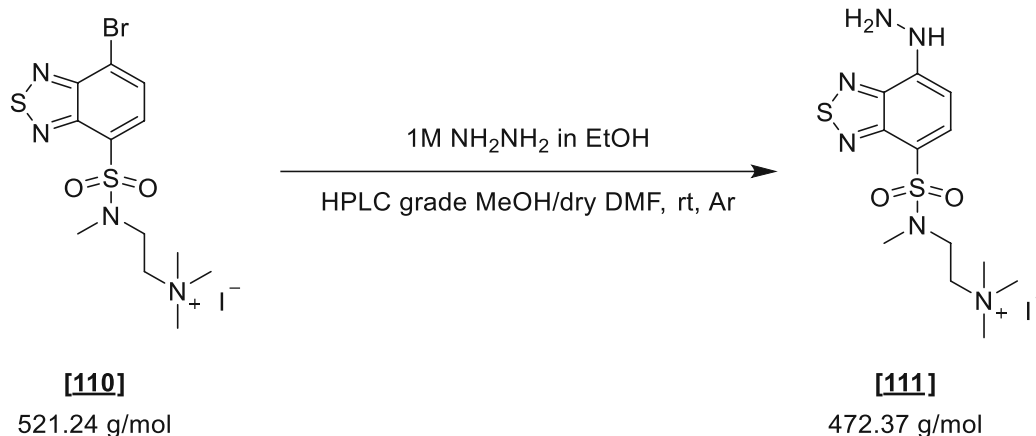


2-((7-bromo-N-methylbenzo[c][1,2,5]thiadiazole)-4-sulfonamido)-N,N,N-trimethylethan-1-aminium iodide **[110]** was synthesized according to general procedure J using 7-bromo-N-(2-(dimethylamino)ethyl)-N-methylbenzo[c][1,2,5]thiadiazole-4-sulfonamide **[107]** (0.65 g, 1.72 mmol). The product could be used for further experimentation without additional purification.

Yield	0.80 g (90 %)
Appearance	yellow solid

Reaction scale	0.65 g (1.72 mmol)
Substrate concentration	0.11 M
Purification	pure after work-up
Sum formula, m.w.	C ₁₂ H ₁₈ BrIN ₄ O ₂ S ₂ , 521.24 g/mol
M.p.	232 - 238 °C
¹ H-NMR (400 MHz, DMSO- <i>d</i> ₆)	δ 2.88 (s, 3H, -NCH ₃), 3.18 (s, 9H, -N(CH ₃) ₃), 3.64 (t, <i>J</i> = 6.8 Hz, 2H, -CH ₂ -N(CH ₃) ₃), 3.75 (t, <i>J</i> = 6.8 Hz, 2H, -SO ₂ N-CH ₂ -), 8.16 (d, <i>J</i> = 7.7 Hz, 1H, H5), 8.24 (d, <i>J</i> = 7.7 Hz, 1H, H6).
¹³ C-NMR (101 MHz, DMSO- <i>d</i> ₆)	δ 35.1 (q, -NCH ₃), 44.3 (t, -SO ₂ N-CH ₂ -), 52.6 (q, 3C, -N(CH ₃) ₃), 61.5 (t, -CH ₂ -N(CH ₃) ₃), 119.9 (C7), 128.4 (s, C4), 131.3 (d, C6), 133.1 (d, C5), 148.5 (s, C3a), 153.5 (s, C7a).
HRMS (ESI)	calc. for C ₁₂ H ₁₈ BrN ₄ O ₂ S ₂ ⁺ [M-I] ⁺ 393.0073, found 393.0049 – Δ = 6.00 ppm.

E III.5.14 2-((7-Hydrazineyl-N-methylbenzo[c][1,2,5]thiadiazole)-4-sulfonamido)-N,N,N-trimethylethan-1-aminium iodide **[111]**

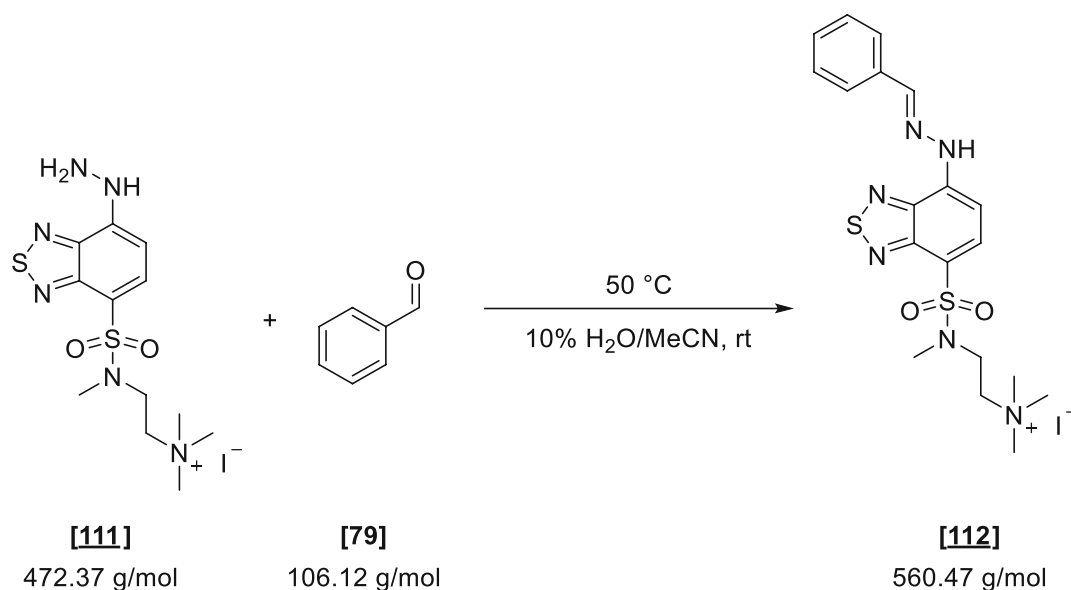


Procedure: A flame-dried 8 mL screw cap vial was charged with 2-((7-bromo-N-methylbenzo[c][1,2,5]thiadiazole)-4-sulfonamido)-N,N,N-trimethylethan-1-aminium iodide **[110]** (150 mg, 0.29 mmol, 1.00 equiv.). The atmosphere was exchanged for argon using standard Schlenk techniques upon which anhydrous hydrazine (1 M in EtOH, 2.90 mL, 2.90 mmol, 10.00 equiv.) was added in one portion. Due to the insolubility of the starting material, HPLC grade MeOH (1 mL – no change) and then dry DMF (2 mL – minimal dissolution) was added. The light-yellow suspension was stirred at room temperature under argon for two days. As HPLC-MS (C₁₈, acidic) analysis still confirmed only partial conversion, the reaction was heated to 50 °C, which caused the complete dissolution of solids after 15 minutes. The reaction was stirred for 8 hours at this temperature, upon which HPLC-MS (C₁₈, acidic) indicated full conversion of starting materials.

Work-up: The crude solution was placed in the freezer, which enabled crystallization after two days. The product was collected by suction filtration and washed thoroughly with MeOH (3 x 3 mL) and then Et₂O (3 x 5 mL). The solids were dried *in vacuo* to yield 56 mg (36 %) of 2-((7-hydrazineyl-N-methylbenzo[c][1,2,5]thiadiazole)-4-sulfonamido)-N,N,N-trimethylethan-1-aminium iodide **[111]** as orange-brown solid. Due to the presence of dimethylamine in all commercial DMF sources, the arylamine product could also be isolated *via* preparative HPLC (C₁₈, acidic) of the filtrate. The target product was used for further experimentation without further purification.

Yield	56 mg (36 %)
Appearance	orange-brown solid
Reaction scale	150 mg (0.29 mmol)
Substrate concentration	final conc. 0.05 M
Purification	pure after work-up
Sum formula, m.w.	C ₁₂ H ₂₁ N ₆ O ₂ S ₂ , 472.37 g/mol
M.p.	142 – 145 °C
¹H-NMR (400 MHz, DMSO-<i>d</i>₆)	δ 2.75 (s, 3H, -NCH ₃), 3.17 (s, 9H, -N(CH ₃) ₃), 3.59 (t, <i>J</i> = 6.0 Hz, 2H, -CH ₂ -N(CH ₃) ₃), 3.66 (t, <i>J</i> = 5.8 Hz, 2H, -SO ₂ N-CH ₂ -), 4.71 (s, 2H, -NH ₂), 6.84 (d, <i>J</i> = 8.5 Hz, 1H, H ₆), 8.05 (d, <i>J</i> = 8.5 Hz, 1H, H ₅), 8.90 (s, 1H, -NH-).
¹³C-NMR (101 MHz, DMSO-<i>d</i>₆)	δ 34.9 (-NCH ₃), 44.6 (t, -SO ₂ N-CH ₂ -), 52.6 (q, 3C, -N(CH ₃) ₃), 61.7 (t, -CH ₂ -N(CH ₃) ₃), 98.9 (d, C ₆), 110.6 (s, C ₄), 137.4 (d, C ₅), 145.1 (s, C _{7a}), 147.0 (s, C ₇), 150.7 (s, C _{3a}).
HRMS (ESI)	calc. for C ₁₂ H ₂₁ N ₆ O ₂ S ₂ ⁺ [M-I] ⁺ 345.1162, found 345.1174 – Δ = 3.39 ppm.

E III.5.15 (E)-2-((7-(2-Benzylidenehydrazineyl)-N-methylbenzo[c][1,2,5]thiadiazole)-4-sulfonamido)-N,N,N-trimethylethan-1-aminium iodide [112]



Procedure: A flame-dried 2 mL screw cap vial was charged with 2-((7-hydrazineyl)-N-methylbenzo[c][1,2,5]thiadiazole)-4-sulfonamido)-N,N,N-trimethylethan-1-aminium iodide [111] (20 mg, 0.04 mmol, 1.00 equiv.) which was suspended in 5 vol% d.H₂O in HPLC grade MeCN (1 mL). The atmosphere was exchanged for argon using standard Schlenk techniques upon which benzaldehyde [79] (13 μL, 14 mg, 0.13 mmol, 3.00 equiv.) was added in one portion. The reaction was stirred at 50 °C for 1 hour, upon which UHPLC-MS (C₁₈, acidic) analysis confirmed full conversion.

Work-up: The product was precipitated with the addition of Et₂O (3 mL) and was placed inside the freezer for 30 minutes. The precipitate was collected by suction filtration and was washed with fresh -20 °C Et₂O (2 x 3 mL). The solids were dried *in vacuo* to yield 20 mg (81 %) of (E)-2-((7-(2-Benzylidenehydrazineyl)-N-methylbenzo[c][1,2,5]thiadiazole)-4-sulfonamido)-N,N,N-trimethylethan-1-aminium iodide [112] as bright orange solids.

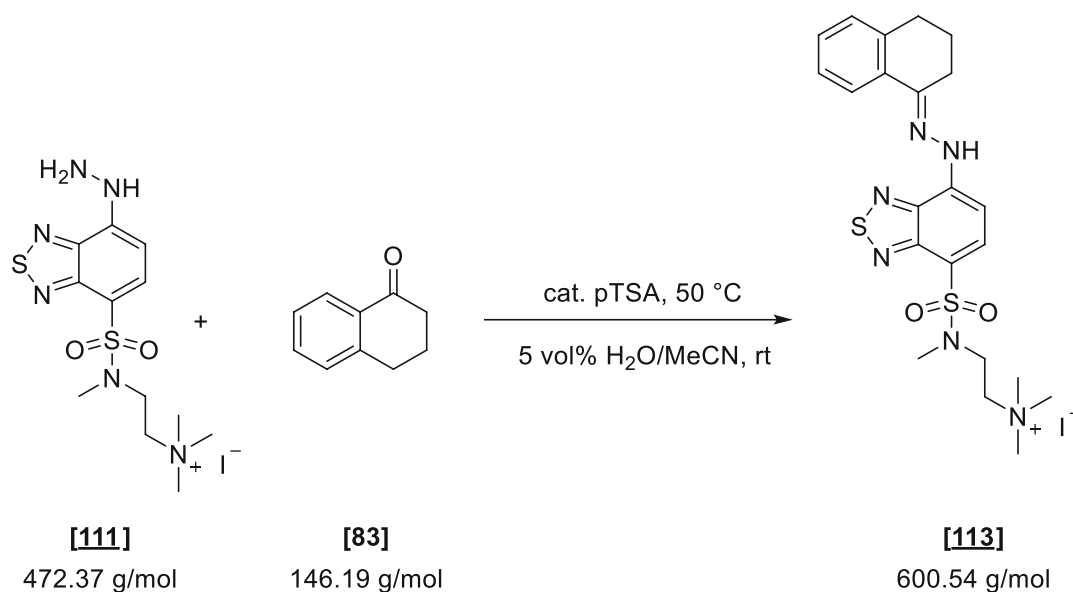
Yield	20 mg (81 %)
Appearance	orange solid
TLC	-
Reaction scale	20 mg (0.04 mmol)
Substrate concentration	0.04 M
Purification	pure after work-up
Sum formula, m.w.	C ₁₉ H ₂₅ IN ₆ O ₂ S ₂ , 560.47 g/mol
M.p.	decomposition > 120 °C

¹H-NMR (400 MHz, DMSO-*d*₆) δ 2.81 (s, 3H, -NCH₃), 3.17 (s, 9H, -N(CH₃)₃), 3.60 (t, J = 6.5 Hz, 2H, -CH₂-N(CH₃)₃), 3.70 (t, J = 6.6 Hz, 2H, -SO₂N-CH₂-), 7.42 (d, J = 8.3 Hz, 1H, H₆), 7.42 – 7.51 (m, 3H, H_{3'}, H_{4'}, H_{5'}), 7.71 – 7.87 (m, 2H, H_{2'}, H_{6'}), 8.17 (d, J = 8.3 Hz, 1H, H₅), 8.56 (s, 1H, -N=CH-Ar), 11.89 (s, 1H, -NH-).

¹³C-NMR (101 MHz, DMSO-*d*₆) δ 35.0 (q, -NCH₃), 44.5 (t, -SO₂N-CH₂-), 52.6 (q, -N(CH₃)₃, 3C), 61.7 (t, -CH₂-N(CH₃)₃), 102.4 (d, C₆), 114.9 (s, C₄), 126.8 (d, C_{2'}, C_{6'}, 2C), 128.9 (d, C_{3'}, C_{5'}, 2C), 129.8 (d, C_{4'}), 134.5 (s, C_{1'}), 136.6 (d, C₅), 141.0 (s, C₇), 145.1 (s, C_{7a}), 145.5 (d, -N=CH-Ar), 150.6 (s, C_{3a}).

HRMS (ESI) calc. for C₁₉H₂₅N₆O₂S₂⁺ [M-I]⁺ 433.1475, found 433.1500 – Δ = 5.78 ppm.

E III.5.16 (*E*)-2-((7-(2-(3,4-Dihydronaphthalen-1(2H)-ylidene)hydrazineyl)-N-methylbenzo[*c*][1,2,5]thiadiazole)-4-sulfonamido)-N,N,N-trimethylethan-1-aminium iodide **[113]**

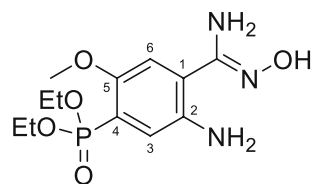


Procedure: A flame-dried 2 mL screw cap vial was charged with 2-((7-hydrazineyl)-N-methylbenzo[*c*][1,2,5]thiadiazole)-4-sulfonamido)-N,N,N-trimethylethan-1-aminium iodide **[111]** (20 mg, 0.04 mmol, 1.00 equiv.) and pTSA (approx. 1 mg) which was suspended in 5 vol% d.H₂O in HPLC grade MeCN (1 mL). The atmosphere was exchanged for argon using standard Schlenk techniques upon which alpha-tetralone **[83]** (18 μL, 20 mg, 0.13 mmol, 3.00 equiv.) was added in one portion. The reaction was stirred at 50 °C for 1 hour, upon which UHPLC-MS (C₁₈, acidic) analysis confirmed full conversion.

Work-up: The product was precipitated with the addition of Et₂O (3 mL) and was placed inside the freezer for 30 minutes. The precipitate was collected by suction filtration and was washed with fresh -20 °C Et₂O (2 x 3 mL). The solids were dried *in vacuo* to yield 19 mg (80 %) of (*E*)-2-((7-(2-(3,4-dihydronaphthalen-1(2H)-ylidene)hydrazineyl)-N-methylbenzo[c][1,2,5]thiadiazole)-4-sulfonamido)-N,N,N-trimethylethan-1-aminium iodide **[113]** as bright orange solids.

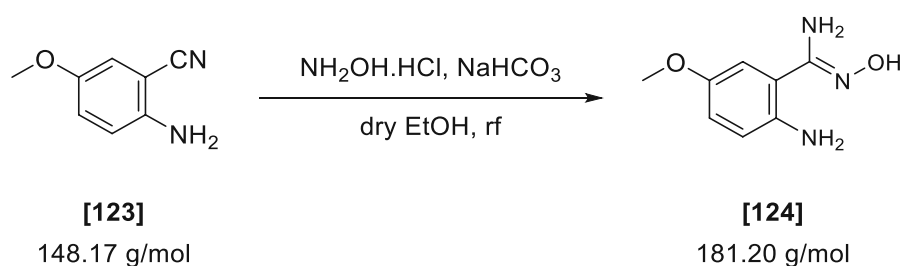
Yield	19 mg (80 %)
Appearance	bright orange solid
TLC	-
Reaction scale	20 mg (0.04 mmol)
Substrate concentration	0.04 M
Purification	pure after work-up
Sum formula, m.w.	C ₂₂ H ₂₉ IN ₆ O ₂ S ₂ , 600.54 g/mol
M.p.	decomposition > 100 °C
¹ H-NMR (400 MHz, DMSO- <i>d</i> ₆)	δ 1.92 (dt, J = 5.4, 12.5 Hz, 2H, -CH ₂ - (H3')), 2.77 – 2.87 (m, 5H, -NCH ₃ , Ar-CH ₂ (H4')), 2.95 (t, J = 6.5 Hz, 2H, -CH ₂ -C=N (H2')), 3.17 (s, 9H, -N(CH ₃) ₃), 3.61 (d, J = 6.5 Hz, 2H, -CH ₂ -N(CH ₃) ₃), 3.71 (t, J = 6.3 Hz, 2H, -SO ₂ N-CH ₂ -), 7.20 – 7.37 (m, 3H, H5', H6', H7'), 7.45 (d, J = 8.3 Hz, 1H, H6), 8.16 – 8.26 (m, 2H, H5, H8'), 10.10 (s, 1H, -NH-).
¹³ C-NMR (101 MHz, DMSO- <i>d</i> ₆)	δ 21.3 (t, -CH ₂ - (C3')), 25.4 (t, -CH ₂ -C=N (C2')), 28.9 (t, Ar-CH ₂ - (C4')), 35.0 (q, -NCH ₃), 44.5 (t, -SO ₂ N-CH ₂ -), 52.7 (q, -N(CH ₃) ₃), 3C), 61.7 (t, -CH ₂ -N(CH ₃) ₃), 103.1 (d, C6), 115.4 (s, C4), 124.4 (d, C8'), 126.4 (d, C7'), 128.7 (s, C5'), 129.2 (s, d, C6'), 132.2 (s, C8a'), 136.5 (d, C5), 139.9 (s, C4a'), 141.4 (s, C7), 145.6 (s, C7a), 150.4 (s, C3a), 151.4 (s, -C=N-).
HRMS (ESI)	calc. for C ₂₂ H ₂₉ N ₆ O ₂ S ₂ ⁺ [M-I] ⁺ 473.1788, found 473.1820 – Δ = 6.74 ppm.

E III.6 Part VI – Improving water solubility of ABAO reagents



NMR assignments of core structures in this chapter were given according to the following example.

E III.6.1 5-Methoxy-2-amino benzamidoxime (5-MeO-ABAO) [124]



The product was synthesized according to a modified literature procedure⁶².

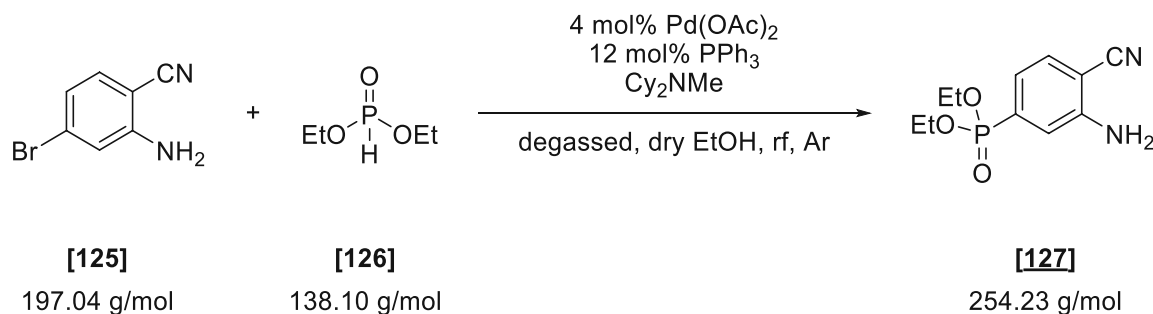
Procedure: 2-Amino-5-methoxybenzonitrile [123] (1.00 g, 6.75 mmol, 1.00 equiv.), hydroxylamine hydrochloride (0.56 g, 4.72 mmol, 1.20 equiv.), and NaHCO₃ (0.85 g, 10.12 mmol, 1.50 equiv.) were suspended in a 25 mL screw-cap vial with dry EtOH (12.5 mL). To solubilize, the base HPLC grade H₂O (4 mL) was added, leading to immediate gas evolution. The resulting suspension was heated to 80 °C for 2 days, upon which TLC indicated full conversion.

Work up: To dissolve all polar or ionic components, dH₂O (4 mL) was added, and the solution was cooled to 0 °C, upon which spontaneous product precipitation occurred. The solids were collected by suction filtration, were washed twice with ice-cold dH₂O (2 x 10 mL), twice with ice-cold EtOH (2 x 5 mL), and with Et₂O (20 mL). The product was dried *in vacuo* to yield 0.99 g (81 %) of 5-MeO-ABAO [124] as an off-white crystalline solid. The target product was used for further experimentation without further purification.

Yield	0.99 g (81 %)
Appearance	off-white crystalline solid
Reaction scale	1.00 g (6.75 mmol)
Substrate concentration	0.54 M
Purification	pure after work-up
Sum formula, m.w.	C ₈ H ₁₁ NO ₂ , 181.20 g/mol
M.p.	156.7 – 157.9 °C (lit.: ⁶² 156 - 157 °C)

- ¹H-NMR (400 MHz, DMSO-*d*₆)** δ 3.67 (s, 3H, -OCH₃), 5.73 (s, 2H, -NH₂), 5.74 (s, 2H, -NH₂), 6.61 (d, *J* = 8.7 Hz, 1H, H3), 6.70 (dd, *J* = 2.9, 8.8 Hz, 1H, H4), 6.94 (d, *J* = 2.9 Hz, 1H, H6), 9.56 (s, 1H, -OH).
- ¹³C-NMR (101 MHz, DMSO-*d*₆)** δ 55.5 (q, -OCH₃), 112.2 (d, C6), 114.9 (s, C1), 116.0 (d, C4), 116.7 (d, C3), 140.8 (s, C2), 149.8 (s, C5), 152.6 (s, -C=NOH).

E III.6.2 Diethyl (3-amino-4-cyanophenyl)phosphonate [127]



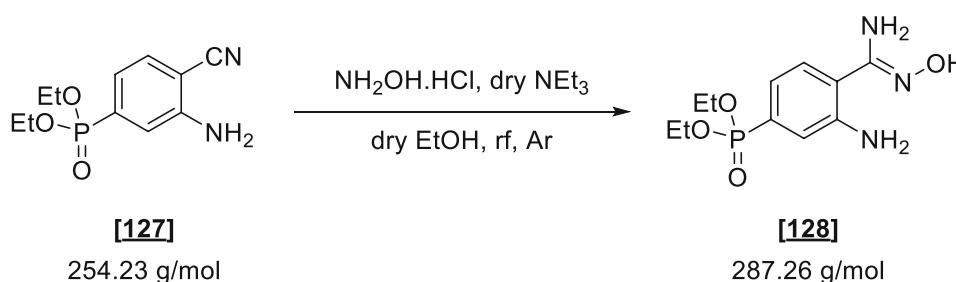
The product was synthesized according to a literature procedure^{243,244}.

Procedure: A flame-dried, argon purged 100 mL Schlenk-flask was charged with dry EtOH (60 mL), which was degassed by the freeze-thaw method in three cycles. Pd(OAc)₂ (0.14 g, 0.61 mmol, 0.04 equiv.) and PPh₃, (0.48 g, 1.83 mmol, 0.12 equiv.) were subsequently added, and the bright yellow suspension was stirred at room temperature for 1 hour under argon until most of the solids were dissolved. Subsequently, 2-amino-4-bromobenzonitrile [125] (3.00 g, 15.23 mmol, 1.00 equiv.), freshly distilled Cy₂NMe (4.89 mL, 4.46 g, 22.84 mmol, 1.50 equiv.) and freshly distilled diethyl phosphite [126] (2.35 mL, 2.52 g, 18.27 mmol, 1.20 equiv.) were added successively with gentle argon counterflow, which led to a slight darkening of the suspension after the addition of the base. The reaction mixture was additionally degassed three times by applying a mild vacuum to the suspension until the solvent started to boil, followed by an immediate argon purge. The yellow suspension was then heated to 80 °C for 18 hours, upon which TLC and GC-MS (method B) indicated full conversion. Complete dissolution of all particulates was generally observed after 1 hour.

Work-up: The solvent was removed *in vacuo*, and the resulting oily residue was taken up in EtOAc (50 mL) and washed with twice 1N HCl (2 x 100 mL). The aqueous phase was re-extracted twice with EtOAc (2 x 100 mL). The combined organic layers were washed with sat. NaHCO₃ (100 mL), brine (100 mL), dried over Na₂SO₄ and concentrated. The crude product was further purified *via* column chromatography (LP/EtOAc – 4:1) to yield 3.07 g (79 %) of diethyl (3-amino-4-cyanophenyl)phosphonate [127] as a colorless crystalline solid. Minimal contaminations with triphenylphosphine oxide (approx. 5 %) were impossible to remove by chromatography. The product was nevertheless used for the next steps without additional purification. In order to remove the oxidized ligand, an additional washing with ice-cold 1:1 CH₂Cl₂/Et₂O was necessary, enabling the isolation of a highly pure product albeit with diminished yield (approx. 40 - 50 %).

Yield	3.07 g (79 %)
Appearance	colorless crystalline solid
Reaction scale	3.00 g (15.73 mmol)
Substrate concentration	0.25 M
Purification	column chromatography (silica) LP/EtOAc 1:4
Sum formula, m.w.	C ₁₁ H ₁₅ N ₂ O ₃ P, 254.23 g/mol
M.p.	101 – 102 °C
¹H-NMR (600 MHz, CDCl₃)	δ 1.32 (t, <i>J</i> = 7.1 Hz, 6H, -CH ₃), 4.02 – 4.19 (m, 4H, -O-CH ₂ -), 4.80 (s, 2H, -NH ₂), 7.05 (ddd, <i>J</i> = 1.2, 7.9, 12.3 Hz, 1H, H5), 7.31 (dd, <i>J</i> = 1.2, 15.3 Hz, 1H, H3), 7.45 (dd, <i>J</i> = 4.5, 7.9 Hz, 1H, H6).
¹³C-NMR (151 MHz, CDCl₃)	δ 16.4 (qd, ³ <i>J</i> _{C-P} = 6.4 Hz, 2C, -CH ₃), 62.7 (td, ² <i>J</i> _{C-P} = 5.7 Hz, 2C, -O-CH ₂ -), 98.9 (d, ⁴ <i>J</i> _{C-P} = 3.5 Hz, C1), 116.9 (s, -CN), 118.9 (dd, ² <i>J</i> _{C-P} = 11.8 Hz, C3), 119.6 (dd, ² <i>J</i> _{C-P} = 8.8 Hz, C5), 132.6 (dd, ³ <i>J</i> _{C-P} = 16.2 Hz, C6), 134.5 (d, ¹ <i>J</i> _{C-P} = 184.7 Hz, C4), 149.7 (d, ³ <i>J</i> _{C-P} = 18.4 Hz, C2).
³¹P NMR (243 MHz, CDCl₃)	δ 16.5 (-P(O)(OEt) ₂).
HRMS (ESI)	calc. for C ₁₁ H ₁₆ N ₂ O ₃ P ⁺ [M+H] ⁺ 255.0893, found 255.0859 – Δ = -13.25 ppm.

E III.6.3 Diethyl (3-amino-4-(N'-hydroxycarbamimidoyl)phenyl)phosphonate [128]



Diethyl (3-amino-4-(N'-hydroxycarbamimidoyl)phenyl)phosphonate [128] was synthesized according to general procedure L using diethyl (3-amino-4-cyanophenyl)phosphonate [127] (1.00 g, 3.93 mmol).

Yield	0.80 (71 %)
Appearance	light-yellow solid
Reaction scale	1.00 g (3.93 mmol)
Substrate concentration	0.44 M
Purification	column chromatography (silica) EtOAc
Sum formula, m.w.	C ₁₁ H ₁₈ N ₃ O ₄ P, 287.26 g/mol
M.p.	139 – 141 °C

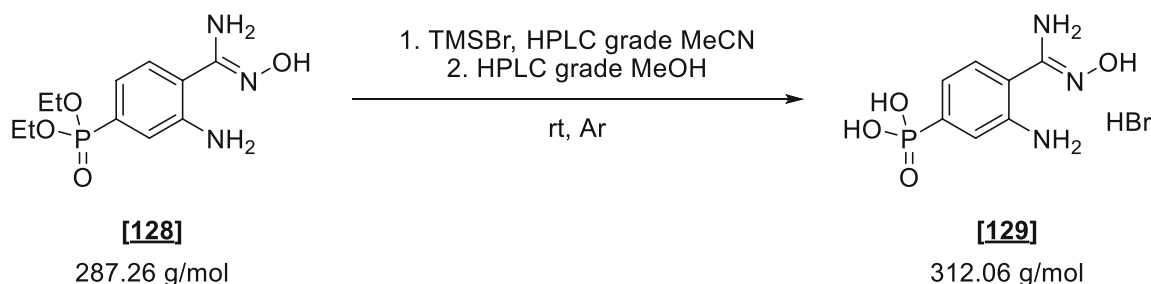
¹H-NMR (400 MHz, DMSO-*d*₆) δ 1.23 (t, *J* = 7.1 Hz, 6H, -CH₃), 3.87 – 4.13 (m, 4H, -O-CH₂-), 5.83 (s, 2H, -NH₂), 6.54 (s, 2H, -NH₂), 6.80 (ddd, *J* = 1.5, 8.0, 12.3 Hz, 1H, H5), 7.06 (dd, *J* = 1.5, 15.0 Hz, 1H, H3), 7.49 (dd, *J* = 4.9, 8.0 Hz, 1H, H6), 9.79 (s, 1H, -OH).

¹³C-NMR (101 MHz, DMSO-*d*₆) δ 16.2 (qd, ³*J*_{C-P} = 6.1 Hz, 2C, -CH₃), 61.5 (td, ²*J*_{C-P} = 5.3 Hz, 2C, -O-CH₂-), 116.8 (dd, ²*J*_{C-P} = 9.3 Hz, C5), 117.2 (d, ⁴*J*_{C-P} = 3.2 Hz, C1), 118.2 (dd, ²*J*_{C-P} = 11.8 Hz, C3), 127.6 (dd, ³*J*_{C-P} = 16.4 Hz, C6), 128.3 (d, ¹*J*_{C-P} = 184.5 Hz, C4), 146.7 (d, ³*J*_{C-P} = 17.5 Hz, C2), 152.3 (s, C_{oxim}).

³¹P NMR (243 MHz, DMSO-*d*₆) δ 18.7 (-P(O)(OEt)₂).

HRMS (ESI) calc. for C₁₁H₁₈N₃O₄P⁺ [M+H]⁺ 287.1108, found 288.1079 – Δ = -9.79 ppm.

E III.6.4 (3-Amino-4-(*N*'-hydroxycarbamimidoyl)phenyl)phosphonic acid (4-P-ABAO) [129]

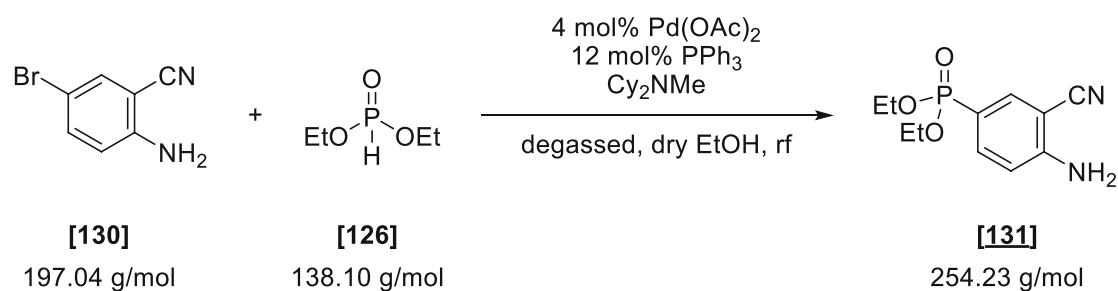


(3-Amino-4-(*N*'-hydroxycarbamimidoyl)phenyl)phosphonic acid [129] was synthesized according to general procedure **M** using diethyl (3-amino-4-(*N*'-hydroxycarbamimidoyl)phenyl)phosphonate [128] (0.50 g, 1.74 mmol). NMR analysis of the crude product indicated high purity. Hence subsequent washing steps were not performed, and the crude product was directly used for further experimentation.

Yield	0.54 g (95 %)
Appearance	light-yellow solid
TLC	-
Reaction scale	0.50 g (1.74 mmol)
Substrate concentration	0.35 M
Purification	-
Sum formula, m.w.	C ₇ H ₁₁ BrN ₃ O ₄ P, 312.06 g/mol
M.p.	decomp. > 150 °C

- ¹H-NMR (400 MHz, DMSO-*d*₆)** δ 6.89 (ddd, *J* = 1.3, 7.8, 12.2 Hz, 1H, H5), 7.16 (dd, *J* = 1.2, 14.8 Hz, 1H, H3), 7.17 (dd, *J* = 4.2, 7.8 Hz, 1H, H6), 8.09 (br s, 4H, 2x -NH₂), 9.07 (s, 1H, -OH).
- ¹³C-NMR (101 MHz, DMSO-*d*₆)** δ 111.7 (d, ⁴*J*_{C-P} = 3.2 Hz, C1), 117.4 (dd, ²*J*_{C-P} = 9.4 Hz, C5), 118.4 (dd, ²*J*_{C-P} = 11.1 Hz, C3), 129.4 (dd, ³*J*_{C-P} = 15.5 Hz, C6), 138.6 (d, ¹*J*_{C-P} = 178.5 Hz, C4), 146.1 (d, ³*J*_{C-P} = 16.9 Hz, C2), 158.6 (s, C_{oxim}).
- ³¹P NMR (243 MHz, DMSO-*d*₆)** δ 12.1 (-P(O)(OH)₂).

E III.6.5 Diethyl (4-amino-3-cyanophenyl)phosphonate [131]



Diethyl (4-amino-3-cyanophenyl)phosphonate [131] was synthesized according to the same procedure used for the synthesis of diethyl (3-amino-4-cyanophenyl)phosphonate [127] using 2-amino-5-bromobenzonitrile [130] (3.00 g, 15.23 mmol).

Yield 3.06 g (79 %)
Appearance colorless crystalline solid

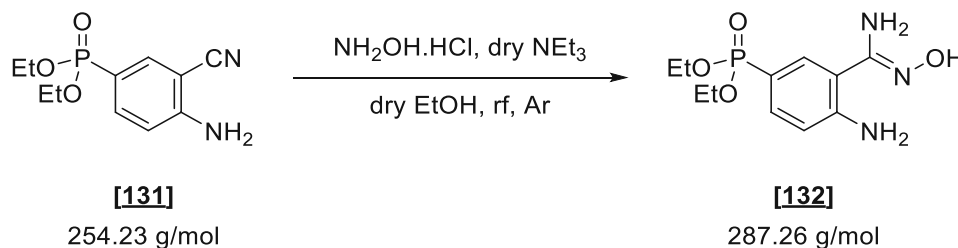
Reaction scale 3.00 g (15.73 mmol)
Substrate concentration 0.25 M
Purification column chromatography (silica) LP/EtOAc 1:4
Sum formula, m.w. C₁₁H₁₅N₂O₃P, 254.23 g/mol
M.p. 108 – 109 °C

¹H-NMR (600 MHz, CDCl₃) δ 1.20 (t, *J* = 7.1 Hz, 6H, -CH₃), 3.82 – 4.03 (m, 4H, -O-CH₂-), 6.79 (s, 2H, -NH₂), 6.86 (dd, *J* = 3.4, 8.7 Hz, 1H, H3), 7.52 (ddd, *J* = 1.9, 8.7, 11.7 Hz, 1H, H4), 7.65 (dd, *J* = 1.9, 13.5 Hz, 1H, H6).

¹³C-NMR (151 MHz, CDCl₃) δ 16.6 (qd, ³*J*_{C-P} = 6.1 Hz, 2C, -CH₃), 61.9 (td, ²*J*_{C-P} = 5.3 Hz, 2C, -O-CH₂-), 93.6 (d, ³*J*_{C-P} = 18.5 Hz, C1), 114.3 (d, ¹*J*_{C-P} = 199.2 Hz, C5), 115.6 (dd, ³*J*_{C-P} = 14.6 Hz, C3), 117.6 (d, ⁴*J*_{C-P} = 1.1 Hz, -CN), 136.7 (dd, ²*J*_{C-P} = 10.6 Hz, C4), 137.6 (dd, ²*J*_{C-P} = 12.6 Hz, C6), 154.7 (d, ⁴*J*_{C-P} = 2.5 Hz, C2).

³¹P NMR (243 MHz, CDCl₃) δ 17.7 (-P(O)(OEt)₂).

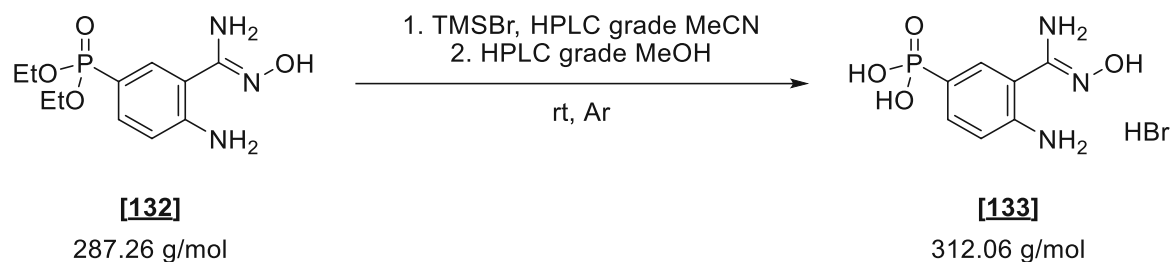
HRMS (ESI) calc. for C₁₁H₁₆N₂O₃P⁺ [M+H]⁺ 255.0893, found 255.0862 – Δ = -12.19 ppm.

E III.6.6 Diethyl (4-amino-3-(N'-hydroxycarbamimidoyl)phenyl)phosphonate **[132]**

Diethyl (3-amino-4-(N'-hydroxycarbamimidoyl)phenyl)phosphonate **[132]** was synthesized according to general procedure L using diethyl (4-amino-3-cyanophenyl)phosphonate **[131]** (1.60 g, 6.29 mmol).

Yield	1.13 g (71 %)
Appearance	light-yellow solid
Reaction scale	1.60 g (6.29 mmol)
Substrate concentration	0.54 M
Purification	column chromatography (silica) EtOAc
Sum formula, m.w.	C ₇ H ₁₈ N ₃ O ₄ P, 287.26 g/mol
M.p.	142 – 143 °C
¹H-NMR (400 MHz, DMSO-<i>d</i>₆)	δ 1.21 (t, <i>J</i> = 7.0 Hz, 6H, -CH ₃), 3.87 – 4.00 (m, 4H, -O-CH ₂ -), 5.82 (s, 2H, -NH ₂), 6.75 (dd, <i>J</i> = 4.1, 8.4 Hz, 1H, H ₃), 6.88 (s, 2H, -NH ₂), 7.30 (ddd, <i>J</i> = 1.8, 8.3, 12.0 Hz, 1H, H ₄), 7.68 (dd, <i>J</i> = 1.8, 14.1 Hz, 1H, H ₆), 9.72 (s, 1H, -OH).
¹³C-NMR (101 MHz, DMSO-<i>d</i>₆)	δ 16.2 (qd, ³ <i>J</i> _{C-P} = 6.1 Hz, 2C, -CH ₃), 61.0 (td, ² <i>J</i> _{C-P} = 5.2 Hz, 2C, -O-CH ₂ -), 111.8 (d, ¹ <i>J</i> _{C-P} = 198.6 Hz, C5), 113.7 (d, ³ <i>J</i> _{C-P} = 15.9 Hz, C1), 115.0 (dd, ³ <i>J</i> _{C-P} = 15.3 Hz, C3), 131.6 (dd, ² <i>J</i> _{C-P} = 12.8 Hz, C6), 132.1 (dd, ² <i>J</i> _{C-P} = 10.6 Hz, C4), 150.3 (d, ⁴ <i>J</i> _{C-P} = 2.6 Hz, C2), 152.4 (s, -C=NOH).
³¹P NMR (243 MHz, DMSO-<i>d</i>₆)	δ 20.6 (-P(O)(OEt) ₂).
HRMS (ESI)	calc. for C ₇ H ₁₉ N ₃ O ₄ P ⁺ [M+H] ⁺ 288.1108, found 288.1082 – Δ = -8.78 ppm.

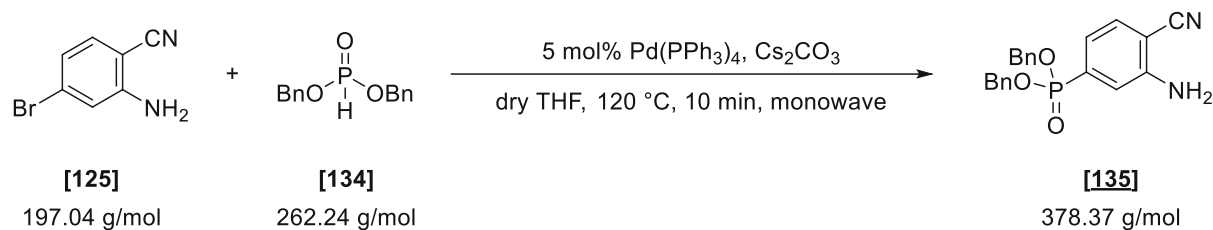
E III.6.7 (3-Amino-4-(N'-hydroxycarbamimidoyl)phenyl)phosphonic acid (5-P-ABAO) [133]



(3-Amino-4-(N'-hydroxycarbamimidoyl)phenyl)phosphonic acid [133] was synthesized according to general procedure **M** using diethyl (3-amino-4-(N'-hydroxycarbamimidoyl)phenyl)phosphonate [132] (0.60 g, 2.09 mmol). As NMR analysis indicated increased side product formation, repeated washing steps were needed for the isolation of pure product, diminishing the overall yield.

Yield	0.33 g (51 %)
Appearance	light-yellow solid
Reaction scale	0.50 g (1.74 mmol)
Substrate concentration	0.35 M
Purification	trituration in ice-cold EtOH
Sum formula, m.w.	C ₇ H ₁₁ BrN ₃ O ₄ P, 312.06 231.15 g/mol
M.p.	decomp. > 150 °C
¹H-NMR (400 MHz, DMSO-<i>d</i>₆)	δ 6.89 (ddd, <i>J</i> = 1.3, 7.8, 12.2 Hz, 1H, H5), 7.16 (dd, <i>J</i> = 1.2, 14.8 Hz, 1H, H3), 7.17 (dd, <i>J</i> = 4.2, 7.8 Hz, 1H, H6), 8.09 (br s, 4H, 2x -NH ₂), 9.07 (s, 1H, -OH).
¹³C-NMR (101 MHz, DMSO-<i>d</i>₆)	δ 111.7 (d, ⁴ <i>J</i> _{C-P} = 3.2 Hz, C1), 117.4 (dd, ² <i>J</i> _{C-P} = 9.4 Hz, C5), 118.4 (dd, ² <i>J</i> _{C-P} = 11.1 Hz, C3), 129.4 (dd, ³ <i>J</i> _{C-P} = 15.5 Hz, C6), 138.6 (d, ¹ <i>J</i> _{C-P} = 178.5 Hz, C4), 146.1 (d, ³ <i>J</i> _{C-P} = 16.9 Hz, C2), 158.6 (s, C _{oxim}).
³¹P NMR (243 MHz, DMSO-<i>d</i>₆)	δ 12.1 (-P(O)(OH) ₂).
HRMS (ESI)	not found

E III.6.8 Dibenzyl (3-amino-4-cyanophenyl)phosphonate [135]



The product was synthesized according to a modified literature procedure^{243,244}.

Procedure: A 10 mL Monowave vial was charged with 2-amino-4-bromobenzonitrile **[125]** (0.25 g, 1.25 mmol, 1.00 equiv.), Cs₂CO₃ (0.49 g, 1.50 mmol, 1.10 equiv.) and Pd(PPh₃)₄ (72 mg, 0.06 mmol, 0.05 equiv.) which were suspended in dry THF (5 mL). Subsequently, dibenzyl phosphite **[134]** (0.30 mL, 0.36 g, 1.38 mmol, 1.10 equiv.) was added, and the suspension was degassed for 30 minutes under sonication by bubbling argon through it. The vial was capped, and the mixture was heated at 120 °C for 10 minutes in a Monowave 50 reactor. The reaction was allowed to reach room temperature, upon which TLC confirmed full conversion.

Work-up: The suspension was immediately flashed over a pad of Celite and concentrated to leave a deep yellow oil. The crude product was further purified *via* column chromatography (LP/EtOAc – 1:1) to yield 0.27 g (58 %) of dibenzyl (3-amino-4-cyanophenyl)phosphonate **[135]** as a brown oil.

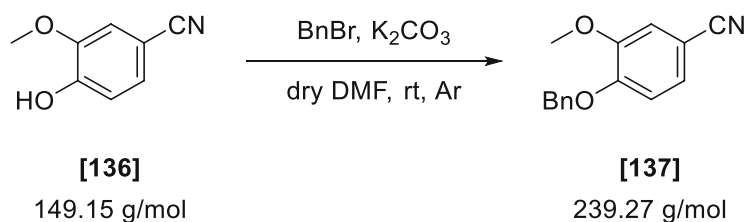
Yield	0.27 g (58 %)
Appearance	brown oil
TLC	R _f (LP/EtOAc – 1:1) = 0.15 (anisaldehyde)
Reaction scale	0.25 g (15.73 mmol)
Substrate concentration	0.25 M
Purification	column chromatography (silica) LP/EtOAc 1:1
Sum formula, m.w.	C ₂₁ H ₁₉ N ₂ O ₃ P, 378.37 g/mol

¹H-NMR (600 MHz, CDCl₃) δ 4.71 (s, 2H, -NH₂), 4.99 – 5.11 (m, 4H, -O-CH₂-), 7.04 (ddd, *J* = 1.3, 7.9, 12.5 Hz, 1H, H5), 7.22 (dd, *J* = 1.2, 15.6 Hz, 1H, H3), 7.28 – 7.35 (m, 10H, HAr), 7.40 (dd, *J* = 4.7, 7.9 Hz, 1H, H6).

¹³C-NMR (151 MHz, CDCl₃) δ 68.1 (td, ²*J*_{C-P} = 5.5 Hz, -O-CH₂-), 99.1 (d, ⁴*J*_{C-P} = 3.6 Hz, C1), 116.8 (s, -CN), 118.8 (dd, ²*J*_{C-P} = 11.9 Hz, C3), 119.8 (dd, ²*J*_{C-P} = 9.1 Hz, C5), 128.1 (d, 4C, C2', C6'), 128.7 (d, 6C, 2x C3', C5', C4'), 132.6 (dd, ³*J*_{C-P} = 16.5 Hz, C6), 134.0 (d, ¹*J*_{C-P} = 186.5 Hz, C4), 135.8 (d, ³*J*_{C-P} = 6.5 Hz, C1'), 149.5 (d, ³*J*_{C-P} = 18.6 Hz, C2).

³¹P NMR (243 MHz, CDCl₃) δ 20.1 (-P(O)(OBn)₂).

E III.6.9 4-(Benzyloxy)-3-methoxybenzonitrile [137]



The product was synthesized according to a literature procedure²⁴⁸.

Procedure: A 250 mL RBF was charged with 4-hydroxy-3-methoxybenzonitrile **[136]** (10.00 g, 67.05 mmol, 1.00 equiv.), which was dissolved in dry DMF (130 mL) under argon atmosphere using standard Schlenk techniques. Anhydrous K_2CO_3 (13.90 g, 100.57 mmol, 1.50 equiv.) and benzyl bromide (13.74 g, 80.31 mmol, 1.20 equiv.) were added, and the reaction was stirred at room temperature for 24 hours, upon which TLC indicated full conversion.

Work-up: The reaction mixture was poured onto brine (150 mL), causing immediate product precipitation. The solids were collected by suction filtration and washed thoroughly with dH_2O (3 x 50 mL) and $-20\text{ }^\circ\text{C}$ EtOH (2 x 10 mL). The resulting colorless solids were dried *in vacuo* to yield 15.40 g (96 %) of 4-(benzyloxy)-3-methoxybenzonitrile **[137]** as a colorless solid. The product could be used for further experimentation without additional purification.

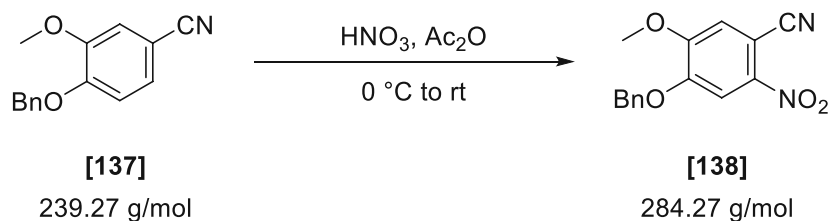
Yield	15.40 g (96 %)
Appearance	colorless solid
TLC	R_f (LP/EtOAc – 5:1) = 0.45 (UV)

Reaction scale	10.00 g (67.05 mmol)
Substrate concentration	0.50 M
Purification	-
Sum formula, m.w.	$\text{C}_{15}\text{H}_{13}\text{NO}_2$, 239.27 g/mol
M.p.	90.5 - 91 $^\circ\text{C}$ (lit. ²⁷⁸ 90 $^\circ\text{C}$)

$^1\text{H-NMR}$ (600 MHz, CDCl_3) δ 3.90 (s, 3H, $-\text{OCH}_3$), 5.20 (s, 2H, $-\text{O-CH}_2-$), 6.91 (d, $J = 8.3$ Hz, 1H, H3), 7.10 (d, $J = 1.9$ Hz, 1H, H6), 7.21 (dd, $J = 1.9, 8.3$ Hz, 1H, H2), 7.31 – 7.35 (m, 1H, H1'), 7.38 (m, $J = 1.3, 6.6, 7.7$ Hz, 2H, H3', H5'), 7.40 – 7.44 (m, 2H, H2', H6').

$^{13}\text{C-NMR}$ (151 MHz, CDCl_3) δ 56.3 (q, $-\text{OCH}_3$), 71.0 (t, $-\text{O-CH}_2-$), 104.3 ($-\text{C}1$), 113.4 (d, C3), 114.5 (d, C6), 119.3 (s, $-\text{CN}$), 126.4 (d, C2), 127.3 (d, 2C, C2', C6'), 128.4 (d, C4'), 128.9 (d, 2C, C3, C5'), 135.9 (s, C1'), 149.8 (s, C5), 152.1 (s, C4).

E III.6.10 4-(Benzyloxy)-5-methoxy-2-nitrobenzonitrile [138]



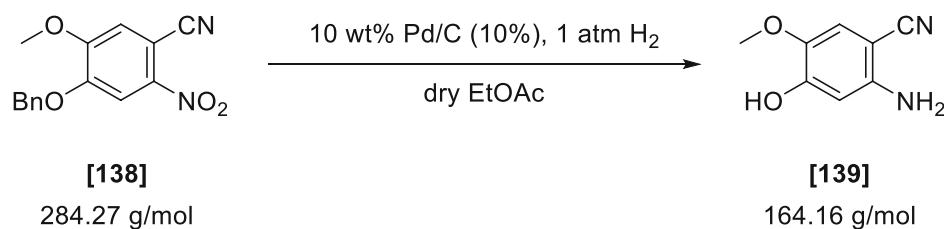
The product was synthesized according to a literature procedure²⁴⁸.

Procedure: A 100 mL three-necked RBF was charged with 4-(benzyloxy)-3-methoxybenzonitrile [137] (15.40 g, 64.36 mmol, 1.00 equiv.), which was dissolved in acetic anhydride (180 mL). One part of the flask was connected directly to the exhaust of the fume hood to limit the exposure of nitrous gases during the reaction. The mixture was cooled *via* ice bath to < 5 °C, followed by the dropwise addition of fuming 90 % HNO₃ (12.00 mL, 18.20 g, 289.63 mmol, 4.50 equiv.) *via* dropping funnel over a period of 30 minutes. The reaction was then allowed to warm to room temperature by stirring in the cooling bath and was continued to stir for another 2 days.

Work-up: The reaction was quenched by pouring the deep yellow suspension into ice-water (200 mL), causing immediate precipitation of the product. The solids were collected by suction filtration and washed thoroughly with ice water (3 x 100 mL) and twice with EtOH (2 x 100 mL). The resulting colorless solids were dried *in vacuo* to yield 12.20 g (67 %) of 4-(benzyloxy)-5-methoxy-2-nitrobenzonitrile [138] as a colorless solid. The product could be used for further experimentation without additional purification.

Yield	12.20 g (67 %)
Appearance	colorless solid
TLC	R _f (LP/EtOAc – 1:1) = 0.30 (UV)
Reaction scale	15.40 g (64.36 mmol)
Substrate concentration	0.36 M
Purification	-
Sum formula, m.w.	C ₁₅ H ₁₂ N ₂ O ₄ , 284.27 g/mol
M.p.	184 – 185 °C (lit. ²⁴⁸ 159 – 162 °C)
¹H-NMR (600 MHz, CDCl₃)	δ 4.01 (s, 3H, -OCH ₃), 5.27 (s, 2H, -O-CH ₂ -), 7.21 (s, 1H, H ₆), 7.34 – 7.41 (m, 1H, H _{4'}), 7.40 – 7.42 (m, 2H, H _{3'} , H _{5'}), 7.43 – 7.46 (m, 2H, H _{2'} , H _{6'}), 7.85 (s, 1H, H ₃).
¹³C-NMR (151 MHz, CDCl₃)	δ 57.0 (q, -OCH ₃), 71.7 (t, -O-CH ₂ -), 101.0 (s, C ₁), 109.5 (d, C ₃), 115.5 (s, -CN), 115.7 (d, C ₆), 127.7 (d, 2C, C _{3'} , C _{5'}), 128.9 (d, C _{4'}), 129.0 (d, 2C, C _{2'} , C _{6'}), 134.4 (s, C _{1'}), 142.6 (s, C ₂), 151.2 (s, C ₄), 153.8 (s, C ₅).

E III.6.11 2-Amino-4-hydroxy-5-methoxybenzonitrile [139]

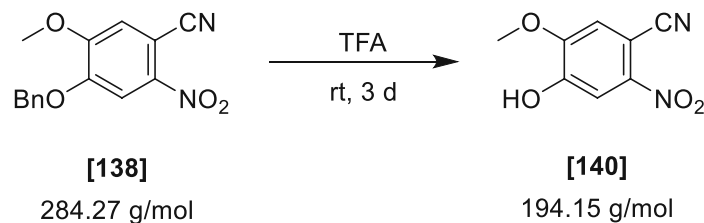


Procedure: A 250 mL three-necked RBF was charged with 4-(benzyloxy)-5-methoxy-2-nitrobenzonitrile **[138]** (5.00 g, 17.59 mmol, 1.00 equiv.) and 10% Pd/C (10 wt%; 0.50 g). The flask was evacuated and backfilled with argon using standard Schlenk techniques. The catalyst and starting material were suspended in HPLC grade EtOAc (50 mL), and hydrogen was introduced into the reaction by alternately applying 5 vacuum and hydrogen purges. The reaction was kept at room temperature with strong stirring for 1 day, upon which TLC indicated full conversion. During the reaction, complete dissolution of the starting material (3 hours) and subsequent precipitation of the product was observed.

Work-up: MeOH (200 mL) was added to solubilize the product, and the dark suspension was filtered over a large pad of Celite. The pad was thoroughly flushed with fresh MeOH (approx. 1 L) until complete product elution was confirmed *via* TLC. The collected colorless filtrate exhibited immediate darkening upon continuous exposure to air and light. Hence, the solvent was quickly evaporated to dryness to leave a dark brown viscous oil. The crude product was further purified *via* column chromatography (CH₂Cl₂/MeOH – 50:1 to 15:1). As no dissolution of the product was possible in any CH₂Cl₂ mixtures, the crude was dissolved in MeOH and subjected to the column preconditioned with pure CH₂Cl₂. Upon evaporation of the solvent, 1.95 g (68 %) of 2-amino-4-hydroxy-5-methoxybenzonitrile **[139]** was isolated as ochre solid that quickly tarnished upon contact with air. The product was therefore stored at -20 °C under argon.

Yield	1.95 g (68 %)
Appearance	ochre solids that tarnish immediately upon contact with air
TLC	R _f (EtOAc) = 0.45 (UV)
Reaction scale	5.00 g (17.59 mmol)
Substrate concentration	0.34 M
Purification	column chromatography (silica) CH ₂ Cl ₂ /MeOH 50:1 to 15:1
Sum formula, m.w.	C ₈ H ₉ N ₂ O ₂ , 164.16 g/mol
M.p.	decomposition in air
¹H-NMR (600 MHz, CDCl₃)	δ 3.80 (s, 3H, -OCH ₃), 4.16 (br s, 3H, -NH ₂), 6.29 (s, 1H, H3), 6.77 (s, 1H, H6).
¹³C-NMR (151 MHz, CDCl₃)	δ 56.5 (q, -OCH ₃), 86.3 (s, C1), 102.0 (d, C3), 113.0 (d, C6), 118.3 (s, -CN), 139.7 (s, C5), 146.5 (s, C2), 151.6 (s, C4).

E III.6.12 4-Hydroxy-5-methoxy-2-nitrobenzonitrile [140]



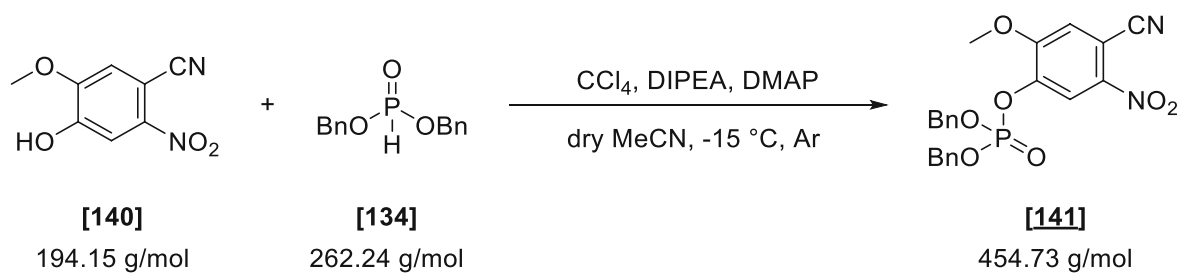
The product was synthesized according to a literature procedure²⁴⁹.

Procedure: A 250 mL RBF was charged with 4-(benzyloxy)-5-methoxy-2-nitrobenzonitrile **[138]** (5.00 g, 17.59 mmol, 1.00 equiv.), which was dissolved in TFA (100 mL). The reaction was stirred at room temperature for 3 days, upon which TLC indicated full conversion.

Work-up: The solvent was removed *in vacuo*, and the crude was taken up in d.H₂O (100 mL) and CH₂Cl₂ (400 mL). The aqueous phase was extracted twice with fresh CH₂Cl₂ (2 x 100 mL), and the combined organic layers were washed with brine (200 mL), dried over Na₂SO₄, and concentrated to leave a dark green/greyish, waxy solid. The crude was adsorbed onto Celite with a mixture of 1:1 CH₂Cl₂/MeOH and was purified *via* column chromatography (CH₂Cl₂/MeOH – 50:1 to 20:1) to yield 2.21 g (65 %) of 2-amino-4-hydroxy-5-methoxybenzonitrile **[140]** as crystalline off-white solid.

Yield	2.21 g (67 %)
Appearance	crystalline off-white solid
Reaction scale	5.00 g (17.59 mmol)
Substrate concentration	0.18 M
Purification	column chromatography (silica) CH ₂ Cl ₂ /MeOH 50:1 to 20:1
Sum formula, m.w.	C ₈ H ₆ N ₂ O ₄ , 194.15 g/mol
M.p.	decomp. > 150 °C
¹H-NMR (600 MHz, DMSO-<i>d</i>₆)	δ 3.96 (s, 3H, -OCH ₃), 7.64 (s, 1H, H ₆), 7.71 (s, 1H, H ₃), 11.32 (s, 1H, -OH).
¹³C-NMR (151 MHz, DMSO-<i>d</i>₆)	δ 56.9 (q, -OCH ₃), 97.7 (s, C ₁), 112.0 (d, C ₃), 116.1 (s, -CN), 117.2 (d, C ₆), 142.2 (s, C ₂), 150.8 (s, C ₄), 152.5 (s, C ₅).

E III.6.13 Dibenzyl (4-cyano-2-methoxy-5-nitrophenyl) phosphate [141]



The product was synthesized according to a modified literature procedure²⁴².

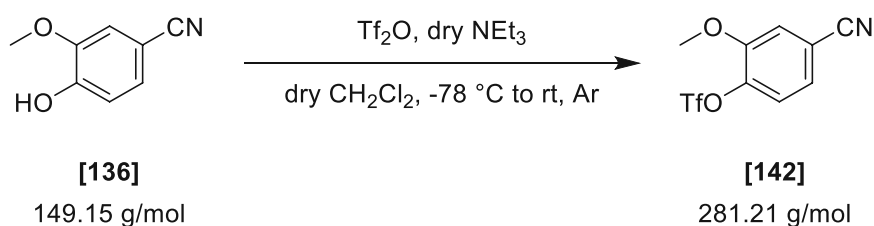
Procedure: A flame-dried 30 mL three-necked RBF was charged with 2-amino-4-hydroxy-5-methoxybenzonitrile [140] (0.20 g, 1.03 mmol, 1.00 equiv.) and then evacuated and purged with argon using standard Schlenk techniques. The solids were suspended in dry MECN (6 mL), and dry DIPEA (0.38 mL, 0.28 g, 2.16 mmol, 2.10 equiv.) was added at room temperature, which led to immediate dissolution and a strong red color change of the solution. Subsequently, CCl_4 (0.50 mL, 0.79 g, 5.15 mmol, 5.00 equiv.) followed by DMAP (12 mg, 0.10 mmol, 0.10 equiv.) were added in with gentle argon counterflow, and the solution was cooled to $-15 \text{ }^\circ\text{C}$ by stirring in an ice/NaCl/water bath. Dropwise addition of dibenzyl phosphite [134] (0.33 mL, 0.39 g, 1.49 mmol, 1.45 equiv.) over a period of 2 minutes gradually brightened the solution until a deep yellow color persisted. The reaction was then stirred for 1 hour at $-15 \text{ }^\circ\text{C}$, upon which TLC indicated full conversion.

Work-up: The reaction was quenched with the addition of 0.5 M KH_2PO_4 (2 mL). The layers were separated, and the aqueous phase was extracted with EtOAc (5 mL). The combined organics were washed with 1 N HCl (20 mL) and brine (20 mL), dried over Na_2SO_4 and concentrated. The crude product was further purified *via* column chromatography (LP/EtOAc – 1.5:1) to yield 0.31 g (64 %) of dibenzyl (3-amino-4-cyanophenyl)phosphonate [141] as a colorless oil that solidified upon standing.

Yield	0.31 g (64 %)
Appearance	colorless crystalline solid
Reaction scale	0.20 g (1.03 mmol)
Substrate concentration	0.17 M
Purification	column chromatography (silica) LP/EtOAc – 1.5:1
Sum formula, m.w.	$\text{C}_{22}\text{H}_{19}\text{N}_2\text{O}_7\text{P}$, 454.73 g/mol
M.p.	$81 - 84 \text{ }^\circ\text{C}$

$^1\text{H-NMR}$ (600 MHz, CDCl_3)	δ 3.91 (s, 3H, $-\text{CH}_3$), 5.19 (qd, $J = 11.6, 9.4$ Hz, 4H, $-\text{O-CH}_2-$), 7.23 (s, 1H, H3), 7.33 – 7.39 (m, 10H, PhH), 8.02 (d, $J = 1.3$ Hz, 1H, H6).
$^{13}\text{C-NMR}$ (151 MHz, CDCl_3)	δ 57.2 (q, $-\text{CH}_3$), 70.9 (td, $^2J_{\text{C-P}} = 6.0$ Hz, 2C, $-\text{O-CH}_2-$), 105.9 (s, C1), 114.8 (s, $-\text{CN}$), 117.5 (s, C6), 119.2 (dd, $^3J_{\text{C-P}} = 3.0$ Hz, C3), 128.3 (d, 4C, C2', C6'), 128.8 (d, 4C, 2x C3', C5'), 129.2 (d, 2C, 2x C4'), 134.9 (d, $^3J_{\text{C-P}} = 6.1$ Hz, 2C, 2x C1'), 141.7 (s, C2), 142.4 (d, $^2J_{\text{C-P}} = 6.6$ Hz, C4), 155.4 (d, $^3J_{\text{C-P}} = 5.4$ Hz, C5).
$^{31}\text{P NMR}$ (243 MHz, CDCl_3)	δ -6.7 ($-\text{O-P(O)(OBn)}_2$).
HRMS (ESI)	mass not found.

E III.6.14 4-Cyano-2-methoxyphenyl trifluoromethanesulfonate [142]



The product was synthesized according to a literature procedure²⁵².

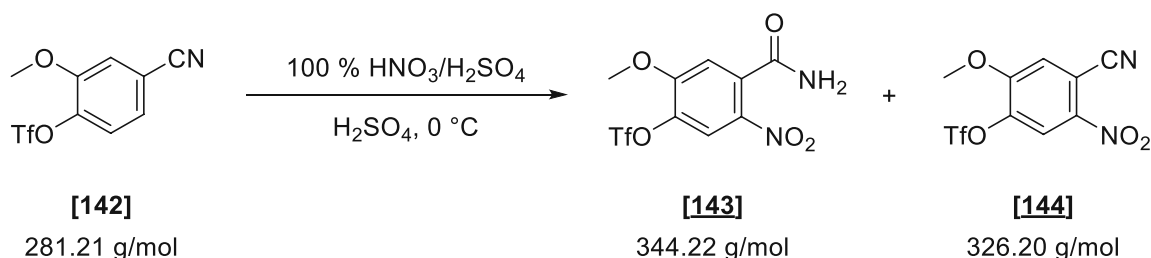
Procedure: A flame-dried 250 mL three-necked RBF was charged with 4-hydroxy-3-methoxybenzonitrile [136] (10.00 g, 67.11 mmol, 1.00 equiv.) and then evacuated and backfilled with argon using standard Schlenk techniques. Subsequently, dry CH_2Cl_2 (120 mL) and dry triethylamine (28 mL, 20 g, 201 mmol, 3.00 equiv.) were added, and the reaction was cooled down to $< -75^\circ\text{C}$ with an acetone/liquid N_2 cooling bath. Tf_2O (12.5 mL, 21.0 g, 74.3 mmol, 1.10 equiv.) was added over a period of 40 minutes *via* a dropping funnel turning the solution reddish-brown and viscous. The suspension was then gradually warmed by stirring in the cooling bath. During warming, improved stirring and minor precipitation of bright solids were observed. The dark solution was then stirred at room temperature for 12 hours, upon which TLC indicated full conversion.

Procedure: The reaction was quenched with the addition of dH_2O (200 mL). The phases were separated, and the aqueous phase was extracted three times with CH_2Cl_2 (3 x 100 mL). The combined organic layers were washed with brine (250 mL), dried over Na_2SO_4 , and concentrated. The crude product was further purified *via* flash chromatography (CH_2Cl_2) to yield 18.27 g (97 %) of 4-cyano-2-methoxyphenyl trifluoromethanesulfonate [142] as a colorless or yellowish oil that solidified upon standing.

Yield	18.27 g (97 %)
Appearance	colorless or yellowish crystalline solid
TLC	R_f (LP/EtOAc – 3:1) = 0.64 (KMnO_4)

Reaction scale	10.00 g (67.11 mmol)
Substrate concentration	0.56 M
Purification	flash chromatography (silica) CH ₂ Cl ₂
Sum formula, m.w.	C ₉ H ₆ F ₃ NO ₄ S, 281.21 g/mol
M.p.	50.6 – 51.9 °C (lit. ²⁷⁹ 51 – 53 °C)
¹ H-NMR (600 MHz, CDCl ₃)	δ 3.92 (s, 3H, -OCH ₃), 7.25 (d, <i>J</i> = 1.6 Hz, 1H, H ₆), 7.28 (dd, <i>J</i> = 1.1, 2.3 Hz, 2H, H ₂ , H ₃).
¹³ C-NMR (151 MHz, CDCl ₃)	δ 56.8 (q, -OCH ₃), 113.4 (-C1), 116.7 (d, C ₆), 117.5 (s, -CN), 118.7 (q, ¹ <i>J</i> _{C-F} = 320.5 Hz, -CF ₃), 123.8 (d, C ₃), 125.4 (d, C ₂), 141.7 (s, C ₄), 152.1 (s, C ₅).
¹⁹ F NMR (565 MHz, CDCl ₃)	δ -73.7 (-CF ₃).

E III.6.15 4-Carbamoyl-2-methoxy-5-nitrophenyl trifluoromethanesulfonate **[143]** and 4-cyano-2-methoxy-5-nitrophenyl trifluoromethanesulfonate **[144]**



Procedure: A 250 mL three-necked RBF was charged with 4-cyano-2-methoxyphenyl trifluoromethanesulfonate **[142]** (13.00 g, 46.23 mmol, 1.00 equiv.), which was dissolved in conc. H₂SO₄ (100 mL) applying mild heating. Upon full dissolution, the gold-colored mixture was cooled to < 5 °C *via* ice/water bath. While cooling a mixture of 90 % HNO₃ (4.80 mL, 7.28 g, 115.57 mmol, 2.50 equiv.) in conc. H₂SO₄ (12 mL) was prepared in a separate vial. The nitrating agent was then added dropwise to the cooled solution at < 5 °C *via* dropping funnel in approximately 15 minutes. Immediate darkening of the reaction was observed at the first contact of the reagent. Upon completed addition, the mixture was stirred for 30 minutes at 0 °C, upon which TLC indicated full conversion.

Work-up: The dark red reaction mixture was poured onto a freshly prepared solid ice/solid NaHCO₃ (approx. 500 g) mixture in a 2 L glass beaker. The waxy orange product immediately precipitated and deposited on the walls of the beaker. Neutralization of the strongly acidic solution was achieved with the addition of copious amounts of solid NaHCO₃ under strong stirring. At neutral pH, EtOAc (400 mL) was added, and the phases were separated. The aqueous phase was extracted twice with EtOAc (2 x 200 mL). The combined organic layers were washed with brine (250 mL), dried over Na₂SO₄, and the solvent was evaporated in *vacuo*. The resulting pinkish solids were sonicated in diisopropyl ether (50 mL) for 5 minutes and collected by suction filtration. Repeated washing with diisopropyl ether (3 x 40 mL) yielded 7.26 g (46 %) of the corresponding amide **[143]** as off-white solids.

Evaporation of the filtrate revealed the desired product. The crude was further purified *via* flash chromatography (CH₂Cl₂) to yield 4.41 g (29 %) of 4-cyano-2-methoxy-5-nitrophenyl trifluoromethanesulfonate [144] as a light-yellow solid.

Reaction scale	13.00 g (46.23 mmol)
Substrate concentration	0.45 M
Purification	flash chromatography (silica) CH ₂ Cl ₂

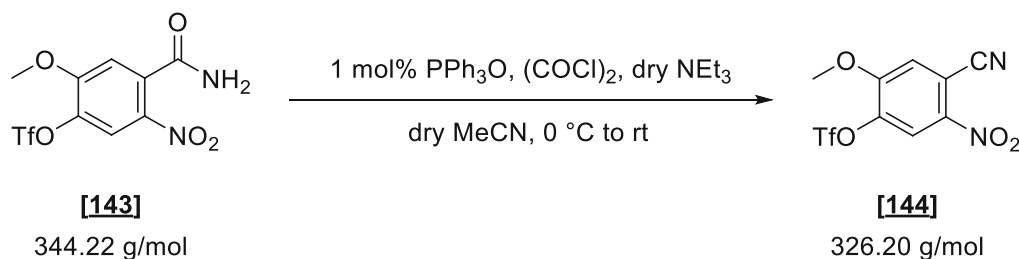
Nitrile [144]:

Yield	4.41 g (29 %)
Appearance	light-yellow solid
TLC	R _f (CH ₂ Cl ₂) = 0.75 (KMnO ₄)
Sum formula, m.w.	C ₉ H ₅ F ₃ N ₂ O ₆ S, 326.20 g/mol
¹ H-NMR (600 MHz, CDCl ₃)	δ 4.13 (s, 3H, -OCH ₃), 7.51 (s, 1H, H ₆), 8.25 (s, 1H, H ₃).
¹³ C-NMR (151 MHz, CDCl ₃)	δ 58.0 (q, -OCH ₃), 109.7 (s, C1), 114.0 (s, -CN), 118.7 (q, ¹ J _{C-F} = 320.9 Hz, -CF ₃), 118.7 (d, C6), 121.1 (d, C3), 140.2 (s, C2), 141.6 (s, C4), 156.3 (s, C5).
¹⁹ F NMR (565 MHz, CDCl ₃)	δ -73.1 (-CF ₃).

Amide [143]:

Yield	7.26 g (46 %)
Appearance	off-white solid
TLC	R _f (CH ₂ Cl ₂) = 0.10 (KMnO ₄)
Sum formula, m.w.	C ₉ H ₇ F ₃ N ₂ O ₇ S, 344.22 g/mol
¹ H-NMR (600 MHz, DMSO- <i>d</i> ₆)	δ 4.06 (s, 3H, -OCH ₃), 7.52 (s, 1H, H ₆), 7.85 (s, 1H, -CONH ₂), 8.15 (s, 1H, -CONH ₂), 8.34 (s, 1H, H ₃).
¹³ C-NMR (151 MHz, DMSO- <i>d</i> ₆)	δ 57.94 (q, -OCH ₃), 113.74 (d, C3), 118.13 (q, ¹ J _{C-F} = 320.6 Hz, -CF ₃), 119.79 (d, C6), 135.67 (s, C1), 136.49 (s, C2), 138.43 (s, C4), 154.72 (s, C5), 166.04 (-CONH ₂).
¹⁹ F NMR (565 MHz, DMSO- <i>d</i> ₆)	δ -73.5 (-CF ₃).

E III.6.16 4-Cyano-2-methoxy-5-nitrophenyl trifluoromethanesulfonate [144]



The product was synthesized according to a modified literature procedure²⁵¹.

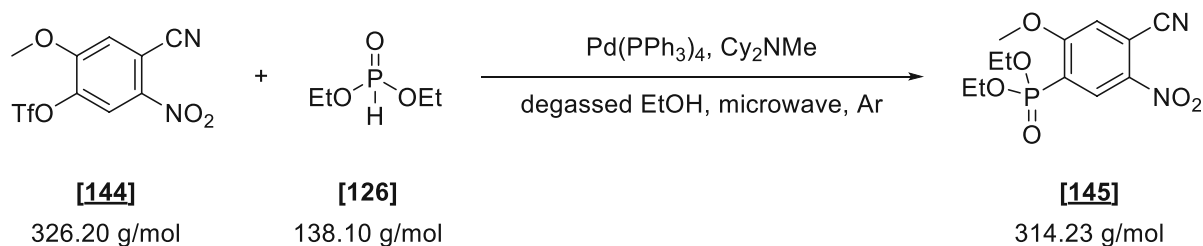
Procedure: A flame-dried 250 mL three-necked RBF was charged with 4-carbamoyl-2-methoxy-5-nitrophenyl trifluoromethanesulfonate [143] (8.00 g, 23.24 mmol, 1.00 equiv.) and triphenylphosphine oxide (65 mg, 0.23 mmol, 0.01 equiv.). The atmosphere was exchanged for argon using standard Schlenk techniques. Subsequently, dry MeCN (100 mL) and dry triethylamine (9.60 mL, 7.00 g, 69.72 mmol, 3.00 equiv.) were added, which upon addition of base led to a slight darkening of the solution. After cooling the reaction mixture to < -5 °C *via* acetone/ice bath, oxalyl chloride (4.00 mL, 5.90 g, 46.48 mmol, 2.00 equiv.) was added *via* syringe pump in 1 hour directly into a vigorously stirred solution. Careful temperature control was important to maintain a high yielding process. Upon contact with each drop, immediate bubbling and precipitation of solids were observed. Following the completed addition, the temperature was raised to 0 °C, which triggered an increasing reddish discoloring of the suspension. The reaction was stirred for 1 hour, upon which TLC indicated full conversion.

Work-up: The solids were removed by filtration, and the filtrate was evaporated to dryness, leaving a reddish suspension. The crude was taken up in CH₂Cl₂ and was purified *via* flash chromatography (CH₂Cl₂) to yield 6.01 g (79 %) of 4-cyano-2-methoxyphenyl trifluoromethanesulfonate [144] as orange oil that solidified upon standing.

Yield	6.01 g (79 %)
Appearance	light orange crystalline solid
TLC	R _f (CH ₂ Cl ₂) = 0.64 (KMnO ₄)
Reaction scale	8.00 g (23.24 mmol)
Substrate concentration	0.24 M
Purification	flash chromatography (silica) CH ₂ Cl ₂
Sum formula, m.w.	C ₉ H ₆ F ₃ N ₂ O ₆ S, 326.20 g/mol

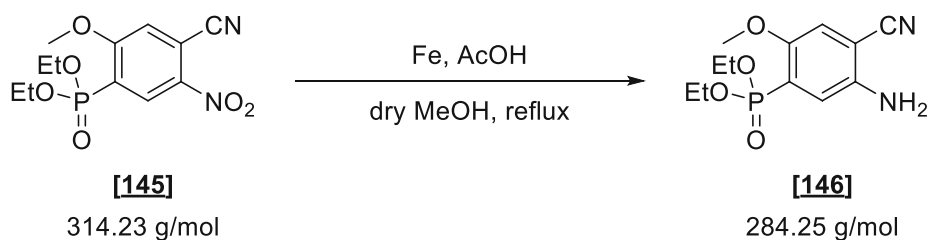
Spectral data in accordance with E III.6.15.

E III.6.17 Diethyl (4-cyano-2-methoxy-5-nitrophenyl)phosphonate [145]



Diethyl (4-cyano-2-methoxy-5-nitrophenyl)phosphonate [145] was synthesized according to general procedure K using 4-cyano-2-methoxyphenyl trifluoromethanesulfonate [144] (0.20 g, 0.61 mmol) and diethyl phosphite [126] (0.12 mL, 0.13 g, 0.92 mmol).

Yield	0.11 g (58 %)
Appearance	colorless crystalline solid
TLC	R_f (EtOAc) = 0.41 (anisaldehyde)
Reaction scale	0.20 g (0.61 mmol)
Substrate concentration	0.26 M
Purification	column chromatography (silica) EtOAc, trituration with -20 °C Et ₂ O
Sum formula, m.w.	C ₁₂ H ₁₅ N ₂ O ₆ P, 314.23 g/mol
M.p.	92 – 93 °C
¹H-NMR (600 MHz, CDCl₃)	δ 1.38 (t, <i>J</i> = 7.1 Hz, 6H, -CH ₃), 4.08 (s, 3H, -OCH ₃), 4.16 – 4.32 (m, 4H, -O-CH ₂ -), 7.36 (d, <i>J</i> = 6.0 Hz, 1H, H ₆), 8.74 (d, <i>J</i> = 15.6 Hz, 1H, H ₃).
¹³C-NMR (151 MHz, CDCl₃)	δ 16.5 (qd, ³ <i>J</i> _{C-P} = 6.0 Hz, 2C, -CH ₃), 57.6 (q, -OCH ₃), 63.5 (td, ² <i>J</i> _{C-P} = 6.0 Hz, 2C, -O-CH ₂), 113.4 (d, ⁴ <i>J</i> _{C-P} = 2.4 Hz, C1), 114.6 (s, -CN), 117.3 (dd, ³ <i>J</i> _{C-P} = 9.3 Hz, C6), 123.7 (d, ¹ <i>J</i> _{C-P} = 189.5 Hz, C4), 132.4 (dd, ² <i>J</i> _{C-P} = 8.3 Hz, C3), 141.1 (d, ³ <i>J</i> _{C-P} = 16.4 Hz, C2), 164.6 (d, ² <i>J</i> _{C-P} = 2.8 Hz, C5).
³¹P NMR (243 MHz, CDCl₃)	δ 9.8 (-P(O)(OEt) ₂).
HRMS (ESI)	calc. for C ₁₂ H ₁₆ N ₂ O ₆ P ⁺ [M+H] ⁺ 315.0741, found 315.0732 – Δ = -2.86 ppm.

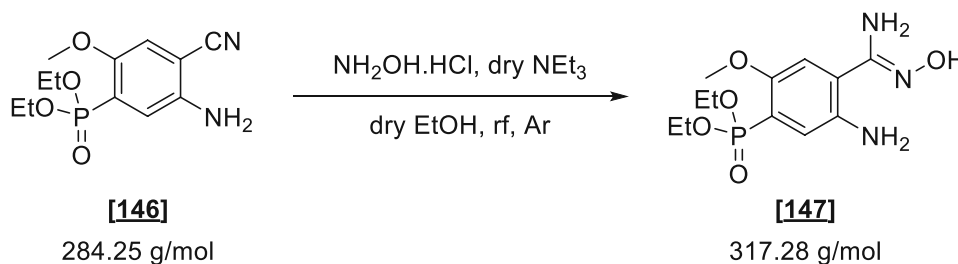
E III.6.18 Diethyl (5-amino-4-cyano-2-methoxyphenyl)phosphonate **[146]**

The product was synthesized according to a modified literature procedure⁶².

Procedure: A flame-dried 250 mL three-necked RBF was charged with diethyl (4-cyano-2-methoxy-5-nitrophenyl)phosphonate **[145]** (0.70 g, 2.23 mmol, 1.00 equiv.) and iron powder (0.34 g, 5.79 mmol, 2.61 equiv.). The atmosphere was exchanged for argon using standard Schlenk techniques. After the addition of dry MeOH (110 mL) and acetic acid (1.65 mL, 1.73 g, 28.96 mmol, 5.00 eq), the reaction was heated to reflux. Precipitation of yellow solids occurred during the reaction after approx. 30 minutes. The suspension was heated for 2 hours until TLC and GC-MS confirmed complete conversion.

Work-up: The crude was filtered over a pad of Celite, and the pad was thoroughly washed with HPLC grade MeOH. The filtrate was concentrated *in vacuo*, leaving a dark-red oily residue which was taken up in EtOAc (100 mL) and washed twice with sat. NaHCO₃ (2 x 100 mL). The aqueous phase was re-extracted three times with EtOAc (3 x 50 mL), and the combined organic layers were dried over Na₂SO₄ and concentrated. The crude was further purified *via* column chromatography (EtOAc) to yield 0.55 g (87 %) of diethyl (5-amino-4-cyano-2-methoxyphenyl)phosphonate **[146]** as a light-yellow crystalline solid.

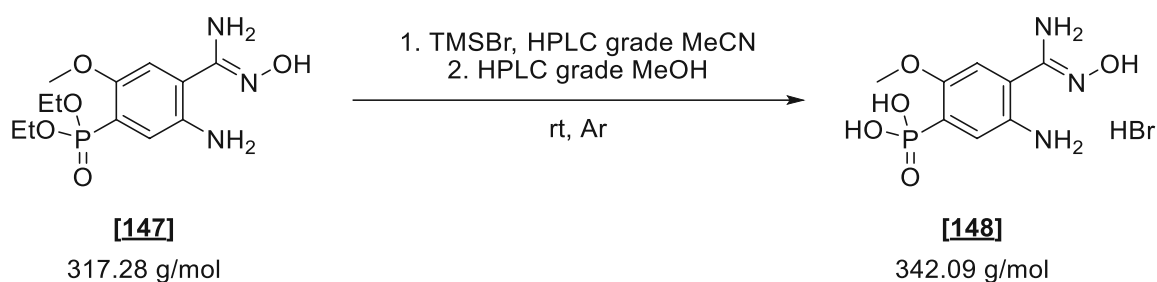
Yield	0.55 g (87 %)
Appearance	light-yellow crystalline solid
TLC	R _f (EtOAc) = 0.25 (KMnO ₄)
Reaction scale	0.70 g (2.23 mmol)
Substrate concentration	0.14 M
Purification	column chromatography (silica) EtOAc
Sum formula, m.w.	C ₁₂ H ₁₇ N ₂ O ₄ P, 284.25 g/mol
M.p.	122 – 124 °C
¹H-NMR (600 MHz, CDCl₃)	δ 1.23 (t, <i>J</i> = 7.0 Hz, 6H, -CH ₃), 3.73 (s, 3H, -OCH ₃), 3.95 – 4.08 (m, 4H, -O-CH ₂), 5.87 (s, 2H, -NH ₂), 7.16 (d, <i>J</i> = 7.0 Hz, 1H, H ₆), 7.23 (d, <i>J</i> = 16.5 Hz, 1H, H ₃).
¹³C-NMR (151 MHz, CDCl₃)	δ 16.2 (qd, ³ J _{C-P} = 6.0 Hz, 2C, -CH ₃), 56.5 (q, -OCH ₃), 61.9 (td, ² J _{C-P} = 5.6 Hz, 2C, -O-CH ₂ -), 96.8 (d, ⁴ J _{C-P} = 2.8 Hz, C1), 114.6 (dd, ³ J _{C-P} = 10.0 Hz, C6), 117.3 (s, -CN), 121.6 (dd, ² J _{C-P} = 7.7 Hz, C3), 124.1 (d, ¹ J _{C-P} = 181.2 Hz, C4), 145.7 (d, ³ J _{C-P} = 16.8 Hz, C2), 150.4 (d, ² J _{C-P} = 2.1 Hz, C5).
³¹P NMR (243 MHz, CDCl₃)	δ 18.9 (-P(O)(OEt) ₂).
HRMS (ESI)	calc. for C ₁₂ H ₁₈ N ₂ O ₄ ⁺ [M+H] ⁺ 285.0999, found 285.0970 – Δ = -10.2 ppm.

E III.6.19 Diethyl (5-amino-4-(N'-hydroxycarbamimidoyl)-2-methoxyphenyl)phosphonate **[147]**

Diethyl (5-amino-4-(N'-hydroxycarbamimidoyl)-2-methoxyphenyl)phosphonate **[147]** was synthesized according to general procedure L using diethyl (5-amino-4-cyano-2-methoxyphenyl)phosphonate **[146]** (0.45 g, 1.57 mmol).

Yield	0.35 g (69 %)
Appearance	light-yellow solid
TLC	R_f (EtOAc + 5 % MeOH) = 0.30 (anisaldehyde)
Reaction scale	0.45 g (1.57 mmol)
Substrate concentration	0.54 M
Purification	column chromatography (silica) EtOAc + 5 % MeOH
Sum formula, m.w.	$C_{12}H_{20}N_3O_5P$, 317.28 g/mol
M.p.	139 – 140.5 °C
1H-NMR (600 MHz, DMSO-d_6)	δ 1.23 (t, J = 7.1 Hz, 6H, -CH ₃), 3.75 (s, 3H, -OCH ₃), 3.93 – 4.05 (m, 4H, -O-CH ₂ -), 5.91 (s, 2H, -NH ₂), 6.03 (s, 2H, -NH ₂), 7.06 (d, J = 16.0 Hz, 1H, H3), 7.08 (d, J = 7.2 Hz, 1H, H6), 9.78 (s, 1H, -OH).
^{13}C-NMR (151 MHz, DMSO-d_6)	δ 16.2 (qd, $^3J_{C-P}$ = 6.1 Hz, 2C, -CH ₃), 56.5 (q, -OCH ₃), 61.4 (td, $^2J_{C-P}$ = 5.5 Hz, 2C, -O-CH ₂ -), 111.6 (dd, $^3J_{C-P}$ = 10.5 Hz, C6), 117.5 (d, $^1J_{C-P}$ = 184.2 Hz, C4), 118.4 (d, $^4J_{C-P}$ = 2.8 Hz, C1), 121.2 (dd, $^2J_{C-P}$ = 8.5 Hz, C3), 140.4 (d, $^3J_{C-P}$ = 16.5 Hz, C2), 150.8 (d, $^2J_{C-P}$ = 2.1 Hz, C5), 152.1 (s, -C=NOH).
^{31}P NMR (243 MHz, DMSO-d_6)	δ 16.4 (-P(O)(OEt) ₂).
HRMS (ESI)	calc. for $C_{12}H_{21}N_3O_5P^+$ [M+H] ⁺ 318.1213, found 318.1216 – Δ = 0.77 ppm.

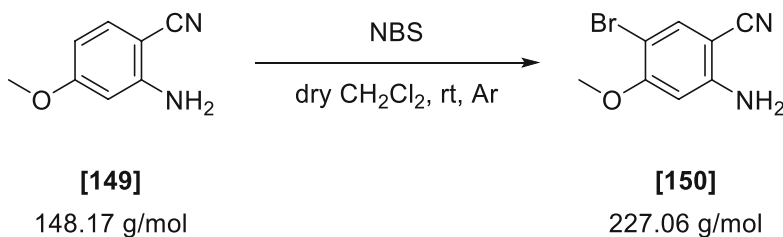
E III.6.20 (5-Amino-4-(N'-hydroxycarbamimidoyl)-2-methoxyphenyl)phosphonic acid (4,5-P-MeO-ABAO) [148]



(5-amino-4-(N'-hydroxycarbamimidoyl)-2-methoxyphenyl)phosphonic acid [148] was synthesized according to general procedure **M** using diethyl (5-amino-4-(N'-hydroxycarbamimidoyl)-2-methoxyphenyl)phosphonate [147] (0.35 g, 1.09 mmol). As NMR analysis indicated increased side product formation, repeated washing steps were needed for the isolation of pure product, diminishing the overall yield.

Yield	0.12 g (32 %)
Appearance	off-white solid
Reaction scale	0.35 g (1.09 mmol)
Substrate concentration	0.47 M
Purification	-
Sum formula, m.w.	C ₈ H ₁₃ BrN ₃ O ₅ P, 342.09 g/mol
M.p.	decomp. > 180 °C
¹H-NMR (400 MHz, DMSO-<i>d</i>₆)	δ 3.74 (s, 3H, -OCH ₃), 6.93 (d, <i>J</i> = 6.4 Hz, 1H, H6), 7.30 (d, <i>J</i> = 15.7 Hz, 1H, H3), 8.21 (s, 4H, -NH ₂), 10.58 (s, 1H, -OH).
¹³C-NMR (101 MHz, DMSO-<i>d</i>₆)	δ 56.8 (q, -OCH ₃), 112.8 (dd, ³ <i>J</i> _{C-P} = 9.3 Hz, C6), 116.8 (s, C1), 124.0 (dd, ² <i>J</i> _{C-P} = 7.9 Hz, C3), 126.9 (d, ¹ <i>J</i> _{C-P} = 178.1 Hz, C4), 137.3 (s, C2), 153.5 (s, C5), 156.8 (s, C=NOH).
³¹P NMR (162 MHz, DMSO-<i>d</i>₆)	δ 9.0 (-P(O)(OH) ₂).
HRMS (ESI)	not found

E III.6.21 2-Amino-5-bromo-4-methoxybenzonitrile [150]



Procedure: A 50 mL RBF was charged with 2-amino-4-methoxybenzonitrile **[149]** (1.50 g, 10.10 mmol, 1.00 equiv.), which was dissolved in dry CH_2Cl_2 (30 mL). The solution was cooled to $< 2^\circ\text{C}$ *via* ice/water bath followed by the addition of NBS (1.89 g, 10.62 mmol, 1.05 equiv.) in one portion. The reaction was stirred at 0°C for 30 minutes, upon which TLC indicated full conversion.

Work-up: The solvent was concentrated *in vacuo*, and the crude was immediately purified *via* flash chromatography (CH_2Cl_2) to yield 1.95 g (85 %) of 2-amino-3-bromo-5-methoxybenzonitrile **[150]** as orange solid.

Yield 1.95 g (85 %)

Appearance orange solid

Reaction scale 1.50 g (10.10 mmol)

Substrate concentration 0.34 M

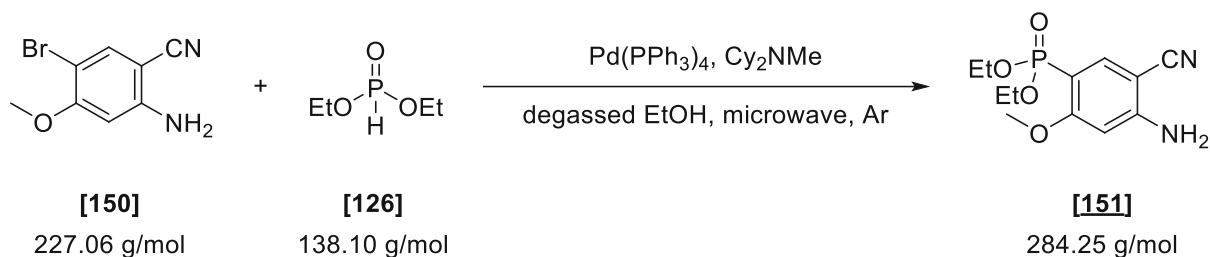
Purification flash chromatography (silica) CH_2Cl_2

Sum formula, m.w. $\text{C}_8\text{H}_7\text{BrN}_2\text{O}$, 227.06 g/mol

M.p. decomp. $> 120^\circ\text{C}$

$^1\text{H-NMR}$ (600 MHz, CDCl_3) δ 3.88 (s, 3H, - OCH_3), 4.47 (s, 2H, - NH_2), 6.22 (s, 1H, H3), 7.50 (s, 1H, H6).

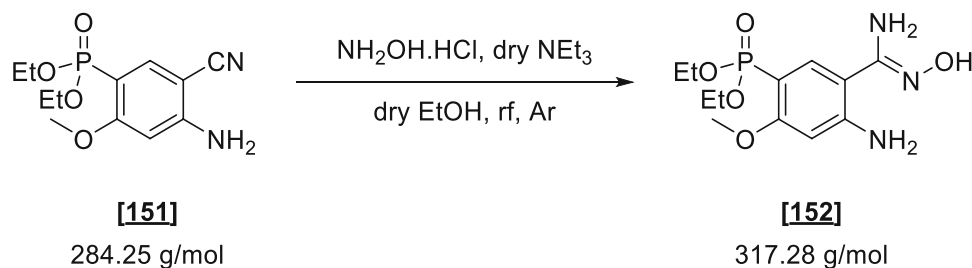
$^{13}\text{C-NMR}$ (151 MHz, CDCl_3) δ 56.4 (q, - OCH_3), 89.6 (s, C1), 98.1 (d, C3), 99.9 (s, C5), 116.9 (s, -CN), 136.0 (d, C6), 151.1 (s, C2), 160.3 (s, C4).

E III.6.22 Diethyl (4-amino-5-cyano-2-methoxyphenyl)phosphonate **[151]**

Diethyl (4-amino-5-cyano-2-methoxyphenyl)phosphonate **[151]** was synthesized according to general procedure **K** using 2-amino-5-bromo-4-methoxybenzonitrile **[150]** (1.45 g, 6.39 mmol) and diethyl phosphite **[126]** (1.24 mL, 1.33 g, 9.59 mmol).

Yield	1.82 g (90 %)
Appearance	colorless crystalline solid
TLC	R_f (EtOAc) = 0.14 (anisaldehyde)
Reaction scale	1.45 g (6.39 mmol)
Substrate concentration	0.26 M
Purification	column chromatography (silica) EtOAc
Sum formula, m.w.	$C_{12}H_{17}N_2O_4P$, 284.25 g/mol
M.p.	206 – 209 °C
$^1\text{H-NMR}$ (600 MHz, CDCl_3)	δ 1.30 (t, J = 7.0 Hz, 6H, $-\text{CH}_3$), 3.82 (s, 3H, $-\text{OCH}_3$), 4.01 – 4.16 (m, 4H, $-\text{O-CH}_2-$), 5.08 (s, 2H, $-\text{NH}_2$), 6.24 (d, J = 5.7 Hz, 1H, H3), 7.81 (d, J = 15.1 Hz, 1H, H6).
$^{13}\text{C-NMR}$ (151 MHz, CDCl_3)	δ 16.4 (qd, $^3J_{\text{C-P}}$ = 6.5 Hz, 2C, $-\text{CH}_3$), 56.0 (q, $-\text{OCH}_3$), 62.3 (td, $^2J_{\text{C-P}}$ = 5.5 Hz, 2C, $-\text{O-CH}_2-$), 88.2 (d, $^3J_{\text{C-P}}$ = 17.6 Hz, C1), 96.6 (dd, $^3J_{\text{C-P}}$ = 9.2 Hz, C3), 106.7 (d, $^1J_{\text{C-P}}$ = 199.0 Hz, C5), 117.2 (s, $-\text{CN}$), 140.7 (dd, $^2J_{\text{C-P}}$ = 9.0 Hz, C6), 155.2 (d, $^4J_{\text{C-P}}$ = 2.1 Hz, C2), 165.4 (d, $^2J_{\text{C-P}}$ = 3.7 Hz, C4).
$^{31}\text{P NMR}$ (243 MHz, CDCl_3)	δ 15.4 ($-\text{P}(\text{O})(\text{OEt})_2$).
HRMS (ESI)	calc. for $C_{12}H_{18}N_2O_4P^+$ $[\text{M}+\text{H}]^+$ 285.0966, found 285.0999 – Δ = -11.49 ppm.

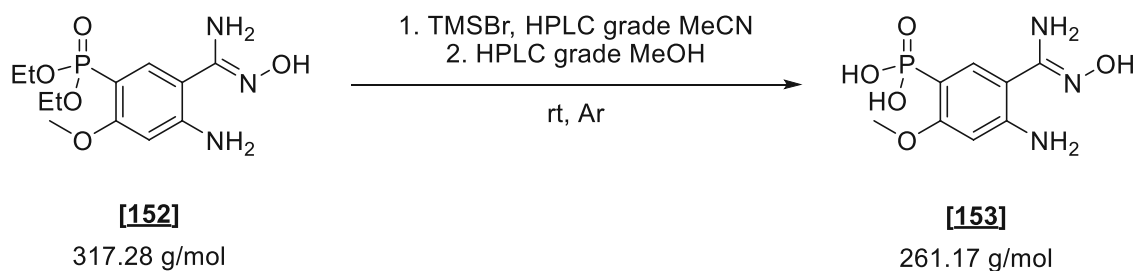
E III.6.23 Diethyl (4-amino-5-(N'-hydroxycarbamimidoyl)-2-methoxyphenyl)phosphonate [152]



Diethyl (4-amino-5-(N'-hydroxycarbamimidoyl)-2-methoxyphenyl)phosphonate [152] was synthesized according to general procedure L using diethyl (4-amino-5-cyano-2-methoxyphenyl)phosphonate [151] (1.00 g, 3.52 mmol).

Yield	1.00 g (90 %)
Appearance	light-yellow solid
TLC	R_f (EtOAc) = 0.10 (anisaldehyde)
Reaction scale	1.00 g (3.52 mmol)
Substrate concentration	0.54 M
Purification	column chromatography (silica) EtOAc + 5% MeOH
Sum formula, m.w.	$C_{12}H_{20}N_3O_5P$, 317.28 g/mol
M.p.	decomp. > 130 °C
1H-NMR (600 MHz, DMSO-d_6)	δ 1.19 (t, J = 7.1 Hz, 6H, -CH ₃), 3.73 (s, 3H, -OCH ₃), 3.93 (dq, J = 5.1, 7.1, 8.7 Hz, 4H, -O-CH ₂ -), 5.66 (s, 2H, -NH ₂), 6.31 (d, J = 6.5 Hz, 1H, H3), 6.88 (s, 2H, -NH ₂), 7.63 (d, J = 15.5 Hz, 1H, H6), 9.52 (s, 1H, -OH).
^{13}C-NMR (151 MHz, DMSO-d_6)	δ 16.2 (qd, $^3J_{C-P}$ = 6.3 Hz, 2C, -CH ₃), 55.3 (q, -OCH ₃), 60.9 (td, $^2J_{C-P}$ = 5.3 Hz, 2C, -O-CH ₂ -), 96.9 (dd, $^3J_{C-P}$ = 9.6 Hz, C3), 101.3 (d, $^1J_{C-P}$ = 197.5 Hz, C5), 107.0 (d, $^3J_{C-P}$ = 14.8 Hz, C1), 134.9 (dd, $^2J_{C-P}$ = 9.6 Hz, C6), 152.4 (d, $^4J_{C-P}$ = 2.0 Hz, C2), 152.4 (s, -C=NOH), 161.6 (d, $^2J_{C-P}$ = 3.5 Hz, C4).
^{31}P NMR (243 MHz, DMSO-d_6)	δ 18.7 (-P(O)(OEt) ₂).
HRMS (ESI)	calc. for $C_{12}H_{21}N_3O_5P^+$ [M+H] ⁺ 318.1213, found 318.1210 – Δ = -1.13 ppm.

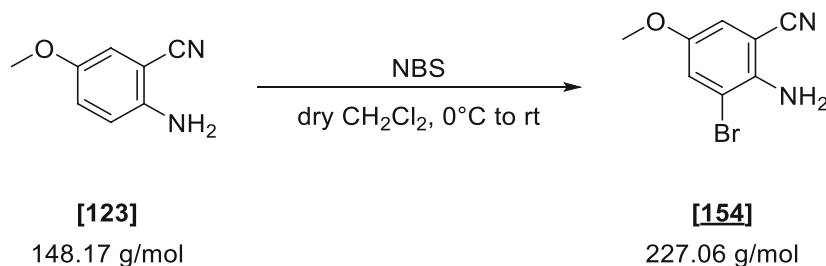
E III.6.24 (4-Amino-5-(N'-hydroxycarbamimidoyl)-2-methoxyphenyl)phosphonic acid [153]



(4-amino-5-(N'-hydroxycarbamimidoyl)-2-methoxyphenyl)phosphonic acid [153] was synthesized according to general procedure **M** using diethyl (4-amino-5-(N'-hydroxycarbamimidoyl)-2-methoxyphenyl)phosphonate [152] (0.60 g, 1.89 mmol). As NMR analysis indicated increased side product formation, repeated washing steps were needed for the isolation of pure product, diminishing the overall yield.

Yield	0.22 g (34 %)
Appearance	yellow solid
Reaction scale	0.60 g (1.89 mmol)
Substrate concentration	0.19 M
Purification	-
Sum formula, m.w.	C ₈ H ₁₂ N ₃ O ₅ P, 261.17 g/mol
M.p.	decomp. > 180 °C
¹H-NMR (400 MHz, DMSO-<i>d</i>₆)	δ 3.73 (s, 3H, -OCH ₃), 6.36 (d, <i>J</i> = 5.5 Hz, 1H, H3), 7.36 (d, <i>J</i> = 15.0 Hz, 1H, H6), 8.11 (s, 2H, -NH ₂), 8.79 (s, 1H, -NH _{2,oxime}), 9.08 (s, 1H, -NH _{2,oxime}), 10.69 (s, 1H, -OH).
¹³C-NMR (101 MHz, DMSO-<i>d</i>₆)	δ 55.5 (q, -OCH ₃), 97.4 (d, ³ <i>J</i> _{C-P} = 8.1 Hz, C3), 101.1 (d, ³ <i>J</i> _{C-P} = 15.5 Hz, C1), 108.5 (d, ¹ <i>J</i> _{C-P} = 193.3 Hz, C5), 135.6 (d, ² <i>J</i> _{C-P} = 9.2 Hz, C6), 151.8 (C=NOH), 158.8 (s, C2), 164.0 (d, ² <i>J</i> _{C-P} = 2.9 Hz, C4).
³¹P NMR (162 MHz, DMSO-<i>d</i>₆)	δ 10.8 (-P(O)(OH) ₂).
HRMS (ESI)	calc. for C ₈ H ₁₄ N ₃ O ₅ P ⁺ [M+H] ⁺ 262.0588, found 262.0543 – Δ = -17.17 ppm.

E III.6.25 2-Amino-3-bromo-5-methoxybenzonitrile [154]

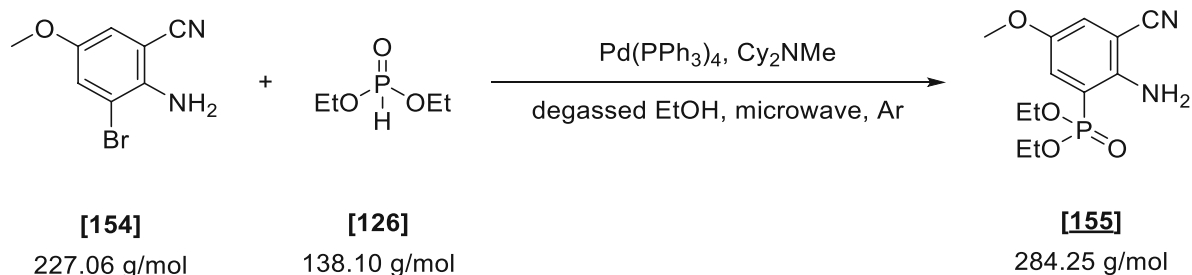


Procedure: A 8 mL screw cap vial was charged with 2-amino-5-methoxybenzonitrile [123] (0.60 g, 4.05 mmol, 1.00 equiv.), which was dissolved in dry CH₂Cl₂ (13.5 mL). The solution was cooled to < 2 °C *via* ice/water bath followed by the addition of NBS (0.76 g, 4.25 mmol, 1.05 equiv.) in one portion, which triggered an immediately deep violet color change. The reaction was stirred at 0 °C for 30 minutes, upon which TLC indicated complete conversion.

Work-up: The solvent was concentrated *in vacuo*, and the crude was immediately purified *via* flash chromatography (CH₂Cl₂) to yield 0.55 g (57 %) of 2-amino-3-bromo-5-methoxybenzonitrile [154] as ochre crystalline solid.

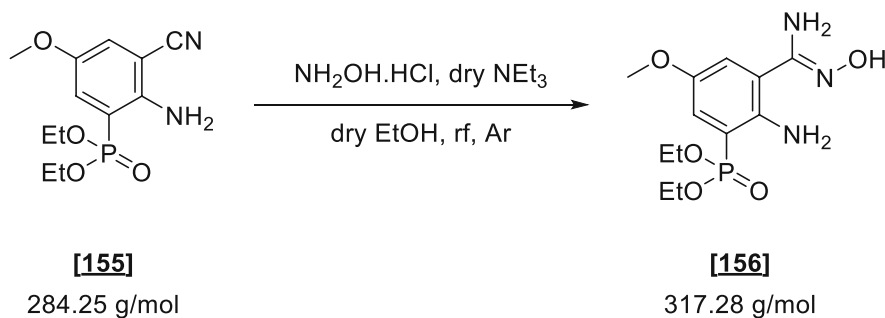
Yield	0.55 g (57 %)
Appearance	ochre crystalline solid
Reaction scale	0.60 g (4.05 mmol)
Substrate concentration	0.30 M
Purification	flash chromatography (silica) CH ₂ Cl ₂
Sum formula, m.w.	C ₈ H ₇ BrN ₂ O, 227.06 g/mol
M.p.	157 – 159 °C
¹H-NMR (400 MHz, CDCl₃)	δ 3.74 (s, 3H, -OCH ₃), 4.52 (s, 2H, -NH ₂), 6.90 (d, <i>J</i> = 2.8 Hz, 1H, H ₆), 7.27 (d, <i>J</i> = 2.9 Hz, 1H, H ₃).
¹³C-NMR (101 MHz, CDCl₃)	δ 56.3 (q, -OCH ₃), 97.0 (s, C ₁), 110.3 (s, C ₃), 115.5 (d, C ₆), 117.0 (s, -CN), 125.3 (d, C ₄), 141.8 (s, C ₂), 151.4 (s, C ₅).
HRMS (ESI)	calc. for C ₈ H ₈ BrN ₂ O ⁺ [M+H] ⁺ 226.9723, found 226.9815 – Δ = -40.53 ppm.

E III.6.26 Diethyl (2-amino-3-cyano-5-methoxyphenyl)phosphonate [155]



Diethyl (2-amino-3-cyano-5-methoxyphenyl)phosphonate [155] was synthesized according to general procedure K using 2-amino-3-bromo-5-methoxybenzonitrile [154] (0.52 g, 2.29 mmol) and diethyl phosphite [126] (0.44 mL, 0.47 g, 3.44 mmol).

Yield	0.45 g (69 %)
Appearance	colorless crystalline solid
TLC	R_f (EtOAc) = 0.15 (anisaldehyde)
Reaction scale	0.52 g (6.39 mmol)
Substrate concentration	0.26 M
Purification	column chromatography (silica) EtOAc
Sum formula, m.w.	$\text{C}_{12}\text{H}_{17}\text{N}_2\text{O}_4\text{P}$, 284.25 g/mol
M.p.	94 – 96 °C
$^1\text{H-NMR}$ (400 MHz, CDCl_3)	δ 1.33 (td, $J = 0.6, 7.1$ Hz, 6H, $-\text{CH}_3$), 3.75 (s, 3H, $-\text{OCH}_3$), 4.00 – 4.23 (m, 4H, $-\text{O-CH}_2-$), 5.62 (s, 2H, $-\text{NH}_2$), 7.08 (dd, $J = 0.8, 3.0$ Hz, 1H, H6), 7.27 (dd, $J = 3.0, 15.9$ Hz, 1H, H4).
$^{13}\text{C-NMR}$ (101 MHz, CDCl_3)	δ 16.4 (qd, $^3J_{\text{C-P}} = 6.6$ Hz, 2C, $-\text{CH}_3$), 56.3 (q, $-\text{OCH}_3$), 62.8 (td, $^2J_{\text{C-P}} = 5.1$ Hz, 2C, $-\text{O-CH}_2-$), 98.1 (d, $^3J_{\text{C-P}} = 17.7$ Hz, C1), 111.9 (d, $^1J_{\text{C-P}} = 185.1$ Hz, C3), 116.9 (d, $^4J_{\text{C-P}} = 4.4$ Hz, $-\text{CN}$), 121.7 (dd, $^4J_{\text{C-P}} = 3.0$ Hz, C6), 125.3 (dd, $^2J_{\text{C-P}} = 7.3$ Hz, C4), 147.6 (d, $^2J_{\text{C-P}} = 9.3$ Hz, C2), 150.1 (d, $^3J_{\text{C-P}} = 17.7$ Hz, C5).
$^{31}\text{P NMR}$ (162 MHz, CDCl_3)	δ 17.4 ($-\text{P}(\text{O})(\text{OEt})_2$).
HRMS (ESI)	calc. for $\text{C}_{12}\text{H}_{18}\text{N}_2\text{O}_4^+$ $[\text{M}+\text{H}]^+$ 285.0999, found 285.0970 – $\Delta = -10.08$ ppm.

E III.6.27 Diethyl (2-amino-3-(N'-hydroxycarbamimidoyl)-5-methoxyphenyl)phosphonate **[156]**

Diethyl (2-amino-3-(N'-hydroxycarbamimidoyl)-5-methoxyphenyl)phosphonate **[156]** was synthesized according to general procedure L using diethyl (2-amino-3-cyano-5-methoxyphenyl)phosphonate **[155]** (0.41 g, 1.44 mmol).

Yield 0.35 g (76 %)
Appearance off-white crystalline solid
TLC R_f (EtOAc) = 0.10 (anisaldehyde)

Reaction scale 0.41 g (1.44 mmol)
Substrate concentration 0.54 M
Purification column chromatography (silica) EtOAc
Sum formula, m.w. $C_{12}H_{20}N_3O_5P$, 317.28 g/mol
M.p. 127 – 128 °C

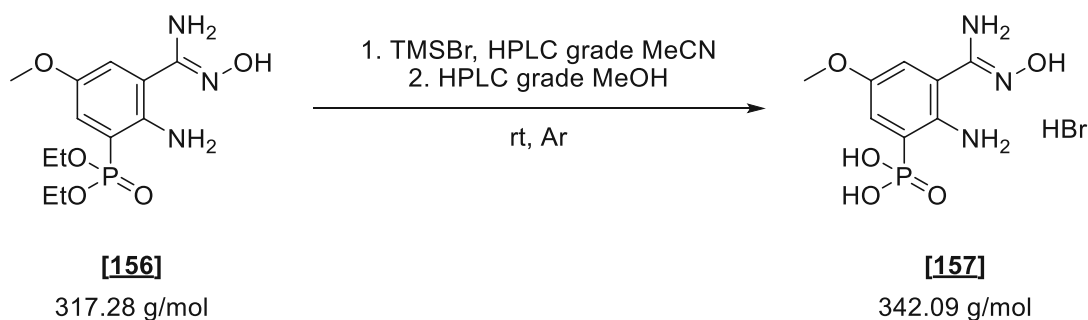
1H -NMR (400 MHz, DMSO- d_6) δ 1.23 (t, J = 7.1 Hz, 6H, -CH₃), 3.71 (s, 3H, -OCH₃), 3.90 – 4.09 (m, 4H, -O-CH₂-), 5.91 (s, 2H, -NH₂), 6.63 (s, 2H, -NH₂), 6.91 (dd, J = 3.0, 15.6 Hz, 1H, H4), 7.25 (d, J = 3.0 Hz, 1H, H6), 9.80 (s, 1H, -OH).

^{13}C -NMR (101 MHz, DMSO- d_6) δ 16.1 (qd, $^3J_{C-P}$ = 6.2 Hz, 2C, -CH₃), 55.7 (q, -OCH₃), 61.7 (td, $^2J_{C-P}$ = 5.2 Hz, 2C, -O-CH₂-), 109.0 (d, $^1J_{C-P}$ = 182.0 Hz, C3), 117.6 (d, $^3J_{C-P}$ = 15.8 Hz, C1), 117.9 (dd, $^2J_{C-P}$ = 8.1 Hz, C4), 119.5 (dd, $^4J_{C-P}$ = 2.8 Hz, C6), 144.0 (d, $^2J_{C-P}$ = 9.4 Hz, C2), 148.6 (d, $^3J_{C-P}$ = 18.7 Hz, C5), 151.9 (d, $^4J_{C-P}$ = 3.5 Hz, -C=NOH).

^{31}P NMR (162 MHz, DMSO- d_6) δ 20.0 (-P(O)(OEt)₂).

HRMS (ESI) calc. for $C_{12}H_{21}N_3O_5P^+$ [M+H]⁺ 318.1213, found 318.1208 – Δ = -1.52 ppm.

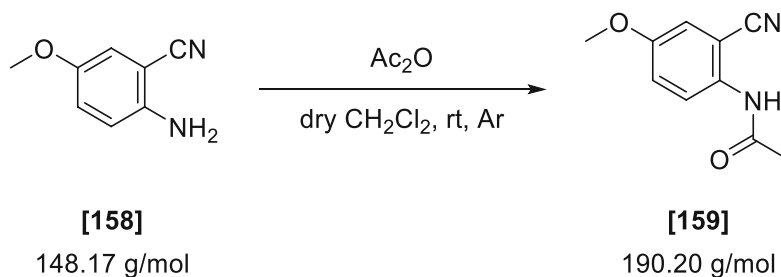
E III.6.28 (2-Amino-3-(N'-hydroxycarbamimidoyl)-5-methoxyphenyl)phosphonic acid (3,5-P-MeO-ABAO) [157]



(2-Amino-3-(N'-hydroxycarbamimidoyl)-5-methoxyphenyl)phosphonic acid [157] was synthesized according to general procedure **M** using diethyl (2-amino-3-(N'-hydroxycarbamimidoyl)-5-methoxyphenyl)phosphonate [156] (0.30 g, 0.95 mmol). As NMR analysis indicated increased side product formation, repeated washing steps were needed for the isolation of pure product, diminishing the overall yield.

Yield	0.19 g (62 %)
Appearance	yellow solid
TLC	-
Reaction scale	0.30 g (0.95 mmol)
Substrate concentration	0.25 M
Purification	-
Sum formula, m.w.	C ₈ H ₁₃ BrN ₃ O ₅ P, 342.09 g/mol
M.p.	decomp. > 180 °C
¹H-NMR (400 MHz, DMSO-<i>d</i>₆)	δ 3.69 (s, 3H, -OCH ₃), 6.97 (d, <i>J</i> = 3.0 Hz, 1H, H6), 7.20 (dd, <i>J</i> = 3.0, 15.7 Hz, 1H, H4), 7.81 (s, 2H, -NH ₂), 9.11 (s, 2H, -NH ₂), 10.83 (s, 1H, -OH).
¹³C-NMR (101 MHz, DMSO-<i>d</i>₆)	δ 56.3 (q, -OCH ₃), 113.2 (d, ³ <i>J</i> _{C-P} = 15.2 Hz, C1), 118.4 (dd, ¹ <i>J</i> _{C-P} = 178.0 Hz, C3), 119.0 (d, ⁴ <i>J</i> _{C-P} = 2.2 Hz, C6), 122.4 (dd, ² <i>J</i> _{C-P} = 8.3 Hz, C4), 142.5 (d, ² <i>J</i> _{C-P} = 8.9 Hz, C2), 149.4 (d, ³ <i>J</i> _{C-P} = 17.3 Hz, C5), 158.1 (s, C=NOH).
³¹P NMR (162 MHz, DMSO-<i>d</i>₆)	δ 12.3 (-P(O)(OH) ₂).
HRMS (ESI)	calc. for C ₈ H ₁₄ N ₃ O ₅ P ⁺ [M+H] ⁺ 262.0588, found 262.0532 – Δ = -21.37 ppm.

E III.6.29 N-(2-cyano-4-methoxyphenyl)acetamide [159]



Procedure: A 25 mL screw-cap vial was charged with 2-amino-5-methoxybenzonitrile **[158]** (0.60 g, 4.05 mmol, 1.00 equiv.), which was dissolved in dry CH₂Cl₂ (10 mL). Acetic anhydride (0.44 mL, 0.47 g, 4.68 mmol, 1.15 equiv.) was added to the solution, and the reaction was stirred at room temperature. Precipitation of colorless crystalline solids was observed during the reaction after 1 hour. TLC analysis after 2 hours confirmed full conversion.

Work-up: To complete precipitation, n-hexane (10 mL) was added, and the product was collected by suction filtration. The solids were washed with ice-cold 80% n-hexane/CH₂Cl₂ (2 x 5 mL) and were dried *in vacuo* to yield 0.71 g (92 %) of N-(2-cyano-4-methoxyphenyl)acetamide **[159]** as a colorless crystalline solid.

Yield	0.71 g (96 %)
Appearance	colorless crystalline solid
TLC	R _f (LP/EtOAc – 2:1) = 0.25 (anisaldehyde)
Reaction scale	0.60 g (4.05 mmol)
Substrate concentration	0.40 M
Purification	-
Sum formula, m.w.	C ₁₀ H ₁₀ N ₂ O ₂ , 204.22 g/mol
M.p.	178 – 179 °C (lit. ²⁸⁰ 179 – 180 °C)
¹H-NMR (400 MHz, CDCl₃)	δ 2.23 (s, 3H, -COCH ₃), 3.80 (s, 3H, -OCH ₃), 7.04 (d, J = 3.0 Hz, 1H, H6), 7.13 (dd, J = 3.0, 9.2 Hz, 1H, H4), 7.53 (s, 1H, -CONH), 8.14 (d, J = 9.2 Hz, 1H, H3).
¹³C-NMR (101 MHz, CDCl₃)	δ 24.6 (-COCH ₃), 55.9 (-OCH ₃), 103.8 (C1), 116.1 (d, C6), 116.4 (-CN), 120.8 (d, C4), 124.1 (d, C3), 133.9 (C2), 156.0 (C5), 168.7 (-CONH).

E IV Biotransformation of SHC variants

E IV.1 Standard media preparations

Table 16: Compositions of applied buffers and components thereof.

Lyse buffer for 400 mL		Reaction buffer for 100 mL		50 x 5052 for 80 mL		40x salt solution for 80 mL	
20.7 g	Na-citrate	1.3 g	Na-citrate	20 mL	glycerol	11.36 g	Na ₂ HPO ₄
40 mL	glycerol			2 g	glucose	10.89 g	KH ₂ PO ₄
	<i>Adjusted with 2N HCl to pH 6.0</i>			8 g	lactose	8.56 g	NH ₄ Cl
						3.71 g	Na ₂ SO ₄ ·5 H ₂ O

Table 17: Compositions of applied media.

LB medium for 1 L		ZYM-5052 medium for 800 mL		Expression ZYM 5052 medium for 100 mL	
10 g	bacto-peptone	8 g	tryptone	2.5 mL	40x salt solution
4 g	yeast extract	4 g	yeast extract	2 mL	50x 5052
10 g	NaCl	8 g	lactose	95.5 mL	ZYM-5052
				0.2 mL	1 M MgSO ₄

E IV.2 *Zymomonas mobilis* (Zmo)

E IV.2.1 Expression of the *Z. mobilis* SHC variants in *Escherichia coli*

Z. mobilis SHC variants (F II) were expressed in *E. coli* BL21 (DE3). The respective cryostock was used for inoculation of the preculture. While keeping cryostocks on ice, a pipette tip was used to take up some cell material and inoculate 5 mL LB medium (100 µg/mL ampicillin), which was incubated overnight at 37 °C and 180 r.p.m. That culture was used to inoculate 250 mL of “Expression ZYM-5052 medium” (100 µg/mL ampicillin) in a 1-L baffled Erlenmeyer flasks at an OD₅₉₀ of approx. 0.05. Auto-induction was used while incubating for 4 h at 37 °C and then 18 h at 20 °C (180 r.p.m.). Cells were harvested at 4 °C for 10 minutes (9000 r.p.m.) and stored at 4 °C until further usage. Before starting the “Cell treatment”, it is advisable to do an SDS-PAGE at an OD₅₉₀ of 7. The bands for ZMOW555Y, ZMOF486C, and ZMOF438C should be observed at 83.1, 82.0, and 75.3 kDa.

E IV.2.2 Cell treatment before the biotransformation

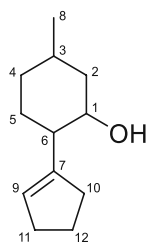
The cell pellet (in a culture of 300 mL) was washed with 0.1 M potassium phosphate-buffer at pH 7 (6 mL per gram wet pellet), centrifuged (9000 r. p. m., 10 minutes, 4 °C), and then resuspended in lysis buffer (6 mL per gram wet pellet), placed into a glass beaker and homogenized by stirring it for several minutes until no clumps could be observed anymore. The suspension was then disrupted by ultrasonic treatment (amplitude 40%, 35s/35s for 30 min) and then centrifuged (16000 r.p.m., 40 minutes, 4 °C). Afterward, the supernatant was discarded, and the pellet was kept for the following biotransformation.

E IV.2.3 Biotransformation

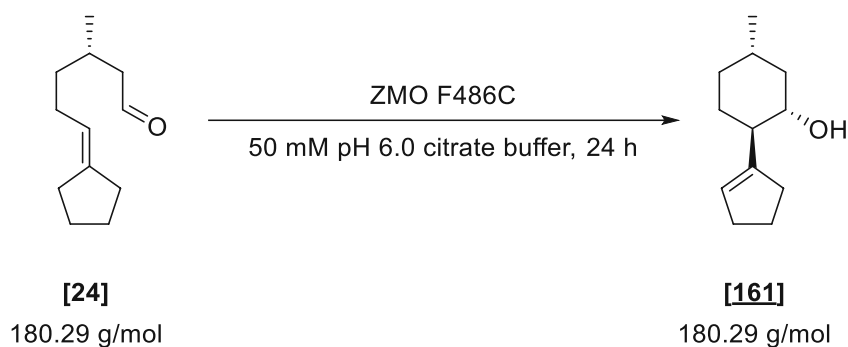
The biotransformation was typically performed with resuspended cells in 50 mM citrate buffer at pH = 6.0 - 6.1, OD₅₉₀ = 20 - 25 and 3-4 mM (final concentration) of substrate. The reaction was performed under vigorous shaking (250 r.p.m. in a multitron HT incubator) at 25 °C in a glass vial. The reaction was continuously monitored *via* GC-MS, and as soon as no substrate could be detected, the work-up was started.

To perform a GC-MS analysis, 200 µL of the cell suspension were placed into a 1.5 mL Eppendorf tube and extracted once with 800 µL EtOAc with 1 mM methyl benzoate as internal standard. The organic layer was dried over Na₂SO₄ and analyzed by GC-MS using „Method B“ or calibrated GC.

Upon confirmation of complete conversion, the solution was centrifuged at 10000 r.p.m. for 15 min. Since the pellet was not reused, the centrifugation was carried out at room temperature. The supernatant containing the product was decanted into a flask, and the cell pellet was discarded. The extraction of the products from the supernatant was done three times with Et₂O in a 50 mL falcon tube (the used amount of Et₂O was two-thirds of the used biotransformation solution). The two-phase system was separated by centrifugation at 15000 r.p.m. for 5 min. If an emulsion was still present, the process was repeated for 10 minutes with the same settings as described above. The ethereal layers were combined, dried over Na₂SO₄, and the solvent was evaporated (max. 300 mbar). The crude product was further purified *via* column chromatography (LP/EtOAc – 20:1; crude mass:SiO₂ = 1:100) to yield the cyclized isopulegol derivatives as colorless oils.

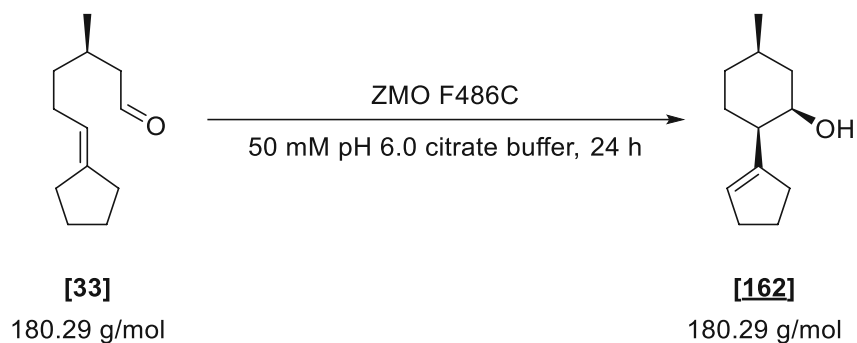


NMR assignments of core structures in this chapter were given according to the following example.

E IV.2.4 Biotransformation of (*S*)-6-cyclopentylidene-3-methylhexanal [24] with ZMO variant F486C to (1*S*,2*R*,5*S*)-2-(cyclopent-1-en-1-yl)-5-methylcyclohexan-1-ol [161]

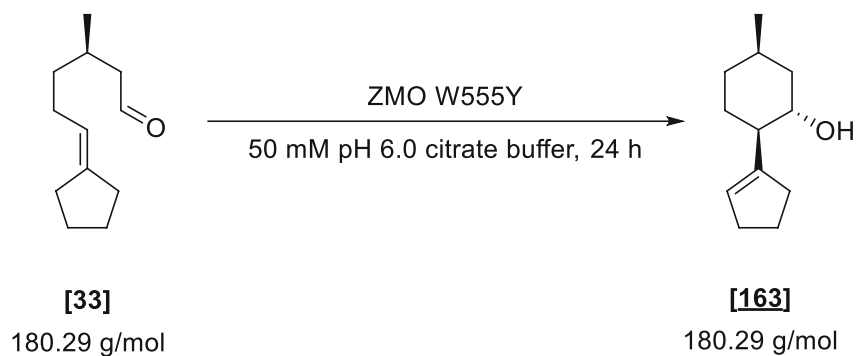
(1*S*,2*R*,5*S*)-2-(cyclopent-1-en-1-yl)-5-methylcyclohexan-1-ol [161] was synthesized according to protocol E IV.2.3 using (*S*)-6-cyclopentylidene-3-methylhexanal [24] (16.2 mg, 90 μmol).

Yield	5.2 mg (32 %)
Appearance	yellowish oil
TLC	R_f (LP/EtOAc – 20:1) = 0.47 (anisaldehyde)
Reaction scale	16.2 mg (90 μmol)
Substrate concentration	3 mM
Purification	column chromatography (silica) LP/EtOAc 20:1
Sum formula, m.w.	$C_{12}H_{20}O$, 180.29 g/mol
$^1\text{H-NMR}$ (600 MHz, CDCl_3)	δ 0.79 – 1.06 (m, 5H, H2', H4', H8), 1.16 – 1.36 (m, 1H, H5'), 1.44 – 1.54 (m, 1H, H3), 1.59 – 1.74 (m, 2H, H4, H5), 1.77 – 1.94 (m, 2H, H12), 1.99 – 2.09 (m, 2H, H2, H6), 2.19 – 2.29 (m, 2H, H10), 2.30 – 2.38 (m, 2H, H11), 3.44 (td, $J = 4.2, 10.3$ Hz, 1H, H1), 5.51 – 5.57 (m, 1H, H9).
$^{13}\text{C-NMR}$ (151 MHz, CDCl_3)	δ 22.4 (q, C8), 23.3 (t, C12), 29.9 (t, C5), 31.6 (d, C3), 31.9 (t, C10), 32.3 (t, C11), 34.4 (t, C4), 42.7 (t, C2), 48.4 (d, C6), 71.1 (s, C1), 126.7 (d, C9), 145.8 (s, C7).
GC-MS (method C)	$t_R = 4.95$ minutes, main fragments 180 (7, M+), 162 (44), 147 (32), 94 (49), 81 (100), 79 (91), 67 (53)

E IV.2.5 Biotransformation of (*R*)-6-cyclopentylidene-3-methylhexanal [33] with ZMO variant F486C to (1*R*,2*R*,5*R*)-2-(cyclopent-1-en-1-yl)-5-methylcyclohexan-1-ol [162]

(1*R*,2*R*,5*R*)-2-(cyclopent-1-en-1-yl)-5-methylcyclohexan-1-ol **[162]** was synthesized according to protocol E IV.2.3 using (*S*)-6-cyclopentylidene-3-methylhexanal **[33]** (16.2 mg, 90 μ mol).

Yield	3.0 mg (19 %)
Appearance	yellowish oil
TLC	R_f (LP/EtOAc – 5:1) = 0.53 (anisaldehyde)
Reaction scale	16.2 mg (90 μ mol)
Substrate concentration	3 mM
Purification	column chromatography (silica) LP/EtOAc 20:1
Sum formula, m.w.	$C_{12}H_{20}O$, 180.29 g/mol
$^1\text{H-NMR}$ (600 MHz, CDCl_3)	δ 0.88 (d, J = 6.6 Hz, 3H, H8), 0.89 – 0.99 (m, 1H, H4'), 1.11 (ddd, J = 2.6, 12.3, 13.7 Hz, 1H, H2'), 1.52 – 1.58 (m, 1H, H5'), 1.65 – 1.76 (m, 2H, H5, H4'), 1.75 – 1.85 (m, 1H, H3), 1.81 – 1.92 (m, 2H, H12), 1.94 (dtd, J = 2.2, 3.5, 13.8 Hz, 1H, H2), 2.09 (d, J = 12.5 Hz, 1H, H6), 2.15 – 2.23 (m, 1H, H10'), 2.35 (ddp, J = 2.2, 6.9, 9.6 Hz, 2H, H11), 2.37 – 2.46 (m, 1H, H10), 4.00 (q, J = 2.7 Hz, 1H, H1), 5.50 (h, J = 2.0 Hz, 1H, H9).
$^{13}\text{C-NMR}$ (151 MHz, CDCl_3)	δ 22.5 (q, C8), 23.2 (t, C12), 24.6 (t, C5), 25.9 (d, C3), 32.7 (t, C11), 34.5 (t, C10), 34.9 (t, C4), 40.8 (t, C2), 43.9 (d, C6), 66.9 (d, C1), 125.6 (d, C9), 146.5 (s, C7).
GC-MS (method C)	t_R = 5.03 minutes, main fragments 180 (7, M ⁺), 162 (42), 147 (24), 94 (53), 81 (82), 79 (100), 67 (57)

E IV.2.6 Biotransformation of (*R*)-6-cyclopentylidene-3-methylhexanal [33] with ZMO variant W555Y to (1*S*,2*R*,5*R*)-2-(cyclopent-1-en-1-yl)-5-methylcyclohexan-1-ol [163]

(1*S*,2*R*,5*R*)-2-(cyclopent-1-en-1-yl)-5-methylcyclohexan-1-ol [163] was synthesized according to protocol E IV.2.3 using (*S*)-6-cyclopentylidene-3-methylhexanal [33] (14.4 mg, 80 μ mol).

Yield	2.8 mg (19 %)
Appearance	yellowish oil
TLC	R_f (LP/EtOAc – 40:1) = 0.39 (anisaldehyde)
Reaction scale	14.4 mg (80 μ mol)
Substrate concentration	4 mM
Purification	column chromatography (silica) LP/EtOAc 20:1
Sum formula, m.w.	$C_{12}H_{20}O$, 180.29 g/mol
$^1\text{H-NMR}$ (600 MHz, CDCl_3)	δ 0.99 (d, $J = 7.2$ Hz, 3H, H8), 1.37 – 1.49 (m, 2H, H2', H4'), 1.49 – 1.64 (m, 3H, H4, H5), 1.78 – 1.94 (m, 3H, H2, H12), 2.04 – 2.15 (m, 2H, H3, H6), 2.19 – 2.31 (m, 2H, H10), 2.31 – 2.38 (m, 2H, H11), 3.74 (td, $J = 4.1, 9.7$ Hz, 1H, H1), 5.53 (pd, $J = 0.8, 2.1$ Hz, 1H, H9).
$^{13}\text{C-NMR}$ (151 MHz, CDCl_3)	δ 19.1 (q, C8), 23.3 (t, C12), 24.9 (t, C5), 28.2 (d, C3), 30.9 (t, C4), 32.4 (t, C10), 32.4 (t, C11), 39.3 (t, C2), 48.4 (d, C6), 67.4 (d, C1), 126.2 (d, C9), 145.7 (s, C7).
GC-MS (method C)	$t_R = 5.08$ minutes, main fragments 180 (7, M^+), 162 (33), 147 (25), 93 (46), 81 (89), 79 (100), 67 (58)

E V Assembly and application of the FADS system

E V.1 Equipment set-up

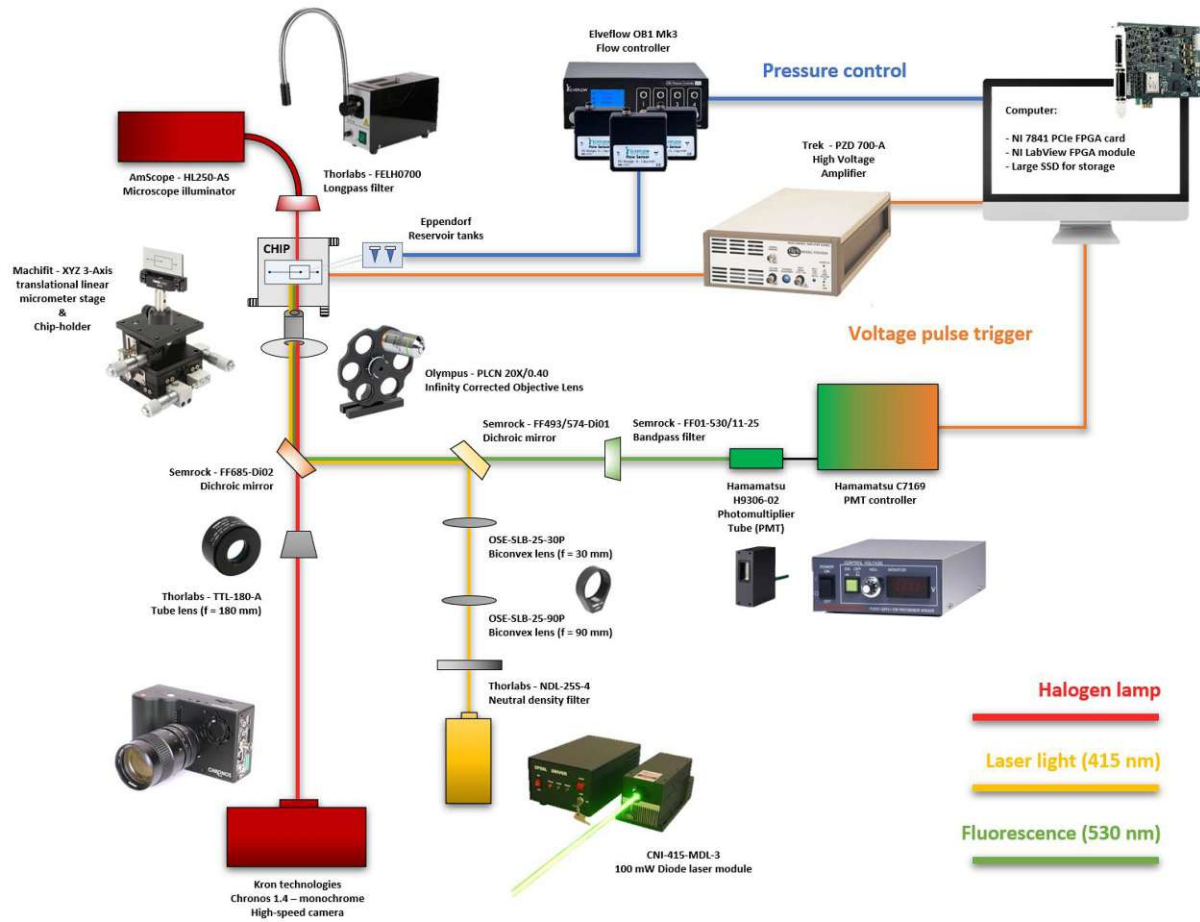


Fig. 103: Schematic overview of the custom-built FADS assembly. Light paths of the different emission sources are marked in different colors. The red path illustrates the backlight illumination of the chip with the halogen lamp; The yellow path describes the optical train of the laser beam through the optical set-up; The green path describes the route of the emitted fluorescence signal to the photomultiplier tube.

The components needed for the final assembly can be divided into several categories depending on their application in the system (Fig. 103). Optomechanical components represent the core structure of the whole setup. They enable the interplay of all optical components and are crucial elements for the special alignment and the correct guidance of the laser and the respective fluorescence signal through the system. Optical elements are responsible for the manipulation of light either for visual control of the sorting processes or the generation and measurement of optical signals. These comprise the emission, focusing, deflection, filtering, and amplification of light. Flow control elements entail all parts that are needed for the pressure-driven control of the applied flow rates and thus sorting speeds of the microfluidic chip system. The droplet analysis and sorting category includes all hardware and software components that are necessary for high-throughput analysis and interpretation of the fluorescence signals and the triggering of sorting events by high voltage pulses.

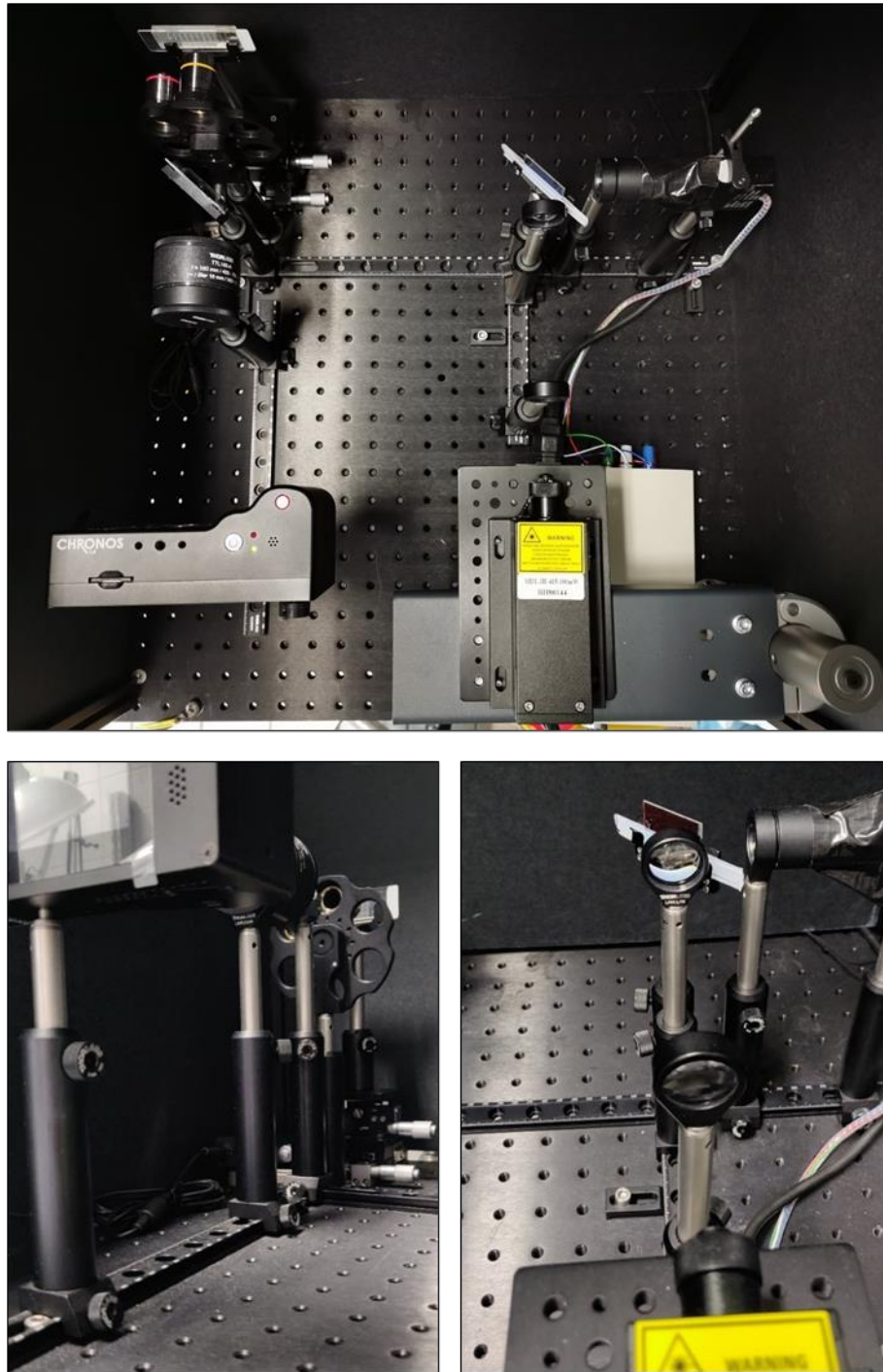


Fig. 104 top: Top view of the optomechanical assembly, including all mounted optical components; **bottom left:** Detailed view of the custom infinity-corrected microscope assembly along the RLA300/M 300 mm optical rail; **bottom right:** Detailed view of the beginning of the optical train guiding the laser beam through the assembly.

All optomechanical components were set up as depicted in Fig. 82 (c.f. top view with Fig. 103), using mainly Thorlabs components. There were either mounted to the MB6060/M breadboard *via* RC1 dovetail rail carriers on RLA optical rails or *via* BE1/M studded pedestal base adapters fixed with CF175C/M clamping forks (Fig. 105 left). Especially rail carriers allowed for exact distance adjustments due to their flexible one-dimensional movement. The Machifit 3-axis translational stage was centered at the end of the 300 mm rail and mounted directly to the breadboard (Fig. 82 bottom left). PH50/PH100

optical posts holders were connected to the respective bases and equipped with individual TR50/TR100 optical posts (Fig. 105 right).

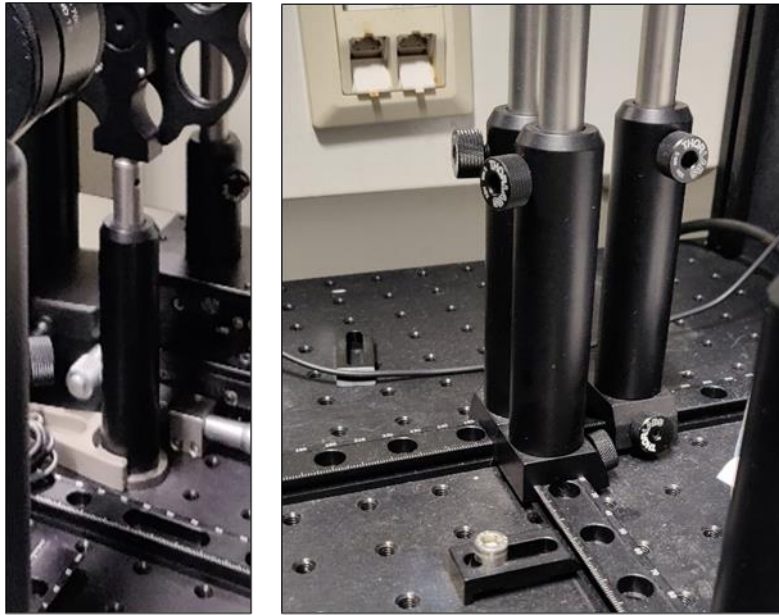


Fig. 105 left: Mounting PH100 optical post holders with the respective TR100 optical posts via CF175C clamping forks and BE1/M pedestal bases; **right:** Mounting via RC1 dovetail rail carriers on RLA optical rails.

Due to the size and weight of the laser, a separate pedestal was needed. Therefore a second mini breadboard MSB1015/M was mounted on a P250/M post via the PSY321/S mounting bracket, which enabled sufficient rigidity of the system. The laser diode was fixed to the breadboard and easily height adjusted by loosening the hinged clamps. (Fig. 106)



Fig. 106: Additional pedestal for flexible adjustment of the laser diode system – hinged clamps attached to the P250/M pole could be easily loosened to adjust the height of the assembly.

The casing was assembled using the XE25L structural rails and the RM1S construction cubes (Fig. 107 expansion). To enable facile access to the system, a flexible lid was envisioned. For this purpose, three XE25L500 500 mm rails had to be cut to 475 mm and fitted with M6 threads. These three rails connected via construction cubes to their 300 mm or 500 mm counterparts represented the core of the lid. The remainder of the casing was assembled in a straightforward fashion forming a cubical

structure. The hardboard covers were cut to appropriate sizes and pushed into the holes of the rails. Finally, the lid was mounted on the middle bar using the XE25H enclosure hinges, and the BBH1 lifting handles were installed (Fig. 107).



Fig. 107: Closed and opened from the whole set-up – back cover missing in open form due to easy accessibility during the construction process. All crucial instruments (high voltage amplifier, laser diode controller, PMT controller, ..) are mounted on an elevated stage below the covered optical assembly. **Expansion:** Close-up of the connectivity of the general cubical structure via RM15 construction cubes and XE25L structural rails

The whole system was later remodeled into a two-level structure to prevent damage due to a possible leak of aqueous material. Critical hardware was placed on an elevated stand below the optical assembly using a separate MB4560/M breadboard and custom-made rail spacers. Herein Frank Johannes from the TU Wien workshop helped with the planning and construction.

E V.1.1 Optical alignment

The Thorlabs RLA300/M optical rail was used for the alignment of the custom-built infinity-corrected microscope. Here exact placement of the optical components was necessary to enable a correct visual read-out. Using the thread for the camera tripod, a centered installation of the camera was easily possible. The tube lens was mounted via the Thorlabs LMR2S/M mounting ring, whereas the Thorlabs FW1A 6-hole filter wheel was fitted with all three microscope objective lenses (see. Table 18). However, due to the incompatibility of the lens thread with the filter wheel, an RMS to SM1 adapter was necessary.

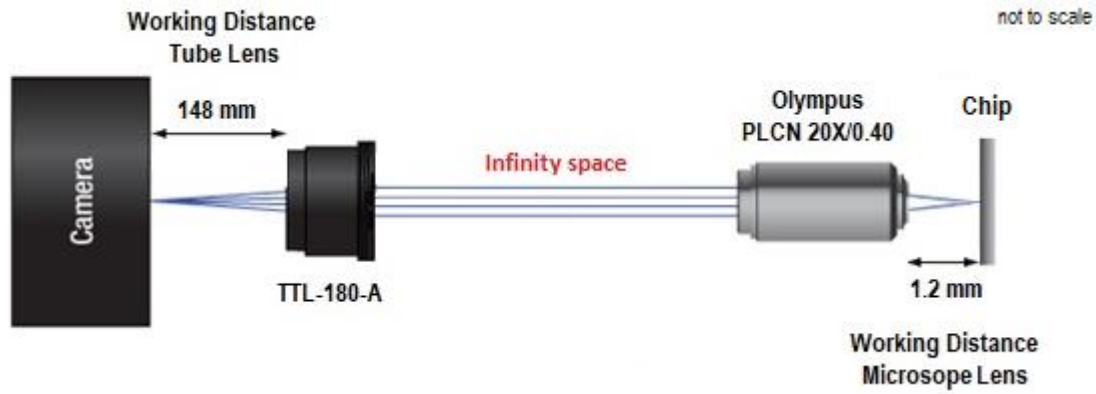


Fig. 108: Spatial alignment of the infinity-corrected microscope – section between the tube lens and the microscope lens represents the infinity space which provides a path of parallel light rays into which complex optical components can be placed without distortion of the visual readout. (not to scale)

The distances between the camera sensor, the tube lens, as well as the microscope objective, and the chip needed to be carefully adhered to (Fig. 81). Minimal adjustments of the gap to the microfluidic device were possible by fine-tuning the Z coordinate of the translational micrometer stage. The in Fig. 81 depicted setup was used for the final irradiation of the chip with the laser source due to the necessity of a 20x magnification (c.f. explanation in Fig. 83). If a broader section of the chip was to be examined, the microscope lens had to be swapped, impacting the required distance to the chip (Table 18).

Table 18: Impact of magnification on working distance and the application of selected microscope lenses

Lens (Olympus)	Magnification	Working distance [mm]	Application
PLCN 4X/0.10	4 x	18.5	droplet formation / defect tracking
PLCN 10X/0.20	10 x	10.6	droplet formation
PLCN 20X/0.40	20 x	1.2	droplet sorting

This was possible by rotating the 6-hole filter wheel to the appropriate position and repeated adjustment of the micrometer stage. For optimal illumination of the chip, the gooseneck of the AmScope HL250-AS microscope illuminator was pointed directly at the microscope lens (Fig. 109). The shutter setting on the camera was set in such a way that limited overexposure and enable a clear visual readout.



Fig. 109: Backlight illumination of the microfluidic chips with the flexible HL250-AS single fiber gooseneck microscope illuminator

For the alignment of the laser light path, all lenses and dichroic mirrors were installed on their respective holders (25 mm lens *via* the Thorlabs LMR1S/M lens mount, 6 mm lens *via* the Thorlabs LMR6/M lens mount, and dichroic mirrors *via* Thorlabs FFM1 filter mount) as depicted in Fig. 110 (top). A dummy chip was mounted to see the impact center of the laser spot (Fig. 111 right). The Hamamatsu Photonics H9306-2 photomultiplier tube was also attached and connected *via* a Thorlabs SM1L20 lens tube to the Semrock SEM-FF01-530/11-25 band-pass filter. A stray light exposition was minimized by wrapping the sensor and the connections with black masking tape Fig. 110 (bottom).

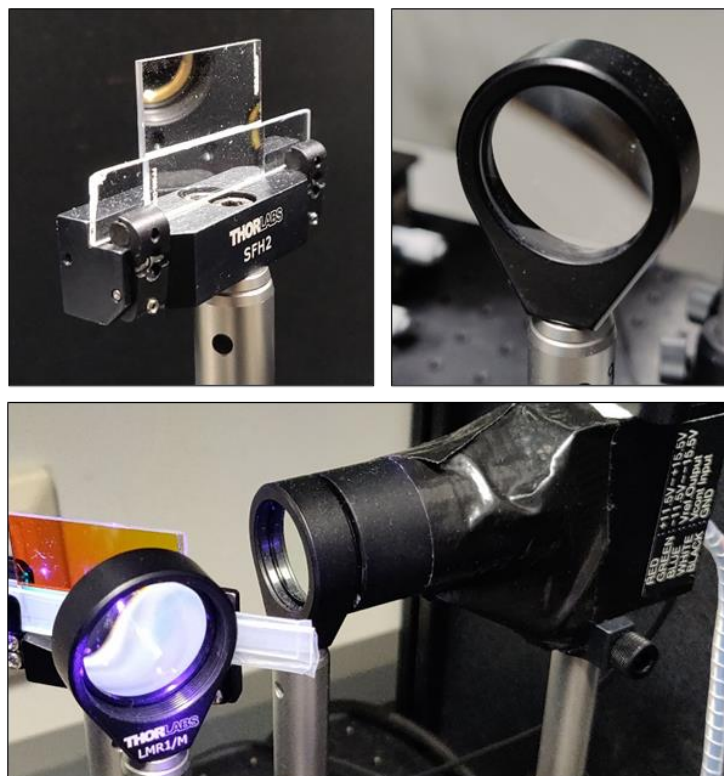


Fig. 110 top left: FFM1 filter mount with the Semrock FF685-Di02-22x29 dichroic mirror; **top right:** LMR1S/M lens mount with the OSE-SLB-25-120PM biconvex lens; **bottom:** Attachment of the H9306-2 photomultiplier tube to the SEM-FF01-530/11-25 band-pass filter *via* the SM1L20 lens tube, which enabled further minimization of stray light and thus the improvement of the signal/noise ratio.

From this moment, all steps were performed using appropriate laser safety goggles that were certified for the applied laser energy output and wavelength (Uvex F42P1E01). The components were aligned starting from the laser and working towards the microfluidic chip using a standard 40 cm ruler. This was done by adjusting the height, the position, and the angle of tilt of every part by steadily checking for parallelism (height) of the laser beam throughout the light path. Centered positioning of the laser spot in all optical components was estimated with the naked eye and was proven to be sufficient (Fig. 111 left). A combination of the OSE-SLB-25-120PM and OSE-SLB-06-08PM biconvex lenses thus magnified the laser and reflected it with the Semrock FF493/574-Di01-25x36 and Semrock FF685-Di02-22x29 dichroic mirrors through the respective microscope lens onto the chip. Using the Olympus PLCN 10X/0.40 lens, a total 150-fold magnification of the laser beam was possible, creating an approx. 25 μm spot on the microfluidic chip. The emitted fluorescence signal was reflected off the Semrock FF685-Di02-22x29 nm longpass mirror, passed through the Semrock FF01-530/11-25 and Semrock FF493/574-Di01-25x36 bandpass filters, and was finally picked up by the Hamamatsu H9306-2 photomultiplier tube (c.f. Fig. 103).

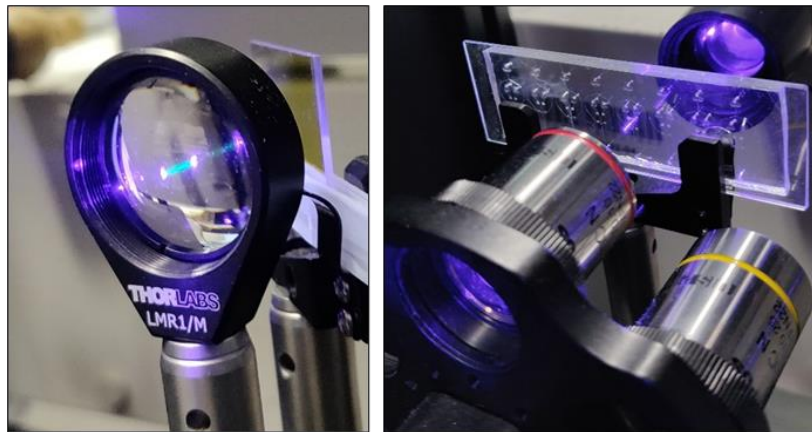


Fig. 111 left: Visible laser spot on the OSE-SLB-25-120PM biconvex lens; **right:** Laser beam passing through the Olympus PLCN 4X/0.10 creating a visible imprint on the microfluidic chip.

The final fine adjustment of the XY-coordinates of the micrometer stage allowed for the exact positioning of the laser beam directed to a specific location preceding the sorting fork of the droplet sorting chip (Fig. 112).

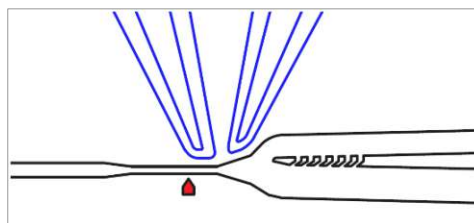


Fig. 112: Schematic structure of the sorting fork on the microfluidic chip: The red arrow represents the location of the laser spot. Dark lines depict the walls and blue lines of the electrode channels on the microfluidic device. Values on differently sized channels are in μm .

The correct alignment could be affirmed in two ways. Direct observation of the centered laser spot using visual control with the high-speed camera was still possible despite the installed dichroic mirror. Alternatively, a positive periodic fluorescence read-out during droplet manipulations on the chip pointed to a correctly set light path. (c.f. Fig. 126)

E V.1.2 Flow controller pressure connection

The operation of the Elveflow Obi Mk3 2000 mbar pressure control units required access to a high-pressure source (1.5 bar to 10 bar). Therefore, the system was connected to the in-house compressed air supply by appropriate high-pressure connectors and hosing (Fig. 113, left, Elveflow LVF-KFI-16, Landefeld polyurethane hose). To omit any particle contamination of the air stream, an Elveflow LVF-KXX-08 particle filter had to be installed prior to entry into the flow controller (Fig. 113, right).

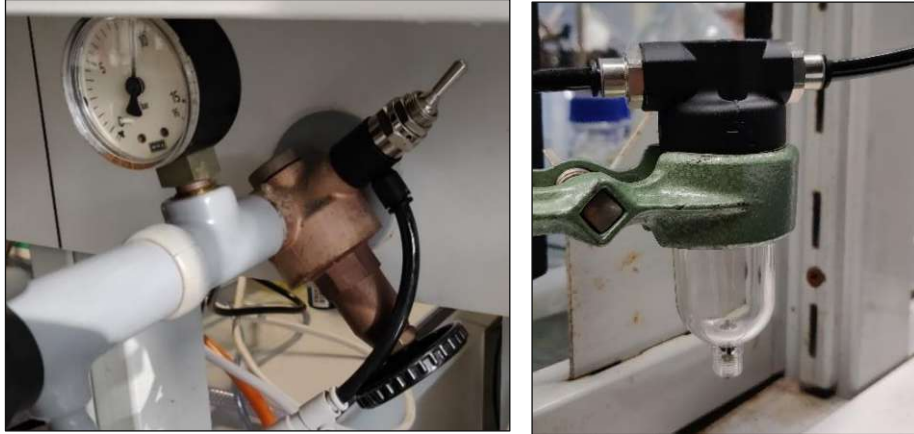


Fig. 113 left: Attachment of the pressure connection to the in-house compressed air supply - lever is used to pressurize and depressurize the system prior and after use; **right:** KXX-08 particle filter is installed to limit any moisture and dust contamination of the Elveflow OB1 Mk3.

E V.2 Manufacturing of microfluidic PDMS chips

All microfluidic devices were fabricated in PDMS using standard soft lithography techniques. For this purpose, already existing AutoCAD designs of the microfluidic chips were printed on a chrome-based photomask with the abovementioned specs (see F I) by Jena Compugraphics (Fig. 84). These photomasks were employed for the repeated manufacture of silicon master molds and could be generally used for several years without any deterioration of quality.

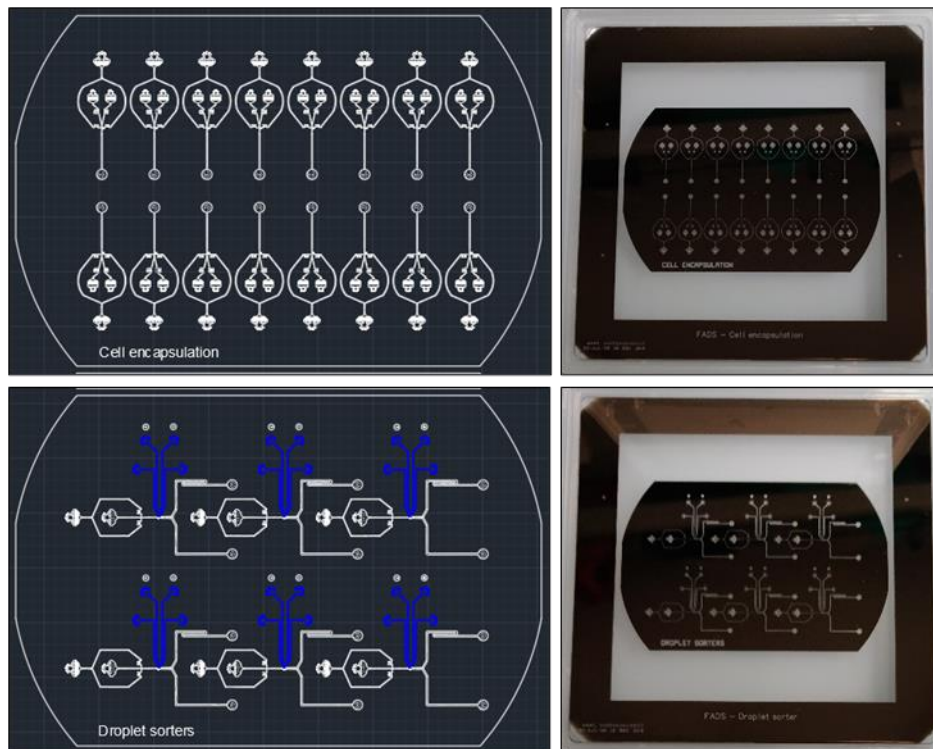


Fig. 114: AutoCAD designs of the microfluidic encapsulation (top) and sorting (bottom) chips and the respective printed chrome-based photomasks used in this thesis.

Any manipulations of wafers, PDMS slabs, and glass slides should be performed exclusively with gloves and minimal contact to their surface. Especially wafers should be only handled with plastic tweezers so that the material is not harmed. By adhering to these rules, contaminations were limited, and reproducible results were guaranteed.

E V.2.1 Master mold fabrication

For the fabrication of the master molds, the refrigerated SU-2025 photoresist (1 mL per inch of wafer diameter + additional 2 mL) was drawn into 10 mL syringes (1 per wafer) to warm to room temperature overnight. Typically, 8 mL were withdrawn and stored capped in an upright position in the dark (Fig. 115 left). This approach allowed for the settling of any bubbles that were trapped in the viscous mixture.

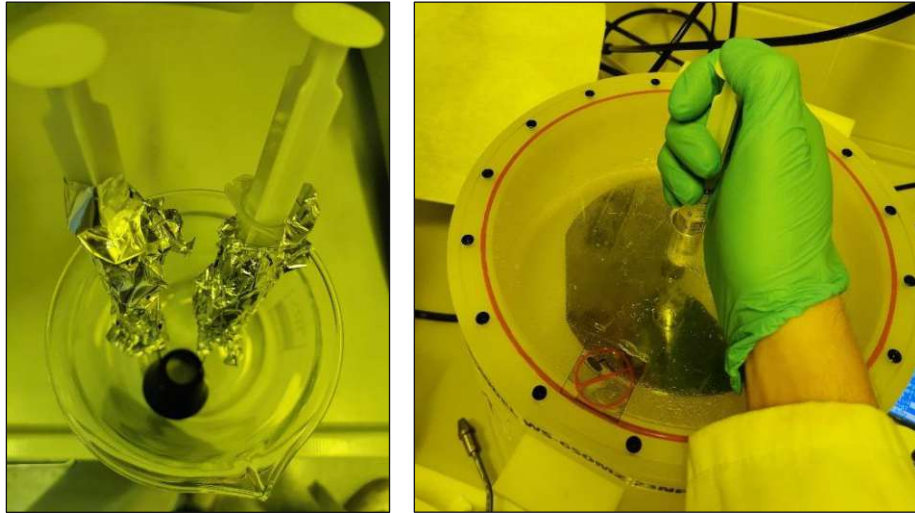


Fig. 115 left: SU-2025 pre-filled syringes covered in aluminum foil to prevent premature decomposition of the photoresist; **right:** injection of the photoresist onto the wafers loaded in the Laurel WS-650MZ-23NPPB spin-coater.

On the next day, all new wafers were dehydrated on a hotplate at 145 °C for at least 15-20 minutes. The wafers were then cooled to room temperature and, prior to plasma treatment, blown dust-free with pressurized N₂. Activation of the wafers was performed using the Harrick Plasma - PDF-002-CE plasma cleaner at high settings for 5 minutes. The wafers were then transferred with a correctly sized wafer fork (6") into the Laurel WS-650MZ-23NPPB and spin-coated with a 25 μm thick layer of the prepared SU-8 2025 photoresist using a predefined spinning program (10 s @ 500 rpm, then 30 s @ 3000 rpm). For this purpose, the contents of the syringes were injected rapidly (2-3 s) without the introduction of any bubbles onto the center of the wafer through the top hole of the spin-coater (Fig. 115 right). The spinning program was immediately started after the completed addition. Prolonged waiting caused an uneven coating of the epoxy resin. Coated wafers were then soft-baked on hotplates at 90 °C for 5-6 minutes.

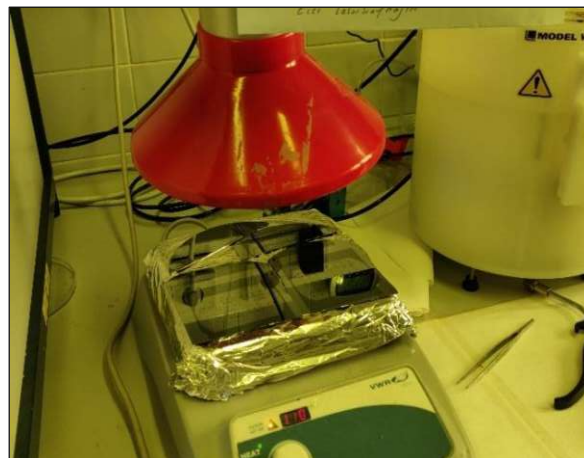


Fig. 116: Soft-bake of the freshly coated wafers under the movable fume hood to limit dust particle exposition.

To omit particle contaminations on the sticky surface, the freshly coated wafers were handled in the most optimal dust-free environment possible. Thus a movable fume hood was directly positioned above the hotplate during the hardening process (Fig. 116). The wafers were additionally covered with a plastic dish while cooling back to room temperature (not shown). Due to the size of the wafers and

the limited space in the UV exposer, the wafers had to be cut to a smaller size (4" maximum). Therefore, overhanging areas were masked with a thin silicon sheet, and the wafers were placed upside down on a dust-free cloth. Areas that exhibited the least dust contaminations were preferably removed using a diamond cutter with two perpendicular cuts.

The wafers were then introduced into the Kloé - UV-KUB 2 masking system (Fig. 117 left) and covered with the respective photomask with the chrome side facing down onto the wafer. UV irradiation was performed using a defined setting for the thickness of the 25 μm structures (7 s @ 23.8 mW/cm² - corresponding to 50 % intensity).



Fig. 117 left: Insertion of the appropriately cut wafers into the Kloé - UV-KUB 2 UV exposer; **right:** Development of the UV exposed wafers using the mr-Dev 600 SU-8 developer in a large glass petri dish – structures can be already distinguished after short treatment times.

The wafers were taken from the instrument and following a 5–6-minute post-exposure bake at 90 °C, developed by submerging them in mr-Dev 600 SU-8 developer (1-2 cm height of solution) for 5 minutes. A constant swirling of the bath improved the dissolution of the UV exposed material. Already after 1 minute, all structures became visible to the naked eye (Fig. 117 right). The wafers were then thoroughly rinsed with HPLC grade iPrOH, whereas residual solvent was removed with pressurized N₂. The integrity of the structures and the efficiency of the development process were checked under the microscope. If any remaining unexposed photoresist was noticed, the process was redone until only sharp edges were detectable. The wafers were then hard-baked for 30 minutes at 200 °C to harden, smoothen, and improve SU-8 adhesion.

Finally, the silicon wafers were treated with tridecafluoro-1,1,2,2-tetrahydrooctyl)trichlorosilane in a vacuum desiccator for 5 minutes to further improve a later PDMS detachment. This was done by dispensing 4 μL of the perfluorinating reagent onto the bottom of a petri dish. The wafers were then glued upside down onto the cover, and the dish was placed loosely sealed inside the vacuum chamber. Following the perfluorination, the wafers were baked once more for 30 minutes at 90 °C, finishing the master mold production. The molds could be stored at room temperature for several > 12 months and were repeatedly used to produce PDMS chips without any decrease in quality.

E V.2.2 PDMS chips fabrication

For the fabrication of the microfluidic chips, 40 mL of Sylgard 184 pre-polymer and curing agent were thoroughly mixed in a small beaker at a ratio of 10:1 (v/v). Intense opaqueness caused by the suspension of bubbles in the solution indicated sufficient mixing. The beaker was then placed in a vacuum desiccator and degassed for at least 15 minutes. The largely bubble-free viscous mixture was poured onto the patterned silicon wafer in a petri dish (Fig. 118 left). Residual bubbles were removed by careful brushing with a plastic pipette without touching the surface of the wafer. The last check for trapped bubbled was performed after the polymer mixture was heated for 5 minutes in the 80 °C drying oven. Once complete transparency of the surface was confirmed, the PDMS pre-polymer was placed back into the oven and cured for 2 hours.

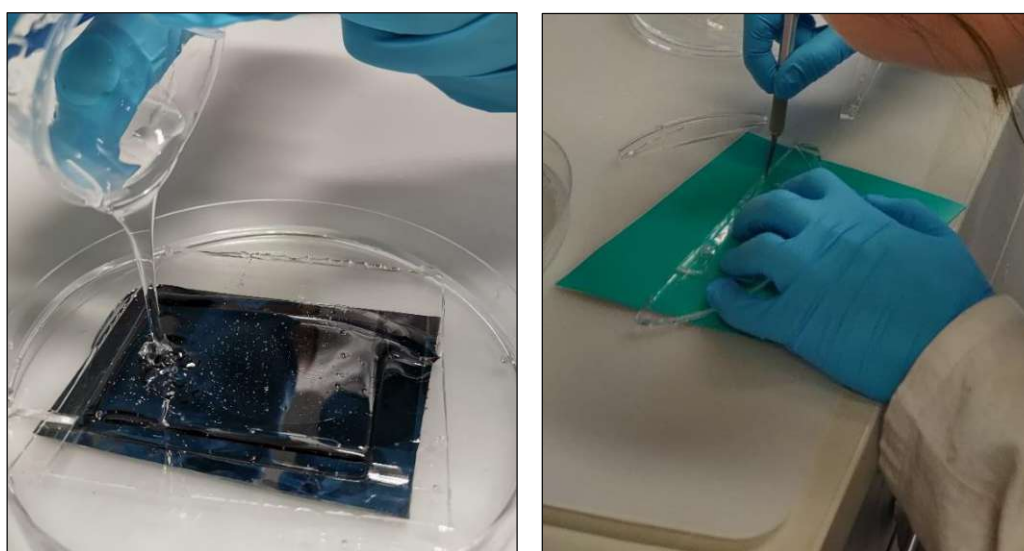


Fig. 118: Pouring of the degassed PDMS pre-polymer onto the patterned wafers; **right:** Precise cutting of the cured PDMS slabs using sharp razor blades – discarded material is reused as mold in subsequent pours to save PDMS.

After the curing process, the still warm PDMS slabs were carefully peeled of the wafers and cut to the sizes of the final microfluidic chips with the use of razor blades (Fig. 118 right). Inlet and outlet tubing holes for liquids and electrodes were punctured into the device using a WPI biopsy puncher ($\varnothing = 0.75$ mm) at the plotted markings. The thus formed debris was removed using scotch tape, and the chip was thoroughly washed with HPLC grade iPrOH. The bulk solvent was removed with pressurized N_2 , and the chips were placed in the oven for additional 30 minutes. Cover glass slides (non-coated for droplet encapsulation, ITO (indium tin oxide) coated for droplet sorting) were cleaned in an ultrasonic bath in an aqueous 2 vol% Hellmanex™ III solution for 5 minutes, then rinsed with dH_2O (3x), sonicated for 5 minutes in dH_2O , rinsed again with dH_2O (3x), then sonicated in HPLC grade iPrOH for 5 minutes and dried using pressurized N_2 . Residual solvent was also removed by placing the glass slides for 30 minutes in the 80 °C oven.

Both a cleaned glass slide and a PDMS chip were then placed inside the PDF-002-CE plasma cleaner and activated for 4 minutes at high settings. If an ITO-coated glass slide was used, the ITO coating should be facing downward. After the treatment, the glass slide was lifted and pressed onto the PDMS chip. A second scotch-tape wrapped glass slide was used as opposite resistance (creating a “glass sandwich”) so that enough force could be applied. Too intense pressure or commonly performed

clamping of the chips led to a collapse of the microfluidic channels. Clean surfaces circumvented the necessity for high pressure and triggered immediate strong adhesion. Following this protocol, all manufactured chips were then placed in the 80 °C oven and irreversibly bonded over the course of two days. Final products were recovered from the oven and wrapped in scotch tape to prevent any contaminations of the channels. All manufactured microfluidic chips were stored at room temperature for further steps.

E V.2.3 Chip preparation and electronics

E V.2.3.1 Silanization

Prior to any application, all internal surfaces of the chips (encapsulation & sorting) were silanized to create fluorophilic channel walls. For this purpose, 10 μL of the perfluorinating agent was mixed with 1 mL of HFE-7500 and syringe-filtered into a clean 1.5 mL Eppendorf tube. The tubes were connected *via* the XS reservoir tanks (Fig. 119 bottom left) to one of the pressure channels of the Elveflow flow controller (Fig. 119 top) and *via* the 0.012" ID x 0.030" OD PTFE tubing to the microfluidic device. Before the insertion of the tubing, the tip was freshly cut off to further limit contamination of the chip with particulate matter. Insertion of 1-2 mm of the tubing into the chip was sufficient to prevent any detachment during any liquid manipulations, even at high pressures. All other outlets were mounted with 23G steel tubing to monitor liquid leakage (Fig. 119, bottom right).

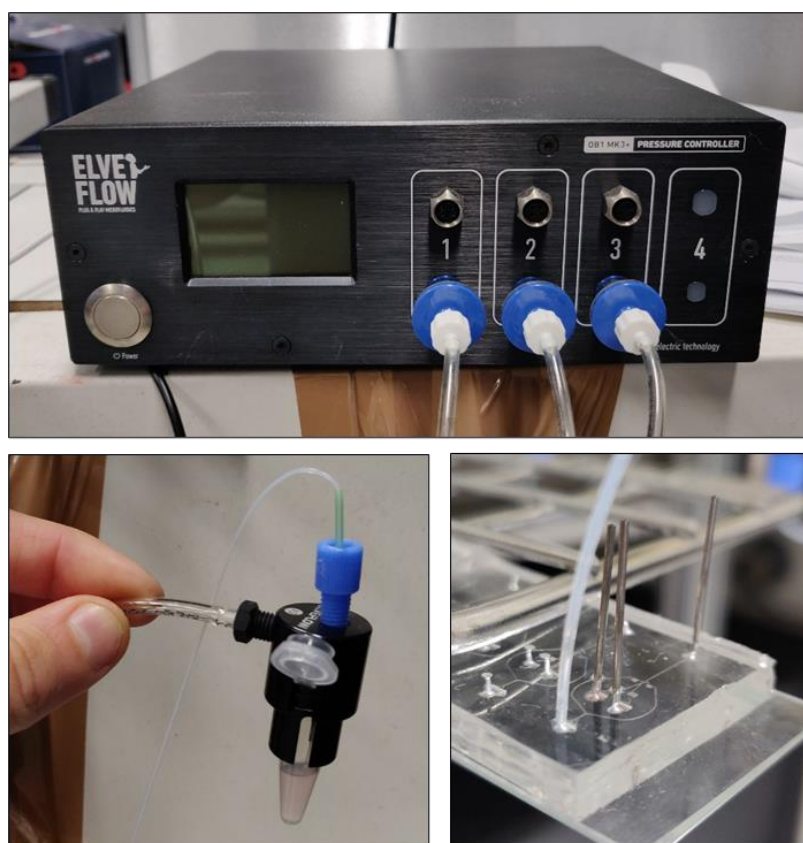


Fig. 119 top: Elveflow OBI Mk3 with three 2000 mbar pressure channels connected *via* 5 μm Luer lock filters and male Luer integral lock to 3/32" OD barbed adapters; **bottom left:** Fully assembled XS reservoir tank – connection to the microfluidic chip *via* 0.030" OD PTFE tubing using a 1/32" to 1/16" OD sleeve and 1/4"-28 fitting, connection to flow controller *via* 4 mm OD PU tubing and 1/4"-28 barbed fitting; **bottom right:** Silanization of the droplet encapsulation chip – reagent is injected through the oil channel of the chip (see. Fig. HFE-7500 & surfactant inlet). All other inlets and outlets are equipped with 23 g steel tubing for improved control of liquid outflow.

The introduction of the reagent was necessarily performed using inlets with incorporated microfluidic filters to prevent blockages of the channels by small debris (Fig. 120). If the backpressure of the microfluidic system prevented outflow of the reagent of all exits, the least flow resistant steel tubing was plugged with a finger until beginning leakage of all other channels was observed. Silanization of the whole system was performed for 5 minutes at 700-1000 mbar, then the reagent was flushed with fresh syringe-filtered HFE-7500, and the chip was dried using pressurized air. Both steps were performed using the Elveflow pressure controller employing individual XS reservoir tanks. In the latter case, an empty Eppendorf tube was employed.

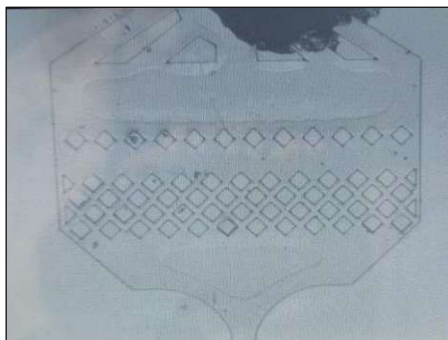


Fig. 120: Magnified image of a microfluidic filter

E V.2.3.2 Electrode manufacturing

The chip was placed on a 90 °C hotplate for 5 minutes, and the electrode channels were filled with low-temperature solder wire (Field's metal, 51In, 32.5Bi, 16.5Sn - Indalloy #19, The Indium Corporation of America). Filling of the channels was performed by pushing approx. 1-2 cm of the wire into the electrode channels until leakage from the outlet was observed. A 10 cm copper wire was then inserted into the still molten alloy, and the chip was allowed to reach room temperature by shutting off the heating (Fig. 121). The slow cooling of the liquid metal allowed for a uniform distribution of the solder inside the channels.

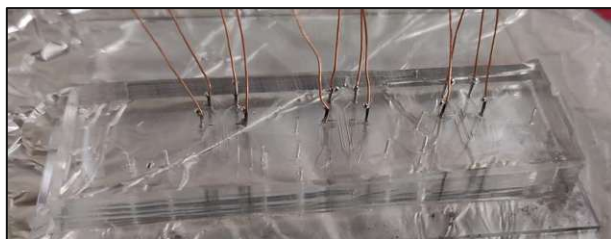


Fig. 121: Electrode channels filled with low-temperature solder inserted with copper wires for electrical connectivity to the Trek PZD700 high voltage amplifier.

E V.2.3.3 Electrical connectivity

The sorting events were triggered using a custom LabView 2019 (see. Fig. 100) program and a National Instruments PCIe-7841 FPGA card. In this assembly, the emitted fluorescence signal was picked up by the PMT and forwarded as corresponding voltage read-out to the FPGA card *via* the SCB-68A connector pane. The wires of the PMT were connected, as depicted in Fig. 122, to the AI0+ and AIGND ports, and the S1 jumpers were set accordingly. To enable the sorting process, analog output

(transferring the voltage trigger pulses) was wired from the AO 0 to the voltage input of the high-voltage amplifier. Using appropriate high-voltage connectors and clamps, the amplified signal was forwarded to the electrodes mounted on the chip. For this purpose, the phase conductor was wired to the positive terminal, whereas the ground was connected to the negative pole and was additionally attached to the backside of the chip using adhesive tape (Fig. 122, right). The aforementioned conductive ITO layer on the glass prevented a buildup of charges which would result in a coalescence of droplets during the sorting process.

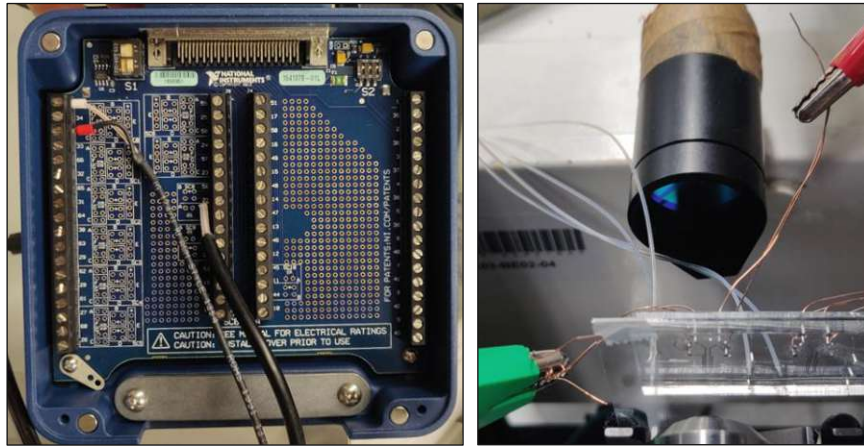


Fig. 122 – *left*: PMT signal cables wired to the SCB-68A connector pane – signal output was connected to AI 0+, the ground is connected to AI GND. S1 jumper settings: 1 – low, 2 – high; *right*: high voltage clamps connected to the electrodes microfluidic chips, the ground electrode was additionally taped onto the backside on the chip to enable connectivity with the ITO layer.

E V.3 Droplet encapsulation

For the droplet encapsulation, the PTFE tubing was connected in a similar fashion used for the silanization of the chip (see Fig. 119 bottom) to the XS reservoirs and the respective inlets and outlets as depicted in Fig. 123. A stock solution of 1% (w/w) 008-FluoroSurfactant (RAN Biotechnologies) = “008FS-Stock” in HFE-7500 (5 g) was prepared as a carrier oil, whereas 1 mL aliquots were syringe filtered and used for singular experiments. The produced droplets were collected under a 200-300 μ L 008FS-Stock layer by submerging the outlet tubing in a pre-filled Eppendorf tube (see Fig. 124). To omit evaporation of the contents, the tubing was guided through a drilled hole of the Eppendorf tube cover. The droplets typically accumulated as a milky layer on top of the oil phase.

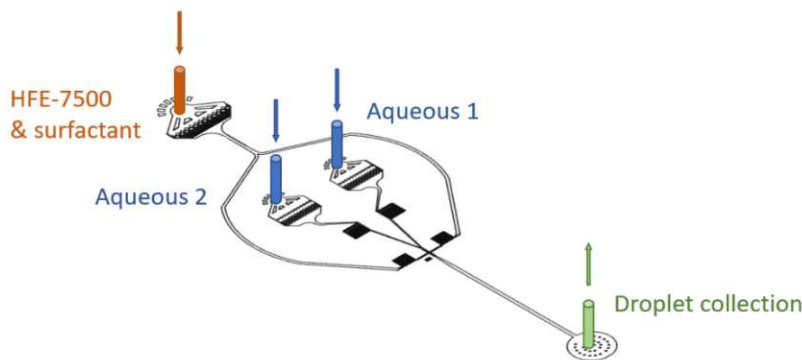


Fig. 123: Schematic of the droplet encapsulation chip - inlets should be connected to the respective XS reservoir tanks via 0.012" ID x 0.030" OD PTFE tubing; the outlet should be connected to a pre-drilled Eppendorf tube (c.f. Fig. 124).



Fig. 124 - left: GUI of the Elveflow® microfluidic control software; middle: pre-drilled Eppendorf tube used to collect formed droplets during the encapsulation stage; right: Eppendorf tube containing the milky droplet layer on top of the transparent buffer oil phase.

The whole process was controlled using the Elveflow ESI Microfluidic Software application. Using different pressure settings for the aqueous and oil phase, different encapsulations frequencies and droplet volumes could be achieved (Table 19). Collections were performed up to 12 hours without a drop in quality, even for droplet formations rates of up to 1-2 kHz.

Table 19: Encapsulation rate and droplet volume depending on oil and aqueous channel pressures.

oil channel pressure [mbar]	aqueous channel pressures [mbar]	encapsulation rate [s^{-1}]	droplet volume [μL]
400	200/200	500	25
600	300/300	750	25
800	400/400	950	25
1000	500/500	1200	25
800	500/500	850	40
600	500/500	600	100

E V.4 Droplet sorting

Unfortunately, due to failed droplet sorting experiments, no definitive standard operation procedure can be written down. However, all preparations towards a successful sorting will still be summarized in this chapter.

For droplet sorting of the encapsulated reagents were reinjected into the prepared sorting chip (silanized & fitted with electrodes – see E V.2.3.1 & E V.2.3.2) using the same setup as for the encapsulation albeit only two inlets were connected as depicted in Fig. 96. The introduction of the droplets was enabled by the correct positioning of the tubing inside the Eppendorf tubes contained in the XS reservoir, placing the PTFE tubing slightly above the lower edge of the milky droplet layer. The pressures were adjusted identically to the encapsulation experiment *via* the Elveflow® GUI.

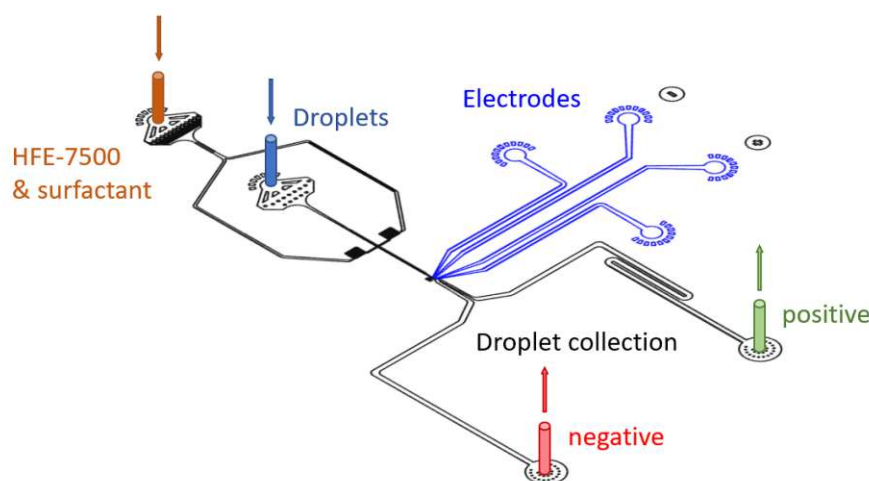


Fig. 125: Schematic of the droplet sorting chip - inlets should be connected to the respective XS reservoir tanks via 0.012" ID x 0.030" OD PTFE tubing; outlets should be connected to separate Eppendorf tubes.

Before any actual sorting, the system was allowed to equilibrate for 10 minutes at constant pressures without switching on the laser diode, the photomultiplier, and the high voltage amplifier. After visual confirmation of stable flow, all optoelectronics were turned on, and the LabView FPGA program was launched. The PDMS chip was aligned in such a way (see Fig. 112) that the fluorescence of the droplets (containing a fluorophore) was confirmed by following the fluorescence emission on the high-speed camera as well with the recording of the PMT voltage data *via* the LabView program (Fig. 126).

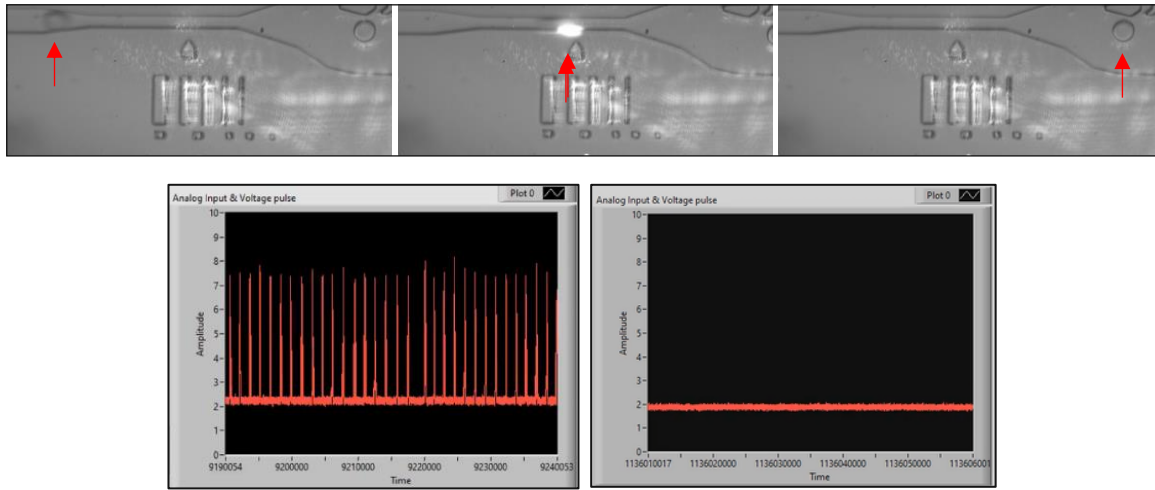


Fig. 126 top: Visual read-out of a positive droplet passing the laser beam; **bottom:** Representation of signal read-out of the same event on the GUI (graphical user interface) – **left:** droplets passing the laser, **right:** only detection of background signal.

The sensitivity of the PMT could be adjusted during the first minutes of the reinjection process by turning the control voltage knob of the Hamamatsu C7169 PMT controller to match a sufficient S/N ratio. The electrodes were subsequently connected to the high voltage amplifier as described in E V.2.3.3.

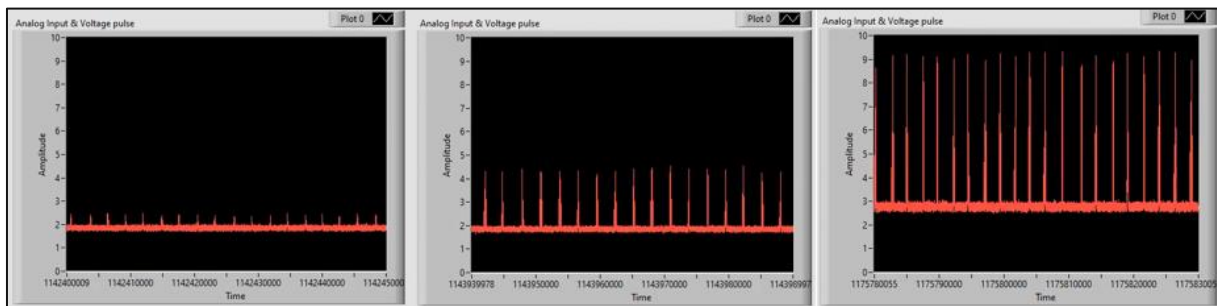


Fig. 127: Gradual increase of the control voltage of the Hamamatsu C7169 PMT controller dramatically increases the S/N ratio (0.05 to 0.3 V).

At this status, the system would be theoretically ready for a sorting experiment. This would be performed by setting the appropriate values for voltage pulse height (V_s), trigger delay (t_0) at defined flow rates of the system by switching the program into “sorting mode” by unticking the “No sorting” box of the GUI (Fig. 102). If a ‘positive’ droplet were detected *via* the PMT, the resulting high-voltage pulse would deflect the droplets into the positive channel. Both negative and positive populations would be collected in the same manner as for the encapsulation stage. The droplets could be subsequently analyzed *via* histogram on the GUI or by taking samples of the sorted populations and observation using a fluorescence microscope with the appropriate excitation wavelength.

E V.5 (Failed) Proof of sorting

For a proof of concept of the whole system, two different populations of droplets containing either 20 mM 4-MeO,5-P-ABAO-octanal adduct [160] or unreacted and thus non-fluorescent 4-P,5-MeO-ABAO [148] in 50 mM pH 5.5 NH₄OAc buffer were produced. The adduct was prepared in an 8 mL brown-glass screw cap vial by weighing 10.45 mg of the ABAO and dissolving it with 1.9 mL of buffer. 100 μ L octanal [XC] as 420 mM stock solution in DMSO was added (1.05 equivalents) to reach a final concentration of 5 % DMSO in buffer. Droplets without a carbonyl source were prepared in the same fashion by dilution with pure DMSO.

Both populations were formed using the settings summarized in Table 20, whereas droplet encapsulations were performed for approximately 2 hours resulting in approx. 10 million droplets per experiment. The two populations were mixed by carefully transferring the milky droplet layer with a plastic pipette (glass pipettes are detrimental to droplet stability) into a new Eppendorf tube. Although reinjection into the sorting chip worked without problems, no deflection of droplets was observed inside the channels using any combinations of voltage pulse height and trigger delay.

Table 20: Summarized settings for droplet encapsulation and sorting for the proof-of-concept system.

Droplet encapsulation	settings
Pressure oil channel	1500 mbar
Pressure aqueous channel 1	800 mbar
Pressure aqueous channel 2	800 mbar
Encapsulation frequency	2200 Hz
Droplet sorting	
Pressure oil channel	160 mbar
Pressure aqueous channel	80 mbar
Sorting frequency	50 Hz
Threshold voltage	sufficient for trigger
Voltage pulse height	300-700 V
Trigger delay	1-100 μ s
Sampling frequency	100.000 kHz
Transfer rate	10.000

F Appendix

F I List of materials for the FADS

Optomechanical components

- General hardware (*Thorlabs*)
 - MB6060/M – breadboard (600 mm x 600 mm x 12.7 mm)
 - MB4560/M – breadboard (450 mm x 600 mm x 12.7 mm)
 - Casing (525 mm x 525 mm x 525 mm)
 - XE25L525/M – 525 mm structural rails (8x)
 - XE25L500/M – 500 mm structural rails (5x)
 - XE25L300/M – 300 mm structural rails (2x)
 - RM1S – 1" construction cube (10x)
 - TB4 – 3/16 black hardboard (610 mm x 610 mm) (2x3)
 - XE25H – enclosure hinges
 - BBH1 – lifting handles
 - Laser holder
 - MSB1015/M – mini-series breadboard (150 mm x 100 mm)
 - PSY321/S – breadboard bracket
 - P250/M – solid post (250 mm x 28 mm \varnothing)
 - PB1 - mounting post base
 - Optical rails
 - RLA150/M – small optical rails 150mm
 - RLA300/M – small optical rails 300mm
 - RLA450/M – small optical rails 450mm
 - CL6 – rail clamps (8x)
 - RC1 – dovetail rail carrier (8x)
 - Optical posts
 - TR100/M-P5 – 100 mm optical post (8x)
 - TR50/M-P5 – 50 mm optical post (2x)
 - PH100/M – 100 mm metric post holder (8x)
 - PH50/M – 50 mm metric post holder (2x)
 - CF175C/M - large clamping fork (2x)
 - BE1/M - studded pedestal base adapter (2x)
- Optical mounts (*Thorlabs*)
 - LMR2S/M – lens mounting ring for 2" optic
 - LMR1S/M – lens mounting ring for 25 mm optic (3x)
 - LMR6/M – lens mounting ring for 6 mm optic
 - FH2 – filter mount for rectangular optic

- FFM1 – 30-mm-cage-compatible rectangular filter mount (2x)
- FW1A – 6-hole filter wheel with base assembly
 - SM1A3TS – thermally stable SM1 to RMS adapter (3x)
- SM1L20 - stackable lens tube (2x)
- 53272 – filter translational mount (*Edmund Optics*)
- XYZ 3-axis translational linear 60 mm x 60 mm micrometer stage (*Machifit*)
- Screws and adapters (mostly M6 & M4 threads)

Optical components

- CNI-415-MDL-3 – 100 mW 415 nm laser, including power supply PSU-III-FDA (*CNI*)
- H9306-2 – photomultiplier tube with C7169 power supply (*Hamamatsu Photonics*)
- Chronos 1.4 – high-speed camera, monochrome, 32 GB (*Kron Technologies*)
- TTL-180-A – tube lens, $f = 180$ mm (*Thorlabs*)
- Infinity corrected objective lenses (*Olympus*)
 - PLCN 10X/0.25
 - PLCN 4X/0.10
- Dichroic beam splitters (*Semrock*)
 - SEM-FF493/574-Di01-25x36 – 493/574 nm dichroic bandpass mirror
 - SEM-FF685-Di02-22x29 – 685 nm dichroic longpass mirror
- Band-/ Longpass filters
 - SEM-FF01-530/11-25 – 530 nm bandpass filter (*Semrock*)
 - FELH0700 – 700 nm longpass filter (*Thorlabs*)
- NDL-25S-4 – linear step neutral density filter (*Thorlabs*)
- Focusing lenses (*Laser2000*)
 - OSE-SLB-25-120PM – 25 mm \varnothing biconvex lens, BK7, AR coated ($f = 120$ mm)
 - OSE-SLB-06-08PM – 6 mm \varnothing biconvex lens, BK7, AR coated ($f = 8$ mm)
 - OSE-SLB-06-10PM – 6 mm \varnothing biconvex lens, BK7, AR coated ($f = 10$ mm)
 - OSE-SLB-06-20PM – 6 mm \varnothing biconvex lens, BK7, AR coated ($f = 20$ mm)
- HL250-AS – single fiber gooseneck microscope illuminator 150W (*AmScope*)

Flow control

- Microfluidic flow controller OB1 Mk3 incl. 3x OB1 Mk3 Channel 2000 mbar (*Elveflow*)
- Pressure equipment (*Elveflow*)
 - LVF-KFI-16 – pressure source quick connection kit
 - LVF-KXX-08 – microfluidic air pressure source cleaner kit
- Connectors and adapters (*Elveflow*)
 - KRXS-V2 – reservoir tank XS for 1.5 mL Eppendorf tubes (3x)
 - KRS1 – reservoir tank S for 15 mL Falcon tubes (2x)
 - KTTS – 1/32" to 1/16" outer \varnothing adapter sleeves + 1/32" outer \varnothing tubing
 - KTSS-23G – fittings 23 g steel fluidic adapters

- STARTPACKLUER – starter pack luer
- Landefeld – polyurethane high-pressure hose (Landefeld)

Droplet analysis and sorting (National Instruments, Trek)

- PCIe-7841 – Virtex-5 LX30 FPGA card (*National Instruments*)
- SCB-68A – 68-pin shielded I/O connector block & R-series cable (*National Instruments*)
- PZD700 – high voltage amplifier (*Trek*)
- Computer incl. large SSD, LabView 2019 incl. LabView FPGA module (*National Instruments*)

Microfluidic chip fabrication

- Equipment
 - PDF-002-CE – expanded plasma cleaner (*Harrick Plasma*)
 - WS-650MZ-23NPPB – spin coater (*Laurell Technologies*)
 - UV-KUB 2 UV-LED – exposure and masking system (*Kloé*)
 - FDL 115 – drying oven (*Binder*)
 - Hot plate (90 – 200 °C temperature range)
 - Vacuum desiccator
- Materials
 - Chrome photomask for droplet sorter & droplet maker (*Jena Compugraphics*)
 - soda-lime-glass 4" x 4", low reflective chrome, defect density 0,5/cm², minimum dimensions: > 1 µm, dimensional tolerances: 0,3 µm
 - Silicon wafers (6" Ø, undoped, 650 µm thickness) – generously supplied by *Infineon*, 1 mm thick wafers are also tolerated
 - SU-8 2025 – permanent negative epoxy photoresist (*Kayaku Advanced Materials*)
 - mr-Dev 600 – SU-8 developer (*micro resist technology*)
 - Sylgard 184 PDMS base (*Dow*)
 - Sylgard 184 PDMS curing agent (*Dow*)
 - 0.75 mm Ø biopsy puncher (*WPI*)
 - Hellmanex III cleaning concentrate (*Hellma*)
 - Glass microscope slides 76 mm x 26 mm (*Marienfeld*)
 - ITO coated microscope slides CG-81IN-S207 (*Delta Technologies*)
 - HFE-7500 (*Fluorochem*)
 - Tridecafluoro-1,1,2,2-tetrahydrooctyl)trichlorosilane (*Fluorochem*)
 - 1H,1H,2H,2H-Perfluorooctan-1-ol (*Fluorochem*)
 - 008-FluoroSurfactant (*RAN Biotechnologies*)
 - Wirebn-53307 - Low-melting-temperature solder wire (composition 51.0 In, 32.5 Bi, 16.5 Sn, 0.020 mm Ø; *The Indium Corporation of America*)

F II Gene sequences

Genes were subcloned into vector pET22b(+) (ampicillin resistance) using restriction enzymes BamHI & NdeI.

ZMO-SHC2_0872_F438C (wild-type, GenBank: AAV89496.1)

ATGACTGTATCGACTTCCTCGGCTTTTCATCATAGCCCGTTGTCTGATGATGTTGAGCCGATTATCCAAA
 AGGCCACCCGTGCCTTGCTTGAGAAGCAGCAGCAGGATGGCCATTGGGTTTTGAATTGGAAGCCGATGCAAC
 CATTCCCGCTGAATACATCCTGTTAAAGCATTATTTGGGTGAACCCGAAGATTTAGAAATAGAGGCCAAGATAG
 GTCGCTATTTGCGTCGTATTCAGGGCGAGCATGGCGGATGGTCTTTGTTTTATGGTGGTGTCTTGATTTGAGC
 GCCACGGTCAAAGCCTATTTGCTTGAAAATGATCGGAGATTCTCCTGATGCGCCTCATATGCTTCGAGCCAGA
 AATGAAATTTGGCACGGGGTGGGGCGATGCGTGCCAATGTCTTTACACGTATTCAATTAGCTCTGTTCCGGGC
 AATGTCATGGGAGCATGTCCCTCAAATGCCCGTAGAGTTGATGTTGATGCCGGAATGGTTCCGGTTCACATCA
 ATAAAATGGCCTATTGGGCAAGAACCGTTTTAGTCCCGTTATTGGTTTTACAGGCGTTAAAGCCTGTCGCCCGTA
 ATCGGCGCGGTATCTTGTTGATGAATTATTTGTGCCGGATGTTTTACCGACCCCTCAGGAAAGCGGTGACCCCT
 ATATGGCGTCGTTTTTTTTCGGCACCTGATAAGGTATTGCATAAAGTAGAACCTTATTGGCCGAAAAATATGCGC
 GCGAAGGCTATTCATAGCTGTGTCCATTTGTGACCGAGCGTTGAATGGTGAAGACGGGTTGGGTGCTATTTA
 TCCGGCGATTGCCAATAGCGTCATGATGTATGATGCCTGGGATATCCCGAAAACCATCCAGAAAGAGCCATTG
 CCCGTCGGGCTGTCGAAAAATTGATGGTGTAGATGGCACGGAAGATCAGGGTGATAAAGAAGTCTACTGTCA
 GCCTTGTTATCCCCGATTGGGATACCGCTTTGGTTGCCCATGCCATGTTGGAAGTCGGAGGCGATGAGGCTG
 AAAAATCGGCTATTTCTGCCTTGAGCTGGTTAAAGCCGCAACAAATTTGGATGTAAAGGGCGATTGGGCATGG
 CGGCGGCCTGATCTCAGACCCGGGGATGGGCCTTCAATATAGAAATGACTATTATCCCGATGTCGATGATAC
 GGCTGTTGTGACTATGGCGATGGATCGAGCCGCAAAATTGTCGGATCTTCACGATGATTTTGAGGAATCTAAAG
 CGCGTGCCATGGAATGGACCATTGGGATGCAAAGCGATAATGGCGGTTGGGGCGCTTGTGATGCCAATAACAG
 CTATACTTATCTGAATAATATTCCCTTTGCTGATCATGGCGGTTACTTGATCCGCCAACGGTTCGATGTCTCGGCA
 CGCTGCGTTTTCAATGATGGCGCAAGCCGGTATCTCGATTACAGATCCCAAATGAAAGCGGCAGTTGATTATCT
 TCTGAAAGAGCAAGAAGAGGATGGTAGCTGGTTCGGGCGTTGGGGTGTCAATTACATATATGGCACATGGTCG
 GCCTTATGTGCATTGAATGTGGCCGCTTACCCCATGATCATTTAGCTGTTCCAGAAAGCTGTGGCTTGGCTGAAA
 ACTATTCAAATGAAGATGGTGGTTGGGGTGAATAATTGCGATAGCTATGCCCTTGATTATAGCGGATACGAGCC
 GATGGATTCGACGGCTTCCCAAACAGCATGGGCTTTATTGGGCTTGATGGCTGTTGGGGAAGCTAATCCGAG
 GCCGTGACAAAGGTATAAACTGGTTGGCACAAATCAGGATGAAGAAGGATTGTGGAAAGAAGATTATTATA
 GTGGCGGTGGTTTTCCCGTGTTTTTATCTTCGGTATCACGGTTATTCCAAATATTTCTCTTTGGGCTTTAGC
 GCGCTATCGCAATTTGAAAAAGCCAATCAGCCGATTGTTCAATTATGGGATGTAA

ZMO-SHC1_1548_W555Y (wild-type, GenBank: AAV90172.1)

ATGGGTATTGACAGAATGAATAGCTTAAGTCGCTTGTTAATGAAGAAGATTTTCGGGGCTGAAAAAAC
 CTCGTATAAACCGGCTTCCGATACCATAATCGGAACGGATACCCTGAAAAGACCGAACCGGCGGCCTGAACCG
 ACGGCAAAAGTCGACAAAACGATATTCAAGACTATGGGGAATAGTCTGAATAATACCCTGTTTCAGCCTGTGA
 CTGGTTGATCGGACAACAAAAGCCCGATGGTCATTGGGTCGGTGCCGTGGAATCCAATGCTTCGATGGAAGCA
 GAATGGTGTCTGGCCTTGTGGTTTTTGGGTCTGGAAGATCATCCGCTTCGTCCAAGATTGGGCAATGCTCTTTG
 GAAATGCAGCGGGAAGATGGCTCTTGGGGAGTCTATTTCCGGCGCTGGAATGGCGATATCAATGCCACGGTTG
 AAGCCTATGCGGCCTTGCGGTCTTTGGGGTATTCTGCCGATAATCCTGTTTTGAAAAAGCGGCAGCATGGATT

GCTGAAAAAGGCGGATTA AAAAATATCCGTGTCTTTACCCGTTATTGGCTGGCGTTGATCGGGGAATGGCCTTG
GGAAAAGACCCCTAACCTTCCCCTGAAATTATCTGGTTCCCTGATAATTTTGTCTTTTCGATTTATAATTTTGCCC
AATGGGCGCGGGCAACCATGGTGCCGATTGCTATTCTGTCCGCGAGACGACCAAGCCGCCGCTGCGCCCTCA
AGACCGATTGGATGAACTGTTTCCAGAAGGCCGCGCTCGCTTTGATTATGAATTGCCGAAAAAAGAAGGCATCG
ATCTTTGGTCGCAATTTTTCCGAACCACTGACCGTGGATTACATTGGGTTCACTCAATCTGTTAAAGCGCAATA
GCTTGCGTGAAGCCGCTATCCGTCATGTTTTGGAATGGATTATCCGGCATCAGGATGCCGATGGCGTTGGGG
TGGAATTCAGCCACCTTGGGTCTATGGTTTGGTGGCGTTACATGGTGAAGGCTATCAGCTTTATCATCCGGTGT
GGCCAAGGCTTTGTCGGCTTTGGATGATCCCGTTGGCGACATGACAGAGGCGAGTCTTCTGGATACAGGCC
ACCAATAGTCCGGTATGGGATACAATGTTGGCCTTGTGGCGTTAAAAGACGCCAAGGCCGAGGATCGTTTTAC
GCCGAAAATGGATAAGGCCGCCGATTGGCTTTTGGCTCGACAGGTCAAAGTCAAAGGCGATTGGTCAATCAAA
CTGCCCCGATGTTGAACCCGGTGGATGGGCATTTGAATATGCCAATGATCGCTATCCCGATACCGATGATACCGC
CGTCGCTTTGATCGCCCTTCTCTTATCGTGATAAGGAGGAGTGGCAAAGAAAGGCGTTGAGGACGCCATTA
CCCGTGGGGTTAATTGGTTGATCGCCATGCAAAGCGAATGTGGCGTTGGGGAGCCTTTGATAAGGATAATAA
CAGAAGTATCCTTCCAAAATCCTTTTTGTGATTTCCGAGAATCTATTGATCCGCCTTCAGTCGATGTAACGGCG
CATGTTTTAGAGGCCTTTGGCACCTTGGGACTGTCCCGCATATGCCGGTCAAAAAAGCGATCGACTATGT
CCGTTCCGAACAGGAAGCCGAAGGCGCGTGGTTTGGTGGTATGGCGTTAATTATATCTATGGCACCGGTGCG
GTTCTGCCTGCTTTGGCGGCGATCGGTGAAGATATGACCCAGCCTTACATACCAAGGCTTGGCATTGGCTGGT
CGCACATCAGCAGGAAGACGGCGGTTGGGGCGAAAGCTGCTTCTATATGGAGATTGATTCCATTGGGAAG
GGCCAACACGCGTCCCAGACTGCTTGGGCTTTGATGGGGTTGATCGCGGCAATCGTCCCGAAGATTATGA
AGCCATTGCCAAGGATGCCATTATCTGATTGATCGCCAAGAGCAGGATGGTAGCTGGAAGAAGAAGAATTC
ACCGGCACCGATTCCCCGTTATGGCGTGGGTGACGATCAAGTTGGATGATCCGGCTTTATCGAAACGATT
GCTTCAAGGCGCTGAACTGTACGGGCGTTTATGCTGCGTTATGATTTTTATCGGCAATCTTCCCCGATTATGGC
GTTAAGTCGGGCAGAGAGACTGATTGATTTGAATAATTGA

ZMO-SHC1_1548_F486C (wild-type, GenBank: AAV90172.1)

ATGGGTATTGACAGAATGAATAGCTTAAGTCGCTTGTTAATGAAGAAGATTTTCGGGGCTGAAAAAAC
CTCGTATAAACCGGCTTCCGATACCATAATCGGAACGGATACCCTGAAAAGACCGAACCGGCGGCCTGAACCG
ACGGCAAAAGTCGACAAAACGATATTCAAGACTATGGGGAATAGTCTGAATAATACCCTTGTTTCAGCCTGTGA
CTGGTTGATCGGACAACAAAAGCCCGATGGTCATTGGGTGCGTGGCCTGGAATCCAATGCTTCGATGGAAGCA
GAATGGTGTCTGGCCTTGTGGTTTTTGGTCTGGAAGATCATCCGCTTCGTCCAAGATTGGGCAATGCTCTTTTG
GAAATGCAGCGGGAAGATGGCTCTTGGGGAGTCTATTTCCGCGCTGGAAATGGCGATATCAATGCCACGGTTG
AAGCCTATGCGGCCTTGGCGTCTTTGGGGTATTCTGCCGATAATCCTGTTTTGAAAAAGCGGCAGCATGGATT
GCTGAAAAAGGCGGATTA AAAAATATCCGTGTCTTTACCCGTTATTGGCTGGCGTTGATCGGGGAATGGCCTTG
GGAAAAGACCCCTAACCTTCCCCTGAAATTATCTGGTTCCCTGATAATTTTGTCTTTTCGATTTATAATTTTGCCC
AATGGGCGCGGGCAACCATGGTGCCGATTGCTATTCTGTCCGCGAGACGACCAAGCCGCCGCTGCGCCCTCA
AGACCGATTGGATGAACTGTTTCCAGAAGGCCGCGCTCGCTTTGATTATGAATTGCCGAAAAAAGAAGGCATCG
ATCTTTGGTCGCAATTTTTCCGAACCACTGACCGTGGATTACATTGGGTTCACTCAATCTGTTAAAGCGCAATA
GCTTGCGTGAAGCCGCTATCCGTCATGTTTTGGAATGGATTATCCGGCATCAGGATGCCGATGGCGTTGGGG
TGGAATTCAGCCACCTTGGGTCTATGGTTTGGTGGCGTTACATGGTGAAGGCTATCAGCTTTATCATCCGGTGT
GGCCAAGGCTTTGTCGGCTTTGGATGATCCCGTTGGCGACATGACAGAGGCGAGTCTTCTGGATACAGGCC
ACCAATAGTCCGGTATGGGATACAATGTTGGCCTTGTGGCGTTAAAAGACGCCAAGGCCGAGGATCGTTTTAC
GCCGAAAATGGATAAGGCCGCCGATTGGCTTTTGGCTCGACAGGTCAAAGTCAAAGGCGATTGGTCAATCAAA

CTGCCCCGATGTTGAACCCGGTGGATGGGCATTTGAATATGCCAATGATCGCTATCCCGATAACCGATGATACCGC
CGTCGCTTTGATCGCCCTTCTCTTATCGTGATAAGGAGGAGTGGCAAAGAAAGGCGTTGAGGACGCCATTA
CCCGTGGGGTTAATTGGTTGATCGCCATGCAAAGCGAATGTGGCGGTTGGGGAGCCTGTGATAAGGATAATAA
CAGAAGTATCCTTCCAAAATTCCTTTTTGTGATTCGGAGAATCTATTGATCCGCCTTCAGTCGATGTAACGGCG
CATGTTTTAGAGGCCTTGGCACCTTGGGACTGTCCCGCGATATGCCGGTCATCCAAAAGCGATCGACTATGT
CCGTTCCGAACAGGAAGCCGAAGGCGCGTGGTTTGGTCGTTGGGGCGTTAATTATATCTATGGCACCGGTGCG
GTTCTGCCTGCTTGGCGGCGATCGGTGAAGATATGACCCAGCCTTACATCACCAAGGCTTGCGATTGGCTGGT
CGCACATCAGCAGGAAGACGGCGGTTGGGGCGAAAGCTGCTTCTATATGGAGATTGATTCCATTGGGAAG
GGCCCAACACGCGTCCCAGACTGCTTGGGCTTGTGATGGGGTTGATCGCGGCCAATCGTCCCGAAGATTATGA
AGCCATTGCCAAGGGATGCCATTATCTGATTGATCGCCAAGAGCAGGATGGTAGCTGGAAAGAAGAAGAATTC
ACCGGCACCGGATTCCCCGTTATGGCGTGGGTCAGACGATCAAGTTGGATGATCCGGCTTTATCGAAACGATT
GCTTCAAGGCGCTGAACTGTACGGGCGTTTATGCTGCGTTATGATTTTTATCGGCAATTCCTCCCGATTATGGC
GTTAAGTCGGGCAGAGAGACTGATTGATTTGAATAATTGA

F III List of abbreviations

ABAO	2-amino benzamidoxime	(u)HTS	(ultra-)high-throughput screening
<i>Aac</i>	<i>Alicyclobacillus acidocaldarius</i>	iPrOH	isopropanol
ABThD	ammonium benzothiazdiazoles	ITO	Indium tin oxide
Ac	acetyl	LIF	Laser-induced fluorescence
Ac ₂ O	acetic anhydride	LP	light petroleum
AcOH	acetic acid	Me, Et, Bn	methyl, ethyl, benzyl
aq.	aqueous	MeCN	acetonitrile
Ar	argon	MeO	methoxy
atm	atmosphere	MeOH	methanol
BAIB	bis(acetoxy)iodobenzene	MsCl	mesyl chloride
BSA	bovine serum albumin	n.d. / n.a.	not determined / not available
CAR	carboxylic acid reductase	NBD	7-nitro-2,1,3-benzoxadiazole
COSY	correlated spectroscopy	NBS	N-bromosuccinimid
DIPEA	diisopropylethylamine	n-BuLi	n-butyllithium
DMAP	4-dimethylaminopyridine	NMR	nuclear magnetic resonance
DMF	dimethylformamide	PDMS	polydimethylsiloxane
DMSO	dimethylsulfoxide	PMT	photomultiplier
EDCI	1-Ethyl-3-(3-dimethylaminopropyl)carbodiimide	ppm	parts per million
epPCR	error-prone PCR	pTSA	<i>p</i> -toluenesulfonic acid
equiv.	molar equivalents	quant.	quantitative
Et ₂ O	diethyl ether	sat.	saturated
EtOAc	ethyl acetate	SHC	squalene hopene cyclase
FACS	fluorescence-activated cell sorting	TBAF	tetrabutylammonium fluoride
FADS	fluorescence-activated droplet sorting	TBS	<i>tert</i> -butyldimethylsilyl
FCA	Friedel-Crafts acylation	TEMPO	2,2,6,6-Tetramethylpiperidin-1-yl)oxyl
FPGA	field programmable gate array	Tf	triflate
FRET	Förster resonance energy transfer	TFA	trifluoroacetic acid
GC(-MS)	gas chromatography (mass spectrometry)	THF	tetrahydrofuran
GFP	green fluorescent protein	TLC	thin-layer chromatography
GUI	graphical user interface	TMS	trimethylsilyl
HPLC	high-performance liquid chromatography	TOCSY	total correlation spectroscopy
HR-MS	high resolution mass spectrometry	UV/Vis	ultra violett / visible spectroscopy
(u)HTA	(ultra-)high-throughput assays	<i>Zmo</i>	<i>Zymomonas mobilis</i>

F IV Curriculum vitae

Dipl. Ing. Sebastian Hecko BSc.

Newaldgasse 3/36
1090, Vienna (Austria)

Mobile + 43 660 150 98 98 Birthday 03/11/1990
E-mail sebastian.hecko@tuwien.ac.at Nationality Austrian, Slovakian



Professional Experience

- 02/2017 – today **University Assistant – Teaching assistant - TU Wien**, Vienna (Austria)
Department: Institute of Applied Synthetic Chemistry
- Concurrent participation in research and teaching in the course of the doctoral program
 - Supervision and administration of students at examinations, practical trainings and lab courses
 - Assistance in organization of conferences, meetings and symposiums
- 2015, 2016 (summer term) **Student Assistant - TU Wien**, Vienna (Austria)
Supervision of students and general administrative tasks during the lab course "Fundamentals of Chemistry" at the Institute of Applied Synthetic Chemistry
- 09/2013 – 11/2013 **Internship - Octapharma HGmbH**, Vienna (Austria)
Department: Quality Control
- Analytical activities for routine testing of in-process and final container samples
 - Documentation and revision of all relevant activities
 - General administrative activities (management of records, storage management, etc.)
- 10/2009 – 06/2010 **Paramedic - Johanniter-Unfall-Hilfe**, Vienna (Austria)
Training as part of the Austrian community service

Academic Career

- 02/2017 – today **Doctoral Programme in Engineering Sciences (PhD) - TU Wien**, Vienna (Austria)
Dissertation field: Technical Chemistry - Focus on Bioorganic Synthetic Chemistry
Supervisor: Prof. Florian Rudroff, Prof. Marko D. Mihovilovic
- Title of degree dissertation: "Development of Carbonyl-Sensing Assays for the Application in Fluorescence Activated Droplet Sorting"
- 09/2015 – 02/2016 **ETH Zurich**, Zurich (Switzerland)
Exchange semester in the framework of the **Erasmus scholarship**
Research project in research group Prof. Erick Carreira
- 11/2014 – 02/2017 **Master Programme in Engineering Sciences (Dipl. Ing.) - TU Wien**, Vienna (Austria)
Dissertation field: Applied Synthetic Chemistry - Focus on Advanced Organic Synthetic Chemistry
Supervisor: Prof. Marko D. Mihovilovic
- Title of degree dissertation: "Total Synthesis of Potential Anti-inflammatory Drug Lead Candidate (±)-Kadsurenin-F"
Grade point average: 1.20 – *passed with distinction*
- 10/2010 – 10/2014 **Bachelor Programme (B.Sc.) - TU Wien**, Vienna (Austria)
Technical Chemistry
Grade point average: 1.49 – *passed with distinction*
- 09/2001 – 09/2009 **Albertus Magnus Gymnasium (AHS - higher general education school)**, Vienna (Austria)
Higher education entrance qualification, emphasis on natural sciences
Grade point average: 1.50 – *passed with distinction*

Scientific Contributions

11/2020	Cell-free in vitro reduction of carboxylates to aldehydes: with crude enzyme preparations to a key pharmaceutical building block. Anna Schwarz, Sebastian Hecko, Florian Rudroff, Jeffrey Kohrt, Roger Howard, Margit Winkler <i>Biotechnol. J.</i> 2021;16:2000315.
02/2020	12th ÖGMBT Annual Meeting , online – Short oral Sebastian Hecko, Marko D. Mihovilovic, Prof. Florian Rudroff - <i>Modification of fluorophore backbones for the application in FADS systems for directed evolution of aldehyde producing enzymes</i>
08/2017	VII Meeting of the Paul Ehrlich Euro-PhD Network , Vienna (Austria) – Short oral Sebastian Hecko, Marko D. Mihovilovic - <i>Development of synthetic strategies towards neolignans</i>

Extra Curricular Activities

2021	Acceptance into the TU Wien incubator program for future start-up Velaex technologies
02/2021	İc STARTacademy 2021 – Winner of 2 nd and 4 th price for the pitch challenge
2017 – 2019	TEDxTUWien – Co-Organizer, Head of Finances & Sponsoring Main organizer of the event, responsible for administration and coordination of all sub-teams, treasury and acquisition of sponsors
2016 – 2019	Treasurer for the alumni association of the Albertus Magnus Gymnasium
2018 – today	Chairman for the “Association of Friends of the Austrian Chemistry Olympiad” (VFÖC)

Skills

EDP	MS Office: Word, PowerPoint, Outlook and Excel (European Computer Driving Licence)			
Languages	<i>Slovak:</i>	Mother Tongue	<i>German:</i>	C2
	<i>English:</i>	C2	<i>French:</i>	A2
Driving license	B			

Personal Interests & Hobbys

Outdoor sports (running, cycling, bouldering, climbing, skiing)
 Poker (online & live)
 Hardware, software – keeping up-to-date with the newest developments
 Crypto-enthusiast

F V References

- (1) Pasteur, L. Transformation of the two kinds of tartaric acid into racemic acid. Discovery of inactive tartaric acid. New method of separating racemic acid into the two tartaric acids, right and left. *C.R. Acad. Sci.* **1858**, *46*, 615-8.
- (2) Fischer, E. Einfluss der configuration auf die wirkung der enzyme. *Ber. Dtsch. Chem. Ges.* **1894**, *27* (3), 2985-93.
- (3) Michaelis, L.; Menten, M. L. The kinetics of the inversion effect. *Biochem. Z* **1913**, *49*, 333-69.
- (4) Buchner, E. Alkoholische gahrung ohne hefezellen. *Ber. Dtsch. Chem. Ges.* **1897**, *30* (1), 117-24.
- (5) Bornscheuer, U. T.; Huisman, G. W.; Kazlauskas, R. J.; Lutz, S.; Moore, J. C.; Robins, K. Engineering the third wave of biocatalysis. *Nature* **2012**, *485* (7397), 185-94.
- (6) Rosenthaler, L. Durch enzyme bewirkte asymmetrische synthesen. 2. Mitteilung. *Biochem. Z* **1909**, *17*, 257.
- (7) Grunwald, P. *Biocatalysis: Biochemical fundamentals and applications*; World Scientific, 2009.
- (8) Griengl, H.; Schwab, H.; Fechter, M. The synthesis of chiral cyanohydrins by oxynitrilases. *Trends Biotechnol.* **2000**, *18* (6), 252-6.
- (9) Nagasawa, T.; Nakamura, T.; Yamada, H. Production of acrylic acid and methacrylic acid using rhodococcus rhodochrous j1 nitrilase. *Appl. Microbiol. Biotechnol.* **1990**, *34* (3), 322-4.
- (10) Stemmer, W. P. DNA shuffling by random fragmentation and reassembly: In vitro recombination for molecular evolution. *Proceedings of the National Academy of Sciences* **1994**, *91* (22), 10747.
- (11) Giver, L.; Gershenson, A.; Freskgard, P. O.; Arnold, F. H. Directed evolution of a thermostable esterase. *Proc Natl Acad Sci U S A* **1998**, *95* (22), 12809-13.
- (12) Garcia-Ruiz, E.; Gonzalez-Perez, D.; Ruiz-Duenas, Francisco J.; Martnez, Angel T.; Alcalde, M. Directed evolution of a temperature-, peroxide- and alkaline ph-tolerant versatile peroxidase. *Biochem. J.* **2011**, *441* (1), 487-98.
- (13) Bessler, C.; Schmitt, J.; Maurer, K.-H.; Schmid, R. D. Directed evolution of a bacterial alpha-amylase: Toward enhanced ph-performance and higher specific activity. *Protein Sci* **2003**, *12* (10), 2141-9.
- (14) Chen, K.; Arnold, F. H. Enzyme engineering for nonaqueous solvents: Random mutagenesis to enhance activity of subtilisin e in polar organic media. *Bio/Technology* **1991**, *9* (11), 1073-7.
- (15) Giver, L.; Gershenson, A.; Freskgard, P.-O.; Arnold, F. H. Directed evolution of a thermostable esterase. *Proceedings of the National Academy of Sciences* **1998**, *95* (22), 12809.
- (16) Leveson-Gower, R. B.; Mayer, C.; Roelfes, G. The importance of catalytic promiscuity for enzyme design and evolution. *Nat. Rev. Chem.* **2019**, *3* (12), 687-705.
- (17) Wang, J.-b.; Li, G.; Reetz, M. T. Enzymatic site-selectivity enabled by structure-guided directed evolution. *ChemComm* **2017**, *53* (28), 3916-28.
- (18) Reetz, M. T. Combinatorial and evolution-based methods in the creation of enantioselective catalysts. *Angew. Chem. Int. Ed.* **2001**, *40* (2), 284-310.
- (19) Brandenberg, O. F.; Prier, C. K.; Chen, K.; Knight, A. M.; Wu, Z.; Arnold, F. H. Stereoselective enzymatic synthesis of heteroatom-substituted cyclopropanes. *ACS Catal.* **2018**, *8* (4), 2629-34.
- (20) Yang, G.; Withers, S. G. Ultrahigh-throughput facs-based screening for directed enzyme evolution. *ChemBioChem* **2009**, *10* (17), 2704-15.
- (21) Olsen, M. J.; Gam, J.; Iverson, B. L.; Georgiou, G. In *Directed enzyme evolution: Screening and selection methods*; Arnold, F. H.; Georgiou, G., Eds.; Humana Press: Totowa, NJ, 2003, DOI:10.1385/1-59259-396-8:329 10.1385/1-59259-396-8:329.
- (22) Olsen, M. J.; Gam, J.; Iverson, B. L.; Georgiou, G. High-throughput facs method for directed evolution of substrate specificity. *Methods Mol. Biol.* **2003**, *230*, 329-42.
- (23) Agresti, J. J.; Antipov, E.; Abate, A. R.; Ahn, K.; Rowat, A. C.; Baret, J.-C.; Marquez, M.; Klibanov, A. M.; Griffiths, A. D.; Weitz, D. A. Ultrahigh-throughput screening in drop-based microfluidics for directed evolution. *Proceedings of the National Academy of Sciences* **2010**, *107* (9), 4004.
- (24) Chiu, F. W. Y.; Stavrakis, S. High-throughput droplet-based microfluidics for directed evolution of enzymes. *Electrophoresis* **2019**, *40* (21), 2860-72.
- (25) Fu, X.; Zhang, Y.; Xu, Q.; Sun, X.; Meng, F. Recent advances of high-throughput on-chip sorting methods in enzyme directed evolution. *Front. Chem.* **2021**, *9*, 168.
- (26) Markel, U.; Essani, K. D.; Besirlioglu, V.; Schiffels, J.; Streit, W. R.; Schwaneberg, U. Advances in ultrahigh-throughput screening for directed enzyme evolution. *Chem. Soc. Rev.* **2020**, *49* (1), 233-62.
- (27) Wang, Y.; Xue, P.; Cao, M.; Yu, T.; Lane, S. T.; Zhao, H. Directed evolution: Methodologies and applications. *ChemRev* **2021**, DOI:10.1021/acs.chemrev.1c00260 10.1021/acs.chemrev.1c00260.
- (28) Bornscheuer, U. T. The fourth wave of biocatalysis is approaching. *Philos. Trans. Ser. A Math. Phys. Eng. Sci.* **2018**, *376* (2110), 20170063.
- (29) Li, C.; Zhang, R.; Wang, J.; Wilson, L. M.; Yan, Y. Protein engineering for improving and diversifying natural product biosynthesis. *Trends Biotechnol.* **2020**, *38* (7), 729-44.
- (30) Kazlauskas, R. Engineering more stable proteins. *Chem. Soc. Rev.* **2018**, *47* (24), 9026-45.
- (31) Behrens, G. A.; Hummel, A.; Padhi, S. K.; Schatzle, S.; Bornscheuer, U. T. Discovery and protein engineering of biocatalysts for organic synthesis. *Adv. Synth. Catal.* **2011**, *353* (13), 2191-215.
- (32) Steiner, K.; Schwab, H. Recent advances in rational approaches for enzyme engineering. *Comput. Struct. Biotechnol* **2012**, *2* (3), e201209010.

- (33) Zeymer, C.; Hilvert, D. Directed evolution of protein catalysts. *Annu. Rev. Biochem.* **2018**, *87* (1), 131-57.
- (34) Arnold, F. H.; Volkov, A. A. Directed evolution of biocatalysts. *Curr. Opin. Chem. Biol.* **1999**, *3* (1), 54-9.
- (35) Arnold, F. H.; Smith, G. P.; Winter, G. P. Directed evolution—bringing the power of evolution to the laboratory: 2018 nobel prize in chemistry. *Curr. Sci.* **2018**, *115* (9), 1627.
- (36) Currin, A.; Swainston, N.; Day, P. J.; Kell, D. B. Synthetic biology for the directed evolution of protein biocatalysts: Navigating sequence space intelligently. *Chem. Soc. Rev.* **2015**, *44* (5), 1172-239.
- (37) Hibbert, E. G.; Dalby, P. A. Directed evolution strategies for improved enzymatic performance. *Microb Cell Fact* **2005**, *4*, 29-.
- (38) Moore, J. C.; Arnold, F. H. Directed evolution of a para-nitrobenzyl esterase for aqueous-organic solvents. *Nat. Biotechnol.* **1996**, *14* (4), 458-67.
- (39) Cobb, R. E.; Chao, R.; Zhao, H. Directed evolution: Past, present, and future. *AIChE J* **2013**, *59* (5), 1432-40.
- (40) Hernandez, K. E.; Renata, H.; Lewis, R. D.; Kan, S. B. J.; Zhang, C.; Forte, J.; Rozzell, D.; McIntosh, J. A.; Arnold, F. H. Highly stereoselective biocatalytic synthesis of key cyclopropane intermediate to ticagrelor. *ACS Catal.* **2016**, *6* (11), 7810-3.
- (41) Preiswerk, N.; Beck, T.; Schulz, J. D.; Milovnik, P.; Mayer, C.; Siegel, J. B.; Baker, D.; Hilvert, D. Impact of scaffold rigidity on the design and evolution of an artificial diels-alderase. *Proceedings of the National Academy of Sciences* **2014**, *111* (22), 8013.
- (42) Brandenburg, O. F.; Fasan, R.; Arnold, F. H. Exploiting and engineering hemoproteins for abiological carbene and nitrene transfer reactions. *Curr. Opin. Biotechnol.* **2017**, *47*, 102-11.
- (43) Hoshino, T.; Sato, T. Squalene-hopene cyclase: Catalytic mechanism and substrate recognition. *ChemComm* **2002**, DOI:10.1039/B108995C 10.1039/B108995C(4), 291-301.
- (44) Sofronov, O. O.; Giubertoni, G.; Pérez de Alba Ortíz, A.; Ensing, B.; Bakker, H. J. Peptide side-cooh groups have two distinct conformations under biorelevant conditions. *J. Phys. Chem. Lett.* **2020**, *11* (9), 3466-72.
- (45) Hoshino, T.; Nakano, S.-i.; Kondo, T.; Sato, T.; Miyoshi, A. Squalene-hopene cyclase: Final deprotonation reaction, conformational analysis for the cyclization of (3*r*,*s*)-2, 3-oxidosqualene and further evidence for the requirement of an isopropylidene moiety both for initiation of the polycyclization cascade and for the formation of the 5-membered e-ring. *Org. Biomol. Chem.* **2004**, *2* (10), 1456-70.
- (46) Nakano, S.-i.; Ohashi, S.; Hoshino, T. Squalene-hopene cyclase: Insight into the role of the methyl group on the squalene backbone upon the polycyclization cascade. Enzymatic cyclization products of squalene analogs lacking a 26-methyl group and possessing a methyl group at c (7) or c (11). *Org. Biomol. Chem.* **2004**, *2* (14), 2012-22.
- (47) Kaneko, I.; Terasawa, Y.; Hoshino, T. Squalene-hopene cyclase: Mechanistic insights into the polycyclization cascades of squalene analogs bearing ethyl and hydroxymethyl groups at the c-2 and c-23 positions. *Chemistry—A European Journal* **2018**, *24* (43), 11139-57.
- (48) Seitz, M.; Klebensberger, J.; Siebenhaller, S.; Breuer, M.; Siedenburg, G.; Jendrossek, D.; Hauer, B. Substrate specificity of a novel squalene-hopene cyclase from *Zymomonas mobilis*. *J. Mol. Catal. B Enzym.* **2012**, *84*, 72-7.
- (49) Hammer, S. C.; Marjanovic, A.; Dominicus, J. M.; Nestl, B. M.; Hauer, B. Squalene hopene cyclases are protonases for stereoselective brønsted acid catalysis. *Nat. Chem. Biol.* **2015**, *11* (2), 121-6.
- (50) Seitz, M.; Syrén, P.-O.; Steiner, L.; Klebensberger, J.; Nestl, B. M.; Hauer, B. Synthesis of heterocyclic terpenoids by promiscuous squalene-hopene cyclases. *ChemBioChem* **2013**, *14* (4), 436-9.
- (51) Siedenburg, G.; Jendrossek, D.; Breuer, M.; Juhl, B.; Pleiss, J.; Seitz, M.; Klebensberger, J.; Hauer, B. Activation-independent cyclization of monoterpenoids. *Appl. Environ. Microbiol.* **2012**, *78* (4), 1055-62.
- (52) Bastian, S. A.; Hammer, S. C.; Kreß, N.; Nestl, B. M.; Hauer, B. Selectivity in the cyclization of citronellal introduced by squalene hopene cyclase variants. *ChemCatChem* **2017**, *9* (23), 4364-8.
- (53) Hammer, S. C.; Dominicus, J. M.; Syrén, P.-O.; Nestl, B. M.; Hauer, B. Stereoselective friedel-crafts alkylation catalyzed by squalene hopene cyclases. *Tetrahedron* **2012**, *68* (37), 7624-9.
- (54) Hoshino, T.; Kumai, Y.; Kudo, I.; Nakano, S.-i.; Ohashi, S. Enzymatic cyclization reactions of geraniol, farnesol and geranylgeraniol, and those of truncated squalene analogs having c 20 and c 25 by recombinant squalene cyclase. *Org. Biomol. Chem.* **2004**, *2* (18), 2650-7.
- (55) Abe, I.; Tanaka, H.; Noguchi, H. Enzymatic formation of an unnatural hexacyclic c35 polyprenoid by bacterial squalene cyclase. *J. Am. Chem. Soc.* **2002**, *124* (49), 14514-5.
- (56) Wendt, K. U.; Poralla, K.; Schulz, G. E. Structure and function of a squalene cyclase. *Science* **1997**, *277* (5333), 1811-5.
- (57) Siedenburg, G.; Breuer, M.; Jendrossek, D. Prokaryotic squalene-hopene cyclases can be converted to citronellal cyclases by single amino acid exchange. *Appl. Microbiol. Biotechnol.* **2013**, *97* (4), 1571-80.
- (58) Gahltho, D.; Dunstan, M. S.; Quaglia, D.; Klumbys, E.; Lockhart-Cairns, M. P.; Hill, A. M.; Derrington, S. R.; Scrutton, N. S.; Turner, N. J.; Leys, D. Structures of carboxylic acid reductase reveal domain dynamics underlying catalysis. *Nat. Chem. Biol.* **2017**, *13* (9), 975-81.
- (59) Finnigan, W.; Thomas, A.; Cromar, H.; Gough, B.; Snajdrova, R.; Adams, J. P.; Littlechild, J. A.; Harmer, N. J. Characterization of carboxylic acid reductases as enzymes in the toolbox for synthetic chemistry. *ChemCatChem* **2017**, *9* (6), 1005-17.
- (60) Butler, N.; Kunjapur, A. M. Carboxylic acid reductases in metabolic engineering. *J. Biotechnol.* **2020**, *307*, 1-14.
- (61) Lahti, R. Microbial inorganic pyrophosphatases. *Microbiol. Rev.* **1983**, *47* (2), 169-78.

- (62) Ressimann, A. K.; Schwendenwein, D.; Leonhartsberger, S.; Mihovilovic, M. D.; Bornscheuer, U. T.; Winkler, M.; Rudroff, F. Substrate-independent high-throughput assay for the quantification of aldehydes. *Adv. Synth. Catal.* **2019**, *361* (11), 2538-43.
- (63) Moura, M.; Pertusi, D.; Lenzini, S.; Bhan, N.; Broadbelt, L. J.; Tyo, K. E. J. Characterizing and predicting carboxylic acid reductase activity for diversifying bioaldehyde production. *Biotechnol. Bioeng.* **2016**, *113* (5), 944-52.
- (64) Khusnutdinova, A. N.; Flick, R.; Popovic, A.; Brown, G.; Tchigvintsev, A.; Nocek, B.; Correia, K.; Joo, J. C.; Mahadevan, R.; Yakunin, A. F. Exploring bacterial carboxylate reductases for the reduction of bifunctional carboxylic acids. *Biotechnol. J.* **2017**, *12* (11), 1600751.
- (65) Stolterfoht, H.; Steinkellner, G.; Schwendenwein, D.; Pavkov-Keller, T.; Gruber, K.; Winkler, M. Identification of key residues for enzymatic carboxylate reduction. *Front. Microbiol.* **2018**, *9*, 250.
- (66) Qu, G.; Liu, B.; Zhang, K.; Jiang, Y.; Guo, J.; Wang, R.; Miao, Y.; Zhai, C.; Sun, Z. Computer-assisted engineering of the catalytic activity of a carboxylic acid reductase. *J. Biotechnol.* **2019**, *306*, 97-104.
- (67) Schwendenwein, D.; Ressimann, A. K.; Doerr, M.; Höhne, M.; Bornscheuer, U. T.; Mihovilovic, M. D.; Rudroff, F.; Winkler, M. Random mutagenesis-driven improvement of carboxylate reductase activity using an amino benzamidoxime-mediated high-throughput assay. *Adv. Synth. Catal.* **2019**, *361* (11), 2544-9.
- (68) Wójcik, M.; Telzerow, A.; Quax, W. J.; Boersma, Y. L. High-throughput screening in protein engineering: Recent advances and future perspectives. *Int. J. Mol. Sci.* **2015**, *16* (10), 24918-45.
- (69) Xiao, H.; Bao, Z.; Zhao, H. High throughput screening and selection methods for directed enzyme evolution. *Ind. Eng. Chem. Res.* **2015**, *54* (16), 4011-20.
- (70) Agresti, J. J.; Antipov, E.; Abate, A. R.; Ahn, K.; Rowat, A. C.; Baret, J.-C.; Marquez, M.; Klibanov, A. M.; Griffiths, A. D.; Weitz, D. A. Ultrahigh-throughput screening in drop-based microfluidics for directed evolution. *Proceedings of the National Academy of Sciences* **2010**, *107* (9), 4004-9.
- (71) Leemhuis, H.; Kelly, R. M.; Dijkhuizen, L. Directed evolution of enzymes: Library screening strategies. *IUBMB Life* **2009**, *61* (3), 222-8.
- (72) Bunzel, H. A.; Garrabou, X.; Pott, M.; Hilvert, D. Speeding up enzyme discovery and engineering with ultrahigh-throughput methods. *Curr. Opin. Struct. Biol.* **2018**, *48*, 149-56.
- (73) Sánchez Barea, J.; Lee, J.; Kang, D.-K. Recent advances in droplet-based microfluidic technologies for biochemistry and molecular biology. *Micromachines* **2019**, *10* (6), 412.
- (74) Mair, P.; Gielen, F.; Hollfelder, F. Exploring sequence space in search of functional enzymes using microfluidic droplets. *Curr. Opin. Chem. Biol.* **2017**, *37*, 137-44.
- (75) Diefenbach, X. W.; Farasat, I.; Guetschow, E. D.; Welch, C. J.; Kennedy, R. T.; Sun, S.; Moore, J. C. Enabling biocatalysis by high-throughput protein engineering using droplet microfluidics coupled to mass spectrometry. *ACS Omega* **2018**, *3* (2), 1498-508.
- (76) Colin, P. Y.; Kintsjes, B.; Gielen, F.; Miton, C. M.; Fischer, G.; Mohamed, M. F.; Hyvonen, M.; Morgavi, D. P.; Janssen, D. B.; Hollfelder, F. Ultrahigh-throughput discovery of promiscuous enzymes by picodroplet functional metagenomics. *Nat. Commun.* **2015**, *6*, 10008.
- (77) Weinmeister, R.; Freeman, E.; Eperon, I. C.; Stuart, A. M.; Hudson, A. J. Single-fluorophore detection in femtoliter droplets generated by flow focusing. *ACS Nano* **2015**, *9* (10), 9718-30.
- (78) Zhang, J.; Chai, X.; He, X.-P.; Kim, H.-J.; Yoon, J.; Tian, H. Fluorogenic probes for disease-relevant enzymes. *Chem. Soc. Rev.* **2019**, *48* (2), 683-722.
- (79) Singh, H.; Tiwari, K.; Tiwari, R.; Pramanik, S. K.; Das, A. Small molecule as fluorescent probes for monitoring intracellular enzymatic transformations. *ChemRev* **2019**, *119* (22), 11718-60.
- (80) Kaur, K.; Saini, R.; Kumar, A.; Luxami, V.; Kaur, N.; Singh, P.; Kumar, S. Chemodosimeters: An approach for detection and estimation of biologically and medically relevant metal ions, anions and thiols. *Coord. Chem. Rev.* **2012**, *256* (17), 1992-2028.
- (81) Obexer, R.; Pott, M.; Zeymer, C.; Griffiths, A. D.; Hilvert, D. Efficient laboratory evolution of computationally designed enzymes with low starting activities using fluorescence-activated droplet sorting. *Protein Eng. Des. Sel.* **2016**, *29* (9), 355-66.
- (82) Wagner, J. M.; Liu, L.; Yuan, S.-F.; Venkataraman, M. V.; Abate, A. R.; Alper, H. S. A comparative analysis of single cell and droplet-based facs for improving production phenotypes: Riboflavin overproduction in *yarrowia lipolytica*. *Metab. Eng.* **2018**, *47*, 346-56.
- (83) Yang, Y.; Zhao, Q.; Feng, W.; Li, F. Luminescent chemodosimeters for bioimaging. *ChemRev* **2013**, *113* (1), 192-270.
- (84) Wu, L.; Sedgwick, A. C.; Sun, X.; Bull, S. D.; He, X. P.; James, T. D. Reaction-based fluorescent probes for the detection and imaging of reactive oxygen, nitrogen, and sulfur species. *Acc. Chem. Res.* **2019**, *52* (9), 2582-97.
- (85) Fu, Y.; Finney, N. S. Small-molecule fluorescent probes and their design. *RSC Adv.* **2018**, *8* (51), 29051-61.
- (86) Chyan, W.; Raines, R. T. Enzyme-activated fluorogenic probes for live-cell and in vivo imaging. *ACS Chem. Biol.* **2018**, *13* (7), 1810-23.
- (87) Bhattacharyya, S.; Ducheyne, P. In *Comprehensive biomaterials ii*; Ducheyne, P., Ed.; Elsevier: Oxford, 2017, DOI:<https://doi.org/10.1016/B978-0-12-803581-8.10211-5> <https://doi.org/10.1016/B978-0-12-803581-8.10211-5>.
- (88) Chan, J.; Dodani, S. C.; Chang, C. J. Reaction-based small-molecule fluorescent probes for chemoselective bioimaging. *Nat. Chem.* **2012**, *4* (12), 973-84.
- (89) Debon, A.; Pott, M.; Obexer, R.; Green, A. P.; Friedrich, L.; Griffiths, A. D.; Hilvert, D. Ultrahigh-throughput screening enables efficient single-round oxidase remodelling. *Nat. Catal.* **2019**, *2* (9), 740-7.

- (90) Moris-Varas, F.; Shah, A.; Aikens, J.; Nadkarni, N. P.; Rozzell, J. D.; Demirjian, D. C. Visualization of enzyme-catalyzed reactions using pH indicators: Rapid screening of hydrolase libraries and estimation of the enantioselectivity. *Bioorg. Med. Chem.* **1999**, *7* (10), 2183-8.
- (91) Janes, L. E.; Löwendahl, A. C.; Kazlauskas, R. J. Quantitative screening of hydrolase libraries using pH indicators: Identifying active and enantioselective hydrolases. *Chem. Eur. J.* **1998**, *4* (11), 2324-31.
- (92) Fox, R. J.; Davis, S. C.; Mundorff, E. C.; Newman, L. M.; Gavriloic, V.; Ma, S. K.; Chung, L. M.; Ching, C.; Tam, S.; Muley, S. et al. Improving catalytic function by prosar-driven enzyme evolution. *Nat. Biotechnol.* **2007**, *25* (3), 338-44.
- (93) Zeng, W.; Du, G.; Chen, J.; Li, J.; Zhou, J. A high-throughput screening procedure for enhancing α -ketoglutaric acid production in *Yarrowia lipolytica* by random mutagenesis. *Process Biochem.* **2015**, *50* (10), 1516-22.
- (94) Meyer, J.; Büldt, A.; Vogel, M.; Karst, U. 4-(n-methylhydrazino)-7-nitro-2,1,3-benzooxadiazole (mnbhd): A novel fluorogenic peroxidase substrate. *Angew. Chem. Int. Ed.* **2000**, *39* (8), 1453-5.
- (95) Forchin, M. C.; Crotti, M.; Gatti, F. G.; Parmeggiani, F.; Brenna, E.; Monti, D. A rapid and high-throughput assay for the estimation of conversions of ene-reductase-catalysed reactions. *ChemBioChem* **2015**, *16* (11), 1571-3.
- (96) Mäkinen, K. K.; Tenovuo, J. Observations on the use of guaiacol and 2,2'-azino-di(3-ethylbenzthiazoline-6-sulfonic acid) as peroxidase substrates. *Anal. Biochem.* **1982**, *126* (1), 100-8.
- (97) Wang, B. L.; Ghaderi, A.; Zhou, H.; Agresti, J.; Weitz, D. A.; Fink, G. R.; Stephanopoulos, G. Microfluidic high-throughput culturing of single cells for selection based on extracellular metabolite production or consumption. *Nat. Biotechnol.* **2014**, *32* (5), 473-8.
- (98) Jiao, X.; Li, Y.; Niu, J.; Xie, X.; Wang, X.; Tang, B. Small-molecule fluorescent probes for imaging and detection of reactive oxygen, nitrogen, and sulfur species in biological systems. *Anal. Chem.* **2018**, *90* (1), 533-55.
- (99) Prasad, A.; Sedlářová, M.; Pospíšil, P. Singlet oxygen imaging using fluorescent probe singlet oxygen sensor green in photosynthetic organisms. *Sci. Rep.* **2018**, *8* (1), 13685.
- (100) Bruemmer, K. J.; Brewer, T. F.; Chang, C. J. Fluorescent probes for imaging formaldehyde in biological systems. *Curr Opin Chem Biol* **2017**, *39*, 17-23.
- (101) Yang, Y.; Chi, Y. T.; Toh, H. H.; Li, Z. Evolving p450_{pyr} monooxygenase for highly regioselective terminal hydroxylation of n-butanol to 1, 4-butanediol. *ChemComm* **2015**, *51* (5), 914-7.
- (102) Vogel, M.; Büldt, A.; Karst, U. Hydrazine reagents as derivatizing agents in environmental analysis – a critical review. *Fresenius J Anal Chem* **2000**, *366* (8), 781-91.
- (103) Jugder, B.-E.; Welch, J.; Braidy, N.; Marquis, C. P. Construction and use of a cupriavidus necator h16 soluble hydrogenase promoter (psh) fusion to GFP (green fluorescent protein). *PeerJ* **2016**, *4*, e2269.
- (104) Lin, J.-L.; Wagner, J. M.; Alper, H. S. Enabling tools for high-throughput detection of metabolites: Metabolic engineering and directed evolution applications. *Biotechnol. Adv.* **2017**, *35* (8), 950-70.
- (105) Woronoff, G.; Ryckelynck, M.; Wessel, J.; Schicke, O.; Griffiths, A. D.; Soumillon, P. Activity-fed translation (aft) assay: A new high-throughput screening strategy for enzymes in droplets. *ChemBioChem* **2015**, *16* (9), 1343-9.
- (106) Pollok, B. A.; Heim, R. Using GFP in FRET-based applications. *Trends Cell Biol.* **1999**, *9* (2), 57-60.
- (107) Wu, L.; Huang, C.; Emery, B. P.; Sedgwick, A. C.; Bull, S. D.; He, X.-P.; Tian, H.; Yoon, J.; Sessler, J. L.; James, T. D. Förster resonance energy transfer (FRET)-based small-molecule sensors and imaging agents. *Chem. Soc. Rev.* **2020**, *49* (15), 5110-39.
- (108) Olsen, M. J.; Stephens, D.; Griffiths, D.; Daugherty, P.; Georgiou, G.; Iverson, B. L. Function-based isolation of novel enzymes from a large library. *Nat. Biotechnol.* **2000**, *18* (10), 1071-4.
- (109) Reymond, J. L. *Enzyme assays*; Wiley, 2006.
- (110) Schmidt-Dannert, C.; Arnold, F. H. Directed evolution of industrial enzymes. *Trends Biotechnol.* **1999**, *17* (4), 135-6.
- (111) Goddard, J.-P.; Reymond, J.-L. Enzyme assays for high-throughput screening. *Curr. Opin. Biotechnol.* **2004**, *15* (4), 314-22.
- (112) Klein, G.; Reymond, J.-L. Enantioselective fluorogenic assay of acetate hydrolysis for detecting lipase catalytic antibodies. *Helv. Chim. Acta* **1999**, *82* (3), 400-7.
- (113) Yang, G.; Rich, J. R.; Gilbert, M.; Wakarchuk, W. W.; Feng, Y.; Withers, S. G. Fluorescence activated cell sorting as a general ultra-high-throughput screening method for directed evolution of glycosyltransferases. *J. Am. Chem. Soc.* **2010**, *132* (30), 10570-7.
- (114) Smeenk, M. L. W. J.; Agramunt, J.; Bongers, K. M. Recent developments in bioorthogonal chemistry and the orthogonality within. *Curr. Opin. Chem. Biol* **2021**, *60*, 79-88.
- (115) Wu, J.; Liu, W.; Ge, J.; Zhang, H.; Wang, P. New sensing mechanisms for design of fluorescent chemosensors emerging in recent years. *Chem. Soc. Rev.* **2011**, *40* (7), 3483-95.
- (116) Gunnlaugsson, T.; Ali, H. D. P.; Glynn, M.; Kruger, P. E.; Hussey, G. M.; Pfeffer, F. M.; dos Santos, C. M. G.; Tierney, J. Fluorescent photoinduced electron transfer (PET) sensors for anions; from design to potential application. *J. Fluoresc.* **2005**, *15* (3), 287-99.
- (117) de Silva, A. P.; Gunaratne, H. Q. N.; Gunnlaugsson, T.; Huxley, A. J. M.; McCoy, C. P.; Rademacher, J. T.; Rice, T. E. Signaling recognition events with fluorescent sensors and switches. *ChemRev* **1997**, *97* (5), 1515-66.
- (118) Valeur, B.; Leray, I. Design principles of fluorescent molecular sensors for cation recognition. *Coord. Chem. Rev.* **2000**, *205* (1), 3-40.
- (119) Martínez-Mañez, R.; Sancenón, F. Fluorogenic and chromogenic chemosensors and reagents for anions. *ChemRev* **2003**, *103* (11), 4419-76.

- (120) Stephanopoulos, N.; Francis, M. B. Choosing an effective protein bioconjugation strategy. *Nat. Chem. Biol.* **2011**, *7* (12), 876-84.
- (121) Spears, R. J.; Fascione, M. A. Site-selective incorporation and ligation of protein aldehydes. *Org. Biomol. Chem.* **2016**, *14* (32), 7622-38.
- (122) Bohlmann, F. Konstitution und lichtabsorption, i. Mitteil.: Carbonyl-derivate. *Chem. Ber.* **1951**, *84* (5-6), 490-504.
- (123) Yang, C.; Ye, L.; Gu, J.; Yang, X.; Li, A.; Yu, H. Directed evolution of mandelate racemase by a novel high-throughput screening method. *Appl. Microbiol. Biotechnol.* **2017**, *101* (3), 1063-72.
- (124) Uzu, S.; Kanda, S.; Imai, K.; Nakashima, K.; Akiyama, S. Fluorogenic reagents: 4-aminosulphonyl-7-hydrazino-2,1,3-benzoxadiazole, 4-(n,n-dimethylaminosulphonyl)-7-hydrazino-2,1,3-benzoxadiazole and 4-hydrazino-7-nitro-2,1,3-benzoxadiazole hydrazine for aldehydes and ketones. *Analyst* **1990**, *115* (11), 1477-82.
- (125) Ali, M. F. B.; Kishikawa, N.; Ohyama, K.; Mohamed, H. A.-M.; Abdel-Wadood, H. M.; Mahmoud, A. M.; Imazato, T.; Ueki, Y.; Wada, M.; Kuroda, N. Chromatographic determination of low-molecular mass unsaturated aliphatic aldehydes with peroxyoxalate chemiluminescence detection after fluorescence labeling with 4-(n,n-dimethylaminosulfonyl)-7-hydrazino-2,1,3-benzoxadiazole. *J. Chromatogr. B* **2014**, *953-954*, 147-52.
- (126) Nakashima, K.; Hidaka, Y.; Yoshida, T.; Kuroda, N.; Akiyama, S. High-performance liquid chromatographic determination of short-chain aliphatic aldehydes using 4-(n,n-dimethylaminosulphonyl)-7-hydrazino-2,1,3-benzoxadiazole as a fluorescence reagent. *J. Chromatogr. B Biomed. Appl.* **1994**, *661* (2), 205-10.
- (127) Büldt, A.; Karst, U. N-methyl-4-hydrazino-7-nitrobenzofurazan as a new reagent for air monitoring of aldehydes and ketones. *Anal. Chem.* **1999**, *71* (9), 1893-8.
- (128) Konarzycka-Bessler, M.; Bornscheuer, U. T. A high-throughput-screening method for determining the synthetic activity of hydrolases. *Angew. Chem. Int. Ed.* **2003**, *42* (12), 1418-20.
- (129) Key, J. A.; Li, C.; Cairo, C. W. Detection of cellular sialic acid content using nitrobenzoxadiazole carbonyl-reactive chromophores. *Bioconjugate Chemistry* **2012**, *23* (3), 363-71.
- (130) Larsen, D.; Pittelkow, M.; Karmakar, S.; Kool, E. T. New organocatalyst scaffolds with high activity in promoting hydrazone and oxime formation at neutral pH. *Org. Lett.* **2015**, *17* (2), 274-7.
- (131) Crisalli, P.; Kool, E. T. Water-soluble organocatalysts for hydrazone and oxime formation. *J. Org. Chem.* **2013**, *78* (3), 1184-9.
- (132) Rashidian, M.; Mahmoodi, M. M.; Shah, R.; Dozier, J. K.; Wagner, C. R.; Distefano, M. D. A highly efficient catalyst for oxime ligation and hydrazone-oxime exchange suitable for bioconjugation. *Bioconjug. Chem.* **2013**, *24* (3), 333-42.
- (133) Crisalli, P.; Kool, E. T. Importance of ortho proton donors in catalysis of hydrazone formation. *Org. Lett.* **2013**, *15* (7), 1646-9.
- (134) Larsen, D.; Kietrys, A. M.; Clark, S. A.; Park, H. S.; Ekebergh, A.; Kool, E. T. Exceptionally rapid oxime and hydrazone formation promoted by catalytic amine buffers with low toxicity. *Chem. Sci.* **2018**, *9* (23), 5252-9.
- (135) Wang, S.; Nawale, G. N.; Kadekar, S.; Oommen, O. P.; Jena, N. K.; Chakraborty, S.; Hilborn, J.; Varghese, O. P. Saline accelerates oxime reaction with aldehyde and keto substrates at physiological pH. *Sci. Rep.* **2018**, *8* (1), 2193.
- (136) Chen, Q.; Chen, X.; Feng, J.; Wu, Q.; Zhu, D.; Ma, Y. Improving and inverting C β -stereoselectivity of threonine aldolase via substrate-binding-guided mutagenesis and a stepwise visual screening. *ACS Catal.* **2019**, *9* (5), 4462-9.
- (137) Anthon, G. E.; Barrett, D. M. Determination of reducing sugars with 3-methyl-2-benzothiazolinonehydrazone. *Anal. Biochem.* **2002**, *305* (2), 287-9.
- (138) Gomez, L. D.; Whitehead, C.; Barakate, A.; Halpin, C.; McQueen-Mason, S. J. Automated saccharification assay for determination of digestibility in plant materials. *Biotechnol. Biofuels* **2010**, *3* (1), 23.
- (139) Fagnani, E.; Melios, C. B.; Pezza, L.; Pezza, H. R. Chromotropic acid-formaldehyde reaction in strongly acidic media. The role of dissolved oxygen and replacement of concentrated sulphuric acid. *Talanta* **2003**, *60* (1), 171-6.
- (140) Gasparini, F.; Weinert, P. L.; Lima, L. S.; Pezza, L.; Pezza, H. R. A simple and green analytical method for the determination of formaldehyde. *J. Braz. Chem. Soc.* **2008**, *19*, 1531-7.
- (141) Schiff, H. Eine neue reihe organischer diamine. *Justus Liebig's Ann. Chem.* **1866**, *140* (1), 92-137.
- (142) Choi, K.-Y.; Jung, E.-O.; Yun, H.; Yang, Y.-H.; Kazlauskas, R. J.; Kim, B.-G. Development of colorimetric hts assay of cytochrome p450 for ortho-specific hydroxylation, and engineering of cyp102d1 with enhanced catalytic activity and regioselectivity. *ChemBioChem* **2013**, *14* (10), 1231-8.
- (143) Matsuoka, M.; Imado, N.; Maki, T.; Banno, K.; Sato, T. Determination of free aliphatic aldehydes in plasma by high-performance liquid chromatography of the 1, 3-cyclohexanedione derivatives. *Chromatographia* **1996**, *43* (9), 501-6.
- (144) Mopper, K.; Stahovec, W. L.; Johnson, L. Trace analysis of aldehydes by reversed-phase high-performance liquid chromatography and precolumn fluorogenic labeling with 5, 5-dimethyl-1, 3-cyclohexanedione. *J. Chromatogr. A* **1983**, *256*, 243-52.
- (145) Nakamura, M.; Toda, M.; Saito, H.; Ohkura, Y. Fluorimetric determination of aromatic aldehydes with 4,5-dimethoxy-1,2-diaminobenzene. *Anal. Chim. Acta* **1982**, *134*, 39-45.
- (146) Imazato, T.; Kanematsu, M.; Kishikawa, N.; Ohyama, K.; Hino, T.; Ueki, Y.; Maehata, E.; Kuroda, N. Determination of acrolein in serum by high-performance liquid chromatography with fluorescence detection after pre-column fluorogenic derivatization using 1, 2-diamino-4, 5-dimethoxybenzene. *Biomed. Chromatogr.* **2015**, *29* (9), 1304-8.
- (147) McLellan, A. C.; Phillips, S. A.; Thornalley, P. J. The assay of methylglyoxal in biological systems by derivatization with 1,2-diamino-4,5-dimethoxybenzene. *Anal. Biochem.* **1992**, *206* (1), 17-23.

- (148) Zurek, G.; Karst, U. Liquid chromatography–mass spectrometry method for the determination of aldehydes derivatized by the hantzsch reaction. *J. Chromatogr. A* **1999**, *864* (2), 191-7.
- (149) Nash, T. The colorimetric estimation of formaldehyde by means of the hantzsch reaction. *Biochem. J.* **1953**, *55* (3), 416-21.
- (150) Al-Moniee, M. A.; Koopal, C.; Akmal, N.; van Veen, S.; Zhu, X.; Sanders, P. F.; Sanders, P. F.; Al-Abeedi, F. N.; Amer, A. M. Applicability of dimedone assays for the development of online aldehyde sensor in seawater flooding systems. *J. Sens. Technol.* **2016**, *6* (04), 101.
- (151) El-Maghrabey, M. H.; Kishikawa, N.; Ohyama, K.; Kuroda, N. Analytical method for lipoperoxidation relevant reactive aldehydes in human sera by high-performance liquid chromatography–fluorescence detection. *Anal. Biochem.* **2014**, *464*, 36-42.
- (152) Fathy Bakr Ali, M.; Kishikawa, N.; Ohyama, K.; Abdel-Mageed Mohamed, H.; Mohamed Abdel-Wadood, H.; Mohamed Mohamed, A.; Kuroda, N. Chromatographic determination of aliphatic aldehydes in human serum after pre-column derivatization using 2,2'-furil, a novel fluorogenic reagent. *J. Chromatogr. A* **2013**, *1300*, 199-203.
- (153) Li, Z.; Xue, Z.; Wu, Z.; Han, J.; Han, S. Chromo-fluorogenic detection of aldehydes with a rhodamine based sensor featuring an intramolecular deoxylactam. *Org. Biomol. Chem.* **2011**, *9* (22), 7652-4.
- (154) Brewer, T. F.; Chang, C. J. An aza-cope reactivity-based fluorescent probe for imaging formaldehyde in living cells. *J. Am. Chem. Soc.* **2015**, *137* (34), 10886-9.
- (155) Kitov, P. I.; Vinals, D. F.; Ng, S.; Tjhung, K. F.; Derda, R. Rapid, hydrolytically stable modification of aldehyde-terminated proteins and phage libraries. *J. Am. Chem. Soc.* **2014**, *136* (23), 8149-52.
- (156) Ressmann, A. K.; Schwendenwein, D.; Leonhartsberger, S.; Mihovilovic, M. D.; Bornscheuer, U. T.; Winkler, M.; Rudroff, F. Substrate-independent high-throughput assay for the quantification of aldehydes. *Adv. Synth. Catal.* **2019**, *361* (11), 2538-43.
- (157) Schwendenwein, D.; Ressmann, A. K.; Doerr, M.; Höhne, M.; Bornscheuer, U. T.; Mihovilovic, M. D.; Rudroff, F.; Winkler, M. Random mutagenesis-driven improvement of carboxylate reductase activity using an amino benzamidoxime-mediated high-throughput assay. *Adv. Synth. Catal.* **2019**, *361* (11), 2544-9.
- (158) Rudroff, F.; Winkler, M.; Schwendenwein, D.; Ressmann, A. K.; Mihovilovic, M. D.; Bornscheuer, U. T.; Dörr, M. Gordon Research Conference Biocatalysis: Biocatalysis Frontiers: From the Microbiome, to Emerging Tools in Structural Biology, to De Novo Pathway Construction, 2018.
- (159) Guo, H.-M.; Tanaka, F. A fluorogenic aldehyde bearing a 1,2,3-triazole moiety for monitoring the progress of aldol reactions. *J. Org. Chem.* **2009**, *74* (6), 2417-24.
- (160) Tanaka, F.; Thayumanavan, R.; Barbas, C. F. Fluorescent detection of carbon–carbon bond formation. *J. Am. Chem. Soc.* **2003**, *125* (28), 8523-8.
- (161) Tanaka, F.; Mase, N.; Barbas, C. F. Design and use of fluorogenic aldehydes for monitoring the progress of aldehyde transformations. *J. Am. Chem. Soc.* **2004**, *126* (12), 3692-3.
- (162) Linares-Pastén, J. A.; Chávez-Lizárraga, G.; Villagomez, R.; Mamo, G.; Hatti-Kaul, R. A method for rapid screening of ketone biotransformations: Detection of whole cell baeyer–villiger monooxygenase activity. *Enzyme Microb. Technol.* **2012**, *50* (2), 101-6.
- (163) Mei, Z.; Zhang, K.; Qu, G.; Li, J.-K.; Liu, B.; Ma, J.-A.; Tu, R.; Sun, Z. High-throughput fluorescence assay for ketone detection and its applications in enzyme mining and protein engineering. *ACS Omega* **2020**, *5* (23), 13588-94.
- (164) Mayr, L. M.; Fuerst, P. The future of high-throughput screening. *J. Biomol. Screen.* **2008**, *13* (6), 443-8.
- (165) Bouzetos, E.; Ganar, K. A.; Mastrobattista, E.; Deshpande, S.; van der Oost, J. (r)evolution-on-a-chip. *Trends Biotechnol.*, DOI:10.1016/j.tibtech.2021.04.009 10.1016/j.tibtech.2021.04.009.
- (166) Baret, J.-C.; Miller, O. J.; Taly, V.; Ryckelynck, M.; El-Harrak, A.; Frenz, L.; Rick, C.; Samuels, M. L.; Hutchison, J. B.; Agresti, J. J. et al. Fluorescence-activated droplet sorting (fads): Efficient microfluidic cell sorting based on enzymatic activity. *Lab Chip* **2009**, *9* (13), 1850-8.
- (167) Larsen, A. C.; Dunn, M. R.; Hatch, A.; Sau, S. P.; Youngbull, C.; Chaput, J. C. A general strategy for expanding polymerase function by droplet microfluidics. *Nat. Commun.* **2016**, *7* (1), 11235.
- (168) Chong, D.; Liu, X.; Ma, H.; Huang, G.; Han, Y. L.; Cui, X.; Yan, J.; Xu, F. Advances in fabricating double-emulsion droplets and their biomedical applications. *Microfluid. Nanofluidics* **2015**, *19* (5), 1071-90.
- (169) Zinchenko, A.; Devenish, S. R. A.; Kintsjes, B.; Colin, P.-Y.; Fischlechner, M.; Hollfelder, F. One in a million: Flow cytometric sorting of single cell-lysate assays in monodisperse picolitre double emulsion droplets for directed evolution. *Anal. Chem.* **2014**, *86* (5), 2526-33.
- (170) Bouzetos, E.; Ganar, K. A.; Mastrobattista, E.; Deshpande, S.; van der Oost, J. (r)evolution-on-a-chip. *Trends Biotechnol.* **2021**, DOI:<https://doi.org/10.1016/j.tibtech.2021.04.009>
- (171) Mazutis, L.; Gilbert, J.; Ung, W. L.; Weitz, D. A.; Griffiths, A. D.; Heyman, J. A. Single-cell analysis and sorting using droplet-based microfluidics. *Nature Protocols* **2013**, *8* (5), 870-91.
- (172) Obexer, R.; Godina, A.; Garrabou, X.; Mittl, P. R. E.; Baker, D.; Griffiths, A. D.; Hilvert, D. Emergence of a catalytic tetrad during evolution of a highly active artificial aldolase. *Nat. Chem.* **2017**, *9* (1), 50-6.
- (173) Schütz, S. S.; Beneyton, T.; Baret, J.-C.; Schneider, T. M. Rational design of a high-throughput droplet sorter. *Lab Chip* **2019**, *19* (13), 2220-32.
- (174) Seemann, R.; Brinkmann, M.; Pfohl, T.; Herminghaus, S. Droplet based microfluidics. *Rep. Prog. Phys.* **2012**, *75* (1), 016601.

- (175) Abate, A. R.; Hung, T.; Mary, P.; Agresti, J. J.; Weitz, D. A. High-throughput injection with microfluidics using picoinjectors. *Proceedings of the National Academy of Sciences* **2010**, *107* (45), 19163.
- (176) Caen, O.; Schütz, S.; Jammalamadaka, M. S. S.; Vrignon, J.; Nizard, P.; Schneider, T. M.; Baret, J.-C.; Taly, V. High-throughput multiplexed fluorescence-activated droplet sorting. *Microsyst. Nanoeng.* **2018**, *4* (1), 33.
- (177) Beneyton, T.; Coldren, F.; Baret, J. C.; Griffiths, A. D.; Taly, V. Cota laccase: High-throughput manipulation and analysis of recombinant enzyme libraries expressed in e. Coli using droplet-based microfluidics. *Analyst* **2014**, *139* (13), 3314-23.
- (178) Woronoff, G.; El Harrak, A.; Mayot, E.; Schicke, O.; Miller, O. J.; Soumillion, P.; Griffiths, A. D.; Ryckelynck, M. New generation of amino coumarin methyl sulfonate-based fluorogenic substrates for amidase assays in droplet-based microfluidic applications. *Anal. Chem.* **2011**, *83* (8), 2852-7.
- (179) Gruner, P.; Riechers, B.; Semin, B.; Lim, J.; Johnston, A.; Short, K.; Baret, J.-C. Controlling molecular transport in minimal emulsions. *Nat. Commun.* **2016**, *7* (1), 10392.
- (180) Mazutis, L.; Baret, J.-C.; Treacy, P.; Skhiri, Y.; Araghi, A. F.; Ryckelynck, M.; Taly, V.; Griffiths, A. D. Multi-step microfluidic droplet processing: Kinetic analysis of an in vitro translated enzyme. *Lab Chip* **2009**, *9* (20), 2902-8.
- (181) Courtois, F.; Olguin, L. F.; Whyte, G.; Theberge, A. B.; Huck, W. T. S.; Hollfelder, F.; Abell, C. Controlling the retention of small molecules in emulsion microdroplets for use in cell-based assays. *Anal. Chem.* **2009**, *81* (8), 3008-16.
- (182) Skhiri, Y.; Gruner, P.; Semin, B.; Brosseau, Q.; Pekin, D.; Mazutis, L.; Goust, V.; Kleinschmidt, F.; El Harrak, A.; Hutchison, J. B. et al. Dynamics of molecular transport by surfactants in emulsions. *Soft Matter* **2012**, *8* (41), 10618-27.
- (183) Pan, M.; Lyu, F.; Tang, S. K. Y. Fluorinated pickering emulsions with nonadsorbing interfaces for droplet-based enzymatic assays. *Anal. Chem.* **2015**, *87* (15), 7938-43.
- (184) Pan, M.; Rosenfeld, L.; Kim, M.; Xu, M.; Lin, E.; Derda, R.; Tang, S. K. Y. Fluorinated pickering emulsions impede interfacial transport and form rigid interface for the growth of anchorage-dependent cells. *ACS Appl. Mater. Interfaces* **2014**, *6* (23), 21446-53.
- (185) Fenneteau, J.; Chauvin, D.; Griffiths, A. D.; Nizak, C.; Cossy, J. Synthesis of new hydrophilic rhodamine based enzymatic substrates compatible with droplet-based microfluidic assays. *ChemComm* **2017**, *53* (39), 5437-40.
- (186) Beneyton, T.; Thomas, S.; Griffiths, A. D.; Nicaud, J.-M.; Drevelle, A.; Rossignol, T. Droplet-based microfluidic high-throughput screening of heterologous enzymes secreted by the yeast *yarrowia lipolytica*. *Microb Cell Fact* **2017**, *16* (1), 18.
- (187) Ma, F.; Chung, M. T.; Yao, Y.; Nidetz, R.; Lee, L. M.; Liu, A. P.; Feng, Y.; Kurabayashi, K.; Yang, G.-Y. Efficient molecular evolution to generate enantioselective enzymes using a dual-channel microfluidic droplet screening platform. *Nat. Commun.* **2018**, *9* (1), 1030.
- (188) Holstein, J. M.; Gylstorff, C.; Hollfelder, F. Cell-free directed evolution of a protease in microdroplets at ultrahigh throughput. *ACS Synth. Biol.* **2021**, *10* (2), 252-7.
- (189) Yadav, J. S.; Subba Reddy, B. V.; Narayana Kumar, G. G. K. S.; Aravind, S. The 'aqueous' prins cyclization: A diastereoselective synthesis of 4-hydroxytetrahydropyran derivatives. *Synthesis* **2008**, *2008* (03), 395-400.
- (190) Doro, F.; Akeroyd, N.; Schiet, F.; Narula, A. The prins reaction in the fragrance industry: 100th anniversary (1919–2019). *Angew. Chem. Int. Ed.* **2019**, *58* (22), 7174-9.
- (191) Liu, L.; Kaib, P. S. J.; Tap, A.; List, B. A general catalytic asymmetric prins cyclization. *J. Am. Chem. Soc.* **2016**, *138* (34), 10822-5.
- (192) Chavre, S. N.; Choo, H.; Lee, J. K.; Pae, A. N.; Kim, Y.; Cho, Y. S. 5- and 6-exocyclic products, cis-2,3,5-trisubstituted tetrahydrofurans, and cis-2,3,6-trisubstituted tetrahydropyrans via prins-type cyclization. *J. Org. Chem.* **2008**, *73* (19), 7467-71.
- (193) Bach, T.; Löbel, J. Selective prins reaction of styrenes and formaldehyde catalyzed by 2,6-di-tert-butylphenoxy(difluoro)borane. *Synthesis* **2002**, *2002* (17), 2521-6.
- (194) Polshettiwar, V.; Varma, R. S. Tandem bis-aldol reaction of ketones: A facile one-pot synthesis of 1,3-dioxanes in aqueous medium. *J. Org. Chem.* **2007**, *72* (19), 7420-2.
- (195) Jacolot, M.; Jean, M.; Levoin, N.; van de Weghe, P. The prins reaction using ketones: Rationalization and application toward the synthesis of the portentol skeleton. *Org. Lett.* **2012**, *14* (1), 58-61.
- (196) Nakatani, Y.; Kawashima, K. A highly stereoselective preparation of l-isopulegol. *Synthesis* **1978**, *1978* (02), 147-8.
- (197) Iwata, T.; Okeda, Y.; Hori, Y.; Takasago International Corporation, Japan . 2002.
- (198) Mäki-Arvela, P.; Kumar, N.; Nieminen, V.; Sjöholm, R.; Salmi, T.; Murzin, D. Y. Cyclization of citronellal over zeolites and mesoporous materials for production of isopulegol. *J. Catal.* **2004**, *225* (1), 155-69.
- (199) Nilewski, C.; Deprez, N. R.; Fessard, T. C.; Li, D. B.; Geisser, R. W.; Carreira, E. M. Synthesis of undecachlorosulfolipid a: Re-evaluation of the nominal structure. *Angew. Chem. Int. Ed.* **2011**, *50* (34), 7940-3.
- (200) Mortensen, M. S.; Osbourn, J. M.; O'Doherty, G. A. De novo formal synthesis of (-)-virginiamycin m2 via the asymmetric hydration of dienolates. *Org. Lett.* **2007**, *9* (16), 3105-8.
- (201) Comito, R. J.; Finelli, F. G.; MacMillan, D. W. C. Enantioselective intramolecular aldehyde α -alkylation with simple olefins: Direct access to homo-ene products. *J. Am. Chem. Soc.* **2013**, *135* (25), 9358-61.
- (202) Omura, K.; Swern, D. Oxidation of alcohols by "activated" dimethyl sulfoxide. A preparative, steric and mechanistic study. *Tetrahedron* **1978**, *34* (11), 1651-60.
- (203) Piancatelli, G.; Leonelli, F. Oxidation of nerol to neral with iodosobenzene and tempo: [(z)-3, 7-dimethyl-2, 6-octadienal]. *Org. Synth.* **2003**, *83*, 18-23.
- (204) Guo, S.; Liu, J.; Ma, D. Total synthesis of leucosceptroids a and b. *Angew. Chem. Int. Ed.* **2015**, *54* (4), 1298-301.

- (205) Kliman, L. T.; Mlynarski, S. N.; Ferris, G. E.; Morken, J. P. Catalytic enantioselective 1,2-diboration of 1,3-dienes: Versatile reagents for stereoselective allylation. *Angew. Chem. Int. Ed.* **2012**, *51* (2), 521-4.
- (206) Shaffer, C. J.; Schröder, D.; Gütz, C.; Lützen, A. Intramolecular C–H bond activation through a flexible ester linkage. *Angew. Chem. Int. Ed.* **2012**, *51* (32), 8097-100.
- (207) Kambe, T.; Maruyama, T.; Naganawa, A.; Asada, M.; Seki, A.; Maruyama, T.; Nakai, H.; Toda, M. Discovery of an 8-aza-5-thiaprostaglandin e1 analog as a highly selective ep4 receptor agonist. *Chem Pharm Bull (Tokyo)* **2011**, *59* (12), 1494-508.
- (208) Lee, K.; Poudel, Y. B.; Glinkerman, C. M.; Boger, D. L. Total synthesis of dihydrolysergic acid and dihydrolysergol: Development of a divergent synthetic strategy applicable to rapid assembly of d-ring analogs. *Tetrahedron* **2015**, *71* (35), 5897-905.
- (209) Betke, T.; Rommelmann, P.; Oike, K.; Asano, Y.; Gröger, H. Cyanide-free and broadly applicable enantioselective synthetic platform for chiral nitriles through a biocatalytic approach. *Angew. Chem. Int. Ed.* **2017**, *56* (40), 12361-6.
- (210) Heretsch, P.; Rabe, S.; Giannis, A. Synthesis of all diastereomers of the piperidine-alkaloid substructure of cyclopamine. *Org. Lett.* **2009**, *11* (23), 5410-2.
- (211) Su, X.; Chen, B.; Wang, S.; Chen, H.; Chen, C. Atom- and step-efficient construction of five-membered carbocycles with alkenes and alkynes catalyzed by AgSbf6. *ACS Catal.* **2018**, *8* (9), 7760-5.
- (212) Lecourt, C.; Boinapally, S.; Dhambri, S.; Boissonnat, G.; Meyer, C.; Cossy, J.; Sautel, F. O.; Massiot, G.; Ardisson, J.; Sorin, G. Elaboration of sterically hindered δ -lactones through ring-closing metathesis: Application to the synthesis of the c1–c27 fragment of hemicalcid. *J. Org. Chem.* **2016**, *81* (24), 12275-90.
- (213) Percec, V.; Peterca, M.; Sienkowska, M. J.; Ilies, M. A.; Aqad, E.; Smidrcal, J.; Heiney, P. A. Synthesis and retrosynthetic analysis of libraries of ab3 and constitutional isomeric ab2 phenylpropyl ether-based supramolecular dendrimers. *J. Am. Chem. Soc.* **2006**, *128* (10), 3324-34.
- (214) Vekariya, R. H.; Aubé, J. Hexafluoro-2-propanol-promoted intermolecular Friedel-Crafts acylation reaction. *Org. Lett.* **2016**, *18* (15), 3534-7.
- (215) Wade Jr., L. G. In *Encyclopedia of reagents for organic synthesis*, DOI:<https://doi.org/10.1002/047084289X.rs107> <https://doi.org/10.1002/047084289X.rs107>.
- (216) Giger, L.; Caner, S.; Obexer, R.; Kast, P.; Baker, D.; Ban, N.; Hilvert, D. Evolution of a designed retro-aldolase leads to complete active site remodeling. *Nat. Chem. Biol.* **2013**, *9* (8), 494-8.
- (217) Pijper, D.; Jongejan, M. G. M.; Meetsma, A.; Feringa, B. L. Light-controlled supramolecular helicity of a liquid crystalline phase using a helical polymer functionalized with a single chiroptical molecular switch. *J. Am. Chem. Soc.* **2008**, *130* (13), 4541-52.
- (218) Zou, Q.; Li, X.; Zhou, J.; Bai, K.; Ågren, H. Synthesis and photochromism of a spirooxazine derivative featuring a carbazole moiety: Fast thermal bleaching and excellent fatigue resistance. *Dyes Pigm.* **2014**, *107*, 174-81.
- (219) McGonigal, P. R.; de León, C.; Wang, Y.; Homs, A.; Solorio-Alvarado, C. R.; Echavarren, A. M. Gold for the generation and control of fluxional barbaralyl cations. *Angew. Chem.* **2012**, *124* (52), 13270-3.
- (220) Ahmed, R.; Altieri, A.; D'Souza, D. M.; Leigh, D. A.; Mullen, K. M.; Pappmeyer, M.; Slawin, A. M.; Wong, J. K.; Woollins, J. D. Phosphorus-based functional groups as hydrogen bonding templates for rotaxane formation. *J. Am. Chem. Soc.* **2011**, *133* (31), 12304-10.
- (221) Stöbel, A.; Schlenk, M.; Hinz, S.; Küppers, P.; Heer, J.; Gütschow, M.; Müller, C. E. Dual targeting of adenosine A2A receptors and monoamine oxidase B by 4h-3,1-benzothiazin-4-ones. *J. Med. Chem.* **2013**, *56* (11), 4580-96.
- (222) Eißler, S.; Bogner, T.; Nahrwold, M.; Sewald, N. Efficient synthesis of cryptophycin-52 and novel para-alkoxymethyl unit analogues. *Chem. Eur. J.* **2009**, *15* (42), 11273-87.
- (223) Blümke, T. D.; Piller, F. M.; Knochel, P. Preparation of highly functionalized alkylzinc halides from alkyl bromides using Mg, ZnCl2 and LiCl. *ChemComm* **2010**, *46* (23), 4082-4.
- (224) Huo, S. Highly efficient, general procedure for the preparation of alkylzinc reagents from unactivated alkyl bromides and chlorides. *Org. Lett.* **2003**, *5* (4), 423-5.
- (225) Tojo, G.; Fernandez, M. I. *Oxidation of alcohols to aldehydes and ketones: A guide to current common practice*; Springer Science & Business Media, 2006.
- (226) Kasturi, T.; Arunachalam, T. Studies in dehydrogenation of 6-methoxy-1-tetralone. Structure of a novel product formed with tetrachloro-1,2-benzoquinone. *Can. J. Chem.* **1968**, *46* (23), 3625-9.
- (227) Drienovská, I.; Mayer, C.; Dulson, C.; Roelfes, G. A designer enzyme for hydrazone and oxime formation featuring an unnatural catalytic aniline residue. *Nat. Chem.* **2018**, *10* (9), 946-52.
- (228) Raindlová, V.; Pohl, R.; Klepetářová, B.; Havran, L.; Šimková, E.; Horáková, P.; Pivoňková, H.; Fojta, M.; Hocek, M. Synthesis of hydrazone-modified nucleotides and their polymerase incorporation onto DNA for redox labeling. *ChemPlusChem* **2012**, *77* (8), 652-62.
- (229) Kölmel, D. K.; Kool, E. T. Oximes and hydrazones in bioconjugation: Mechanism and catalysis. *ChemRev* **2017**, *117* (15), 10358-76.
- (230) Stachissini, A. S.; Do Amaral, L. Kinetics and mechanism of benzaldehyde Girard T hydrazone formation. *J. Org. Chem.* **1991**, *56* (4), 1419-24.
- (231) Jencks, W. Progress in physical organic chemistry. Vol. II, *Interscience, New York* **1964**, 110.
- (232) Wang, C.; Koh, H. J.; Xu, Z.; Liu, X. Theoretical studies on triplet formations in nitrobenzoxadiazole (nbd) derivatives: The impact of donor group and heteroatom substitution. *Results Chem.* **2021**, *3*, 100116.
- (233) Norris, S. R.; Warner, C. C.; Lampkin, B. J.; Bouc, P.; VanVeller, B. Synthesis and spectral properties of push-pull dyes based on isobenzofuran scaffolds. *Org. Lett.* **2019**, *21* (10), 3817-21.

- (234) Benson, S.; Fernandez, A.; Barth, N. D.; de Moliner, F.; Horrocks, M. H.; Herrington, C. S.; Abad, J. L.; Delgado, A.; Kelly, L.; Chang, Z. et al. Scotfluors: Small, conjugatable, orthogonal, and tunable fluorophores for in vivo imaging of cell metabolism. *Angew. Chem. Int. Ed.* **2019**, *58* (21), 6911-5.
- (235) Masuda, M.; Toriumi, C.; Santa, T.; Imai, K. Fluorogenic derivatization reagents suitable for isolation and identification of cysteine-containing proteins utilizing high-performance liquid chromatography–tandem mass spectrometry. *Anal. Chem.* **2004**, *76* (3), 728-35.
- (236) Wu, Y.; Chen, Z.; Yang, Y.; Zhu, W.; Zhou, B. Rh(iii)-catalyzed redox-neutral unsymmetrical C-H alkylation and amidation reactions of N-phenoxyacetamides. *J. Am. Chem. Soc.* **2018**, *140* (1), 42-5.
- (237) Brahmachari, G. Microwave-assisted Hirao reaction: Recent developments. *ChemTexts* **2015**, *1* (3), 15.
- (238) Gao, H.; Xu, Q.-L.; Keene, C.; Kuerti, L. Scalable, transition-metal-free direct oxime O-arylation. Rapid access to O-arylhydroxylamines and substituted benzo[b]furans. *Chem. - Eur. J.* **2014**, *20* (29), 8883-7.
- (239) Kalas, H.; Reichetseder, A.; Scheibelreiter, V.; Rudroff, F.; Stanetty, C.; Mihovilovic, M. D. A kinetic photometric assay for the quantification of the open-chain content of aldoses. *Eur. J. Org. Chem.* **2021**, *2021* (18), 2589-93.
- (240) Xiong, Y.; Li, F.; Babault, N.; Dong, A.; Zeng, H.; Wu, H.; Chen, X.; Arrowsmith, C. H.; Brown, P. J.; Liu, J. Discovery of potent and selective inhibitors for g9a-like protein (glp) lysine methyltransferase. *J. Med. Chem.* **2017**, *60* (5), 1876-91.
- (241) Orlandi, M.; Brenna, D.; Harms, R.; Jost, S.; Benaglia, M. Recent developments in the reduction of aromatic and aliphatic nitro compounds to amines. *Org. Process Res. Dev.* **2018**, *22* (4), 430-45.
- (242) Silverberg, L. J.; Dillon, J. L.; Vemishetti, P. A simple, rapid and efficient protocol for the selective phosphorylation of phenols with dibenzyl phosphite. *Tetrahedron Letters* **1996**, *37* (6), 771-4.
- (243) Goossen, L. J.; Dezfuli, M. K. Practical protocol for the palladium-catalyzed synthesis of arylphosphonates from bromoarenes and diethyl phosphite. *Synlett* **2005**, *2005* (03), 445-8.
- (244) Kalek, M.; Ziadi, A.; Stawinski, J. Microwave-assisted palladium-catalyzed cross-coupling of aryl and vinyl halides with h-phosphonate diesters. *Org. Lett.* **2008**, *10* (20), 4637-40.
- (245) Leypold, M.; Wallace, P. W.; Kljajic, M.; Schittmayer, M.; Pletz, J.; Illaszewicz-Trattner, C.; Guebitz, G. M.; Birner-Gruenberger, R.; Breinbauer, R. A robust and simple protocol for the synthesis of arylfluorophosphonates. *Tetrahedron Letters* **2015**, *56* (41), 5619-22.
- (246) McKenna, C. E.; Schmidhuser, J. Functional selectivity in phosphonate ester dealkylation with bromotrimethylsilane. *J. Chem. Soc., Chem. Commun.* **1979**, DOI:10.1039/C39790000739 10.1039/C39790000739(17), 739-.
- (247) Li, L.; Li, A.; Song, L.; Wang, Z.-H.; Zhou, X.-H.; Yang, T.; Huang, W. Synthesis, structure and properties of a tetranuclear europium(iii) complex based on 9,9-dimethylfluorene-2,7-diphosphonic acid. *J. Mol. Struct.* **2014**, *1067*, 37-42.
- (248) Brocklesby, K. L.; Waby, J. S.; Cawthorne, C.; Smith, G. An alternative synthesis of vandetanib (caprelsa™) via a microwave accelerated dimroth rearrangement. *Tetrahedron Letters* **2017**, *58* (15), 1467-9.
- (249) Yamamoto, S.; Tochigi, H.; Yamazaki, S.; Nakahama, S.; Yamaguchi, K. Synthesis of amphiphilic diblock copolymer using heterobifunctional linkers, connected by a photodegradable N-(2-nitrobenzyl) imide structure and available for two different click chemistries. *Bull. Chem. Soc. Jpn.* **2016**, *89* (4), 481-9.
- (250) Bowers, G. N., Jr.; McComb, R. B.; Christensen, R. G.; Schaffer, R. High-purity 4-nitrophenol: Purification, characterization, and specifications for use as a spectrophotometric reference material. *Clin. Chem.* **1980**, *26* (6), 724-9.
- (251) Shipilovskikh, S. A.; Vaganov, V. Y.; Denisova, E. I.; Rubtsov, A. E.; Malkov, A. V. Dehydration of amides to nitriles under conditions of a catalytic Appel reaction. *Org. Lett.* **2018**, *20* (3), 728-31.
- (252) Si, T.; Li, B.; Xiong, W.; Xu, B.; Tang, W. Efficient cross-coupling of aryl/alkenyl triflates with acyclic secondary alkylboronic acids. *Org. Biomol. Chem.* **2017**, *15* (46), 9903-9.
- (253) Phakhodee, W.; Duangkamol, C.; Wiriyi, N.; Pattarawarapan, M. A convenient one-pot synthesis of N-substituted amidoximes and their application toward 1,2,4-oxadiazol-5-ones. *RSC Adv.* **2018**, *8* (67), 38281-8.
- (254) Hyland, C. J.; O'Connor, C. J. The acid-catalysed hydrolysis of benzonitrile. *J. Chem. Soc., Perkin Trans. 2* **1973**, DOI:10.1039/P29730000223 10.1039/P29730000223(2), 223-7.
- (255) Fischer, K. Neues verfahren zur maßanalytischen bestimmung des wassergehaltes von flüssigkeiten und festen körnern. *Angew. Chem.* **1935**, *48* (26), 394-6.
- (256) Short, J.; Roberts, J.; Roberts, D.; Hodges, G.; Gutsell, S.; Ward, R. Practical methods for the measurement of log p for surfactants. *Ecotoxicol Environ Saf* **2010**, *73* (6), 1484-9.
- (257) Gielen, F.; Hours, R.; Emond, S.; Fischlechner, M.; Schell, U.; Hollfelder, F. Ultrahigh-throughput-directed enzyme evolution by absorbance-activated droplet sorting (aads). *Proceedings of the National Academy of Sciences* **2016**, *113* (47), E7383-E9.
- (258) Beneyton, T.; Coldren, F.; Baret, J.-C.; Griffiths, A. D.; Taly, V. Cota laccase: High-throughput manipulation and analysis of recombinant enzyme libraries expressed in E. coli using droplet-based microfluidics. *Analyst* **2014**, *139* (13), 3314-23.
- (259) Colin, P.-Y.; Kintses, B.; Gielen, F.; Miton, C. M.; Fischer, G.; Mohamed, M. F.; Hyvönen, M.; Morgavi, D. P.; Janssen, D. B.; Hollfelder, F. Ultrahigh-throughput discovery of promiscuous enzymes by picodroplet functional metagenomics. *Nat. Commun.* **2015**, *6* (1), 10008.
- (260) Weng, L.; Spoonamore, J. E. Droplet microfluidics-enabled high-throughput screening for protein engineering. *Micromachines* **2019**, *10* (11), 734.

- (261) Lake, M.; Narciso, C.; Cowdrick, K.; Storey, T.; Zhang, S.; Zartman, J.; Hoelzle, D. Microfluidic device design, fabrication, and testing protocols. *Protoc. Exch.* **2015**, *10* (10.1038).
- (262) Wyatt Shields Iv, C.; Reyes, C. D.; López, G. P. Microfluidic cell sorting: A review of the advances in the separation of cells from debulking to rare cell isolation. *Lab Chip* **2015**, *15* (5), 1230-49.
- (263) Greb, C. Infinity optical systems: From infinity optics to the infinity port. *Optik & Photonik* **2016**, *11* (1), 34-7.
- (264) Qiao, Y.; Zhao, X.; Zhu, J.; Tu, R.; Dong, L.; Wang, L.; Dong, Z.; Wang, Q.; Du, W. Fluorescence-activated droplet sorting of lipolytic microorganisms using a compact optical system. *Lab Chip* **2018**, *18* (1), 190-6.
- (265) Shembekar, N.; Hu, H.; Eustace, D.; Merten, C. A. Single-cell droplet microfluidic screening for antibodies specifically binding to target cells. *Cell Rep.* **2018**, *22* (8), 2206-15.
- (266) Qiao, Y.; Hu, R.; Chen, D.; Wang, L.; Fu, Y.; Li, C.; Dong, Z.; Weng, Y.; Du, W. Fluorescence-activated droplet sorting of polyethylene terephthalate degrading enzymes. *BioRxiv* **2021**, DOI:10.1101/2021.05.12.443719 10.1101/2021.05.12.443719, 2021.05.12.443719.
- (267) Boutros, A.; Betz, V. Fpga architecture: Principles and progression. *IEEE Circuits Syst. Mag.* **2021**, *21* (2), 4-29.
- (268) Kohout, M.; Svoboda, J.; Novotná, V.; Pocięcha, D.; Glogarová, M.; Gorecka, E. A nematic-polar columnar phase sequence in new bent-shaped liquid crystals based on a 7-hydroxynaphthalene-2-carboxylic acid core. *J. Mater. Chem.* **2009**, *19* (20), 3153-60.
- (269) Jacques, J. Molecular structure and estrogenic activity. Xi. New structural isomers in the allenolic acid series. *Bull. Soc. Chim. Fr.* **1952**, 573.
- (270) Tsuno, Y.; Sawada, M.; Fujii, T.; Yukawa, Y. The substituent effect. 14. The solvolysis of 6-and 7-substituted 1-(2-naphthyl) ethyl chlorides. *Bull. Chem. Soc. Jpn.* **1979**, *52* (10), 3033-42.
- (271) Ahmed, R.; Altieri, A.; D'Souza, D. M.; Leigh, D. A.; Mullen, K. M.; Pappmeyer, M.; Slawin, A. M. Z.; Wong, J. K. Y.; Woollins, J. D. Phosphorus-based functional groups as hydrogen bonding templates for rotaxane formation. *J. Am. Chem. Soc.* **2011**, *133* (31), 12304-10.
- (272) Sibi, M. P.; Dankwardt, J. W.; Snieckus, V. Anionic aromatic ring annelation of o-allyl benzamides. Regiospecific synthesis of naphthols and naphthoquinones. *J. Org. Chem.* **1986**, *51* (2), 271.
- (273) Villani, F. J.; King, M. S.; Papa, D. Selective raney nickel hydrogenation of methyl 4-(6-methoxy-1,2,3,4-tetrahydro-1-naphthylidene)crotonate. Synthesis of 1-oxo-7-methoxy-1,2,3,4,9,10-hexahydrophenanthrene. *J. Org. Chem.* **1953**, *18*, 1578.
- (274) Danishefsky, S.; Harayama, T.; Singh, R. K. Use of β -phenylsulfanyl- α,β -unsaturated carbonyl dienophiles in diels-alder reactions. *J. Am. Chem. Soc.* **1979**, *101* (23), 7008.
- (275) Liu, T.; Jiang, Y.; Liu, Z.; Li, J.; Fang, K.; Zhuang, C.; Du, L.; Fang, H.; Sheng, C.; Li, M. Environment-sensitive turn-on fluorescent probes for p53–mdm2 protein–protein interaction. *MedChemComm* **2017**, *8* (8), 1668-72.
- (276) Tsukamoto, Y.; Santa, T.; Saimaru, H.; Imai, K.; Funatsu, T. Synthesis of benzofurazan derivatization reagents for carboxylic acids and its application to analysis of fatty acids in rat plasma by high-performance liquid chromatography–electrospray ionization mass spectrometry. *Biomed. Chromatogr.* **2005**, *19* (10), 802-8.
- (277) Mikhailitsyn, F. S. Syntheses in the benzo[2,1,3]thiadiazole series. *Chem. Heterocycl. Compd.* **1973**, *9* (3), 293-5.
- (278) Schliemann, W. Synthesis of some derivatives of 3,6-diphenyl-s-tetrazine. *Wiss. Z. - Martin-Luther-Univ. Halle-Wittenberg, Math.-Naturwiss. Reihe* **1981**, *30* (4), 65.
- (279) Patrick, D. A.; Bakunov, S. A.; Bakunova, S. M.; Kumar, E. V. K. S.; Lombardy, R. J.; Jones, S. K.; Bridges, A. S.; Zhirnov, O.; Hall, J. E.; Wenzler, T. et al. Synthesis and in vitro antiprotozoal activities of dicationic 3,5-diphenylisoxazoles. *J. Med. Chem.* **2007**, *50* (10), 2468-85.
- (280) Bartlett, M. F.; Dickel, D. F.; Taylor, W. I. The alkaloids of tabernanthe iboga. Part iv.1 the structures of ibogamine, ibogaine, tabernanthine and voacangine. *J. Am. Chem. Soc.* **1958**, *80* (1), 126-36.